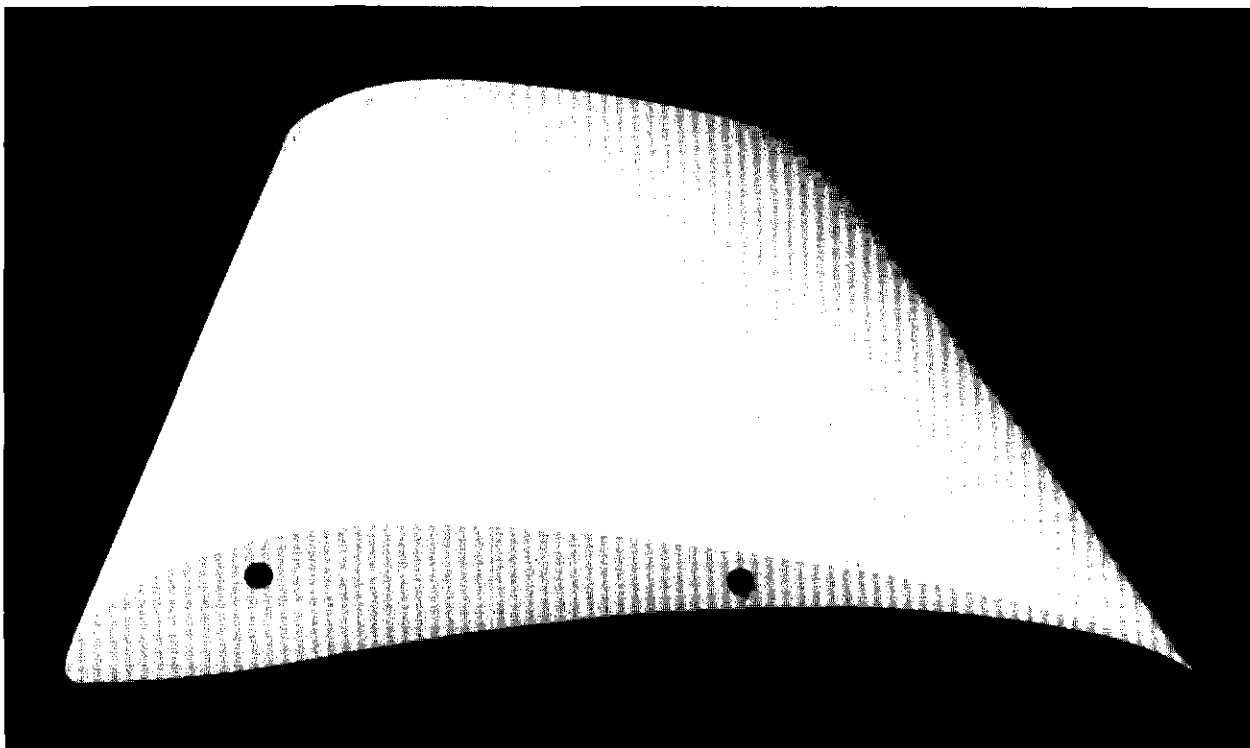


Summary of Low-Speed Airfoil Data

Michael S. Selig, James J. Guglielmo, Andy P. Broeren and Philippe Giguère



Summary of Low-Speed Airfoil Data

Volume 1

About the Authors

DR. MICHAEL S. SELIG, an accomplished applied aerodynamicist and airfoil designer, is an Assistant Professor of Aeronautical and Astronautical Engineering at the University of Illinois at Urbana-Champaign. He received his B.S. (1984) from the University of Illinois, his M.S.E. (1988) from Princeton University and his Ph.D. (1992) from the Pennsylvania State University. His current research areas include low Reynolds number airfoil aerodynamics, multi-point inverse design of slot suction airfoils, horizontal-axis wind-turbine system design and analysis, and flight simulation. He teaches courses in applied aerodynamics and aircraft design.

JAMES J. GUGLIELMO received his Bachelor of Science degree in Aeronautical and Astronautical Engineering from the University of Illinois at Urbana-Champaign in May 1992. Remaining at the University of Illinois for graduate studies, his research has included such topics as experimental supersonic and subsonic wind-tunnel testing, Magnetic Levitation (MagLev) vehicle design, and the conceptual design of a wing-in-ground-effect aircraft. Mr. Guglielmo is also the co-founder and present coordinator of the UIUC Low-Speed Airfoil Tests and is working toward a Master of Science degree in experimental low Reynolds number airfoil aerodynamics. Research interests include applied aerodynamics, flight mechanics, and aircraft conceptual/advanced design.

ANDY P. BROEREN received his Bachelor of Science degree in Mechanical Engineering from the Milwaukee School of Engineering, Milwaukee, Wisconsin in 1993. Several months after beginning graduate study in mechanical engineering at the University of Illinois, he joined Prof. Selig and Mr. Guglielmo in their efforts to establish a program for testing low Reynolds number airfoils. In addition to continuing work in this area, Mr. Broeren is presently working toward a Master of Science degree with thesis research in unsteady fluid mechanics. His interest in aerodynamics, particularly involving high-lift, low Reynolds number airfoil research, results from several years of participation in the Society of Automotive Engineer's (S.A.E.) Aero-Design competition.

PHILIPPE GIGUÈRE received his Bachelor of Mechanical Engineering degree from McGill University, Montreal, Canada in 1992 and his Master of Science degree from Université Laval, Quebec, Canada in 1994. Shortly after receiving his Master's degree, he joined the Department of Aeronautical and Astronautical Engineering at the University of Illinois at Urbana-Champaign. He is currently working toward a Ph.D. degree with research in optimization of wind turbine rotors, wind-tunnel boundary-layer corrections and airfoil performance enhancement. His experience with R/C model airplanes comes from his participation in the Society of Automotive Engineer's (S.A.E.) Aero-Design competition from 1991-1994. He also flies full-scale gliders.

Michael S. Selig
James J. Guglielmo
Andy P. Broeren
Philippe Giguère

*Department of Aeronautical and Astronautical Engineering
University of Illinois at Urbana-Champaign*

Summary of Low-Speed Airfoil Data

Volume 1



SoarTech Publications
Virginia Beach, Virginia

SOARTECH PUBLICATIONS
1504 N. Horseshoe Circle
Virginia Beach, Virginia 23451, USA

Copyright © 1995 by
Michael S. Selig, James J. Guglielmo, Andy P. Broeren, and Philippe Giguère
All rights reserved.

*Cover photograph by Bill Weigand, University of Illinois News Bureau
Wind tunnel model (S1223) by Yvan Tinel, Tinel Technologies, Northbrook, Illinois*

First Printing, June 1995

Library of Congress Cataloging in Publication Data

Selig, Michael Scott
Summary of Low-Speed Airfoil Data, Volume 1 / by Michael Selig,
James Guglielmo, Andy Broeren and Philippe Giguère.

Includes bibliographical references.

1. Aerofoils. 2. Aerodynamics. 3. Airplanes—Models.

I. Model Aviation. II. Title

95-69524

ISBN 0-9646747-1-8

Contents

PREFACE	<i>iii</i>
ACKNOWLEDGMENTS	<i>v</i>
AIRFOIL DATA DISTRIBUTION	<i>ix</i>
LIST OF FIGURES	<i>xi</i>
LIST OF TABLES	<i>xvii</i>
LIST OF SYMBOLS	<i>xix</i>
1 THE AIRFOILS TESTED	1
2 WIND-TUNNEL FACILITY AND MEASUREMENT TECHNIQUES	3
2.1 EXPERIMENTAL FACILITY	3
2.2 MEASUREMENT TECHNIQUES	7
2.2.1 LIFT FORCE MEASUREMENTS	8
2.2.2 DRAG FORCE MEASUREMENTS	9
2.2.3 AIRFOIL MODEL ACCURACY MEASUREMENTS	13
2.2.4 FREESTREAM VELOCITY MEASUREMENTS	13
2.3 DATA REDUCTION	14
2.3.1 WIND-TUNNEL BOUNDARY CORRECTIONS	14
2.3.2 ADDITIONAL VELOCITY CORRECTIONS	16
2.3.3 CORRECTIONS TO MEASURED QUANTITIES	16
2.4 CALIBRATIONS AND UNCERTAINTY ANALYSIS	18
2.5 COMPARISON WITH OTHER FACILITIES	18
3 SUMMARY OF AIRFOIL DATA	23
3.1 AIRFOILS FOR FREE FLIGHT MODELS	27
3.2 AIRFOILS FOR THERMAL DURATION SAILPLANES	31
3.3 AIRFOILS FOR F3B SAILPLANES	34
3.4 AIRFOILS FOR SLOPE RACERS	39
3.5 AIRFOILS FOR TAIL SECTIONS	40
3.6 AIRFOILS FOR QUICKIE 500 PYLON RACERS	42
3.7 AIRFOILS FOR SPORT PLANES	43
3.8 AIRFOILS FOR HEAVY-LIFT CARGO PLANES	45
3.9 AIRFOILS FOR SMALL WIND TURBINES	51
4 AIRFOIL PROFILES AND PERFORMANCE PLOTS	53

ii *Summary of Low-Speed Airfoil Data*

EXTENDED NOTES TO THE TEXT	245
REFERENCES	249
APPENDIX A AIRFOIL COORDINATES	253
APPENDIX B AIRFOIL POLAR DATA	277
APPENDIX C UIUC LOW-SPEED AIRFOIL TESTS MANIFESTO	289

Preface

A reader just discovering airfoil aerodynamics will find it helpful to reference the companion book *Airfoils at Low Speeds* (by Selig, Donovan and Fraser), which was first published as SoarTech 8 in 1989. The book presents the results of wind-tunnel tests conducted at Princeton University on over 60 airfoils for model aircraft (mostly radio controlled sailplanes), and it also introduces the terminology and jargon used here in discussing airfoils at low speeds, specifically, airfoils at low Reynolds numbers.

When the wind-tunnel tests were completed at Princeton in January 1989, no continuation of that effort was planned. In the hope that the tests could be later continued, however, the experimental apparatus and the assorted wind-tunnel models were put in safe storage. Michael Selig continued his graduate studies at Penn State (Ph.D. in Aerospace Engineering) and John Donovan (Ph.D. from Princeton) accepted a position at McDonnell Douglas in St. Louis. Sadly, David Fraser died in an aircraft icing accident in January 1992.

As this book reveals, the opportunity to continue the low-speed airfoil test effort has emerged. In August 1992, Selig joined the faculty in the Department of Aeronautical and Astronautical Engineering at the University of Illinois at Urbana-Champaign. In brief chronological order, re-establishing the airfoil test capability was initiated with the help of two graduate students—Jim Guglielmo (M.S.) and Tony Balow (M.S.). Support from modelers was solicited in December 1993, and the test program was named the UIUC Low-Speed Airfoil Tests. (The tremendous generosity of all those who have contributed to the project is discussed in the acknowledgments.) Preliminary tests were performed in April 1994. Andy Broeren (M.S.) volunteered to join the test team in May 1994. Philippe Giguère (Ph.D.) volunteered to start work on the project in August 1994. The extensive data collection effort mounted for this book took place over a one month period from mid-December 1994 to mid-January 1995. More recently, Cameron Ninham (M.S.) and Ashok Gopalarathnam (Ph.D.) have offered to play a role in future testing. To date, only Jim Guglielmo has been supported (since July 1994) on funds donated by modelers.

This Book and Its Organization

Summary of Low-Speed Airfoil Data is only the first in what should be a series of volumes that document the ongoing low Reynolds number airfoil tests at the University of Illinois at Urbana-Champaign. In this volume, the airfoils tested cover a broad spectrum that includes airfoils for free flight model aircraft, heavy lift R/C aircraft and, of course, R/C sailplanes, to name just a few. As an overview, the 34 airfoils tested are briefly introduced in Chapter 1.

iv *Summary of Low-Speed Airfoil Data*

Chapter 2 is devoted to a discussion of the wind-tunnel test facility and the experimental procedures. This chapter can be skipped by those less interested in the myriad of issues that arise in wind-tunnel testing. Of course, the importance of the methods used in taking and reducing the data cannot be over-emphasized. Although the data collection effort was performed in little more than a month, nearly two and a half years were spent in preparation for the tests. Fortunately, future tests will not require as much preparation time.

This book is primarily designed to be used as a reference for low Reynolds number airfoil data. In Chapter 3, a discussion of all the airfoils is given first; then the figures (airfoil plots and performance data) are presented in Chapter 4. The discussion is organized according to the application (i.e., free flight model airfoils are first discussed, then F3B airfoils and so on for each category). The figures in Chapter 4, however, are organized alphabetically by the airfoil name. For quick referencing of the figures in Chapter 4, the airfoil name is listed in the margin below the page number. Finally, the tabulated airfoil coordinates and performance data (available on diskette) are given in Appendices A and B. Appendix C contains the UIUC Low-Speed Airfoil Tests Manifesto that outlines the scope and purpose of this work.

Acknowledgments

The airfoil testing effort would not have been possible without the support of a large number of people. *To each of them we are indebted.* In particular, for monetary contributions that were used for equipment and a graduate student research assistantship, we are especially grateful to the following organizations, clubs, businesses, individuals and t-shirt patrons. Shown in parentheses for each category is that category's fraction of the total support received. Note that some people are listed more than once since they have helped in different capacities.

- *Organizations (10%):* Academy of Model Aeronautics (with special appreciation to Bob Underwood and others), ISF-International R/C Soaring Forum (with special appreciation to Rolf Girsberger), National Association of Rocketry (Mark Bundick), and National Free Flight Society (with special appreciation to Bob Waterman).
- *Businesses (17%):* Airtronics, Inc. (Bob and Tim Renaud), B² Streamlines (Bill & Bunny Kuhlman), Dan Parsons Products (Dan Parson), F3F Newsletter (Preben Norholm), Gulf R/C (John Rimmer), Kennedy Composites (Barry Kennedy), Landing Products (Fred Burgdorf), Northeast Sailplane Products (Carolyn & Sal DeFranceso), Planeador RC News-Spain (Peter Atkinson, editor) R/C Soaring Digest (Jerry & Judy Slates), Slegers International, Inc. (Ed Slegers), SoarTech Publications (H.A. Stokely) and Websoft, Inc. (Robert Webster).
- *Model Clubs (8%):* B.A.R.C.S., Champaign County Radio Control Club, Clent Soaring Association, Downest Soaring Club, Fairlop Silent Flyers (England), Florida Soaring Society, FMSG Alling/Obb. (Germany), Greek Aeromodelling Federation (Greece), Ivinghoe Soaring Assoc., Lincoln Area Soaring Society, Miniature Aircraft Association of Westchester County (England), North American Scale Soaring Association, Northeast Drone Society, Paducah Aero Modelers, Pasadena Soaring Society, Peninsula Channel Commanders, Portland Area Sailplane Society, Round Valley Radio Control Club, S.E.F.L.I., S.O.A.R., S.W.I.F.T., San Gabriel Valley Radio Control League, Santa Clarita Soaring Assoc., Sheffield Society of Aeromodellers (England), Sundancers R/C Model Club, Tidewater Model Soaring Society, Tri County Aero Club, Tri-Cities Radio Control Modelers Club, Tyler Modelers Club, Victorian Association of Radio Model Soaring (Australia) and W.A. Radio Soarers Club, Inc.,
- *Individuals (58%):* G. Richard Adams, Arnold Angelici, M.D., Thomas Anthony*, Garry Armstrong*, Thomas Atwood, Gary S. Baldwin, Charles Baltzer, Mark Barbee & Charlene Olsen*, Matt Barbian*, Richard Bartkowski, Plenny J. Bates, M.D., David Batey, Jr., Ed Baumgartner, Hans Walter Ben-

der, Byron Blakeslee, Bill Bogart*, Charles Botzko, Chris Bovais*, Arthur J. Boysen*, Ronald Bozzonetti, Phillip Burnside, Wil Byers*, Henry Hain, Kenny Carpenter*, Edward Carter, W.B. Cavanaugh, Paul Clark, Don Coburn, Joseph Conrad*, John Cranmer, Jr.*, Michael J. Cresanta, Michael D. Denton*, Alfred J. DeRenzis*, Armand DeWeese, Dan J. Dobbins, John Donelson, John Drab*, Doug Drullenger*, Chas Dunster*, Hilmar Durden*, Frits Donker Duyvis*, Robert Dyer*, Dr. Don Edberg*, Stefan Eder*, R.J. Edmonds, Nanette & William Entriken, Lars Ericsson*, George L. Fiocca*, Bill Forrey, Norman D. Frank, William S. Friedlander*, Roland Friestad, Myron & Felissa Cagan, David Garwood*, B.I. Gaston*, Robert C. Glover, II, Greg Goldstein, Ed Granger*, Martin Gregorie*, Thomas Gressman*, Charles Griswold, Brian R. Gyles, James Halbert, David L. Hall*, George Harper*, Richard Hognes*, Chuck Hollinger, C.D. Houge, III*, Dale House, Nelson Itterly, Vince Johnkoski*, Darrell Johnson*, Kerry Jones*, Chris Kaiser*, John Kallend*, Michael Lachowski*, James Ladwig, Walter Lareropao*, Benjamin Lawless, Donald Leath, A.G. Lennon, Dr. Robert Livin*, Robert Lockwood, Jr.*, Chuck Lohre, Marco Lorenzomi, Keith C. Love*, Gene Lovejoy*, Warren Lucas*, Steve Lucke, Andrew Macdonald*, Bob Mabli*, G.M. Magarian, Stefano Martini*, Burt Marx, Robert Matheson*, Merlin Meisner, Eric Meyers, Kevin McKiou*, Luther Mitchell*, Owen Morris, Gilbert Morris*, Jeff Morris*, Allen Morse, Tim Mountain, Mark Nankivil*, John D. Newell, M.D.*, Robert Nielsen, Greg Nilsen, Alan Oliver, Bob Peirson*, Paul Penna*, D.N. Penton, John Perry*, James I. Pilkington, Dr. John Ponsford, Ralph Prey, Horst Rabiger, Blaine Beron-Rawdon, David Register, Francis Reynolds, Jerry Robertson, H.J. Rogers*, Dr. Stan Sadorf, David Schenken, Dr. Alan Schwerin*, Allan Scidmore, Marty Selig, Michael S. Selig, Glenn Sembroski*, Robert L. Simon, Arthur Slagle, Charles Smith*, John W. Smith*, Michael Smith*, Howard F. Sosbee, Glen Spackman*, David Steere, Peter Steinmeyer, Helmut Stettmaier, Tim Stover*, R.T. Sunderland*, Jim Tangler, Jose M. Tellez*, Willard L. Teommey, D'Anne Thompson*, G.J. Tonnelli, Jorgen Tonnesen, Gene Trevino*, Craig Uridil, John Vennerholm*, Rick Waitulionis*, Sean Walbank*, Jess Walls*, Garth Warner, Ralph M. Weaver*, I. Jay Welch*, W.D. Williams*, Oliver C. Wilson*, Vern Winston, Graham Woods*, Joe Wurts, Scott Youmans* and Frank Zaic.
(* denotes T-Shirt Patron as well)

- **T-Shirt Patrons (6%):** Anonymous, Dan Abel, David Acker, Les Akers, Helene Anderson, James Armstrong, Peter Averill, Kendra Baier, Robert Barrows, Douglas Barry, Mari K. Bebeau, Dan Bernauer, Carl Bice, Ben Bierman, S.C.M. Blake, Woody Blanchard, William Boisvert, Doug Boyd, Delmar Brengman, Andy P. Broeren, Joyce C. Broeren, Richard Broeren, Sue Broeren, Gary Brokaw, Lois Budill, Chip Bullen, Richard Burns, Roy Bunnell, Gilbert Bureau, John Burke, George Burns, Steve Cameron, Jim Carlton, Bob Champine, Juan Chi, Dale D. Christensen, Michael Christiansen,

Dave Corven, Bruce Cronkhite, Brenden Cyze, David Darling, David Diesen, Ray DiNoble, Brian Dirman, Lawrence Drennan, Peter Dudley, F.G. Durand, David H. Fletcher, Frank Williams, Joel S. Freeman, R. Marc Gellart, Browne Goodwin, Chris Gregg, Kenneth Griffin, W. Grundler, Jim Guglielmo, Don Harris, Pat Hart, Roger Hebner, Bob Harman, George Hilliard, Gary Hyde, Denis Jenkins, Gordon Jennings, Kelly Johnson, Gordon Jones, Douglas Joyce, Stephen J. Kaye, Barry Kennedy, Leon Kincaid, Bruce Kimball, Ron Konicke, Bill Kubiak, Bill & Bunny Kuhlman, Barry Kurath, Michael Laible, Erik Larson, Rick Lacy, Dwayne Lane, Stephen Lee, Sam Lee, Todd Lee, Brian Levy, Carl Luft, Bill Malvey, Skip Miller, William Miller, Myles Moran, Bob Morford, Mark Morimoto, Tom Moritz, Roger Morrell, Chris Munson, Nick Neve, Cameron Ninham, Jerome B. O'Mara, Harold Ochs, Ray Olsen, Richard Orobittg, Steve Pasierb, Don Pesznecker, Pete Peterson, Daryl Pfaff, William L. Potter, Mike Prager, Todd Presley, John Raley, Michael D. Reed, Gary Rexroad, Waid Reynolds, David Rice, John Fulton, Erkko Saviaro, Herm Schmidt, John Schmoll, John Schultz, David Sieger, Jerry Slates, Ed Slegers, Frank Smith, Andy Smith, Karl Sorensen, Bob Steele, Robert Stewart, Larry Storie, Mike Stump Family, Joe Stute, Stephen Syrotiak, Manny Tau, Jose Tellez, Jim Thomas, Keith Thomson, Paul Trist, Jr., Aaron Valdes, Gregory Vasgerosian, Jean Vendette, Roy W. Wampler, Charlie Waugh, Dennis Weatherly, B.J. Weisman, Dr. John B. West, Dr. Frank Wicks, Michael Wilson, Alan Wirth, David Wood, Wayne Yamamoto, John Yee, Gerald Zeigenfuse and Michael Ziaskas.

The meticulous building efforts of the following individuals are greatly appreciated.

- *Wind-Tunnel Model Builders:* Roger Adams (DU 86-084/18*), Mark Allen (FX 63-137, M06-13-128, S822, S823, S1210), Bill Boisvert (S4083*), Ronald Bozzonetti (NACA 2414*), Wil Byers (Quabeck 3.0/10* & 3.0/15*), Bob Champine (RG15), Erik Dahl Christensen (HQW 2/8*, MH30*), Ralph Cooney (A18, MA409, BE50), Charles Fox (MH45), Mike Fox (WASP), William S. Friedlander (R140), Chuck Hollinger (CH 10-48-13, FX 74-CL5-140 MOD), Karl Hutchings (S4083*), Bernd Jäger (flapped SD7037*), Gordon Jones (S7055), Leon Kincaid (K3311), Mike Lachowski (S7012), Bob Matheson (S6062), Harley Michaelis (SD7032), Gilbert Morris (flapped GM-15), Dermot O'Flynn (helicopter blade airfoil*) Charles Smith (John Harem design*), Howard Sosbee (S7055), Leo T. Spychalla (M6*), D'Anne Thompson (SD7037), Tinel Technologies/Yvan Tinel (S1223), Jorgen Tonneson (MH-32*) and Oliver Wilson (S5010*).

(* denotes wind-tunnel models under construction or built after the completion of the most recent wind-tunnel tests)

Those individuals who have helped to promote the airfoil test effort or offered technical assistance include:

- *Other Supporters:* Hermann Andresen, Robert Alexander, Bruce Baker, Serge Barth, Jim Boxmeyer (Boxmeyer Composites), Leornard Burz, Erik Dahl Christiansen, Peter Compton, Dr. Don Edberg, William S. Friedlander, Greg Goldstein, Paul Grassel, Dale House, John Kallend, Michael Laible, Mark Morimoto, Alan Mayhew, Mike McMahon, James Neal, Nick Neve, Mike O'Donnell, Dermot O'Flynn, Paul Penna, John Raley, David Register, Gary Rexroad, John Rimmer (Gulf R/C), Dr. Alan Schwerin, Jörgen Skogh, Charles Smith, Paul Trist, Jr., John West and Scott Winans.

Several others (some already acknowledged) deserve special mention. It is with a deep sense of gratitude that we thank Herk Stokely (SoarTech Publications) for his diligent and ongoing efforts related to distributing *Airfoils at Low Speeds* and now this book. Also, we have been very fortunate to have received a large donation from an anonymous individual to support the purchase of a new computer and additional equipment that has helped to improve and expand the scope of the program. We have benefited greatly from the earlier work of Dr. John Donovan and the late David Fraser, as well as the many other individuals who contributed to the Princeton Tests. The efforts of Cody Robertson in designing the 1994 UIUC LSATs t-shirt is sincerely appreciated. Special thanks are also extended to Karen Evans for her assistance in designing the LSATs logo. We are also appreciative of Gilbert Morris for organizing the construction of the free flight wind-tunnel models. Also, Lisa Selig's efforts and encouragements are greatly appreciated.

Of those at the University of Illinois, we wish to thank Mike Kerho and Stan Berkovich for their help with the data acquisition software. Also, Cameron Ninham is thanked for his considerable help in digitizing the wind-tunnel models. In this regard, we thank Prof. Michael Philpott for the use of his coordinate measuring machine and also Stephen Craggs for initial setup support. Andy Broeren especially wishes to acknowledge his research advisor, Prof. Michael Bragg, for his patience and support throughout the course of this project. We are indebted to Carol Winkler for her efforts in maintaining the mailing lists and processing the donations.

It should be mentioned that some of the work reported here has benefited from other research activities, such as, research sponsored by the Univerisity of Illinois and also research in wind energy supported by the DOE National Renewable Energy Laboratory. Finally, we must apologize to those whom we have inadvertently omitted.

Airfoil Data Distribution

All of the airfoil coordinates and performance data presented in this book (see Chapter 4) are available on IBM and Macintosh compatible diskettes through SoarTech Publications. SoarTech will be returning a portion of the proceeds from all disk and book sales to help support the continuation of these airfoil wind tunnel tests. For more information, write to

SoarTech Publications
c/o Herk Stokely
1504 N. Horseshoe Circle
Virginia Beach, VA 23451
email: herkstok@aol.com

The data is also available on the Internet from the host **opus.aae.uiuc.edu** using anonymous FTP. See the file **/pub/lsat/AIRFOIL.DATA** for directions on which files to copy.

The airfoil performance data is copyrighted, and restrictions are placed on its use. The data may be freely copied and used in any way, e.g., for personal use, in magazine articles or with a commercial product. If the data is used in a magazine article or book, the author must reference this book and state where it can be obtained. If the data is used in a commercial product, there must be no extra charges for providing it—other than the cost of reproduction and distribution. All products that make use of this data must conspicuously state that it was produced under the UIUC Low-Speed Airfoil Test program, and no restrictions can be placed on the recipient with respect to their use of the source data. Furthermore, they must be allowed to copy the original data and freely distribute it as well. It is in this sense that all access to this data is *free*. More details can be found in the general public license that accompanies the data distribution files. A copy of the license, the copyright notice and the UIUC Low-Speed Airfoil Tests Manifesto must be included with each distribution of the data.

If you find the airfoil performance data useful, **please send a donation** to support our work. If you have already made a donation, we hope that you will consider renewing your commitment. Your tax deductible donations (see Appendix C) can be mailed to

Prof. Michael Selig
Dept. of Aeronautical and Astronautical Eng.
University of Illinois at Urbana-Champaign
306 Talbot Laboratory, 104 S. Wright St.
Urbana, IL 61801-2935
email: m-selig@uiuc.edu

x *Summary of Low-Speed Airfoil Data*

List of Figures

1.1	The collection of airfoils tested during Phase I of the UIUC Low-Speed Airfoil Tests (January 1995)	1
2.1	UIUC low-speed subsonic wind tunnel (not to scale)	4
2.2	Photograph of wind-tunnel inlet	4
2.3	Photographs of wind-tunnel test section	5
2.4	Photograph of wind-tunnel fan	6
2.5	Experimental setup (Plexiglas endplates and traverser not shown for clarity)	6
2.6	The x - y traverser system	7
2.7	General wind-tunnel model construction specifications	8
2.8	Control volume for the 2-D momentum deficit method to determine the profile drag	9
2.9	Drag results for the SD6060 airfoil depicting typical spanwise drag variations for the four spanwise stations for $Re = 60,000, 100,000, 200,000$ and $300,000$	11
2.10	Comparison of drag data for the E387 airfoil from various wind-tunnel facilities for $Re = 60,000, 100,000, 200,000$ and $300,000$	19
2.11	Comparison of drag data for the E374 airfoil from the Princeton and UIUC wind-tunnel facilities	21
3.1	Performance characteristics of the S7012 compared with the RG15 and SD7003 for R of 120k	37
3.2	L/D 's for sailplanes based on the S7012, RG15 and SD7003 for R of 120k	38
3.3	Endurance parameters for sailplanes based on the S7012, RG15 and SD7003 for R of 120k	38
3.4	Velocity distributions for the S8052 airfoil for Q-500 competition	43
3.5	Predicted performance characteristics for the S8052	44
3.6	Low Reynolds number airfoil characteristics as a function of the recovery type and pitching moment	49
3.7	$C_{l_{max}}$ characteristics for five Wortmann airfoils (from Ref. 26)	51
4.1	Inviscid velocity distributions for the A18	62
4.2	Comparison between the true and actual A18	62
4.3	Performance characteristics for the A18	63
4.4	Lift characteristics for the A18	64
4.5	Inviscid velocity distributions for the BE50	68
4.6	Comparison between the true and actual BE50	68

4.7	Performance characteristics for the BE50	69
4.8	Lift characteristics for the BE50	70
4.9	Inviscid velocity distributions for the CH 10-48-13	74
4.10	Comparison between the true and actual CH 10-48-13	74
4.11	Performance characteristics for the CH 10-48-13 with a boundary-layer trip	75
4.12	Lift characteristics for the CH 10-48-13 with a boundary-layer trip	76
4.13	Inviscid velocity distributions for the E374 (B)	80
4.14	Comparison between the true and actual E374 (B)	80
4.15	Performance characteristics for the E374 (B)	81
4.16	Lift characteristics for the E374 (B)	82
4.17	Inviscid velocity distributions for the E387 (A)	84
4.18	Comparison between the true and actual E387 (A)	84
4.19	Performance characteristics for the E387 (A)	85
4.20	Lift characteristics for the E387 (A)	86
4.21	Inviscid velocity distributions for the FX 63-137 (B)	88
4.22	Comparison between the true and actual FX 63-137 (B)	88
4.23	Performance characteristics for the FX 63-137 (B)	89
4.24	Lift characteristics for the FX 63-137 (B)	90
4.25	Inviscid velocity distributions for the FX 74-CL5-140 MOD	94
4.26	Comparison between the true and actual FX 74-CL5-140 MOD	94
4.27	Performance characteristics for the FX 74-CL5-140 MOD	95
4.28	Lift characteristics for the FX 74-CL5-140 MOD	96
4.29	Inviscid velocity distributions for the GEMINI	100
4.30	Comparison between the true and actual GEMINI	100
4.31	Performance characteristics for the GEMINI	101
4.32	Lift characteristics for the GEMINI	102
4.33	Spanwise drag characteristics for the GEMINI	103
4.34	Inviscid velocity distributions for the GM15	104
4.35	Reflexed GM15 and comparison between the true and actual GM15	104
4.36	Performance characteristics for the GM15	105
4.37	Lift characteristics for the GM15	106
4.38	Performance characteristics for the reflexed GM15	108
4.39	Lift characteristics for the reflexed GM15	109
4.40	Inviscid velocity distributions for the J5012	112
4.41	Comparison between the true and actual J5012	112
4.42	Lift characteristics for the J5012	113
4.43	Inviscid velocity distributions for the K3311	116
4.44	Comparison between the true and actual K3311	116

4.45	Performance characteristics for the K3311	117
4.46	Lift characteristics for the K3311	118
4.47	Inviscid velocity distributions for the M06-13-128 (B)	120
4.48	Comparison between the true and actual M06-13-128 (B)	120
4.49	Performance characteristics for the M06-13-128 (B)	121
4.50	Lift characteristics for the M06-13-128 (B)	122
4.51	Inviscid velocity distributions for the MA409	126
4.52	Comparison between the true and actual MA409	126
4.53	Performance characteristics for the MA409	127
4.54	Lift characteristics for the MA409	128
4.55	Inviscid velocity distributions for the MB253515	132
4.56	Comparison between the true and actual MB253515	132
4.57	Lift characteristics for the MB253515	133
4.58	Inviscid velocity distributions for the MH45	136
4.59	Comparison between the true and actual MH45	136
4.60	Performance characteristics for the MH45	137
4.61	Lift characteristics for the MH45	138
4.62	Inviscid velocity distributions for the NACA 0009	140
4.63	Comparison between the true and actual NACA 0009	140
4.64	Lift characteristics for the NACA 0009	141
4.65	Inviscid velocity distributions for the NACA 6409	144
4.66	Comparison between the true and actual NACA 6409	144
4.67	Performance characteristics for the NACA 6409	145
4.68	Lift characteristics for the NACA 6409	146
4.69	Spanwise drag characteristics for the NACA 6409	147
4.70	Inviscid velocity distributions for the NACA 64A010	148
4.71	Comparison between the true and actual NACA 64A010	148
4.72	Performance characteristics for the NACA 64A010	149
4.73	Lift characteristics for the NACA 64A010	150
4.74	Inviscid velocity distributions for the R140 (A)	154
4.75	Comparison between the true and actual R140 (A)	154
4.76	Performance characteristics for the R140 (A)	155
4.77	Lift characteristics for the R140 (A)	156
4.78	Inviscid velocity distributions for the RG15 (B)	158
4.79	Comparison between the true and actual RG15 (B)	158
4.80	Performance characteristics for the RG15 (B)	159
4.81	Lift characteristics for the RG15 (B)	160
4.82	Inviscid velocity distributions for the S822	162
4.83	Comparison between the true and actual S822	162

4.84	Performance characteristics for the S822	163
4.85	Lift characteristics for the S822	164
4.86	Inviscid velocity distributions for the S823	166
4.87	Comparison between the true and actual S823	166
4.88	Performance characteristics for the S823	167
4.89	Lift characteristics for the S823	168
4.90	Inviscid velocity distributions for the S1210	170
4.91	Comparison between the true and actual S1210	170
4.92	Performance characteristics for the S1210	171
4.93	Lift characteristics for the S1210	172
4.94	Inviscid velocity distributions for the S1223	176
4.95	Comparison between the true and actual S1223	176
4.96	Performance characteristics for the S1223	177
4.97	Lift characteristics for the S1223	178
4.98	Performance characteristics for the S1223 with vortex generators . .	182
4.99	Lift characteristics for the S1223 with vortex generators	183
4.100	Spanwise drag characteristics for the S1223	187
4.101	Performance characteristics for the S1223 with a Gurney flap . .	188
4.102	Lift characteristics for the S1223 with a Gurney flap	189
4.103	Inviscid velocity distributions for the S6062	190
4.104	Comparison between the true and actual S6062	190
4.105	Performance characteristics for the S6062	191
4.106	Lift characteristics for the S6062	192
4.107	Inviscid velocity distributions for the S7012	194
4.108	Comparison between the true and actual S7012	194
4.109	Performance characteristics for the S7012	195
4.110	Lift characteristics for the S7012	196
4.111	Inviscid velocity distributions for the S7055	198
4.112	Comparison between the true and actual S7055	198
4.113	Performance characteristics for the S7055	199
4.114	Lift characteristics for the S7055	200
4.115	Inviscid velocity distributions for the SD6060	202
4.116	Comparison between the true and actual SD6060	202
4.117	Performance characteristics for the SD6060	203
4.118	Lift characteristics for the SD6060	204
4.119	Inviscid velocity distributions for the SD7003	206
4.120	Comparison between the true and actual SD7003	206
4.121	Performance characteristics for the SD7003	207
4.122	Lift characteristics for the SD7003	208

4.123 Inviscid velocity distributions for the SD7032 (D)	210
4.124 Comparison between the true and actual SD7032 (D)	210
4.125 Performance characteristics for the SD7032 (D)	211
4.126 Lift characteristics for the SD7032 (D)	212
4.127 Inviscid velocity distributions for the SD7032 (E)	214
4.128 Comparison between the true and actual SD7032 (E)	214
4.129 Performance characteristics for the SD7032 (E)	215
4.130 Lift characteristics for the SD7032 (E)	215
4.131 Inviscid velocity distributions for the SD7037 (A)	216
4.132 Comparison between the true and actual SD7037 (A)	216
4.133 Performance characteristics for the SD7037 (A)	217
4.134 Lift characteristics for the SD7037 (A)	218
4.135 Inviscid velocity distributions for the SD7037 (B)	220
4.136 Comparison between the true and actual SD7037 (B)	220
4.137 Performance characteristics for the SD7037 (B)	221
4.138 Lift characteristics for the SD7037 (B)	222
4.139 Inviscid velocity distributions for the SD8000	224
4.140 Comparison between the true and actual SD8000	224
4.141 Performance characteristics for the SD8000	225
4.142 Lift characteristics for the SD8000	226
4.143 Inviscid velocity distributions for the SD8020	228
4.144 Comparison between the true and actual SD8020	228
4.145 Performance characteristics for the SD8020	229
4.146 Lift characteristics for the SD8020	230
4.147 Lift characteristics for the SD8020 with a boundary-layer trip	234
4.148 Performance characteristics for the SD8020 with a boundary-layer trip	237
4.149 Lift characteristics for the SD8020 with a boundary-layer trip	238
4.150 Inviscid velocity distributions for the WASP	240
4.151 Comparison between the true and actual WASP	240
4.152 Performance characteristics for the WASP	241
4.153 Lift characteristics for the WASP	242

List of Tables

3.1	Airfoils Sorted by Category	24
3.2	Summary of Airfoil Data for Free Flight Models	28
3.3	Summary of Airfoil Data for Thermal Duration Sailplanes	32
3.4	Summary of Airfoil Data for F3B Sailplanes	35
3.5	Summary of Airfoil Data for Slope Racers	39
3.6	Summary of Airfoil Data for Tail Sections	41
3.7	Summary of Airfoil Data for Quickie 500 Pylon Racers	42
3.8	Summary of Airfoil Data for Sport Planes	44
3.9	Summary of Airfoil Data for Heavy-Lift Cargo Planes	46
3.10	Summary of Airfoil Data for Small Wind Turbines	51

List of Symbols

A_{ts}	test section area
b	model span
c	airfoil chord
C_l	airfoil lift coefficient, $l/\frac{1}{2}\rho V_\infty^2 c$
C_L	aircraft lift coefficient
$C_{l_{max}}$	maximum lift coefficient
$\Delta C_{l_{sc}}$	change in lift coefficient due to streamline curvature
C_d	airfoil drag coefficient, $d/\frac{1}{2}\rho V_\infty^2 c$
C_D	aircraft drag coefficient
C_{d_0}	zero-lift drag coefficient
C_{d_u}	uncorrected drag coefficient
$C_{m,c/4}$	airfoil pitching moment about the quarter-chord point
d	drag per unit span
h	trip height or Gurney flap height
h_{ts}	test section height
K_1	wind-tunnel correction constant for solid blockage effects (0.74)
K_{vel}	ratio of upstream velocity to velocity at model quarter-chord point
l	lift per unit span
L/D	aircraft lift-to-drag ratio
M_v	model volume
q_∞	freestream dynamic pressure
P_{atm}	atmospheric pressure
P_0	total pressure
$P_{0,1}$	wake total pressure
$P_{0,\infty}$	freestream total pressure
P_s	static pressure
$P_{s,1}$	wake static pressure
$P_{s,\infty}$	freestream static pressure
ΔP_0	total pressure difference between freestream and wake
R	ideal gas constant for air
Re	Reynolds number, $\rho V_\infty c/\mu$
\mathcal{R}	reduced Reynolds number
S	Sutherland's constant or wing area
T	temperature
T_0	reference temperature
u_1	streamwise velocity in wake
V	inviscid local velocity on airfoil surface
V_c	corrected velocity
V_u	uncorrected velocity
V_∞	freestream velocity

W	aircraft weight
x	distance along airfoil chord or along model span
y	vertical distance
α	angle of attack
α_u	uncorrected angle of attack
$\Delta\alpha_{sc}$	change in angle of attack due to streamline curvature
ϵ_b	total blockage correction factor (solid and wake)
ϵ_{sb}	solid blockage correction factor
ϵ_{wb}	wake blockage correction factor
σ	wind-tunnel correction parameter, $(\pi^2/48)(c/h)^2$
μ	fluid viscosity
μ_0	reference fluid viscosity
ρ	fluid density
FF	free flight
HLG	hand-launch glider
MSL	mean sea level
VG's	vortex generators

Chapter 1

The Airfoils Tested

This volume of SoarTech presents the performance characteristics of 34 airfoils (36 wind tunnel models), most of which are intended primarily for model aircraft, although the airfoils and data are expected to have wider application. Figure 1.1 shows by category the collection of airfoils that were tested. The myriad of airfoils depicted reflects the variety of airfoil design requirements that differ widely from one application to the next. These differences are highlighted in the pages that follow.

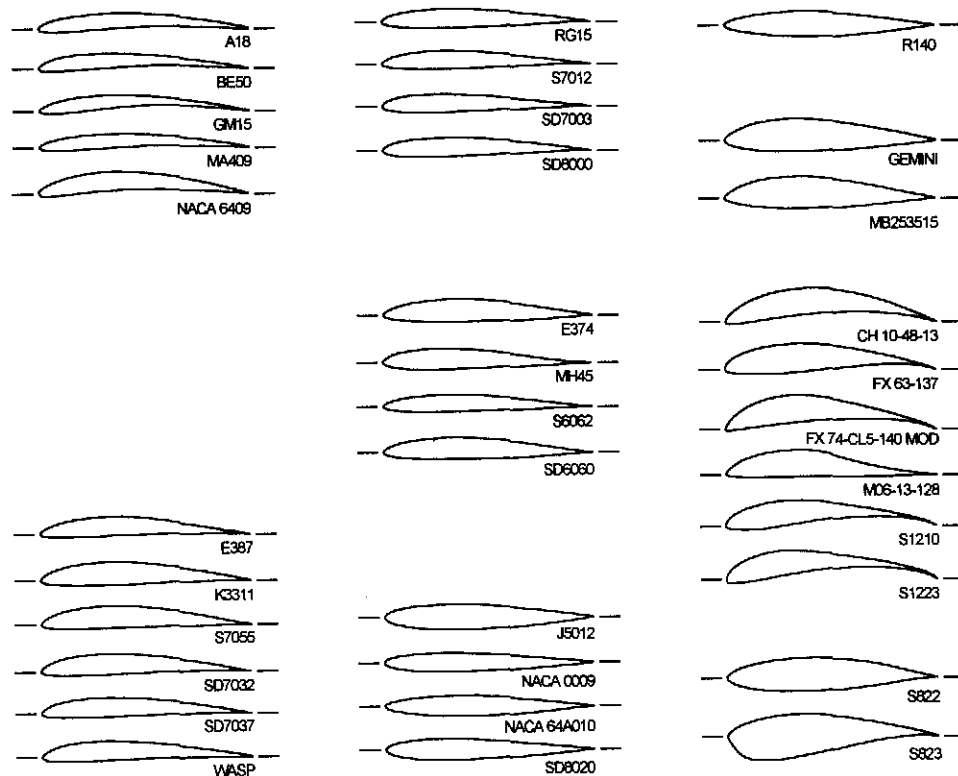


Fig. 1.1 The collection of airfoils tested during Phase I of the UIUC Low-Speed Airfoil Tests (January 1995).

2 *Summary of Low-Speed Airfoil Data*

Chapter 2

Wind-Tunnel Facility and Measurement Techniques

All experiments were performed in the UIUC Department of Aeronautical and Astronautical Engineering Subsonic Aerodynamics Laboratory. Detailed descriptions of the low-speed wind tunnel, lift and drag measurement techniques, data acquisition equipment, and data reduction procedures are presented in this chapter and in Ref. 1.

2.1 Experimental Facility

Research was conducted in the UIUC low-turbulence subsonic wind tunnel shown in Fig. 2.1. The wind tunnel is an open-return type with a 7.5:1 contraction ratio. The rectangular test section is nominally 2.8×4.0 ft in cross section and 8 ft long. Over the length of the test section, the width increases by approximately 0.5 in to account for boundary-layer growth along the tunnel side walls. Test-section speeds are variable up to 160 mph via a 125 horsepower alternating current electric motor connected to a five-bladed fan. For a Reynolds number of 500,000 based on the airfoil chord, the resulting test-section speed was 80 ft/sec (55 mph). Additional photographs of the wind-tunnel inlet, test section and fan are presented in Figs. 2.2–2.4.

Since low Reynolds number airfoil performance is highly dependent on the behavior of the laminar boundary layer, low turbulence levels within the wind tunnel are necessary to ensure that laminar flow does not prematurely transition to turbulent flow over the airfoil surface. In order to ensure good flow quality in the test section, the wind-tunnel settling chamber contains a 4 in thick honeycomb and four anti-turbulence screens, which can be partially removed for cleaning. The turbulence intensity has been measured to be less than 0.1%,² which is sufficient for low Reynolds number airfoil measurements.

The experimental setup is depicted in Fig. 2.5. For the current tests, the airfoil models were mounted horizontally between two 3/8 in thick, 6 ft long Plexiglas endplates (not shown in Fig. 2.5 for clarity) to isolate the ends of the model from the tunnel side-wall boundary layers and the support hardware. Gaps between the model and Plexiglas were nominally 0.05 in. One side of the

4 Summary of Low-Speed Airfoil Data

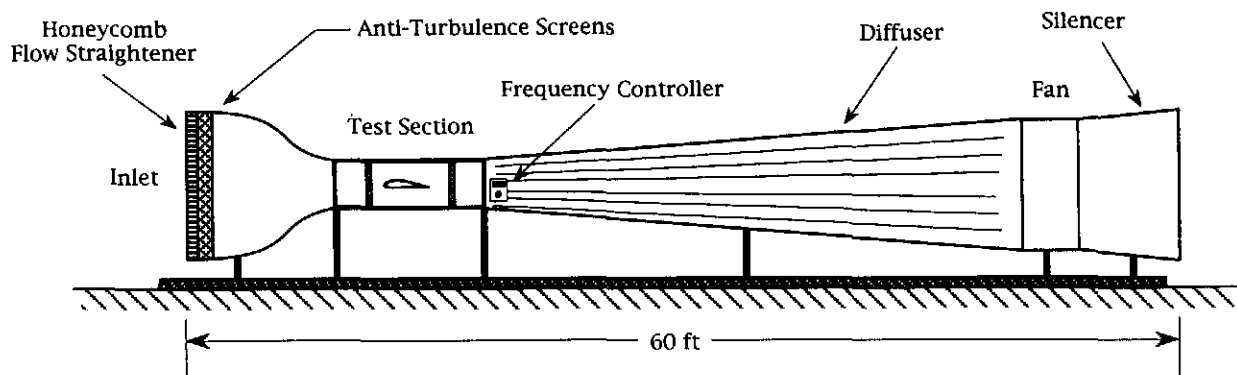


Fig. 2.1 UIUC low-speed subsonic wind tunnel. (not to scale)

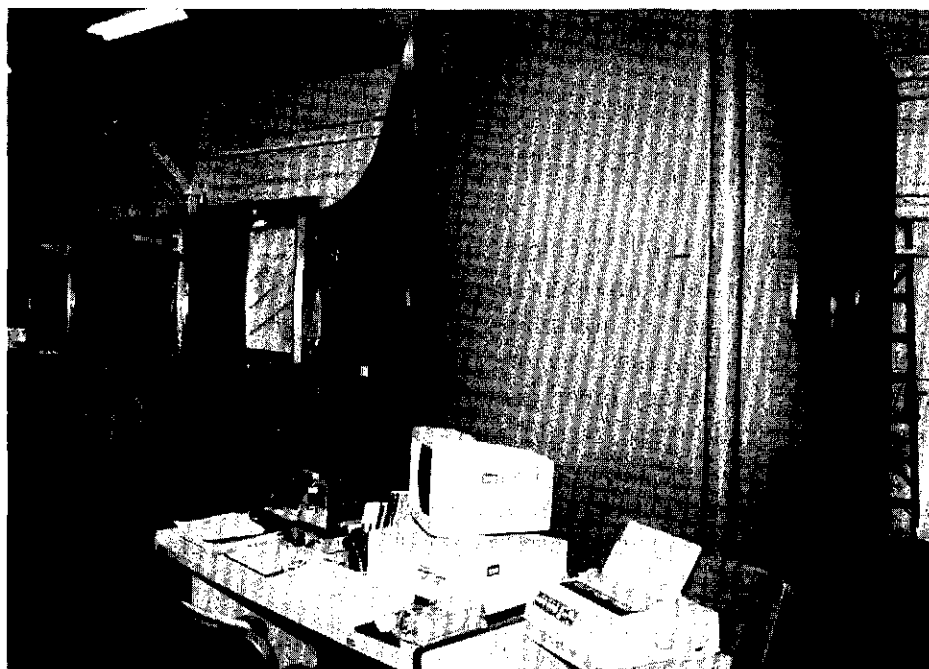


Fig. 2.2 Photograph of wind-tunnel inlet.

airfoil was free to pivot (far side of Fig. 2.5). At this location, the angle of attack was measured using a linear transformer. The other side of the airfoil model was connected to the lift carriage through two steel wing rods that passed through the wing-rod fixture and were anchored to the model through two set screws. At this side, the airfoil model was free to move vertically on a precision ground shaft, but not free to rotate. A feedback-controlled force balance, however, restrained the motion of the model, as discussed later. Linear and spherical ball bearings within the lift carriage helped to minimize any frictional effects.

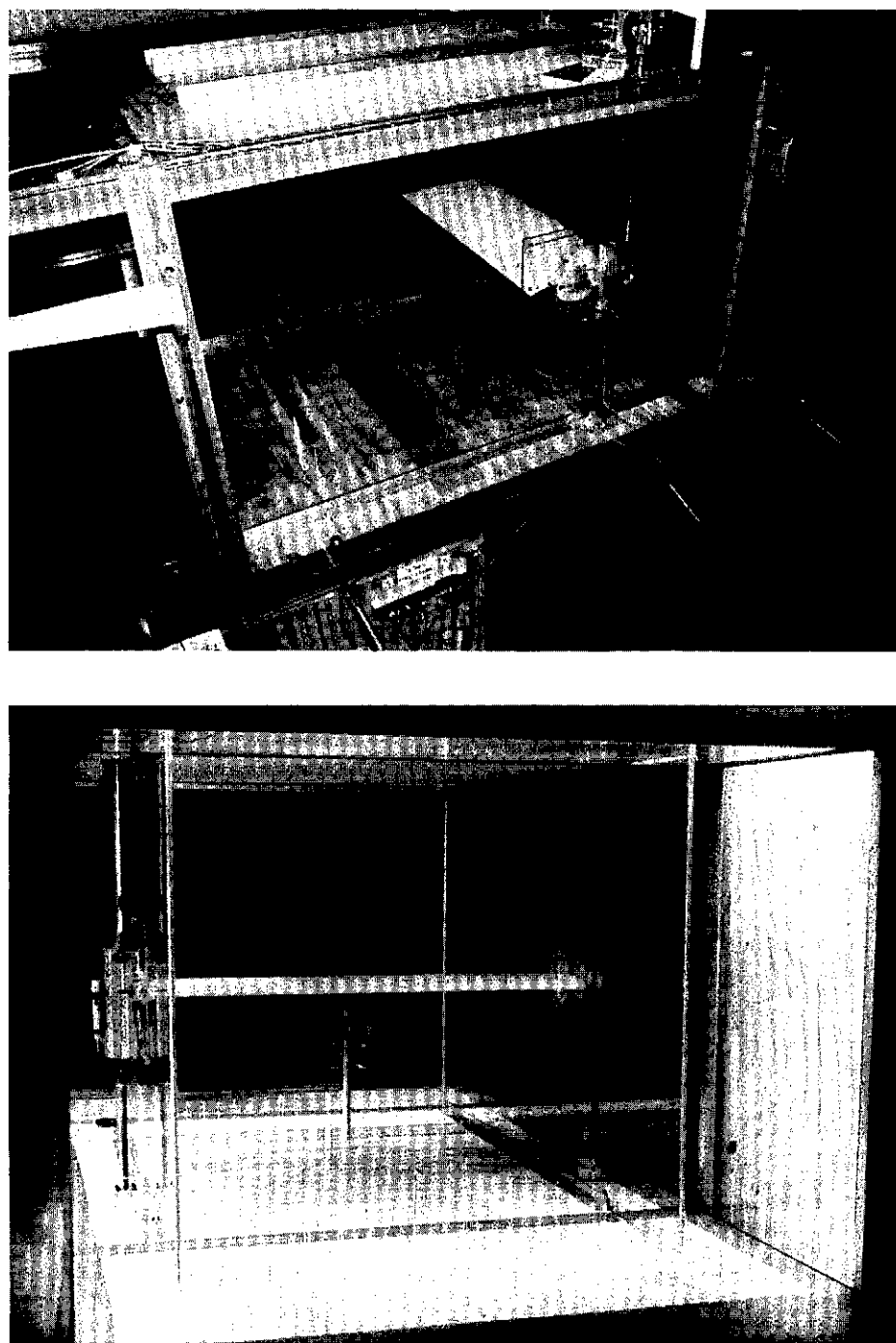


Fig. 2.3 Photographs of wind-tunnel test section.

The two-axis traverser designed and built by the late David Fraser is depicted in Fig. 2.6. Two side-by-side pitot probes (spaced 3.96 in apart in the spanwise x -direction) were connected to the main center post that extended vertically

6 Summary of Low-Speed Airfoil Data

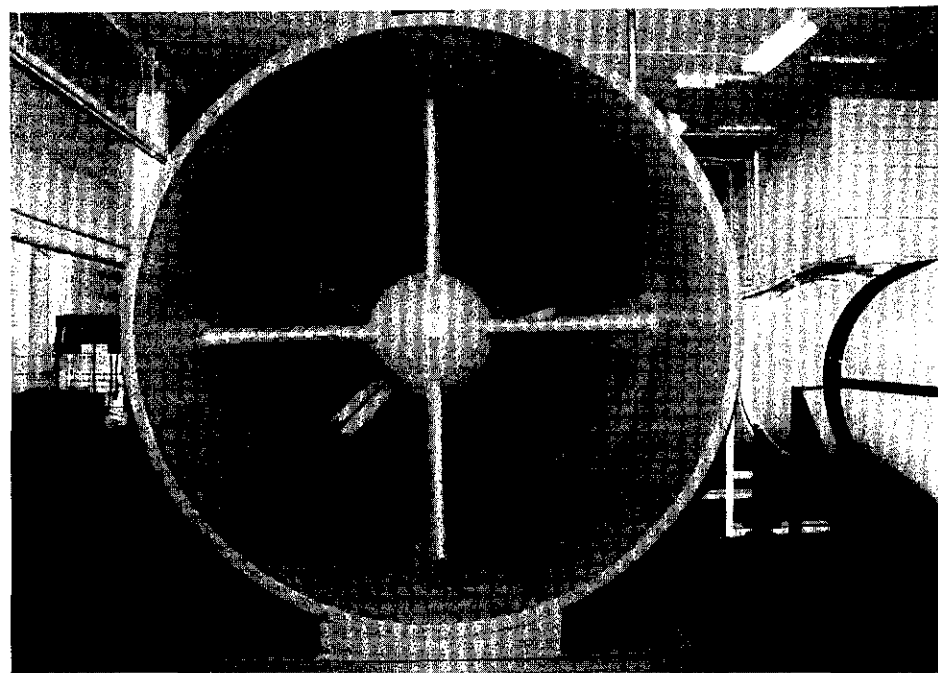


Fig. 2.4 Photograph of wind-tunnel fan.

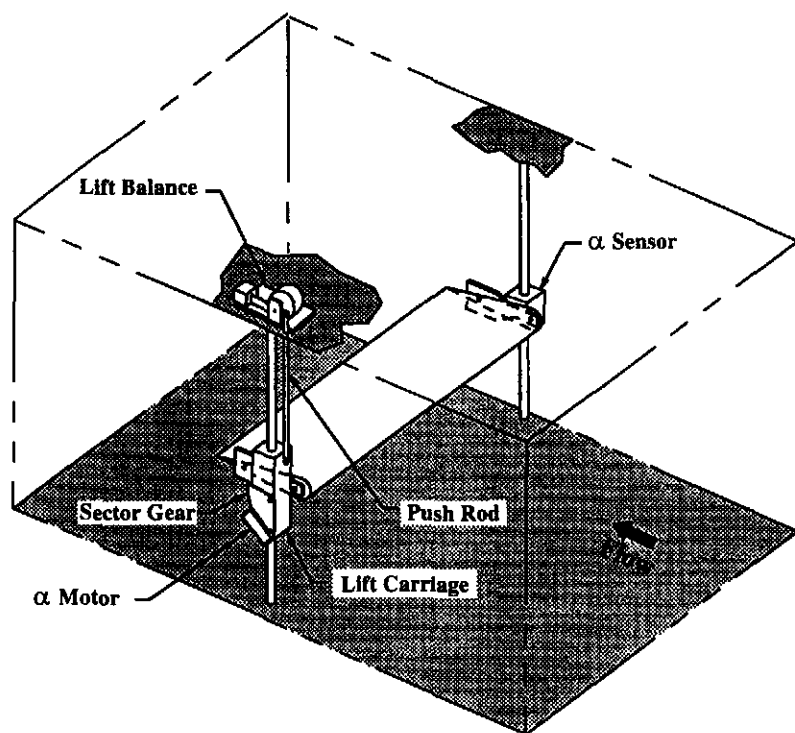


Fig. 2.5 Experimental setup. (Plexiglas endplates and traverser not shown for clarity)

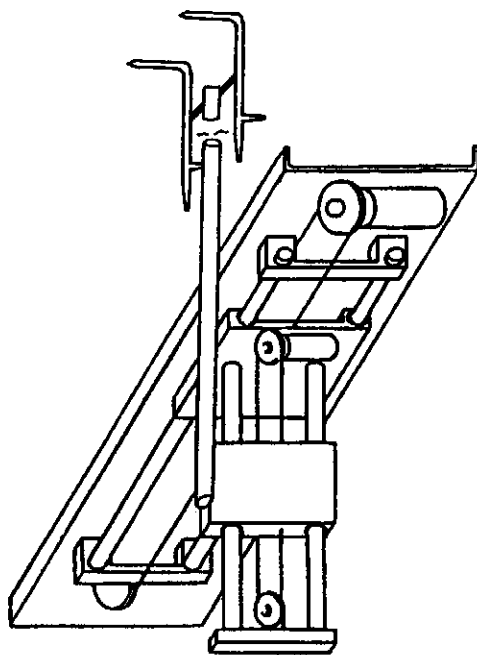


Fig. 2.6 The x - y traverser system.

through the tunnel test-section floor. The whole traversing system was located within a pressure-sealed box underneath the tunnel test section. The resolution and setability of the traverser are less than 0.001 and 0.005 in, respectively, in both the spanwise and vertical directions. Readout accuracy in the spanwise and vertical directions are 0.020 and 0.002 in, respectively.

All wind-tunnel models have a nominal 12 in chord and 33 5/8 in span ($\pm 1/64$ in tolerances), and two brass tubes on each end of the model for mounting. Figure 2.7 depicts the general construction specifications and dimensions of the airfoil models.

2.2 Measurement Techniques

All analog data was recorded on an AT&T 386 computer through a Data Translation DT2836 16-bit analog-to-digital data acquisition board. The DT2836 has a resolution of 0.0015% of full-scale reading, eight differential input channels, and two 16-bit digital-to-analog output channels. Set for a full-scale range of ± 10 volts, the 16-bit resolution of the board provided an accuracy of ± 0.305 mV.

At the low speeds required for low Reynolds number tests, there were small time-dependent fluctuations in tunnel speed due to the inertia of both the drive system and the air. Thus, all quantities (dynamic pressure, total pressure, lift, angle of attack, x -position, y -position, and temperature) were measured simultaneously through a computer controlled data acquisition system. Once a run started, the entire data acquisition process was completely automated, including

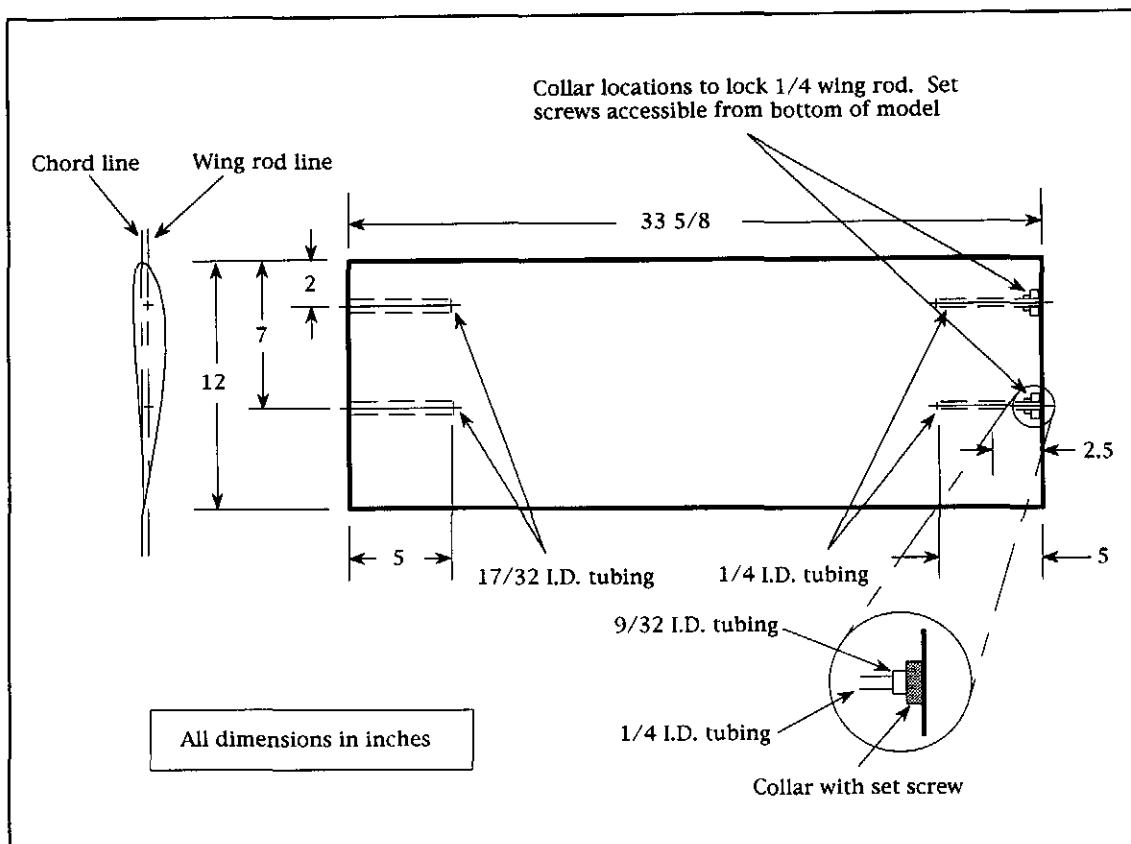


Fig. 2.7 General wind-tunnel model construction specifications.

setting and maintaining a constant Reynolds number within the test section, acquiring data, and plotting raw data graphically to the computer screen and numerically to a printer. All data was also saved to a separate output file for later in-depth data reduction.

2.2.1 Lift Force Measurements

The wind-tunnel model was connected to the lift balance (or force transducer) through a pushrod attached to the lift carriage, as shown in Fig. 2.5. The force transducer was a servo balance rather than a standard strain gauge or load cell. Similar to a standard beam balance, the dead weight of the airfoil and support structure were counter-balanced with weights. The remaining forces (lift and residual imbalance) were then balanced by the torque from a brushless DC torque motor mounted on the beam axis. Any angular displacement from a reference zero was sensed by a linear transformer, and the error signal was used to drive the torque motor until the error was removed.

In general, acquiring only lift data was a relatively quick process. Since no wake measurements were taken, it was possible to cover a full angle of attack

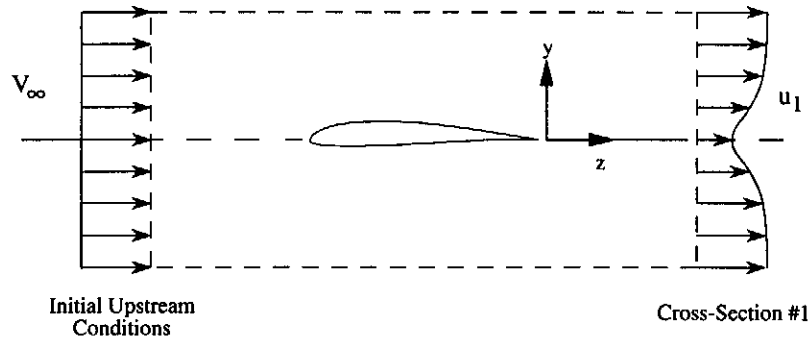


Fig. 2.8 Control volume for the 2-D momentum deficit method to determine the profile drag.

range past stall in a short amount of time. (For example, angle of attack values from -8 deg to 16 deg to -8 deg with increments of 0.5 deg took approximately 15 minutes). Both increasing and decreasing angles of attack were covered to document any aerodynamic hysteresis.

2.2.2 Drag Force Measurements

While the lift force on airfoils at low Reynolds numbers can be obtained with acceptable accuracy through a lift balance, drag forces are often a magnitude less than their lift counterparts. As a result, profile drag is often best obtained by the momentum method instead of a force balance. For the current tests, the profile drag was determined through the method developed by Jones³ (taken from Schlichting⁴).

After application of the two-dimensional momentum and continuity equations to a control volume shown in Fig. 2.8, the drag force per unit span can be calculated from

$$d = \rho \int_{-\infty}^{\infty} u_1 (V_{\infty} - u_1) dy \quad (2.1)$$

Assuming that the location in which the measurements are performed is located sufficiently far enough behind the airfoil such that the static pressure has returned to upstream tunnel static pressure (i.e., $P_{s,1} = P_{s,\infty} = P_s$) and that the downstream flow outside the airfoil wake proceeds without losses (i.e., the total pressure remains constant along every streamline), the total pressure relationships from Bernoulli's equation are

$$P_s + \frac{1}{2} \rho u_1^2 = P_{0,1} \quad (2.2)$$

$$P_s + \frac{1}{2}\rho V_\infty^2 = P_{0,\infty} \quad (2.3)$$

Application of the above relationships to Eq. (2.1) and simplifying

$$d = 2 \int_{-\infty}^{\infty} \{ \sqrt{P_{0,1} - P_s} \sqrt{q_\infty - P_s} - (P_{0,1} - P_s) \} dy \quad (2.4)$$

$$P_{0,1} - P_s = P_{0,1} - P_s - P_{0,\infty} + P_{0,\infty} = q_\infty - \Delta P_0 \quad (2.5)$$

$$d = 2 \int_{-\infty}^{\infty} \sqrt{q_\infty - \Delta P_0} (\sqrt{q_\infty} - \sqrt{q_\infty - \Delta P_0}) dy \quad (2.6)$$

To ensure that the wake had relaxed to tunnel static pressure, the wake measurements were performed 14.8 in (approximately 1.25 chord lengths) downstream of the trailing edge of the airfoil. Each vertical wake traverse consisted of between 20 and 80 total-head pressure measurements (depending on wake thickness) with points nominally spaced 0.08 in apart. No measurements were taken in stall due to the size and unsteadiness of the wake.

Pressure measurements within the wake were made using MKS Baratron Model 220 variable-capacitance differential pressure transducers with a full-scale range of 1 mm Hg (0.02 psia), resolution of 0.01% of full-scale reading, and an accuracy of 0.15% of reading.

In order to obtain an accurate value for the drag coefficient, wake profile measurements were taken at four spanwise locations spaced 4 in apart over the center 12 in of the airfoil. The resulting four drag coefficients were then averaged to obtain the drag at a given angle of attack. This average drag coefficient is presented in Chapter 4 and Appendix B. Figure 2.9 depicts a typical variation in the spanwise drag coefficient at Reynolds numbers from 60,000 to 300,000. For the Re of 60,000 case, the variation could be called “scatter,” which is due partly to the unsteadiness in the wake and the difficulty in resolving such small pressure differences. At the higher Re ’s, however, an intrinsic steady-state variation is present. For the interested reader, a thorough documentation of this phenomenon is presented in Refs. 5 and 6.

It should be noted that for the Re ’s of 60,000 and 100,000 the spanwise drag coefficient for approximately $x = 5.5$ in was often higher than the other three locations. (For reference, the center of the tunnel was $x = 0$ in and the endplates are ± 16.86 in.) The higher spanwise drag value may be related to corner vortices developing at the juncture between the model and endplates, but this is only speculation. While it may be correct to discard this value, it was still included for the average drag coefficient results presented in this book.

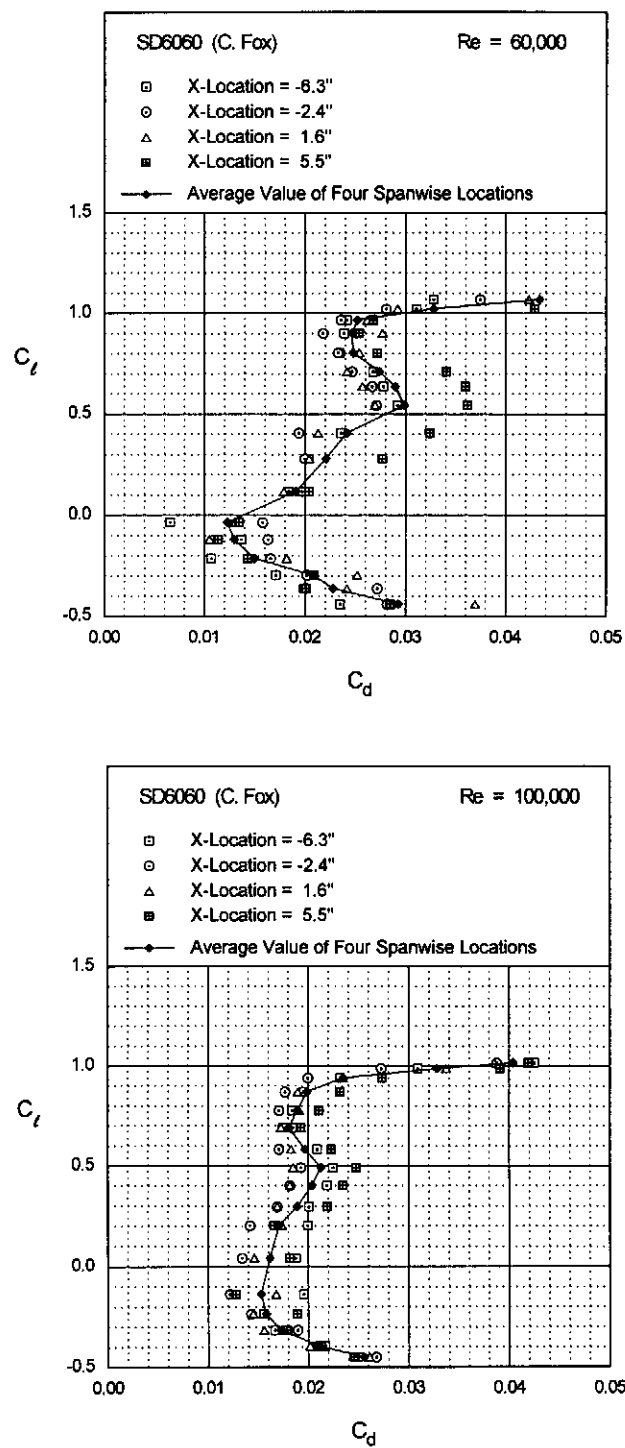


Fig. 2.9 Drag results for the SD6060 airfoil depicting typical spanwise drag variations for the four spanwise stations for $Re = 60,000, 100,000, 200,000$ and $300,000$.

(figure continues)

12 Summary of Low-Speed Airfoil Data

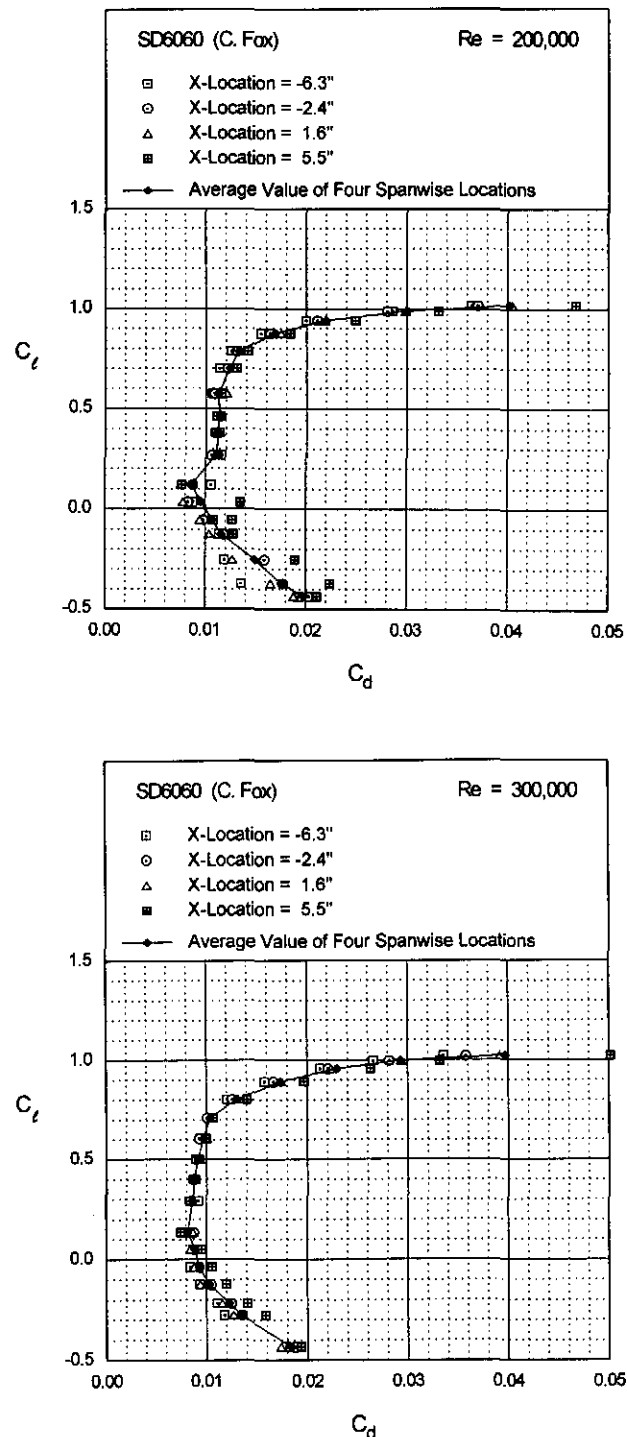


Fig. 2.9 Continued.

For the spanwise drag measurements, primary emphasis was placed on resolving the spanwise profile drag variations, and as a result, detailed vertical (y -direction) surveys through the wake were made at spanwise stations nominally spaced 0.25 in apart. On average, a typical run involving 57 spanwise stations required 2 hours of continuous wind-tunnel operation.

2.2.3 Airfoil Model Accuracy Measurements

In order to determine the accuracy of the wind-tunnel models, each model was digitized using a Brown & Sharpe coordinate measuring machine (CMM) to determine the actual airfoil shape. Approximately 80 points were taken around the airfoil. The spacing was more or less proportional to the local curvature; near the leading and trailing edges the spacing was relatively small, while over the central section it was as large as 0.7 in. Due to constraints on the model/CMM arrangement, the S823, S1223, CH 10-48-13 and FX 74-CL5-140 MOD wind-tunnel models were measured on the left (angle of attack) side of the model. All other models coordinates were measured in the middle of the model.

Section profiles and model accuracy plots are presented Chapter 4. The profiles include both the true airfoil as designed (solid line) compared with the actual digitized model coordinates (dotted line). The model accuracy plots depict the differences between the true airfoil and actual airfoil coordinates for the upper surface (solid line) and lower surface (dotted line) of the airfoil. A displacement above or below the axis means that the model surface lies above or below the nominal, respectively. For instance, the actual SD6060 wind-tunnel model was thinner than the true SD6060 by approximately 0.008 in over the majority of the chord.

2.2.4 Freestream Velocity Measurements

Since the wind-tunnel model was mounted between endplates, the amount of flow (or spillage) between the endplates and the side walls of the test section could not be easily determined. Consequently, measurement of the freestream ahead of the endplates could not be used to determine the true freestream experienced by the model. Rather, the upstream dynamic pressure was measured between the two endplates 15.9 in ahead of the quarter-chord point of the airfoil models, and 5.2 in above the test section floor. Since the upstream pitot-static probe was close to the leading edge of the airfoil, the measured velocity was corrected for circulation effects, as discussed in Section 2.3.2. In order to convert the upstream dynamic pressure into velocity, the air density was calculated from the ideal gas law

$$\rho = \frac{P_{atm}}{RT} \quad (2.7)$$

with ambient temperature obtained from an Omega thermocouple (accurate to within 1 deg Rankine) located next to the wind tunnel. The velocity was then calculated from

$$V_\infty = \sqrt{\frac{2q_\infty}{\rho}} \quad (2.8)$$

The Reynolds number based on the airfoil chord is given by

$$Re = \frac{\rho V_\infty c}{\mu} \quad (2.9)$$

where μ for air was calculated using Sutherland viscosity law⁷ expressed as

$$\frac{\mu}{\mu_0} = \left(\frac{T}{T_0} \right)^{3/2} \left(\frac{T_0 + S}{T + S} \right) \quad (2.10)$$

2.3 Data Reduction

The physical boundaries of a closed test section restrict the flow and, as a result, produce extraneous forces on the model that must be subtracted out. These extraneous aerodynamic forces occur mainly from the fact that the velocity of the air increases as it flows over the model due to the restraining effect of the wind-tunnel boundaries combined with the physical presence of the model and its wake. This effect is minimized when the model is small compared to the size of the test section. Unfortunately, smaller models are more difficult to build accurately. Since experienced model airplane enthusiasts were solicited to build the airfoil models instead of a machine shop, a larger 12 in chord model was selected as a compromise even though it required measuring smaller forces and a more complicated data reduction process.

In the following three sections, only an overview of the two-dimensional wind-tunnel corrections and their causes is presented. A more detailed discussion can be found in a separate report.⁸

2.3.1 Wind-Tunnel Boundary Corrections

The presence of the wind-tunnel walls increase the measured lift, drag and pitching moment due to an increase in velocity at the model. More specifically, the lateral boundaries in a two-dimensional testing context cause four phenomena to occur.

- **Buoyancy:** Buoyancy is an additional drag force that results from a decrease in static pressure along the test section due to the growth of the boundary layer at the walls. Even though buoyancy effects are usually insignificant even for airfoils tested within test sections of constant area,⁹ the main effect of buoyancy was taken into account directly in the corrections of the freestream velocity.
- **Solid Blockage:** The physical presence of a model within a test section is known as solid blockage, which produces a decrease in the effective area. From the continuity and Bernoulli's equation, the velocity of the air must increase as it flows over the model, increasing all aerodynamic forces and moments at a given angle of attack. Solid blockage is a function of the model size and test section dimensions.

$$\varepsilon_{sb} = \frac{K_1 M_v}{A_a^{3/2}} \quad (2.11)$$

- **Wake Blockage:** The second type of blockage is known as wake blockage, which results from a lower velocity within the airfoil wake compared to the freestream velocity. For closed test sections, in order to satisfy the continuity equation the velocity at the model (outside of the wake) must increase. The effect of wake blockage is proportional to the wake size and thus to the measured drag force on the model.

$$\varepsilon_{wb} = \left(\frac{c}{2 h_{ts}} \right) C_{du} \quad (2.12)$$

- **Streamline Curvature:** Due to the physical constraints of the tunnel boundaries, the normal curvature of the free air as it passes over a lifting body (such as an airfoil) is altered, increasing the airfoil effective camber as the streamlines are “squeezed” together. For closed wind-tunnel sections, the increase in camber results in an increase in lift, pitching moment about the quarter-chord point, and angle of attack, while the drag is unaffected. Since no pitching moment measurements were taken, corrections for only lift and angle of attack are presented below.

$$\Delta C_{lsc} = \sigma C_l \quad (2.13)$$

$$\Delta \alpha_{sc} = \frac{57.3 \sigma}{2\pi} (C_l + 4 C_{m,c/4}) \quad (2.14)$$

where

$$\sigma = \frac{\pi^2}{48} \left(\frac{c}{h_{ts}} \right)^2 \quad (2.15)$$

2.3.2 Additional Velocity Corrections

In the case of the UIUC LSATs, the velocity must not only be corrected for solid and wake blockage, but also for other factors which are particular to the present setup. As previously mentioned, the model was mounted between two endplates within the test section. This arrangement minimized the effects of boundary-layer growth (and thus buoyancy) by generating fresh boundary layers at the leading edge of the endplates, isolated the model from the support hardware, but also required the upstream velocity to be measured between the endplates. Since the upstream pitot-static probe was close to the airfoil leading edge, the circulation about the airfoil induced a velocity component that effected the pitot-static probe reading. This circulation effect was directly related to the generation of lift by the model—the higher the lift, the larger the induced velocity. Since all aerodynamic coefficients were normalized by a velocity term, it was important to have an accurate freestream velocity measurement and thus to correct for the circulation effects.

To obtain a mathematical expression to account for the circulation effects, the airfoil was modeled as a single vortex at the quarter-chord point, and the tunnel walls were simulated by an image system. The induced velocity components were then computed at the location of the velocity measuring probe. Since the circulation is also function of the freestream velocity, an iterative method was used to converge on a solution.

Finally, the velocity was also corrected to account for the boundary-layer growth along the tunnel walls, which resulted in a slightly higher-than-freestream velocity at the model. By using a second velocity measuring probe at the model quarter-chord point with the model removed, and measuring the upstream and downstream velocities simultaneously over the full chord Reynolds number range, a calibration curve was obtained. Thus, for a measured upstream velocity, the actual velocity at the model could be calculated.

2.3.3 Corrections to Measured Quantities

The measured quantities that must be corrected can be subdivided into two categories: stream and model quantities. The most important stream quantity is the velocity at the model. This velocity was obtained from the freestream velocity measurements and by applying the proper corrections to account for solid

and wake blockage as well as boundary-layer growth. Combining the velocity corrections in a single expression:

$$V_c = V_u K_{vel} (1 + \varepsilon_{sb} + \varepsilon_{wb}) \quad (2.15)$$

Other stream quantities, such as the Reynolds number and dynamic pressure, were then obtained directly from the corrected value of the velocity.

The model quantities of interest are the lift, drag and the angle of attack, which were corrected in their non-dimensional form to account for solid and wake blockage as well as streamline curvature.

$$C_l = C_{l_u} \frac{1 - \sigma}{(1 + \varepsilon_b)^2} \quad (2.16)$$

$$C_d = C_{d_u} \frac{1 - \varepsilon_{sb}}{(1 + \varepsilon_b)^2} \quad (2.17)$$

$$\alpha = \alpha_u - \frac{57.3\sigma}{2\pi} (C_l + 4C_{m,c/4}) \quad (2.18)$$

It is important to note that drag coefficient data was necessary to correct the model quantities since wake blockage is proportional to the measured drag coefficient. For the lift runs, however, drag was not measured, which has an effect on the lift data reduction. For the lift curves, the wake blockage correction was computed using a constant value for the drag coefficient of 0.04, which was representative for conditions close to maximum lift. This method ensured more accurate values for the maximum lift coefficients even though it over-corrected lift coefficient values in the linear region of the lift curves. This “over-correction” was not significant as can be seen by comparing lift data taken from a lift run with that from a drag run.

A final note concerning these wind-tunnel corrections is that even though the current setup does not provide pitching moment data, airfoil moment coefficients have been determined computationally using either the Eppler,^{10,11} ISES^{12,13} or XFOIL¹⁴ code. These moments are representative over the low drag range and were used to correct the angle of attack measurements. Since quarter-chord pitching moments are relatively constant with angle of attack and since the effect on the wind-tunnel corrections was small, a constant $C_{m,c/4}$ was used for each airfoil. The values used are listed in Chapter 3.

2.4 Calibrations and Uncertainty Analysis

By applying the general uncertainty analysis presented in Coleman & Steele,¹⁵ the uncertainties in the velocity, lift coefficient, and drag coefficient were found in a relatively straight forward manner. Further details describing the uncertainty analysis are presented in Ref. 6.

First, consider the case of measuring the upstream velocity, which is used to normalize the lift and drag forces. The highest uncertainty in the pressure readings due to fluctuations in flow angle is 1%, resulting in a freestream-velocity uncertainty within 0.5%. If no errors related to the probes are included, the uncertainty in pressure readings and the velocity measurements reduce to less than approximately 0.5% and 0.3%, respectively. The lift balance was calibrated over a range that depended on the loads expected for a given run—the higher the Reynolds number, the larger the range. The lift balance calibration slopes over the 1 1/2 month testing period varied by approximately 4%. Of course, this drift did not affect the accuracy of the measurements since the lift balance was repeatedly calibrated. Overall uncertainty in the lift coefficient is estimated to be 1.5%. The accuracy of the lift calibrations was the main contribution to this small error. The drag measurement error comes from three sources: accuracy of the data acquisition instruments, repeatability of the measurements, and the selection of the particular four wake profiles used to determine the average drag coefficient. Based partly on the error analysis method presented in McGhee¹⁶ and Coleman & Steele,¹⁵ the uncertainty due to the instruments and measurement repeatability are less than 1% and 1.5%, respectively. Based on a statistical analysis (for a 95% confidence interval) of the spanwise drag results for the E374 airfoil at $\alpha = 4$ deg (which is representative of the middle range of the drag polars), the uncertainties due to the spanwise variations are estimated at 3% for $Re = 100,000$ and reduce to approximately 1.5% at and above $Re = 200,000$. At $Re = 60,000$ and below, the flow is dominated by laminar separation bubbles that produce large variations in profile drag that make it difficult to confidently assign a measure of accuracy. A more detail discussion of this issue is presented in Ref. 6. For the angle of attack sensor, calibration measurements were taken at six different angles of attack incremented from 0 to 25 deg in 5 deg steps. Overall uncertainty in the angle of attack is estimated at 0.08 deg, based on the calibration results.

2.5 Comparison with Other Facilities

For comparison, drag polar results for the E387 airfoil from tests at NASA-Langley LTPT,¹⁶ Delft,¹⁶ Stuttgart,¹⁷ and UIUC are presented in Fig. 2.10. It should be noted, however, that the E387 from the UIUC tests was slightly decambered and warped at the trailing edge, which has an effect on the results. Drag polar results for the the same E374 airfoil model tested both at the Princeton¹ and UIUC wind tunnels are presented in Fig. 2.11. The agreement between the Princeton and UIUC data is quite good, even at a Reynolds number of 60,000.

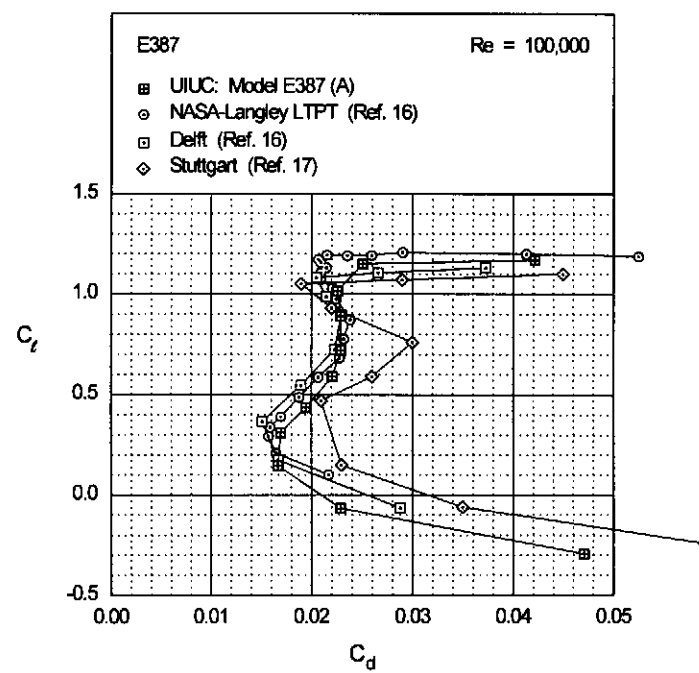
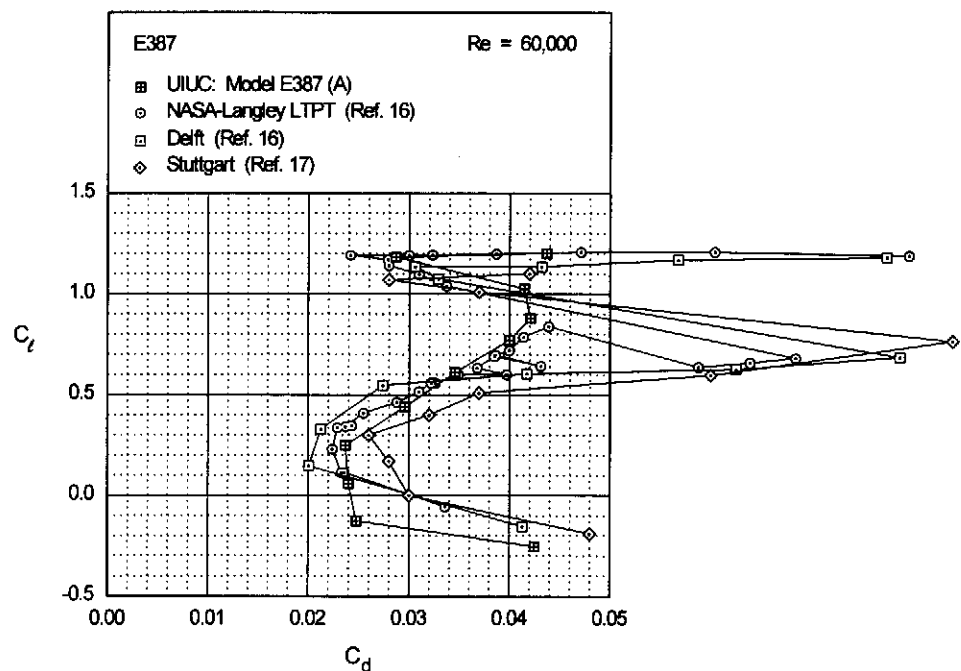


Fig. 2.10 Comparison of drag data for the E387 airfoil from various wind-tunnel facilities for $Re = 60,000, 100,000, 200,000$ and $300,000$.

(figure continues)

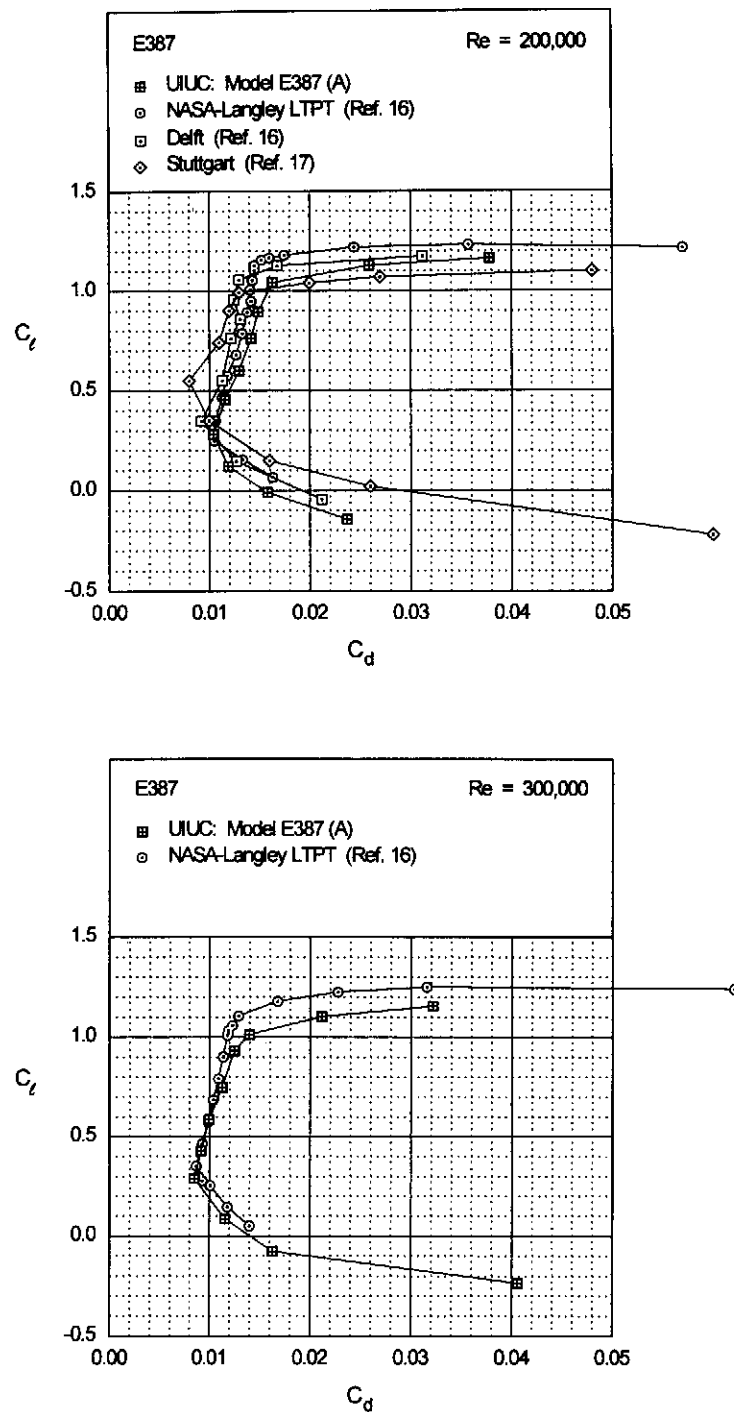


Fig. 2.10 Continued.

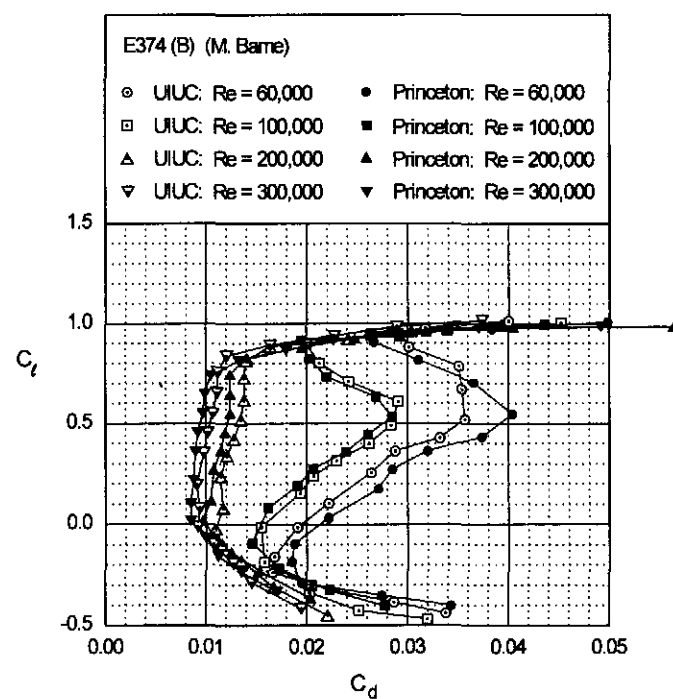


Fig. 2.11 Comparison of drag data for the E374 airfoil from the Princeton and UIUC wind-tunnel facilities.

Chapter 3

Summary of Airfoil Data

In this chapter, the airfoil performance characteristics are discussed. To aid in the navigation of the data, the airfoils are grouped and discussed by category, e.g., airfoils for free flight models, airfoils for thermal soaring, and so on. The categories in order of discussion are listed in Table 3.1 along with the associated airfoils. Also, for reference, Table 3.1 lists the thickness, camber and pitching moment for the true airfoils, as well as the wind-tunnel model construction method, model accuracy and model builder.

Within each category, the discussion is organized according to how the airfoils relate to each other in terms of performance. Tables are included that list each airfoil in the category. For each airfoil, the table then lists the profile plot, the lift and drag data, the configuration of the model (e.g., clean, with boundary-layer trips, etc.), any special data, and the figures and pages pertaining to the data. Occasionally embedded within the discussion of the airfoils are sections on more general but related topics. These special sections are typeset between centered horizontal rules.

Following the discussion of the airfoils by category in this chapter, all of the figures (airfoil profile and performance plots) are included separately in Chapter 4. The figures are organized alphabetically by airfoil name for quick indexing.

As shown in Table 3.1, many of the airfoils listed were previously tested at Princeton.¹ The tests were repeated for several reasons. First, comparisons of the airfoil data from the two facilities can be used to gauge what differences might be expected if those remaining airfoils were tested again at Illinois. Second, the data can also be used in an attempt to ascertain any gross differences in wind-tunnel flow quality. And finally, since data taken on identical airfoils in different wind tunnels can vary, several of the widely used airfoils were re-tested to provide a complete and consistent data set.

Some general comments apply to the data and discussion.

- In *Airfoils at Low Speeds*,¹ the designation “-PT” (for Princeton Tests) was used after the names of the actual airfoils tested to distinguish them from the true airfoils. In this book, no special designation is applied to the airfoil name to make this distinction between the actual and true airfoil. It is important to note, however, that the discussion of each airfoil is based on the actual

Table 3.1: Airfoils Sorted by Category

Airfoils for:	Airfoil	% Thickness	% Camber	$C_{m,c/4}$
Free Flight Models	A18	7.26	3.84	-0.126
	BE50	7.31	3.96	-0.114
	GM15	6.70	4.76	-0.154
	MA409	6.69	3.33	-0.115
	NACA 6409†	9.00	6.00	-0.163
Thermal Duration Sailplanes	E387 (A)†	9.06	3.90	-0.082
	K3311	11.03	3.23	-0.085
	S7055‡	10.50	3.55	-0.068
	SD7032 (D)†	9.95	3.66	-0.099
	SD7032 (E)	9.95	3.66	-0.099
	SD7037 (A)†	9.20	3.02	-0.085
	SD7037 (B)	9.20	3.02	-0.085
F3B Sailplanes	WASP	9.35	2.98	-0.074
	RG15 (B)	8.92	1.76	-0.058
	S7012‡	8.75	2.02	-0.068
	SD7003†	8.51	1.46	-0.035
Slope Racers	SD8000†	8.86	1.71	-0.049
	E374 (B)†	10.91	2.24	-0.056
	MH45	9.84	1.64	-0.006
	S6062	7.95	1.59	-0.040
Tail Sections	SD6060†	10.37	1.84	-0.039
	J5012†	12.00	0.00	0.000
	NACA 0009†	9.00	0.00	0.000
	NACA 64A010†	10.00	0.00	0.000
Quickie 500 Racers	SD8020†	10.10	0.00	0.000
	R140 (A)	12.04	0.45	-0.012
Sport Planes	GEMINI	15.38	2.20	-0.048
	MB253515†	14.96	2.43	-0.050
Heavy Lift Cargo Planes	CH 10-48-13	12.75	10.20	-0.230
	FX 63-137 (B)	13.59	5.94	-0.170
	FX 74-CL5-140 MOD	13.01	9.72	-0.250
	M06-13-128 (B)	12.81	5.16	0.004
	S1210‡	11.87	7.20	-0.250
	S1223‡	11.93	8.67	-0.290
Small Wind Turbines	S822	16.00	1.89	-0.070
	S823	21.00	2.49	-0.150

† Wind-tunnel models tested previously at Princeton¹

‡ New airfoils designed and built for the current test phase

Table 3.1: continued

Airfoil	Surface Finish	Avg. Difference (in)	Builder
A18	smooth	0.0105	Cooney
BE50	smooth	0.0159	Cooney
GM15	monokote over balsa	0.0028*	Morris
MA409	smooth	0.0195	Cooney
NACA 6409	open bay	0.0107	Halsey
E387 (A)	smooth	0.0106	Champine
K3311	monokote over balsa	0.0032*	Kincaid
S7055	smooth	0.0160	Jones
SD7032 (D)	smooth	0.0057	Watson
SD7032 (E)	smooth	0.0152	Michaelis
SD7037 (A)	fiberglass over balsa	0.0119	Michaelis
SD7037 (B)	smooth	0.0081	Thompson
WASP	smooth	0.0018*	M. Fox
RG15 (B)	paint over obechi	0.0049	Champine
S7012	smooth	0.0077	Lachowski
SD7003	smooth	0.0065	Allen
SD8000	smooth	0.0073	Wagner/Olsen
E374 (B)	smooth	0.0083	Bame
MH45	smooth	0.0384	C. Fox
S6062	varnish over balsa	0.0125	Matheson
SD6060	smooth	0.0088	C. Fox
J5012	smooth	0.0130	Raskin
NACA 0009	smooth	0.0105	Nankivil
NACA 64A010	varnish over obechi	0.0062	Champine
SD8020	smooth	0.0041	Wagner/Olsen
R140 (A)	smooth	0.0230	Friedlander
GEMINI	open bay	0.0052*	Bates
MB253515	smooth	0.0046	Bame
CH 10-48-13	smooth	0.0017*	Hollinger
FX 63-137 (B)	smooth	0.0093	Allen
FX 74-CL5-140 MOD	smooth	0.0038*	Hollinger
M06-13-128 (B)	smooth	0.0112	Allen
S1210	smooth	0.0037	Allen
S1223	molded, smooth	0.0100	Tinel
S822	smooth	0.0054	Allen
S823	smooth	0.0073	Allen

* Smoothed model coordinates were taken as true coordinates

contour shape of the model. If the average difference between the actual and true airfoil coordinates is large (greater than approximately 0.010 in, depending on the model), then interpretation of the true airfoil performance from the wind-tunnel test data might be difficult. The accuracy of the lower surface is not as critical as that of the leading and trailing edges, and the upper surface. The useful lift range is most affected by differences at the trailing edge, while inaccuracies along the upper surface contour influence pressure (bubble) drag.

- The suffixes “(A)”, “(B)”, etc. on the airfoil names refer to multiple models of the particular airfoil. If only one version of the airfoil was built for the Princeton Tests and another one was built for the current tests, the models are designated here as versions “(A)” and “(B)” as in the case of the SD7037.
- Coordinates for the airfoils are tabulated in Appendix A. The performance characteristics are tabulated in Appendix B and ordered according to the airfoil name and figure. This data is available in various forms as mentioned in the Section “Airfoil Data Distribution.”
- For some airfoils, the wind-tunnel model coordinates were mathematically smoothed (using the computer program AFSMO¹⁸) and taken as the true airfoil since no “as designed” airfoil coordinates were available. In such cases, the smoothed wind-tunnel model coordinates were then compared with the actual model coordinates as measured. These airfoils are identified in Table 3.1 by the notation “*” in the column for accuracy. As the comparison plots reveal (see Chapter 4), the differences between the smoothed and actual coordinates is nominally 0.003 in, which is in some sense a measure of the surface waviness.
- The nominal Reynolds number is listed in the figures while the actual Reynolds number is listed in the tabulated data in Appendix B.
- If a model was tested with a boundary-layer trip or modified in some other way (e.g., plain flap, Gurney flap), the configuration of the model is listed in the data summary table and drawn on the related figures.
- The airfoil moment coefficients listed in Table 3.1 were determined computationally using either the Eppler,¹⁰ ISES^{12,13} or XFOIL¹⁹ code. The value given is representative of that over the low drag range.
- In Table 3.1, in the column for surface finish, “smooth” indicates that the model finish was produced by either vacuum bagging fiberglass over foam or painted or both.
- Although the airfoils are categorized by application, the airfoils, of course, can have a wider application. For example, some airfoils might fit equally well into two groups. For instance, the GEMINI and MB253515 airfoils were first used on R/C sailplanes but are listed here as airfoils for sport planes.

Also, the MH45 was developed for flying wings, but it is included with the airfoils for slope soaring.

- For airfoils that were previously tested at Princeton, the discussion is sometimes brief, in which case a more thorough discussion of the airfoil can be found in *Airfoils at Low Speeds*.¹
- Velocity distributions for the true airfoils as predicted by the Eppler code¹⁰ are included with the airfoil polars, lift plots, etc. It should be noted that these velocity distributions do not include the effects of the laminar separation bubble; only the inviscid flow is modeled. Nevertheless, with experience, much can be gleaned from this information to help interpret the airfoil polars and lift curves. As can be seen, subtle differences in airfoil shapes can yield significant differences in the velocity distributions.
- For the lift plots, increasing and decreasing angles of attack are denoted by solid-triangle and open-circle symbols, respectively.

3.1 Airfoils for Free Flight Models

As listed in Table 3.2, five free flight (FF) airfoils were tested. The first four airfoils (A18, BE50, GM15 and MA409) are used by leading flyers in F1C competition (“FAI power”). The NACA 6409 airfoil, as described by the builder Harlan I. Halsey, is used on old-timer FF, R/C (SAM) and electric FF.

Prior to discussing the wind-tunnel test results of the F1C airfoils, background information on the airfoils is given as provided by Gilbert Morris (see acknowledgments):

- **A18** The A18 airfoil was designed by Randy Archer (Scottsdale, Arizona) — the current F1C World Champion. The A18 was named after his model 18 used in the 1993 World Championship contest in which he successfully defended his title. As compared with the A15 that was used on his model 15 to win the 1991 title,¹⁹ the A18 is very similar but has slightly less camber. Model 18 has a higher climb but does not glide as well as model 15. In terms of total performance (climb and glide), both models are essentially equal.
- **BE50** The BE50 airfoil was designed by Eugene Verbitsky (Ukraine) — former F1C World Champion. Verbitsky is considered to be one of the most influential F1C designers worldwide. The BE50 was named after his first model employing this airfoil. In 1980, the Russian team unveiled their new F1C design embodying much of the work of Verbitsky—high aspect ratio, thin, undercambered, low dihedral, aluminum foil covered wing, long tail boom, small stab, folding propeller, brake, VIT (variable incidence tail) and the revolutionary “bunt transition.”ⁿ¹

Table 3.2: Summary of Airfoil Data for Free Flight Models

Airfoil	Data	Configuration	Figure/Page
A18	Velocity Dist.		Fig. 4.1/p. 62
	Profile		Fig. 4.2/p. 62
	Drag Polar	Clean	Fig. 4.3/p. 63
	Lift Curves	Clean	Fig. 4.4/p. 64
BE50	Velocity Dist.		Fig. 4.5/p. 68
	Profile		Fig. 4.6/p. 68
	Drag Polar	Clean	Fig. 4.7/p. 69
	Lift Curves	Clean	Fig. 4.8/p. 70
GM15	Velocity Dist.		Fig. 4.34/p. 104
	Profile		Fig. 4.35/p. 104
	Drag Polar	Clean	Fig. 4.36/p. 105
	Lift Curves	Clean	Fig. 4.37/p. 106
	Profile	Clean, Reflexed	Fig. 4.35/p. 104
	Drag Polar	Clean, Reflexed	Fig. 4.38/p. 108
	Lift Curves	Clean, Reflexed	Fig. 4.39/p. 109
MA409	Velocity Dist.		Fig. 4.51/p. 126
	Profile		Fig. 4.52/p. 126
	Drag Polar	Clean	Fig. 4.53/p. 127
	Lift Curves	Clean	Fig. 4.54/p. 128
NACA 6409	Velocity Dist.		Fig. 4.65/p. 144
	Profile		Fig. 4.66/p. 144
	Drag Polar	Clean	Fig. 4.67/p. 145
	Lift Curves	Clean	Fig. 4.68/p. 146
	Planform		Fig. 4.69/p. 147
	Spanwise Drag	Clean	Fig. 4.69/p. 147

- **GM15** The GM15 airfoil was designed by Gilbert Morris (Columbus, Ohio) and named after his model that won the 1994 F1C US Team Selection Finals. Of the six “flapper airfoils” designed by Morris over the past eight years, the GM15 has proven the best to date in giving balance between climb, glide and total endurance. The airfoils was designed by combining three logarithmic spirals: 7% top, 7% undercamber and 2% Phillips entry.
- **MA409** The MA409 airfoil was designed by Michael Achterberg (Sacramento, California) — former US F1C Team Member. This airfoil was designated by his initials followed by maximum camber of “4.09%.” (It actually has 3.33% camber.) The MA409 has proven itself in numerous unlimited flyoffs for fast climb and good glide endurance. It is currently being used by an increasing number of F1C flyers. Achterberg won a team position at the 1994 F1C US Team Selection Finals using this airfoil.

In general, this type of anecdotal background information and personal experience and observations are needed to complement and interpret the wind tunnel test data. The degree to which this information is useful, however, depends on the accuracy of the observations and also the accuracy of the wind-tunnel models. With respect to the latter, the A18, BE50, and MA409 models all had significantly less camber than their respective true airfoils. Thus, for these airfoils, the usefulness of correlating the comments of Gilbert Morris to wind-tunnel data is limited. Therefore, the following comments only pertain to the wind-tunnel model airfoils.

A18 & MA409 Of the four F1C airfoils tested, the A18 and MA409 are quite similar both in shape and in performance as shown in Figs. 4.1–4.4 and 4.51–4.54. A significant difference, however, is that the MA409 has less camber and consequently the polar is shifted downward as compared with the A18. The lower overall lift of the MA409 is probably advantageous for the near vertical climb phase (power condition) during which the C_l is close to zero and the Re is in the range 250k–300k. Thus, low drag at zero C_l and high Re is important for this type of model. From the polars, the C_{d_0} (zero lift C_d) of the MA409 is lower than the A18. In fact, the MA409 had the lowest C_{d_0} of all the F1C airfoils tested.

In F1C competition, there is a tradeoff between the climb and glide: a mediocre climb can be offset by an excellent glide and vice versa. Although the A18 might not launch as high as the MA409 (with all else equal), the A18 probably makes up for this climb handicap in glide performance. The process of finding the best airfoil that optimizes the tradeoff between climb and glide is best determined through flight tests combined with computer simulations that use the wind-tunnel data.

BE50 The performance of the BE50 differs significantly from both the A18 and the MA409. As compared with the A18 at Re of 60k, the drag is lower in the mid-range of the polar. This same trend is observed at 100k. For all Re 's, the polars show a smooth increase in drag over the C_l range from 0.5 to 1. Airfoils with this type of behavior typically offer the best endurance over a fairly broad C_l range, which corresponds to a broad speed range. Thus, the BE50 might be less sensitive to trim changes in glide as compared with the A18 and MA409 airfoils, which exhibit a more “peaky” performance.

GM15 Since climb and glide are the primary flight conditions of importance in F1C competition, one strategy is to use a “flapper airfoil”—an airfoil with a plain flap that is reflexed (low camber) in climb and unflapped (high camber) in glide. The GM15 is an example of such an airfoil. As shown in Fig. 4.36, the unflapped GM15 has the highest C_l of all the F1C airfoils. In this condition, the glide performance probably equals or exceeds that of the other airfoils. With the 33%-chord trailing-edge flap reflexed by approximately $-8\frac{1}{2}$ deg for climb (see Fig. 4.38), the effects of the flap are apparent. The polar is shifted downward

and the C_{d_0} is reduced. There is, however, added drag owing to the disturbed flow around the hinge line. Nevertheless, as compared with the other airfoils, the added drag is small for the zero- C_l condition for climb.

R/C Hand Launch Airfoils Although these airfoils are currently used for F1C, they are probably applicable to R/C hand-launch gliders (R/C HLG). The launch is somewhat similar to the climb/bunt maneuver in F1C. Upon release the glider is put into a steep climb, and then at the top a relatively quick push-over maneuver is performed. At the beginning of the climb, the Re 's are in the 300k range, and then for thermaling the Re 's are in the 80k–100k range. Between R/C HLG and F1C, there is an important difference in the flying mode. R/C HLGs must repeatedly be able to thermal and then cruise to the next thermal. This need to cruise places more emphasis on low drag in the mid- C_l range. In this range, all of the F1C airfoils presented have good performance.

NACA 6409 The NACA 6409 model, which was built originally for the Princeton Tests, had an open-bay construction from the leading edge to trailing edge. As depicted in Fig. 4.69, 1/8 in thick primary ribs were spaced every 3 in (25% chord). In addition, 1/8 in thick leading-edge secondary ribs were located between the main ribs and used on the forward 27% chord. The sagging of the covering was about 0.025 in (0.2%) worst case, and generally much less—0.005 to 0.015 in. Due to the lack of torsional rigidity, data was taken only up to 200k.

The polar and lift curves presented in Fig. 4.67 and Figs. 4.68, respectively, show the effects of a laminar separation bubble at Re of 60k. At an angle of attack near 4 deg, the bubble detaches from the airfoil and the airfoil effectively stalls. At an angle of attack of near 11 deg, however, the bubble reattaches, the airfoil unstalls and the lift reaches a level consistent with that at Re of 100k and 200k. There exists a small hysteresis loopⁿ² between 9 and 11 deg. Just beyond 11 deg, the airfoil exhibits a mild stall.

Detailed spanwise drag measurements were taken to examine the effects of the ribs on the downstream wake profiles, which are used to determine the drag. Since the geometry of the model with ribs is non-uniform, specifically, three-dimensional and periodic, it can be anticipated that a periodic variation will appear in the wake profile drag. Indeed, at an angle of attack of 1.5 deg, downstream of the primary ribs, the drag is highest, while between the primary ribs the drag is lowest. At an angle of attack of 7.5 deg, a similar trend is seen; however, the secondary ribs located midway between the primary ribs also appear to produce on a smaller scale the same peak and valley effect. Also shown in Fig. 4.69 are the four spanwise stations at which measurements were taken to determine the drag presented in Fig. 4.67. It cannot be inferred from this result

that the ribs cause high drag since the profiles were measured approximately 1.25 chord lengths downstream. It is merely an observation (albeit interesting) that the drag is periodic with the rib spacing and highest downstream of the primary ribs. The variation in the drag found downstream is most likely due to the evolution of the three-dimensional wake that is affected by the periodic spatial change of the geometry of the model.

Clearly, for a model with open-bay construction (or some other spanwise variation), if an accurate C_d value is desired, detailed spanwise surveys through the wake should be made. Unfortunately, such extensive surveys are very time consuming. For instance, the data shown in Fig. 4.69 required approximately 3.5 hours of wind-tunnel test time.

3.2 Airfoils for Thermal Duration Sailplanes

Of the seventeen Selig-Donovan airfoils presented in *Airfoils at Low Speeds*,¹ the SD7037 has become the favorite for R/C soaring thermal duration competition. Due to its popularity, the SD7037 will be discussed first and used as a benchmark for comparison with similar thermal duration airfoils listed in Table 3.3.

SD7037 Two models of the SD7037 were tested. Version A was built for the Princeton Tests and tested again for comparison. Owing to improvements in the wind-tunnel data-acquisition and correction techniques (see Chapter 2), the maximum lift at the lower Re 's is slightly increased as compared with the Princeton data. Also, the drag is somewhat higher, which indicates that the UIUC wind tunnel has lower turbulence levels. This trend—higher $C_{l_{max}}$ at lower Reynolds numbers and higher drag overall—is observed in much of the data presented.

Version B is more accurate than version A, which has a slightly reflexed trailing edge and too little thickness on the forward upper surface. The reflexed trailing edge of version A will reduce the overall lift of the airfoil. Moreover, the deviation on the forward upper surface can be expected to reduce the high-lift performance (see the DF101/102/103 airfoil discussion in *Airfoils at Low Speeds*¹). Indeed, as seen in the polars, version A is not as efficient as version B at high lift coefficients. From the polars alone, one would anticipate a substantial difference in $C_{l_{max}}$ between versions A and B. From the lift curves, however, the difference in $C_{l_{max}}$ is only 0.05.

The drag data of versions A and B at Re of 60k (see Figs. 4.133 and 4.137) reveals some of the challenges and mysteries in taking data at low Reynolds numbers. For several angles of attack, the spanwise drag station at x of 5.5 in on the SD7037 (B) yielded values that were far above the average of the other three stations. If this station at x of 5.5 in were ignored, then the average of

Table 3.3: Summary of Airfoil Data for Thermal Duration Sailplanes

Airfoil	Data	Configuration	Figure/Page
E387	Velocity Dist.		Fig. 4.17/p. 84
	Profile		Fig. 4.18/p. 84
	Drag Polar	Clean	Fig. 4.19/p. 85
	Lift Curves	Clean	Fig. 4.20/p. 86
K3311	Velocity Dist.		Fig. 4.43/p. 116
	Profile		Fig. 4.44/p. 116
	Drag Polar	Clean	Fig. 4.45/p. 117
	Lift Curves	Clean	Fig. 4.46/p. 118
S7055	Velocity Dist.		Fig. 4.111/p. 198
	Profile		Fig. 4.112/p. 198
	Drag Polar	Clean	Fig. 4.113/p. 199
	Lift Curves	Clean	Fig. 4.114/p. 200
SD7032 (D)	Velocity Dist.		Fig. 4.123/p. 210
	Profile		Fig. 4.124/p. 210
	Drag Polar	Clean	Fig. 4.125/p. 211
	Lift Curves	Clean	Fig. 4.126/p. 212
SD7032 (E)	Velocity Dist.		Fig. 4.127/p. 214
	Profile		Fig. 4.128/p. 214
	Drag Polar	Clean	Fig. 4.129/p. 215
	Lift Curves	Clean	Fig. 4.130/p. 215
SD7037 (A)	Velocity Dist.		Fig. 4.131/p. 216
	Profile		Fig. 4.132/p. 216
	Drag Polar	Clean	Fig. 4.133/p. 217
	Lift Curves	Clean	Fig. 4.134/p. 218
SD7037 (B)	Velocity Dist.		Fig. 4.135/p. 220
	Profile		Fig. 4.136/p. 220
	Drag Polar	Clean	Fig. 4.137/p. 221
	Lift Curves	Clean	Fig. 4.138/p. 222
WASP	Velocity Dist.		Fig. 4.150/p. 240
	Profile		Fig. 4.151/p. 240
	Drag Polar	Clean	Fig. 4.152/p. 241
	Lift Curves	Clean	Fig. 4.153/p. 242

the remaining three would produce results similar to those of the SD7037 (A). A discussion of this dilemma, its possible causes, the frequency of occurrence, and a strategy to deal with the problem is discussed in Section 2.2.2. For Re above 100k, any bias, if present, was negligible.

The SD7037 is favored for R/C thermal soaring because of its working lift range (the lift range over the low drag region) that begins near a C_l of 0.2 and extends to near C_l of 1.0 where the drag begins to increase more rapidly. Its other attributes include low drag and good flap/aileron response, the latter of which will be quantified during the next series of tests.

WASP The WASP airfoil built and designed by Mike Fox is quite similar to the SD7037 in performance and shape. In many respects, the performance appears to be a mixture of the SD7037 (A) and SD7037 (B). Although Mike Fox uses the airfoil for R/C HLG, it is included here since it has much in common with the SD7037.

K3311 The K3311 airfoil was designed by Leon C. Kincaid and used on his HEAT SEEKER design that placed 1st in Sportsman Multi-Task at the 1992 and 1993 LSF Championships. Leon Kincaid, a retired Model Builder/Machinist for the NACA (now NASA), used his skills to measure the K3311 coordinates off his original wind-tunnel model with a dial indicator with a 1 in throw, mounted on a surface gauge. These original coordinates were mathematically smoothed using AFSMO,¹⁸ from which 79 coordinates (based on a standard x/c data set) were determined. The airfoil differs from the previous two airfoils discussed in that the high-lift (low-speed) corner of the polar is improved at 100k. As a result, the K3311 should have better thermal performance. This advantage is balanced by slightly worse performance at low lift (cruise). It should also be noted that the stall of the K3311 is milder than the SD7037.

E387 Version A of the E387 built by Bob Champine and originally tested at Princeton is included here since it shares much in common with the K3311. It should, however, be noted that this wind-tunnel model had a spanwise twist of approximately 0.22 deg/ft. Also, the overall camber of the model was less than the true E387. Thus, the results do not accurately represent the performance of the true E387.

S7055 Newcomers and casual pilots favor simplicity, which often leads to the choice of a flat-bottomed airfoil. Unfortunately, the selection of flat-bottomed airfoils is limited. Also, few flat-bottomed airfoils have been recently designed with a view toward reducing the bubble drag. The idea to change this situation was motivated through discussions with Tim Renaud of Airtronics who felt that a 10–11% flat-bottomed airfoil (flat past the spar) was needed for thermal soaring. In addition, he recommended that the new airfoil be designed with more lift than the S3021 or E205, which “build up speed too quickly for beginners.” As a result, the new S7055 (10.5%) was designed to fill this niche.

The wind-tunnel results show that the flat-bottomed S7055 does not perform as well as the SD7037, WASP, E387 and K3311—airfoils that are not constrained to be flat. In particular, at low lift, there is a noticeable performance loss.

Nevertheless, the high-lift thermal performance compares well with the other airfoils, and the airfoil has a mild stall.

Flat Bottomed Airfoils The S7055 in comparison with the SD7037 serves to illustrate that when an airfoil is required to be flat bottomed, there is an associated performance penalty. More generally, when the geometry of any portion of the airfoil is constrained, some performance loss can be anticipated because that part of the airfoil cannot be optimized for best aerodynamic performance. The airfoil, however, can be tailored so that the performance loss occurs in less important regions of the polar.

SD7032 The SD7032 is a high-lift variant of the SD7037. As in Figs. 4.123–4.126 (version D), the polar as compared with the SD7037 is shifted upward by a ΔC_l of 0.15. This increment in C_l is enough to substantially improve the thermal performance. The trade-off is reduced L/D performance, which in light-wind conditions is acceptable. Version E of the SD7032 is less accurate than version D, but the performance characteristics are similar.

3.3 Airfoils for F3B Sailplanes

RG15 For F3B flying, the RG15 designed by Rolf Girsberger has become a standard. As compared with the previous group of thermal duration airfoils, the lower lift of the RG15 makes it more ideal for F3B where the distance (L/D performance) and speed tasks are more important than the duration task (thermal performance). Some pilots, however, prefer the RG15 for thermal duration competition, particular in geographical regions noted for having strong thermals in windy conditions. Under such circumstances, the L/D performance is the design driver that favors the RG15 or, more generally, all airfoils in this category.

SD7003 This airfoil designed and tested at Princeton was used by Joe Wurts and Daryl Perkins on their F3B EAGLE models that placed 1st and 2nd, respectively, in the 1991 F3B World Championship. Since that time, interest has shifted away from the SD7003 toward the RG15, which has an advantage in the duration task. Although thermal performance is secondary, this is the key factor that reportedly sets the two airfoils apart. From the polars, little difference is observed at high lift. The high-lift performance shown in the polars is, however, for zero flap deflection. In F3B competition, camber-changing flaps are used in all three tasks. For the duration task, the positive flap settings that are used must improve the performance of the RG15 over the SD7003. To see this effect, these airfoils should be tested with flaps.

Table 3.4: Summary of Airfoil Data for F3B Sailplanes

Airfoil	Data	Configuration	Figure/Page
RG15 (B)	Velocity Dist.	Clean	Fig. 4.78/p. 158
	Profile		Fig. 4.79/p. 158
	Drag Polar		Fig. 4.80/p. 159
	Lift Curves		Fig. 4.81/p. 160
S7012	Velocity Dist.	Clean	Fig. 4.107/p. 194
	Profile		Fig. 4.108/p. 194
	Drag Polar		Fig. 4.109/p. 195
	Lift Curves		Fig. 4.110/p. 196
SD7003	Velocity Dist.	Clean	Fig. 4.119/p. 206
	Profile		Fig. 4.120/p. 206
	Drag Polar		Fig. 4.121/p. 207
	Lift Curves		Fig. 4.122/p. 208
SD8000	Velocity Dist.	Clean	Fig. 4.139/p. 224
	Profile		Fig. 4.140/p. 224
	Drag Polar		Fig. 4.141/p. 225
	Lift Curves		Fig. 4.142/p. 226

SD8000 The SD8000 has a working lift range similar to both the RG15 and SD7003, and it has been used successfully in F3B competition, although without such illustrious results. The thermal performance is known to be better than, but similar to, the SD7003.

S7012 The S7012 is a new F3B airfoil designed to be an improvement over the RG15. Clearly, the RG15 for F3B competition can be classified as an “optimum” airfoil in the sense that it seems that no airfoil can be designed with lower drag everywhere. Therefore, one is left with making tradeoffs. The question then becomes what are the best compromises to make. In particular, where does the RG15 have good performance that can be sacrificed for better performance elsewhere, or in conceptual terms where can the drag be increased for lower drag elsewhere? The strategy taken in the design of the S7012 was to give up performance between the best distance speed and the best thermal speed in exchange for improvements primarily in the speed and thermal tasks. As the following discussion reveals, these goals were achieved at the expense of some performance in the distance task.

Judging Polars Based on Constant Reynolds Numbers Before discussing the S7012 further, a word about interpreting airfoil polars is in order. Judging aircraft performance based on airfoil data for constant Re polars can be difficult. The aircraft Re changes with the flight speed, and therefore it does not follow a constant Re line on the traditional polar. Plotting the performance of the airfoil

as it “flies” through the constant Re polars is much more helpful since it takes into account the change in aircraft speed (and hence Re) with lift coefficient. This aircraft Re that changes with the lift coefficient is called the “reduced Reynolds number,” \mathcal{R} .ⁿ³

Another difficulty in judging aircraft performance based on airfoil data is that the fuselage, tail and induced drag components, which make up a significant contribution to the overall aircraft drag, are not included in the airfoil polar plots. As a result of this additional drag, the $(C_L/C_D)_{max}$ and $(C_L^{3/2}/C_D)_{max}$ for the whole aircraft will not correspond to the same flight condition as the $(C_l/C_d)_{max}$ and $(C_l^{3/2}/C_d)_{max}$ read directly from the airfoil drag polars. For the interested reader, the basics of understanding airfoil polars can be found in Ref. 20.

Seeing the full effect of this additional drag together with the airfoil drag greatly helps in the airfoil selection process. With respect to the design of the S7012, including this additional drag with the airfoil drag helps to determine what tradeoffs are the best ones to make.

Figure 3.1 shows the performance of the S7012 as compared with the RG15 for \mathcal{R} of 120k, which is typical for F3B ships with wing loadings near 12 oz/ft². The SD7003 airfoil data is shown for reference and will be discussed last. Figures 3.2 and 3.3 show two key performance parameters plotted vs. the sailplane lift coefficient, C_L . These performance parameter curves correspond to a typical F3B glider (in particular, one with an aspect ratio of 12.5, a wing span of 112 in and a combined fuselage and tail drag coefficient of approximately 0.003).

The first parameter is the aircraft L/D (sailplane glide slope), where the drag coefficient does include all drag components. As seen, there is clearly a tradeoff. The S7012 is better than the RG15 below a C_L of approximately 0.27—the crossover point. Thus, if the F3B distance run is done below this point, the S7012 will be better, and if above it will be worse. Typically, for sailplanes with the RG15, the distance run is done near a C_L of 0.40 or lower—the lower the C_L , the greater the number of laps in the working time. The benefit of the S7012 will depend on the course conditions: the stronger the lift on course, the lower the C_L , and the better the S7012 relative to the RG15.

The second performance parameter shown in Fig. 3.3 is the aircraft endurance parameter $(C_L^{3/2}/C_D)$. A 5% improvement in the endurance parameter translates into a 5% improvement in duration time. As seen in the figure, the S7012 peak value for the endurance parameter is nearly 2% higher than the RG15. An additional improvement is that the best endurance occurs at a higher lift coefficient, so the best thermal speed is slower and thermal turns can be made tighter.

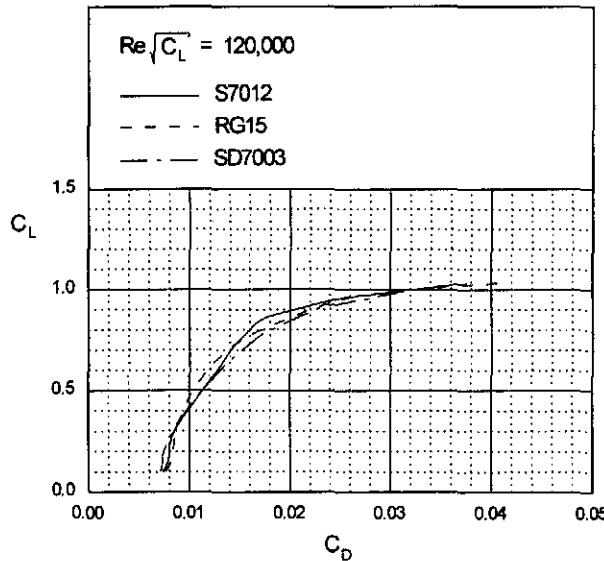


Fig. 3.1 Performance characteristics of the S7012 compared with the RG15 and SD7003 for \mathcal{R} of 120k.

For the F3B speed task, the differences between the S7012 and RG15 are hard to deduce from Figs. 3.2 and 3.3. From the airfoil polars, however, the S7012 has 3% lower drag at a C_L of 0.1, which is close to that for speed task. Thus, the new airfoil should be slightly faster in a straight run. For turn performance during the speed and distance task, the L/D performance is best compared; whereas, for turns in the duration task the endurance performance should be used for comparison. Unfortunately, the comparison in these areas requires testing the airfoils with flaps—tests which have not yet been done.

It is important to emphasize that the S7012 is only better than the RG15 in certain areas of the C_l range, which translate to certain aircraft speeds. The best thermal speed only occurs over a fairly narrow C_l range, so if the speed is not carefully controlled the benefits of the new airfoil will hardly be noticed. If the distance task is flown too slowly, again the benefits will be hard to detect, or worse, there will be no benefit.

Another characteristic of the S7012 should also be mentioned. The thermal performance improves gradually with increasing lift coefficient, but only up to a certain point. Beyond this point, the performance degrades rather quickly, which should send a clear signal to the pilot. Several Eppler airfoils have this characteristic, and it seems to be favored as it provides clear cues to the pilot.

The SD7003 is known for its good high-speed performance and marginal thermal performance. The S7012 is an improvement above a C_L of 0.4 and worse below, which again illustrates that compromises must be made when the performance is near an optimum.

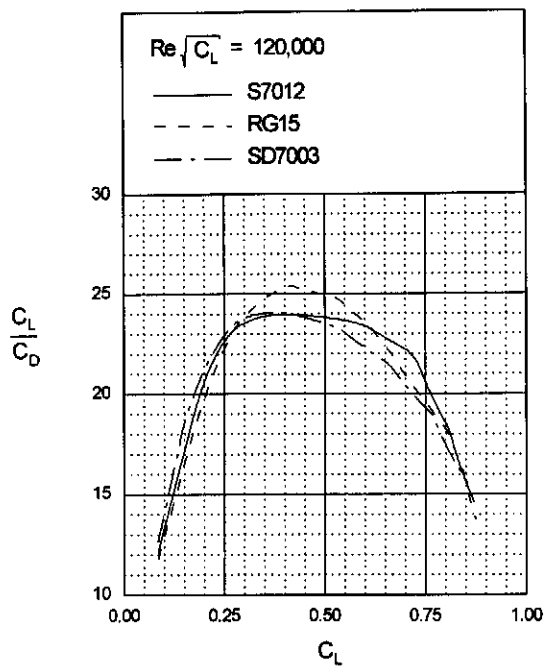


Fig. 3.2 L/D 's for sailplanes based on the S7012, RG15 and SD7003 for \mathcal{R} of 120k.

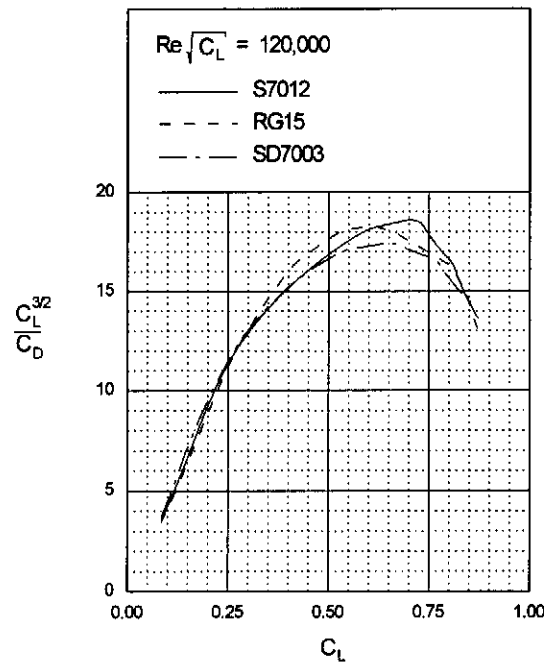


Fig. 3.3 Endurance parameters for sailplanes based on the S7012, RG15 and SD7003 for \mathcal{R} of 120k.

3.4 Airfoils for Slope Racers

Table 3.5: Summary of Airfoil Data for Slope Racers

Airfoil	Data	Configuration	Figure/Page
E374 (B)	Velocity Dist.		Fig. 4.13/p. 80
	Profile		Fig. 4.14/p. 80
	Drag Polar	Clean	Fig. 4.15/p. 81
	Lift Curves	Clean	Fig. 4.16/p. 82
MH45	Velocity Dist.		Fig. 4.58/p. 136
	Profile		Fig. 4.59/p. 136
	Drag Polar	Clean	Fig. 4.60/p. 137
	Lift Curves	Clean	Fig. 4.61/p. 138
S6062	Velocity Dist.		Fig. 4.103/p. 190
	Profile		Fig. 4.104/p. 190
	Drag Polar	Clean	Fig. 4.105/p. 191
	Lift Curves	Clean	Fig. 4.106/p. 192
SD6060	Velocity Dist.		Fig. 4.115/p. 202
	Profile		Fig. 4.116/p. 202
	Drag Polar	Clean	Fig. 4.117/p. 203
	Lift Curves	Clean	Fig. 4.118/p. 204

E374 & SD6060 An extensive discussion of the design philosophy behind the SD6060 was given in *Airfoils at Low Speeds*¹ and also Ref. 21. Briefly, the SD6060 was designed to be an improvement over the E374. The approach was to incorporate into the SD6060 design bubble ramps that were similar to, but longer than, the E374. The effect of these longer ramps was to reduce the drag produced by the laminar separation bubble. As seen in Figs. 4.15 and 4.117, almost everywhere the drag of the SD6060 is lower than the E374. When the drag polars are used to generate data for a constant reduced Reynolds number, \mathcal{R} , the performance is better than the E374 under most R/C slope-soaring conditions.

The performance envelope of these two airfoils is typical of slope-soaring airfoils. The straight-line high-speed performance requires that slope-soaring airfoils have low drag at low lift. Thus, the working range of the polar must extend to zero lift and below to accommodate gusts. The high-lift end of the polar is determined partly by turn performance, but perhaps more importantly by climb performance. Climb is important because the slope racers are allowed a fixed amount of time to gain altitude before entering the course—the higher the start height, the better the speed on course.

The specific amount of high-lift performance, that is, the upper end of the working range, is most easily determined by inspection of the SD6060 and E374 polars, which are very similar to the F3B airfoils previously discussed. Conse-

quently, F3B airfoils are equally applicable to slope racing. For instance, the S7012 as a slope-soaring airfoil is better than the SD6060 in most areas of the performance envelope.

Although these two airfoils are categorized here as airfoils for slope soaring, the E374 and likewise the SD6060 have been used effectively on cross-country sailplanes where the Re 's can be in the 400k–800k range.

S6062 The S6062 is a 8% version of the SD6060 (10.37%) optimized for speed as evidenced by its minimum drag coefficient, which is the lowest of all the airfoils tested. Efficient turn performance will require the use of camber-changing flaps. Interestingly, the S6062 has nearly the same maximum lift coefficient as the SD6060. The S6062 is recommended for use as a tip airfoil in combination with the SD6060 at the root.

MH45 The slightly-reflexed 9.84% thick MH45 was designed by Martin Hepperle for use on flying wings, but it is included in this category since it has much in common with slope soaring airfoils. The airfoil has a wide usable lift range, including good performance at negative lift coefficients required for inverted flight. The generous thickness, wide lift range and predictable stall characteristics make the MH45 a good all-purpose slope airfoil. The true characteristics of the MH45, however, are difficult to ascertain from the polars since the wind-tunnel model was too thick.

3.5 Airfoils for Tail Sections

J5012, NACA 0009, NACA 64A010 & SD8020 These four airfoils were all tested at Princeton¹ and showed to varying degrees nonlinearities in the lift curve about 0 deg. A much more dramatic case of this effect (which gives the airfoil a “deadband” in relative terms) was found by Mueller & Batill on the NACA 66₃-018 airfoil.²² For this airfoil at Re of 130k the lift curve through zero angle of attack actually changed sign over a 3 deg range, that is, an increase in angle of attack produced a decrease in lift. Of the current airfoils tested, the NACA 64A010 exhibited the most pronounced case of this nonlinearity. When such an airfoil is used as a full-flying stabilator, it can adversely impact the aircraft handling qualities, particularly when the Re 's are low and the airfoil operates about zero lift. Consider a special case of a hand-launch glider that uses the NACA 64A010 at a Re of 30k. When the tail surface is deflected 2 deg (in magnitude), the C_l reaches 0.1. A 4 deg deflection, however, produces a C_l of 0.4. This nonlinear C_l - α characteristic will produce a nonlinear control response that is undesirable. (Note that the difference in the lift coefficient for increasing and decreasing angles of attack for Re of 30k is due to transducer and mechanical hysteresis.)

Table 3.6: Summary of Airfoil Data for Tail Sections

Airfoil	Data	Configuration	Figure/Page
J5012	Velocity Dist.	Clean	Fig. 4.40/p. 112
	Profile		Fig. 4.41/p. 112
	Lift Curves		Fig. 4.42/p. 113
NACA 0009	Velocity Dist.	Clean	Fig. 4.62/p. 140
	Profile		Fig. 4.63/p. 140
	Lift Curves		Fig. 4.64/p. 141
NACA 64A010	Velocity Dist.	Clean	Fig. 4.70/p. 148
	Profile		Fig. 4.71/p. 148
	Drag Polar		Fig. 4.72/p. 149
	Lift Curves		Fig. 4.73/p. 150
SD8020	Velocity Dist.	Clean	Fig. 4.143/p. 228
	Profile		Fig. 4.144/p. 228
	Drag Polar	Clean	Fig. 4.145/p. 229
	Lift Curves	Clean	Fig. 4.146/p. 230
	Lift Curves	Tripped	Fig. 4.147/p. 234
	Drag Polar	Clean	Fig. 4.148/p. 237
	Lift Curves	Tripped	Fig. 4.149/p. 238

As compared with the Princeton data, the current results show larger deadband regions. In fact, the SD8020 when tested at Princeton appeared to have no significant deadband; whereas, the current results show that the SD8020 is not an exception after all. (Its lift characteristics are, however, the most linear of the four airfoils). The main cause of the peculiar lift characteristics is related to the interplay between the upper and lower surface laminar separation bubbles. Furthermore, it is known that larger turbulence levels produce smaller laminar separation bubbles and their associated effects, which for these symmetrical airfoils includes the extent of the deadband region. Thus, from the nonlinear behavior of the lift curves, it is clear that the turbulence levels of the current tunnel are lower than they were at Princeton.

Trips can sometimes be used to “repair” otherwise poorly performing airfoils known to be afflicted adversely by bubbles. This axiom was applied in an attempt to improve the characteristics of the SD8020, particularly in regard to the lift characteristics. First, one zig-zag trip type B shown in Fig. 4.147 was placed on both the upper and lower surfaces. The leading edge of the trip was located at 25% chord. As seen in Fig. 4.147, the nonlinearity (deadband) is reduced up to Re of 80k, after which it is completely eliminated. Second, two layers of the zig-zag trip were used, and the effects of the bubbles were eliminated between 60k and 100k (see Fig. 4.149). At 40k, although there is still some nonlinear behavior, the lift characteristics are greatly improved over the baseline case without trips.

It is reasonable to assume that the other three airfoils would likewise benefit in this way from the use of trips. Of course, the drag at the higher Re 's will be increased (see Fig. 4.148).

3.6 Airfoils for Quickie 500 Pylon Racers

Table 3.7: Summary of Airfoil Data for Quickie 500 Pylon Racers

Airfoil	Data	Configuration	Figure/Page
R140 (A)	Velocity Dist.	Clean	Fig. 4.74/p. 154
	Profile		Fig. 4.75/p. 154
	Drag Polar		Fig. 4.76/p. 155
	Lift Curves		Fig. 4.77/p. 156
S8052	Velocity Dist.	Clean	Fig. 3.4/p. 43
	Profile		Fig. 3.4/p. 43
	Drag Polar		Fig. 3.5/p. 44

R140 (A) & S8052 The R140 has been used for Quickie 500 (Q-500) pylon racing. The airfoil thickness is 12.04%, which is close to that required by Q-500 rules (11.88%). Under typical race conditions, the Re 's can reach 1×10^6 (1000k), which is beyond the current wind-tunnel test capability. In order to gain a measure of the performance in this relatively high Re regime, the XFOIL airfoil code¹⁴ (version 6.5) was used to predict the performance at 300k, 600k and 1000k. The results afford a comparison between predictions and experimental results for the Re of 300k. Over the mid-lift range the agreement is relatively good, while at the limits of the polar discrepancies exist. In these regions, the higher drag found in the wind-tunnel tests indicates that transition takes place sooner than predicted. (For reference, the computational results were performed with a turbulence amplification factor, n , of 9—a value consistent with the wind-tunnel turbulence level.)

From the wind-tunnel data, the airfoil operates well at moderately negative lift coefficients, but performance in this range may not be required. Negative lift coefficients are used for inverted flight as encountered in aerobatic maneuvers. Also, in steady level upright flight, gusts can cause the airfoil to operate in the negative range. At high speeds, however, gust effects are reduced and consequently so too is the need for good negative lift performance. Pilot control excursions could cause the model to operate at negative g 's (negative lift coefficients), but top competition pilots flying smooth laps usually keep positive g 's (positive lift coefficients) on the aircraft. In F3B competition, the speed task is somewhat like Q-500 pylon racing and one could assume that the airfoil requirements will be somewhat similar. As deduced partly through trial and error, optimum airfoils for F3B do not have much negative lift performance. The ev-

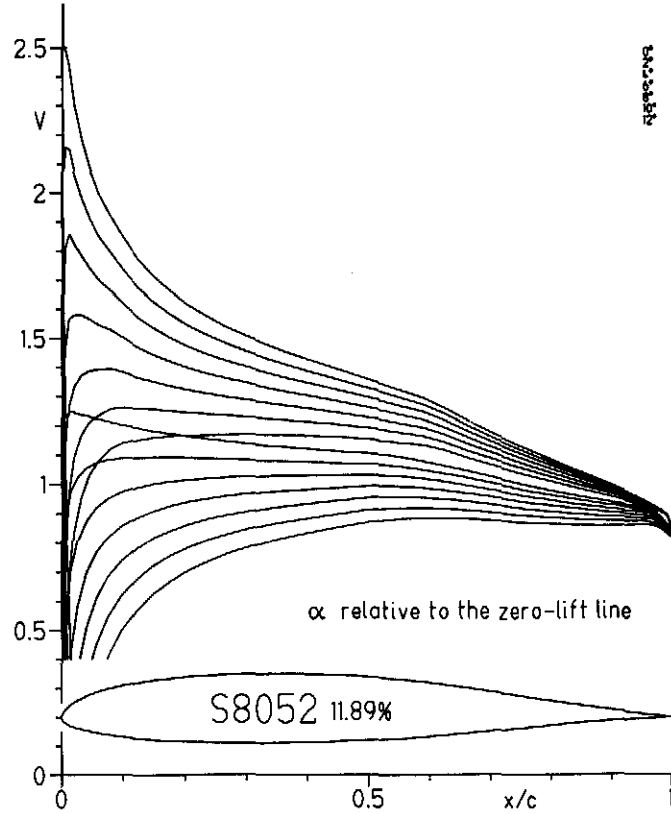


Fig. 3.4 Velocity distributions for the S8052.

idence indicates that very little negative lift performance is required for Q-500 models.

In light of the aforementioned comments related to setting the airfoil design requirements for Q-500 models, a new airfoil, the S8052 shown in Fig. 3.4, was designed for Q-500 pylon racing. Since wind-tunnel tests have not yet been performed, Fig. 3.5 shows the performance predicted by XFOIL. As seen, the new airfoil has less negative lift performance and nearly the same minimum drag coefficient as compared with the R140. The upper limit of the low-drag range is extended to improve turn performance. Camber-changing flaps are not required, but, as has been found useful in F3B competition, camber-changing flaps will prove to be quite beneficial for rapid turn performance. For reference, the airfoil zero-lift angle of attack and pitching moment are approximately -1.5 deg and -0.031 , respectively.

3.7 Airfoils for Sport Planes

GEMINI & MB253515 Both of these semi-symmetrical airfoils were originally used for R/C sailplanes, but they are included here since they have application to powered sport models. The GEMINI airfoil used on the GEMINI

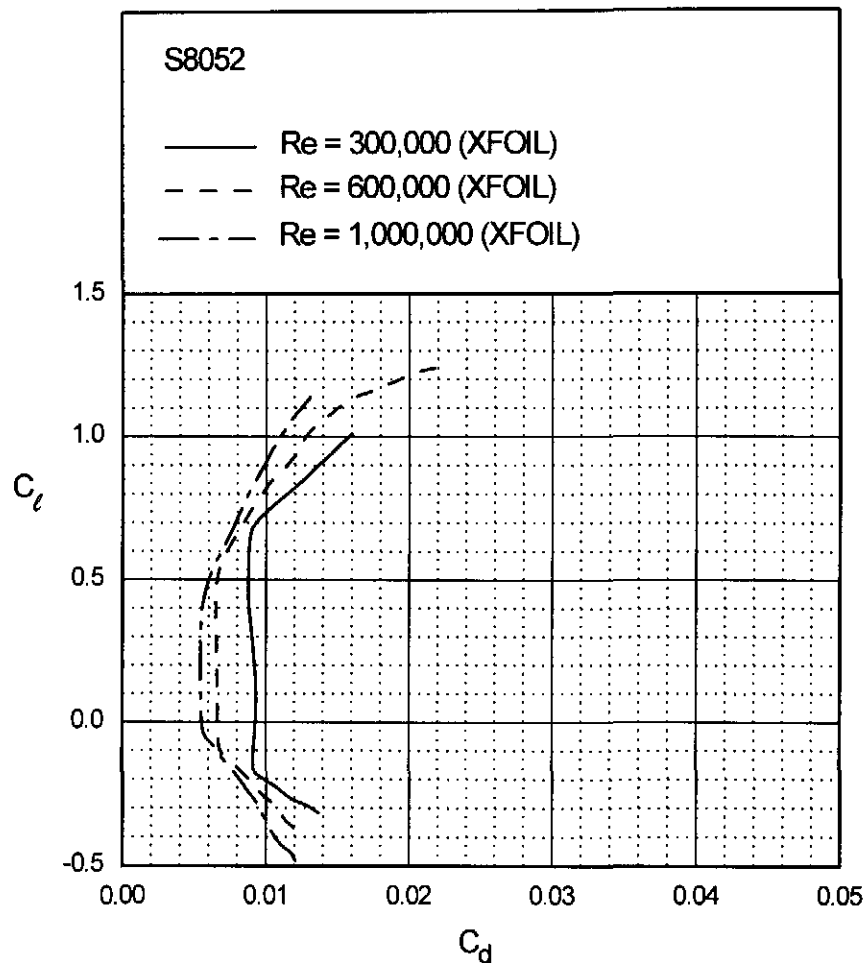


Fig. 3.5 Predicted performance characteristics for the S8052.

Table 3.8: Summary of Airfoil Data for Sport Planes

Airfoil	Data	Configuration	Figure/Page
GEMINI	Velocity Dist.	Clean	Fig. 4.29/p. 100
	Profile		Fig. 4.30/p. 100
	Drag Polar		Fig. 4.31/p. 101
	Lift Curves		Fig. 4.32/p. 102
	Planform		Fig. 4.33/p. 103
	Spanwise Drag		Fig. 4.33/p. 103
MB253515	Velocity Dist.	Clean	Fig. 4.55/p. 132
	Profile		Fig. 4.56/p. 132
	Lift Curves		Fig. 4.57/p. 133

R/C sailplane is intended to be the same as the MB253515, but slight differences exist. Moreover, the GEMINI airfoil model had a D-tube/aft-open bay construction as shown in Fig. 4.33. The 9/32 in wide capstrips on the ribs were spaced every 3 1/8 in (26% chord). The sagging of the covering was between 0.032 and 0.090 in with an average of 0.062 in.

The MB253515 airfoil was tested primarily for comparison with the Princeton lift data. Once again, the effects of the laminar separation bubble are more apparent than at Princeton. The unusual bubble behavior results from the velocity distributions, which as shown in Fig. 4.55 are quite unlike those of all the other airfoils tested. Attempting to described the particular features in the velocity distributions that lead to the kink in the lift curve goes beyond the scope of this book.

As expected, the GEMINI airfoil has performance characteristics much like the MB253515, with some notable exceptions. The lift curve at Re of 100k does not show a kink near 0 deg like the MB253515. Thus, the bubble on the GEMINI airfoil at this condition is probably smaller in size. This hypothesis is supported by the observation that the drag on the GEMINI airfoil is less at this condition. Another important difference is that the $C_{l_{max}}$ of the GEMINI airfoil is greater. These differences combined are probably caused by the sagging of the covering between the ribs.

Detailed spanwise measurements were taken on the GEMINI airfoil to quantify the degree of spanwise drag variation associated with the open-bay construction (see Fig. 4.33). As observed on the NACA 6409, the drag measured downstream of the ribs was higher than between the ribs for reasons that were discussed in Section 3.1.

3.8 Airfoils for Heavy-Lift Cargo Planes

As a result of heavy-lift cargo model competitions gaining popularity (e.g., the SAE Aero-Design Competition), there is a renewed interest in high-lift airfoils for such applications. Also, unmanned aerial vehicles (UAVs) are becoming increasingly important in both civilian (e.g., scientific, meteorology and mapping) and military (e.g., reconnaissance and electronic warfare) roles. Small model aircraft size UAVs are sometimes driven by the need to carry relatively heavy payloads for long periods of time.^{23,24} For example, a mission may include a 24-hour endurance at an altitude at or below 100 ft mean sea level, with flight speeds ranging from 25–40 knots and payload requirements varying from 10–25 lb.²⁴ These objectives are best achieved through the use of efficient high-lift low Reynolds number wings, whose performance depends largely on the airfoils employed.

Table 3.9: Summary of Airfoil Data for Heavy-Lift Cargo Planes

Airfoil	Data	Configuration	Figure/Page
CH 10-48-13	Velocity Dist.	Tripped	Fig. 4.9/p. 74
	Profile		Fig. 4.10/p. 74
	Drag Polar		Fig. 4.11/p. 75
	Lift Curves		Fig. 4.12/p. 76
FX 63-137 (B)	Velocity Dist.	Clean	Fig. 4.21/p. 88
	Profile		Fig. 4.22/p. 88
	Drag Polar		Fig. 4.23/p. 89
	Lift Curves		Fig. 4.24/p. 90
FX 74-CL5-140 MOD	Velocity Dist.	Clean	Fig. 4.25/p. 94
	Profile		Fig. 4.26/p. 94
	Drag Polar		Fig. 4.27/p. 95
	Lift Curves		Fig. 4.28/p. 96
M06-13-128 (B)	Velocity Dist.	Clean	Fig. 4.47/p. 120
	Profile		Fig. 4.48/p. 120
	Drag Polar		Fig. 4.49/p. 121
	Lift Curves		Fig. 4.50/p. 122
S1210	Velocity Dist.	Clean	Fig. 4.90/p. 170
	Profile		Fig. 4.91/p. 170
	Drag Polar		Fig. 4.92/p. 171
	Lift Curves		Fig. 4.93/p. 172
S1223	Velocity Dist.	Clean	Fig. 4.94/p. 176
	Profile		Fig. 4.95/p. 176
	Drag Polar	Clean	Fig. 4.96/p. 177
	Lift Curves	Clean	Fig. 4.97/p. 178
	Drag Polar	Vortex Generators	Fig. 4.98/p. 182
	Lift Curves	Vortex Generators	Fig. 4.99/p. 183
	Spanwise Drag	Vortex Generators	Fig. 4.100/p. 187
	Drag Polar	Gurney Flap	Fig. 4.101/p. 188
	Lift Curves	Gurney Flap	Fig. 4.102/p. 189

Although the existing “library” of low Re ’s airfoils is extensive, to date only a few airfoils are suitable for high-lift low Re applications. Leading the list is often the Wortmann FX 63-137 airfoil, which will be discussed first.

FX 63-137 Currently, the Wortmann FX 63-137 (see Figs. 4.21–4.24) is one of the most desirable airfoils for high-lift low Re models. The high-lift capability ($C_{l_{max}}$ near 1.7 at Re of 200k) and mild-stall characteristics seen in Figs. 4.24 are among its key attributes.

The FX 63-137 was tested down to Re of 60k to explore the limits of its capability. At Re of 60k, an indication of separation on the upper surface is already noticeable at an angle of attack of -2 deg. (Compare 60k data with 300k data). At 80k for increasing angles of attack, the airfoil is stalled at an angle of attack of near 11 deg, just beyond which the flow reattaches and C_l dramatically increases. Trailing-edge stall eventually takes place near 16 deg. For decreasing angles of attack the airfoil unstalls at 16 deg, and then just past 8 deg the flow again separates and effectively stalls the airfoil. This complex stall behavior is shared by many of the high-lift airfoils in this group. At 90k, the hysteresis loop at low angles of attack is beginning to vanish, and only a small remnant is left at 100k, after which the airfoil is fairly well-behaved.

M06-13-128 This airfoil designed by Miley²⁵ was intended for operation at its design Re of 600k. Nevertheless, it has been considered as a high-lift airfoil for application at Re 's below 600k. As seen in the polars for a Re of 300k, the $C_{l_{max}}$ is near 1.5, which is substantial in light of the low pitching-moment constraint. For practical applications, however, the M06-13-128 airfoil should not be given serious consideration at Re 's below 300k owing to its high drag characteristics.

FX 74-CL5-140 MOD The actual wind-tunnel model tested is a modified version of the FX 74-CL5-140. As stated by the builder, Chuck Hollinger, the plot of the FX 74-CL5-140 found in a paper by Wortmann²⁶ on high-lift airfoils was enlarged in order to measure the coordinates. The airfoil was then reduced from 14% thickness to 13%, and the leading-edge nose radius was slightly increased. Other modifications can be deduced from Fig. 4.26.

Although the FX 74-CL5-140 was originally designed for Re 's between 1000k and 3000k, the modified FX 74-CL5-140 does perform well at lower Re 's. In fact, as seen in Fig. 4.28, a $C_{l_{max}}$ of near 2.0 is achieved at Re of 200k. In contrast to the FX 63-137, which was well-behaved at Re of 100k, the modified FX 74-CL5-140 must reach Re of near 175k to avoid inefficient operation within hysteresis loops.

It is interesting to note the unusual nature of the lift characteristics of the modified FX 74-CL5-140. For Re of 100k, the airfoil has a small but abrupt stall near 0 deg. Then at 20 deg the flow reattaches and the C_l increases. This increase in C_l , however, does not occur as a result of fully-attached flow. As seen for Re of 175k, the airfoil at this high angle of attack condition is in the stalled region of the lift curve. As Re increases from 100k to 125k and then from 125k to 150k, the point at which the abrupt stall takes place increases to an angle of attack near 8 deg. For decreasing angles of attack at 175k, the flow first remains attached until 13 deg, then stalls, and reattaches near 1 deg to form a clockwise hysteresis loop in contrast the FX 63-137 that had a counter-clockwise hysteresis loop below the final stall angle of attack.

CH 10-48-13 As described by the designer, Chuck Hollinger, this airfoil was formed by combining a 12.75% thick S4233 thickness distribution around an 10.2% mean camber line. A plain trip at 25% chord on the upper surface was added by Hollinger in an effort to improve the drag characteristics. Lift characteristics show that the airfoil achieves a $C_{l_{max}}$ of 1.95 at Re of 200k. This airfoil also shows hysteresis characteristics much like the FX 74-CL5-140 MOD.

S1223 As described in more detail at the end of this section, the design philosophy employed in the design of the S1223 airfoil involves combining the favorable effects of both a concave pressure recovery and aft loading to achieve maximum lift at a design Reynolds number of 200k.²⁴ The desired aerodynamic characteristics were achieved through the use of a suite of computational tools for airfoil design and analysis.⁷⁴ As shown in Fig. 4.97, the $C_{l_{max}}$ at Re of 200k is 2.11. Below this design Re , hysteresis in the lift curve characteristics appears. The single hysteresis loop is similar to the first hysteresis loop found on the Miley and FX 74-CL5-140 airfoils. This type of hysteresis is expected since the S1223 velocity distribution architecture is similar to the M06-13-128 and FX 74-CL5-140 airfoils.

In an effort to increase the $C_{l_{max}}$ above that of the baseline (clean) airfoil, the S1223 was tested with vortex generators (VGs) located on the airfoil upper surface at 17% chord. The VG geometry is shown in Fig. 4.95. As seen in Fig. 4.99 for Re of 200k, the $C_{l_{max}}$ is increased to 2.19. This slight increase, however, occurs together with a sharp stall and a hysteresis loop, which taken together make the VGs not advantageous. As might be expected from work performed at Delft,²⁸ the VGs do produce a periodic spanwise drag variation downstream as seen in Fig. 4.100.

A 1.04% chord Gurney flap (shown in Fig. 4.95) on the S1223 was also examined, again, in an effort to improve the $C_{l_{max}}$ characteristics. This experiment did prove successful, yielding for Re of 200k a $C_{l_{max}}$ of 2.21—the highest of all the airfoils tested. Although the airfoil was only tested for increasing angles of attack, hysteresis does not appear to be present. A discussion of the effects of Gurney flaps and the physical mechanism related to this simple and intriguing device can be found in Ref. 29.

S1210 The S1210 was designed (before the S1223) to validate the design philosophy, which was later more fully exploited in the design of the S1223. A relatively conservative approach was taken as can be seen by comparing the velocity distributions of the S1210 with the S1223. Not only was the approach successfully validated, the resulting S1210 has performance comparable to the FX 63-137 (if not better). At Re of 200k, the airfoil achieves a $C_{l_{max}}$ of 1.80 together with a surprisingly soft stall. Moreover, the airfoil maintains good performance down to Re of 90k.

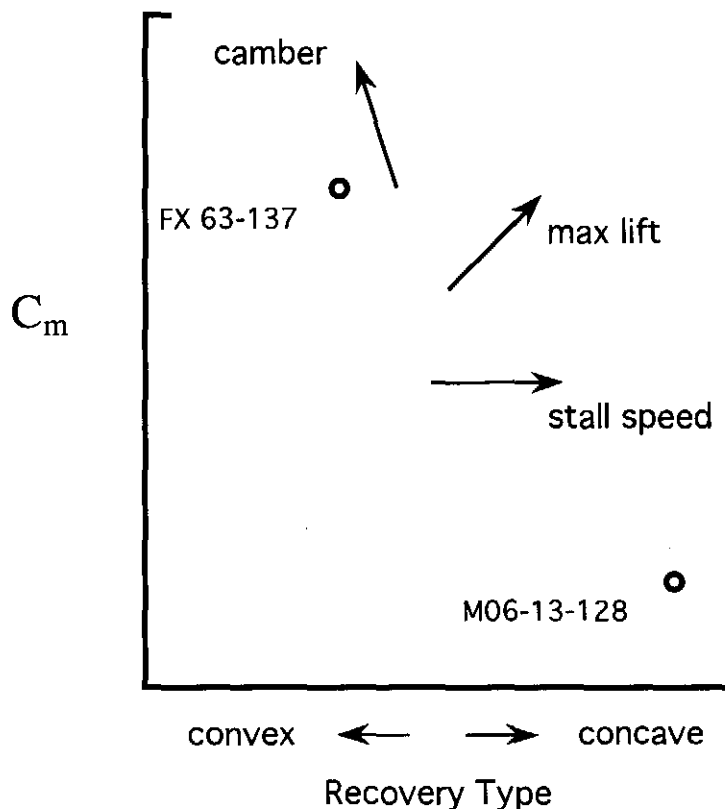


Fig. 3.6 Low Reynolds number airfoil characteristics as a function of the recovery type and pitching moment.

High-Lift Low Reynolds Number Airfoil Design The high-lift S1223 and S1210 were design based on a hypothesis developed from data on the FX 63-137 and M06-13-18 airfoils. These two airfoils can be classified by a number of characteristics as depicted in Fig. 3.6. In the figure, the pitching moment is plotted versus the upper-surface recovery type. Airfoils with concave Stratford-like pressure recoveries and low pitching moments would appear on the lower right, as for example, the M06-13-18 airfoil and some Liebeck airfoils.³⁰ The FX 63-137 with its relatively high pitching moment and convex pressure recovery appears to the upper left in Fig. 3.6.

Also shown in Fig. 3.6 are trend lines. One trend is that the airfoil typically becomes more cambered as the pitching moment increases and as the recovery becomes less concave/more convex. Another trend is that the trailing-edge stall becomes more abrupt as the pressure recovery becomes less convex/more concave.

“Trailing-edge stall speed” as denoted in the figure refers to the shape of the C_l - α curve at stall. The stall of the FX 63-137 is an example of a “slow” trailing-edge stall. The turbulent separation point slowly progresses forward as the angle of attack increases. This slow movement of the separation point produces a plateau in the C_l - α curve past the point of stall initiation (see Fig. 4.24). The stall of the M06-13-128 shown in Fig. 4.50 is an example of a relatively “fast” trailing-edge stall; the C_l - α curve peaks at $C_{l_{max}}$, then falls off more rapidly than the FX 63-137. This characteristic is indicative of a turbulent separation point that moves forward fairly rapidly with increasing angle of attack.

The last trend shown in Fig. 3.6 is that the maximum lift coefficient increases as the pitching moment increases and as the pressure recovery approaches a Stratford distribution. The FX 63-137 is a good example of increasing the $C_{l_{max}}$ primarily through added pitching moment. In contrast, Liebeck type airfoils (such as the M06-13-128) are good examples of increasing the $C_{l_{max}}$ mainly through the use of a Stratford pressure-recovery distribution.

Specifically, the Liebeck high-lift design philosophy³⁰ involves using a Stratford distribution to recover the most pressure without separation at $C_{l_{max}}$. Since separation is avoided completely, that is, up to trailing edge, the prototypical Liebeck airfoil is one with no aft loading, which gives a low pitching moment. The M06-13-128 serves as an example of applying the Liebeck design philosophy at low Re 's. Although the M06-13-128 has a high mid-range bubble drag at the off-design Reynolds numbers of 300k, the $C_{l_{max}}$ is 1.47. This value for $C_{l_{max}}$ is high, especially in light of the intrinsic low pitching-moment constraint.

Eppler¹¹ shows that to achieve maximum lift on an airfoil with concave Stratford-type recovery the low pitching-moment constraint should be relaxed. In particular, through a series of example airfoils, Eppler shows that the lift of an airfoil with a concave recovery can be improved through the use of aft loading. Such airfoils incorporate the favorable effects of both a concave recovery and aft loading to achieve high $C_{l_{max}}$ values. In Fig. 3.6, airfoils of this type would appear between the FX 63-137 and M06-13-128, but displaced in the direction of increased lift.

The high-lift design philosophy described by Eppler¹¹ was employed nearly two decades earlier by Wortmann²⁶ in the design of the FX 74-CL5-140 airfoil, which achieves a $C_{l_{max}}$ of 2.37 at a Reynolds number of 1000k. Figure 3.7 shows the $C_{l_{max}}$ characteristics of the FX 74-CL5-140 along with three other similar high-lift airfoils. In contrast, the FX 63-137 only achieves a $C_{l_{max}}$ of 1.6–1.7. The main difference in the maximum lift is not due to a Reynolds number effect as might be suggested by the figure. Rather, the difference is due to the shape of the recovery distribution—convex vs. concave (compare the inviscid velocity distributions shown in Figs. 4.21 and 4.25). Thus, the FX 63-137 should not be compared with the other airfoils since it is not in the same airfoil “family.”

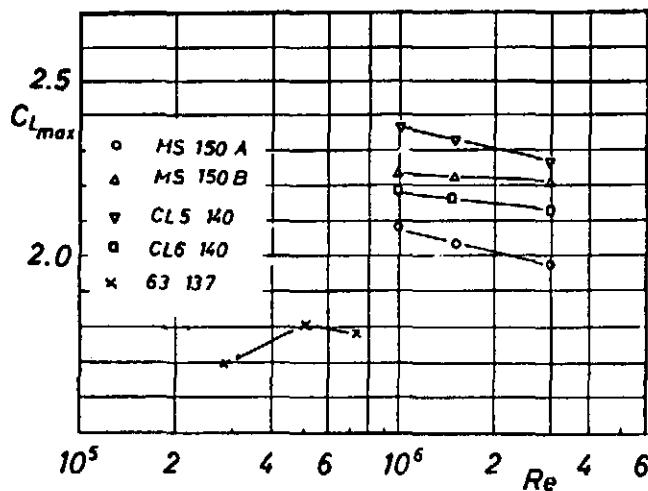


Fig. 3.7 $C_{l_{max}}$ characteristics for five Wortmann airfoils (from Ref. 26).

Since the FX 63-137 should be excluded from consideration in Fig. 3.7, the low Reynolds number high-lift airfoil design problem has yet to be fully explored. The S1223 and S1210, however, are airfoils that fall into this category, that is, airfoils that employ both concave recoveries and aft loading designed for high lift at low R_e 's.. As the S1223 demonstrates, lift coefficients on the order of 2 for R_e of 200k are indeed possible. Moreover, the CH 10-48-13 and modified FX 74-CL5-140 confirm this fact as well. It is interesting to note that although the S1223, CH 10-48-13 and modified FX 74-CL5-140 achieve $C_{l_{max}}$ values near 2, the airfoils differ markedly in shape. Consequently, it can be speculated that future design optimization will lead to a single unique airfoil with an even greater $C_{l_{max}}$ performance.

3.9 Airfoils for Small Wind Turbines

Table 3.10: Summary of Airfoil Data for Small Wind Turbines

Airfoil	Data	Configuration	Figure/Page
S822	Velocity Dist.	Clean	Fig. 4.82/p. 162
	Profile		Fig. 4.83/p. 162
	Drag Polar		Fig. 4.84/p. 163
	Lift Curves		Fig. 4.85/p. 164
S823	Velocity Dist.	Clean	Fig. 4.86/p. 166
	Profile		Fig. 4.87/p. 166
	Drag Polar		Fig. 4.88/p. 167
	Lift Curves		Fig. 4.89/p. 168

S822 & S823 These airfoils,³¹ developed under a joint effort between the National Renewable Energy Laboratory and Airfoils, Inc (D.M. Somers), were specially tailored for use on small horizontal-axis wind turbines, such as the variable-rpm Jacobs 17.5 kW machine. The airfoils have several advantages over those airfoils traditionally used on aircraft. First, the airfoils have a reduced roughness sensitivity for improved energy capture under dirty blade conditions owing to the accumulation of insect debris. Second, the increased section thickness of the root (S823–21%) and tip airfoils (S822–16%) allow for a lower blade weight, lower cost, increased stiffness and improved fatigue resistance. Finally, the restrained $C_{l_{max}}$ improves annual energy production and lower windfarm array losses when used on stall-regulated (fixed-rpm) wind turbines.

Chapter 4

Airfoil Profiles and Performance Plots

In this chapter, the airfoil profiles and performance plots are presented. For reference, the airfoil names are listed beneath the page numbers. Also presented is a table that lists all the data sets and associated figures and page numbers. In the table, a 'T' means that this lift data is not plotted to save space, but it is included with the data distribution disk. As a matter of record, the wind-tunnel run numbers are included in the table, and these also appear with the polar data in Appendix B and also in the data distribution files for cross reference.

Model (Builder) Designer	Config.	Velocity & Profile		Drag Data				Lift Data			
		Fig.	p.	Fig.	p.	Re	Run	Fig.	p.	Re	Run
A18 (Cooney) Archer	Clean	4.1	62	4.3	63	40,000	278	4.4	64	30,000	520
		4.2				60,000	161		65	40,000	519
						100,000	163			60,000	160
						200,000	165/521			100,000	162
						300,000	167/522			200,000	164
BE50 (Cooney) Verbitsky	Clean	4.5	68	4.7	69	60,000	570	4.8	70	30,000	567
		4.6				100,000	572		71	40,000	568
						200,000	574			60,000	569
						300,000	576			100,000	571
CH 10-48-13 (Hollinger) Hollinger	u.s.t. x/c = 40% h/c = 0.20% Plain	4.9	74	4.11	75			4.12	76	100,000	340
		4.10							77	100,000	556
						200,000	156/560			125,000	557
									78	150,000	558
										175,000	559
E374 (B) (Bame) Eppler	Clean	4.13	80	4.15	81	60,000	69	4.16	82	60,000	361
		4.14				100,000	67/503			100,000	363
						150,000	502			150,000	501
						200,000	65			200,000	359
						300,000	63			300,000	62

E387 (A) (Champine) Eppler	Clean	4.17 4.18	84	4.19 	85 	60,000 100,000 150,000 200,000 300,000	209 211 555 213 215	4.20 	■ ■ ■ 86 ■ 87	30,000 40,000 50,000 60,000 100,000 150,000 200,000 300,000	296 294 295 208 210 554 212 214
FX 63-137 (B) (Allen) Wortmann	Clean	4.21 4.22	88	4.23 	89 	100,000 200,000 250,000 300,000	159 154 506 511	4.24 	90 91 92 93	60,000 80,000 90,000 100,000 150,000 200,000 250,000 300,000	504 297 299 158 298 507 508 510
FX 74-CL5-140 MOD (Hollinger) Hollinger	Clean	4.25 4.26	94	4.27 	95 	200,000	185	4.28 	96 97 98	100,000 125,000 150,000 175,000 200,000 300,000	302 304 303 305 579 578
GEMINI (Bates) Bame	Clean	4.29 4.30	100	4.31 	101 	100,000 200,000 300,000	217 219 221	4.32 	102 ■	100,000 200,000 300,000	216 218 220
		4.33	103	200,000							

R140 (A) (Friedlander)	Clean	4.74 4.75	154	4.76	155	100,000	203/531	4.77	156	100,000	202
RG15 (B) (Champine) Grisberger	Clean	4.78 4.79	158	4.80	159	60,000	85	4.81	160	60,000	306
S822 (Allen) Somers	Clean	4.82 4.83	162	4.84	163	100,000	416/417	4.85	164	100,000	415
S823 (Allen) Somers	Clean	4.86 4.87	166	4.88	167	200,000	419	4.89	168	200,000	453
S1210 (Allen) Selig	Clean	4.90 4.91	170	4.92	171	300,000	437		169	300,000	456
						400,000	435			400,000	460
						500,000	420 to 433			400,000	463
						454		4.89	168	100,000	453
						200,000	457/458			200,000	456
						300,000	461/462/465			300,000	460
						400,000	464			400,000	463
						500,000	466 to 475,477				
								4.93	172	60,000	127
									173	80,000	484
										90,000	485
						100,000	129/492			100,000	128
						150,000	488			150,000	545
						200,000	131			200,000	544
						250,000	490/491			250,000	489
						300,000	495			300,000	494

S1223 (Tinel) Selig	Clean	4.94 4.95	176	4.96	177	100,000 150,000 200,000 250,000 300,000	134 590/598 136/588 594 597	4.97	178 179 180 181	60,000 100,000 125,000 150,000 175,000 200,000 250,000 300,000	132 133 336 337 338 339 592 595
	u.s. Vortex Generators x/c = 17% Type A			4.98	182			4.99	183 184 185 186	60,000 80,000 100,000 125,000 150,000 175,000 200,000	354 353 352 346 350 351 344
	Gurney Flap h/c = 1.04%			4.100	187	200,000		4.102	189	200,000	515
				4.101	188	200,000	517				
S6062 (Matheson) Selig	Clean	4.103 4.104	190	4.105	191	100,000 200,000 300,000	142 140/532 138	4.106	192 193	100,000 200,000 300,000	141 139 137
S7012 (Lachowski) Selig	Clean	4.107 4.108	194	4.109	195	60,000 100,000 150,000 200,000 300,000	94 92 565 90 88	4.110	196 197	60,000 100,000 150,000 200,000 300,000	93 91 564 89 87
S7055 (Jones) Selig	Clean	4.111 4.112	198	4.113	199	60,000 100,000 150,000 200,000 300,000	152/547 150 537 148/535/548 146/534/577	4.114	200 201	60,000 100,000 150,000 200,000 300,000	151 149 536 147 145

SD6060 (C. Fox) Selig/Donovan	Clean	4.115	202	4.117	203	60,000	77	4.118	204	60,000	312
SD7003 (Allen) Selig/Donovan	Clean	4.119	206	4.121	207	60,000	169	4.122	208	60,000	168
SD7032 (D) (Watson) Selig/Donovan	Clean	4.123	210	4.125	211	100,000	171	4.126	212	100,000	234
SD7032 (E) (Michaelis)	Clean	4.127	214	4.129	215	150,000	237	4.128	213	150,000	236
SD7037 (A) (Michaelis) Selig/Donovan	Clean	4.131	216	4.133	217	200,000	241	4.130	215	200,000	542
SD7037 (B) (Thompson) Selig/Donovan	Clean	4.135	220	4.137	221	300,000	356	4.134	218	300,000	238
SD8000 (Wagner/ Olsen) Selig/Donovan	Clean	4.139	224	4.141	225	60,000	104	4.138	222	60,000	240
		4.140				100,000	223		219	100,000	355
						150,000	225			150,000	103
						200,000	227			200,000	222
						300,000	325			300,000	224
						60,000	327			60,000	226
						100,000	329			100,000	580
						150,000	331			150,000	99
						200,000	331			200,000	581
						300,000	331			300,000	97
						60,000	331			60,000	95
						100,000	331			100,000	324
						150,000	331			150,000	326
						200,000	331			200,000	328
						300,000	331			300,000	330

SD8020 (Wagner/ Olsen) Selig/Donovan	Clean	4.143	228	4.145	229	60,000	252	4.146	230	30,000	262
		4.144				100,000	254		231	40,000	259
						200,000	256		232	50,000	260
						300,000	258		233	60,000	261
u.s.t./l.s.t. Zig-Zag Type B $x/c = 25\%$ $h/c = 0.16\%$								4.147	234	80,000	263
									235	100,000	264
								4.147	234	200,000	255
									233	300,000	257
u.s.t./l.s.t. Zig-Zag Type B $x/c = 25\%$ $h/c = 0.32\%$				4.148	237	60,000	287	4.149	238	30,000	271
						200,000	289		235	40,000	272
									236	50,000	273
									236	60,000	274
WASP (M. Fox) M. Fox	Clean	4.150	240	4.152	241	60,000	229	4.149	238	80,000	275
		4.151				100,000	144		239	100,000	276
						200,000	231			200,000	277
						300,000	233	4.153	242	60,000	283
									243	100,000	284
										200,000	285
										100,000	286
										200,000	287
										60,000	288
										100,000	289
										200,000	290
										300,000	291

A18

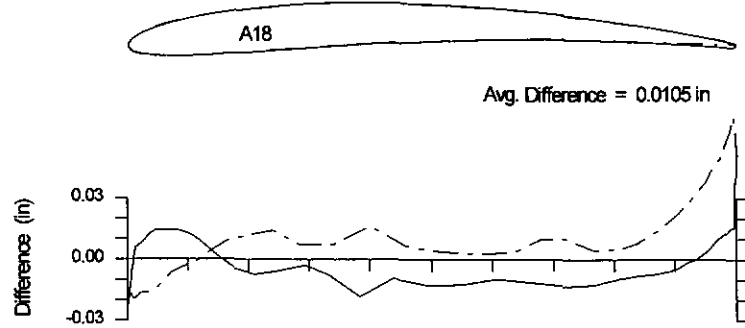
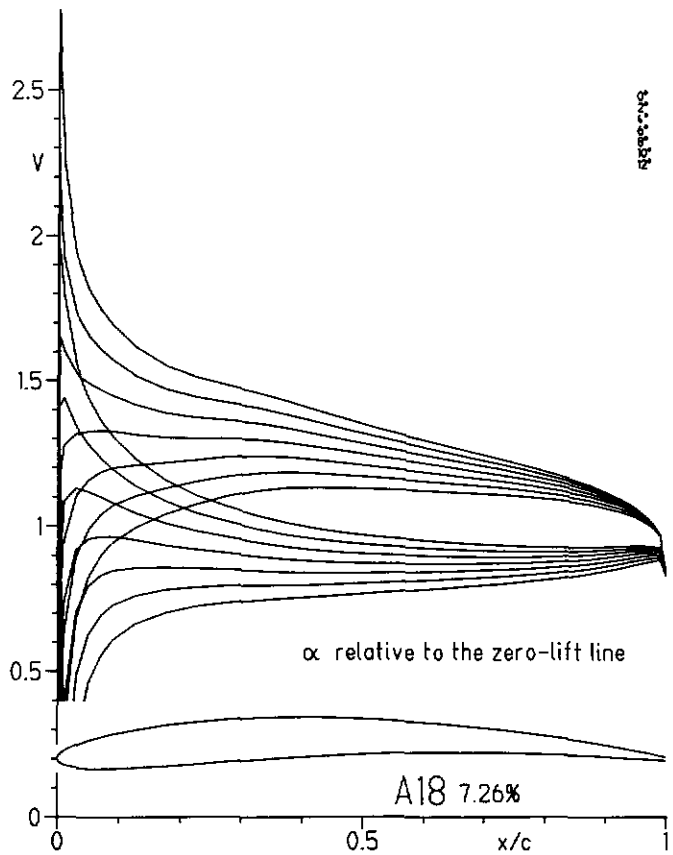
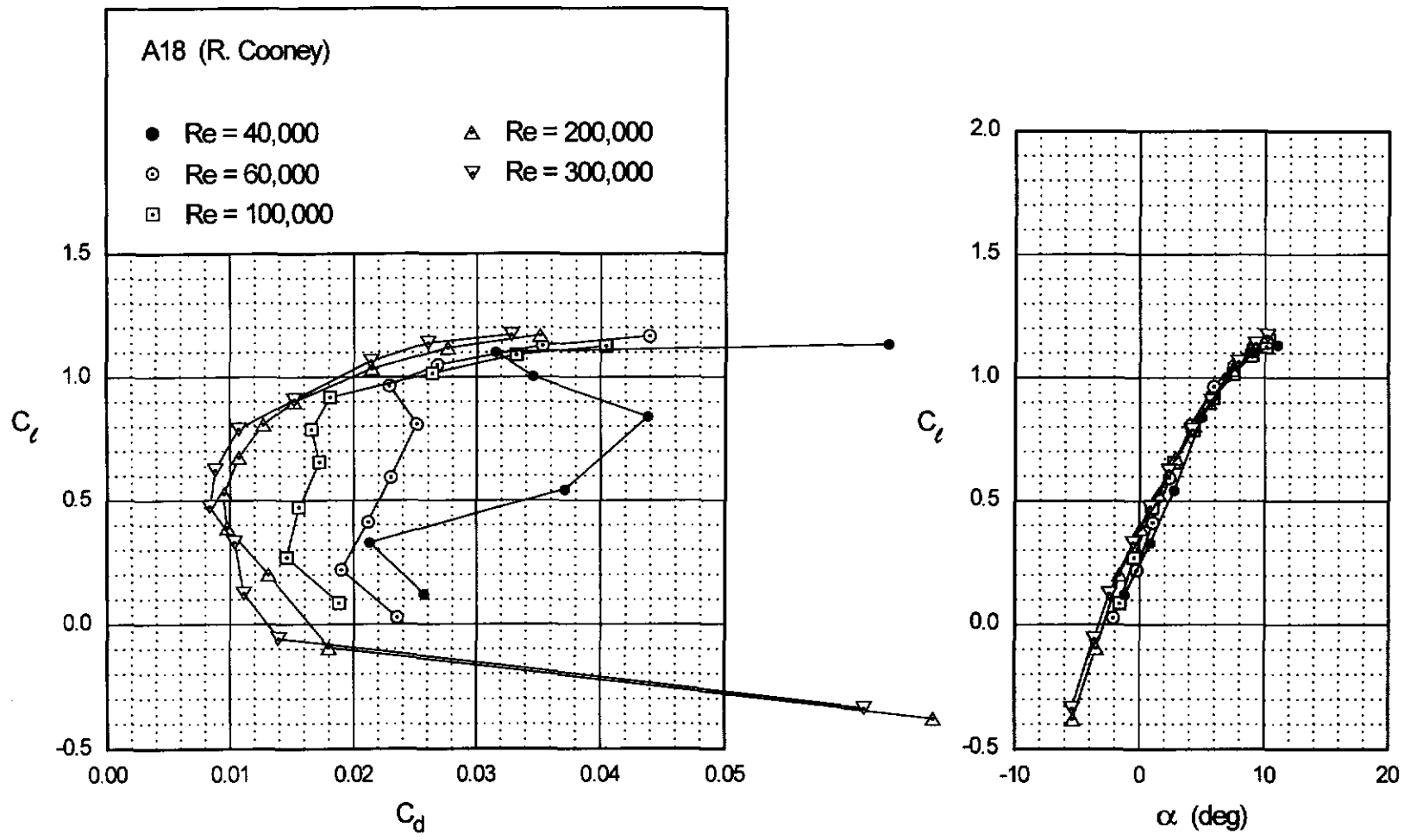


Fig. 4.3

Chapter 4: Airfoil Profiles and Performance Plots 63



A18

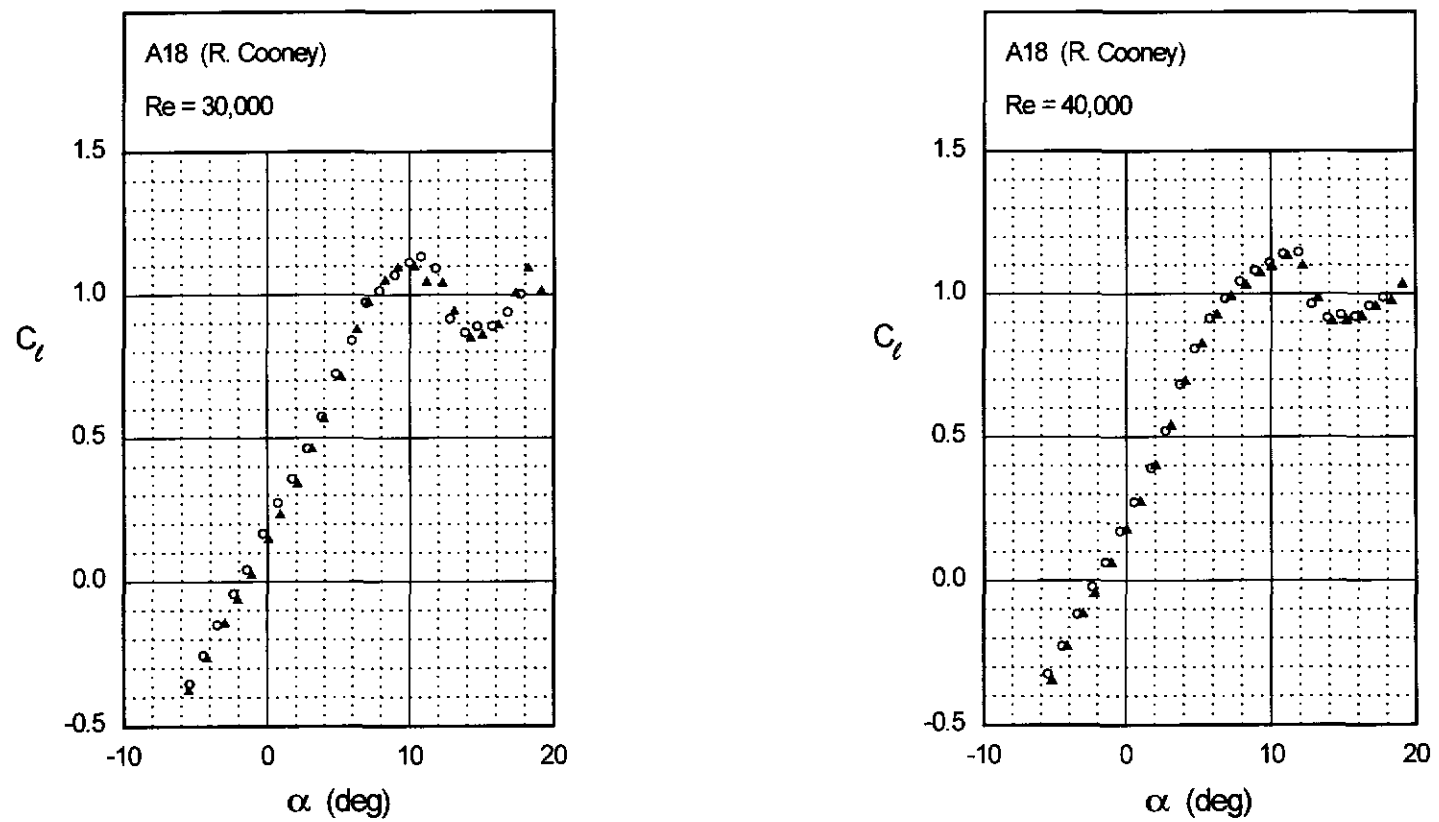
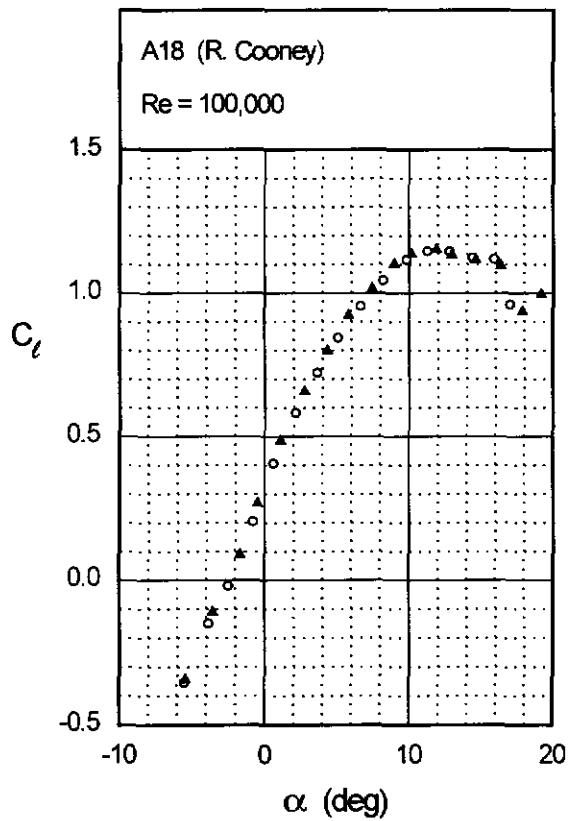
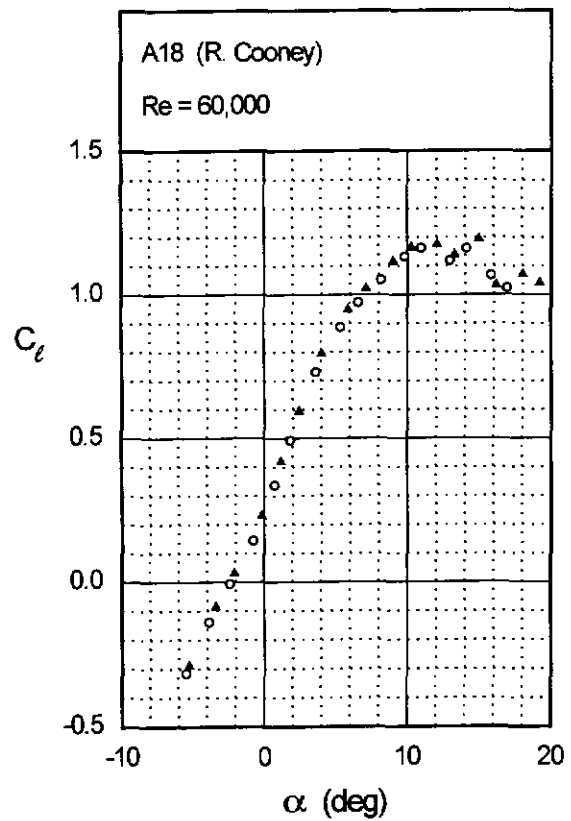


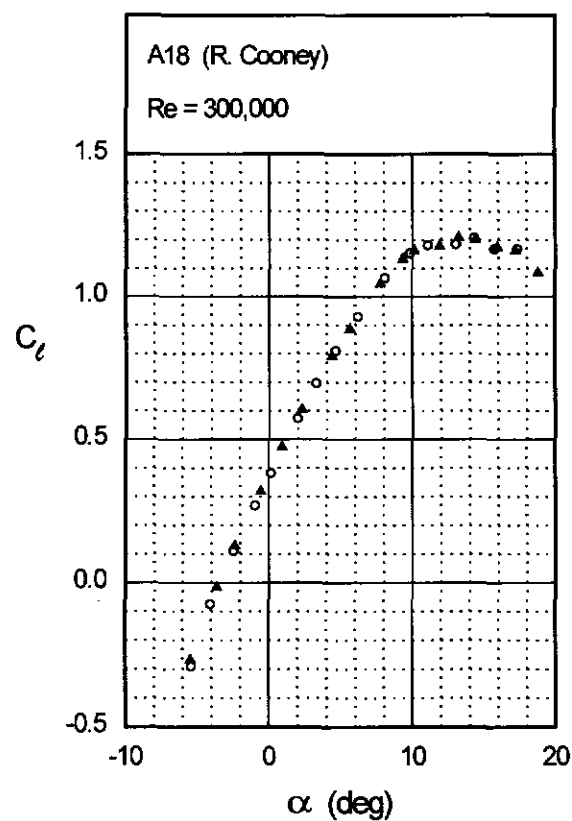
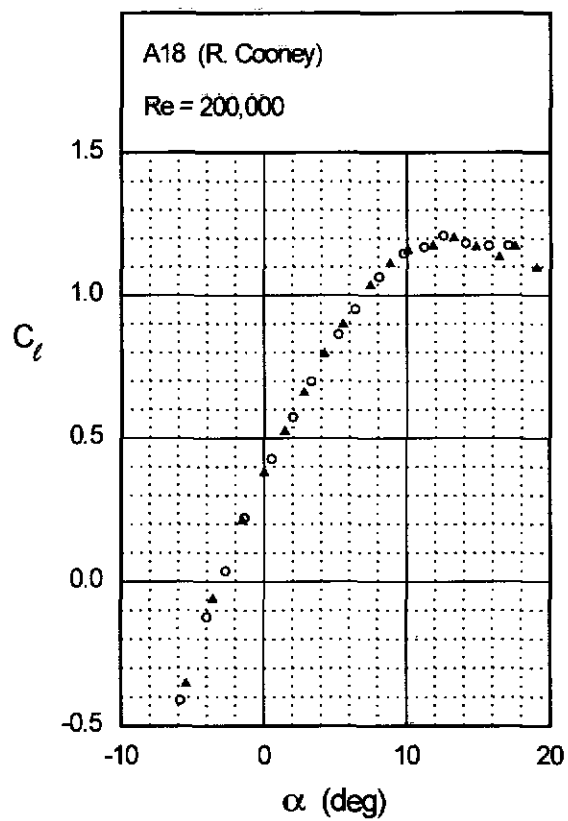
Fig. 4.4

Fig. 4.4 (continued)

A18



A18



BE50

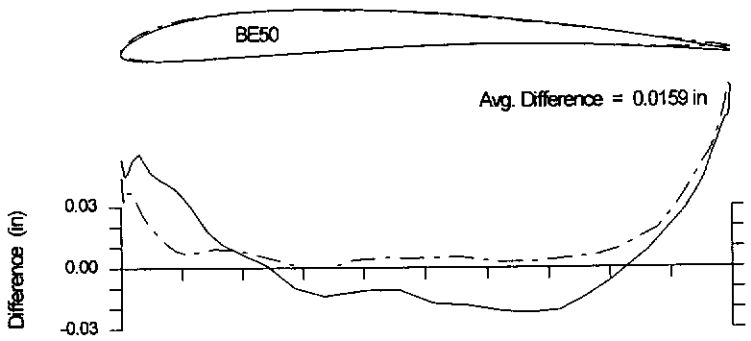
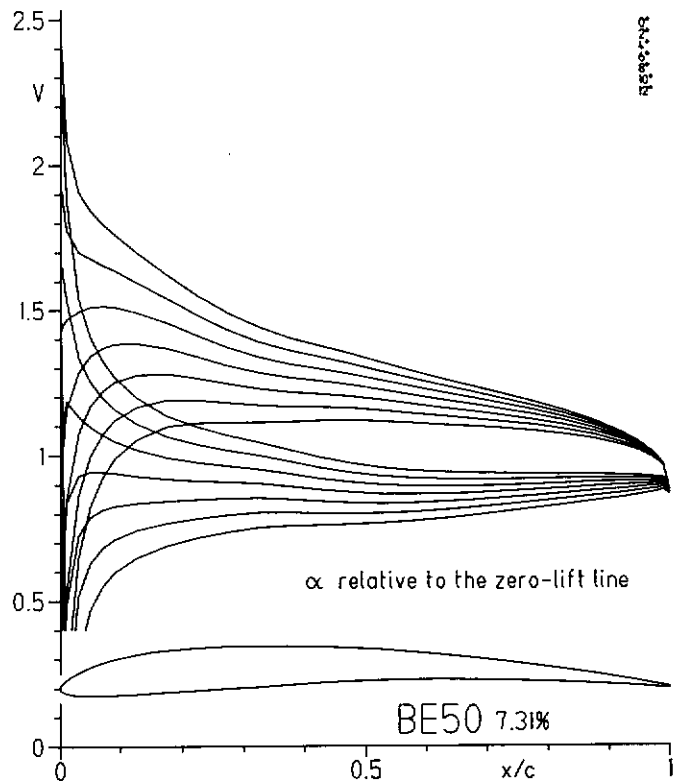
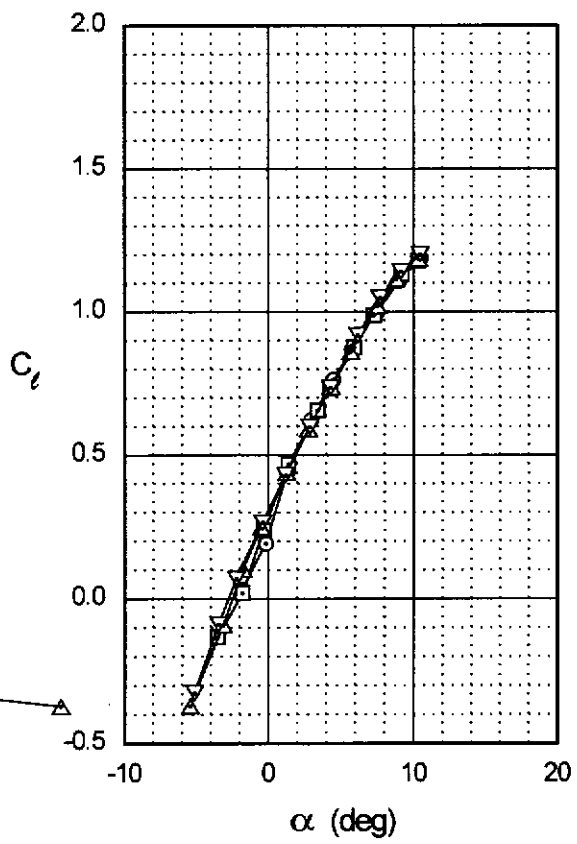
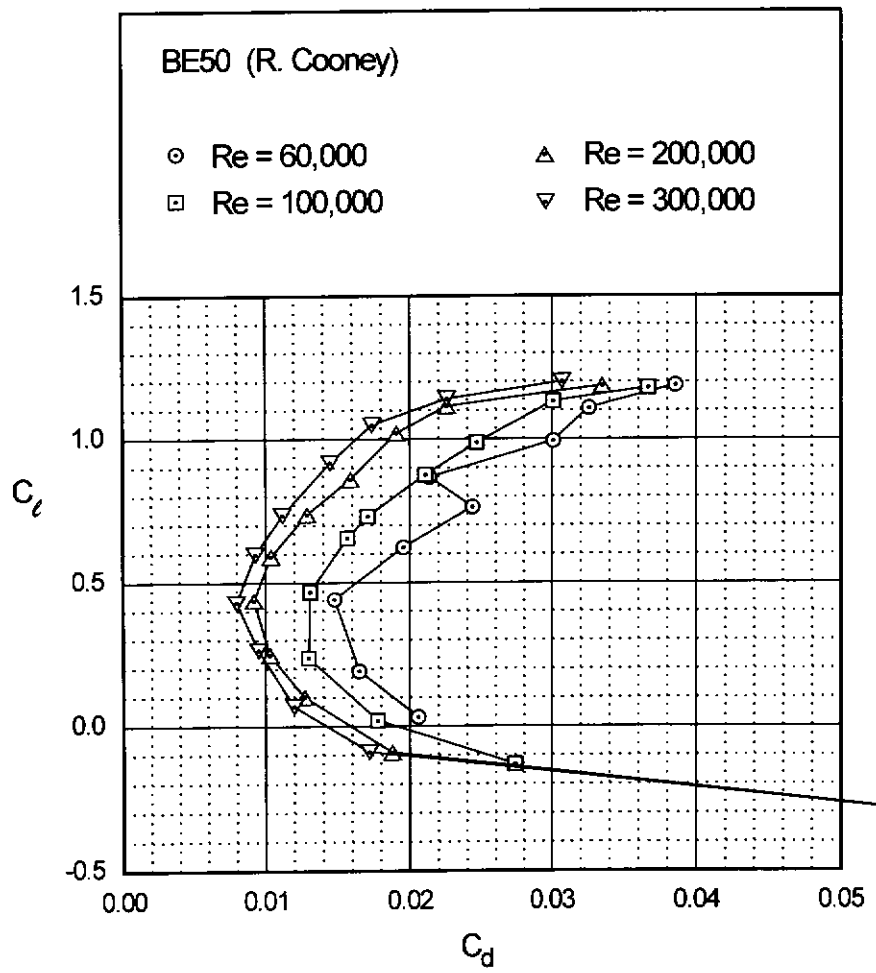


Fig. 4.7

Chapter 4: Airfoil Profiles and Performance Plots 69



BE50

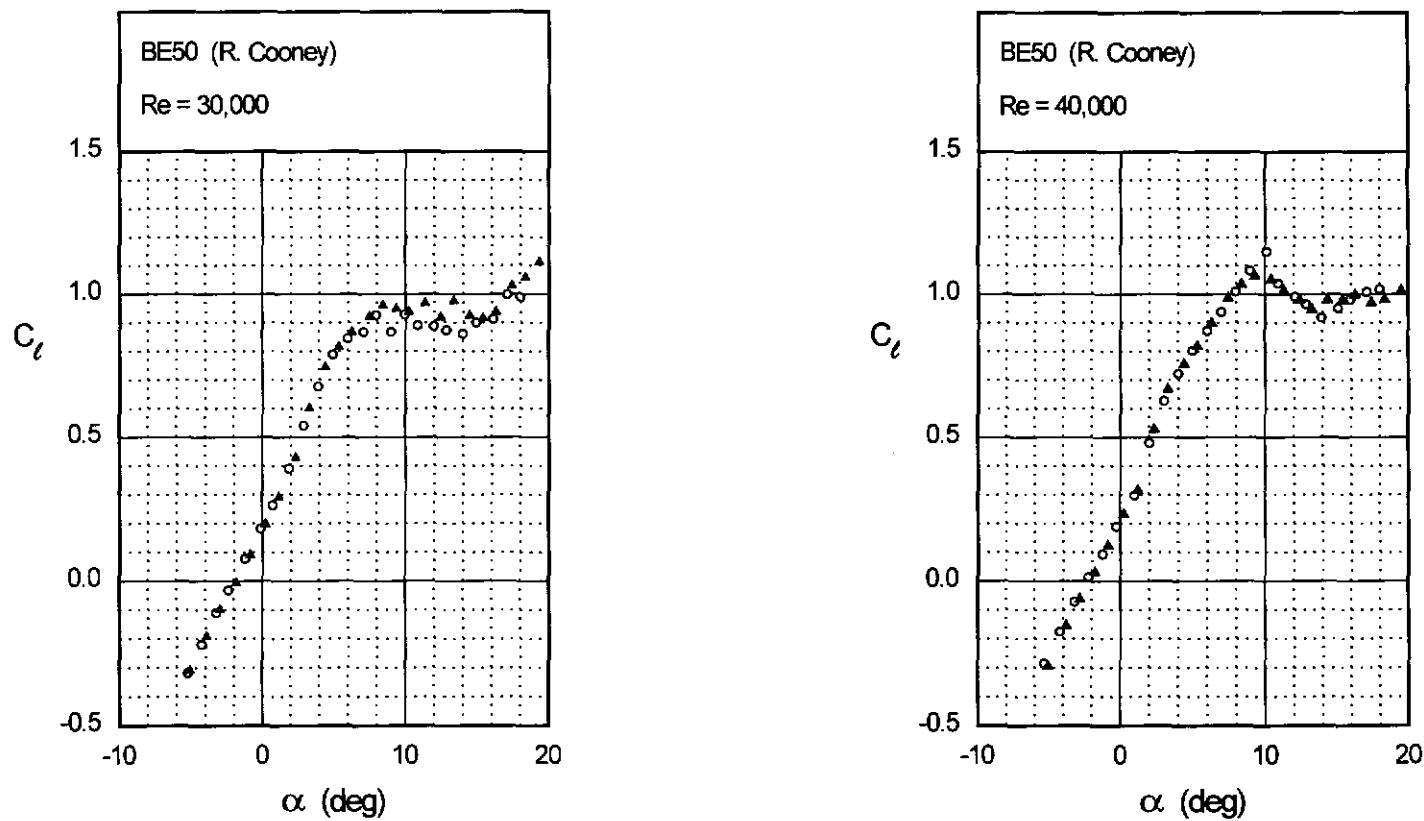


Fig. 4.8 (continued)

Chapter 4: Airfoil Profiles and Performance Plots 71

BE50

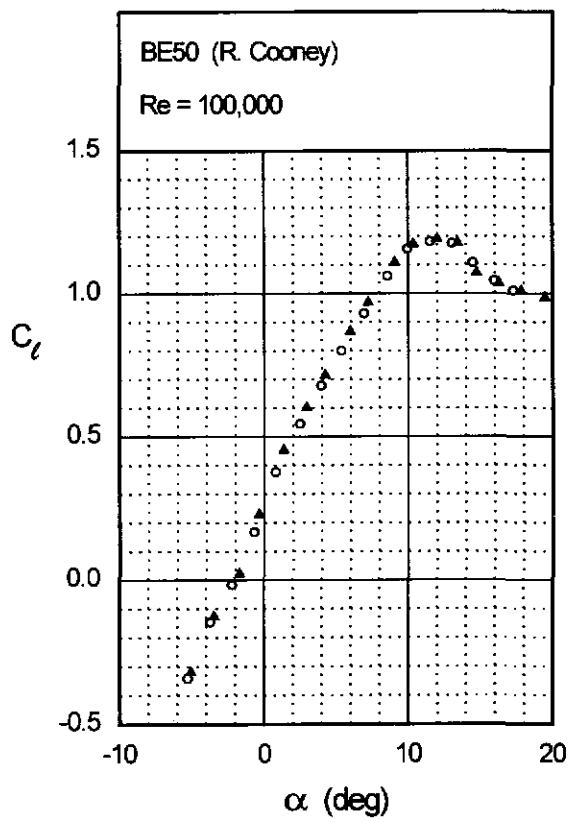
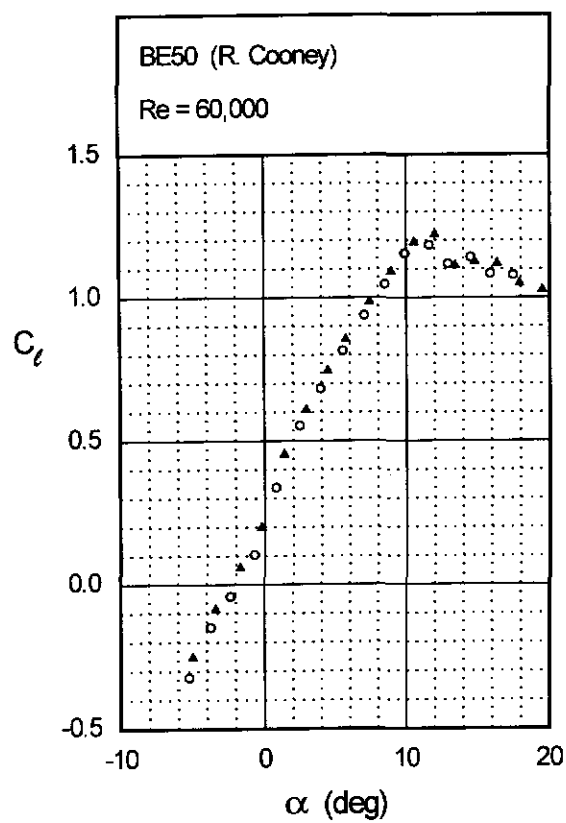
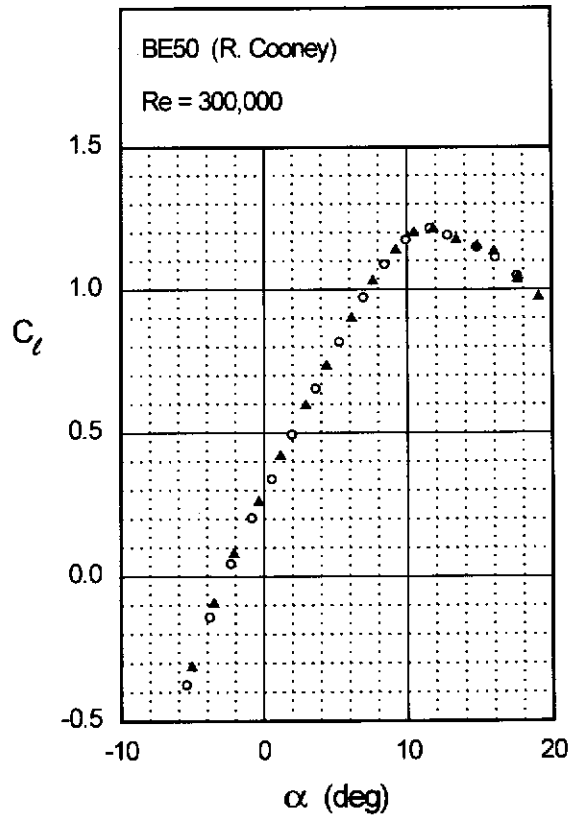
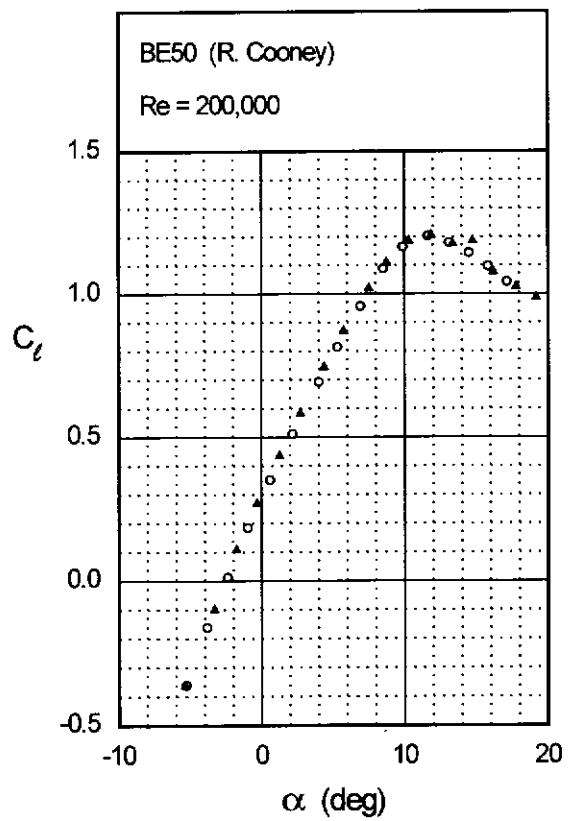


Fig. 4.8 (continued)

BE50



CH 10-48-13

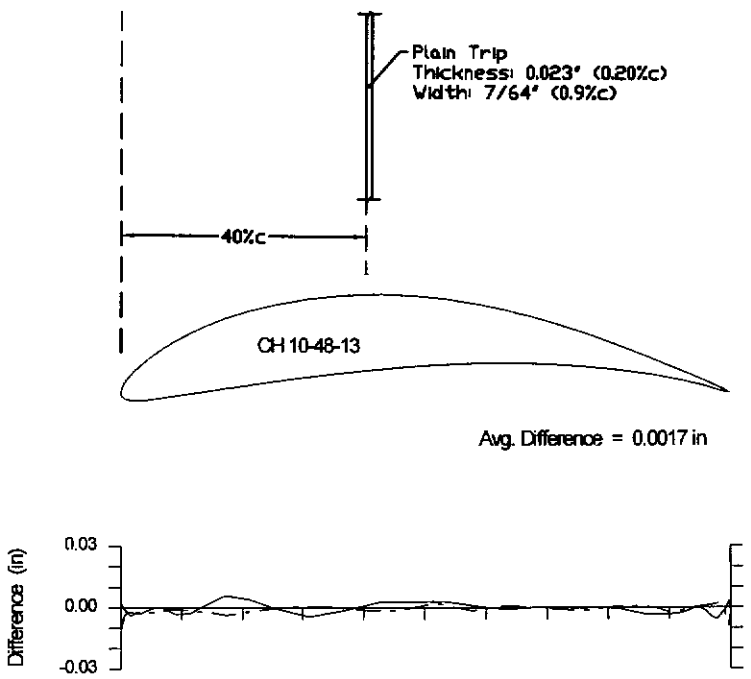
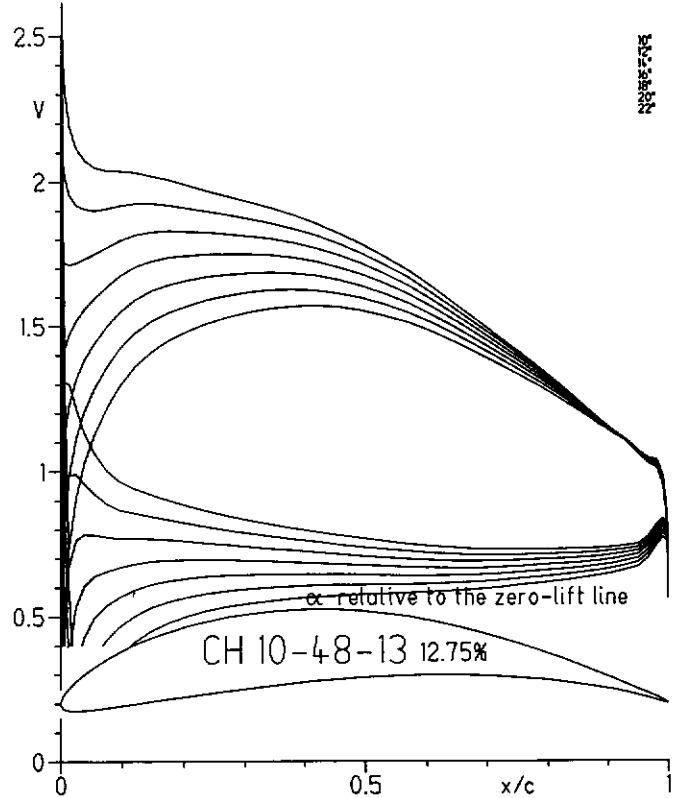
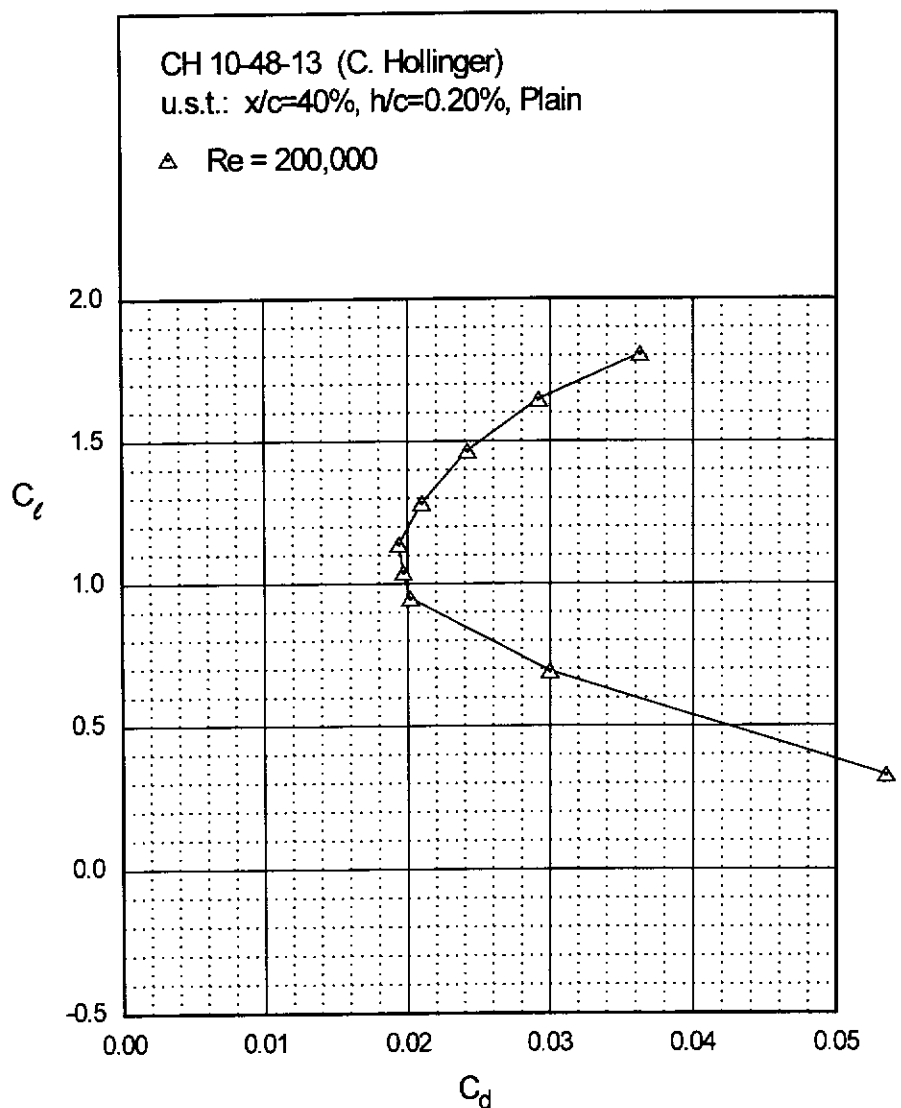
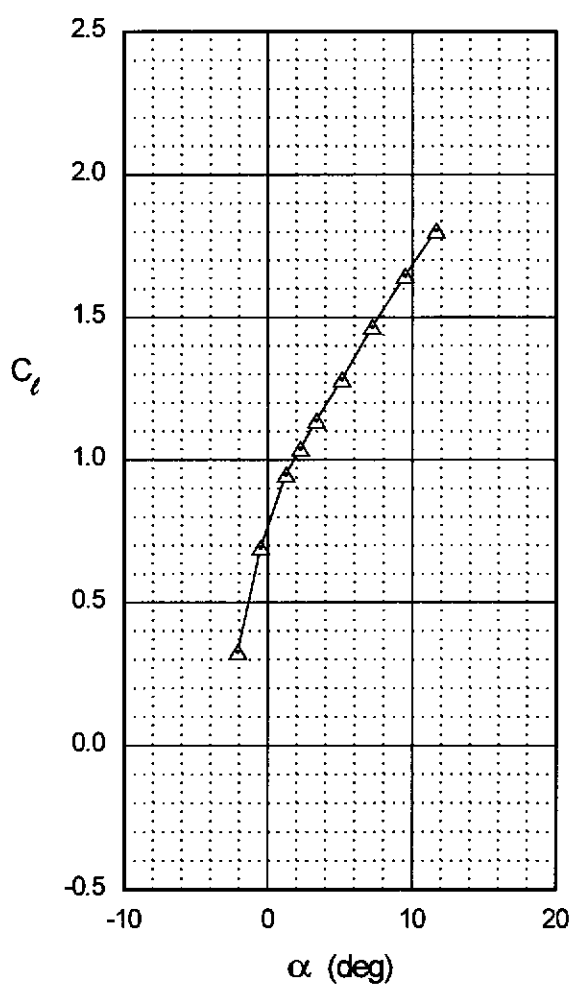


Fig. 4.11

Chapter 4: Airfoil Profiles and Performance Plots 75

CH 10-48-13



CH 10-48-13

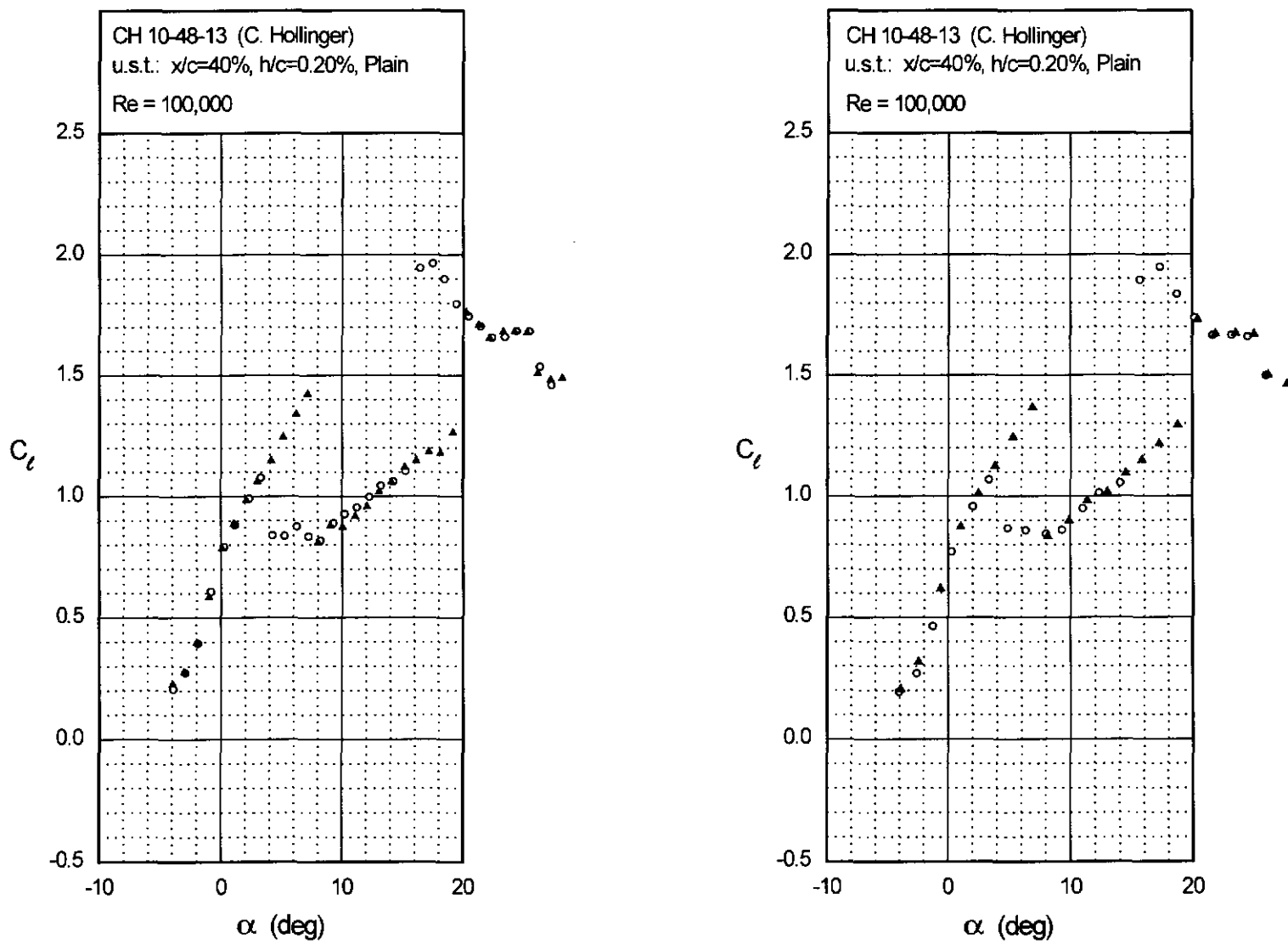


Fig. 4.12 (continued)

Chapter 4: Airfoil Profiles and Performance Plots

77

CH 10-48-13

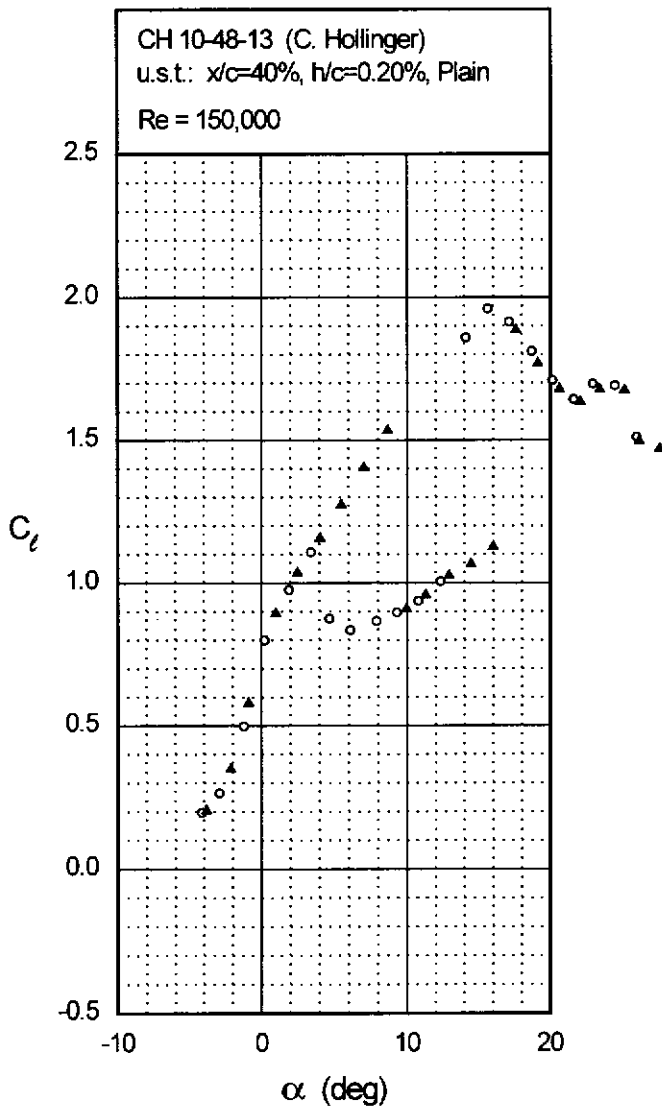
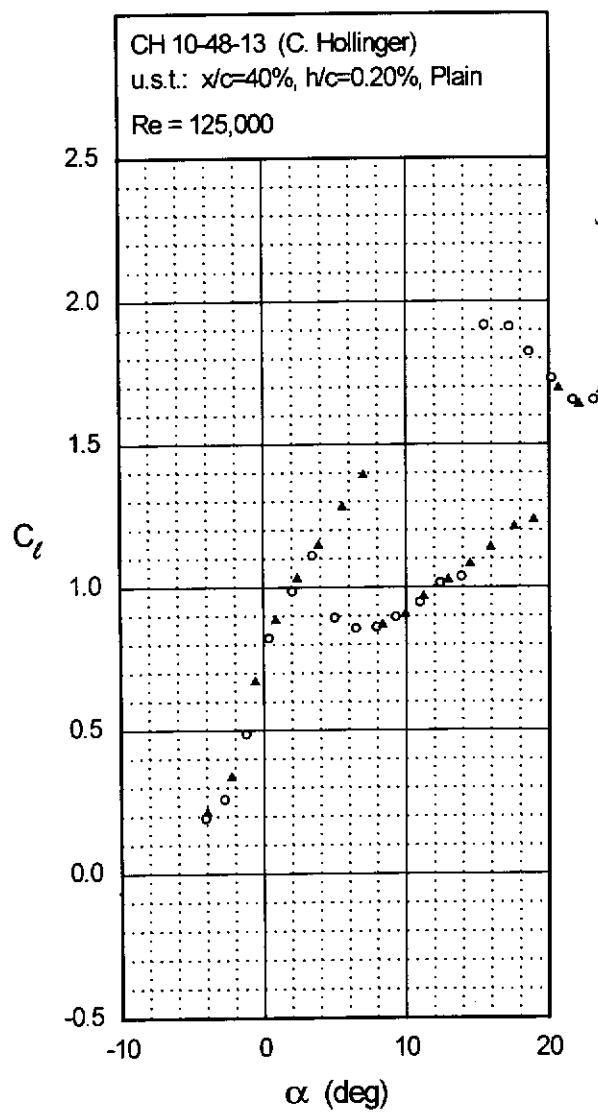
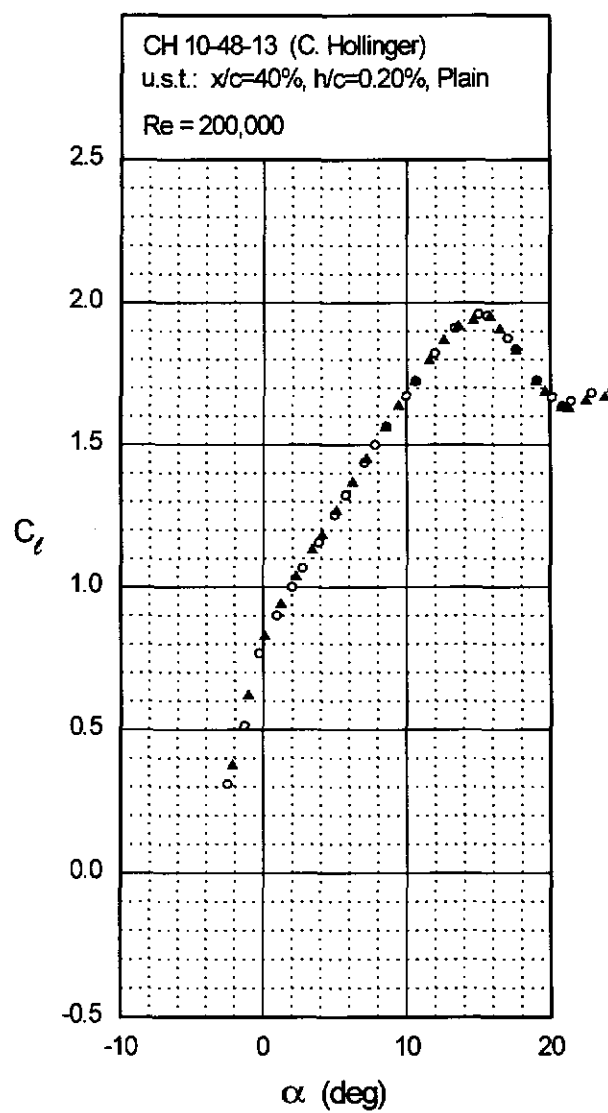
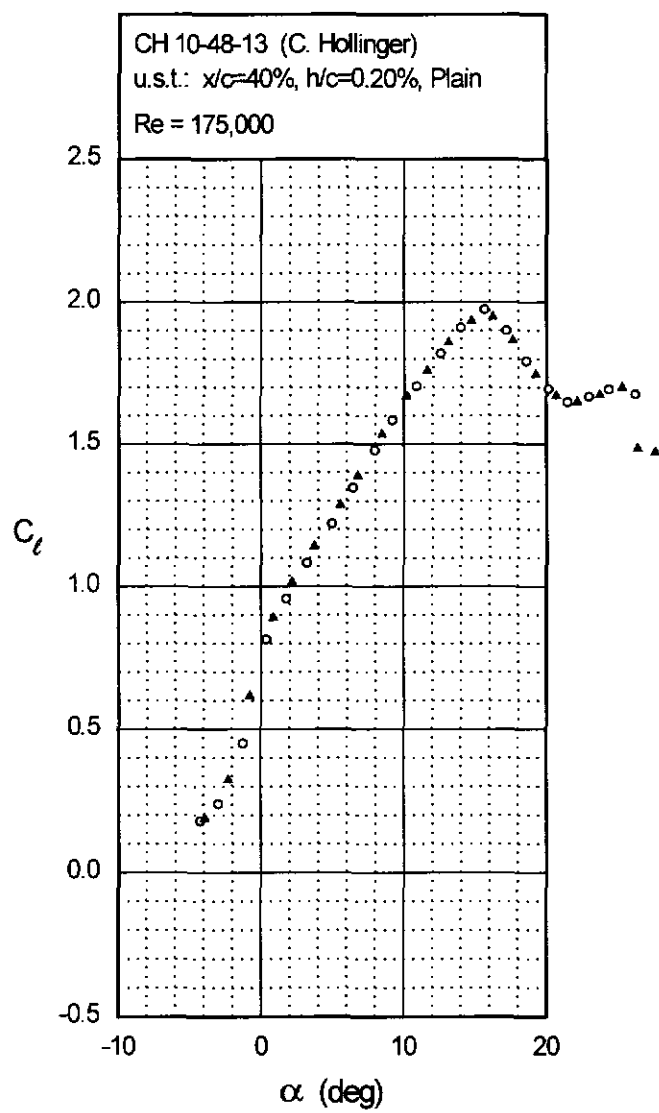
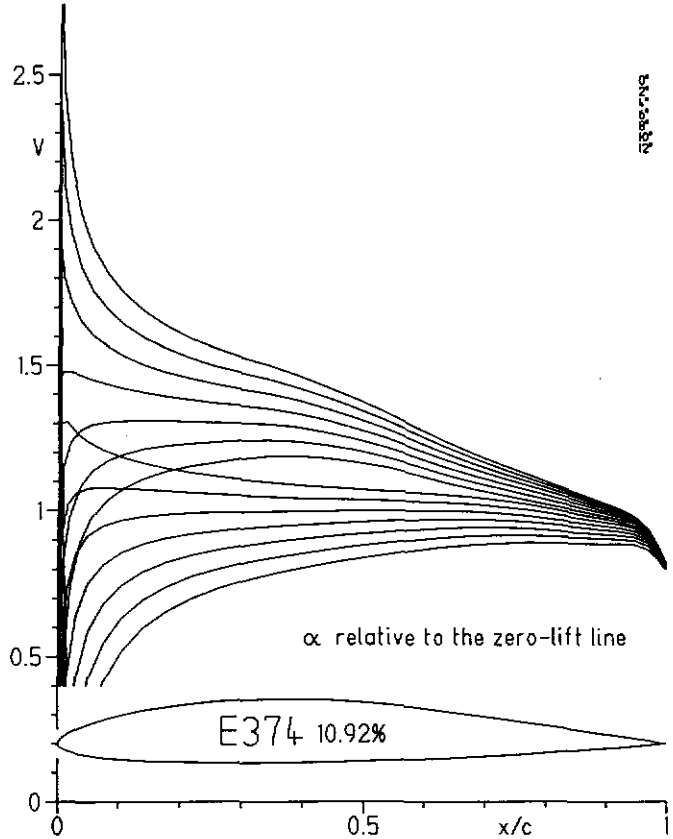


Fig. 4.12 (continued)

CH 10-48-13

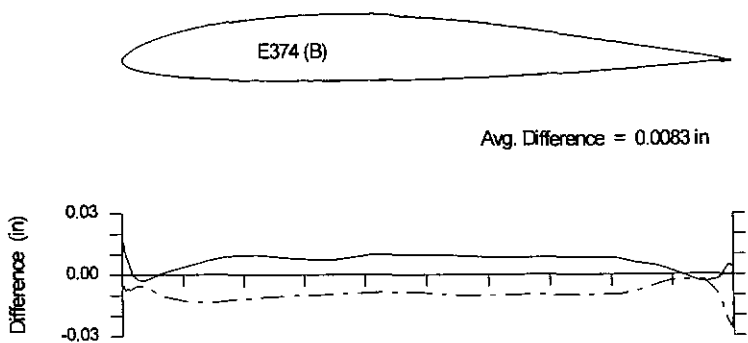


E374 (B)



E374 10.92%

E374 (B)



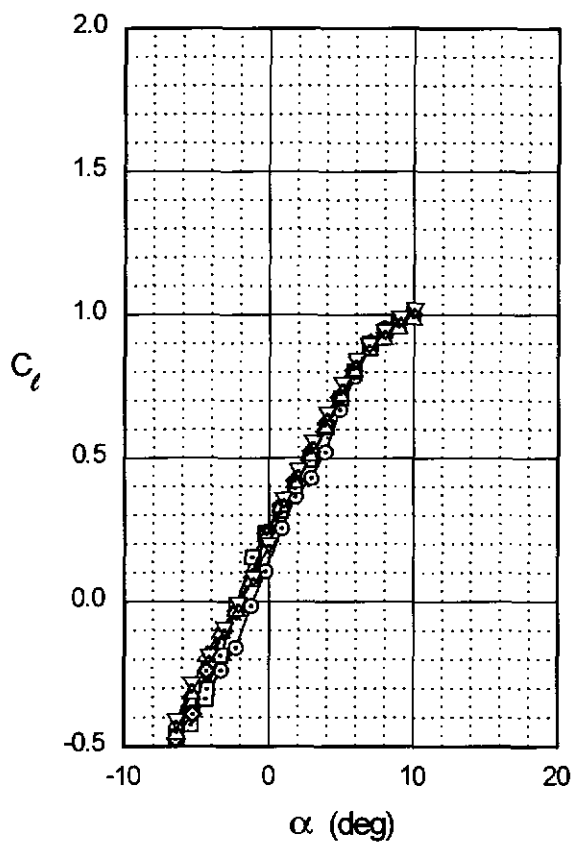
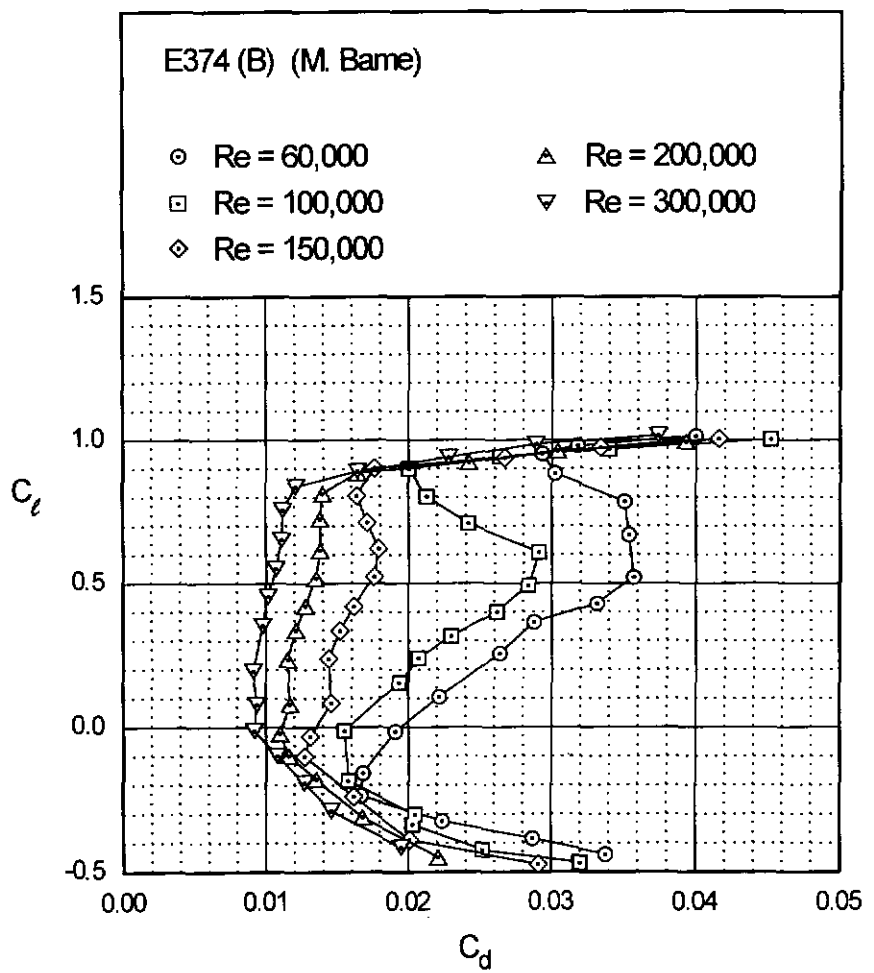
Avg. Difference = 0.0083 in

Fig. 4.15

Chapter 4: Airfoil Profiles and Performance Plots

81

E374 (B)



E374 (B)

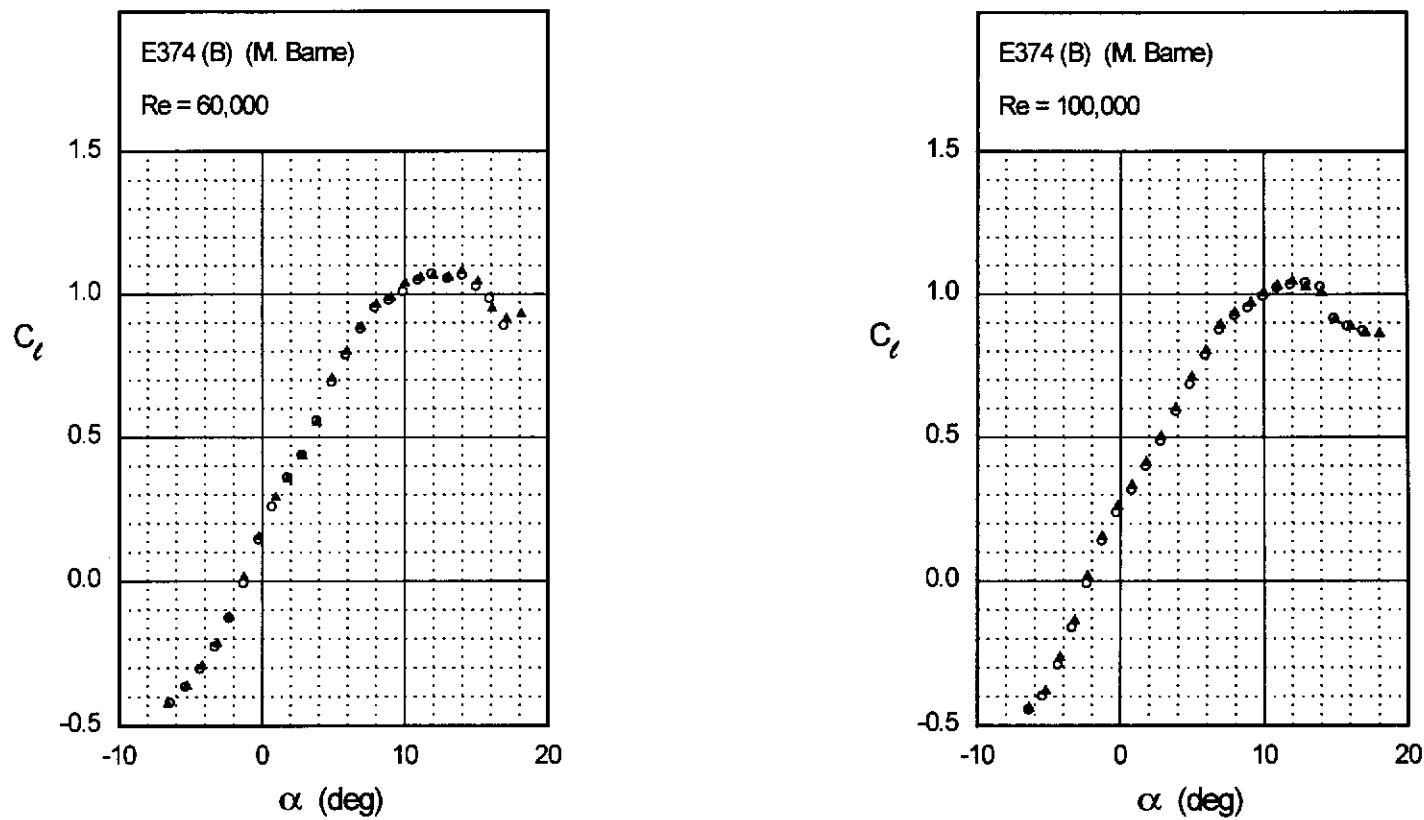
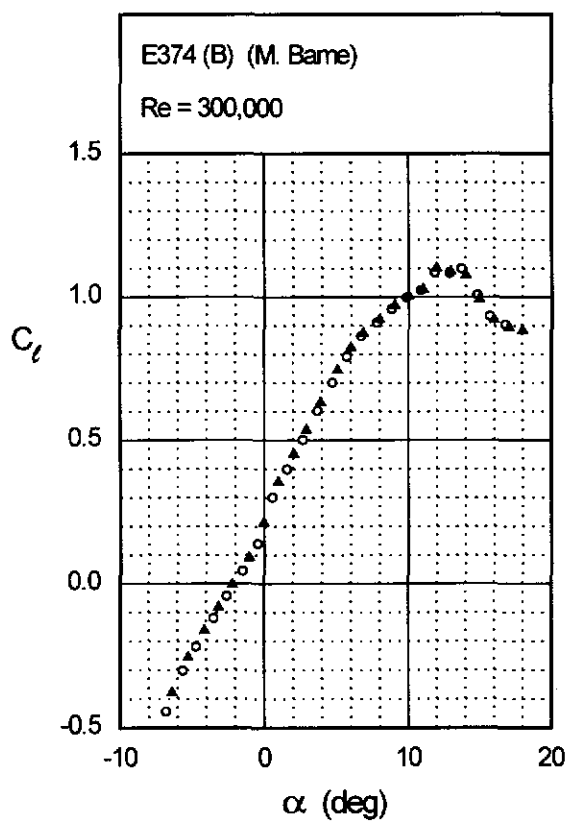
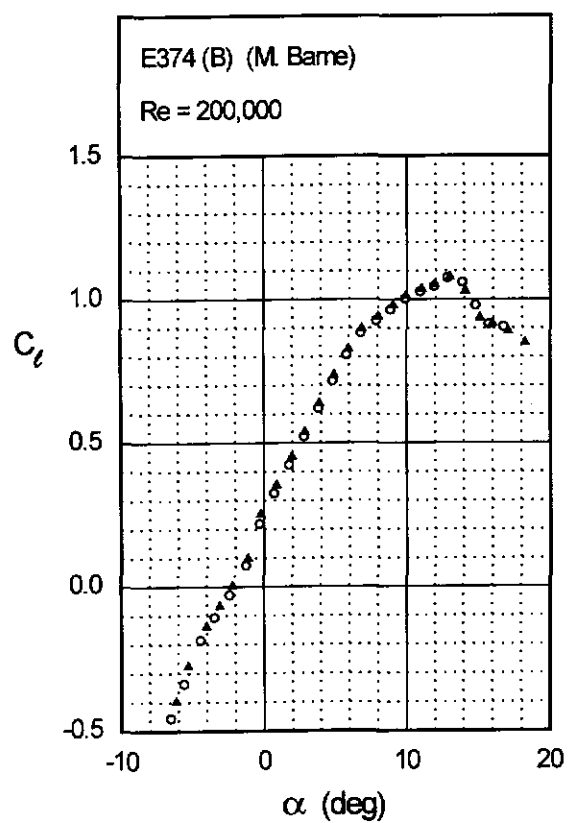


Fig. 4.16

Fig. 4.16 (continued)

Chapter 4: Airfoil Profiles and Performance Plots 83

E374 (B)



E387 (A)

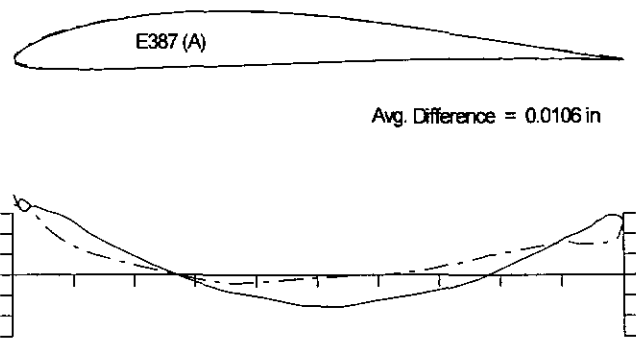
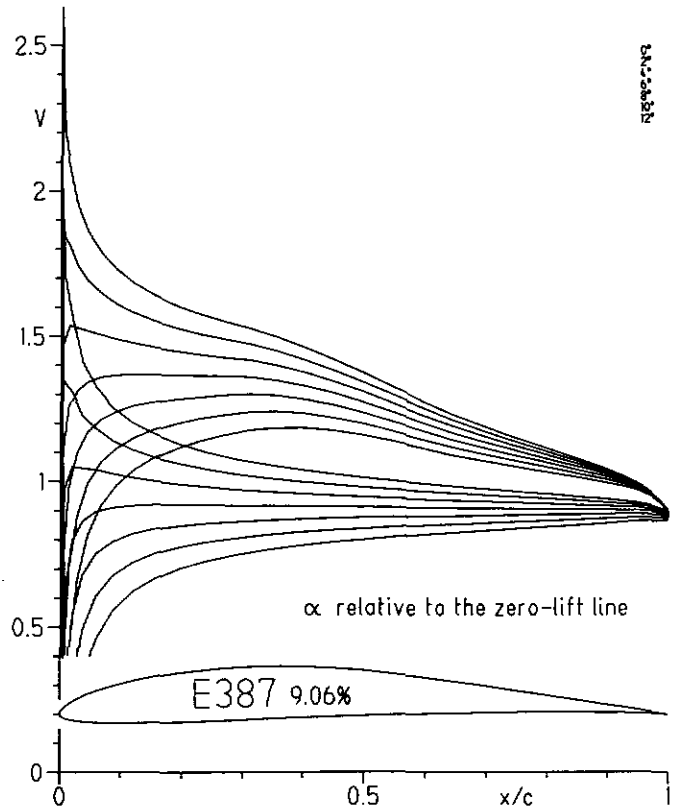
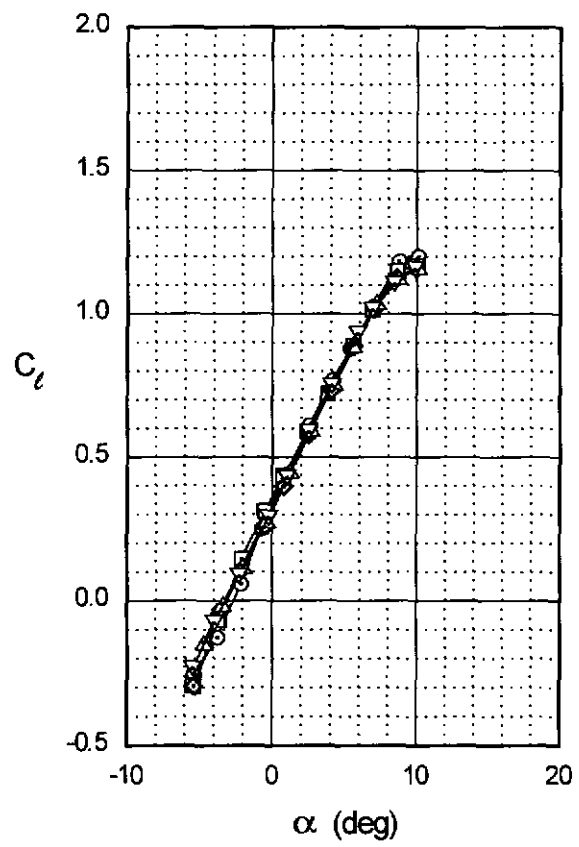
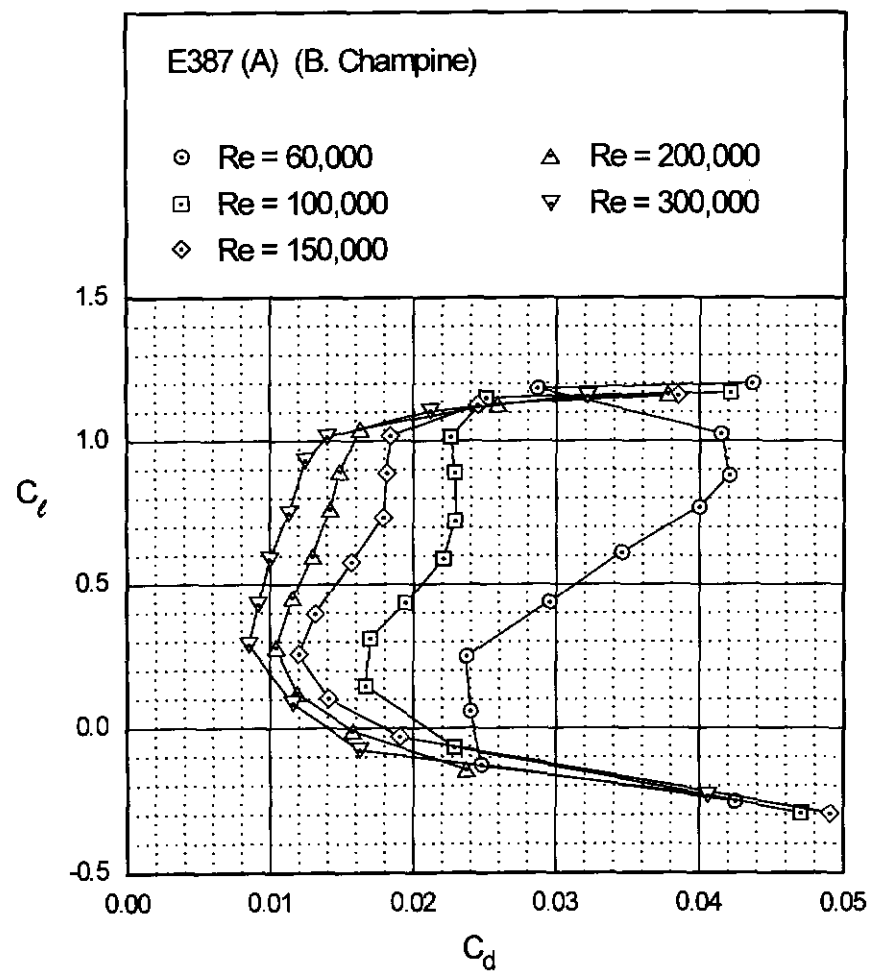


Fig. 4.19

Chapter 4: Airfoil Profiles and Performance Plots 85



E387 (A)

E387 (A)

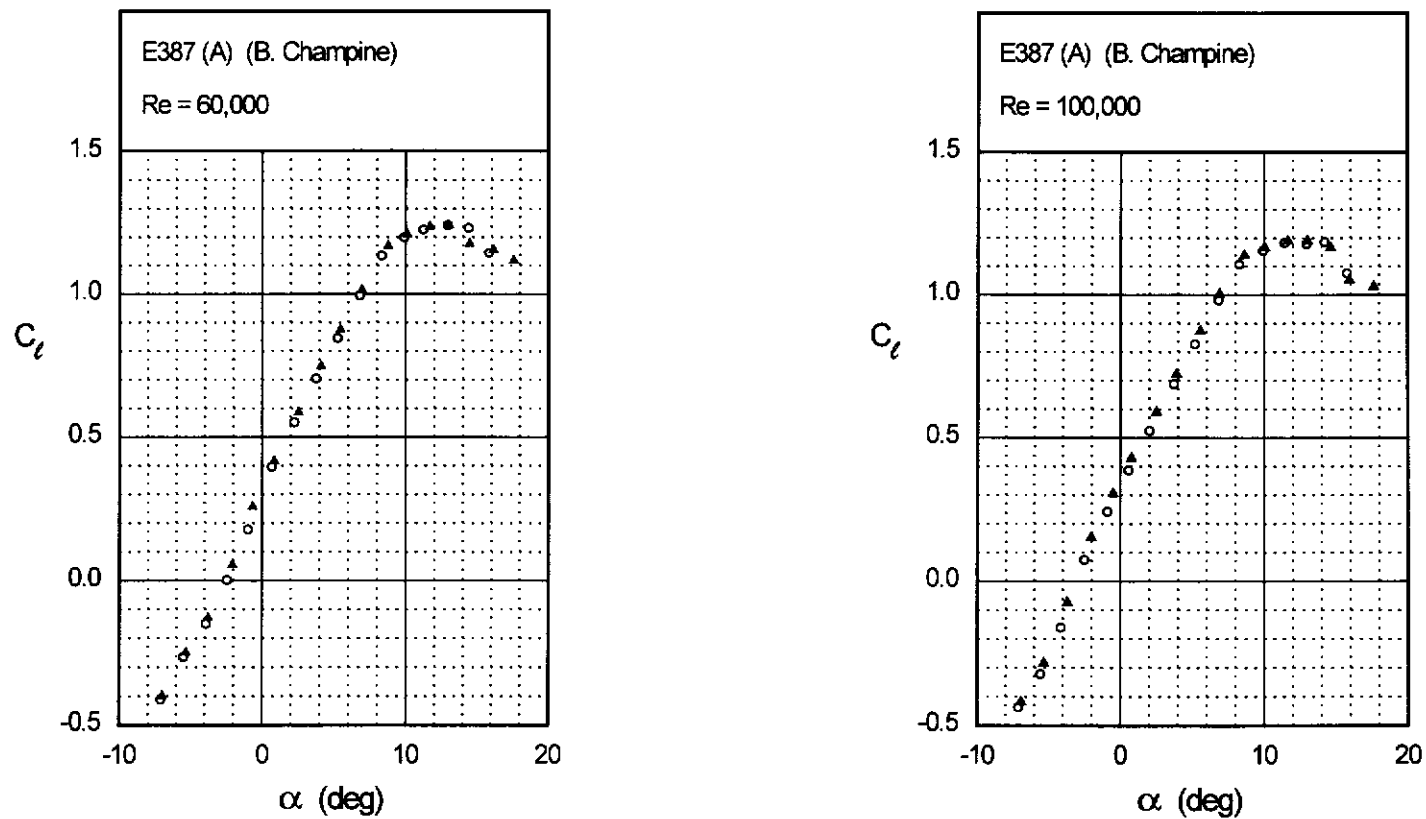


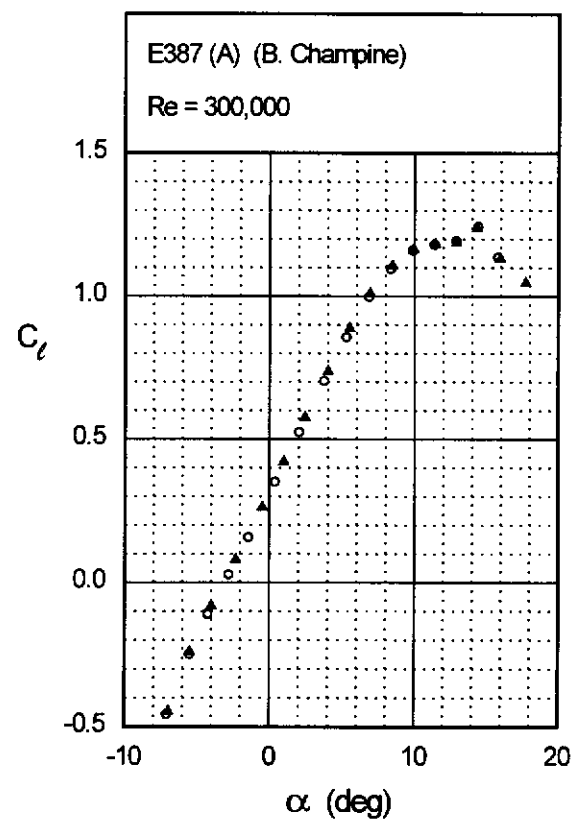
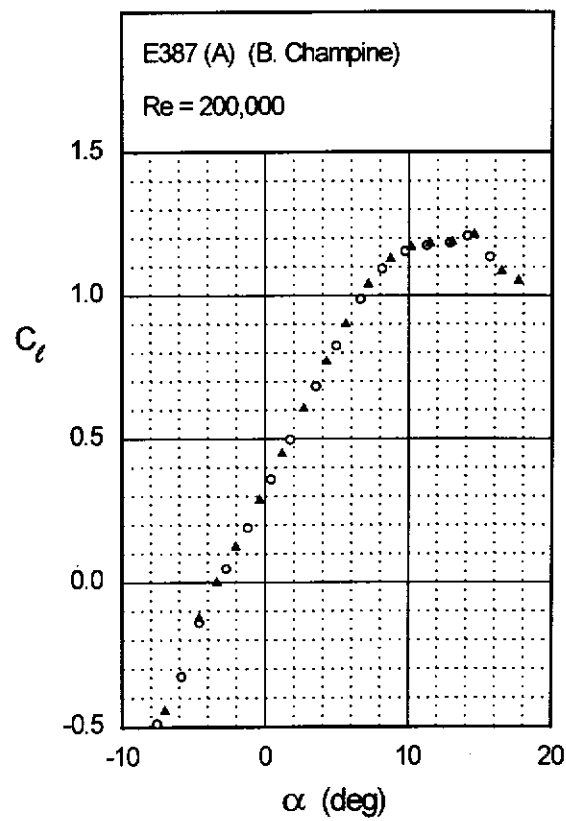
Fig. 4.20

Fig. 4.20 (continued)

Chapter 4: Airfoil Profiles and Performance Plots

87

E387 (A)



Figs. 4.21 & 4.22

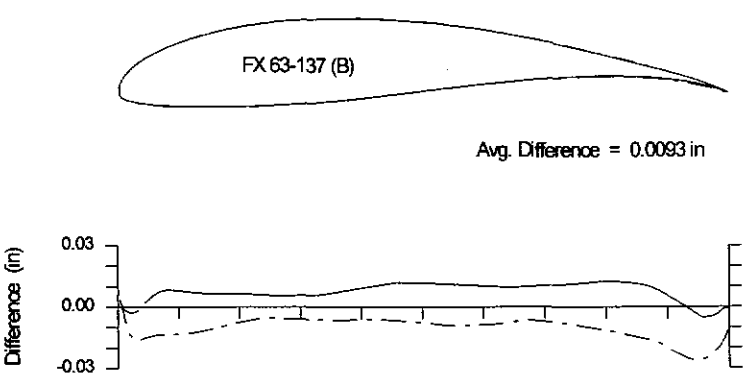
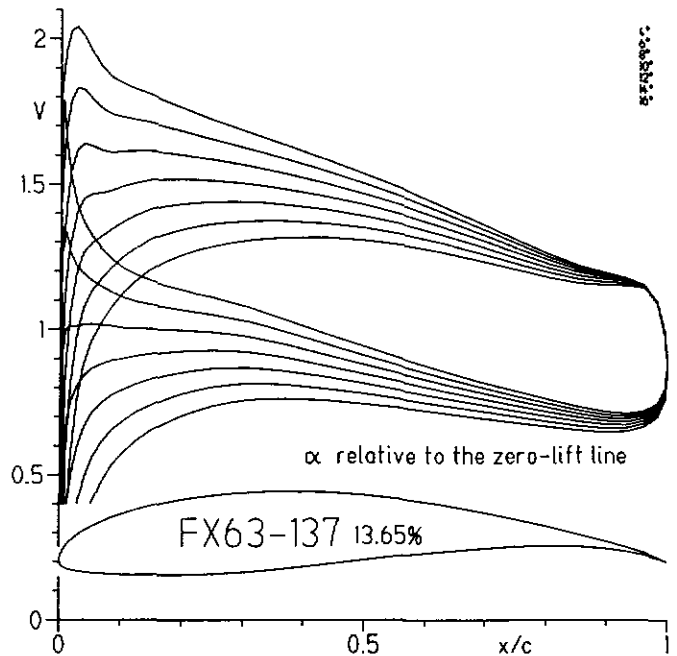
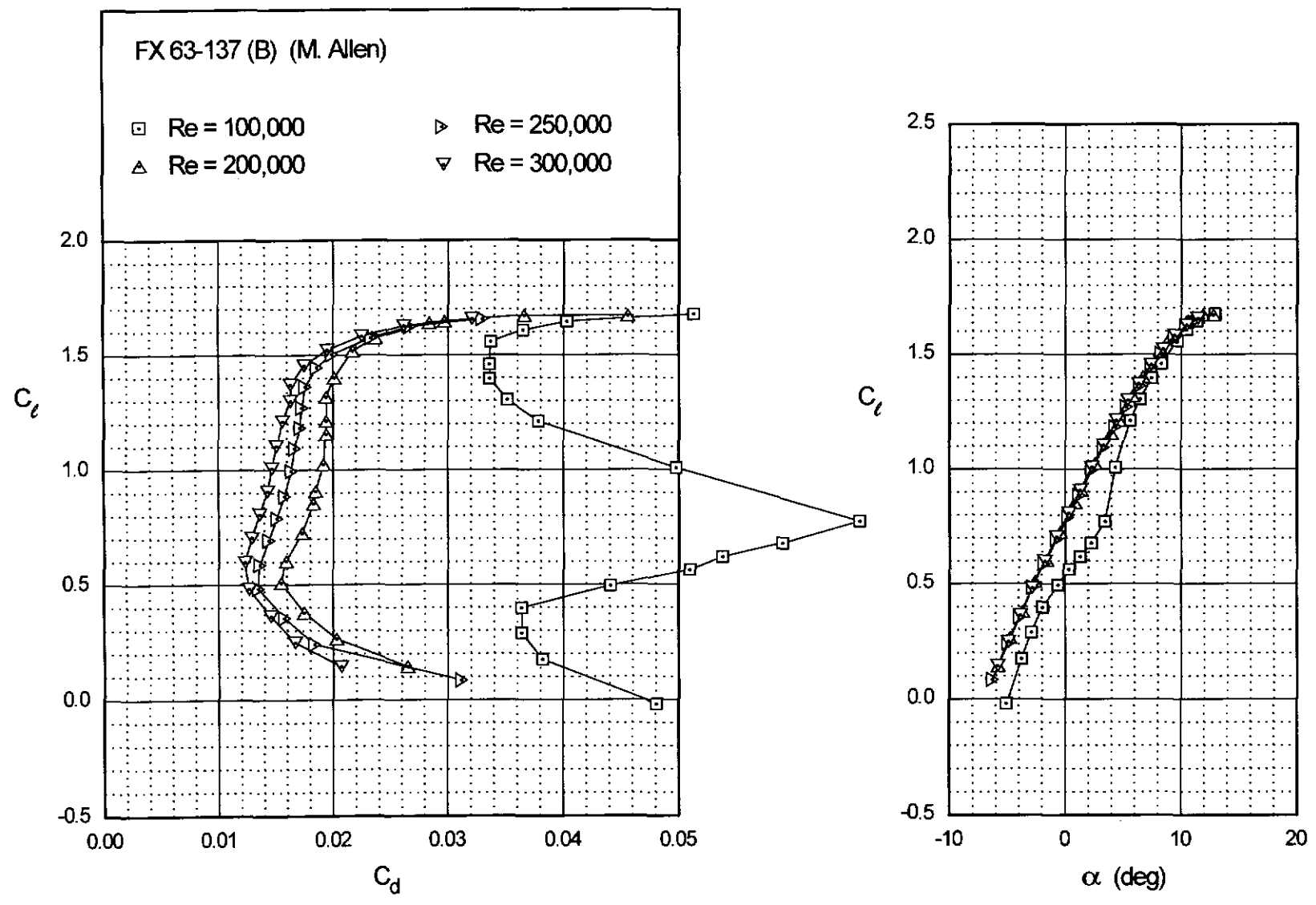


Fig. 4.23

Chapter 4: Airfoil Profiles and Performance Plots 89



FX 63-137 (B)

FX 63-137 (B)

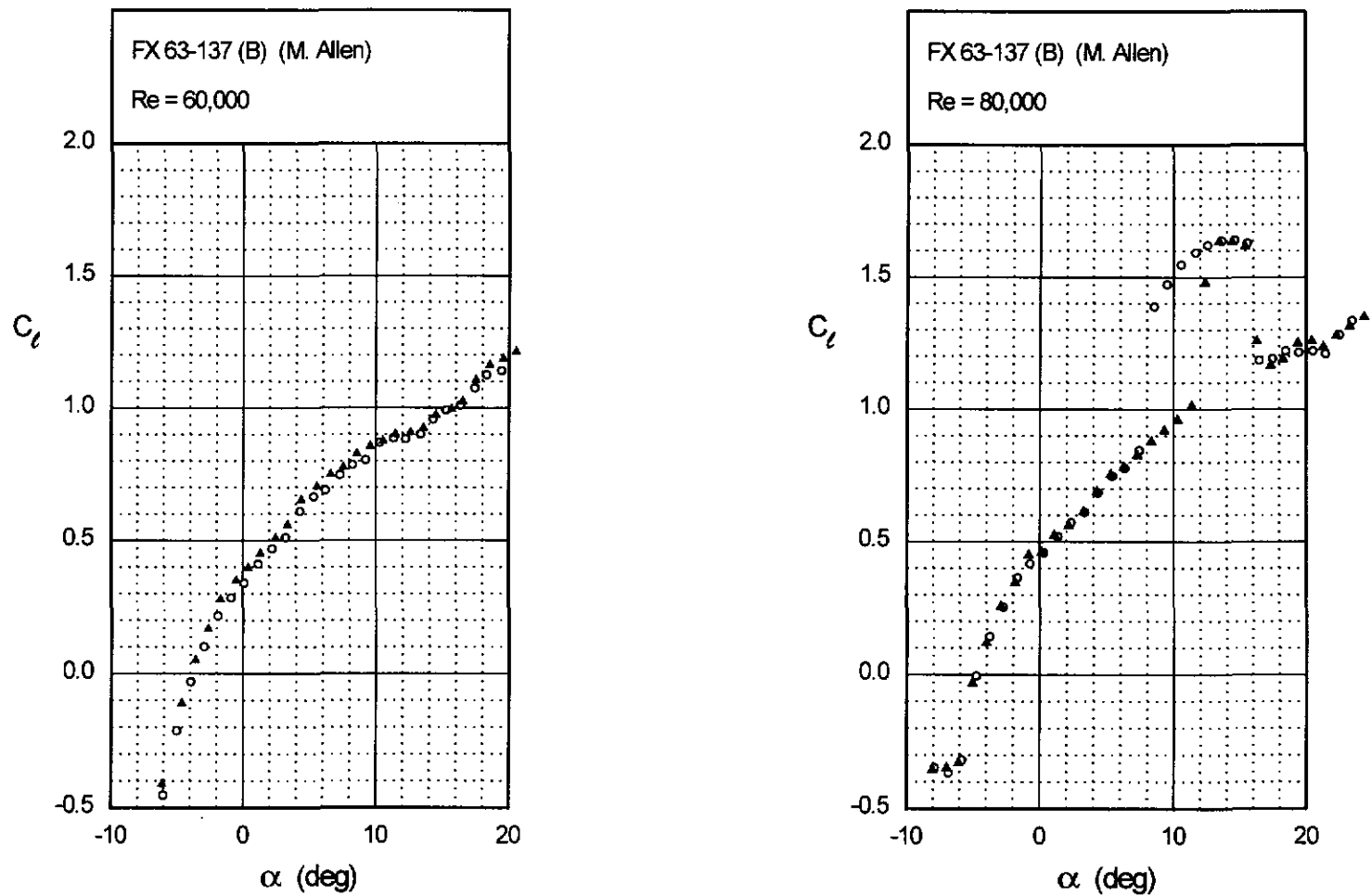
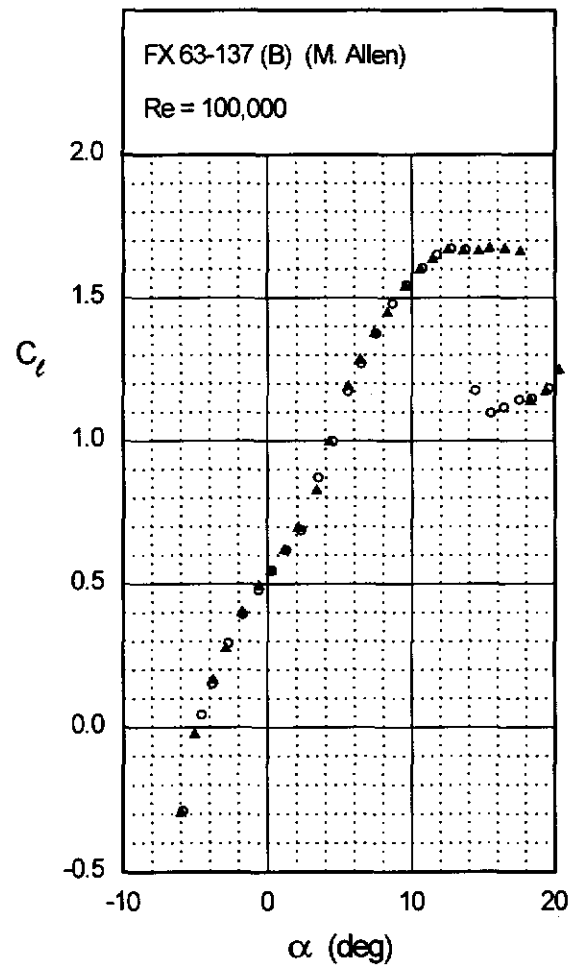
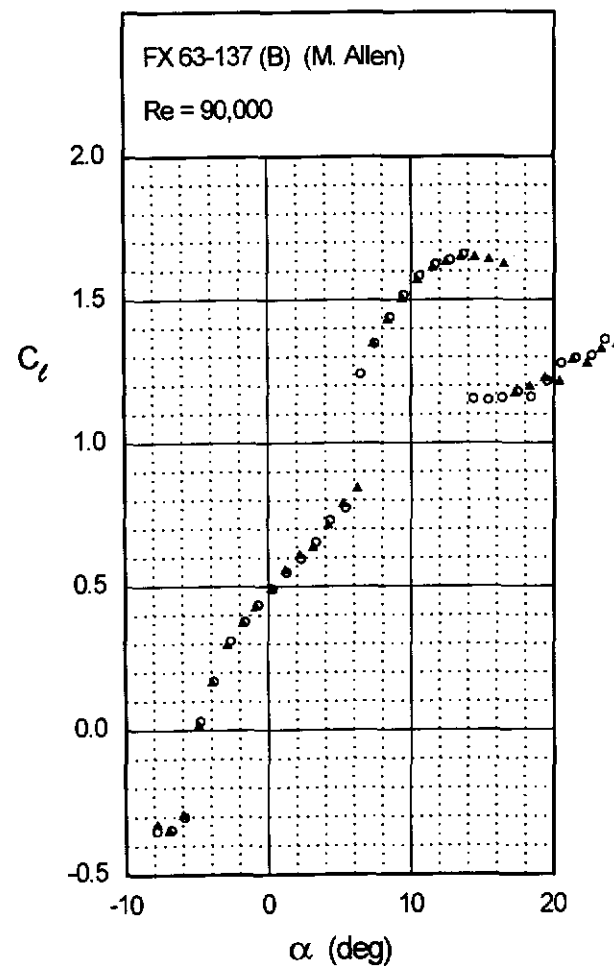


Fig. 4.24 (continued)

Chapter 4: Airfoil Profiles and Performance Plots 91

FX 63-137 (B)



FX 63-137 (B)

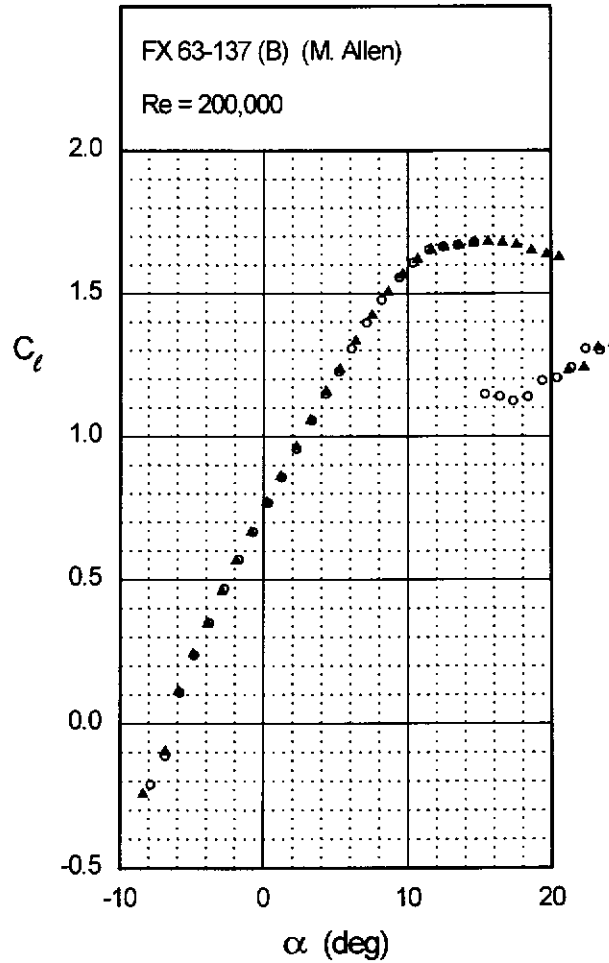
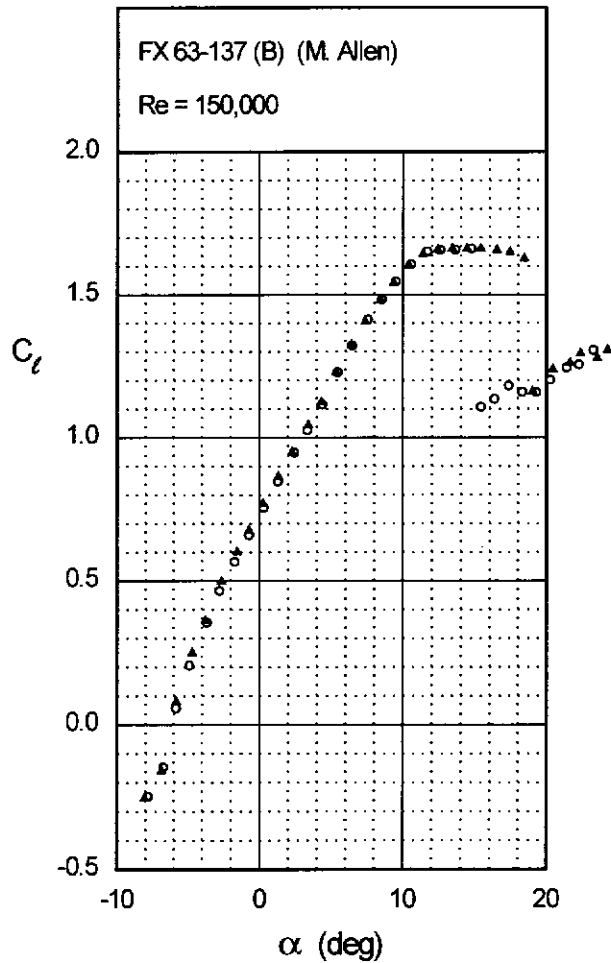
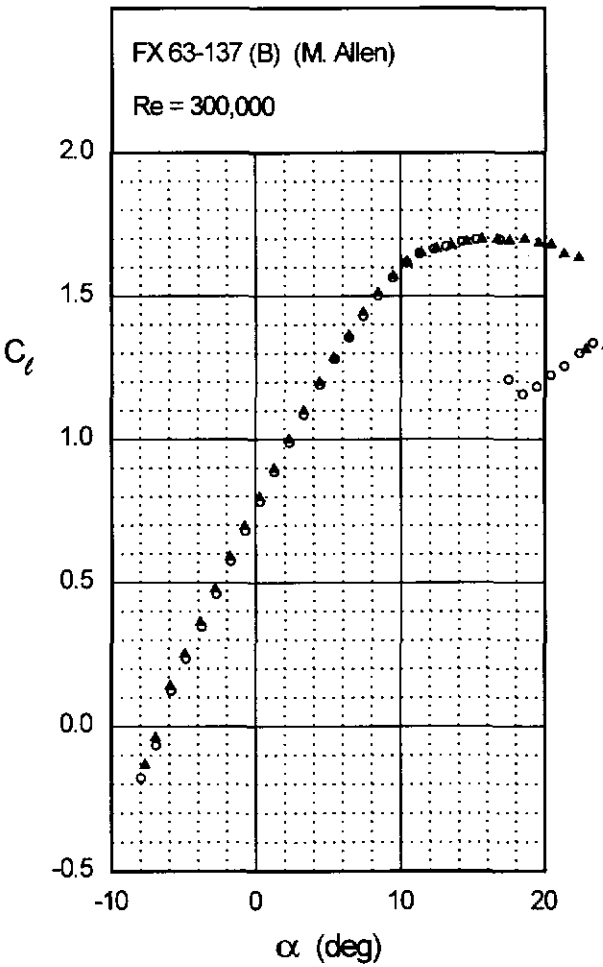
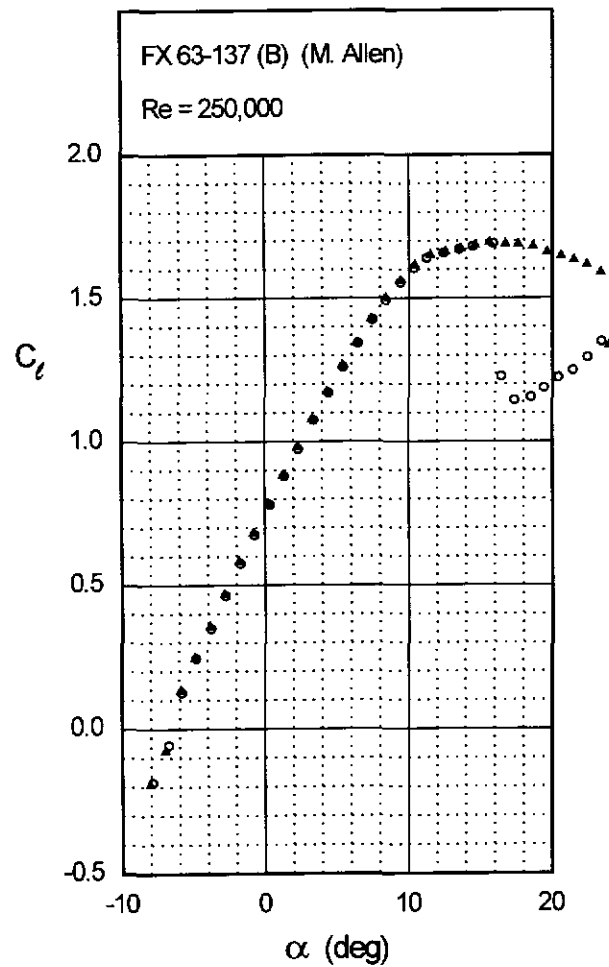


Fig. 4.24 (continued)

Chapter 4: Airfoil Profiles and Performance Plots 93

FX 63-137 (B)



94 Summary of Low-Speed Airfoil Data

FX 74-CL5-140 MOD

Figs. 4.25 & 4.26

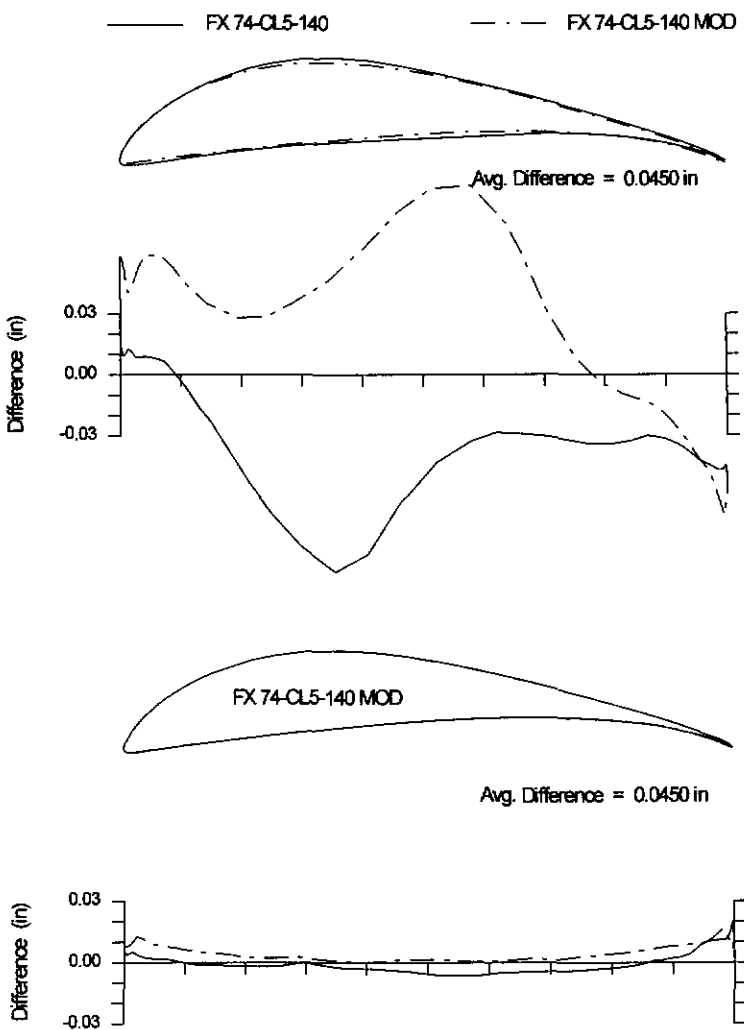
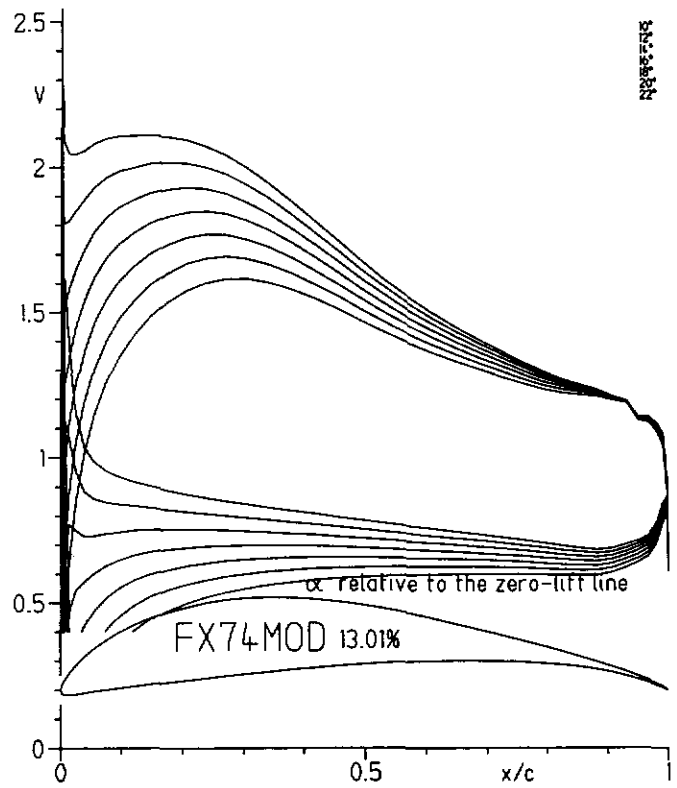
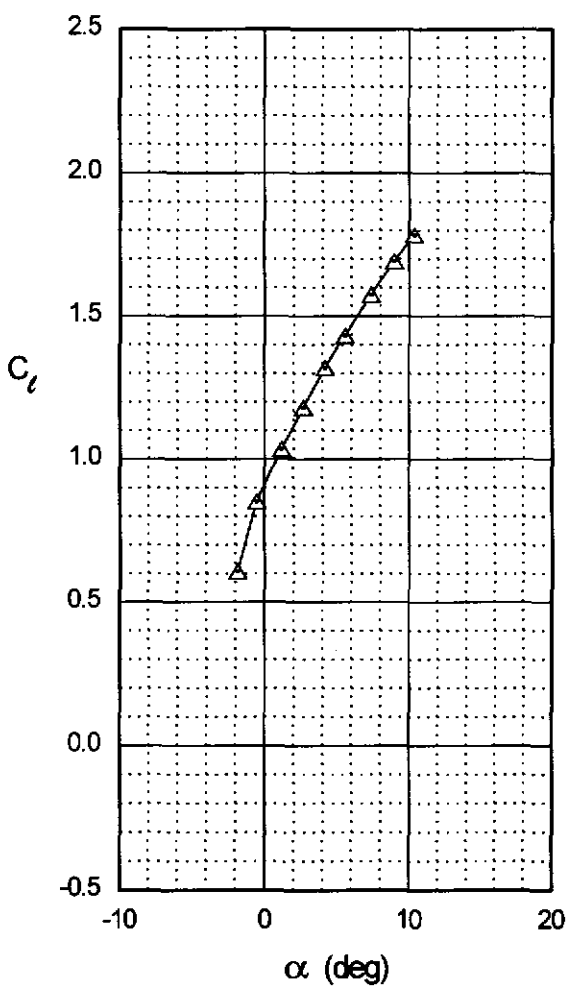
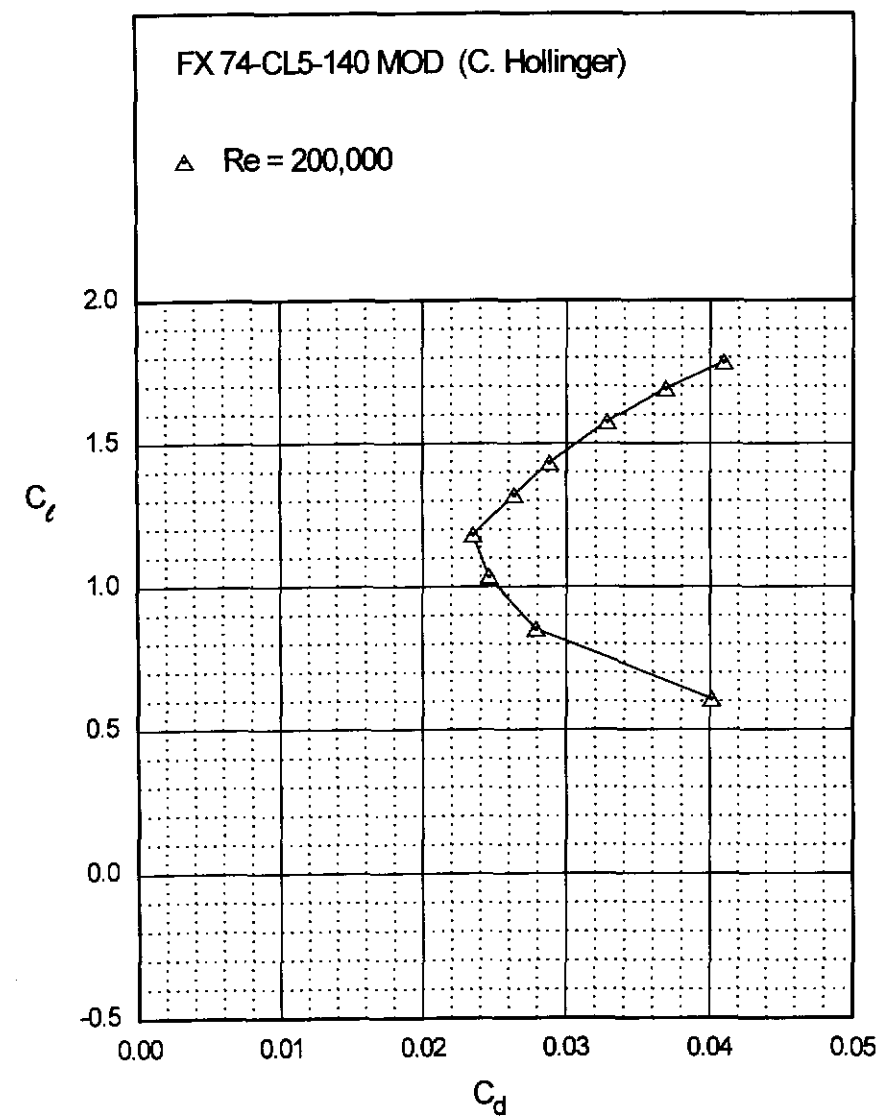


Fig. 4.27

Chapter 4: Airfoil Profiles and Performance Plots 95

FX 74-CL5-140 MOD



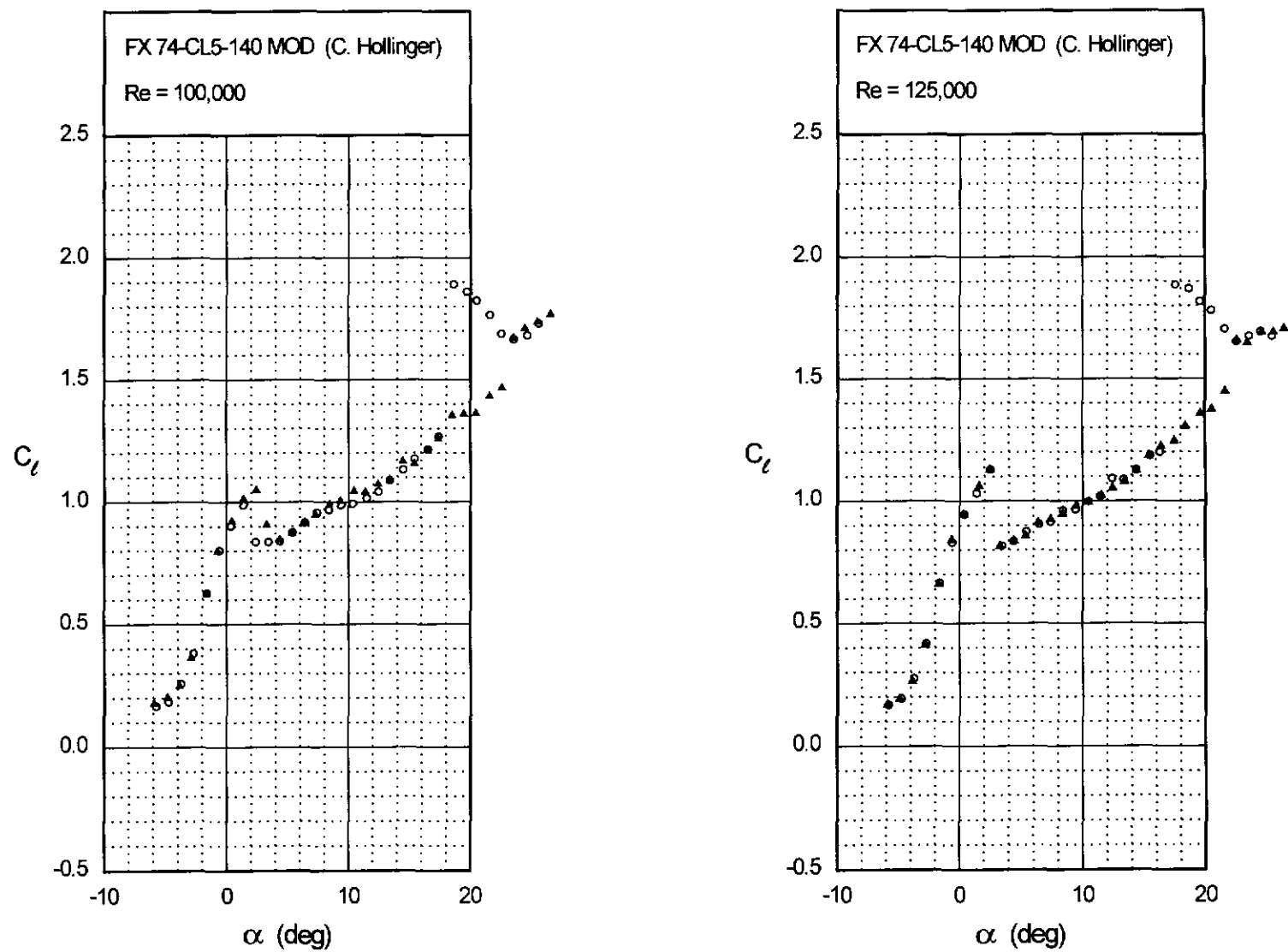


Fig. 4.28

Fig. 4.28 (continued)

Chapter 4: Airfoil Profiles and Performance Plots 97

FX 74-CL5-140 MOD

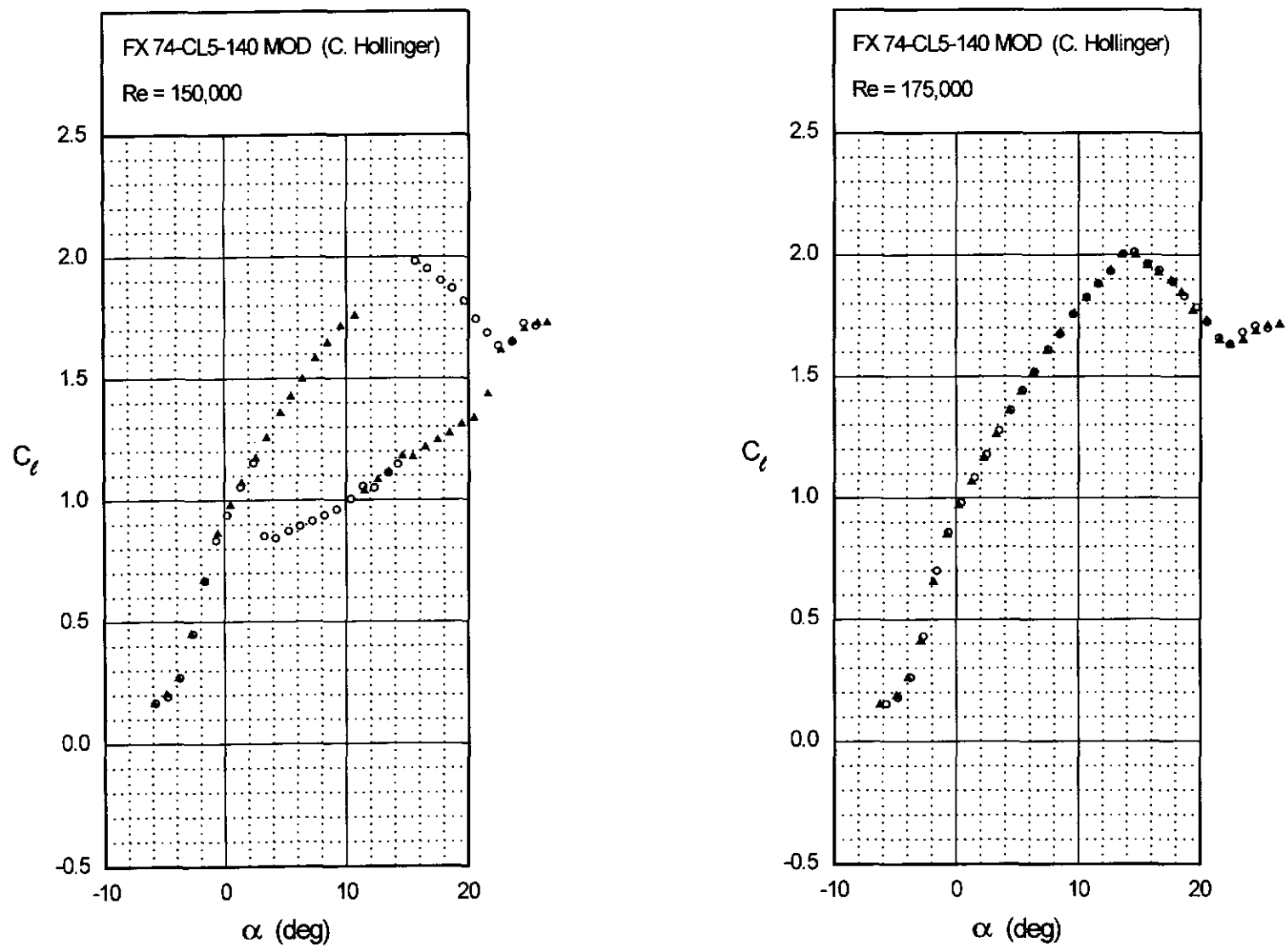
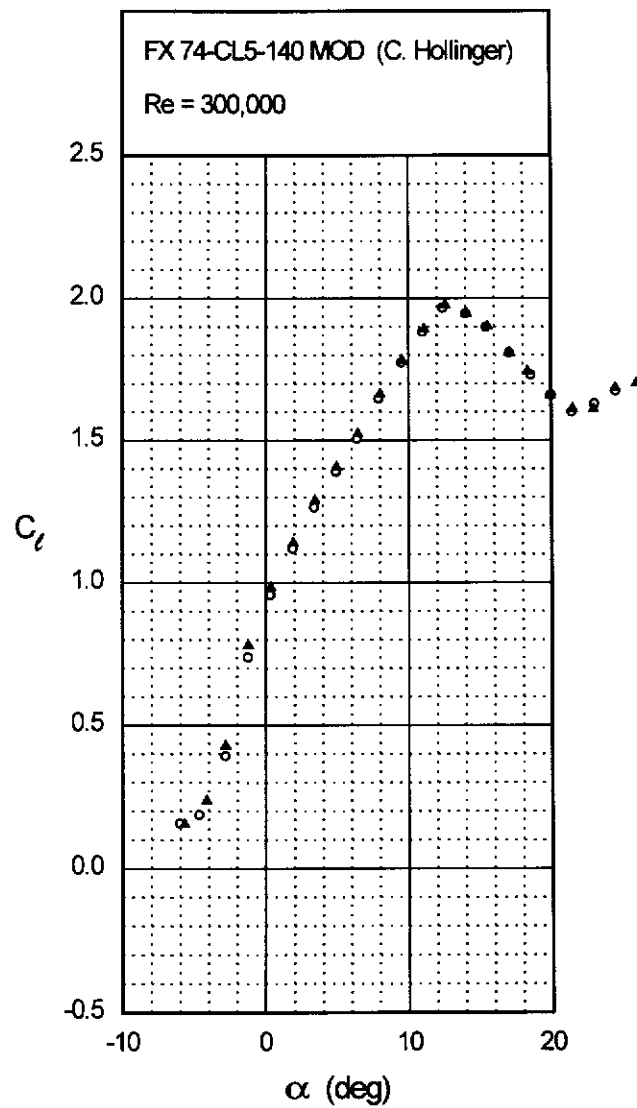
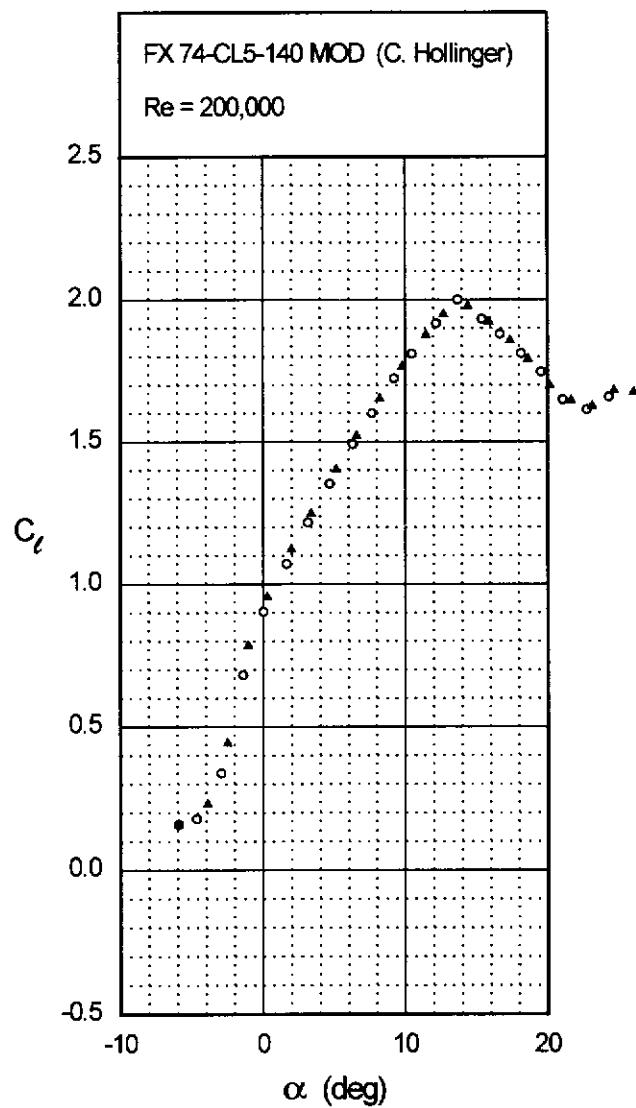


Fig. 4.28 (continued)



GEMINI

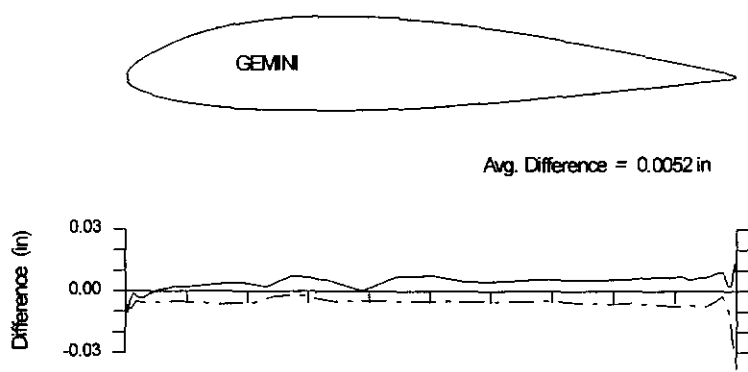
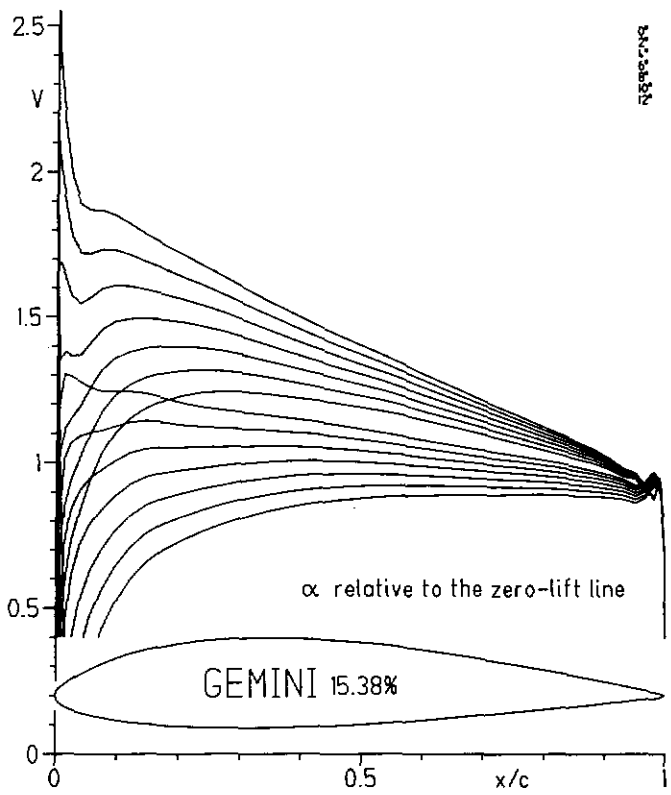
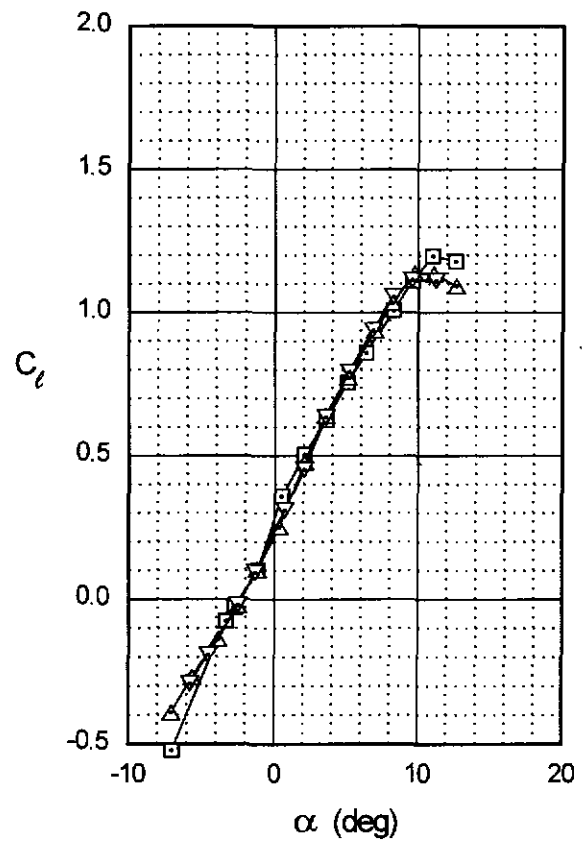
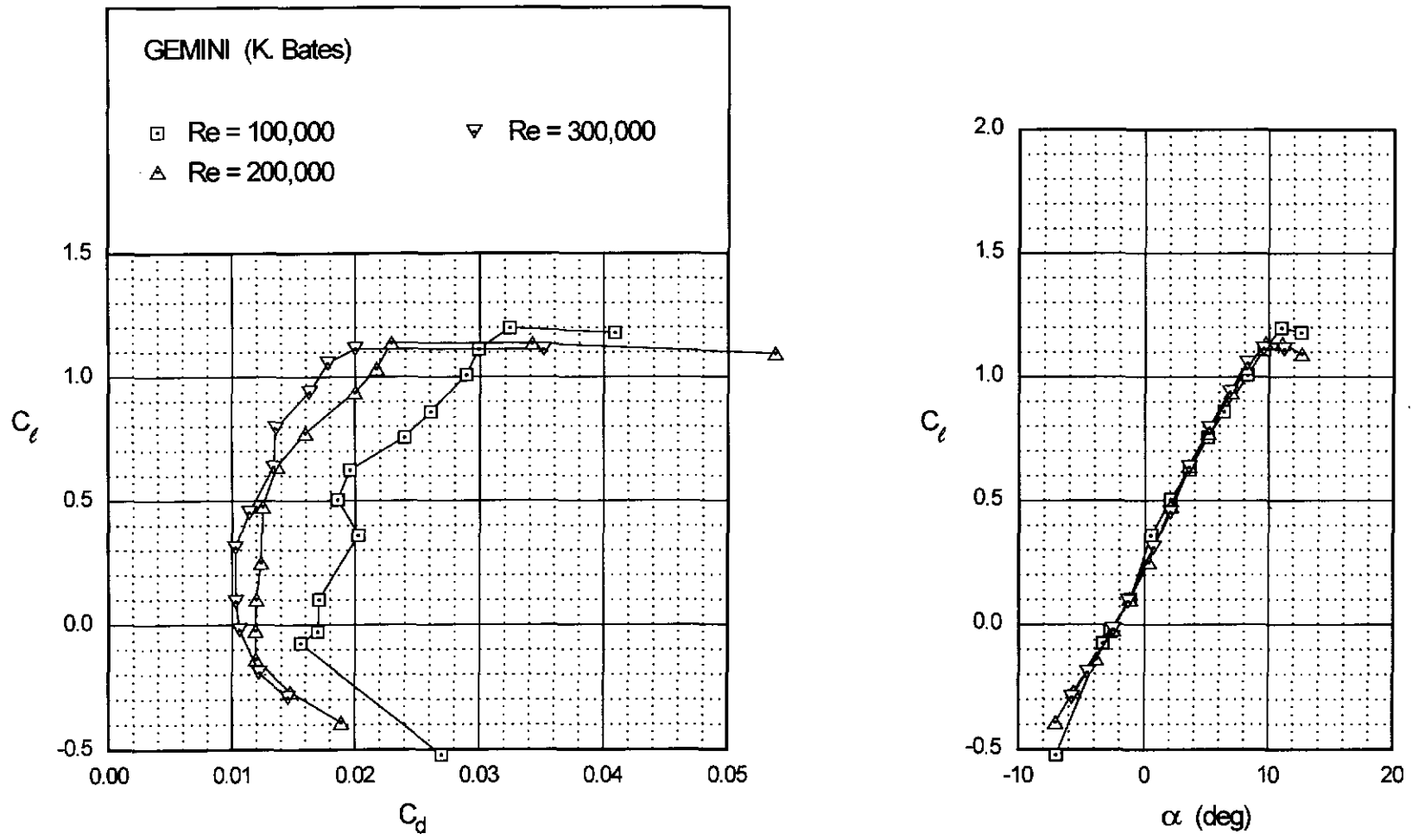


Fig. 4.31

Chapter 4: Airfoil Profiles and Performance Plots 101

GEMINI



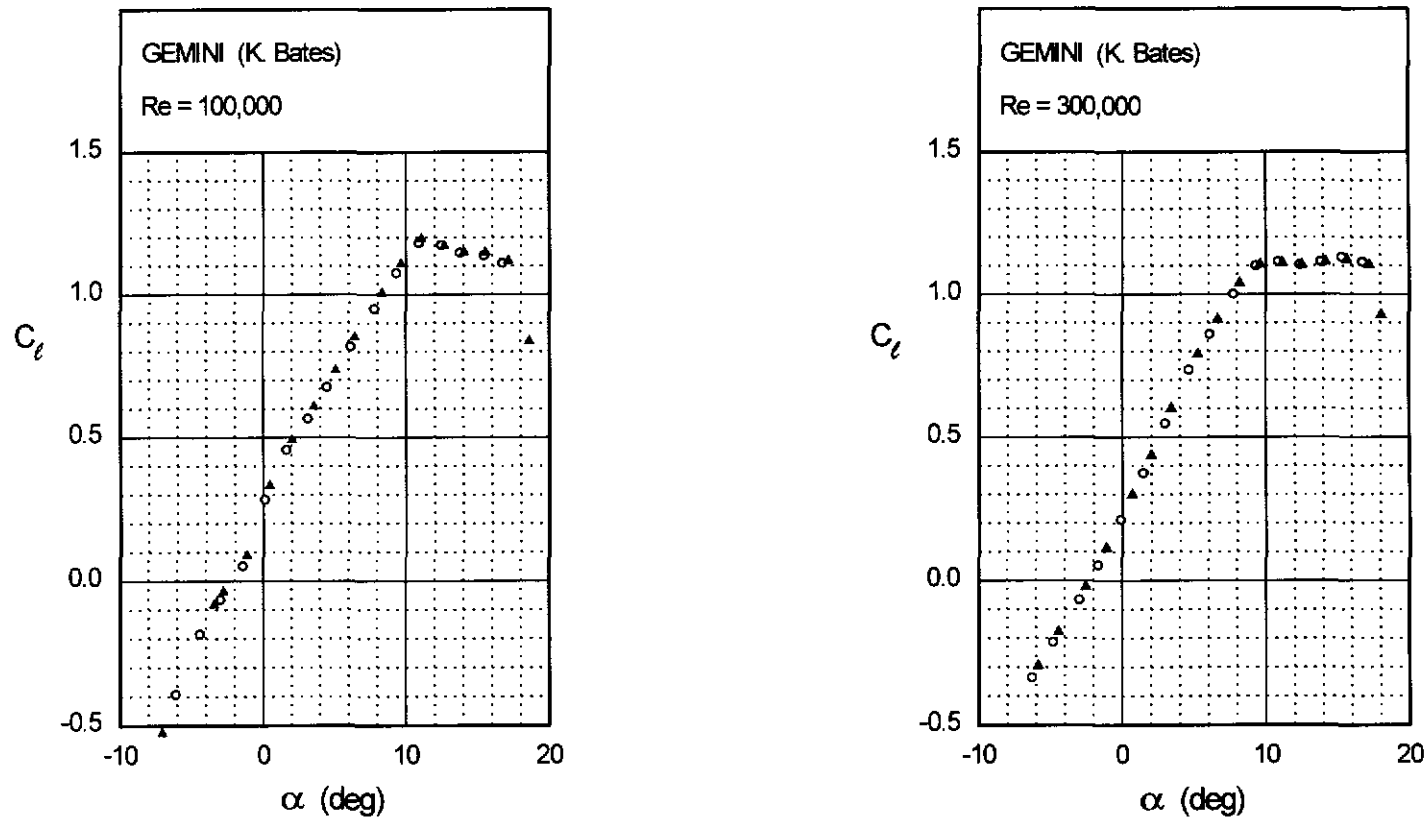
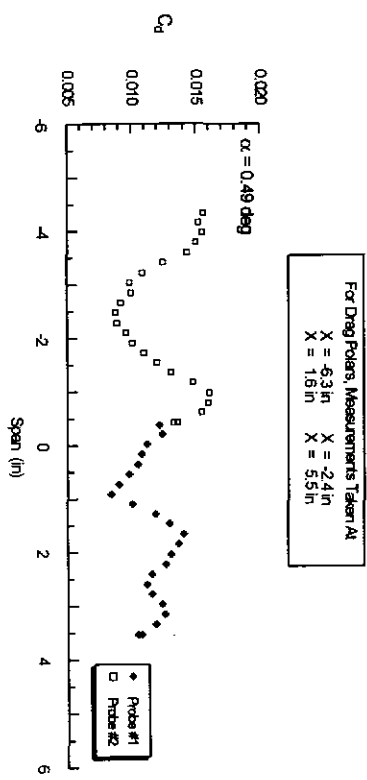
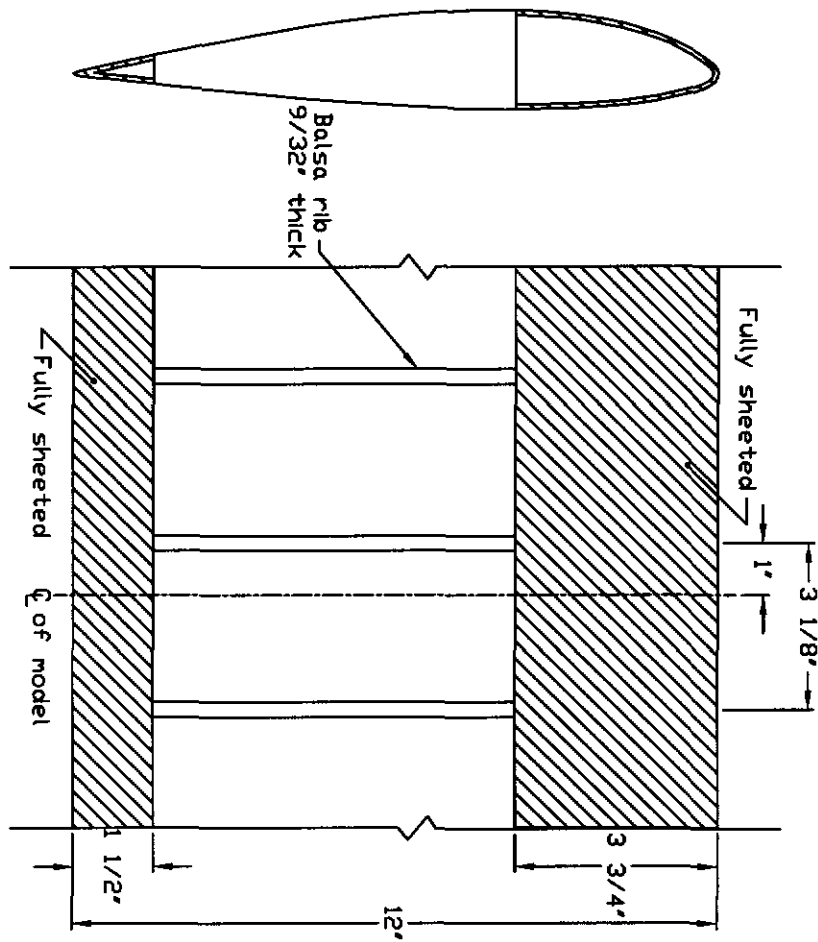


Fig. 4.32

Fig. 4.33

GEMINI



104 Summary of Low-Speed Airfoil Data

Figs. 4.34 & 4.35

GM15

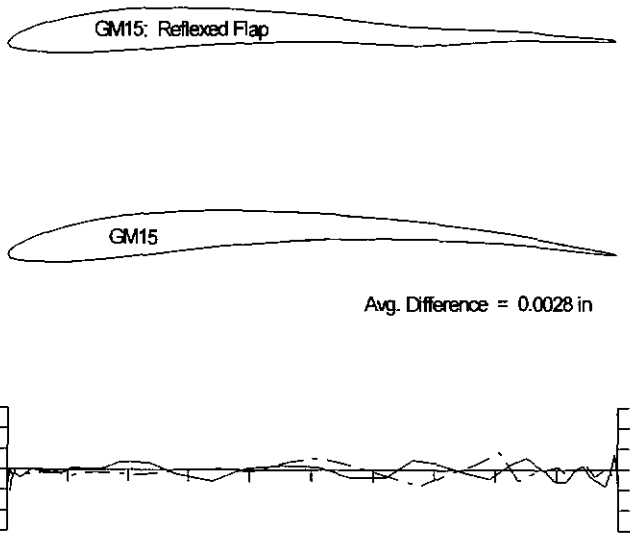
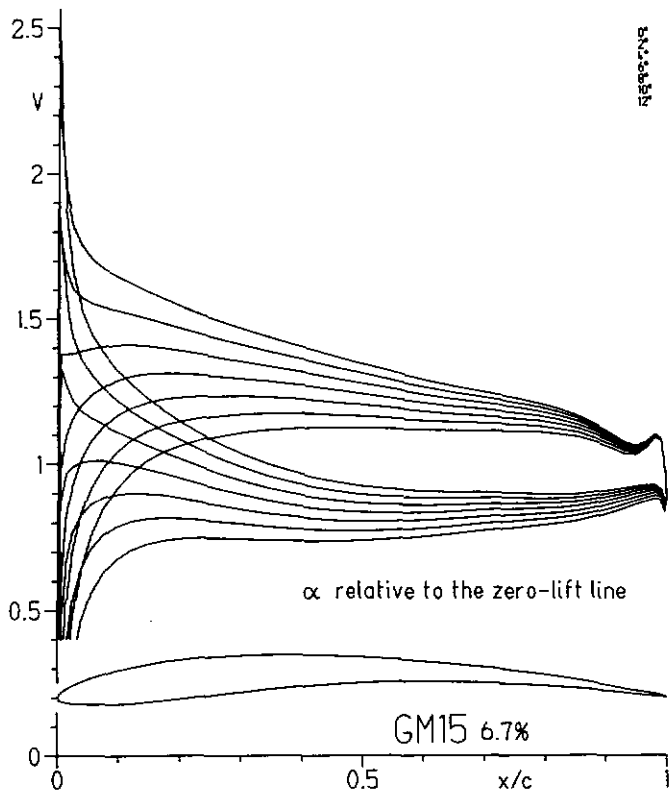
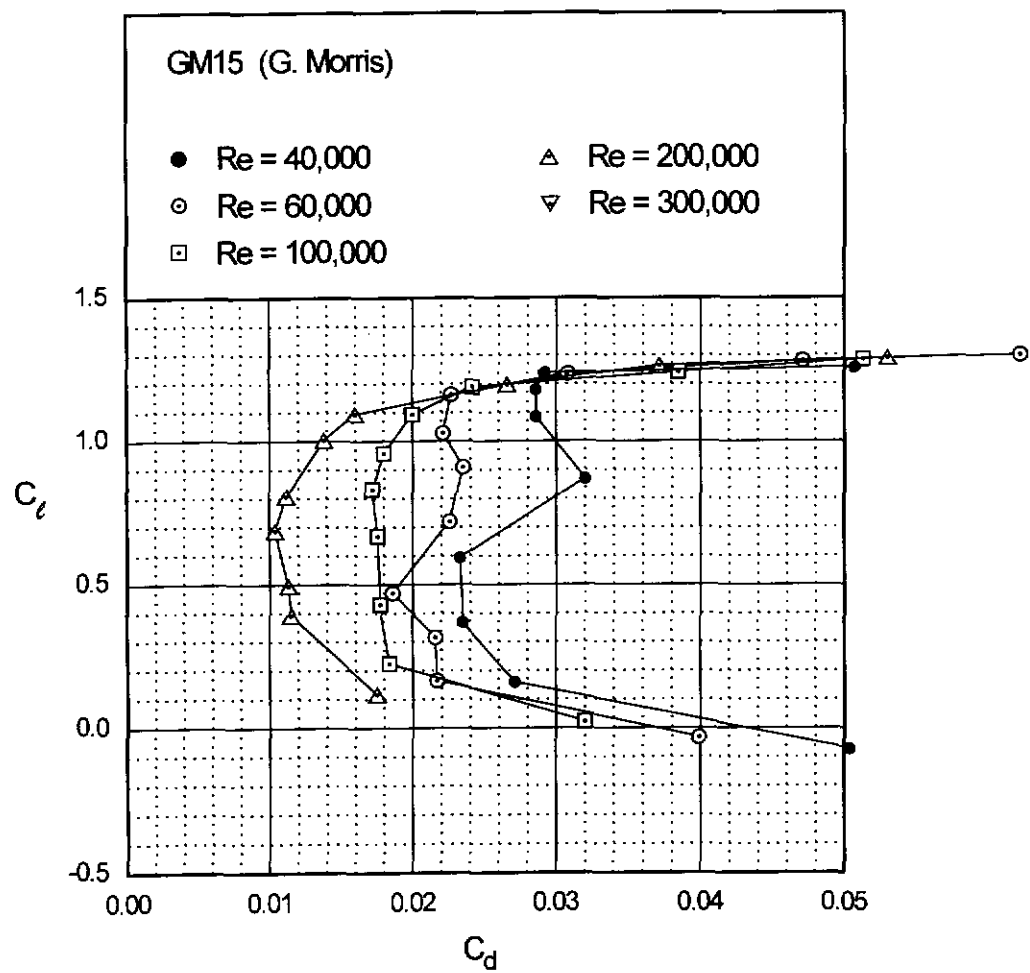
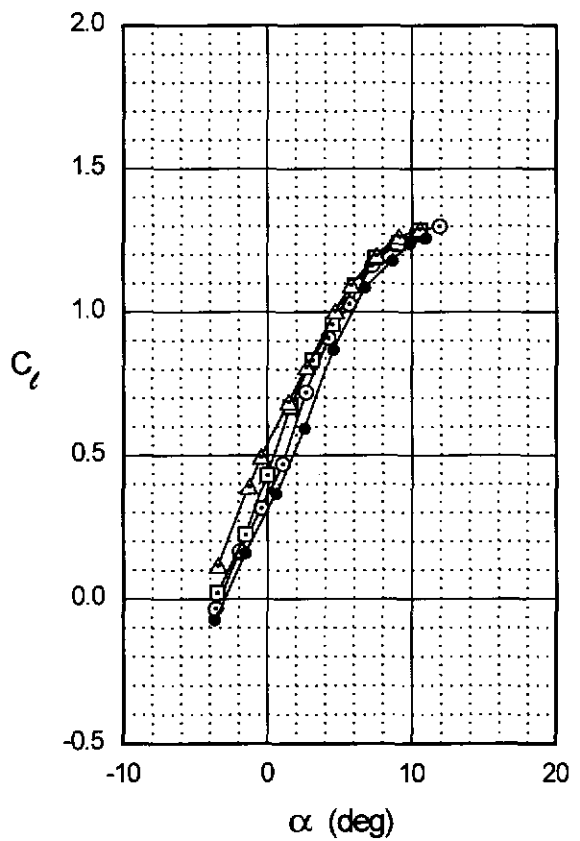


Fig. 4.36

GM15



GM15

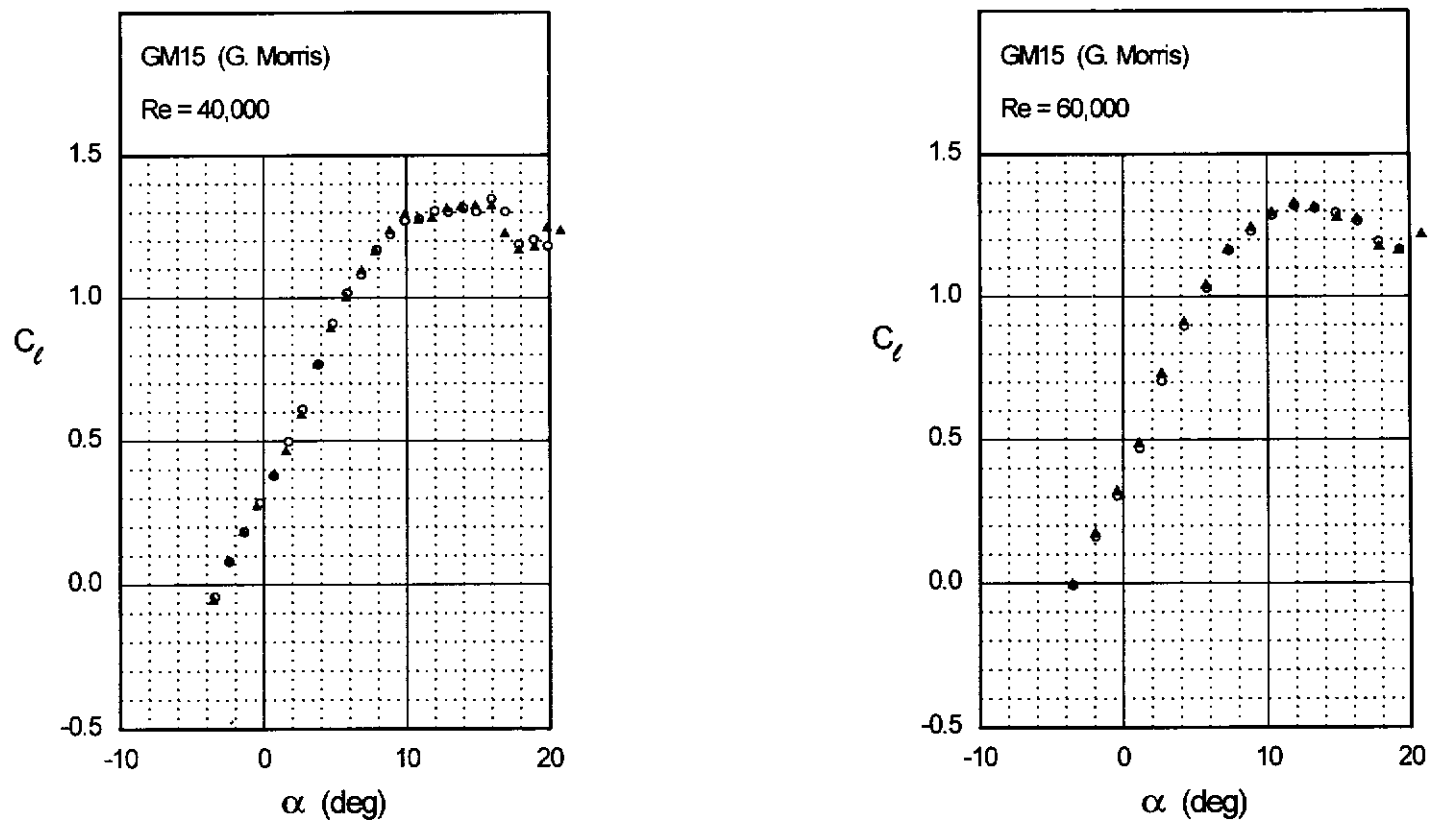
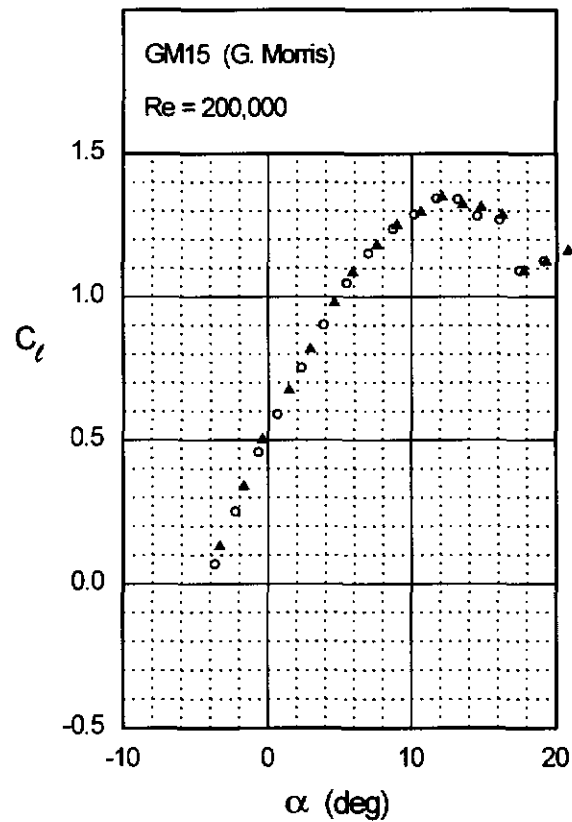
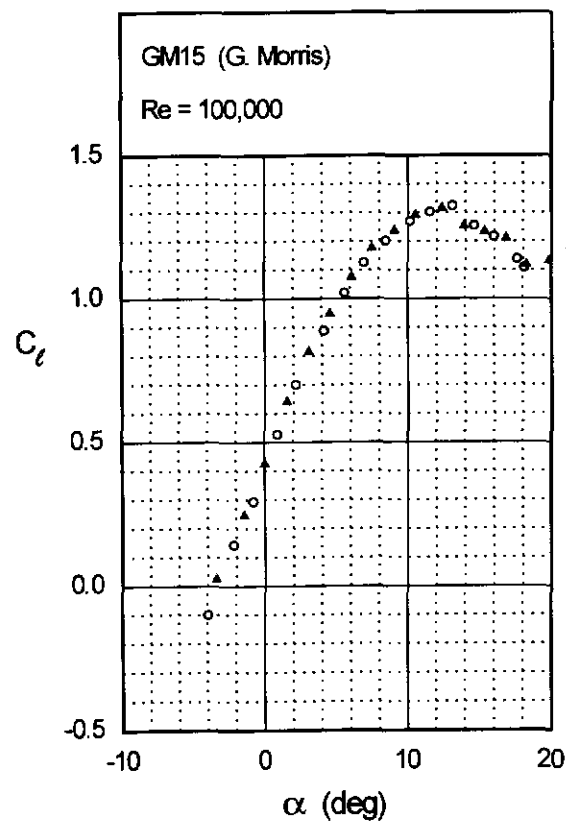


Fig. 4.37

Fig. 4.37 (continued)

GM15



GM15

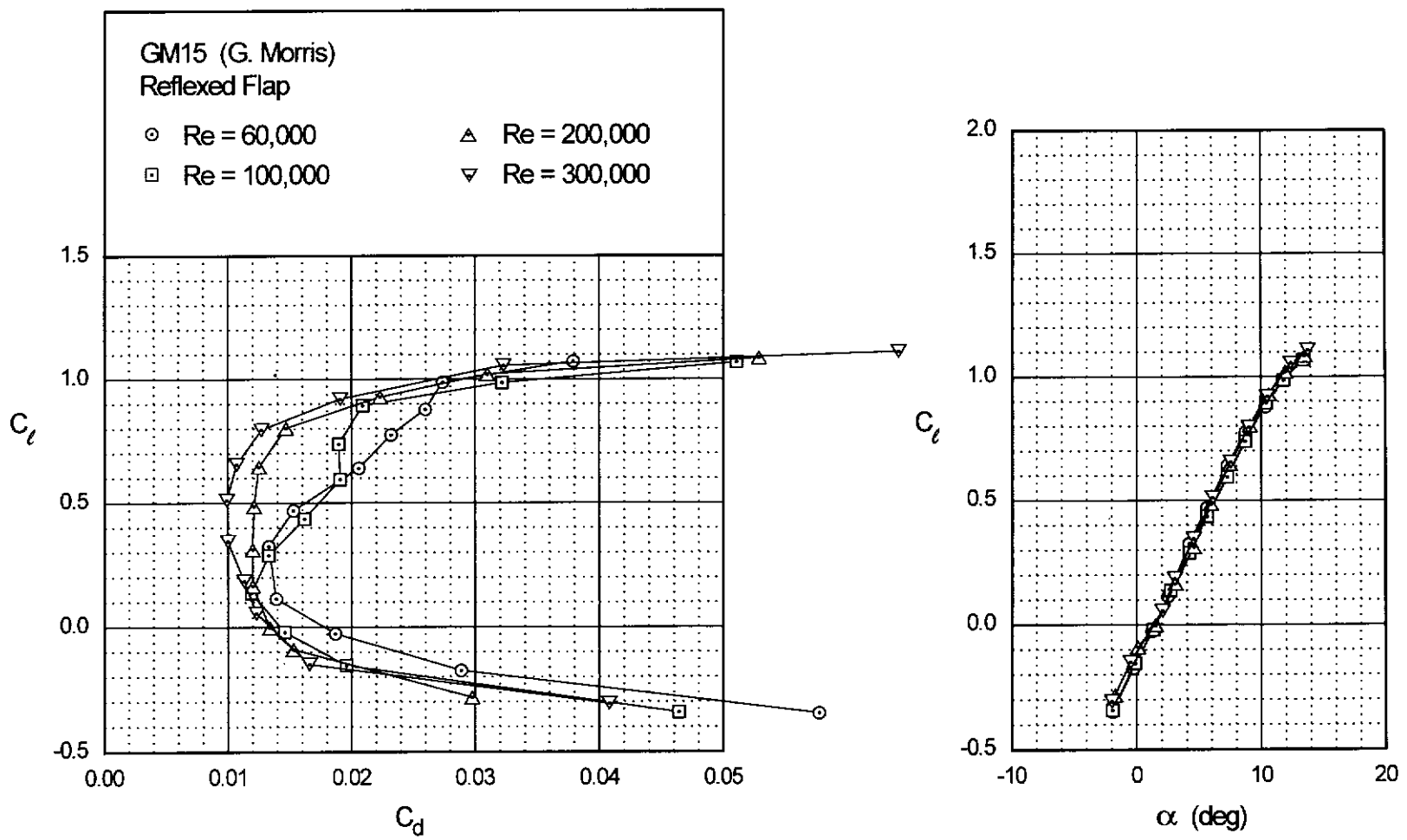


Fig. 4.39

GM15

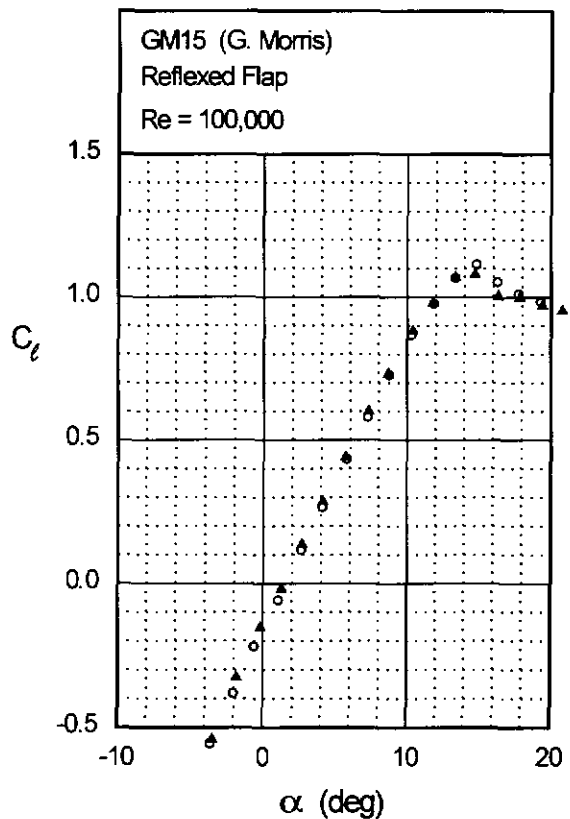
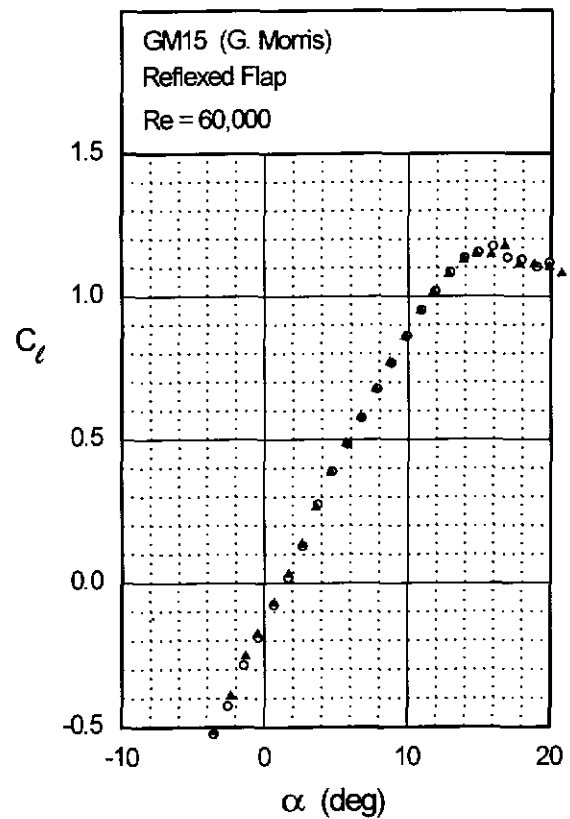
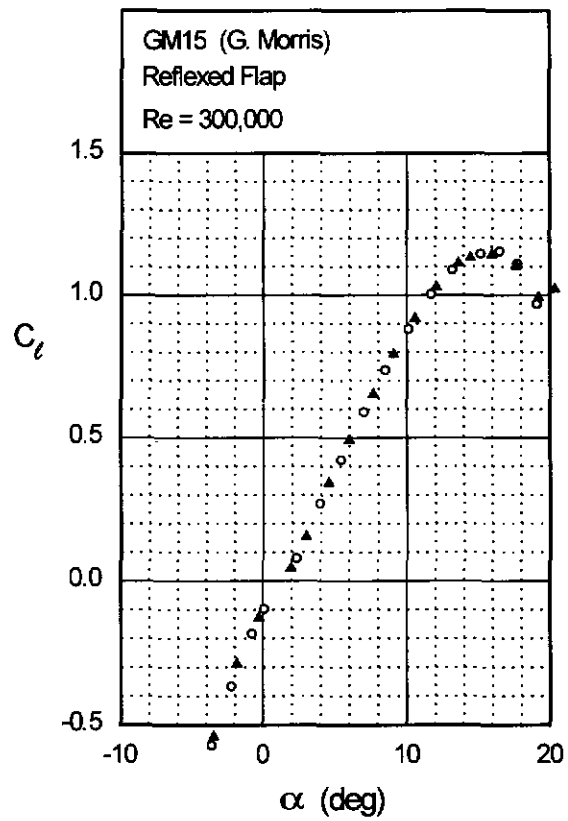
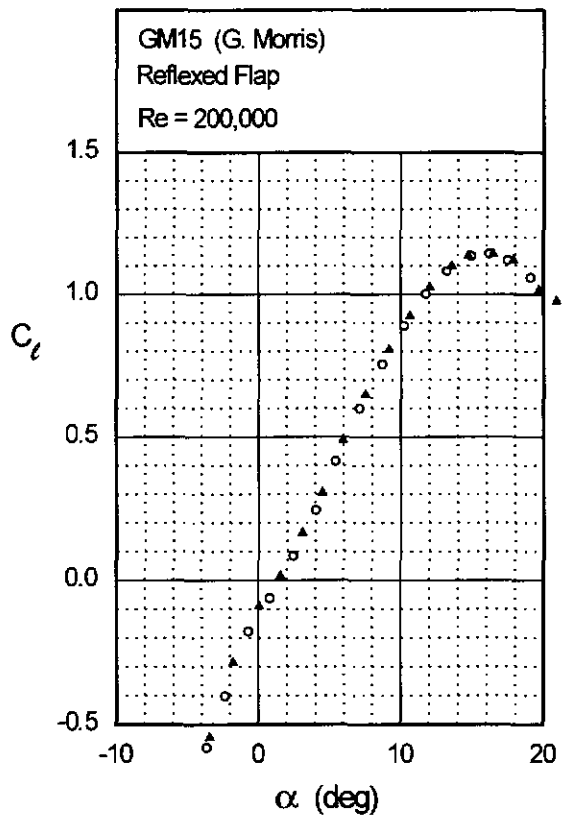


Fig. 4.39 (continued)

GM15



112 Summary of Low-Speed Airfoil Data

Figs. 4.40 & 4.41

J5012

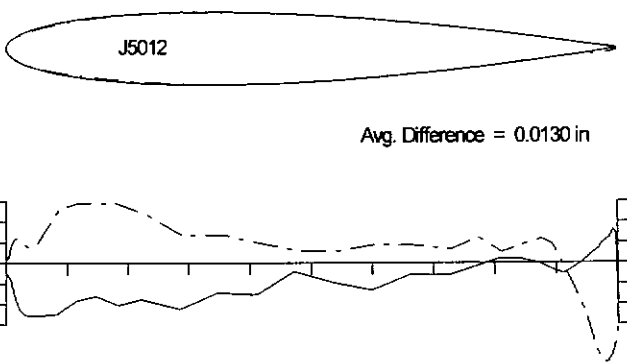
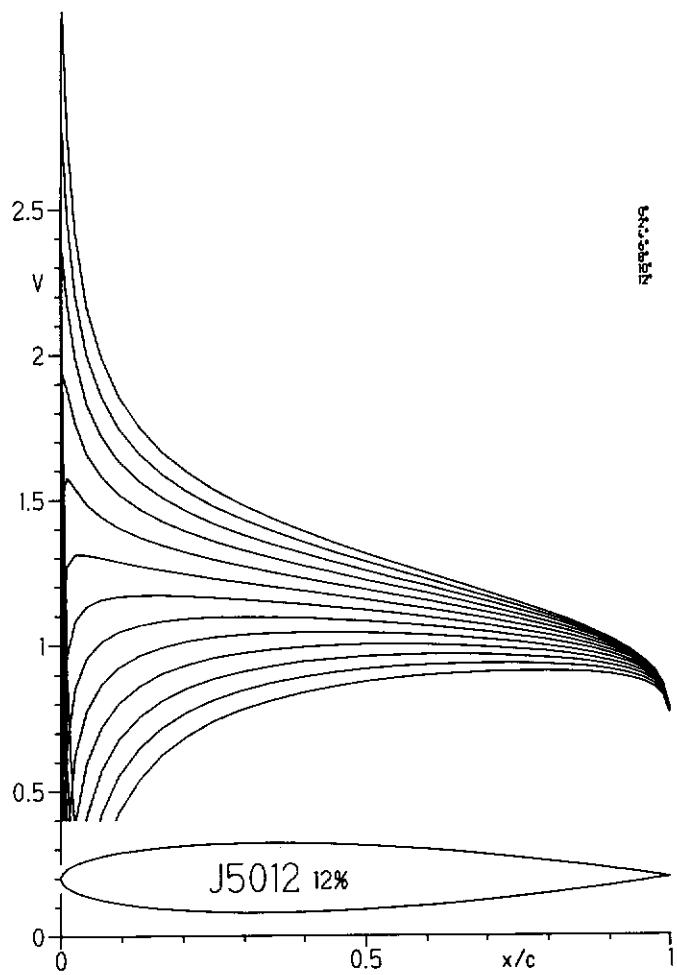
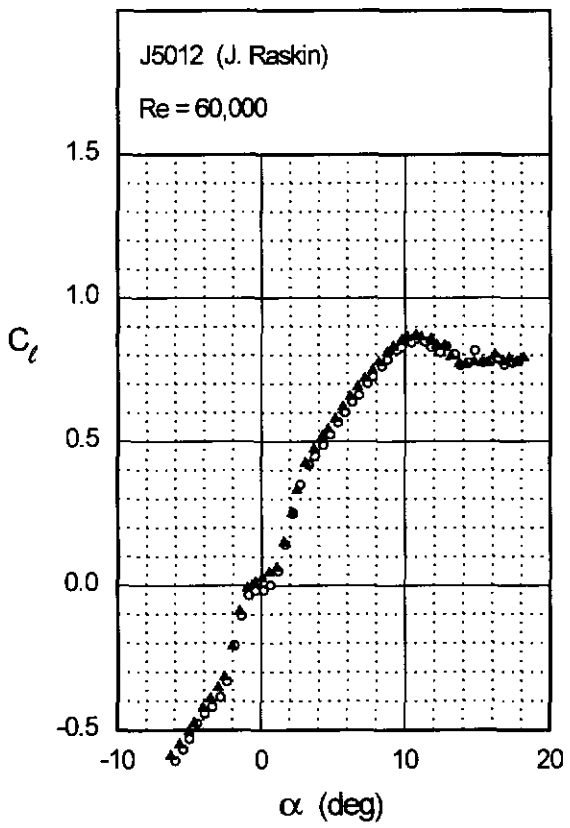
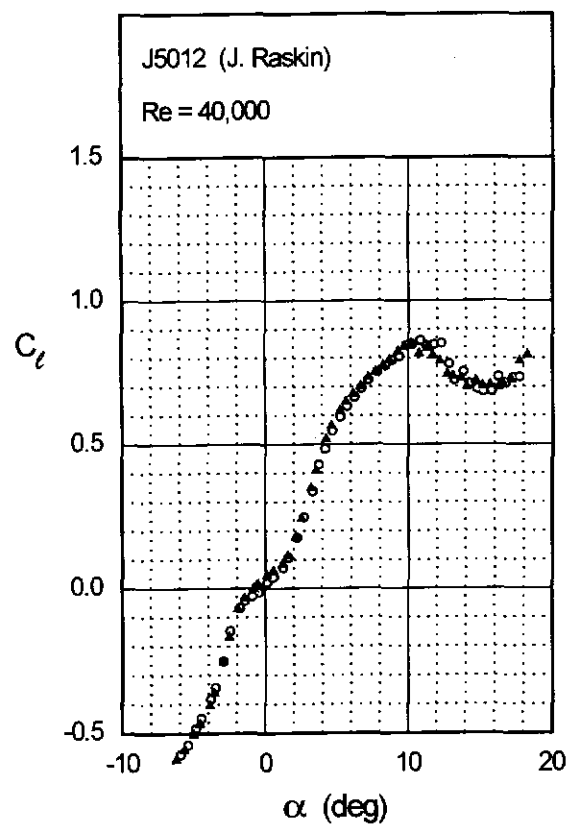


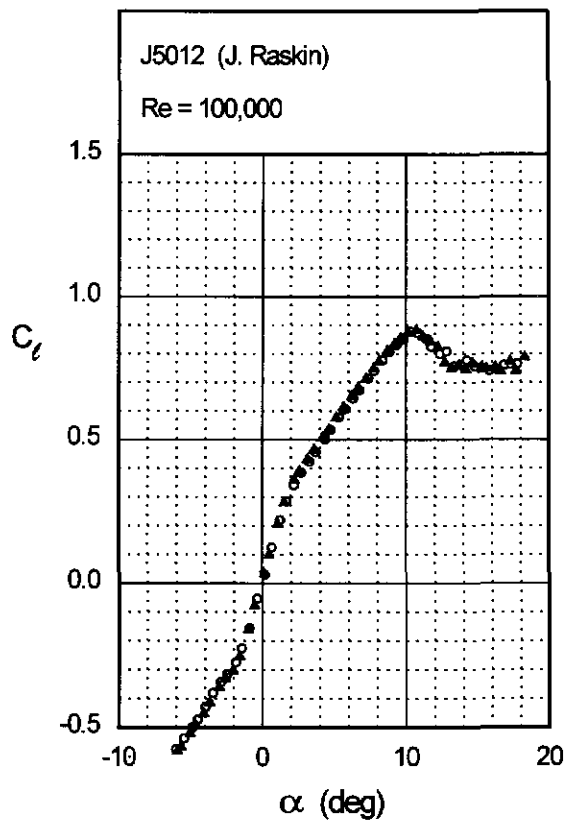
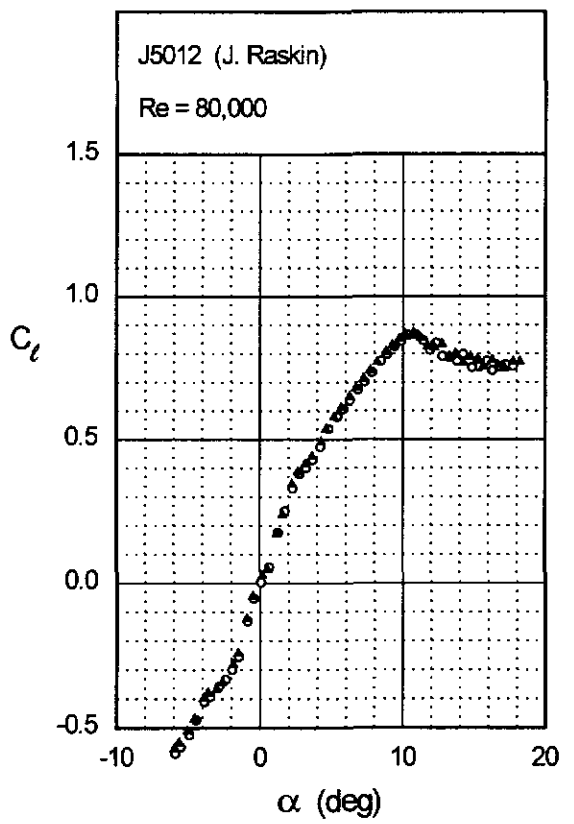
Fig. 4.42

Chapter 4: Airfoil Profiles and Performance Plots 113

J5012



J5012



Figs. 4.43 & 4.44

K3311

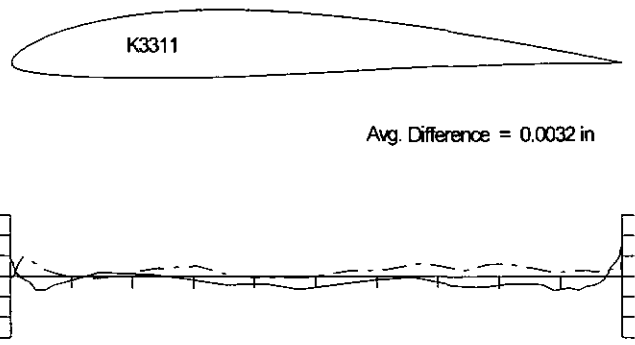
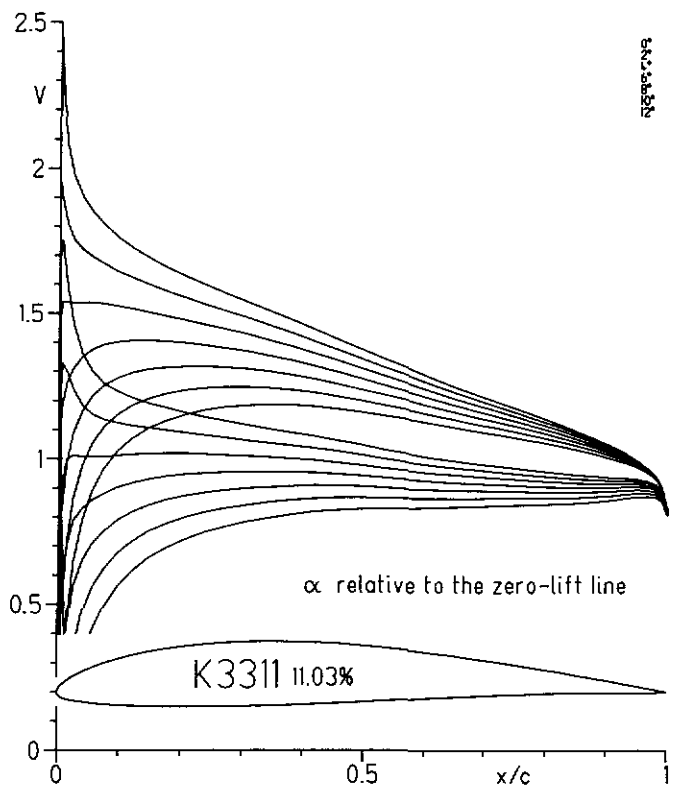
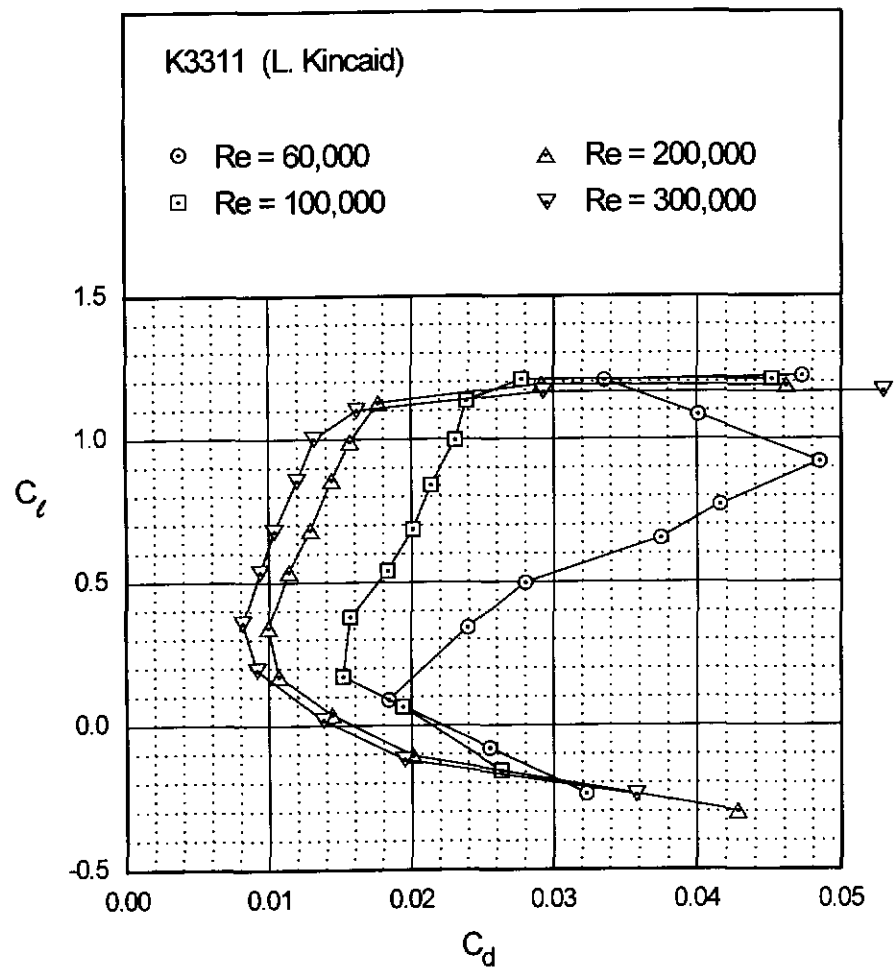
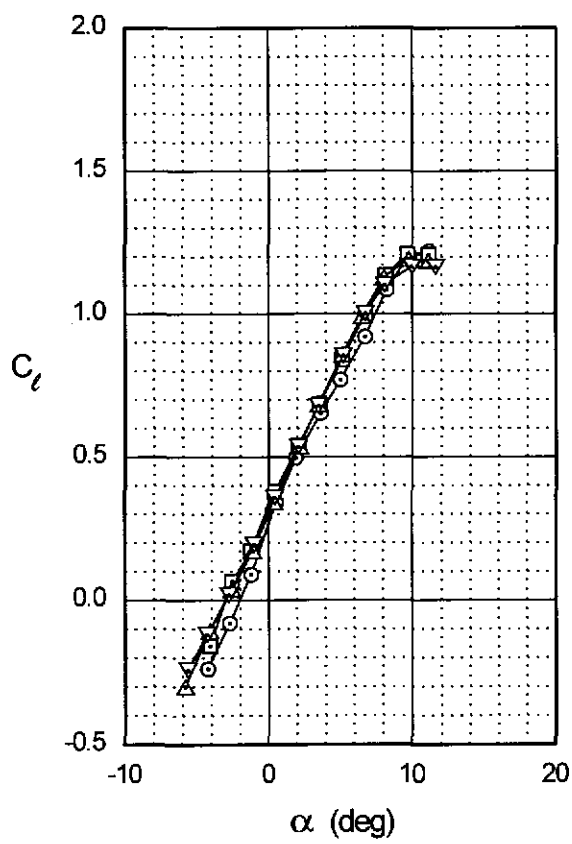


Fig. 4.45

Chapter 4: Airfoil Profiles and Performance Plots 117

K3311



K3311

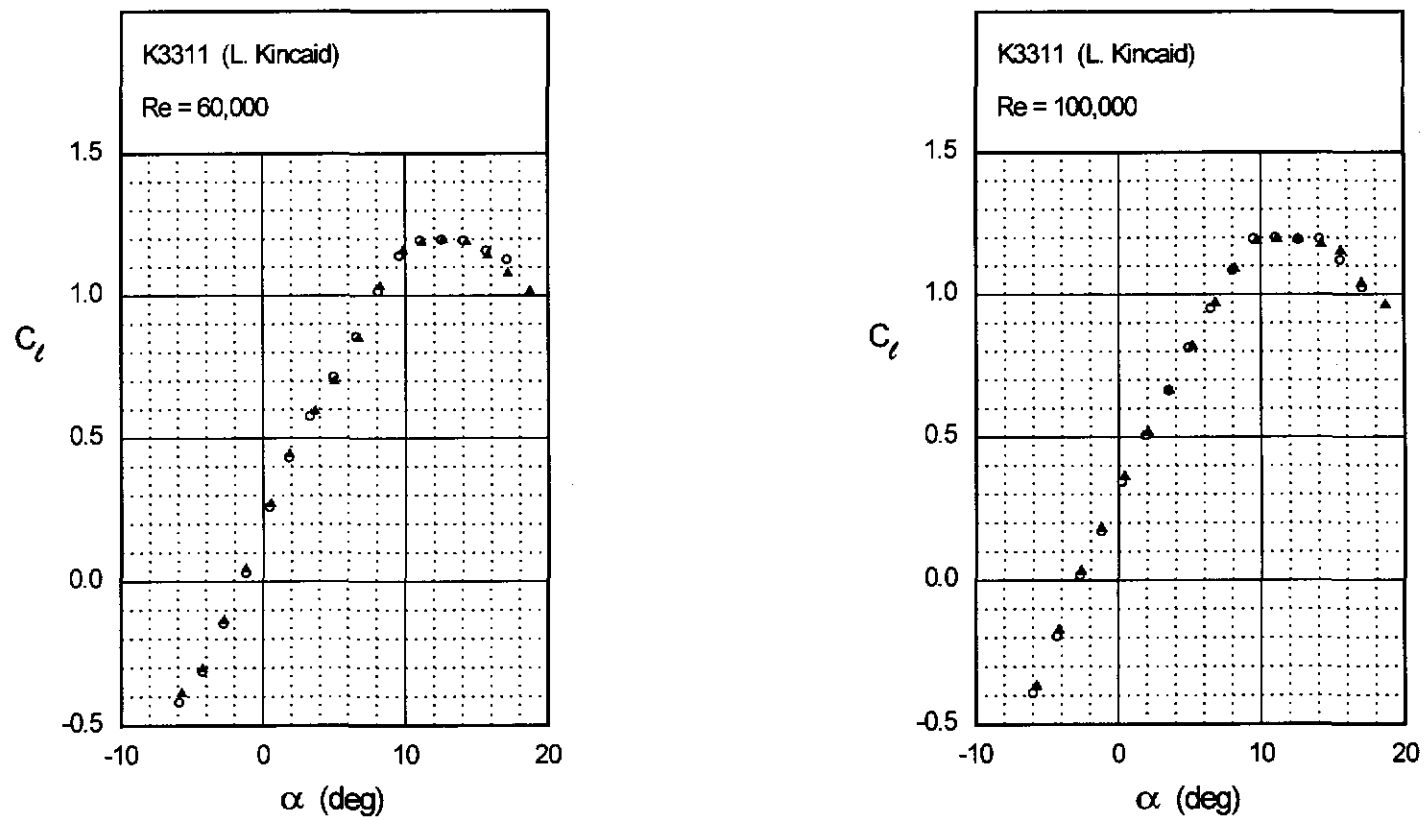
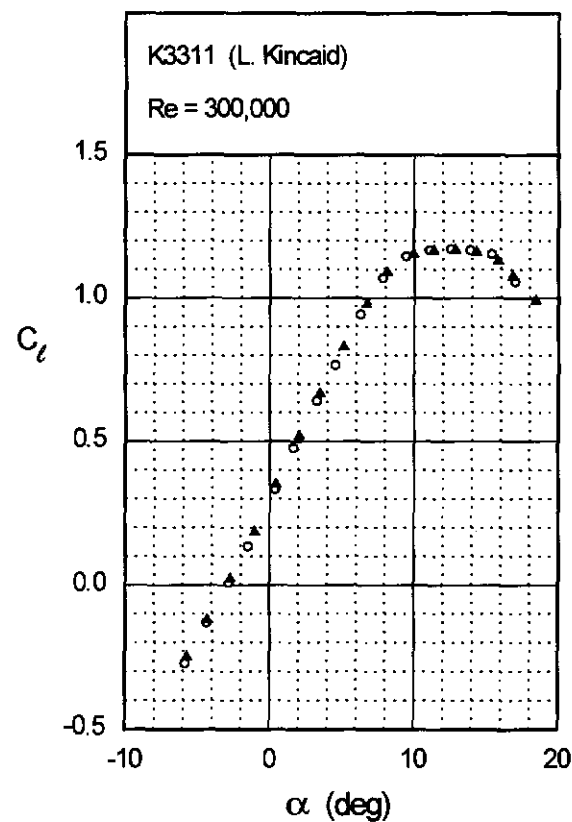
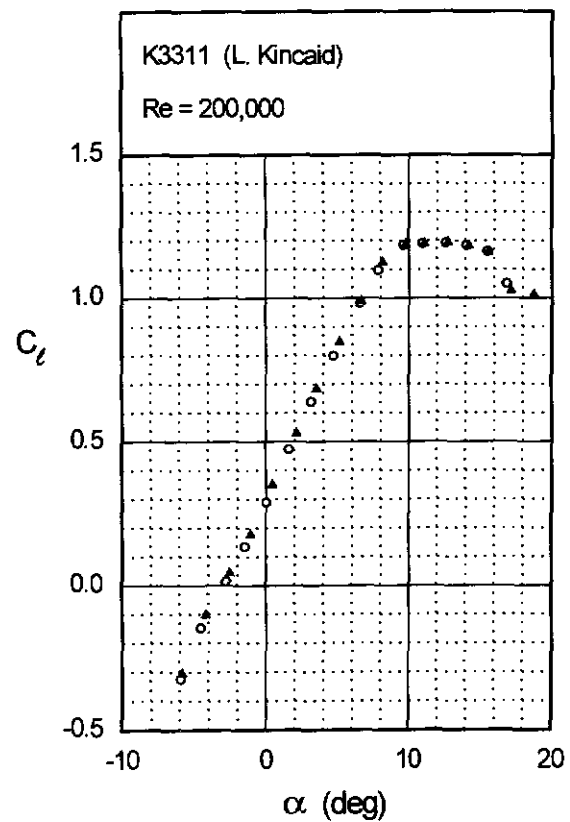


Fig. 4.46

Fig. 4.46 (continued)

Chapter 4: Airfoil Profiles and Performance Plots 119



K3311

M06-13-128 (B)

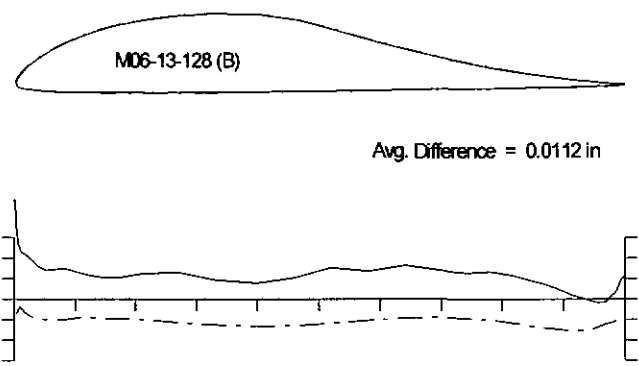
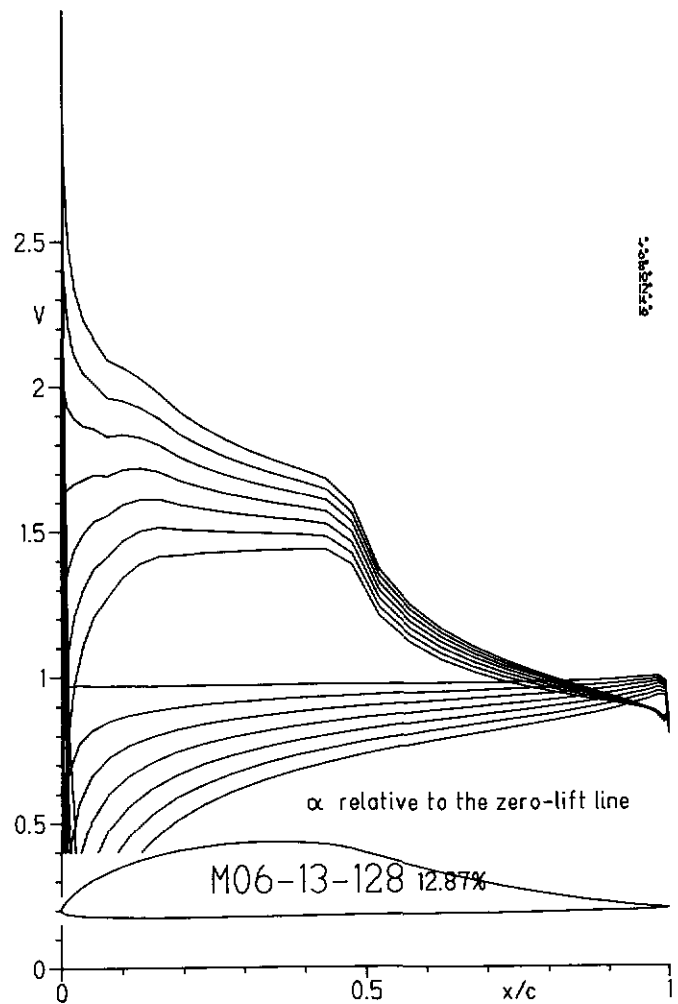
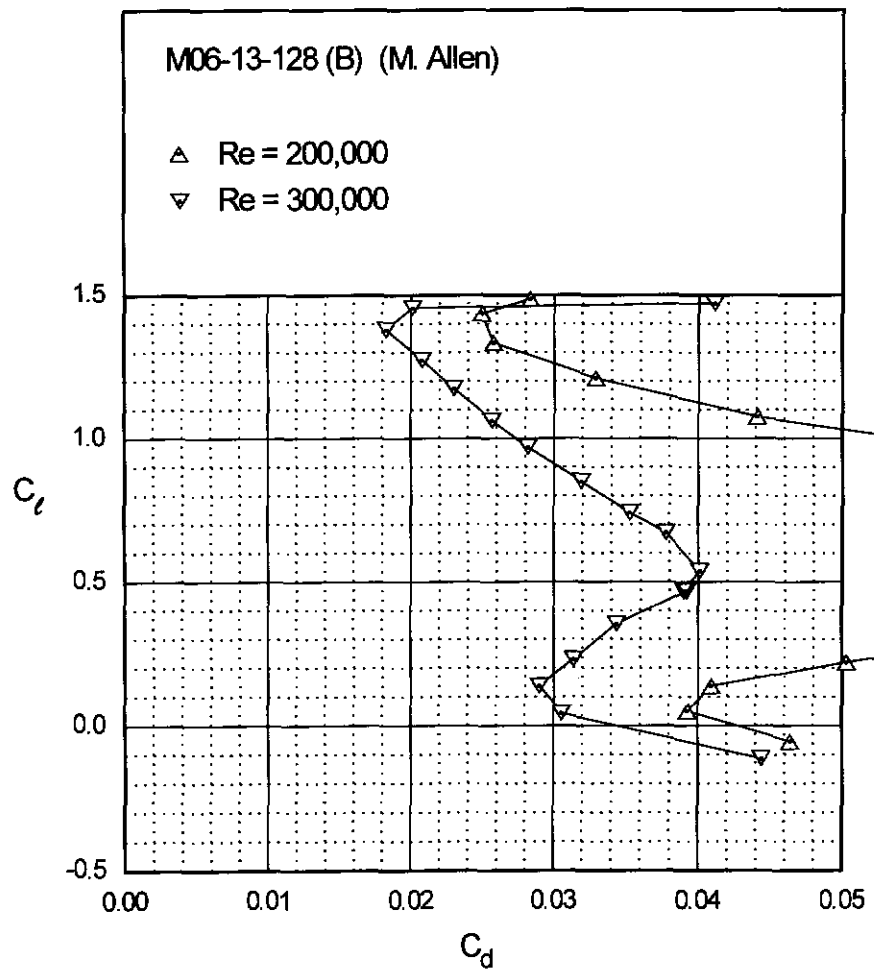
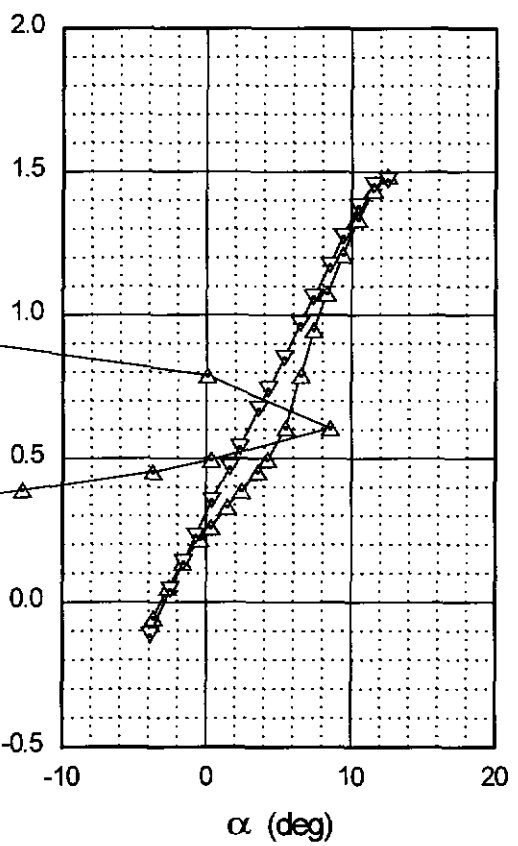


Fig. 4.49

Chapter 4: Airfoil Profiles and Performance Plots 121

M06-13-128 (B)



M06-13-128 (B)

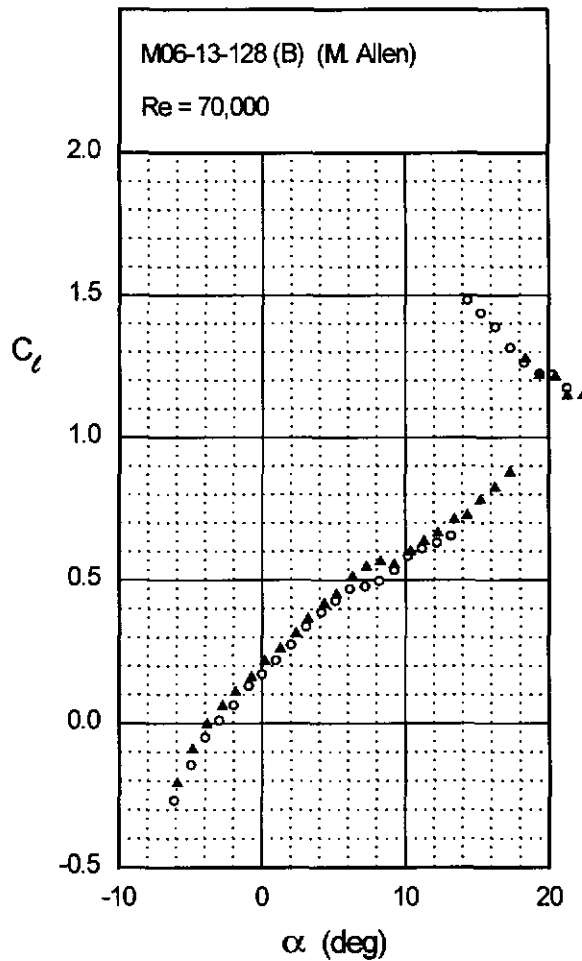
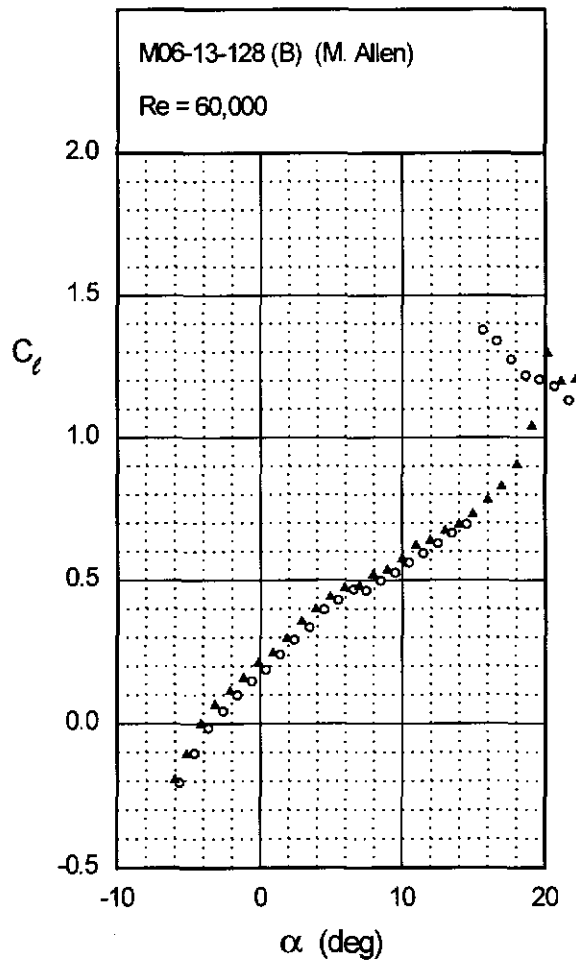
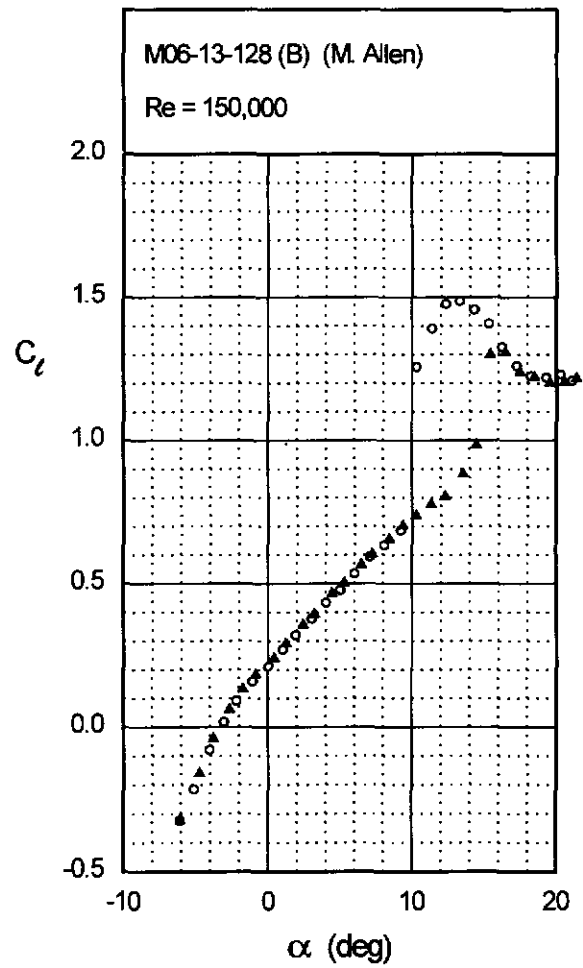
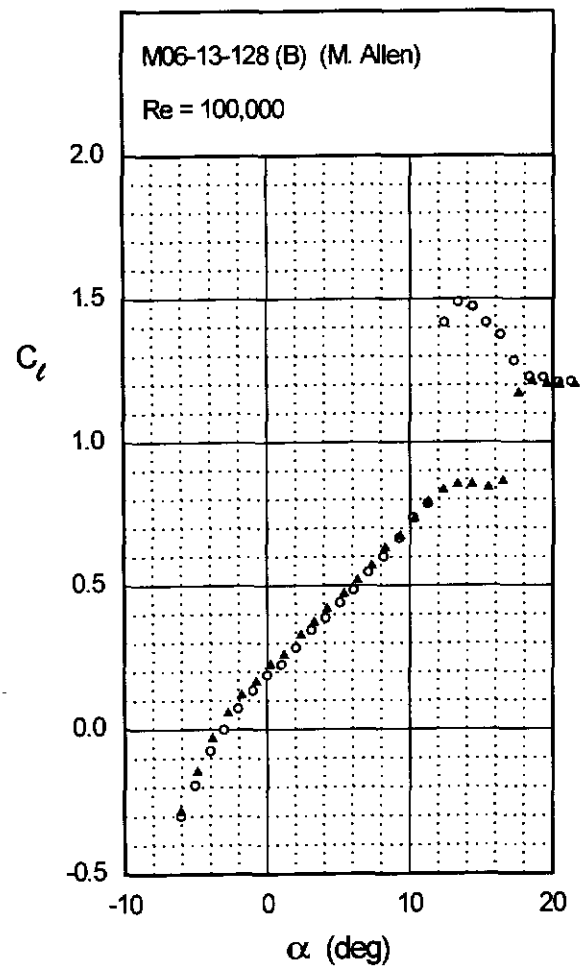


Fig. 4.50 (continued)

Chapter 4: Airfoil Profiles and Performance Plots 123

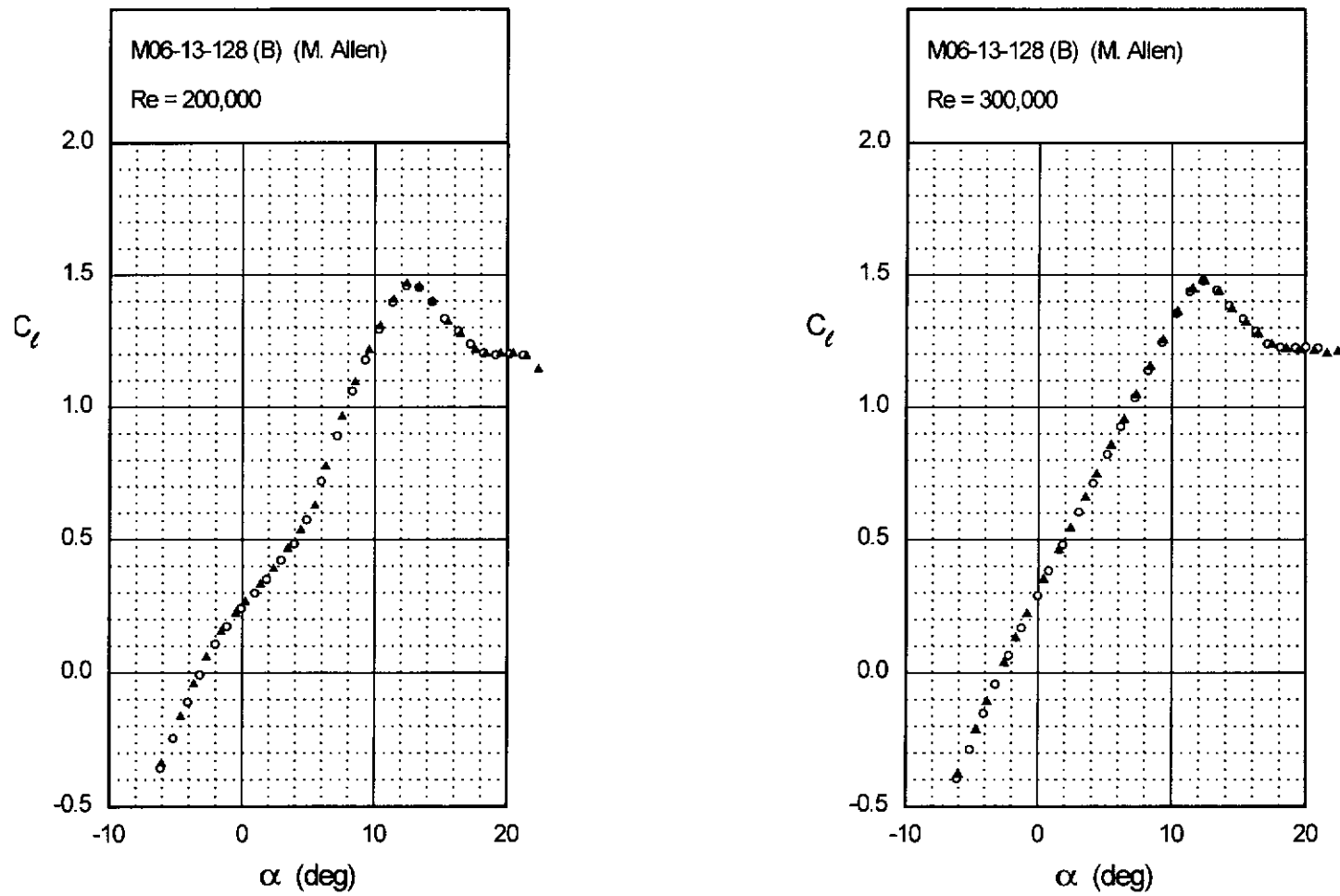
M06-13-128 (B)



124 Summary of Low-Speed Airfoil Data

Fig. 4.50 (continued)

M06-13-128 (B)



MA409

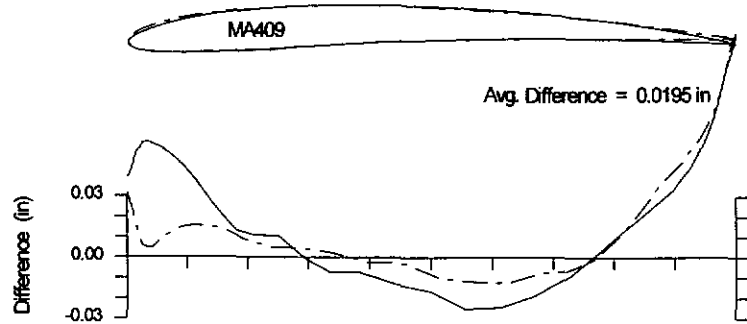
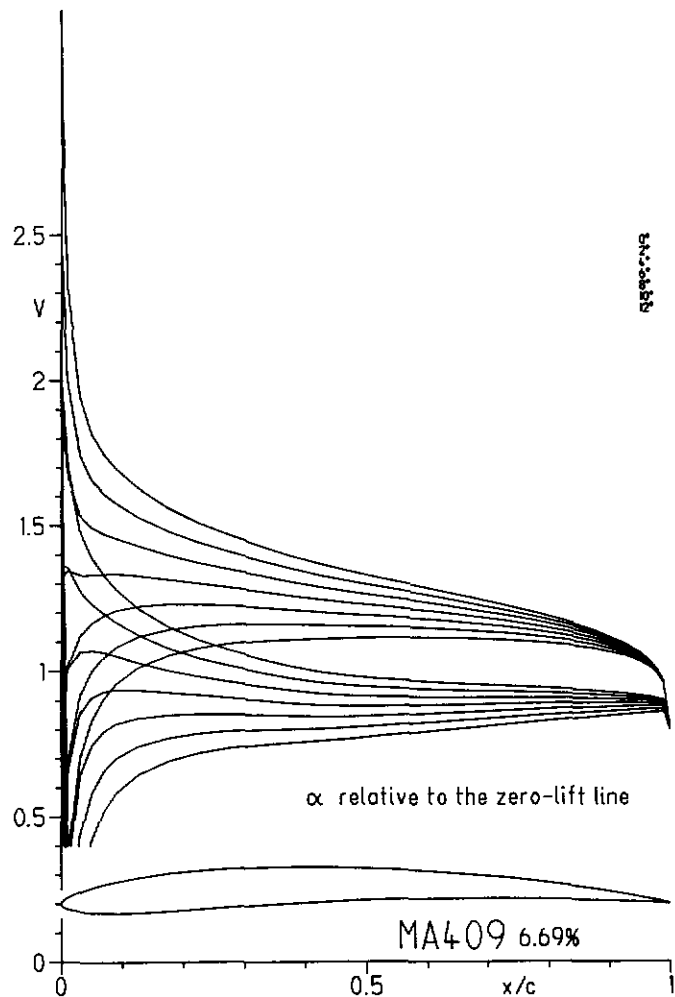
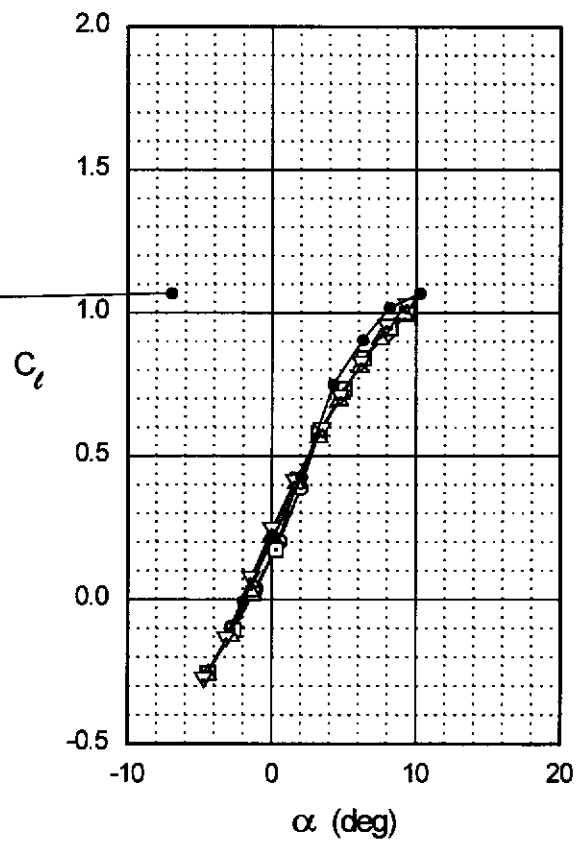
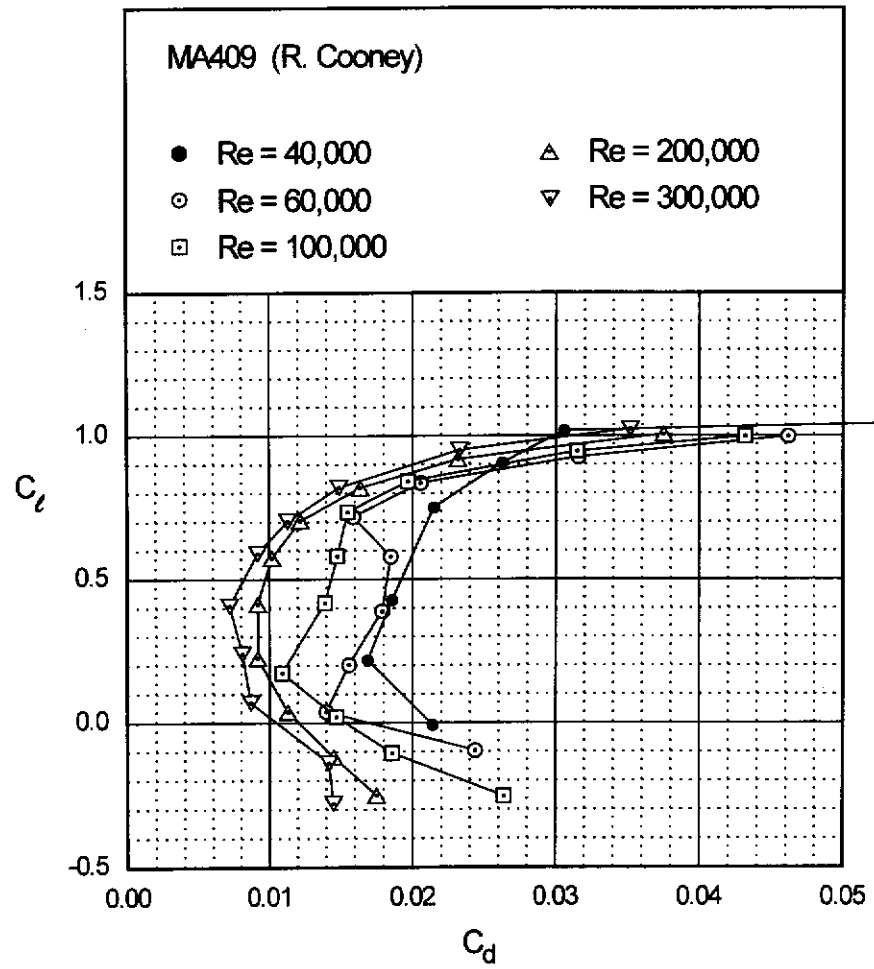


Fig. 4.53

Chapter 4: Airfoil Profiles and Performance Plots 127



MA409

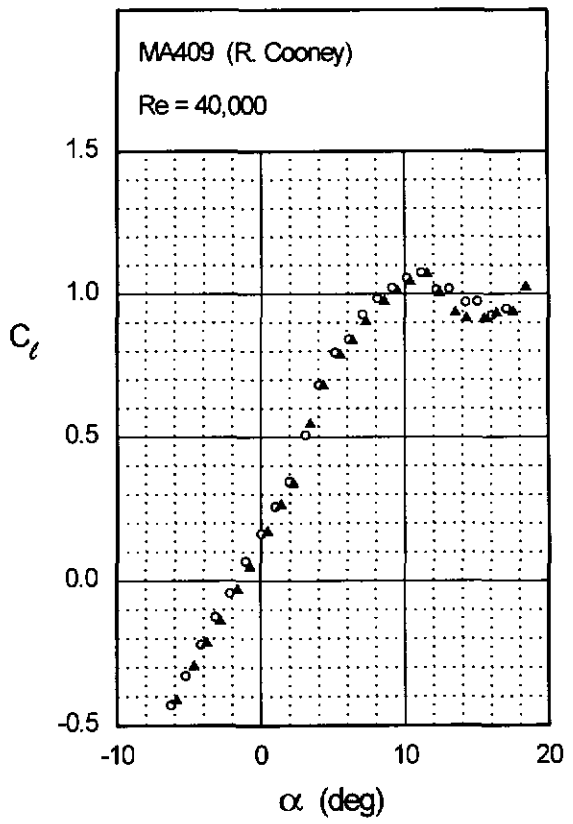
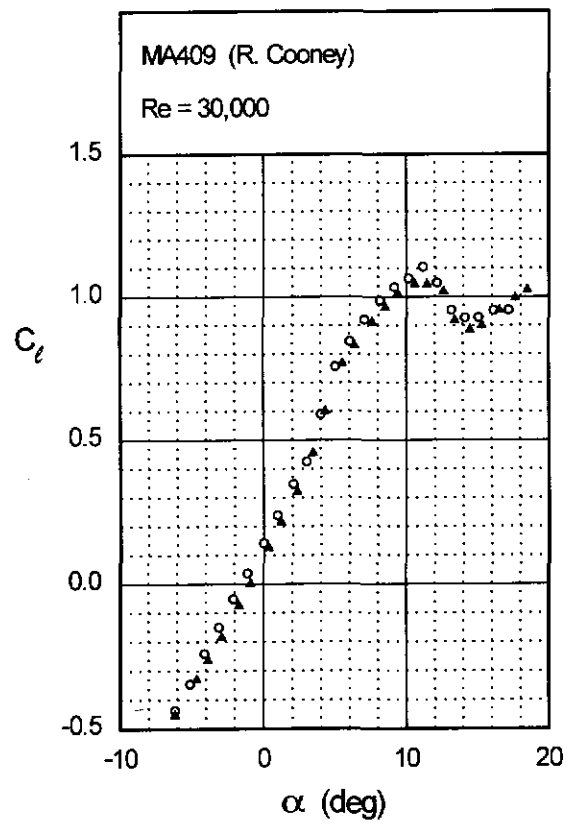
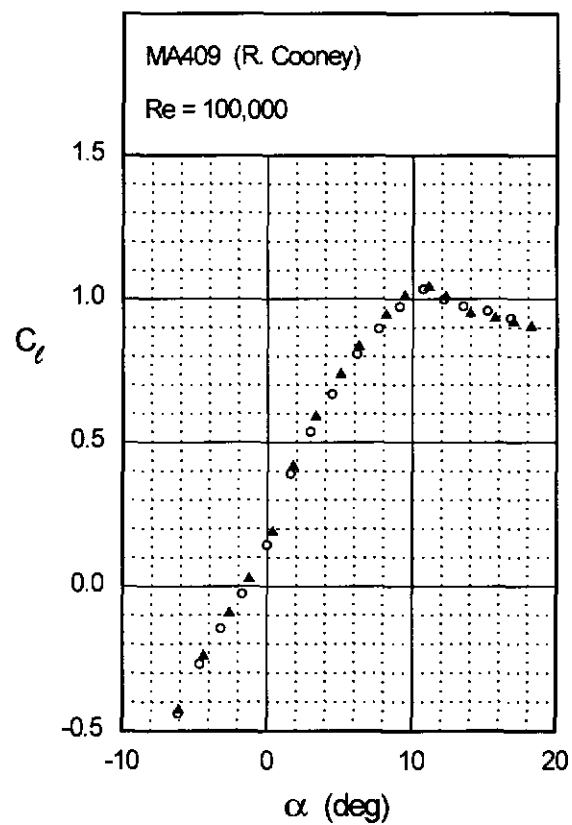
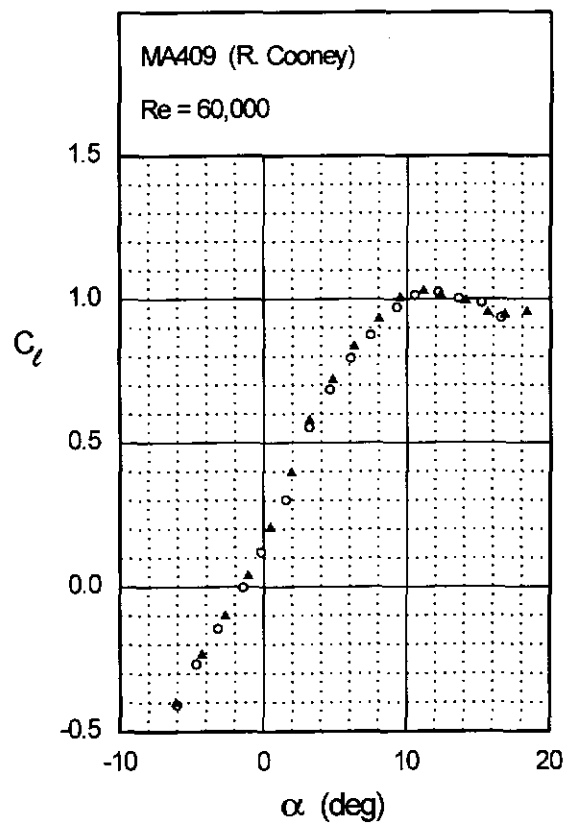


Fig. 4.54 (continued)

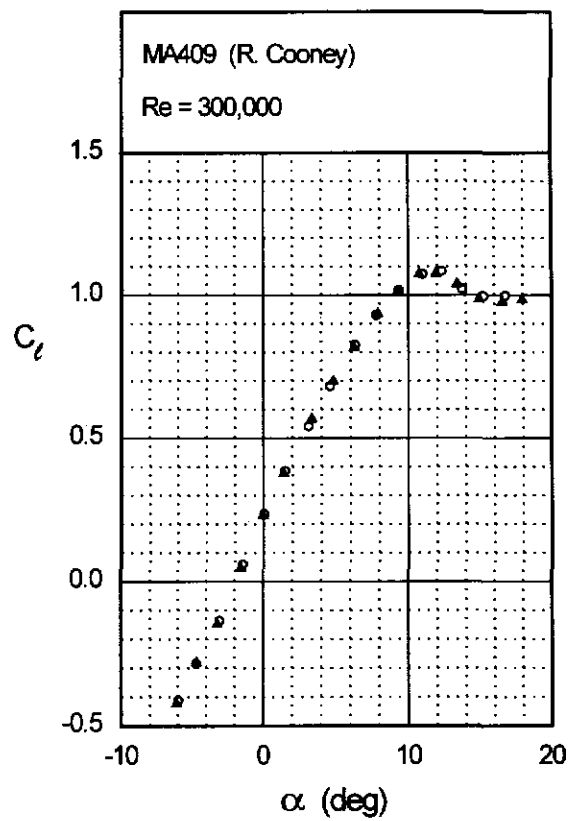
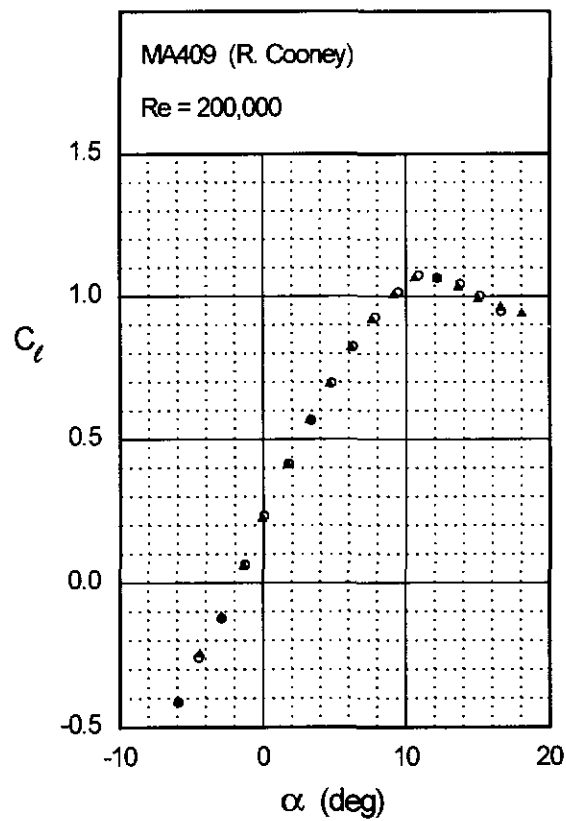
Chapter 4: Airfoil Profiles and Performance Plots

129

MA409



MA409



MB253515

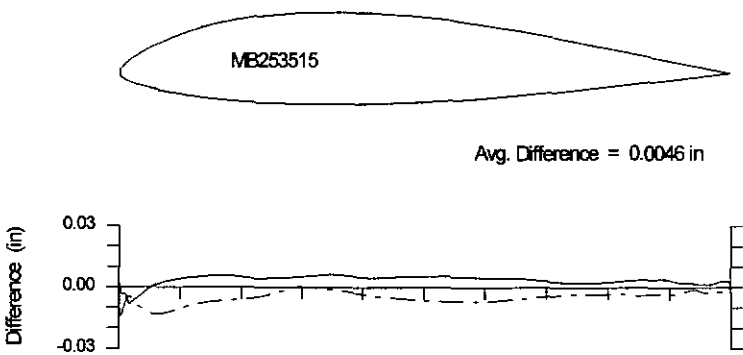
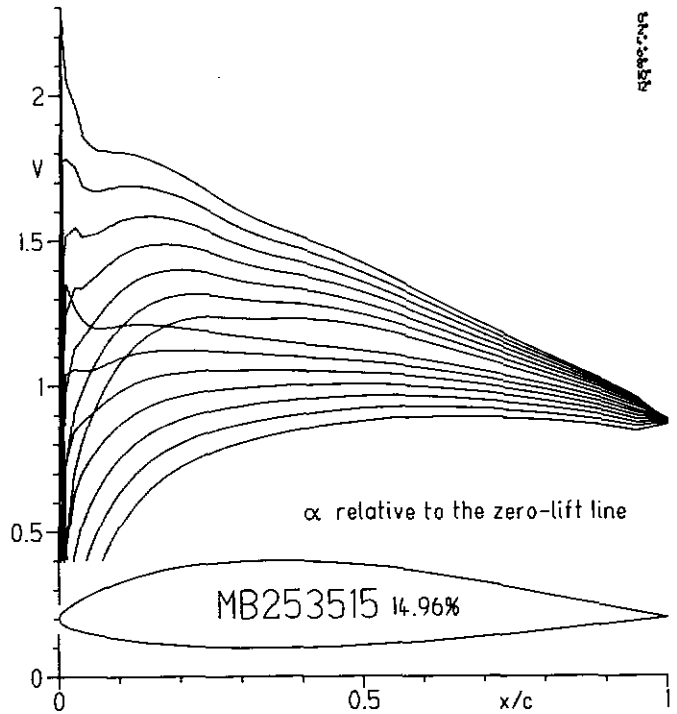
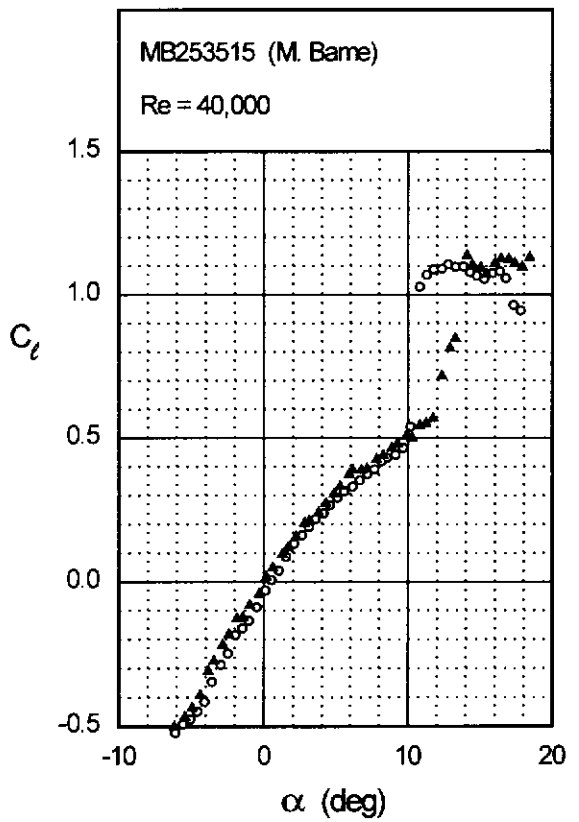
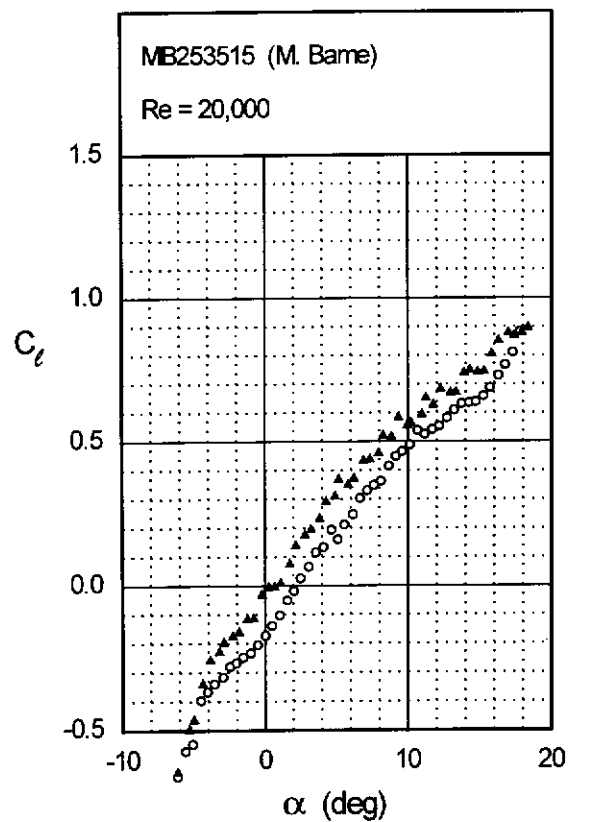


Fig. 4.57

Chapter 4: Airfoil Profiles and Performance Plots 133

MB253515



MB253515

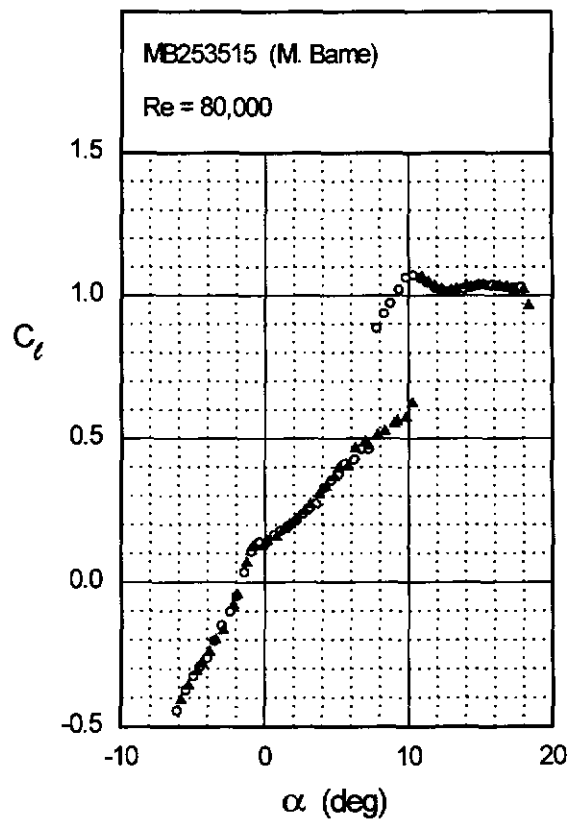
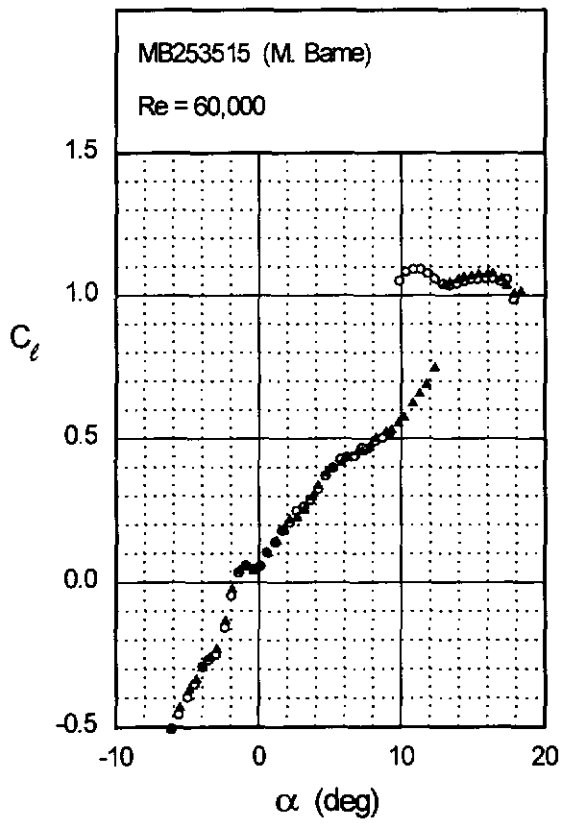
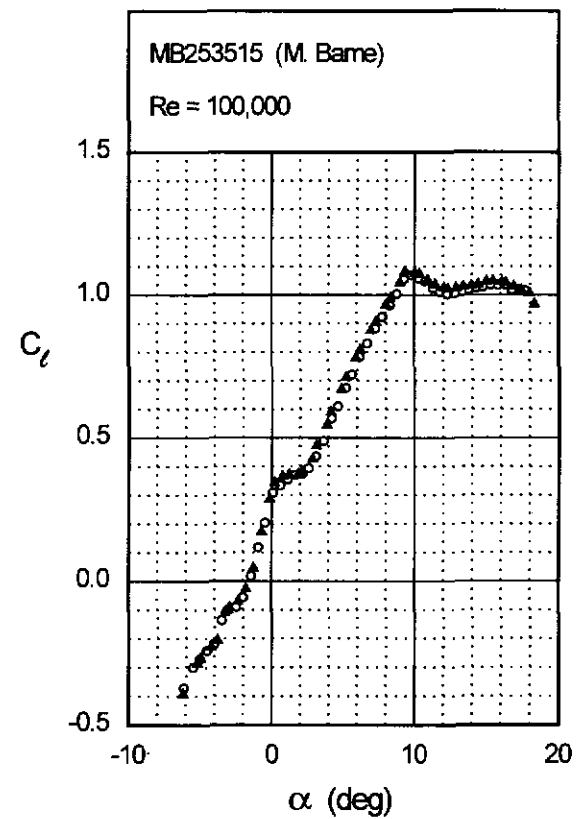


Fig. 4.57 (continued)

Chapter 4: Airfoil Profiles and Performance Plots 135

MB253515



MH45

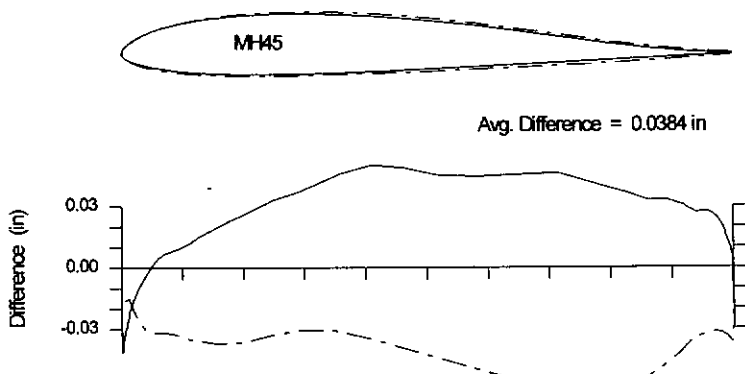
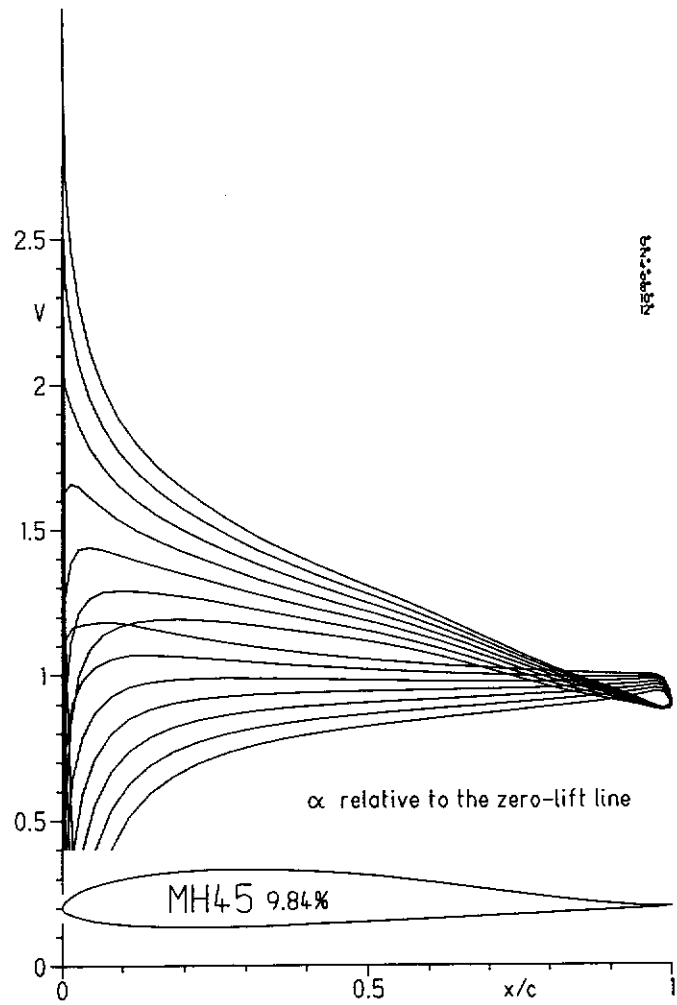
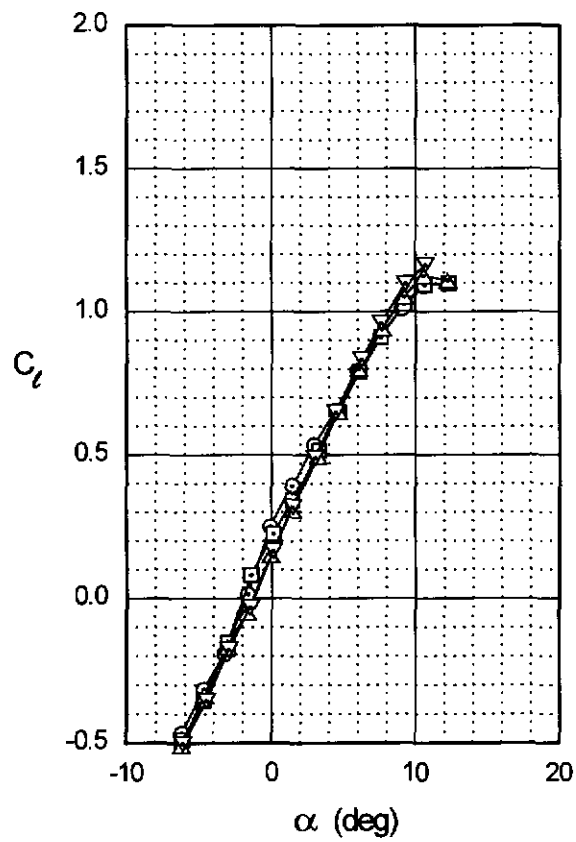
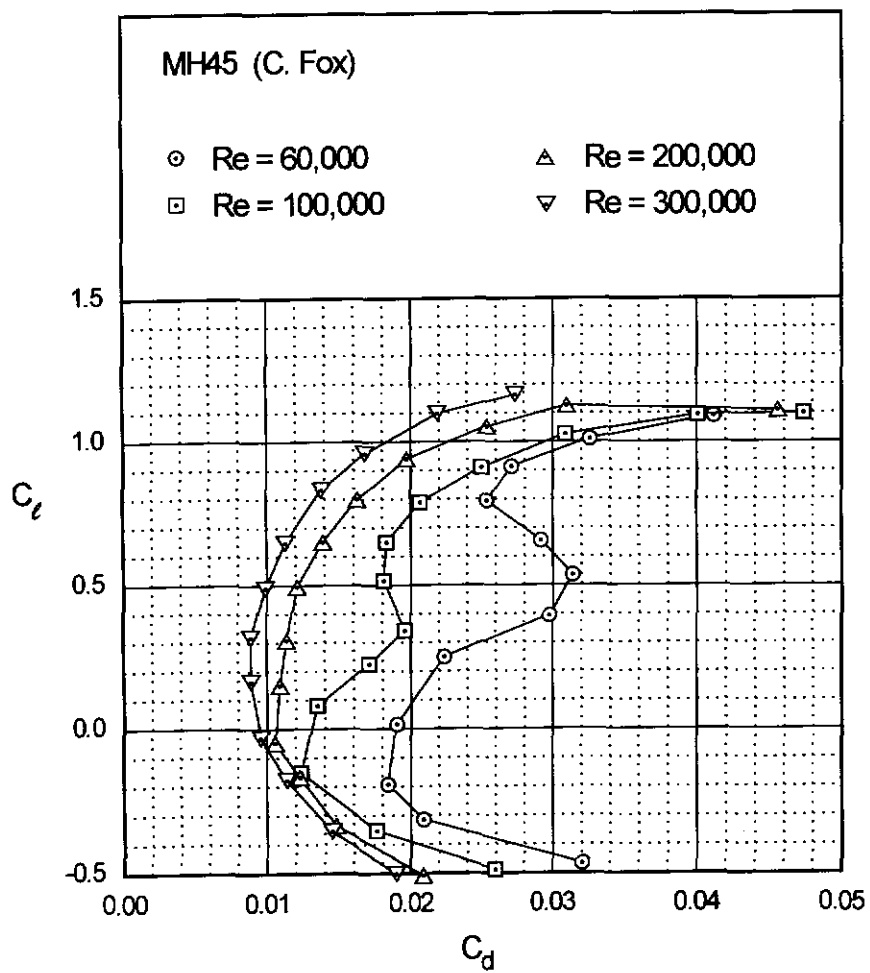


Fig. 4.60

Chapter 4: Airfoil Profiles and Performance Plots 137

MH45



MH45

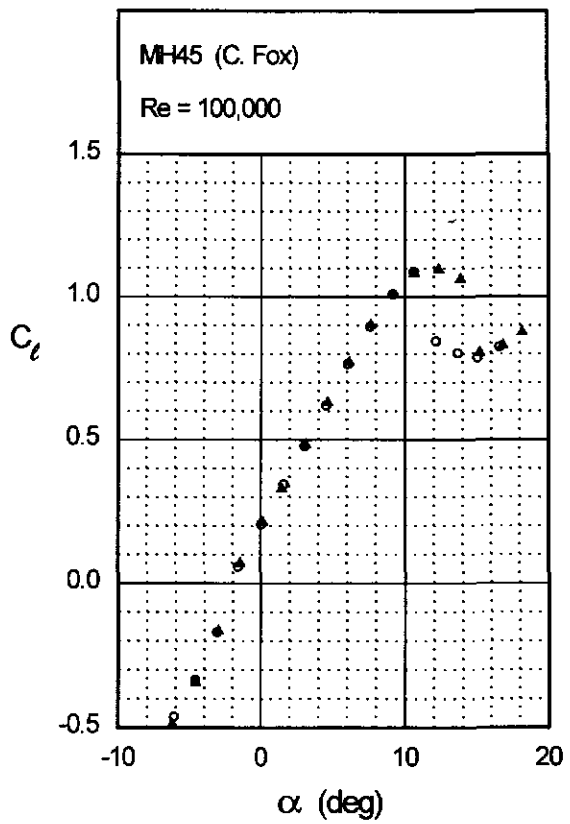
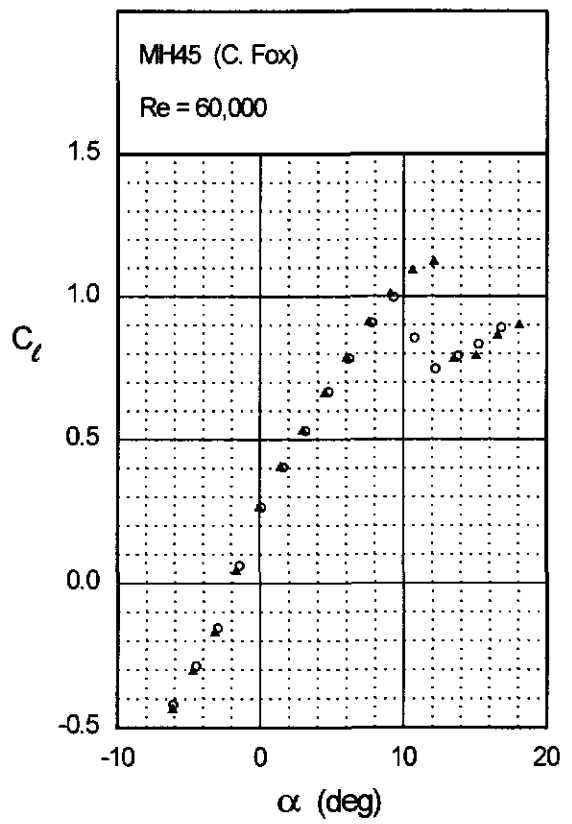
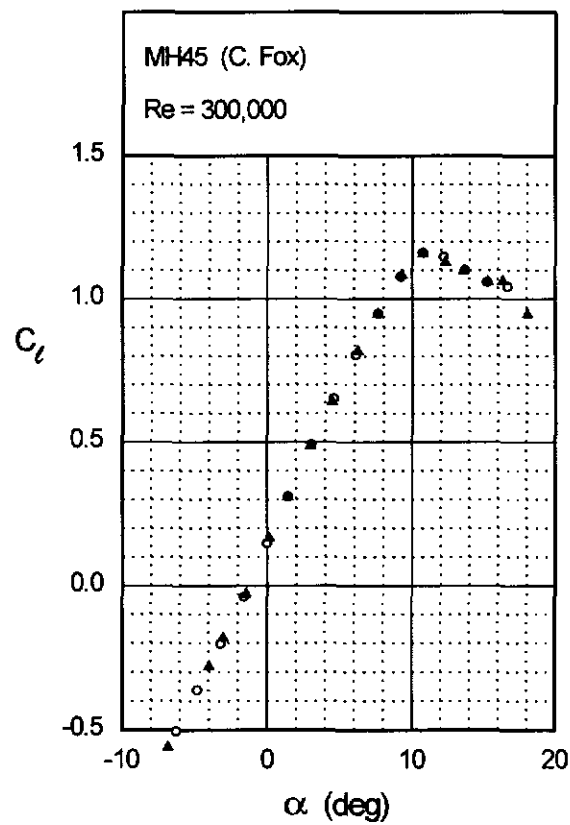
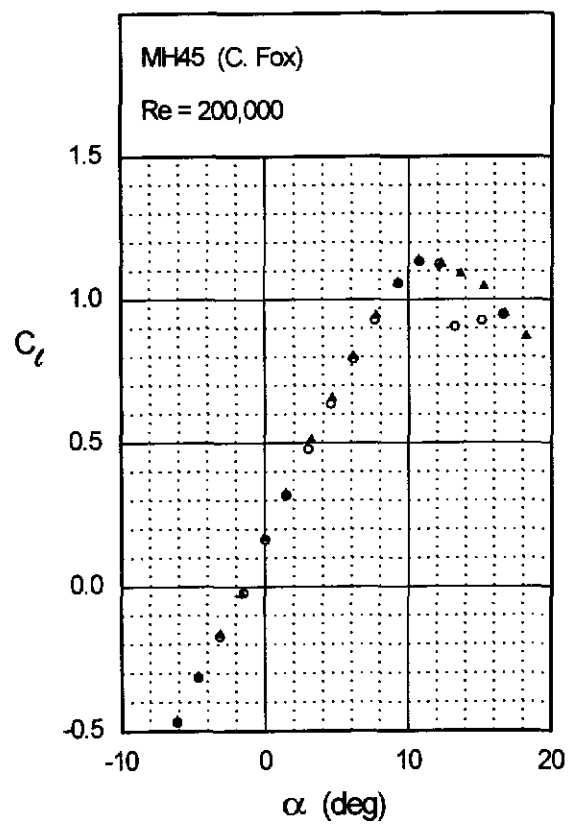


Fig. 4.61 (continued)

Chapter 4: Airfoil Profiles and Performance Plots 139

MH45



NACA 0009

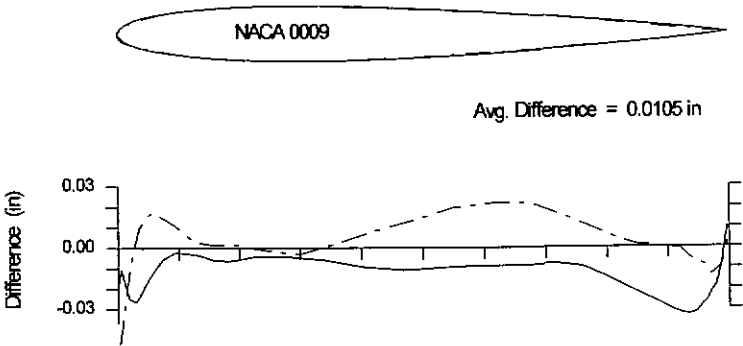
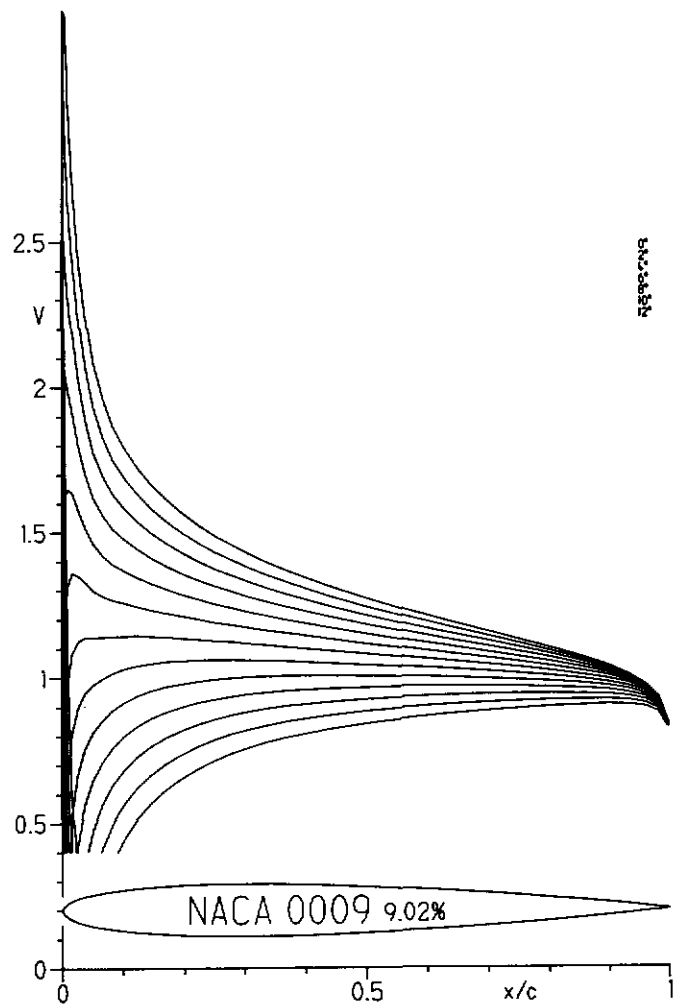


Fig. 4.64

Chapter 4: Airfoil Profiles and Performance Plots 141

NACA 0009

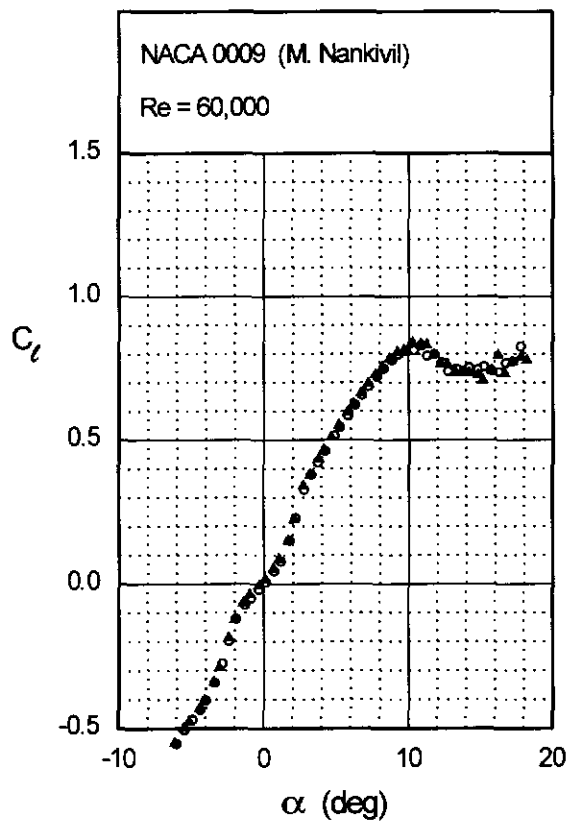
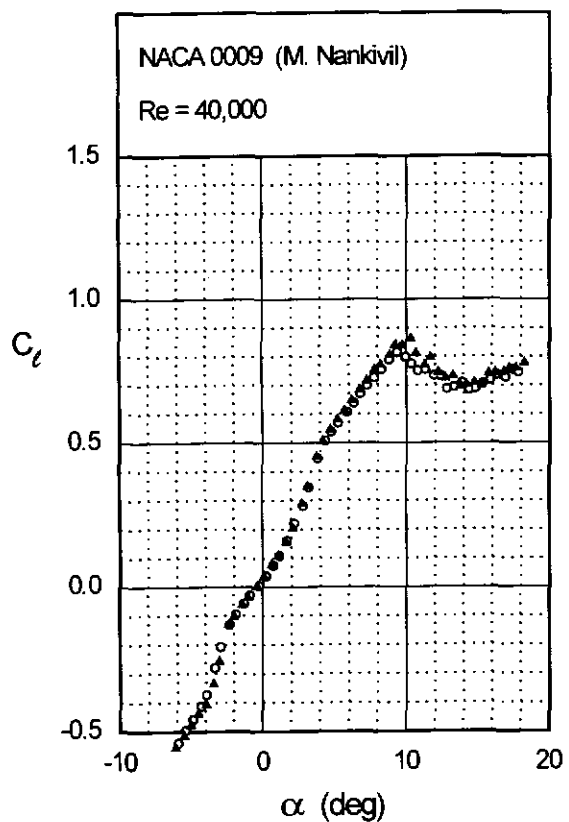
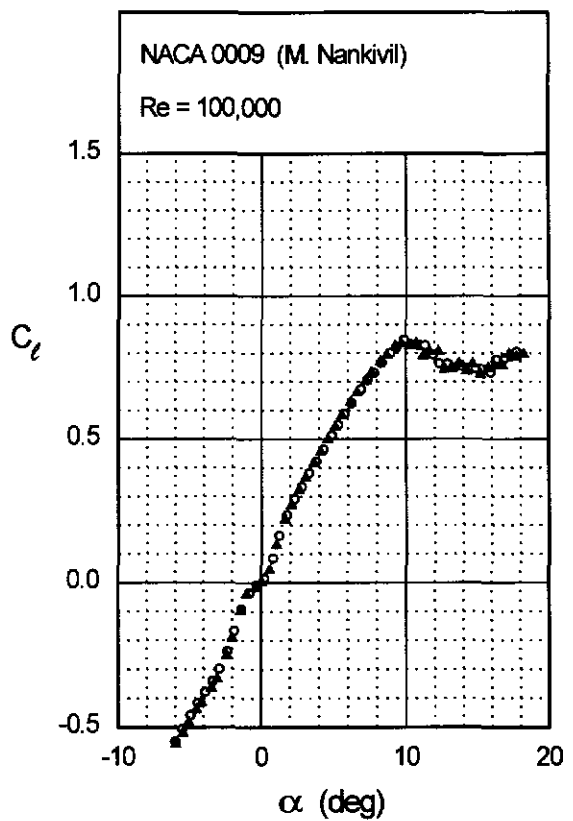
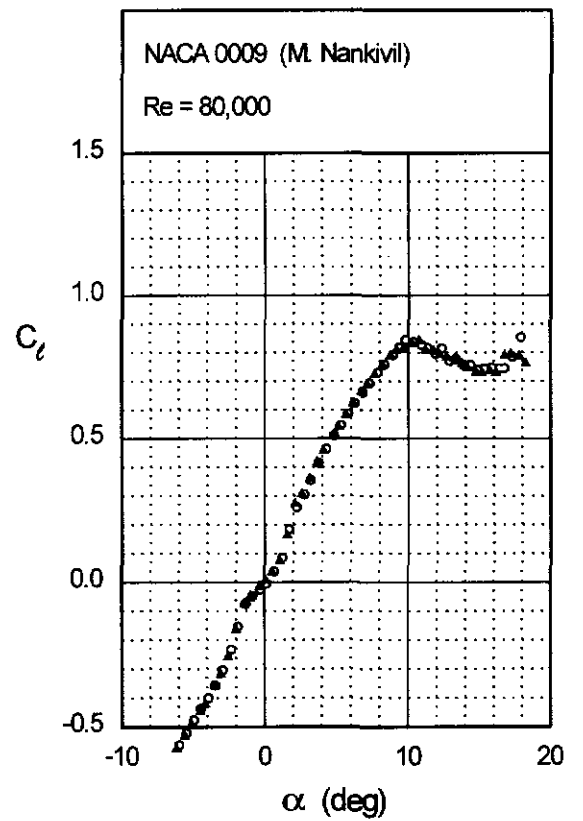


Fig. 4.64 (continued)

NACA 0009



NACA 6409

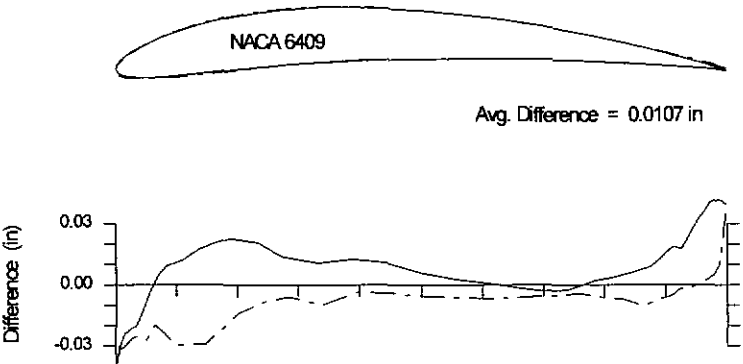
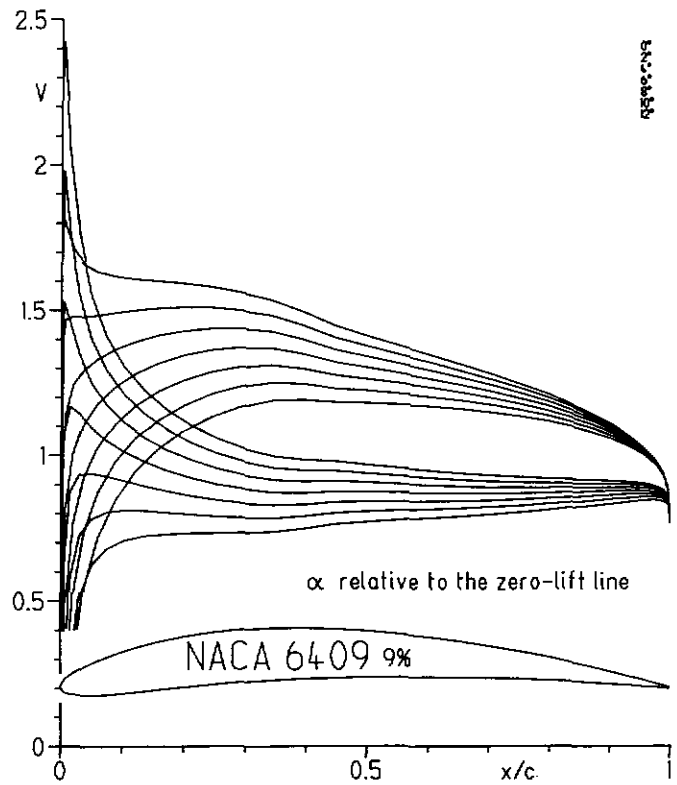
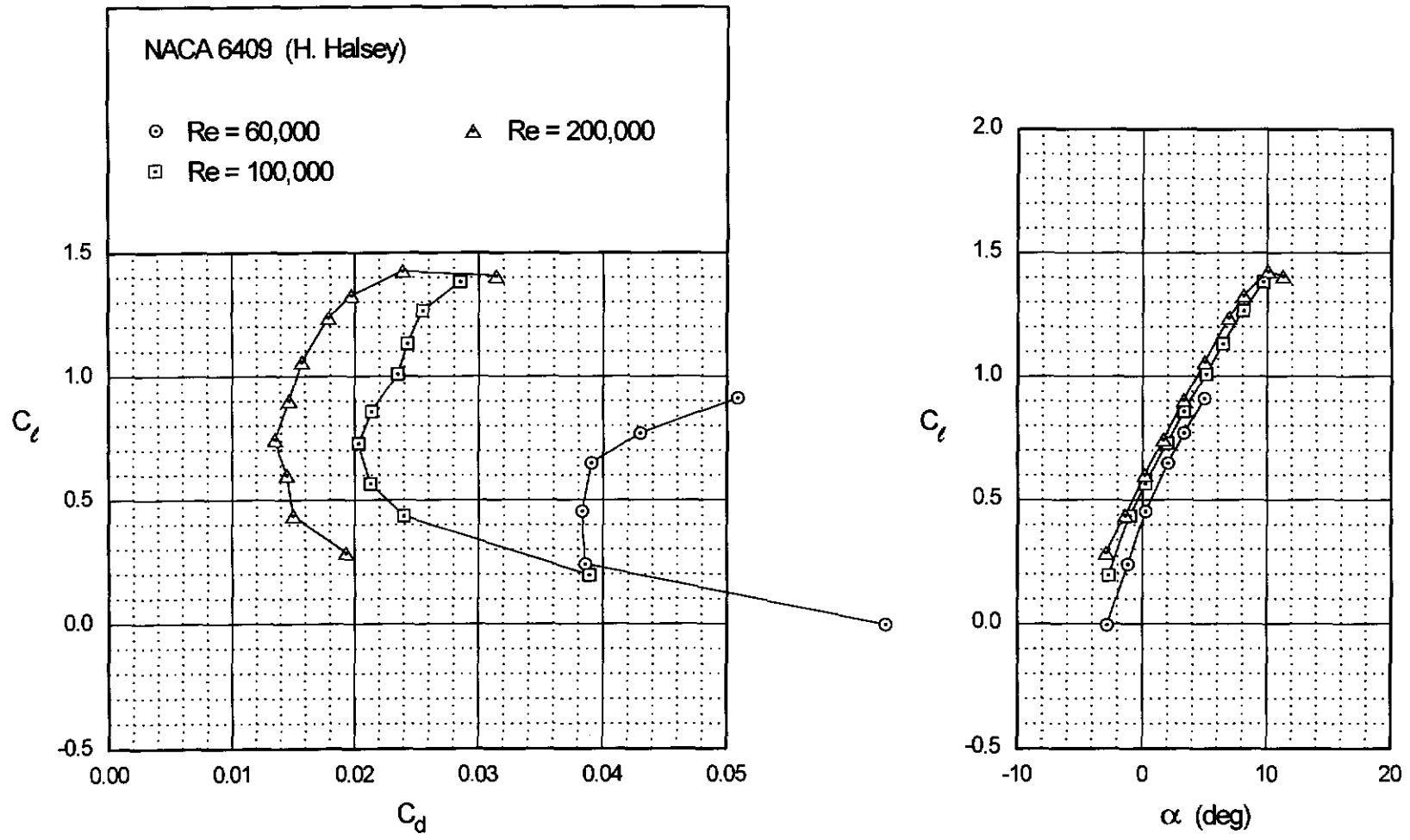


Fig. 4.67

Chapter 4: Airfoil Profiles and Performance Plots

145

NACA 6409



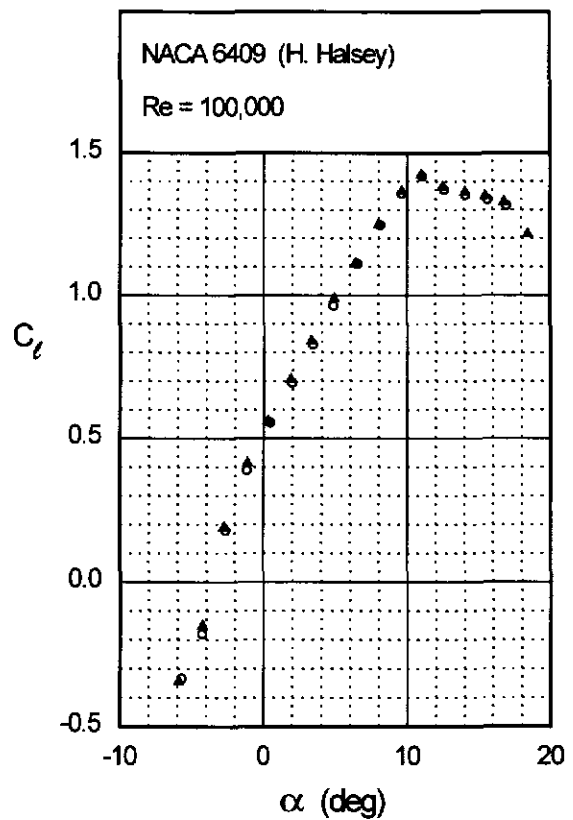
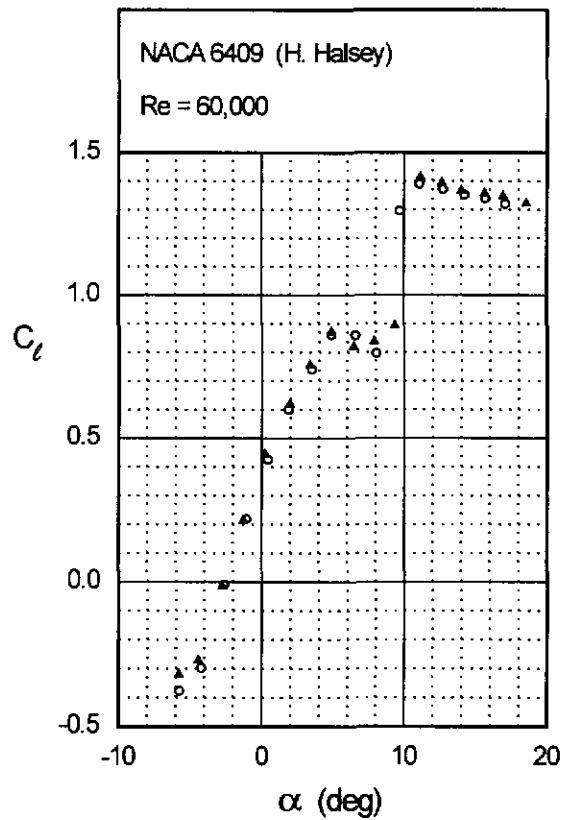
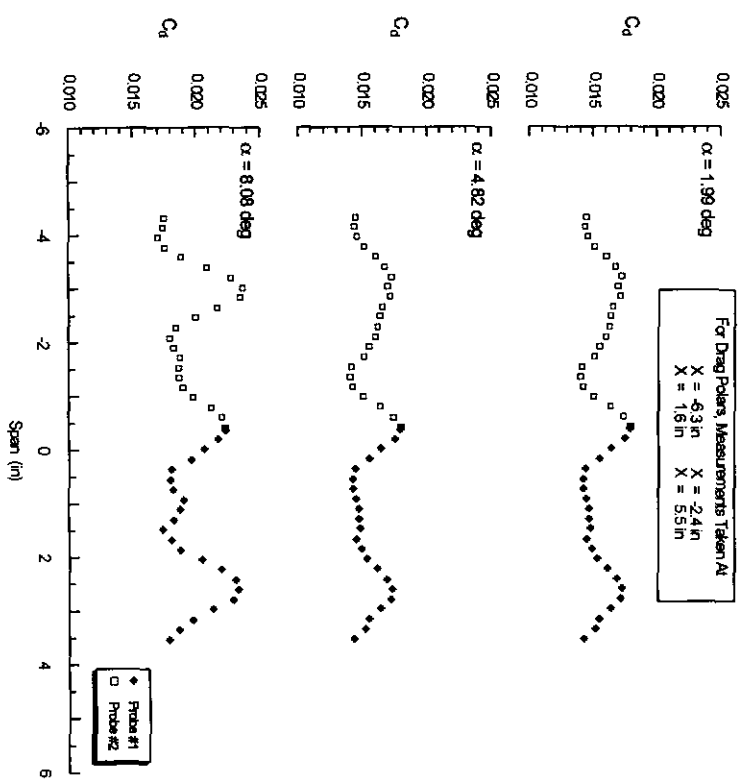
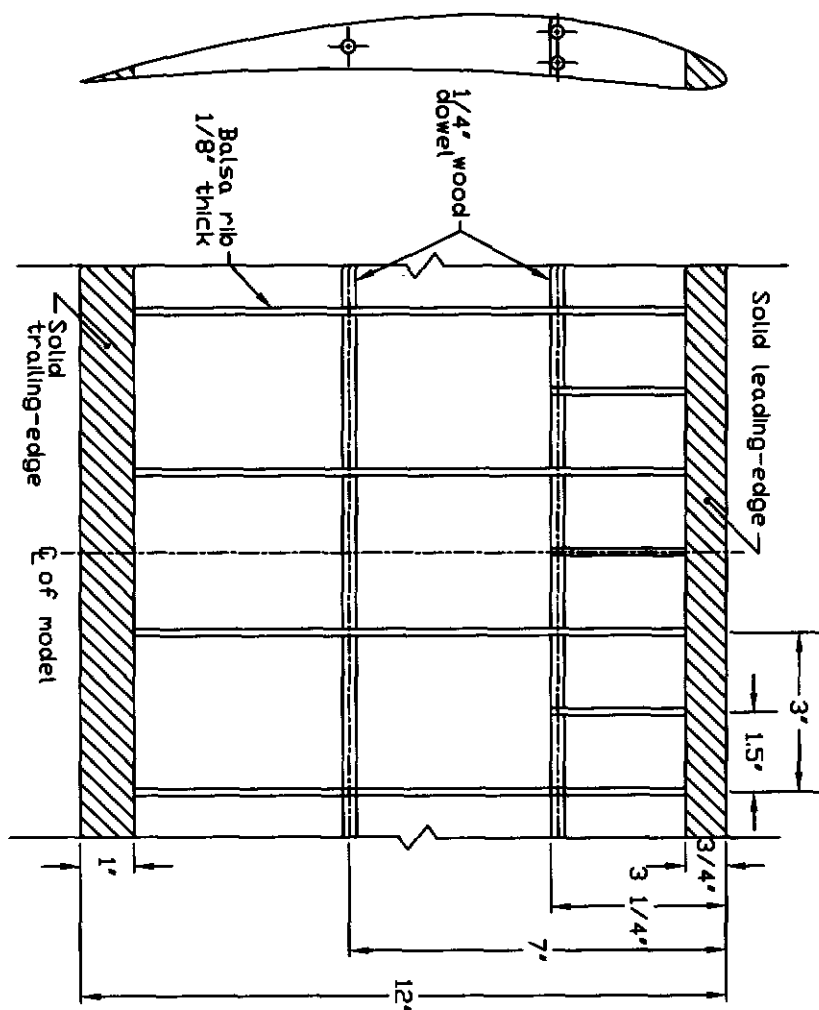


Fig. 4.68

Fig. 4.69

Chapter 4: Airfoil Profiles and Performance Plots 147

NACA 6409



NACA 64A010

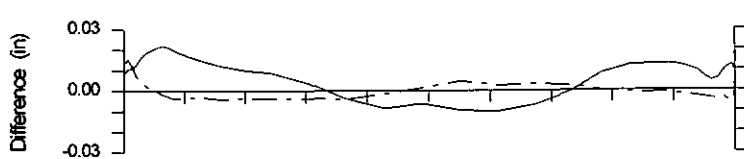
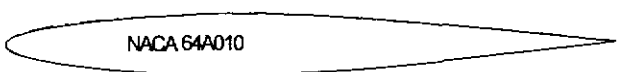
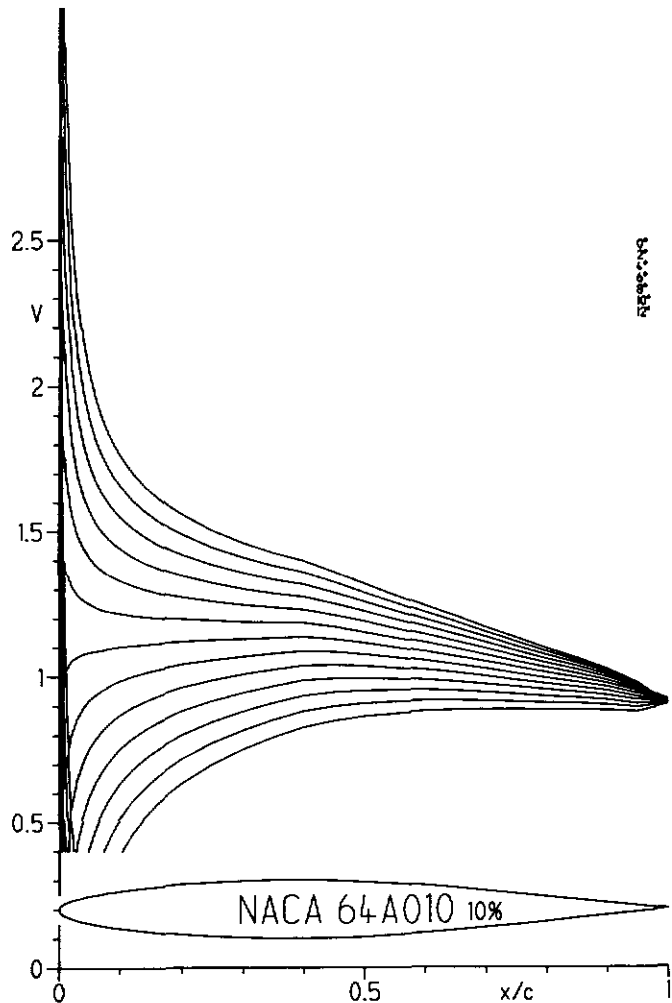
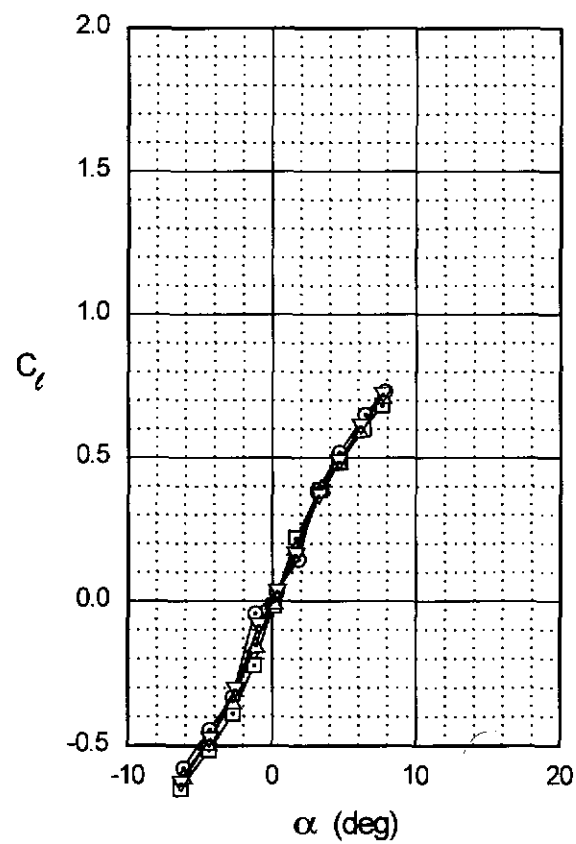
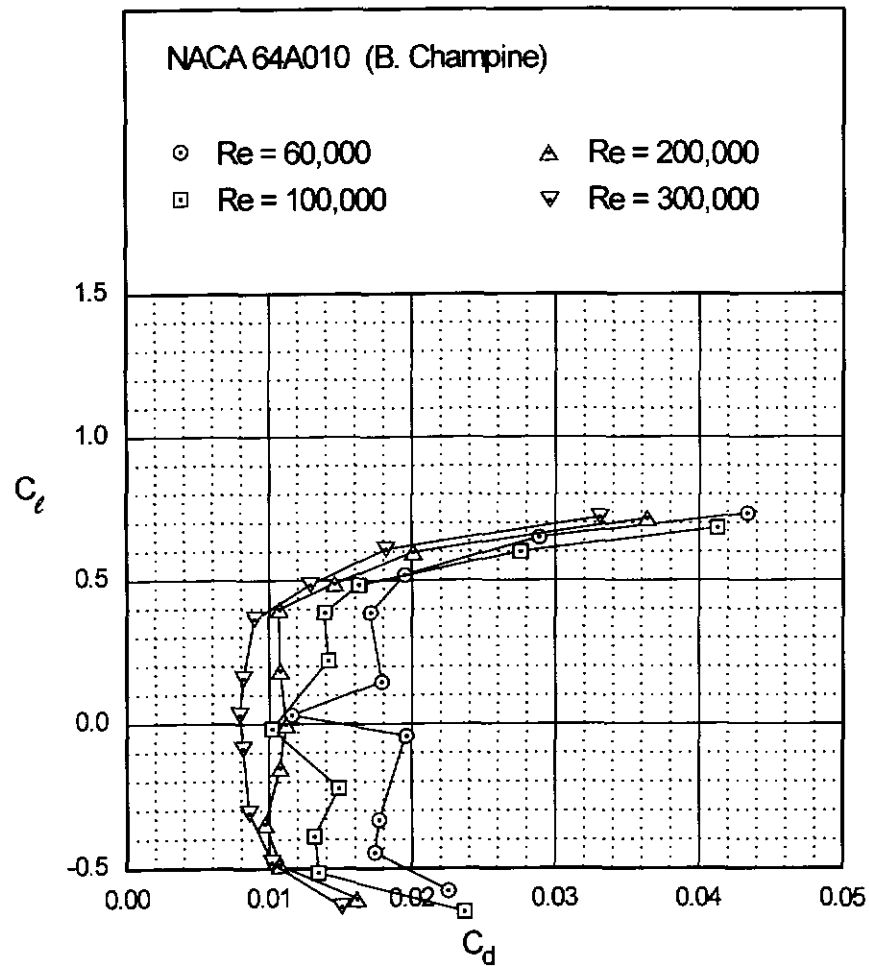


Fig. 4.72

Chapter 4: Airfoil Profiles and Performance Plots 149



NACA 64A010

NACA 64A010

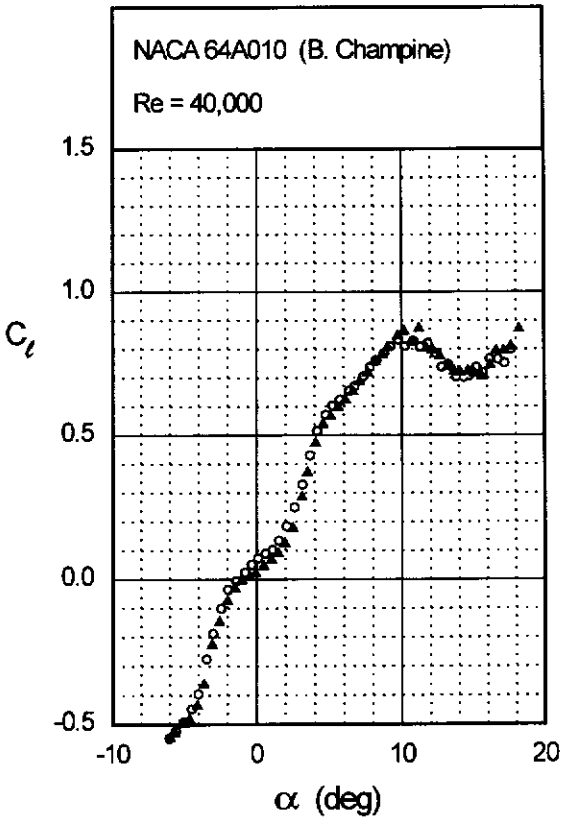
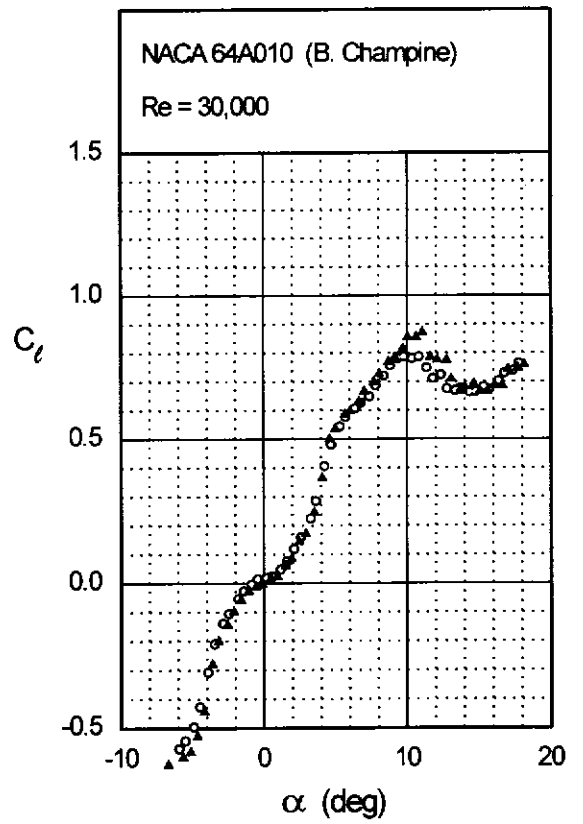
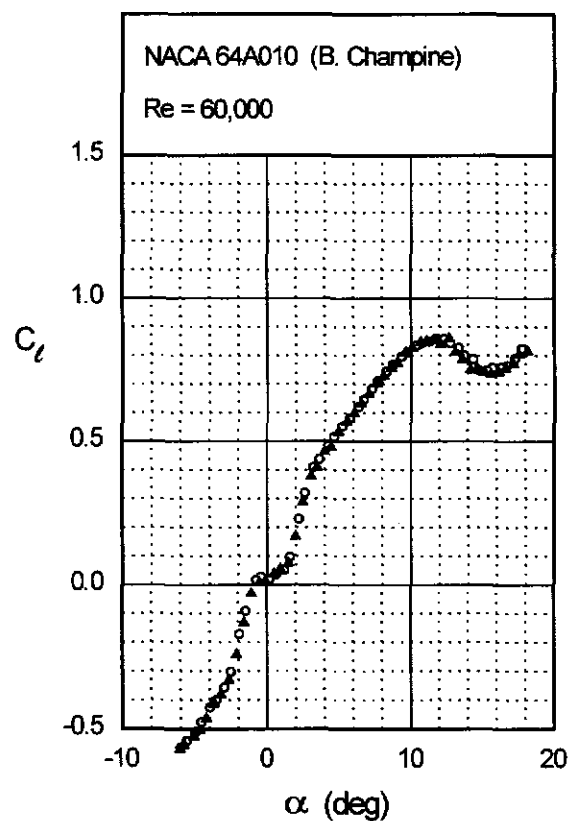
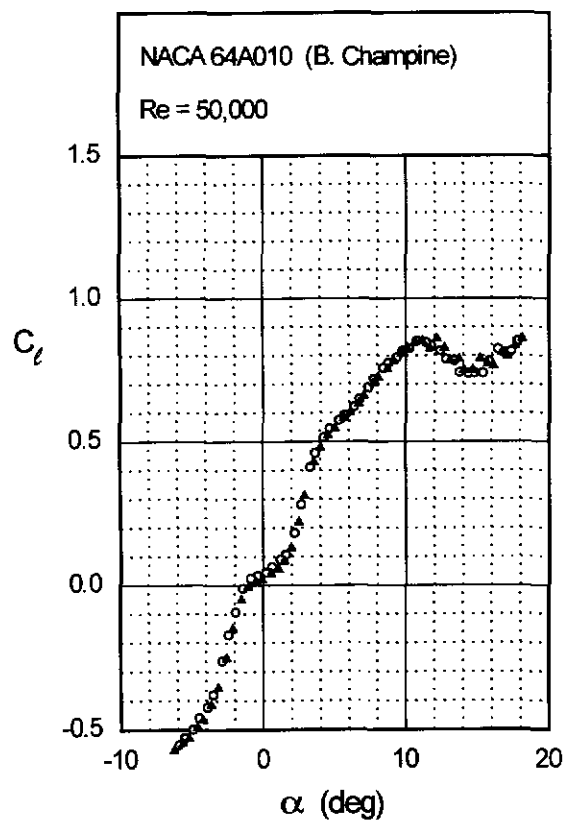


Fig. 4.73 (continued)

Chapter 4: Airfoil Profiles and Performance Plots 151

NACA 64A010



NACA 64A010

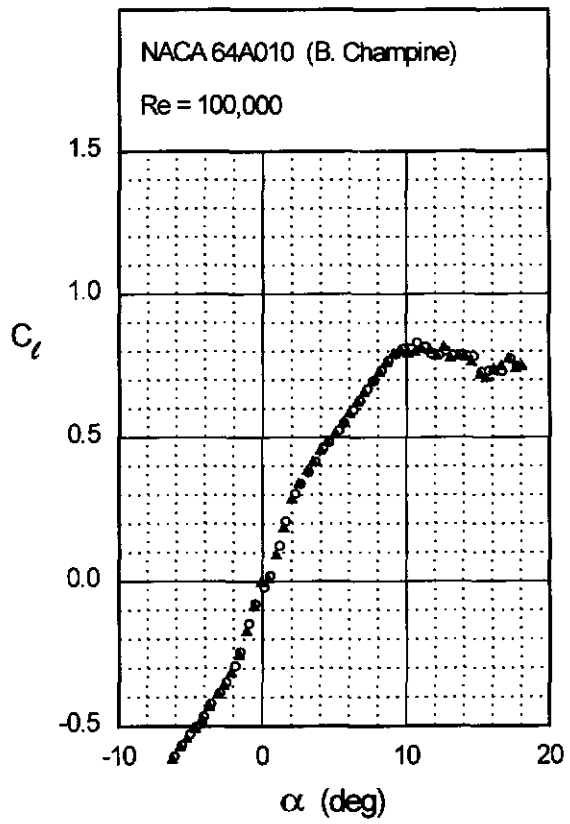
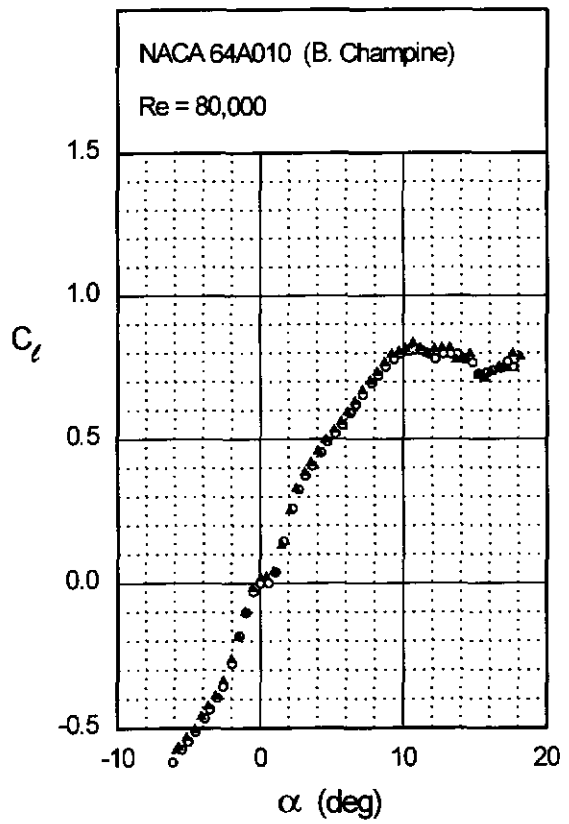
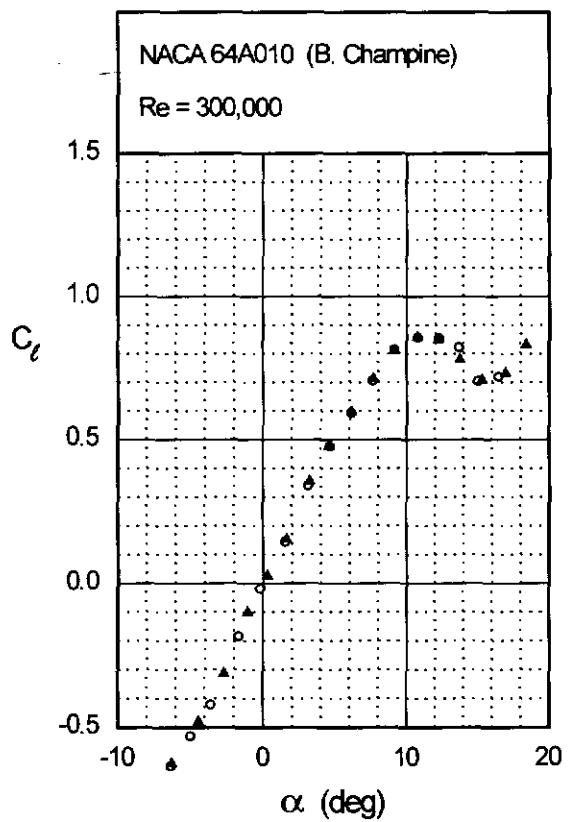
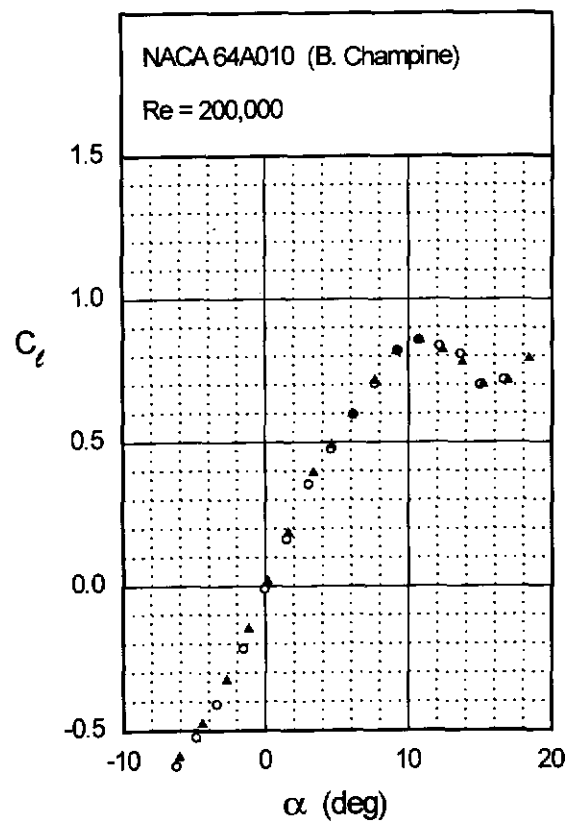


Fig. 4.73 (continued)

Chapter 4: Airfoil Profiles and Performance Plots 153

NACA 64A010



154 Summary of Low-Speed Airfoil Data

Figs. 4.74 & 4.75

R140 (A)

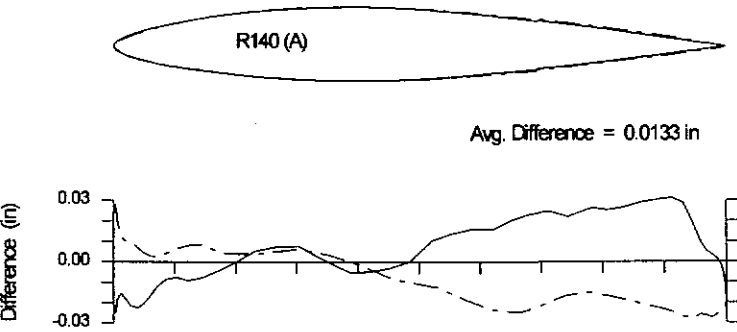
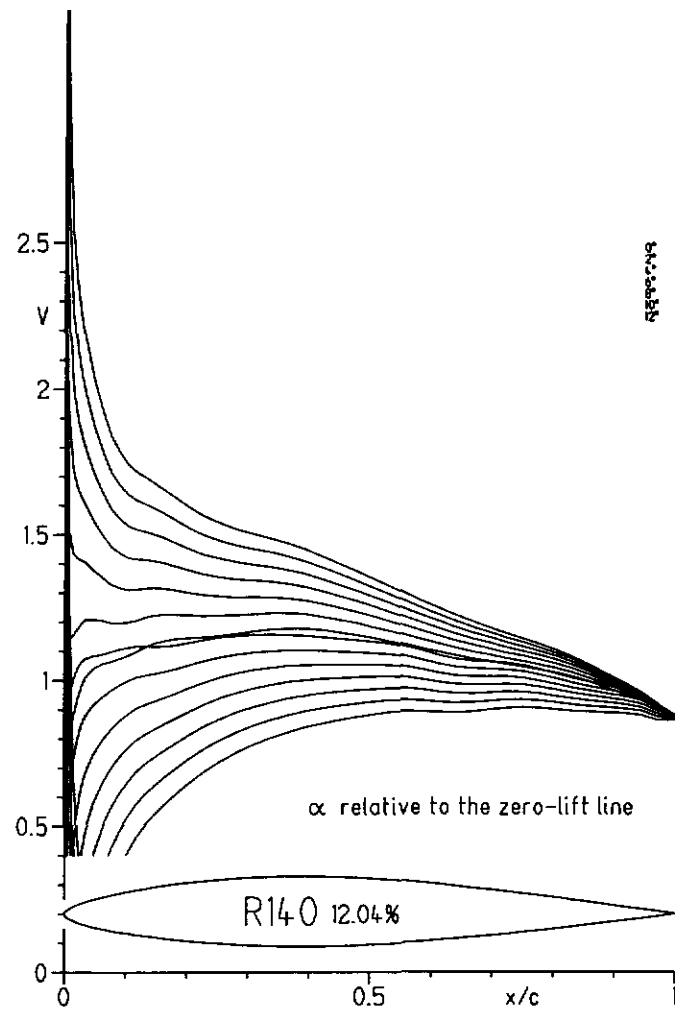
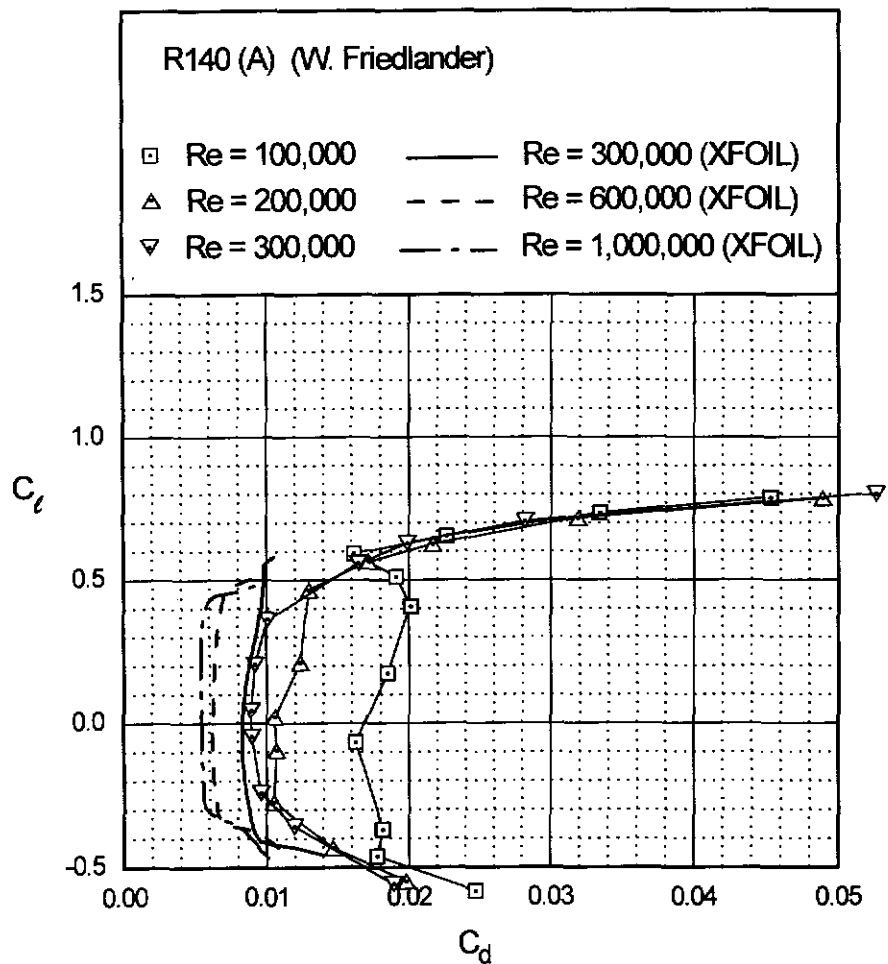
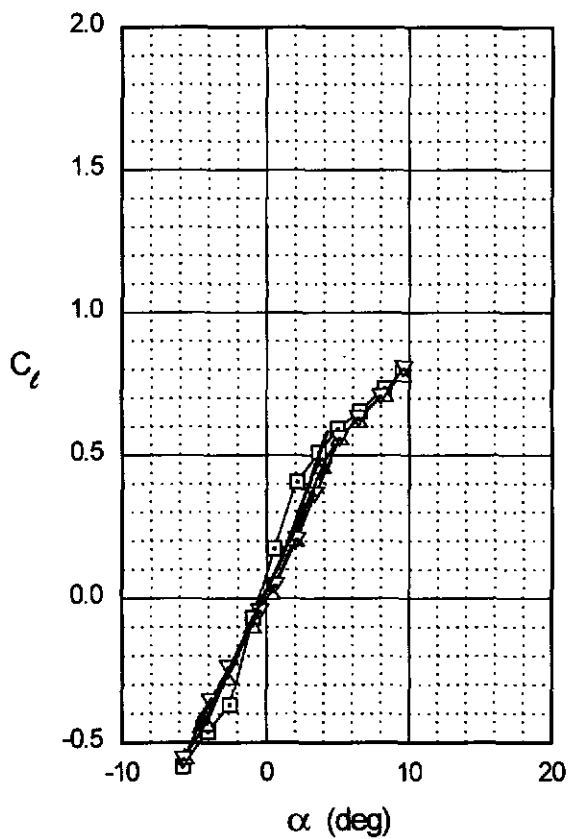


Fig. 4.76

Chapter 4: Airfoil Profiles and Performance Plots 155

R140 (A)



R140 (A)

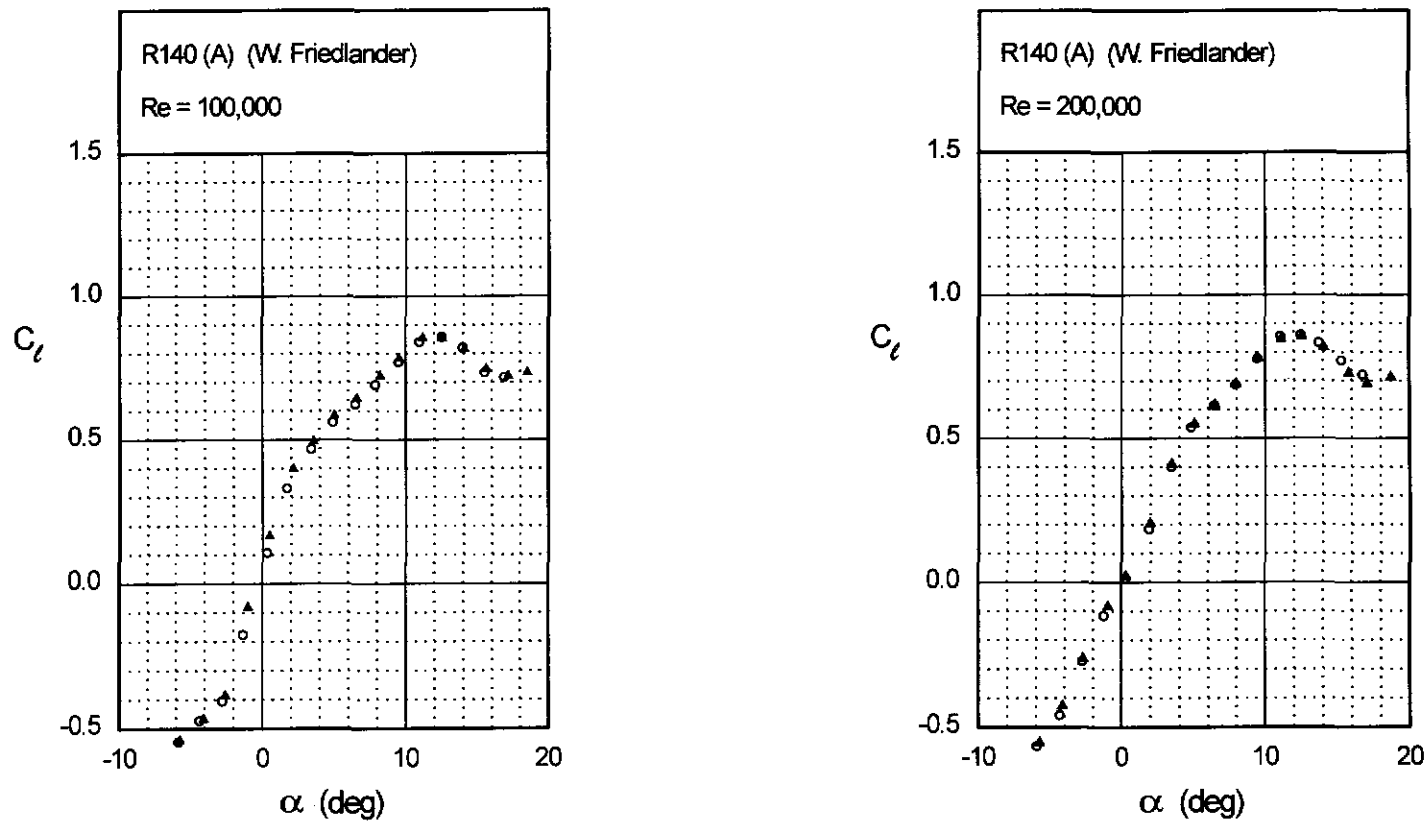
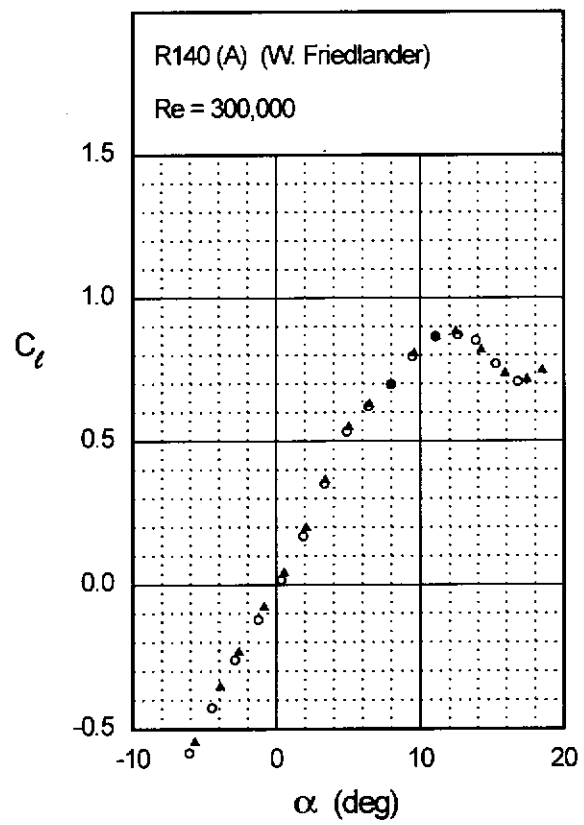


Fig. 4.77

Fig. 4.77 (continued)

Chapter 4: Airfoil Profiles and Performance Plots 157

R140 (A)



RG15 (B)

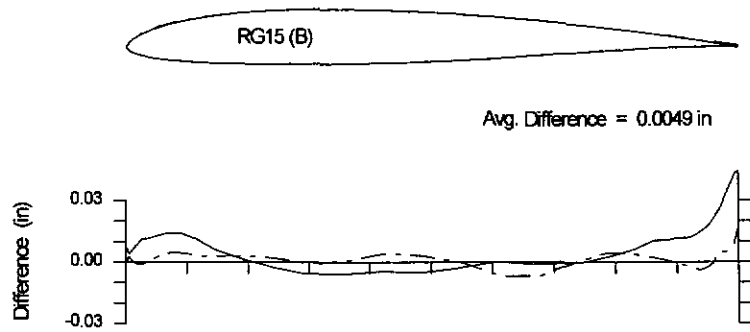
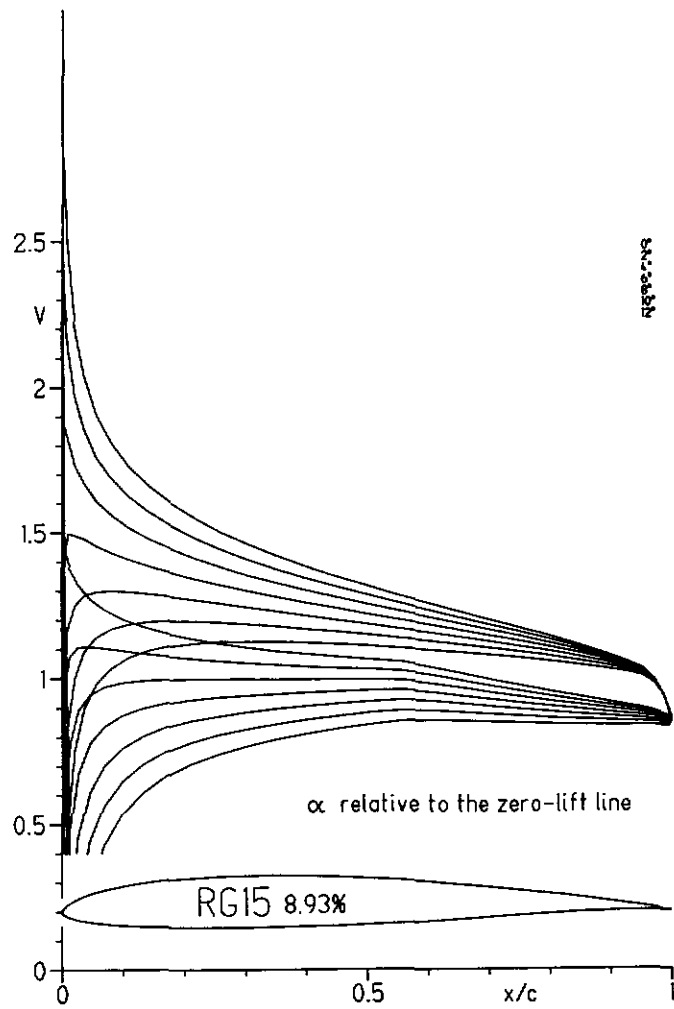
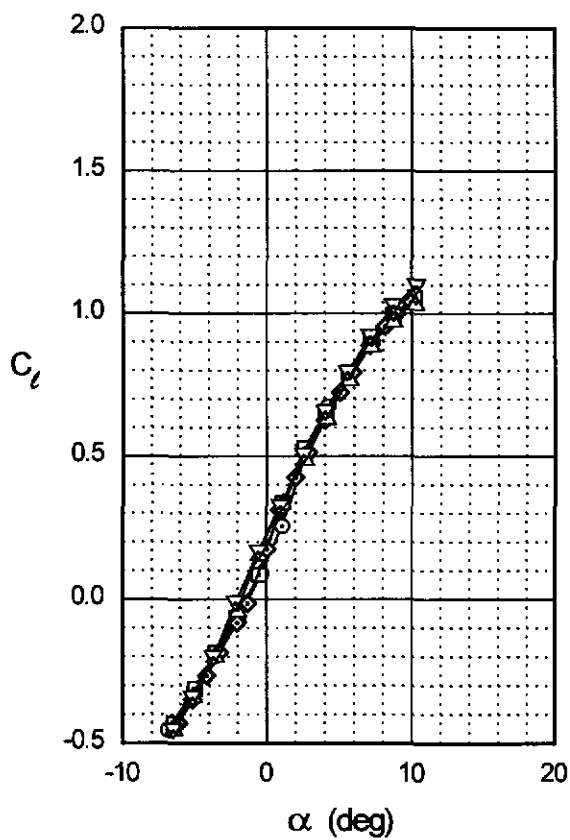
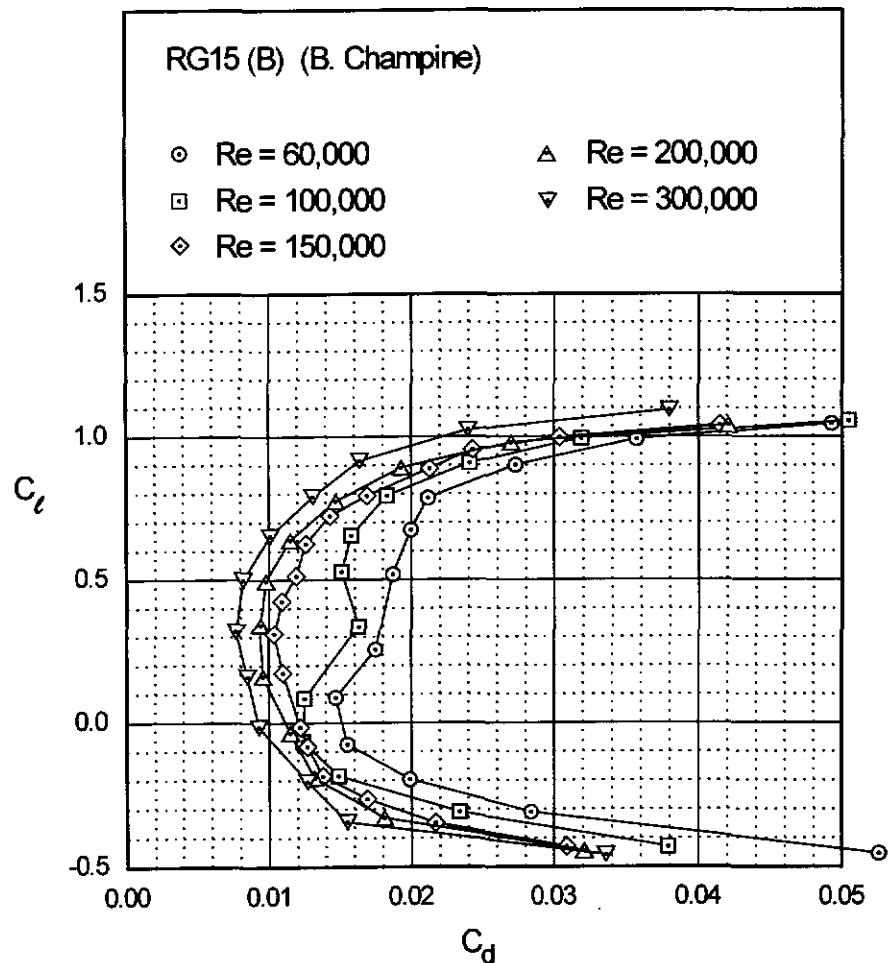


Fig. 4.80

Chapter 4: Airfoil Profiles and Performance Plots 159

RG15 (B)



RG15 (B)

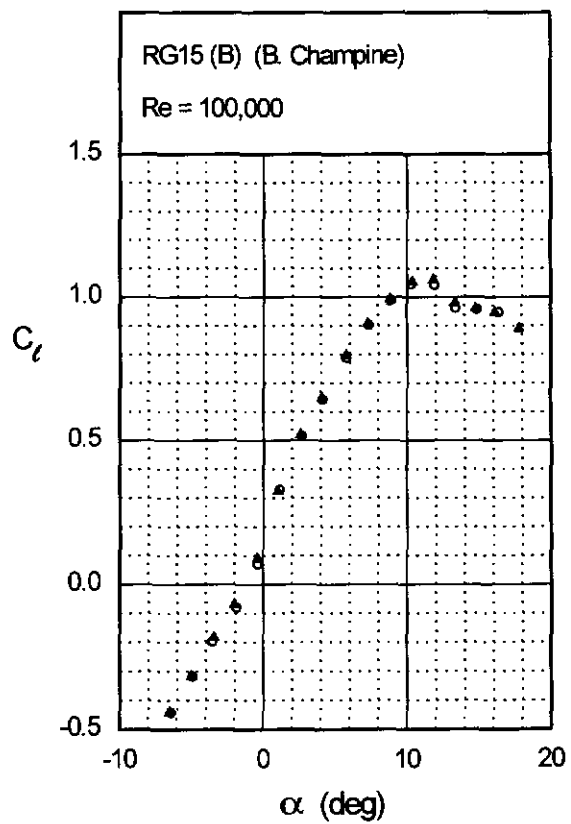
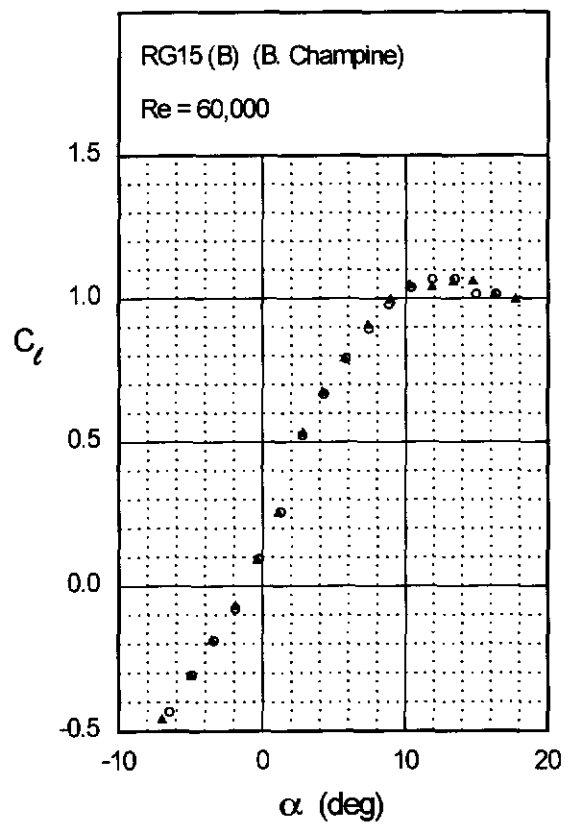
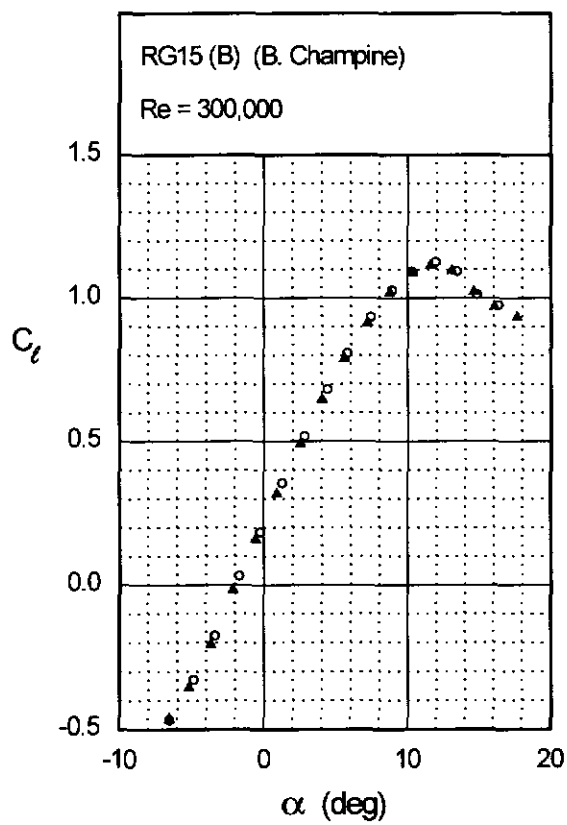
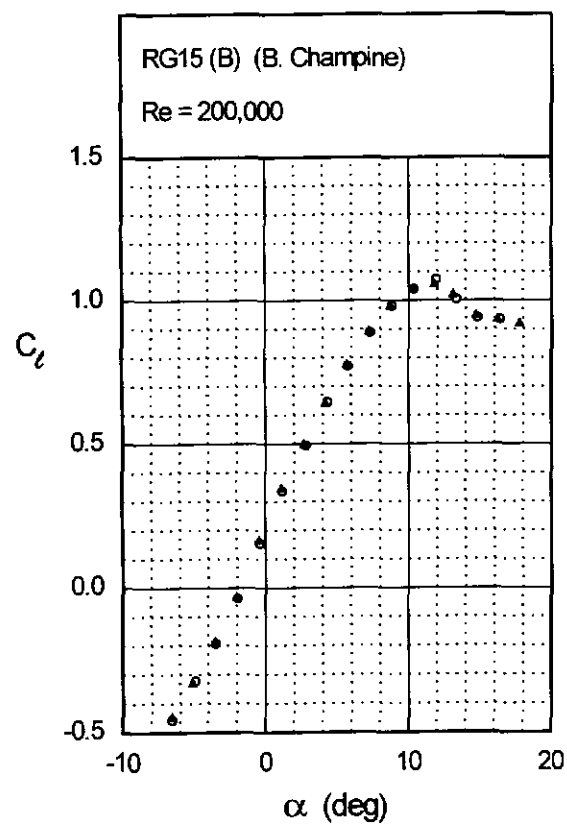


Fig. 4.81

Fig. 4.81 (continued)

Chapter 4: Airfoil Profiles and Performance Plots 161

RG15 (B)



S822

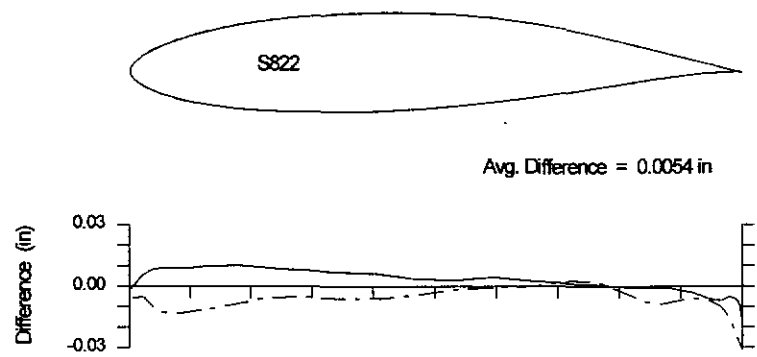
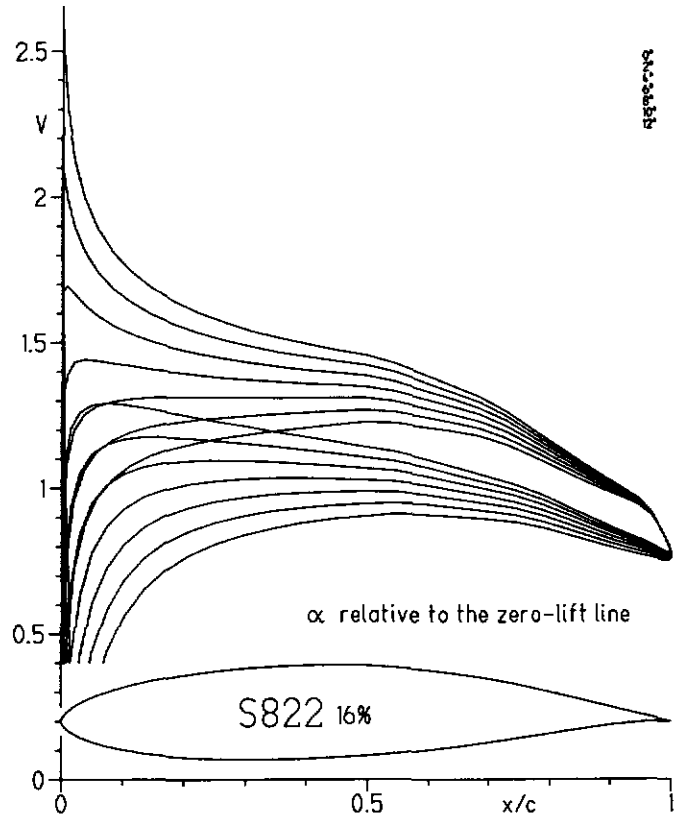
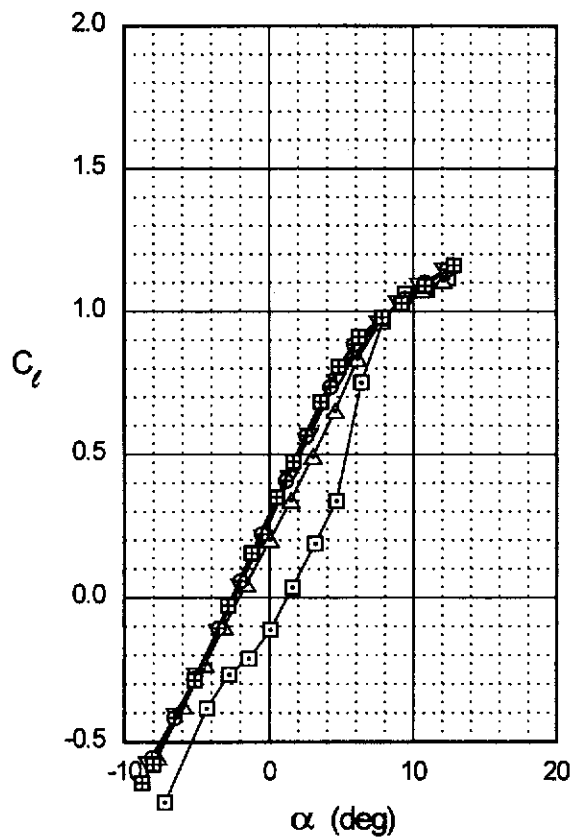
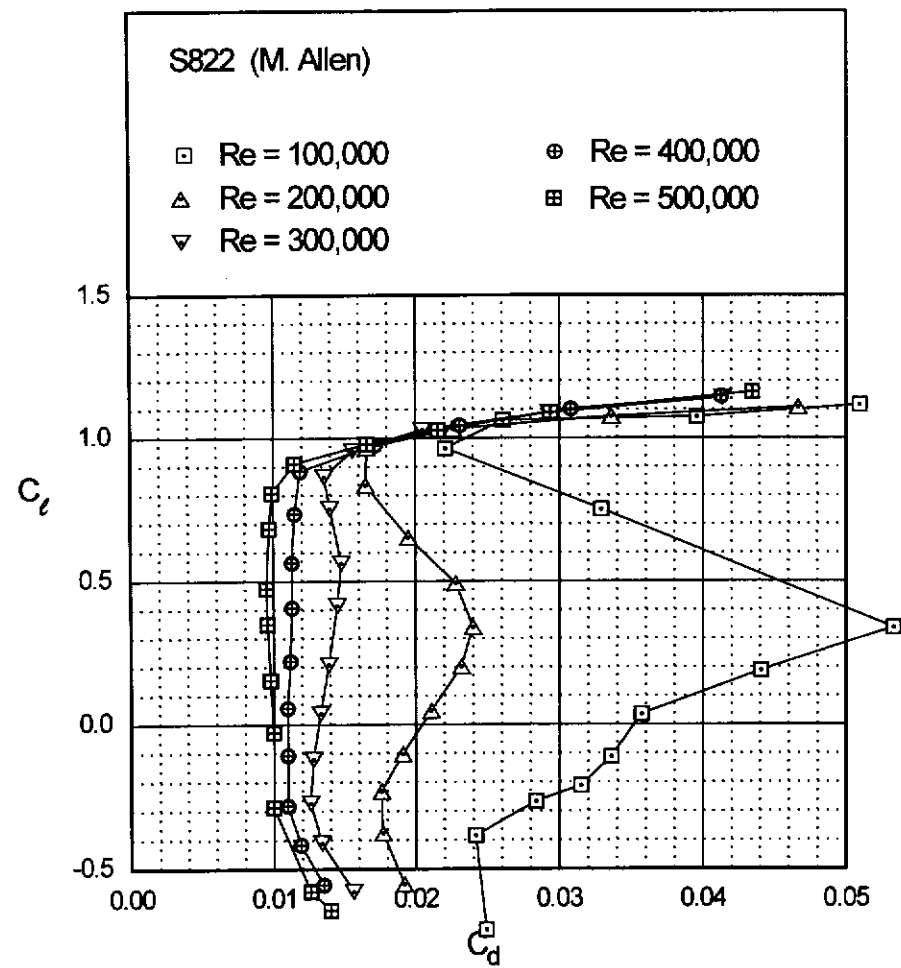


Fig. 4.84

Chapter 4: Airfoil Profiles and Performance Plots 163

S822



S822

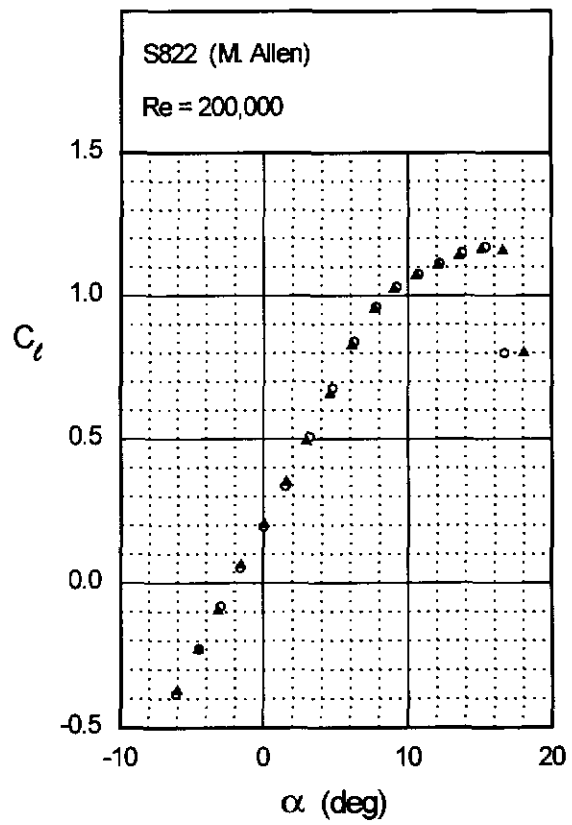
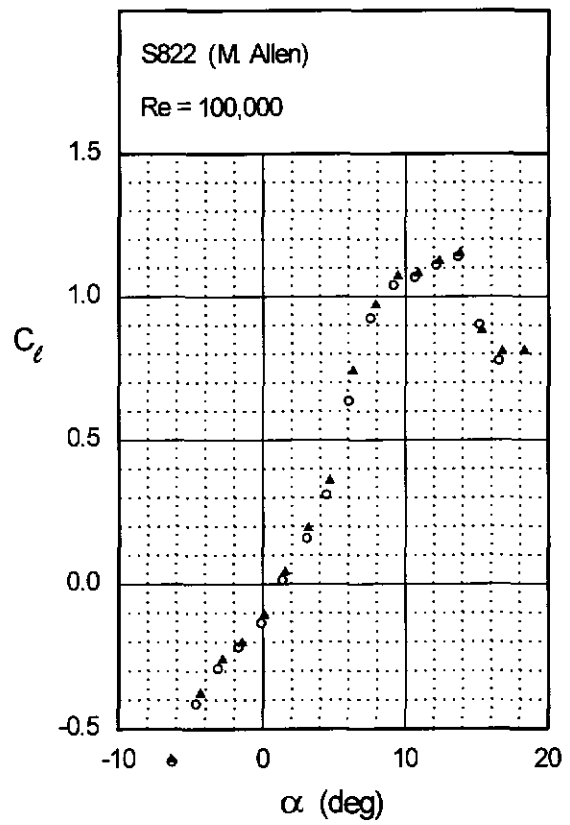
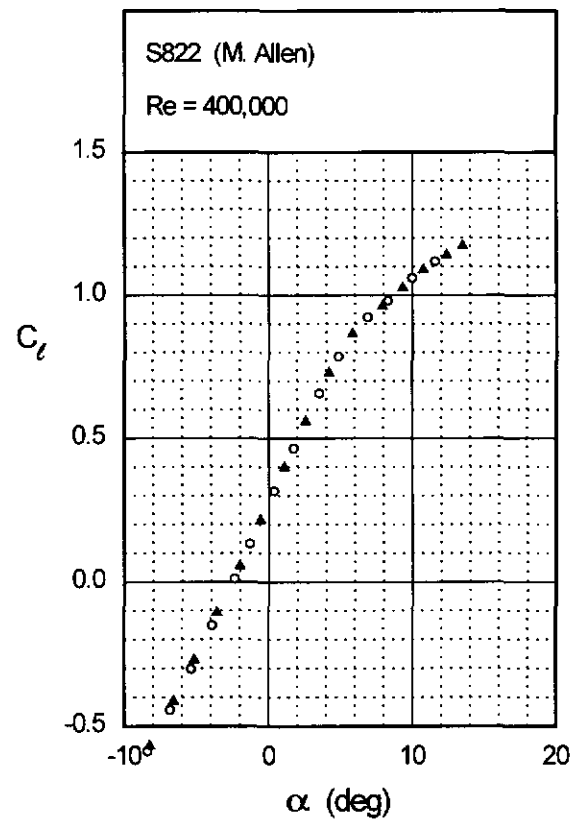
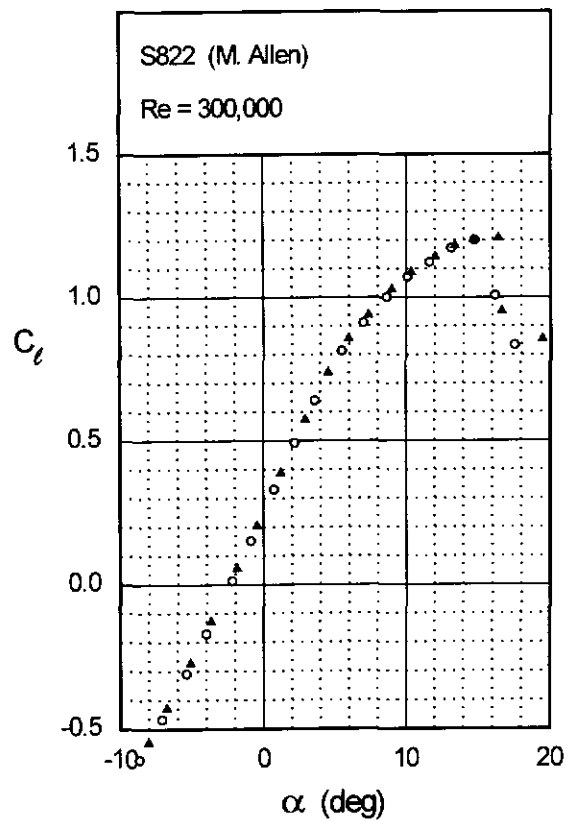


Fig. 4.85

Fig. 4.85 (continued)

Chapter 4: Airfoil Profiles and Performance Plots 165

S822



S823

Figs. 4.86 & 4.87

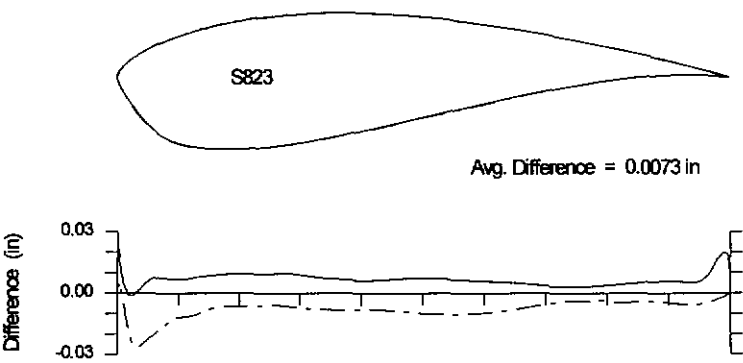
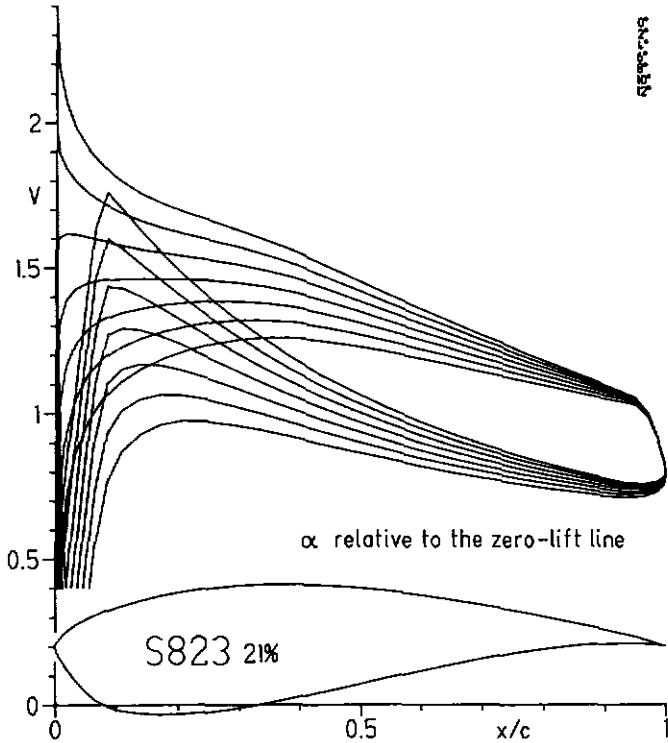
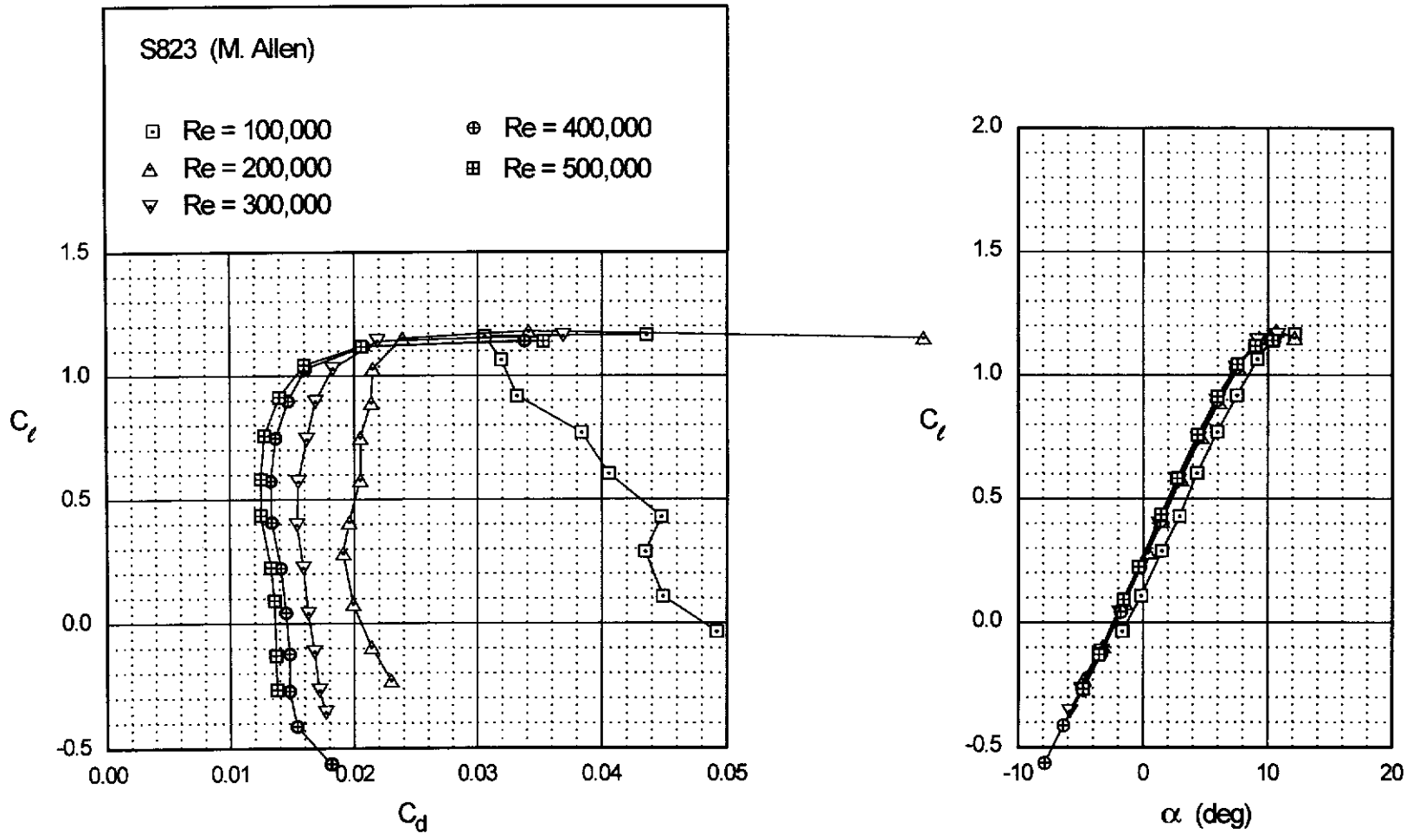


Fig. 4.88

Chapter 4: Airfoil Profiles and Performance Plots

167



S823

S823

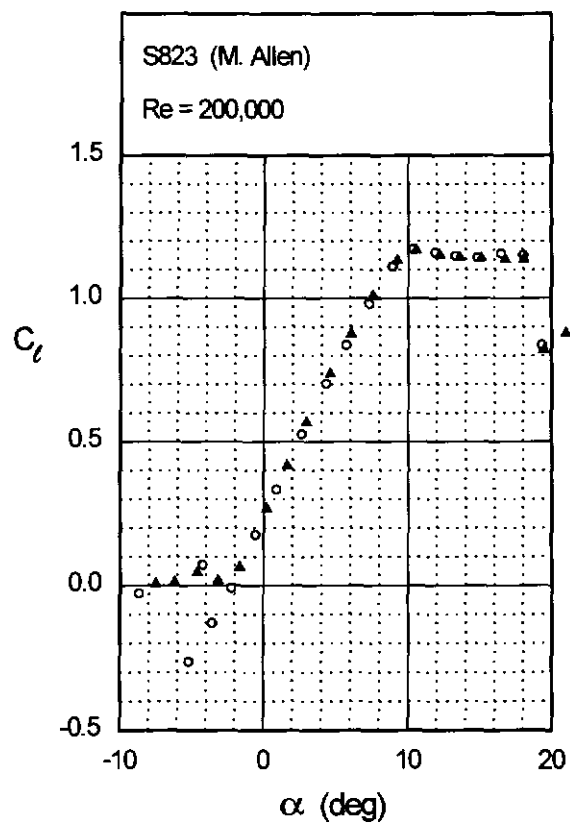
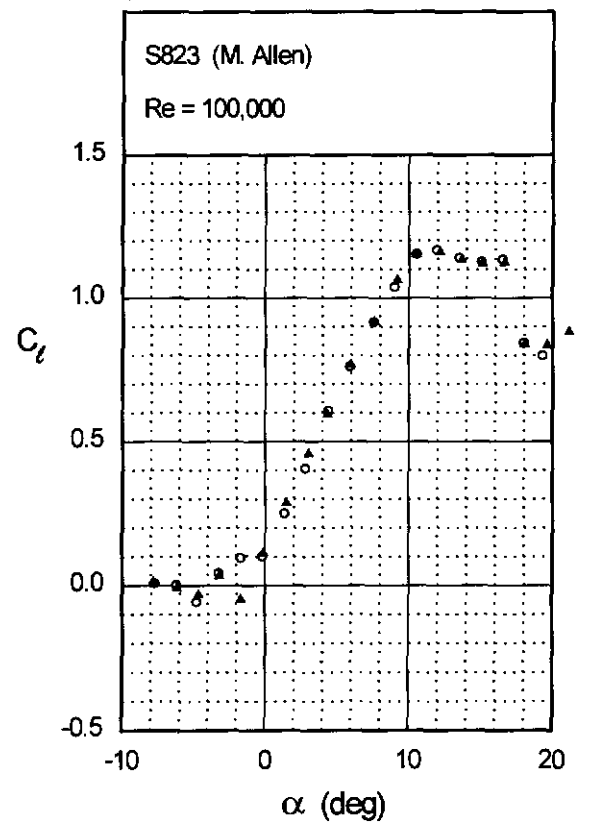
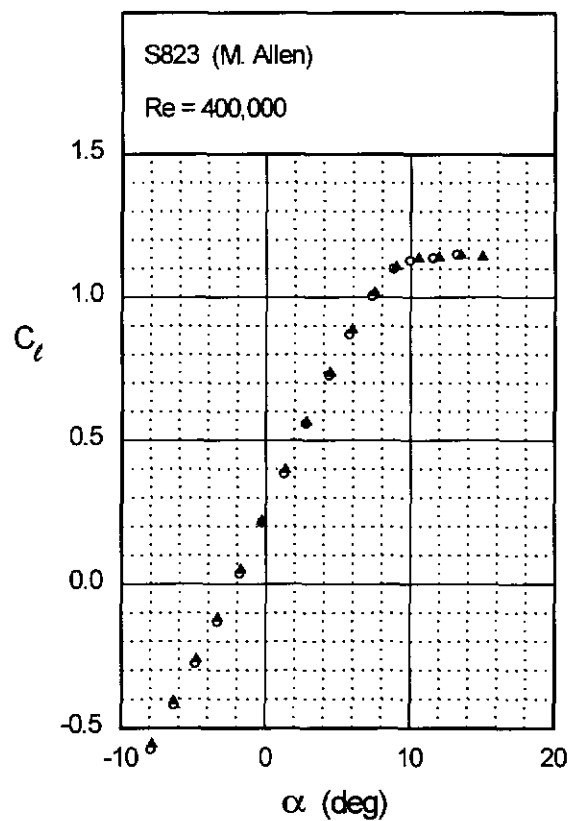
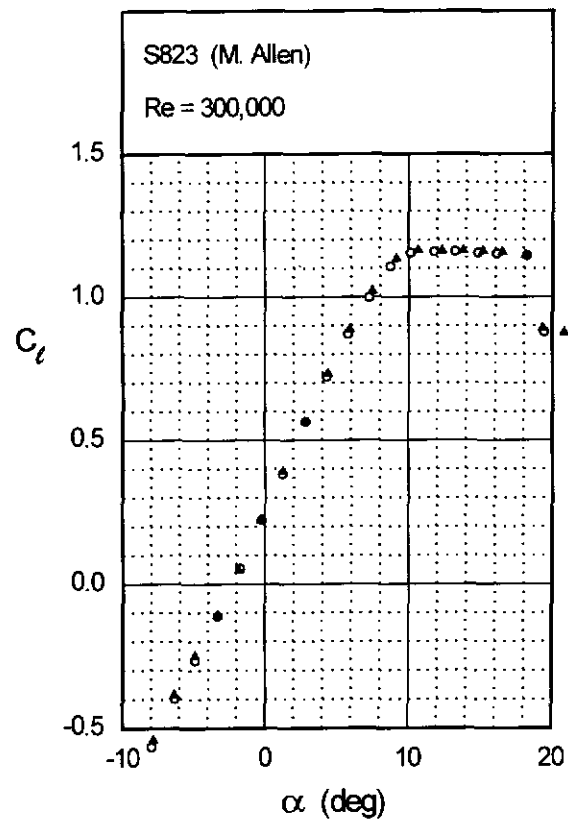


Fig. 4.89

Fig. 4.89 (continued)

Chapter 4: Airfoil Profiles and Performance Plots 169

S823



S1210

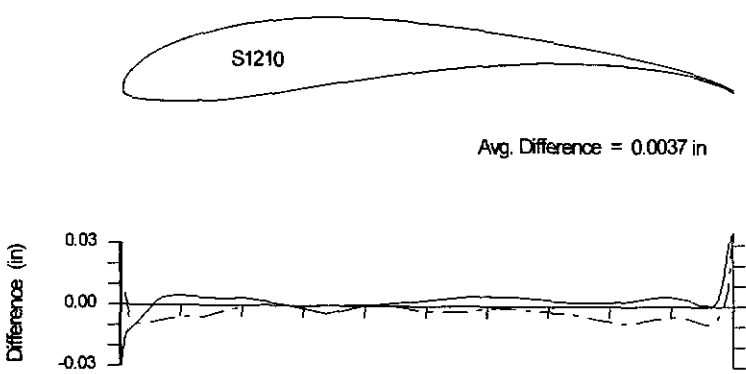
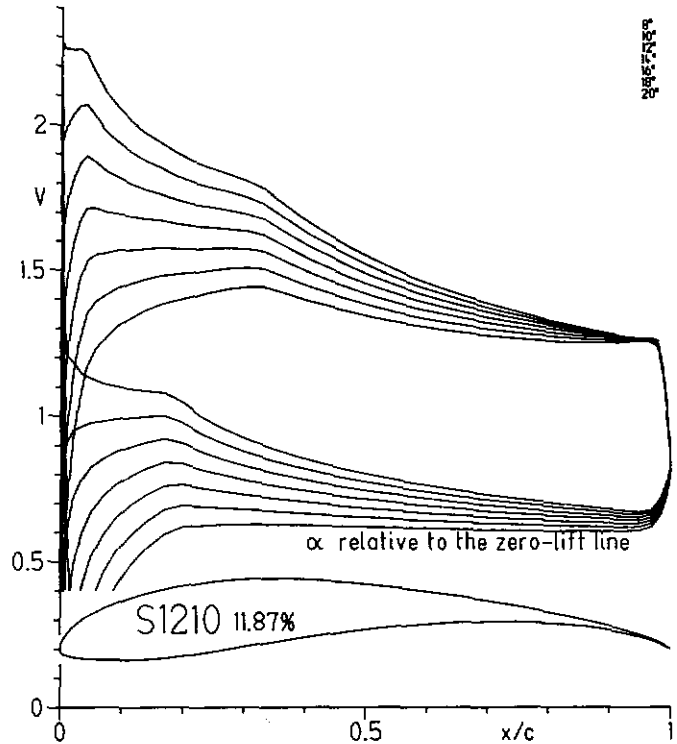
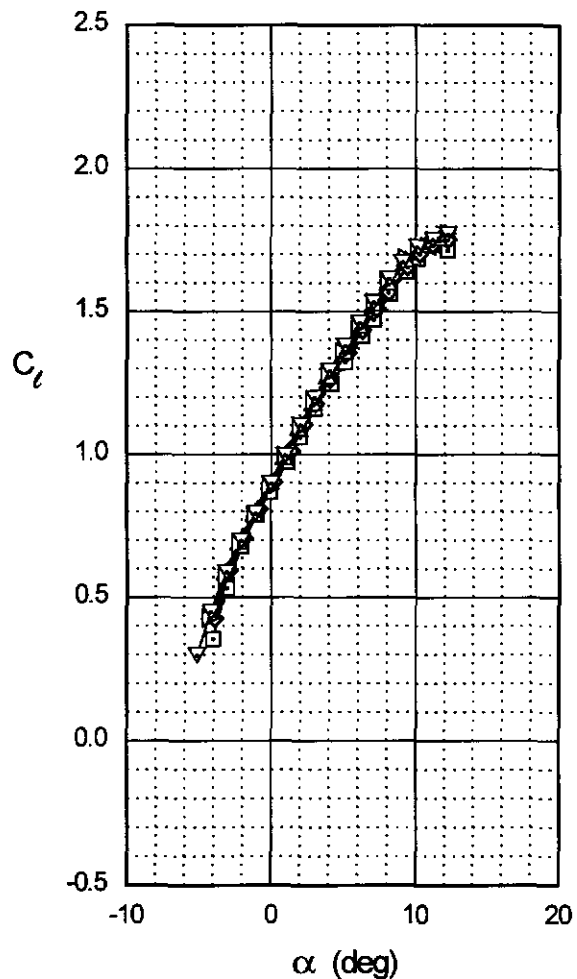
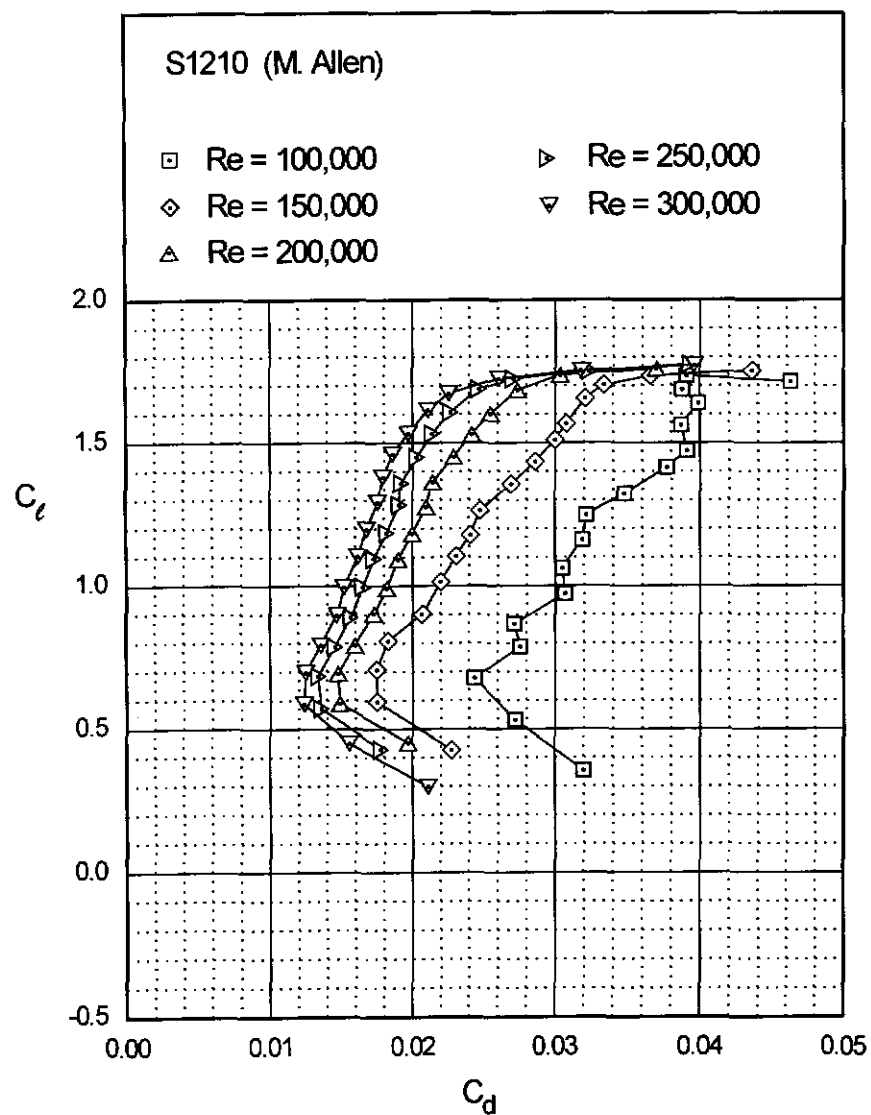


Fig. 4.92

Chapter 4: Airfoil Profiles and Performance Plots 171



S1210

S1210

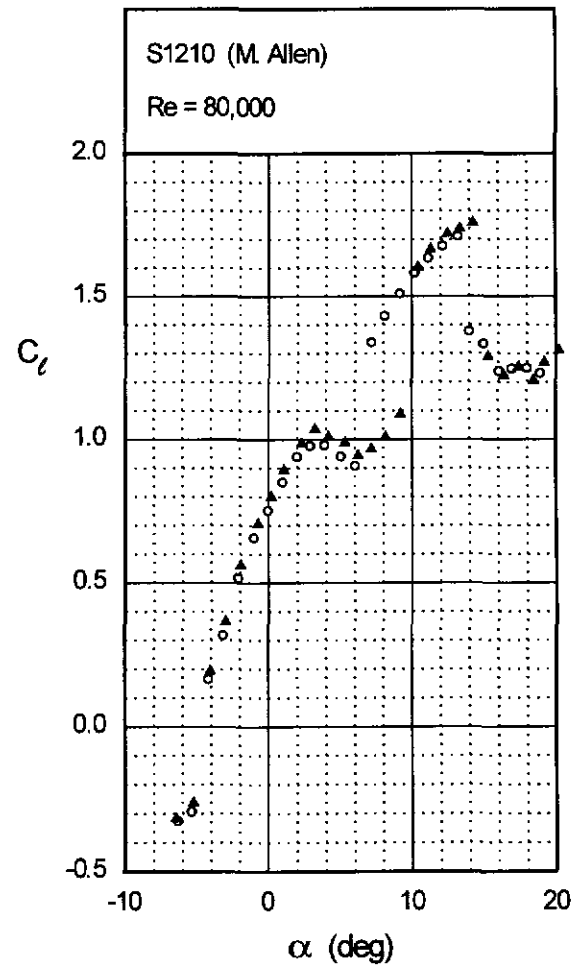
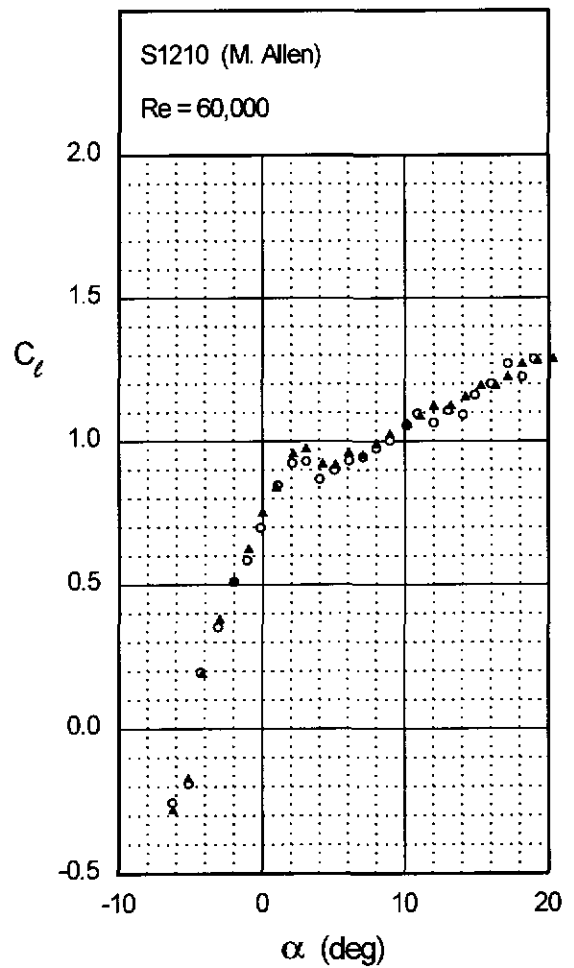
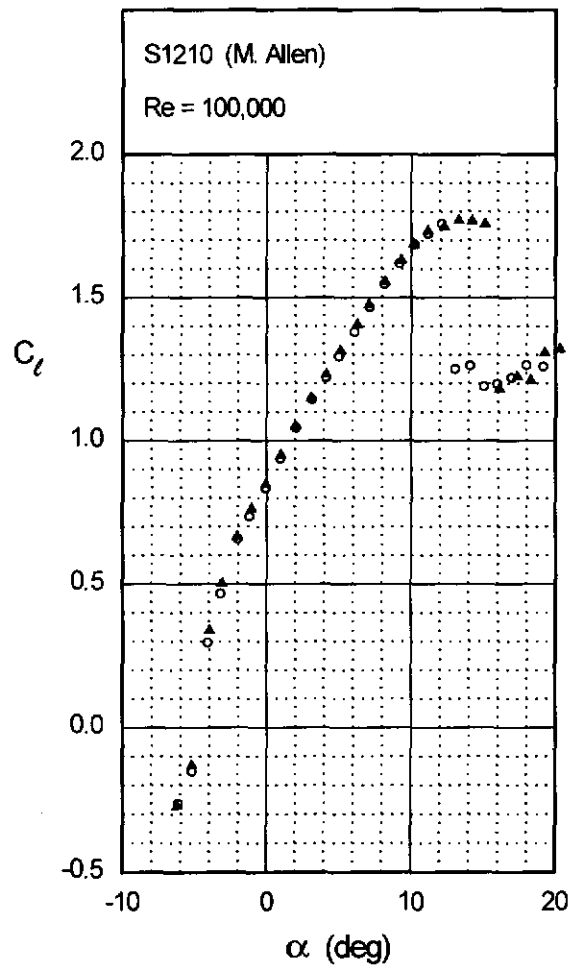
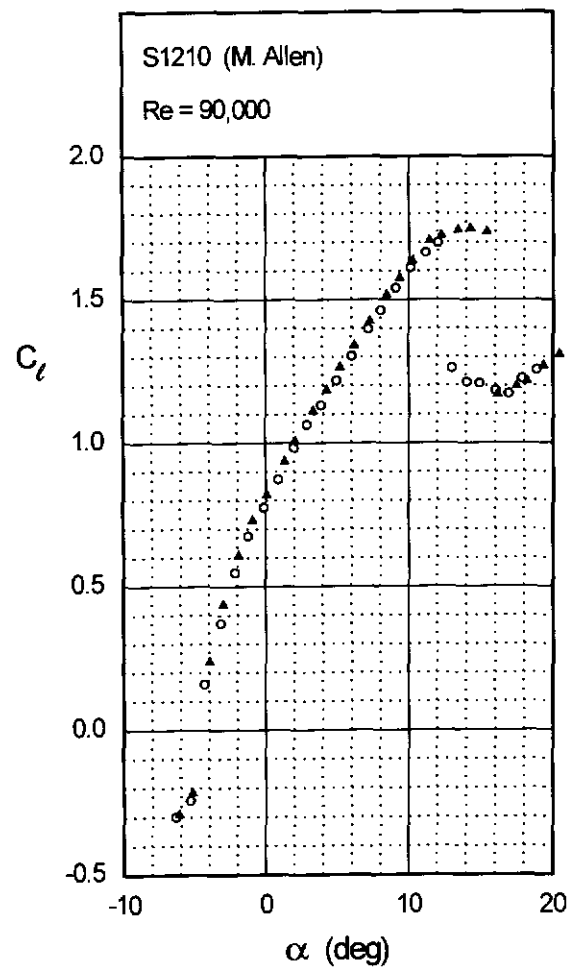


Fig. 4.93 (continued)

Chapter 4: Airfoil Profiles and Performance Plots 173

S1210



S1210

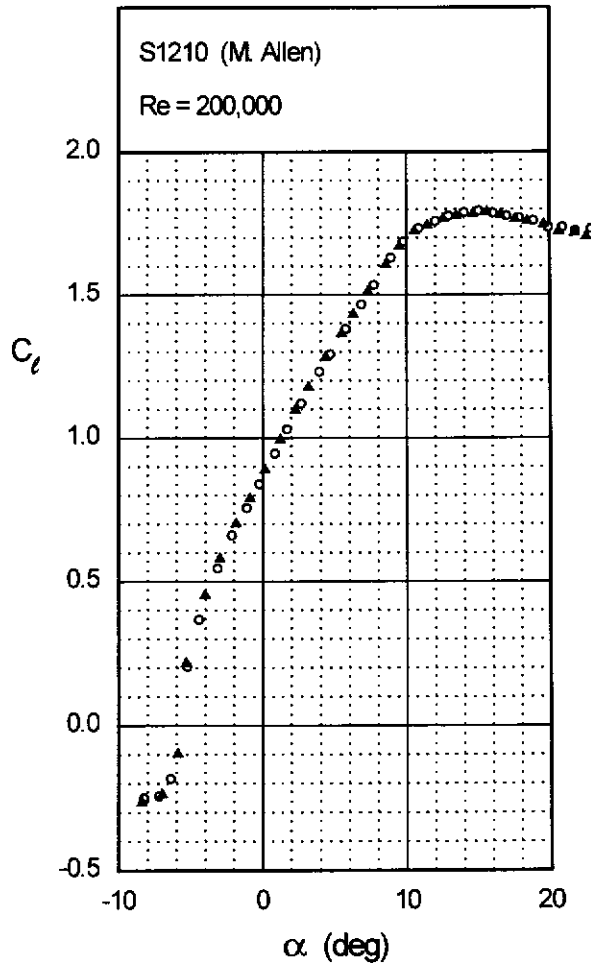
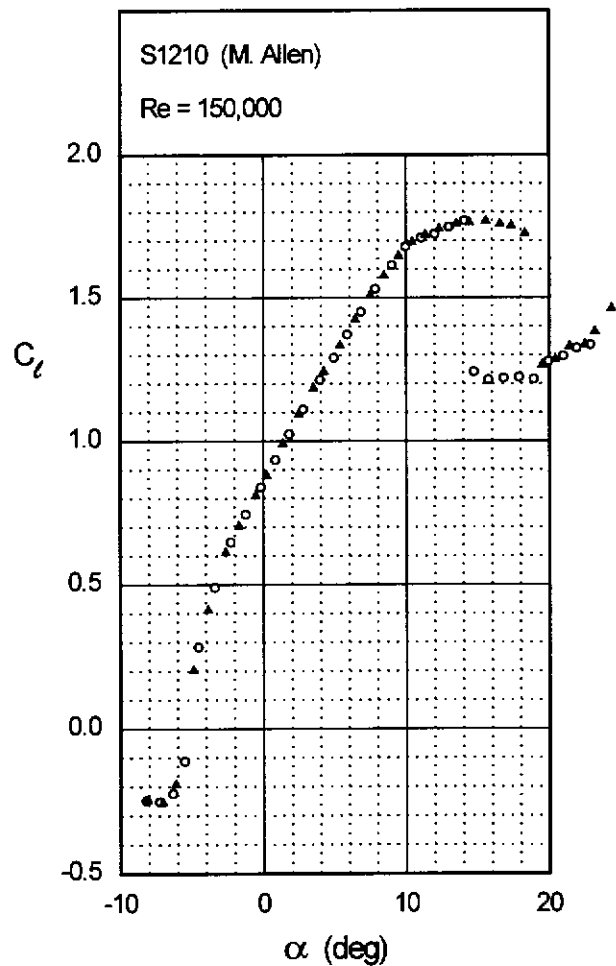
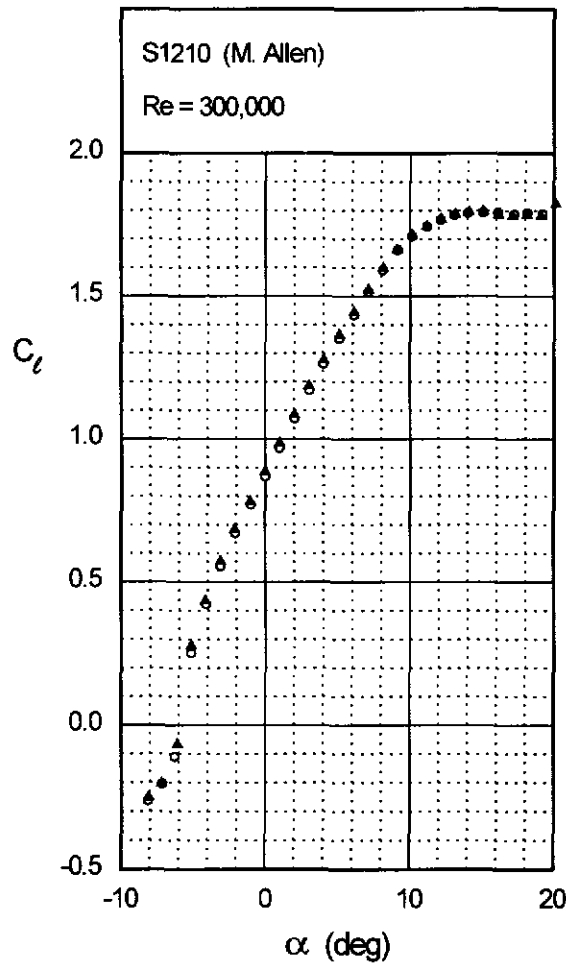
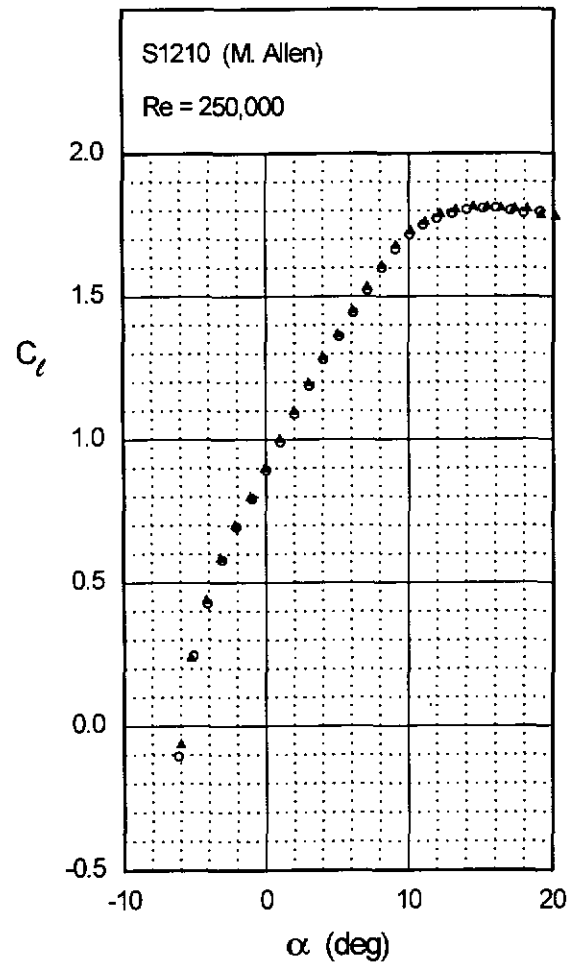


Fig. 4.93 (continued)

Chapter 4: Airfoil Profiles and Performance Plots 175

S1210



S1223

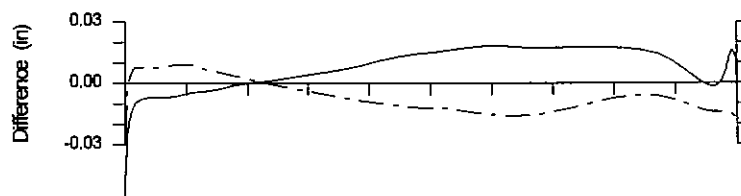
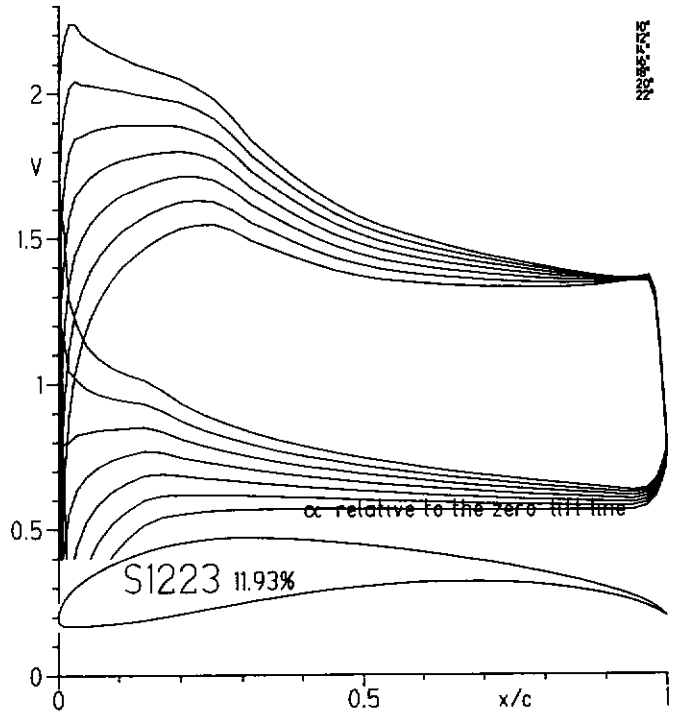
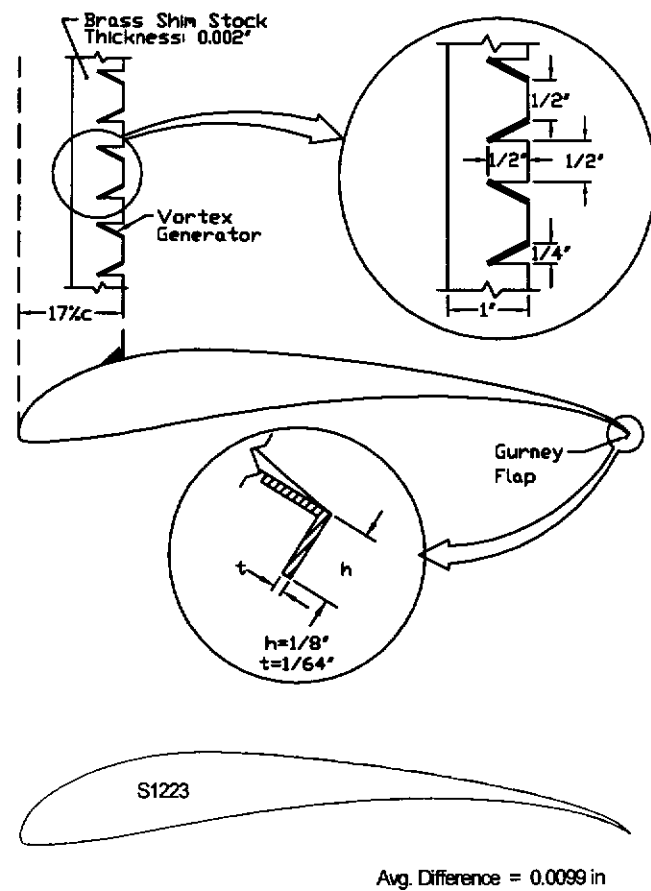
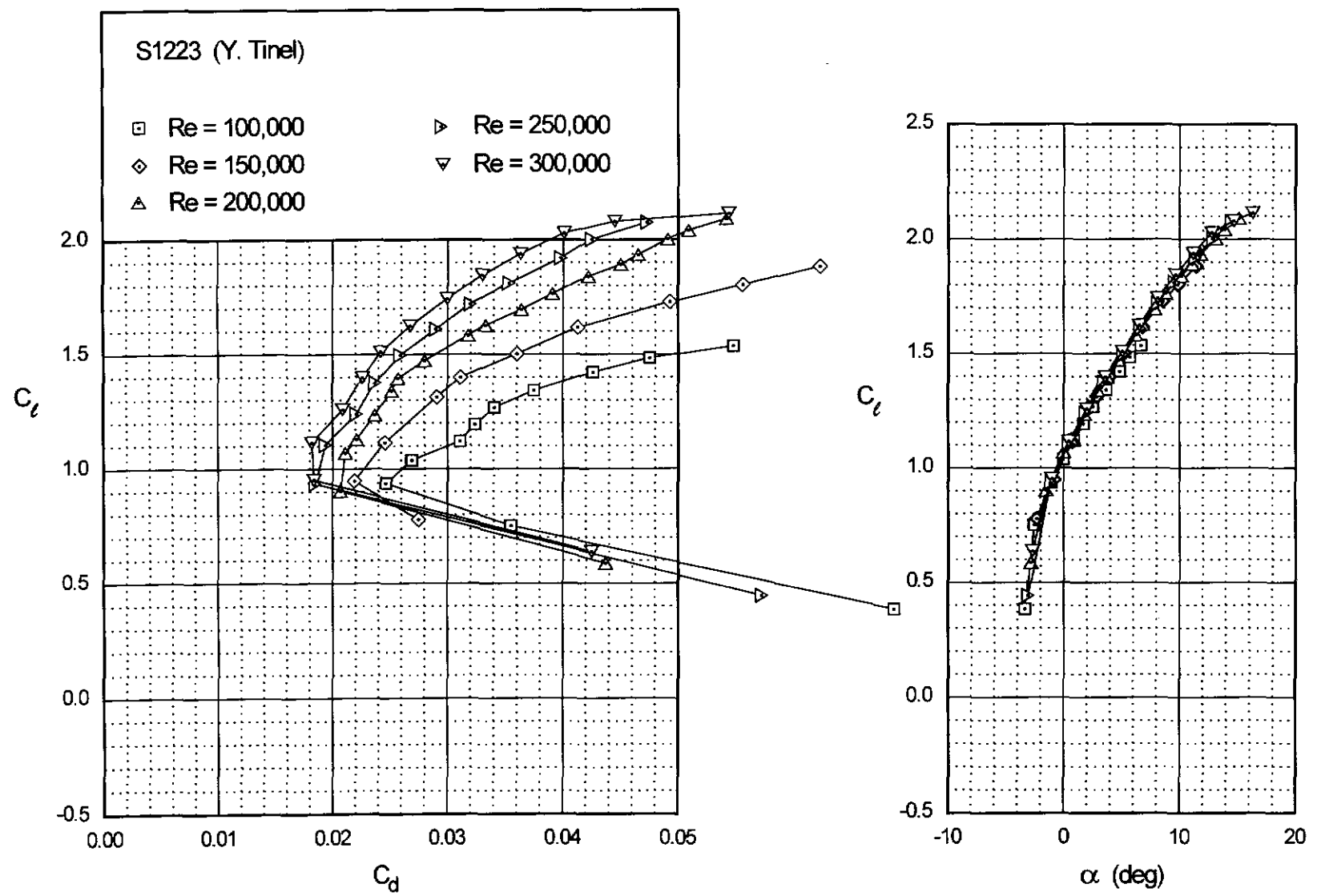


Fig. 4.96

Chapter 4: Airfoil Profiles and Performance Plots 177

S1223



S1223

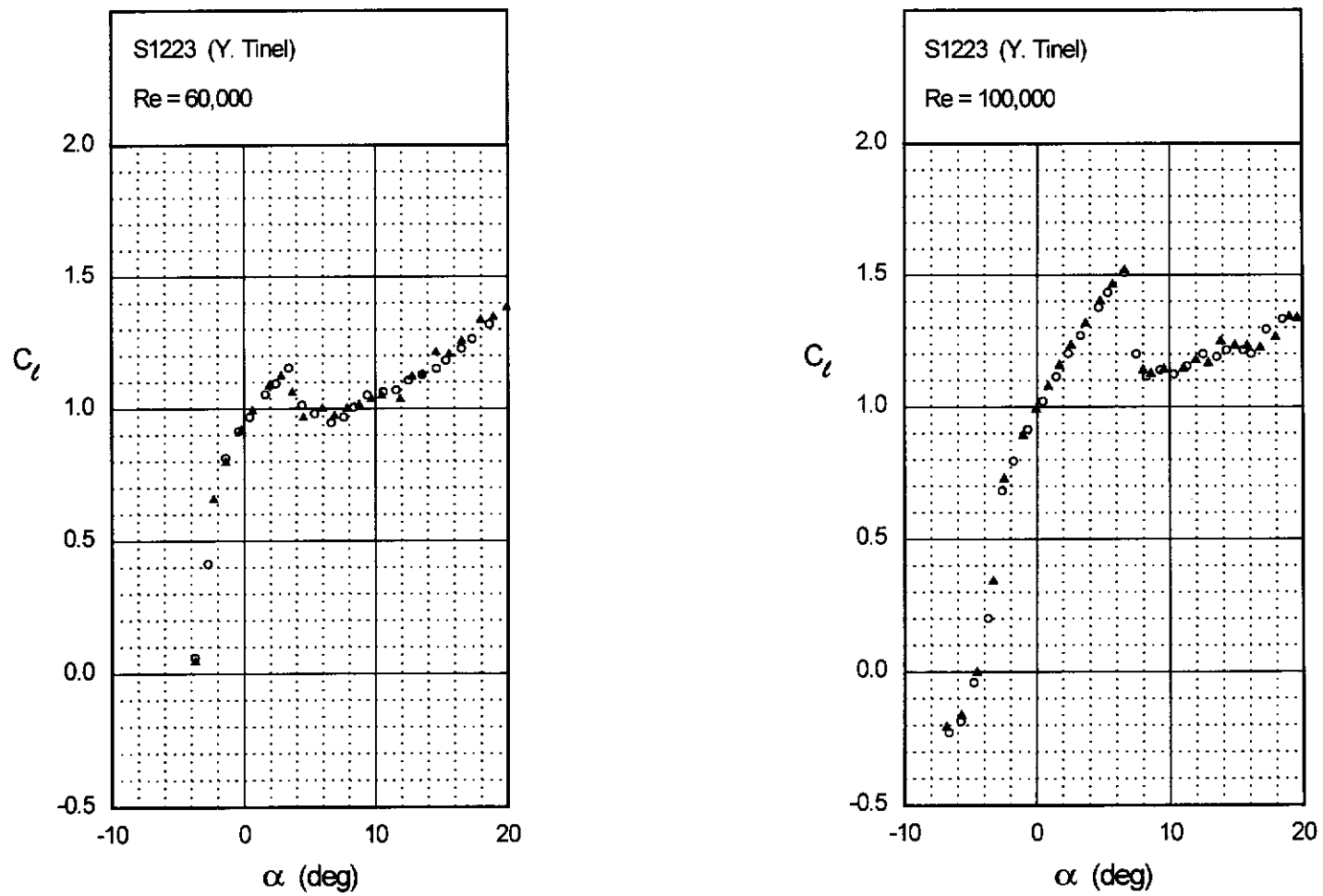


Fig. 4.97 (continued)

Chapter 4: Airfoil Profiles and Performance Plots 179

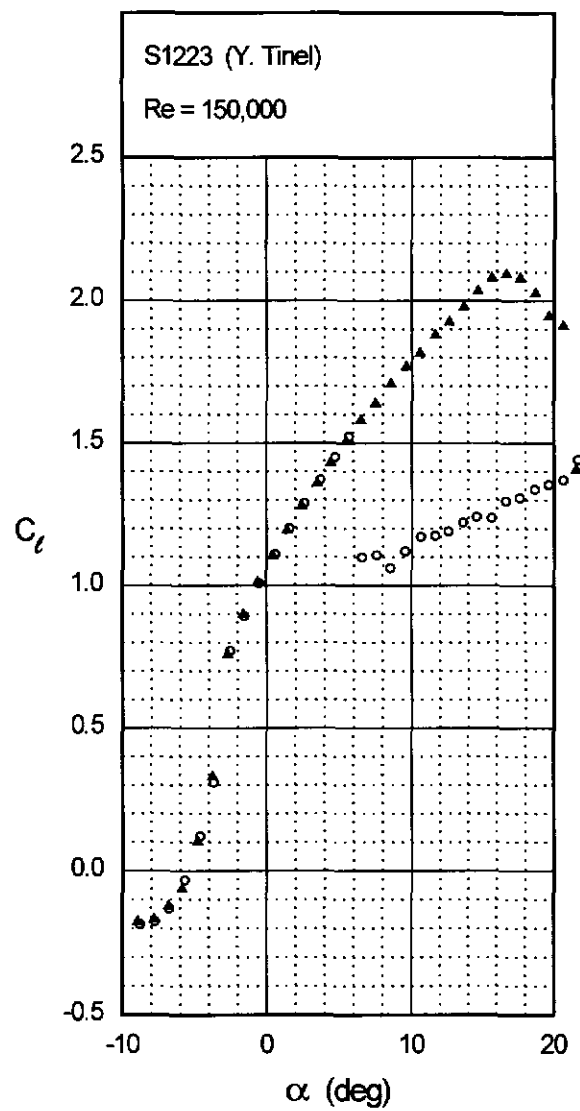
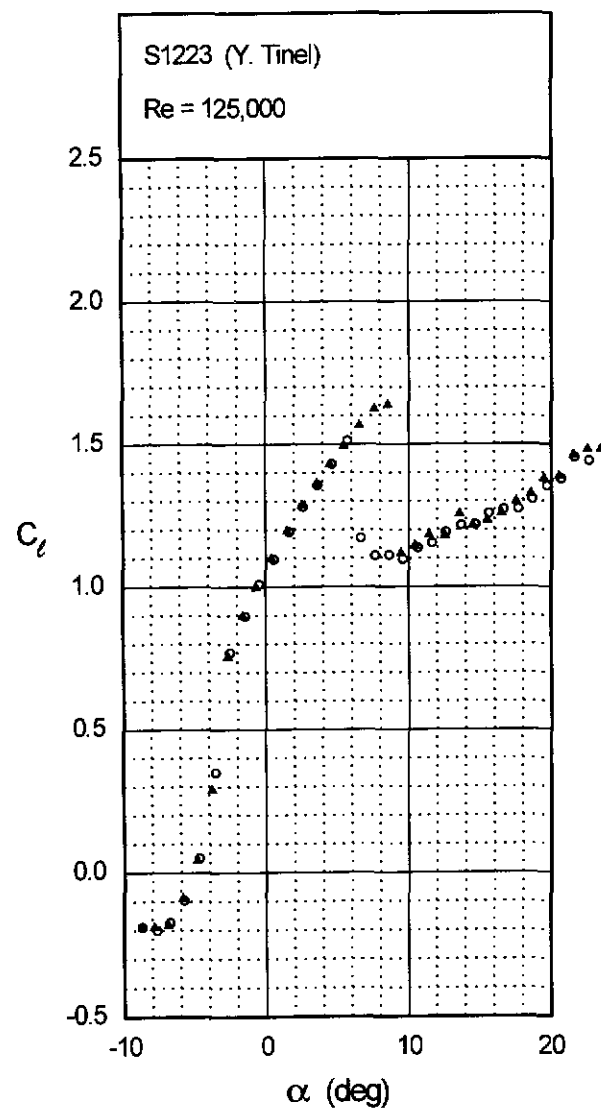


Fig. 4.97 (continued)

S1223

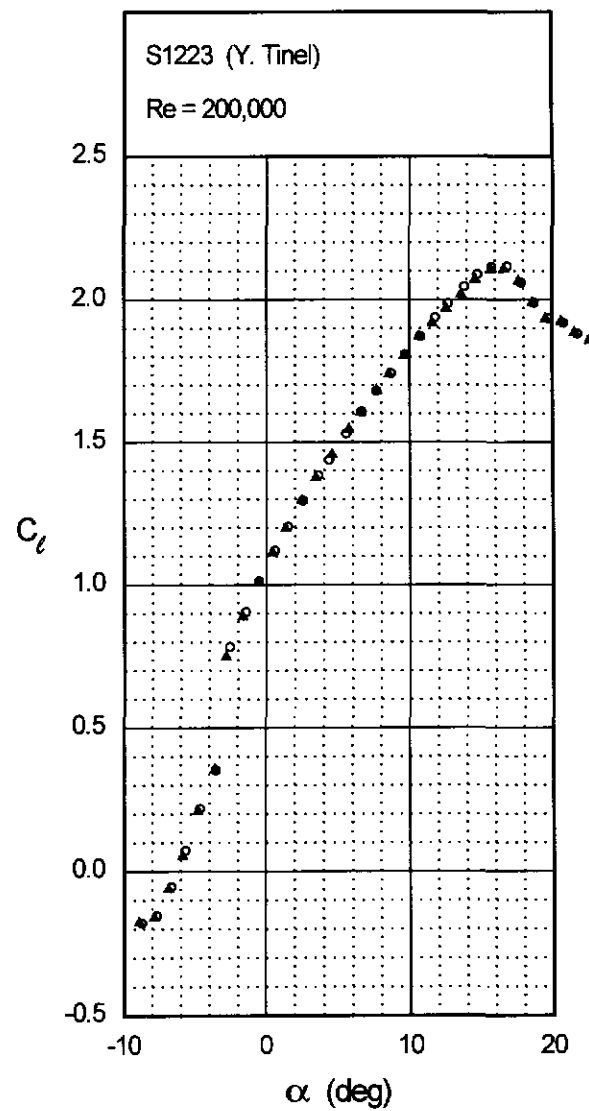
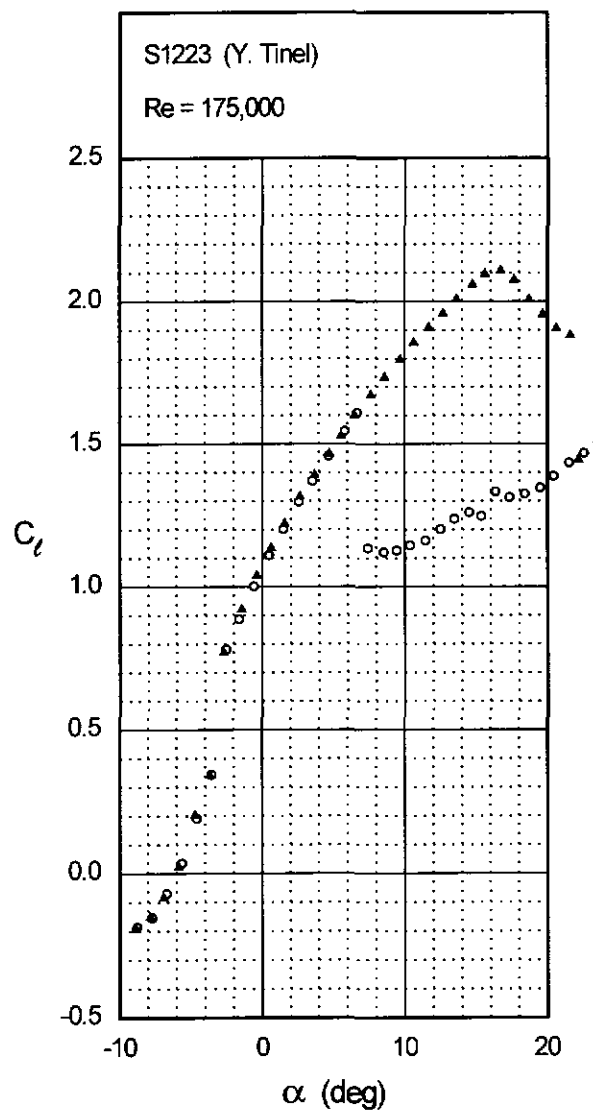


Fig. 4.97 (continued)

Chapter 4: Airfoil Profiles and Performance Plots 181

S1223

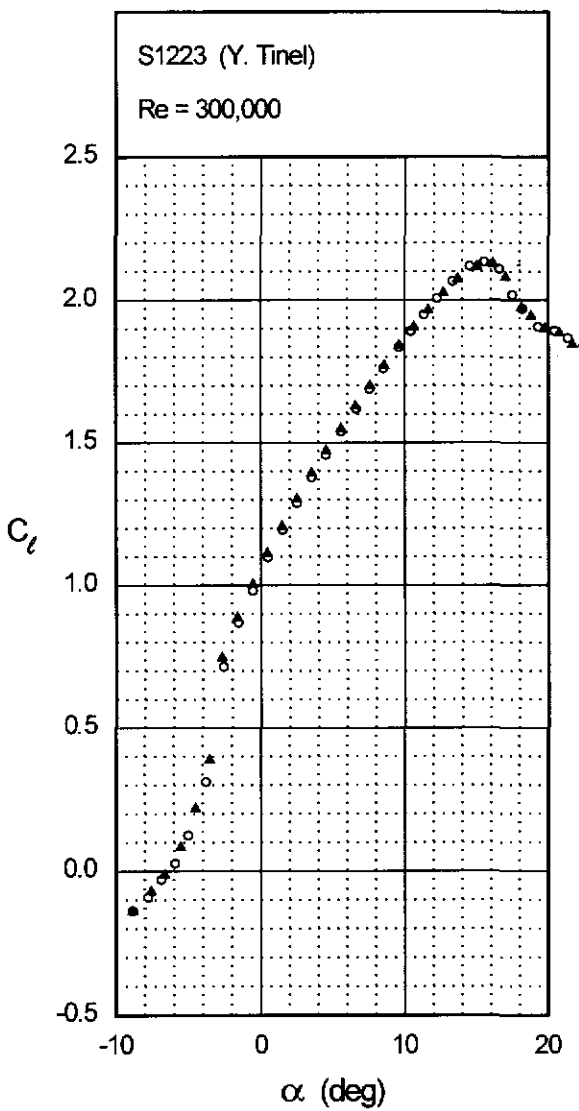
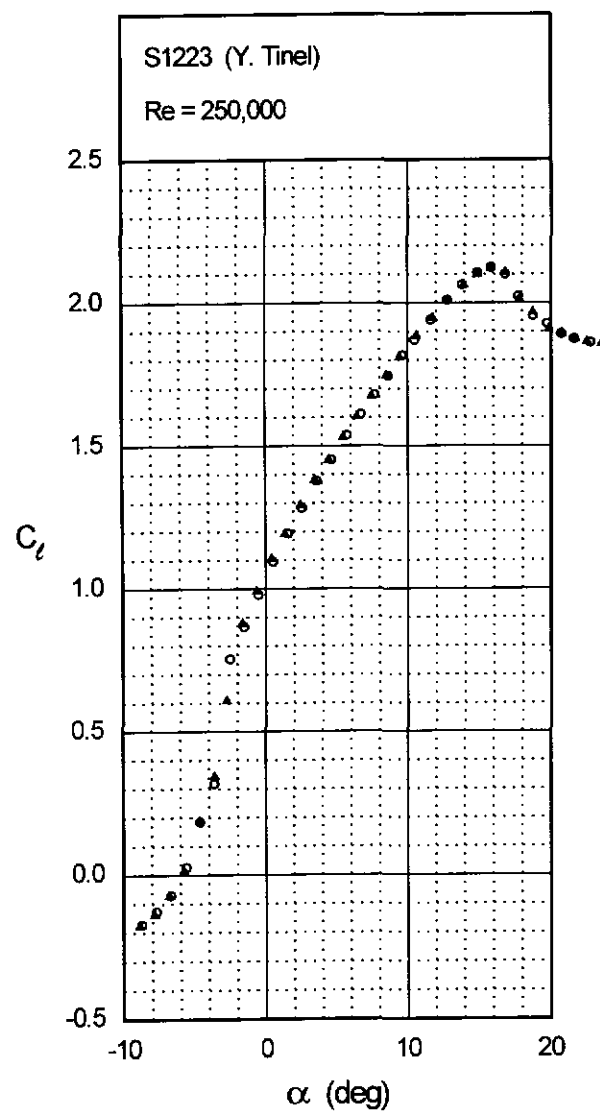


Fig. 4.98

S1223

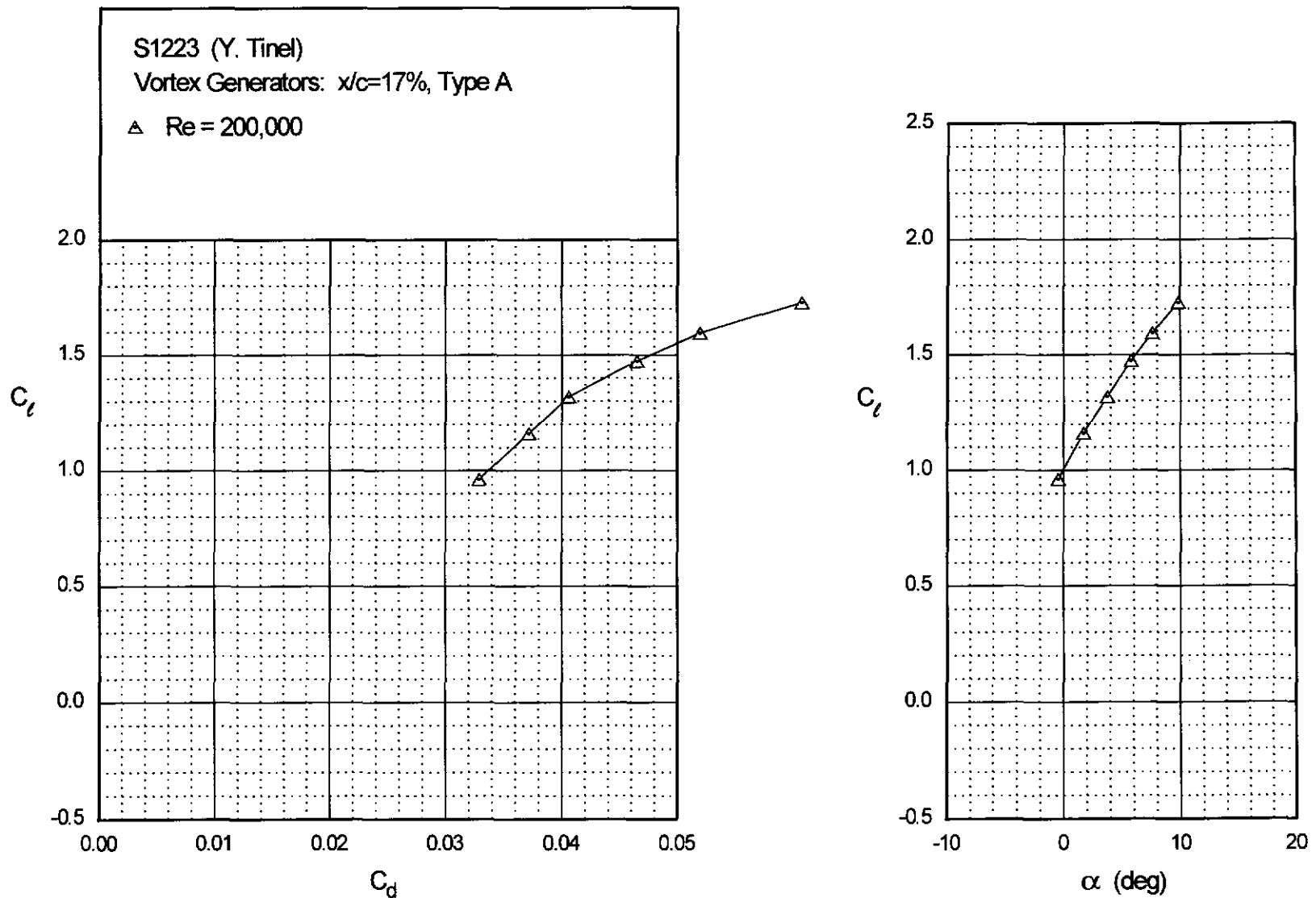
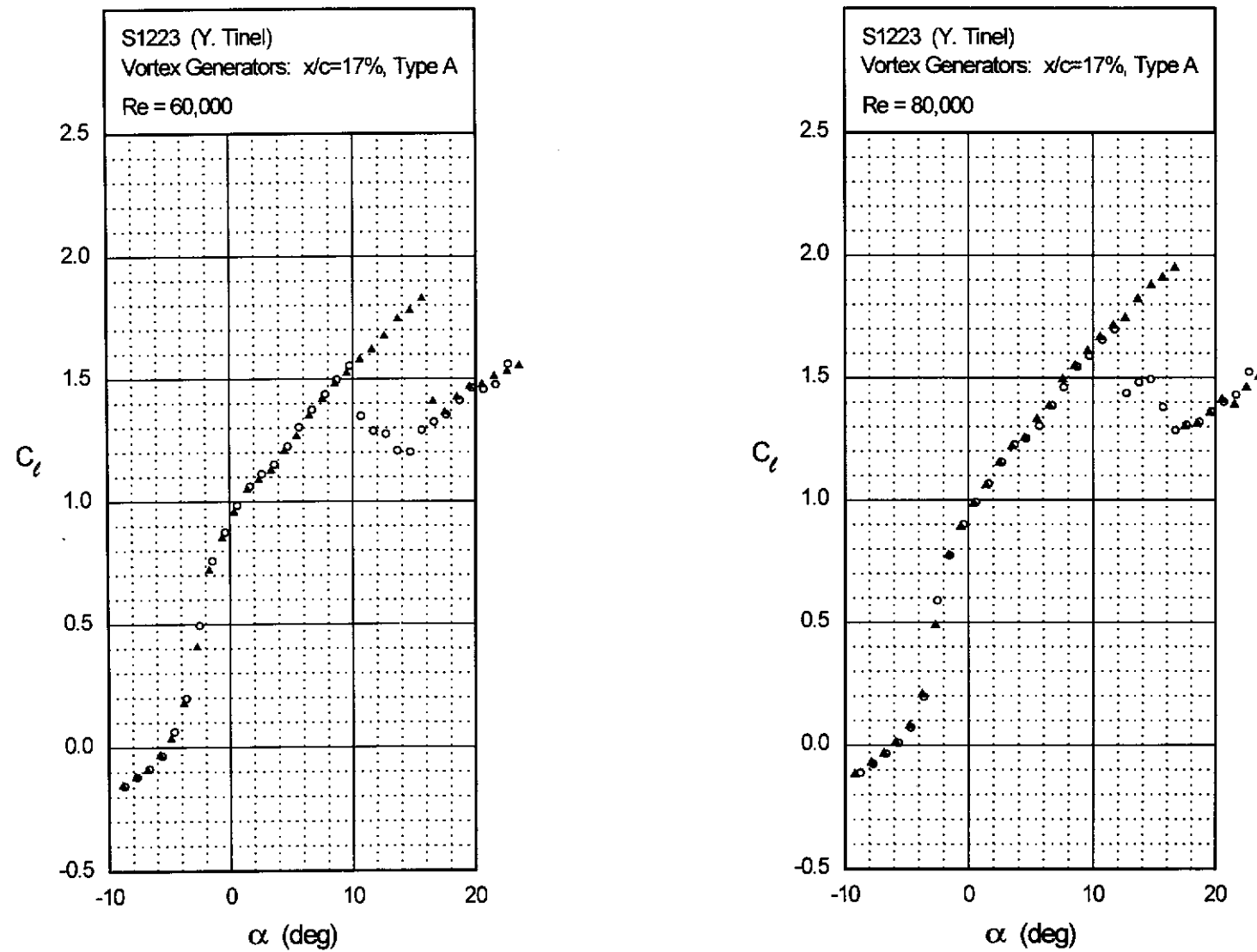


Fig. 4.99

Chapter 4: Airfoil Profiles and Performance Plots

183



S1223

S1223

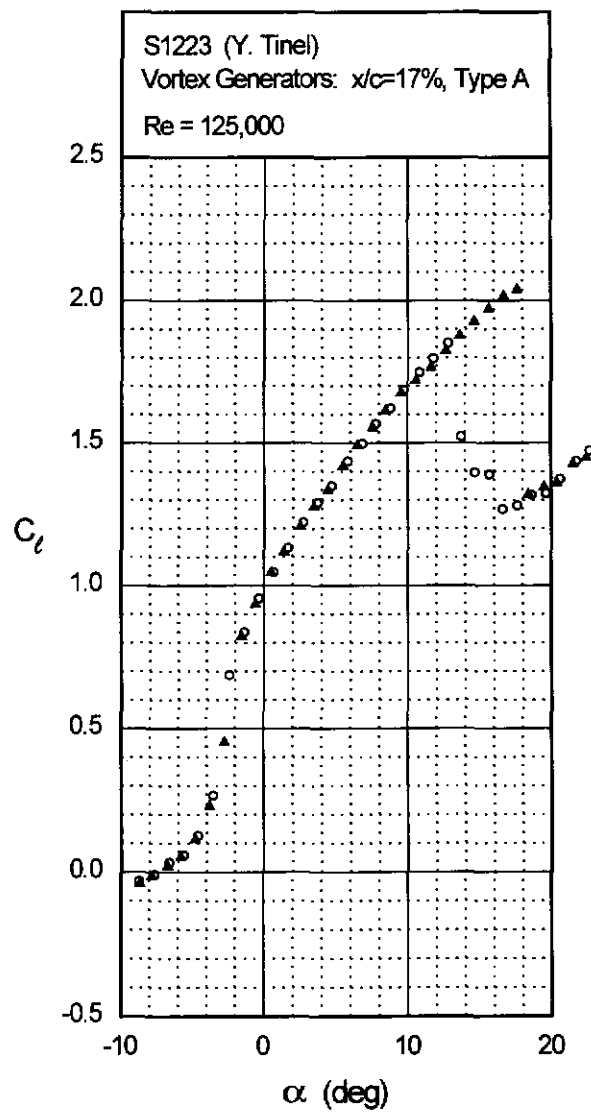
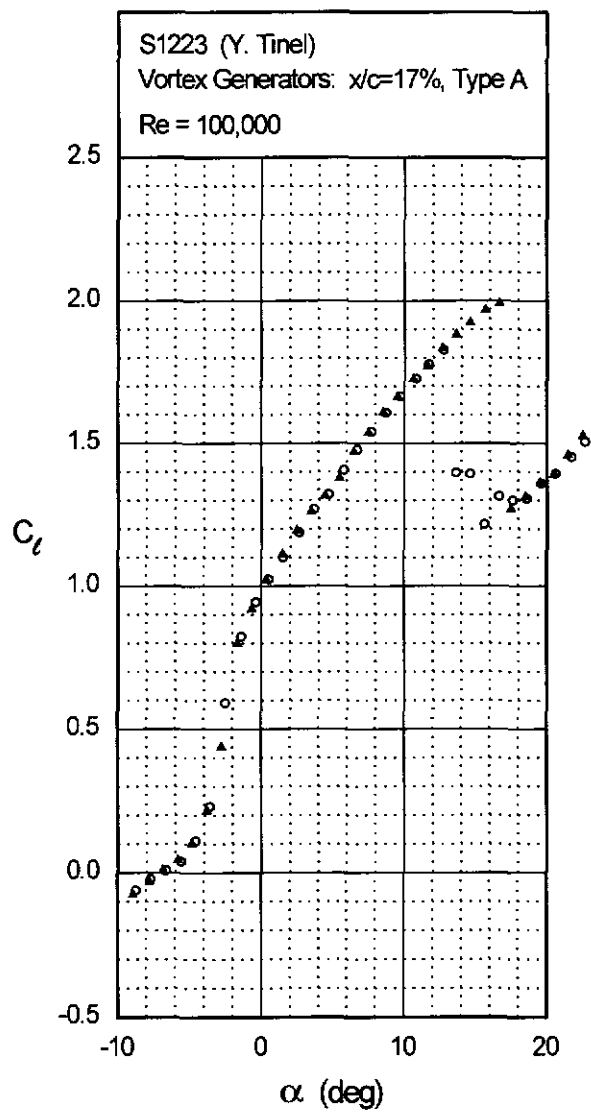
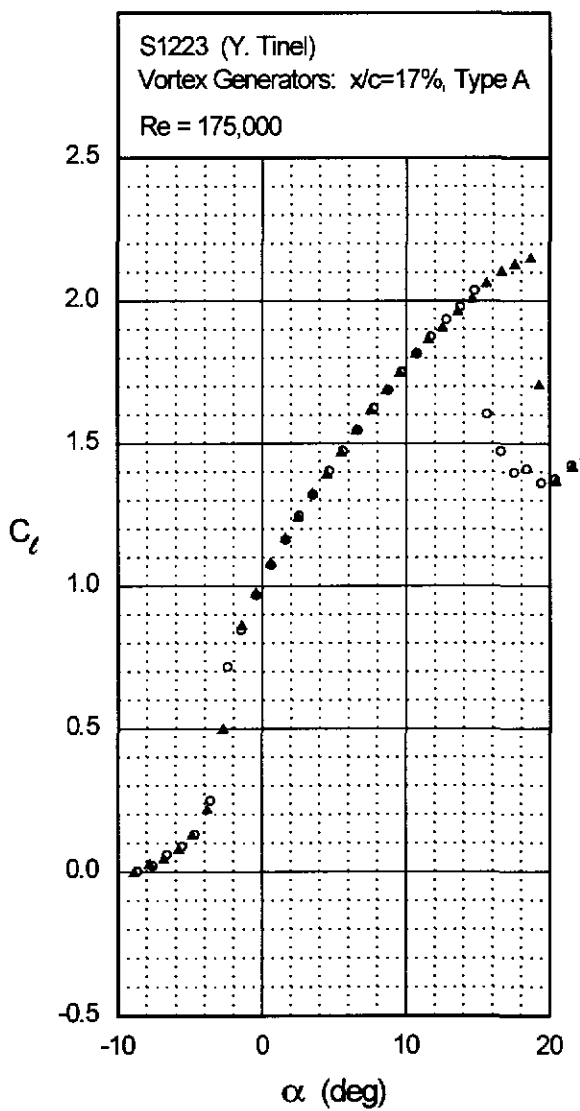
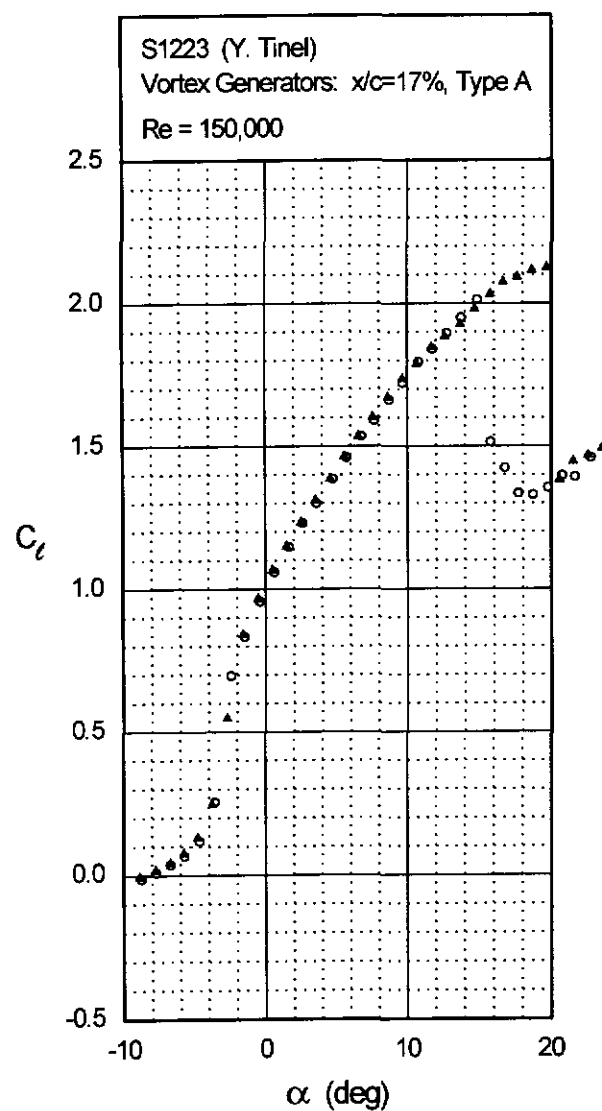


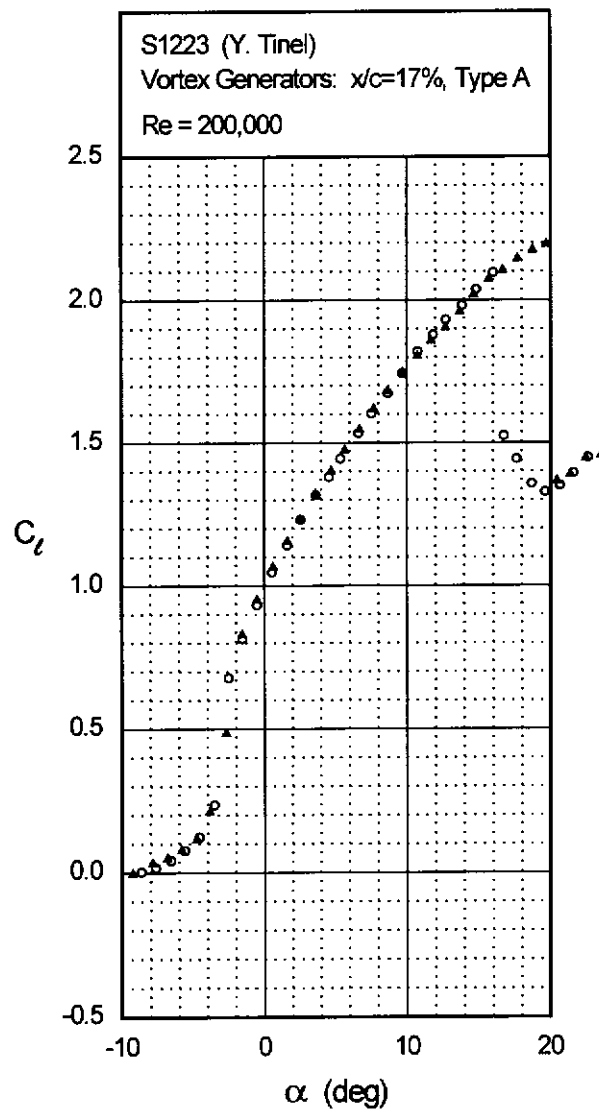
Fig. 4.99 (continued)

Chapter 4: Airfoil Profiles and Performance Plots 185

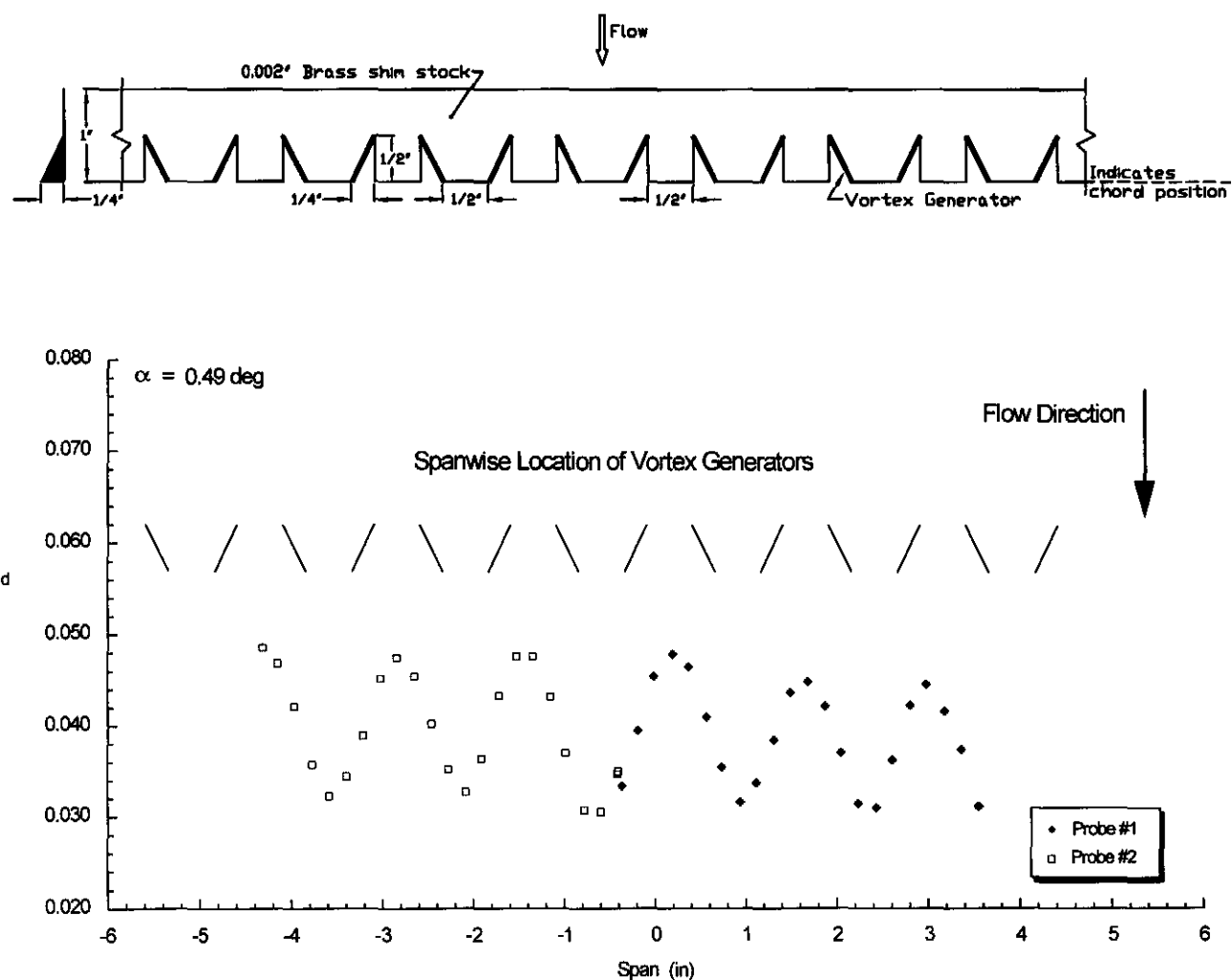
S1223



S1223



S1223



S1223

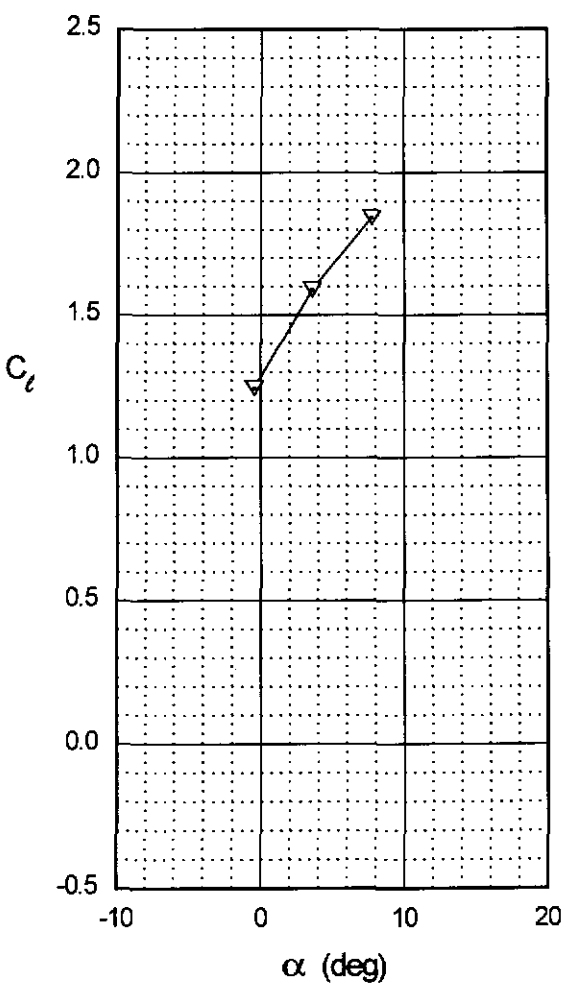
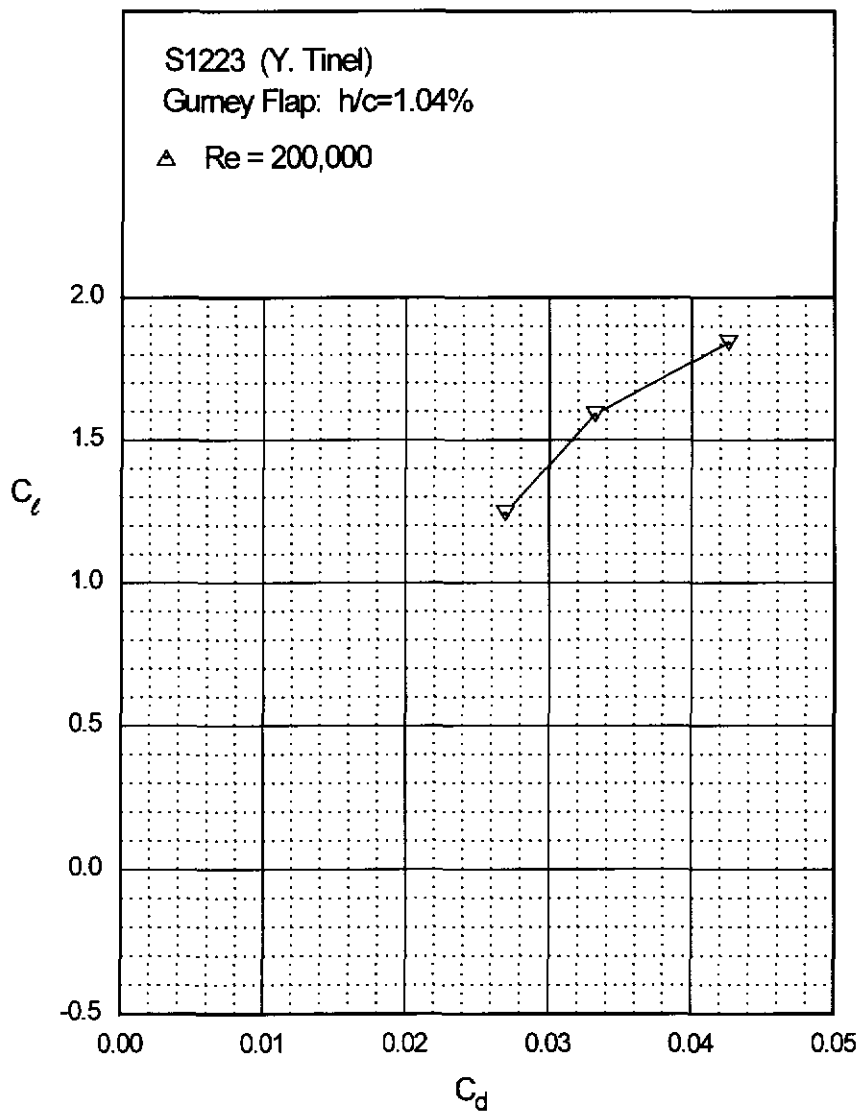
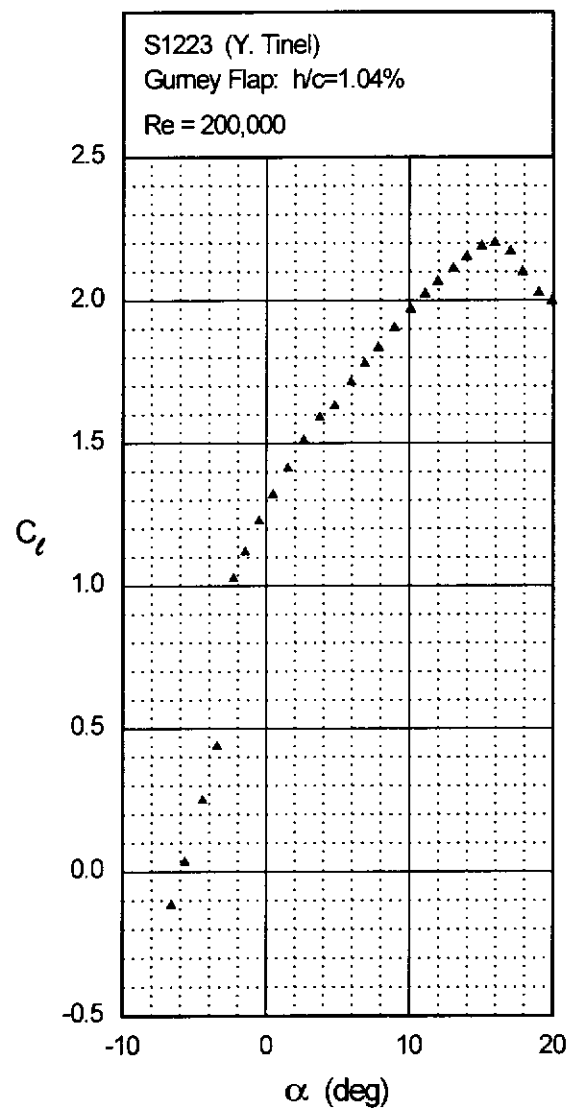


Fig. 4.102

Chapter 4: Airfoil Profiles and Performance Plots 189



S1223

S6062

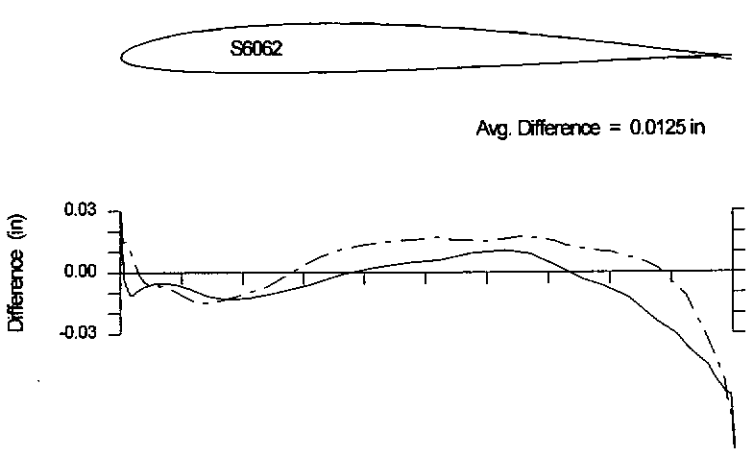
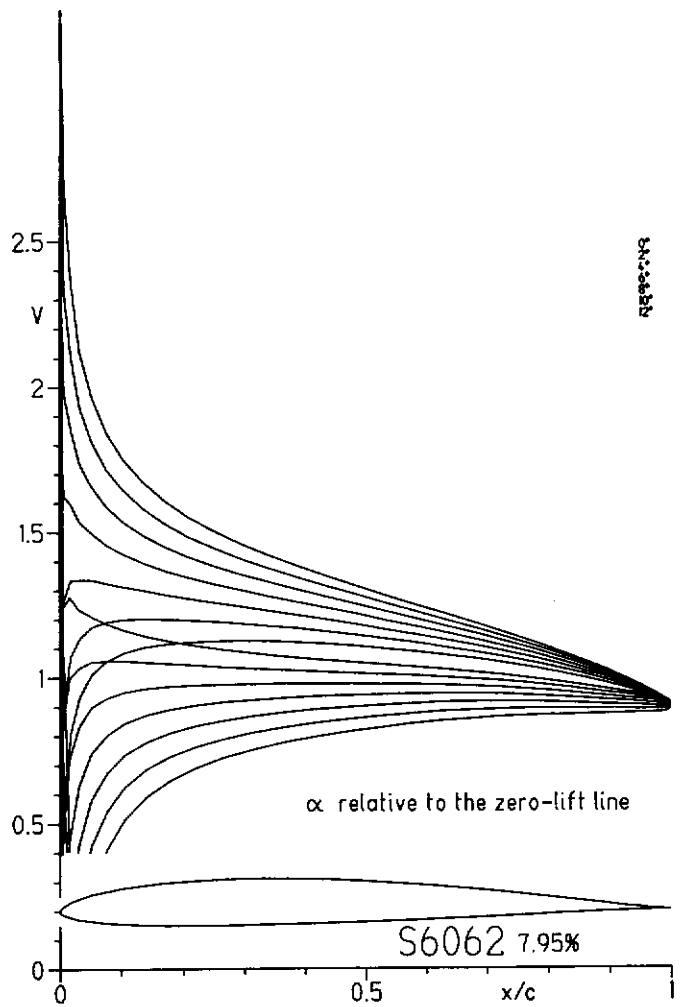


Fig. 4.105

Chapter 4: Airfoil Profiles and Performance Plots

191

S6062

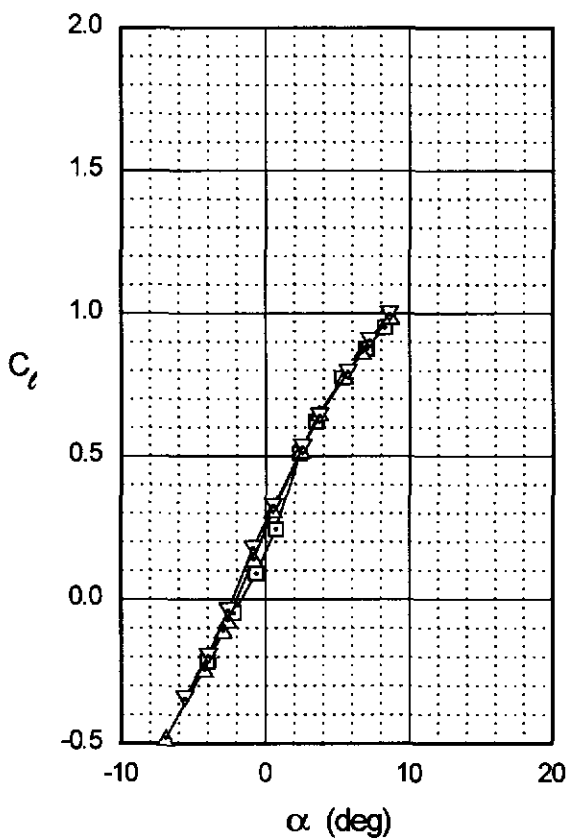
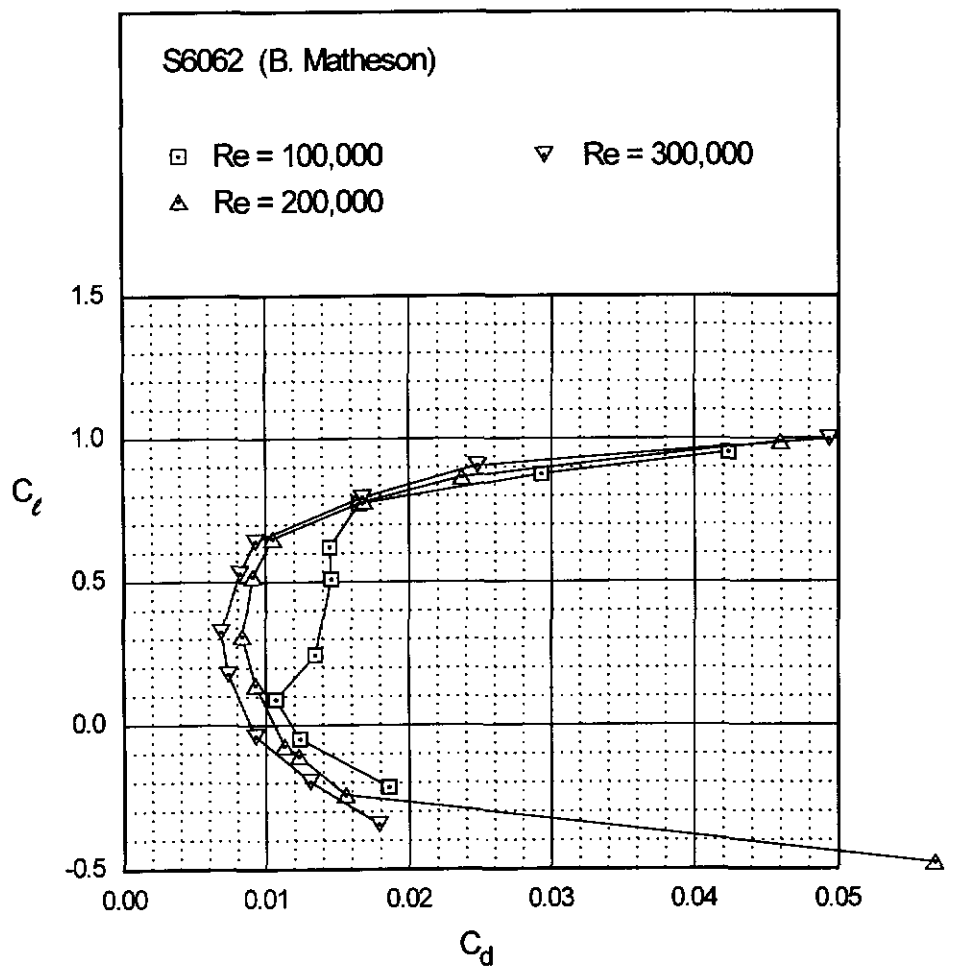


Fig. 4.106

S6062

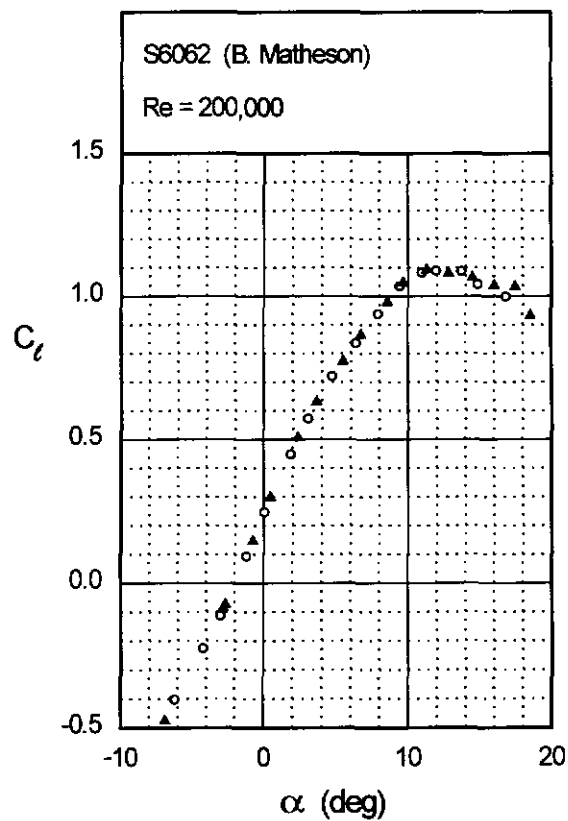
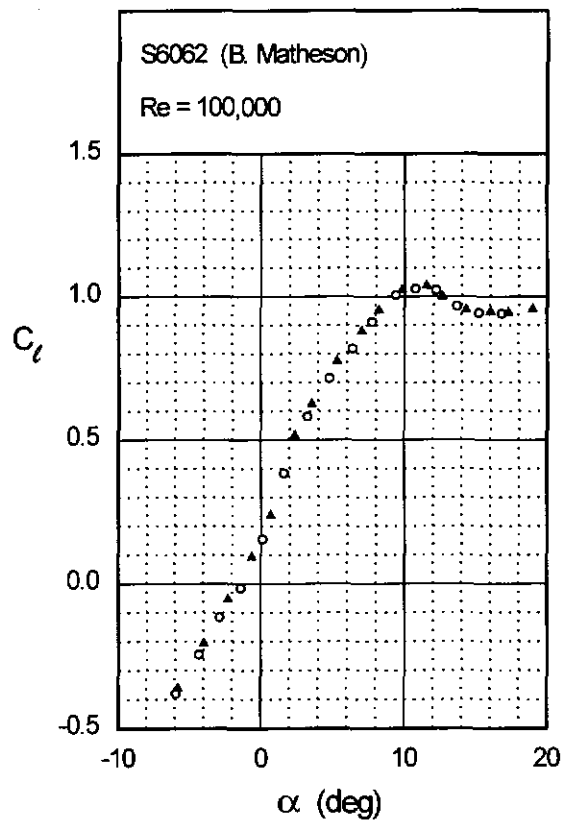
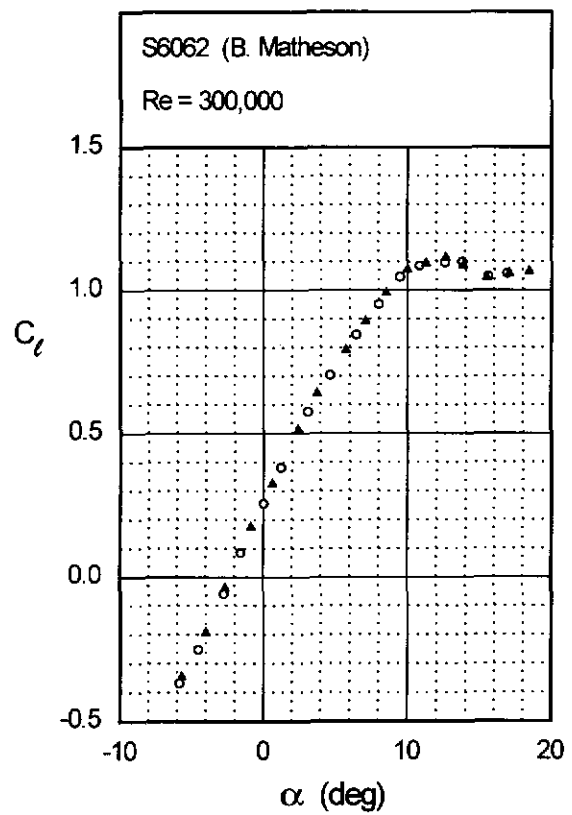


Fig. 4.106 (continued)

Chapter 4: Airfoil Profiles and Performance Plots 193

S6062



S7012

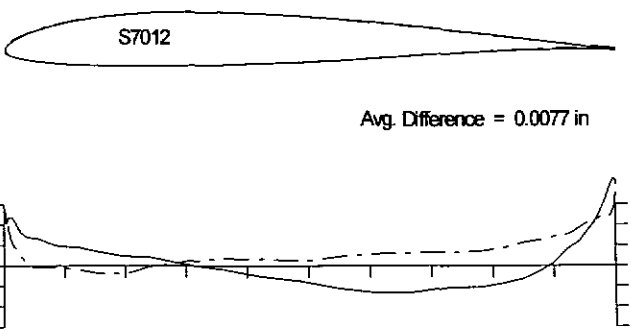
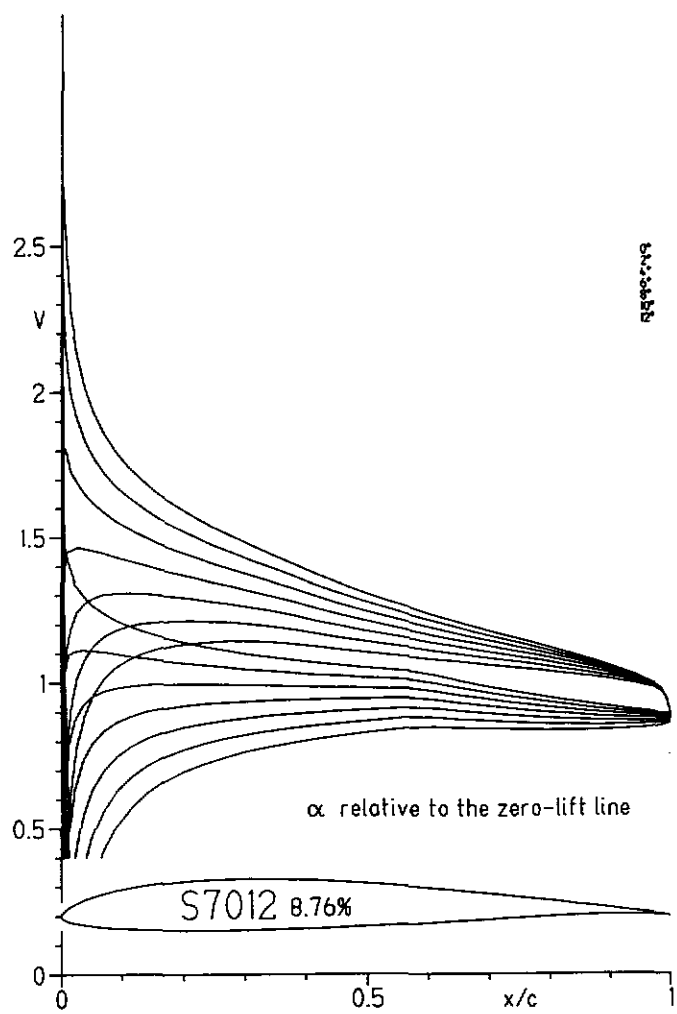
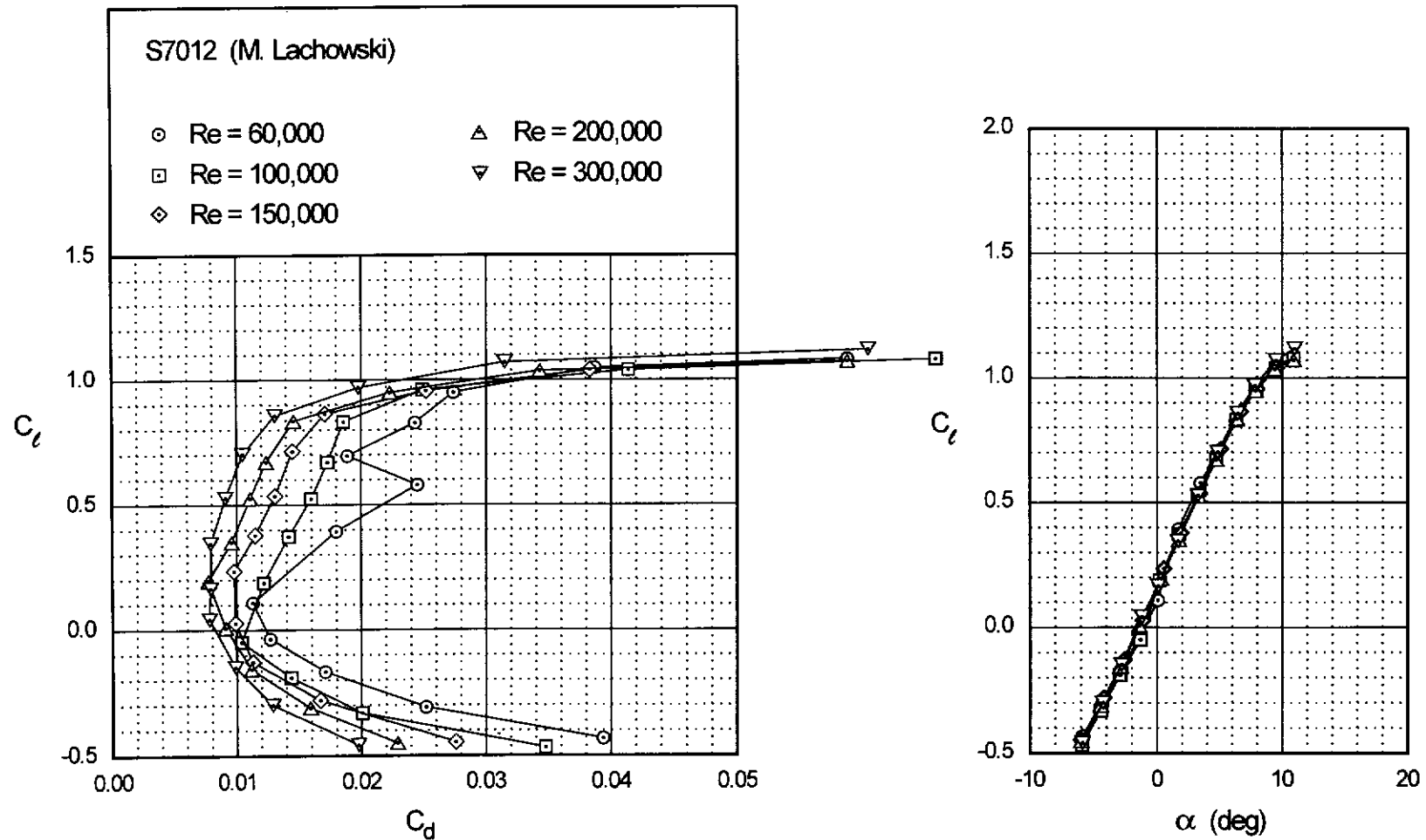


Fig. 4.109

Chapter 4: Airfoil Profiles and Performance Plots 195



S7012

S7012

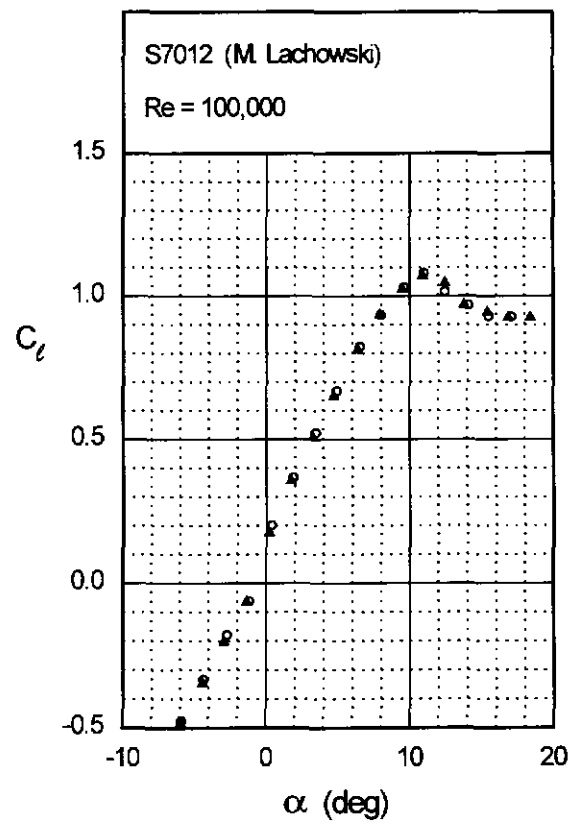
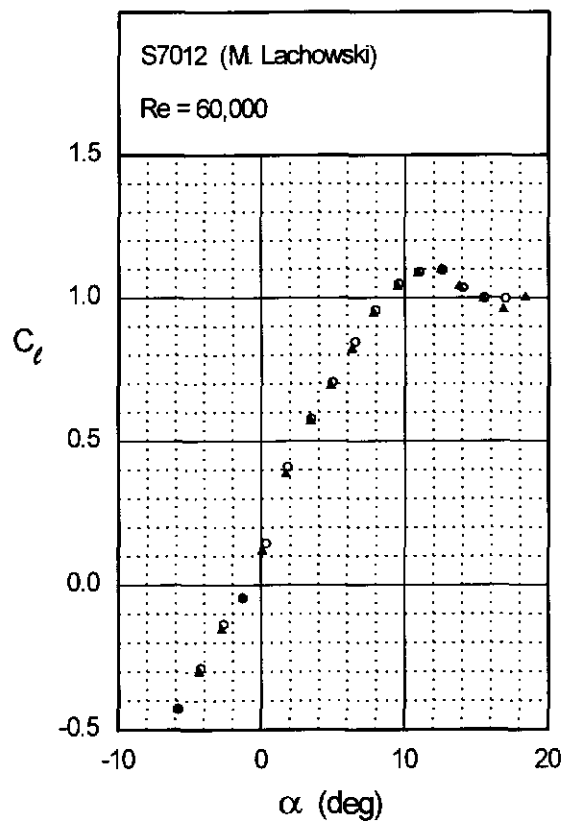
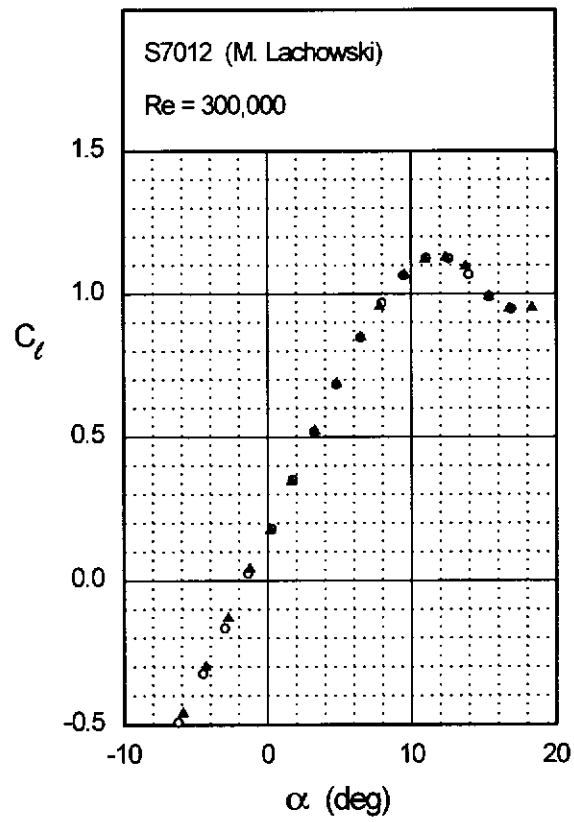
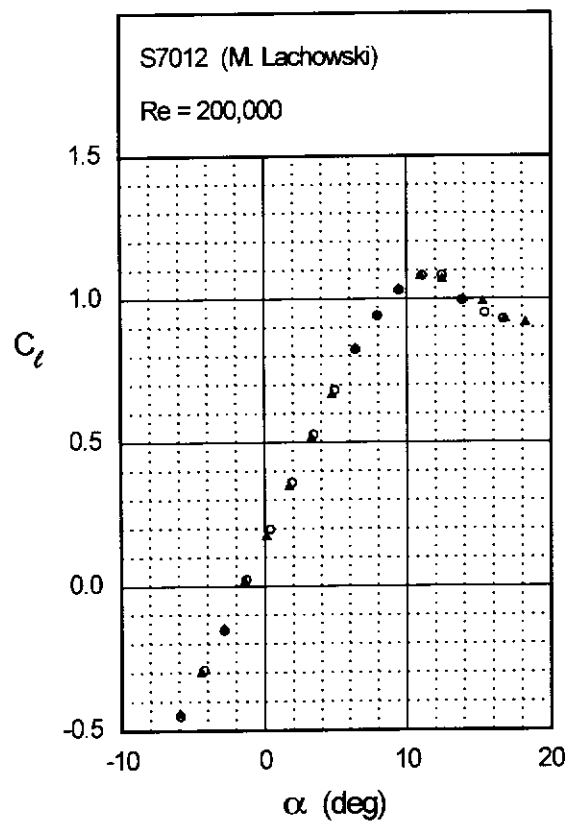


Fig. 4.110 (continued)

Chapter 4: Airfoil Profiles and Performance Plots 197

S7012



S7055

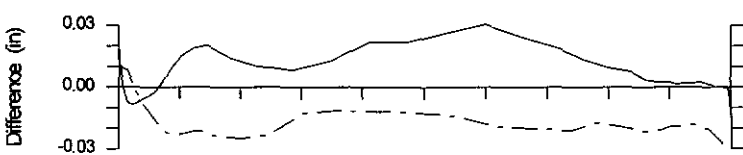
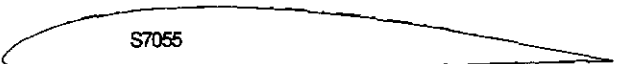
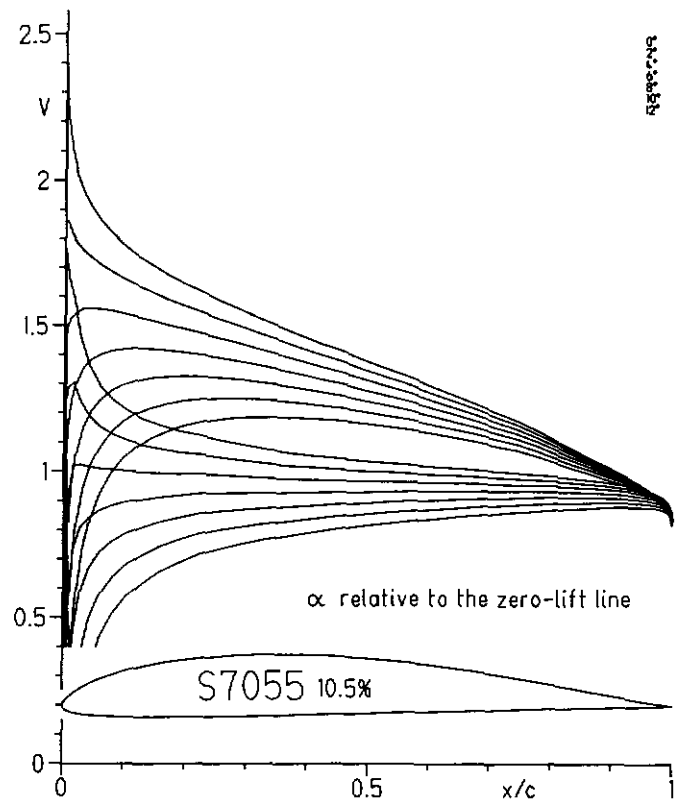
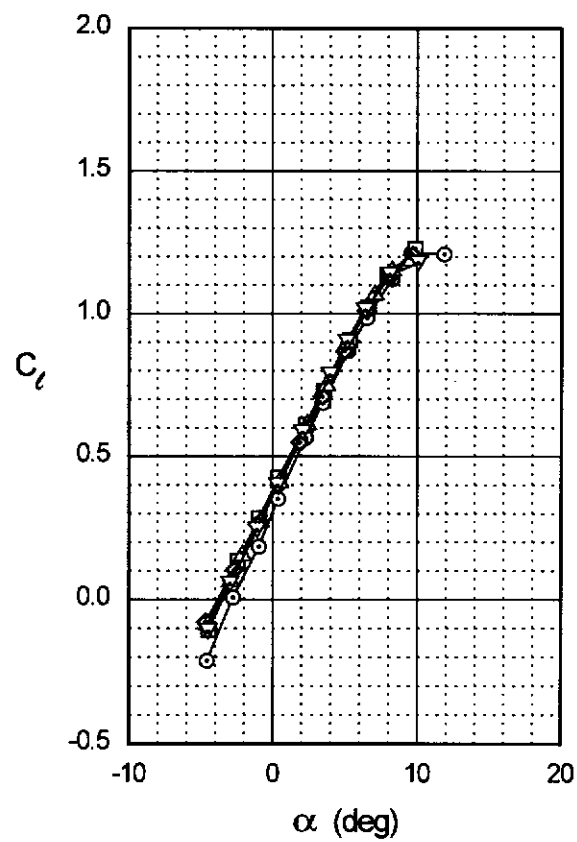
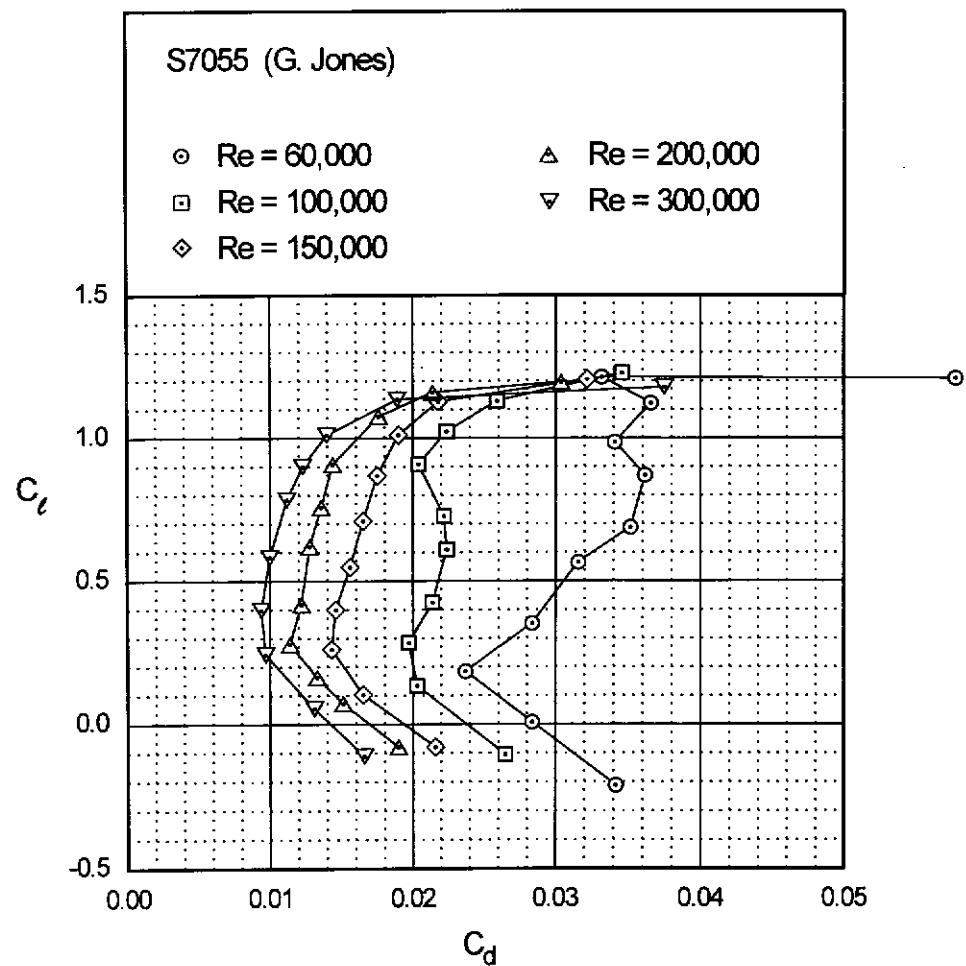


Fig. 4.113

Chapter 4: Airfoil Profiles and Performance Plots

199

S7055



S7055

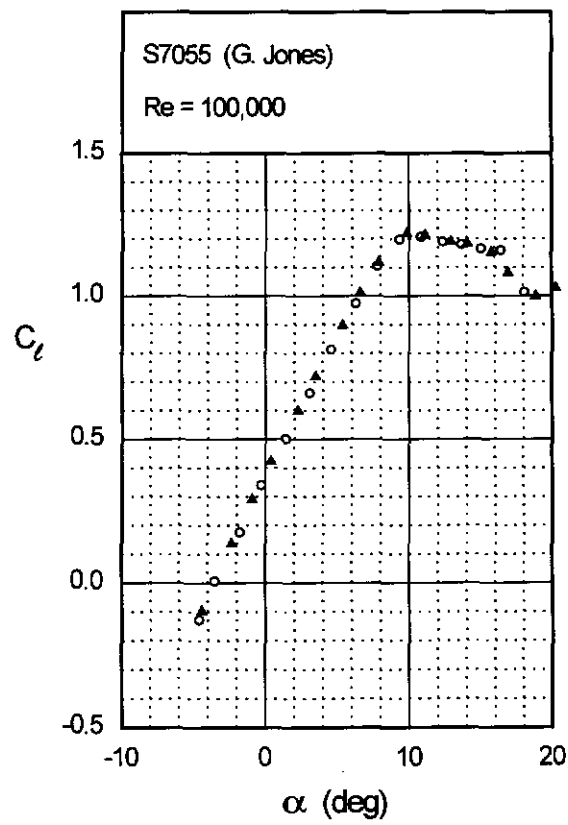
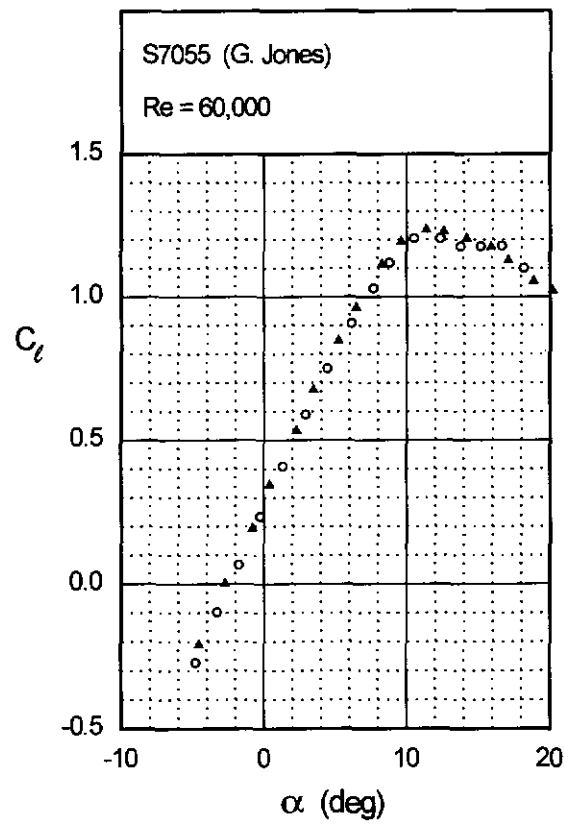
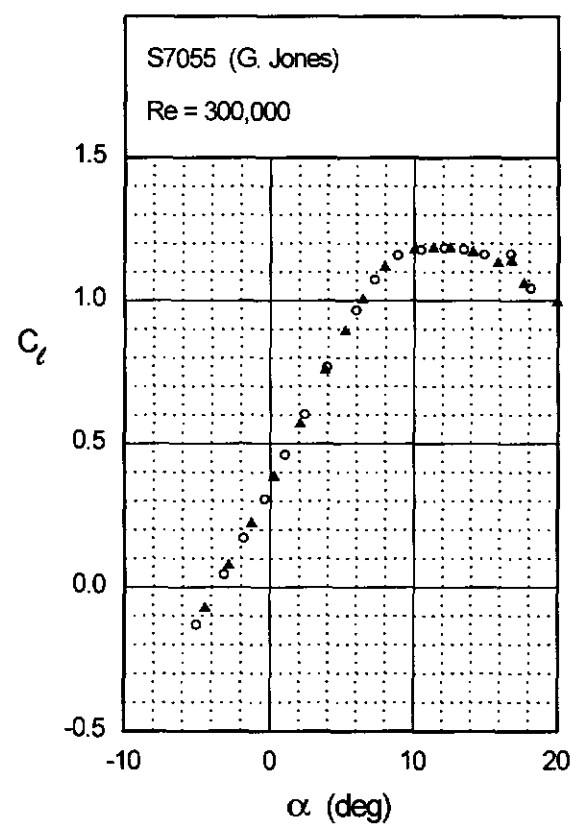
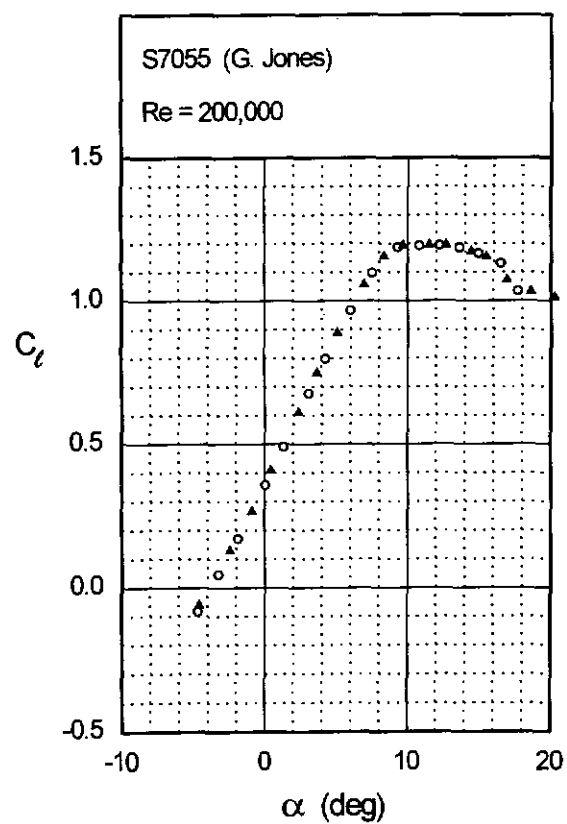


Fig. 4.114 (continued)

Chapter 4: Airfoil Profiles and Performance Plots 201

S7055



SD6060

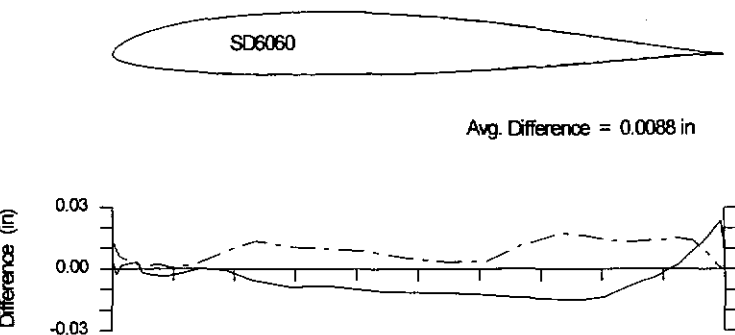
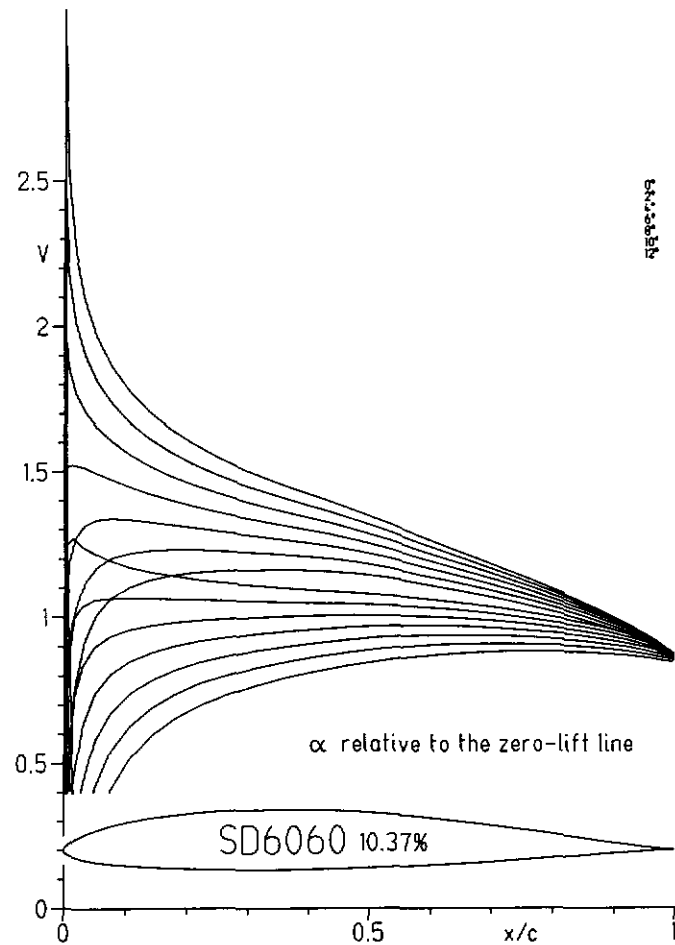
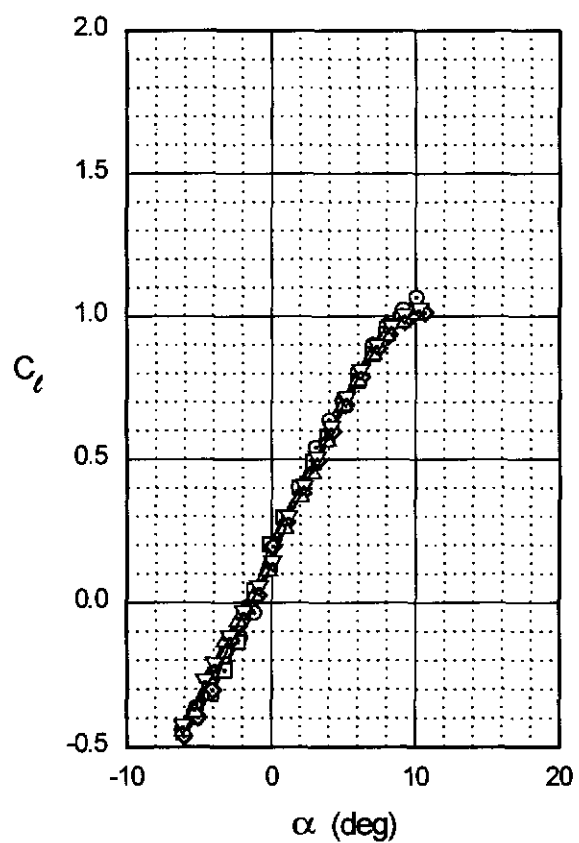
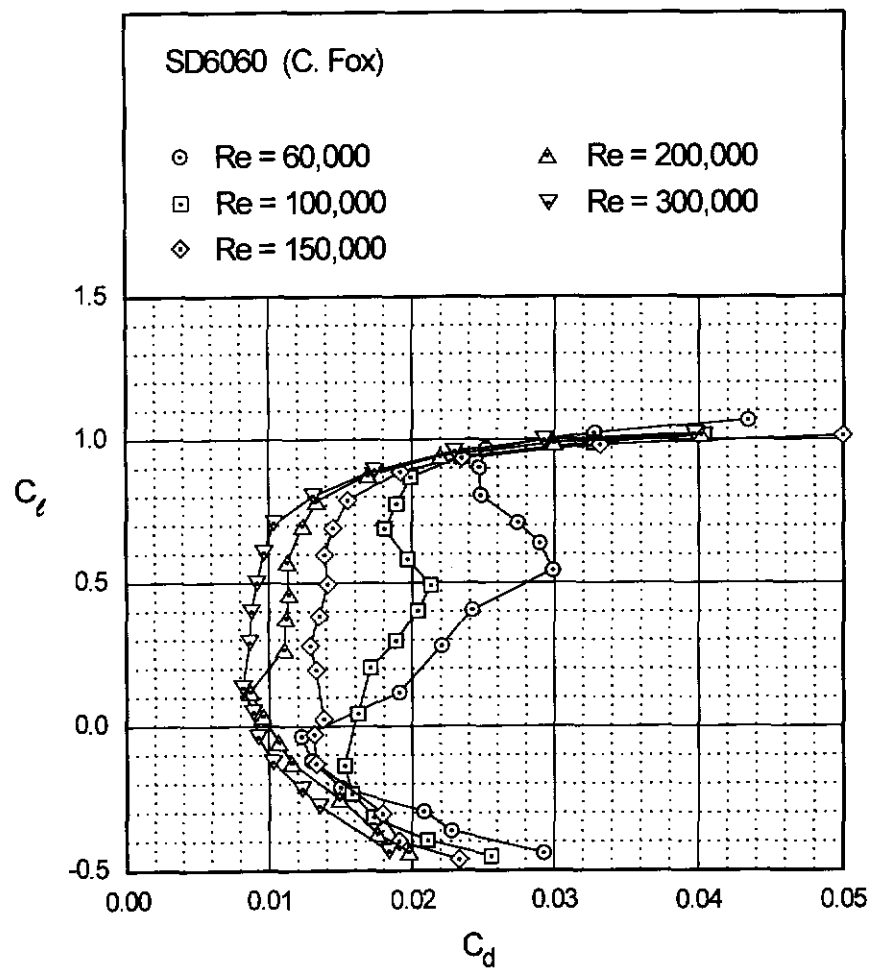


Fig. 4.117

Chapter 4: Airfoil Profiles and Performance Plots 203



SD6060

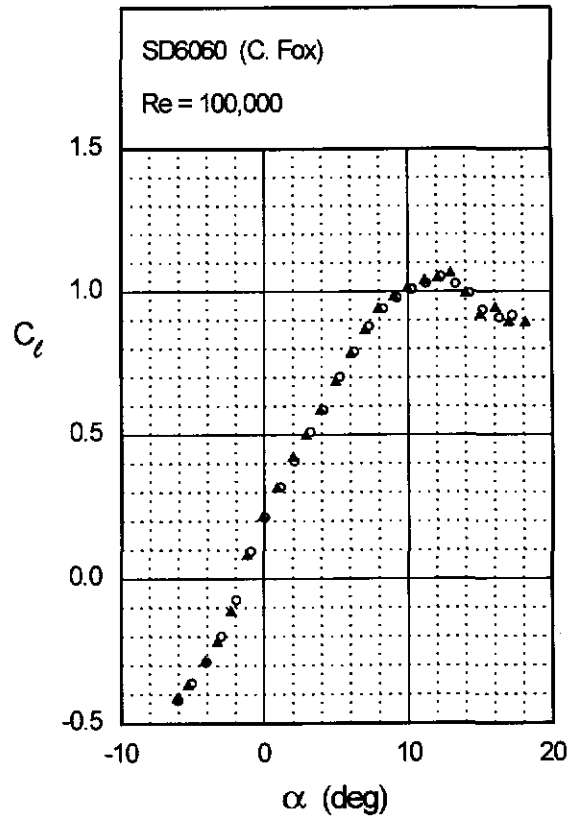
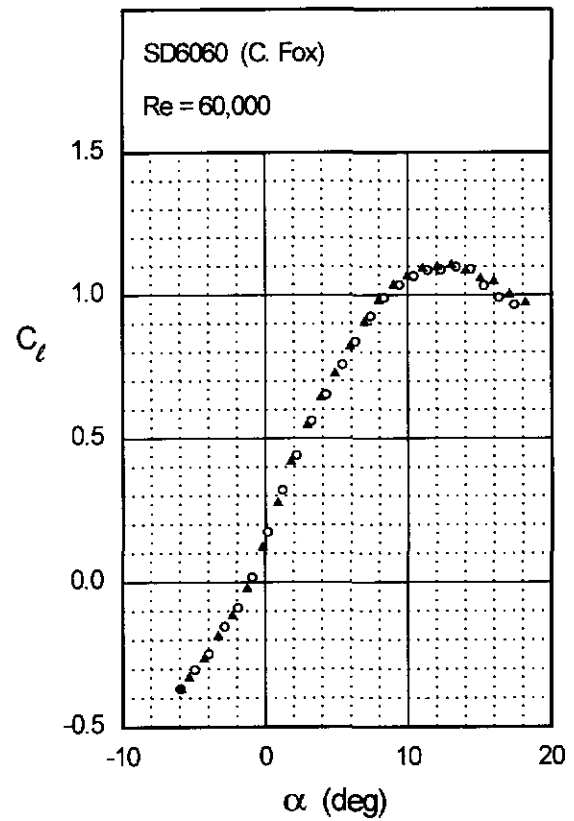
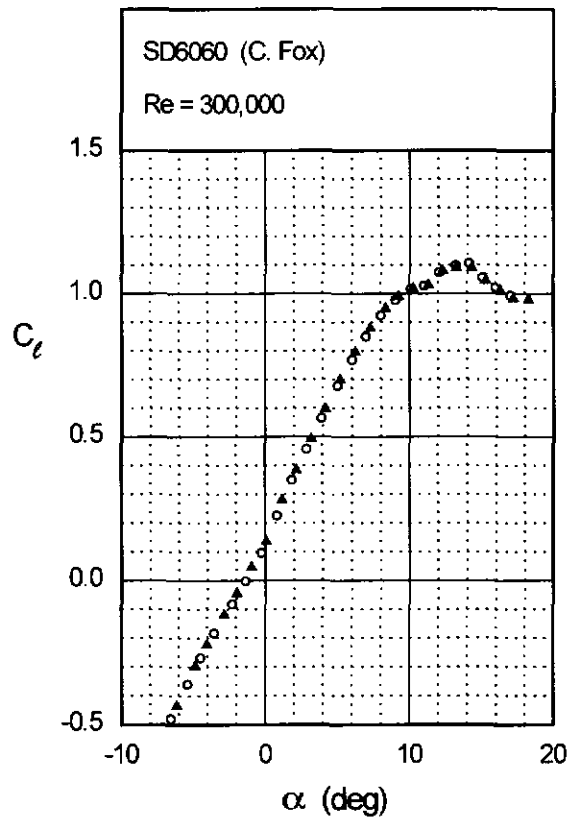
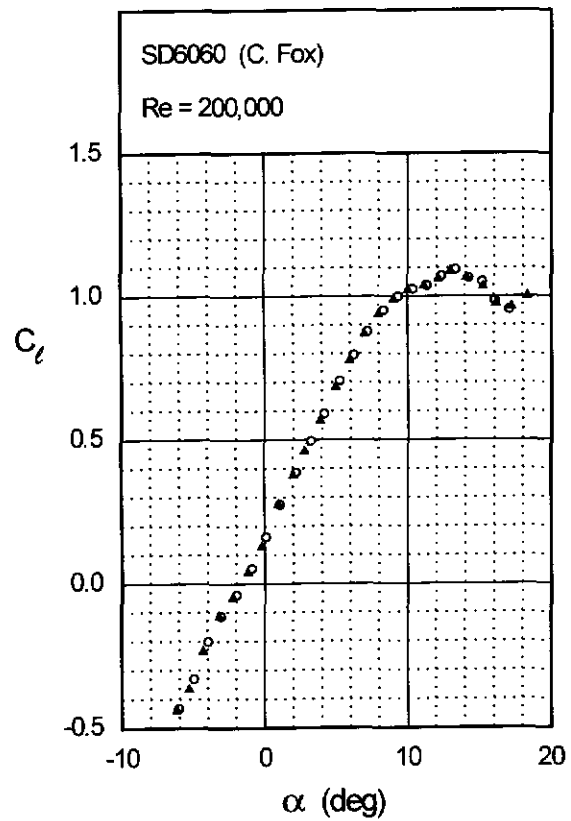


Fig. 4.118 (continued)

Chapter 4: Airfoil Profiles and Performance Plots 205

SD6060



SD7003

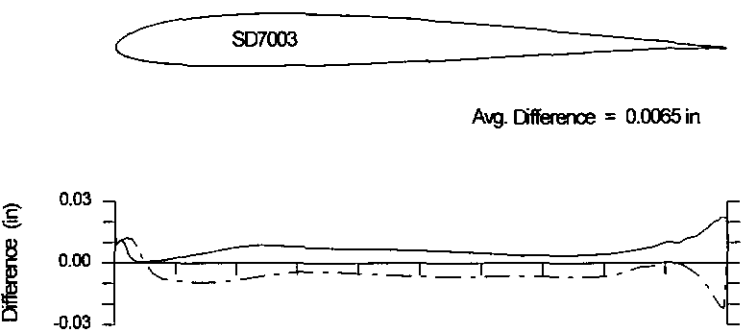
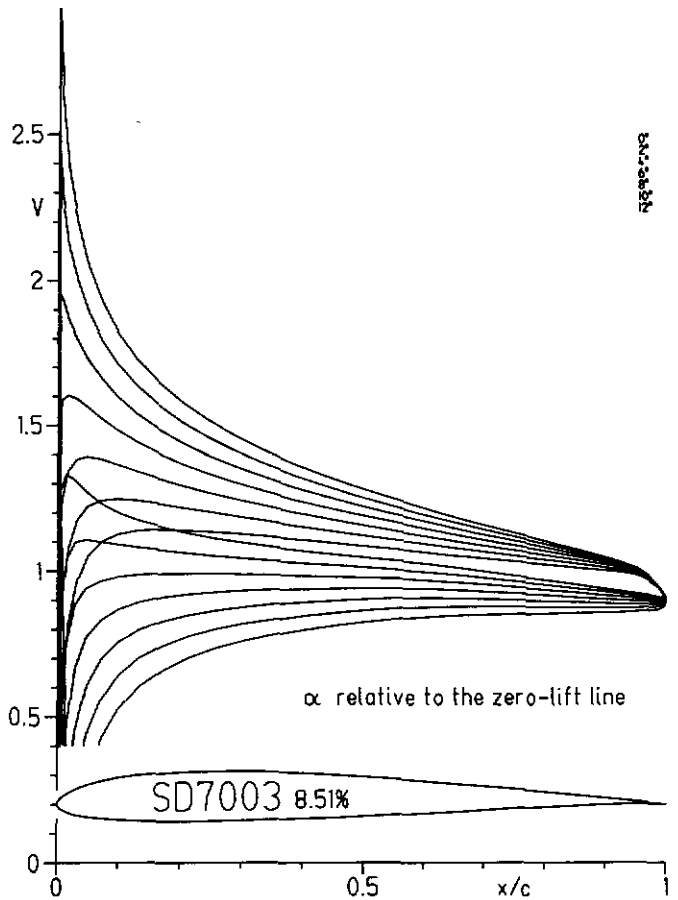
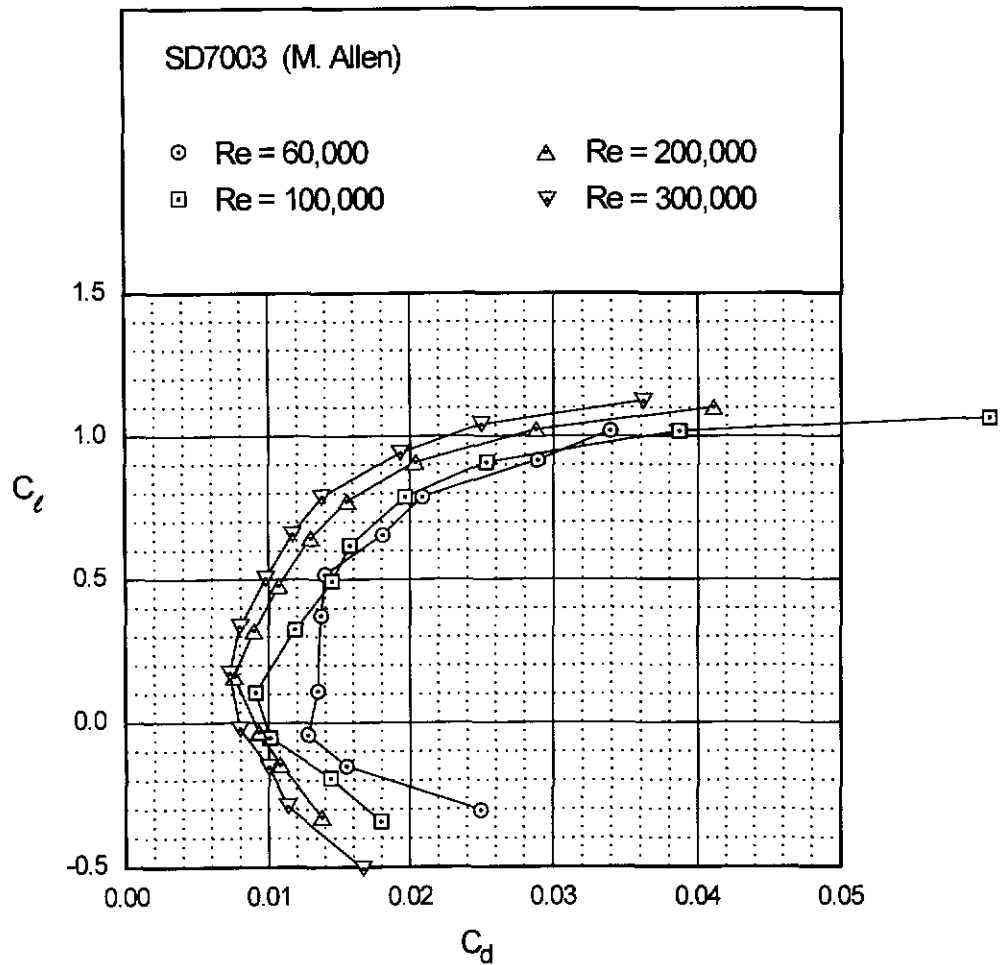
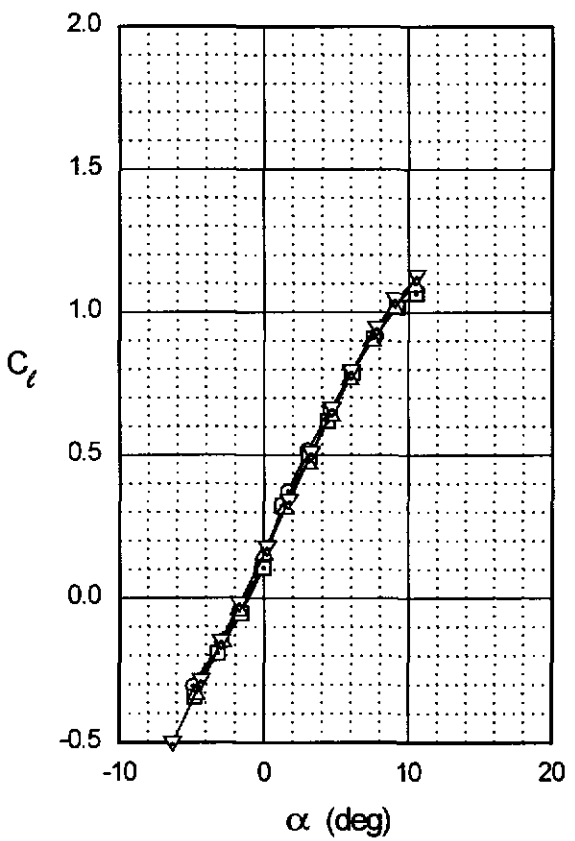


Fig. 4.121

Chapter 4: Airfoil Profiles and Performance Plots 207

SD7003



SD7003

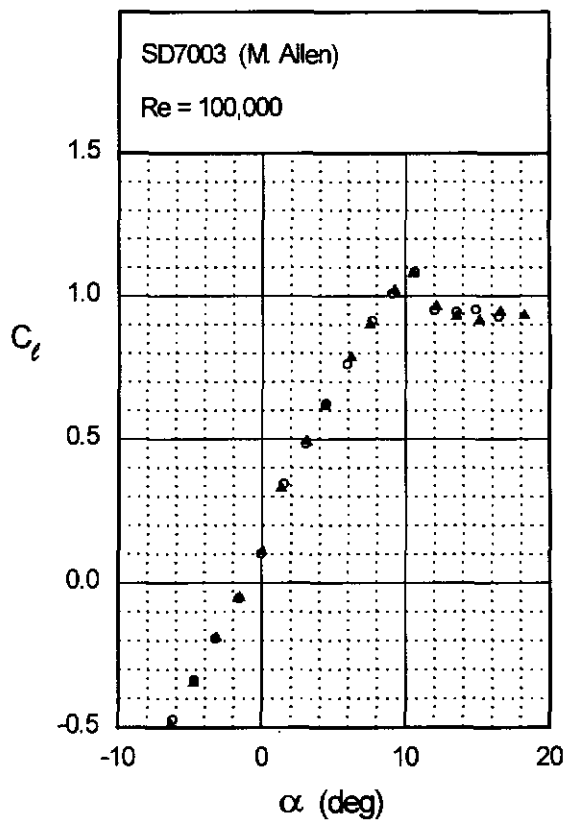
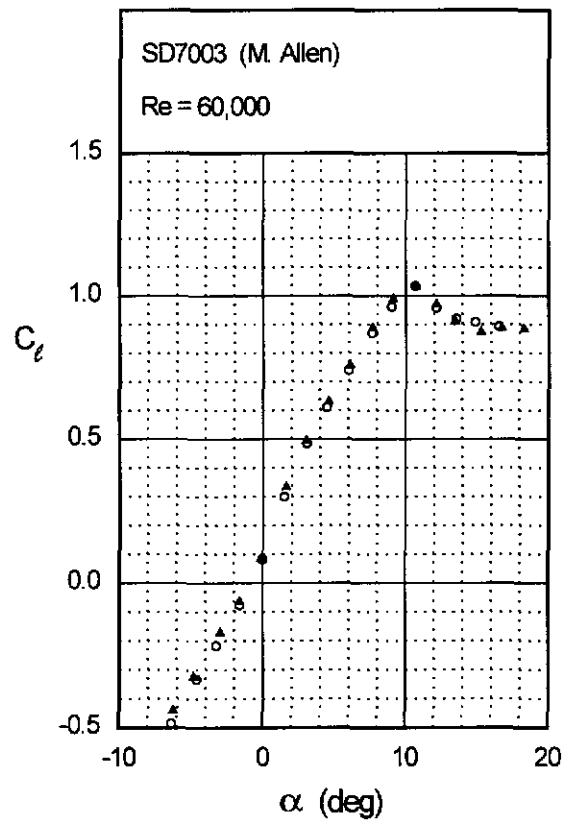
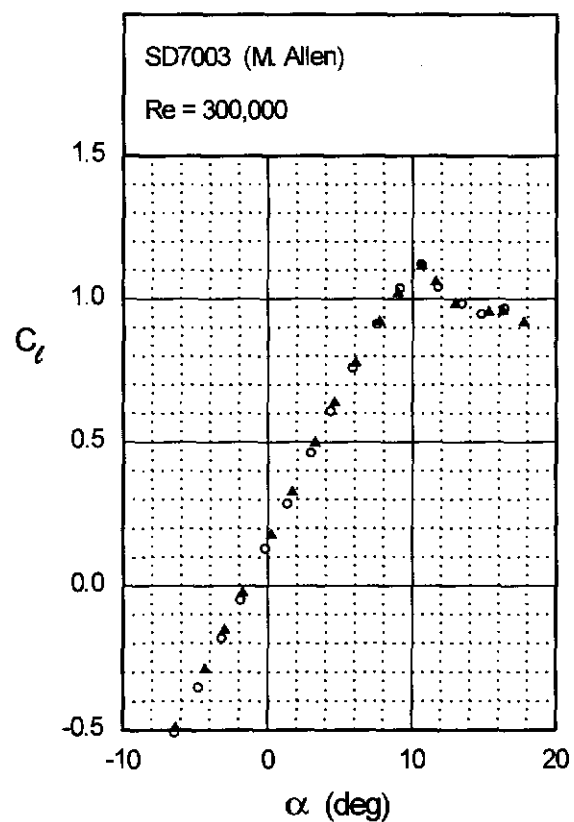
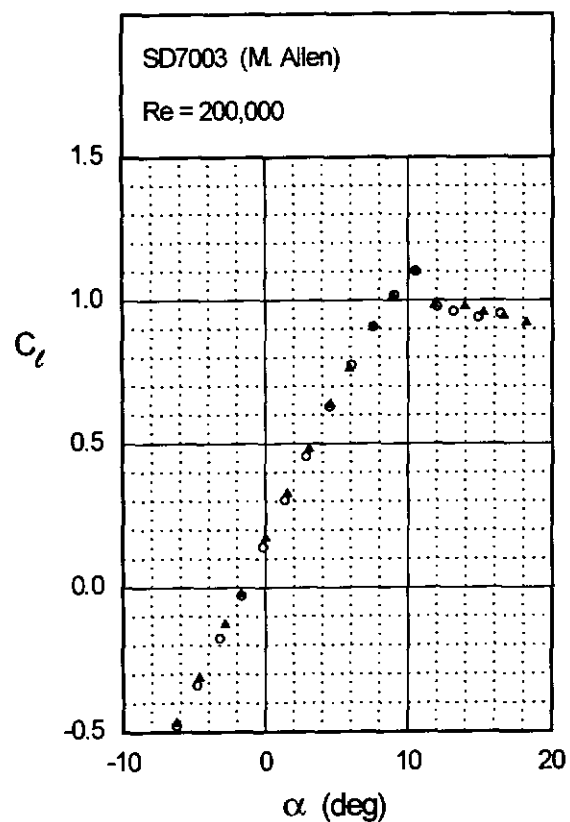


Fig. 4.122 (continued)

Chapter 4: Airfoil Profiles and Performance Plots 209

SD7003



SD7032 (D)

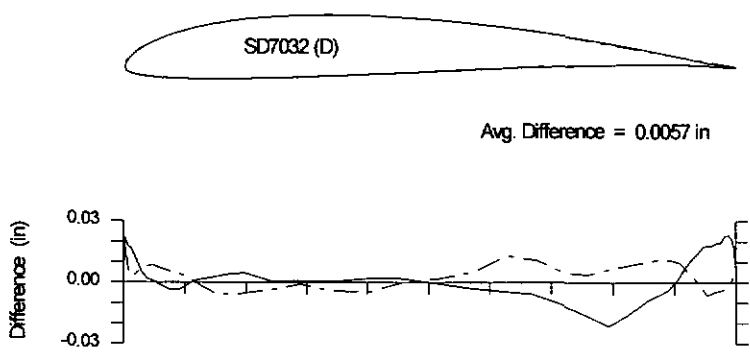
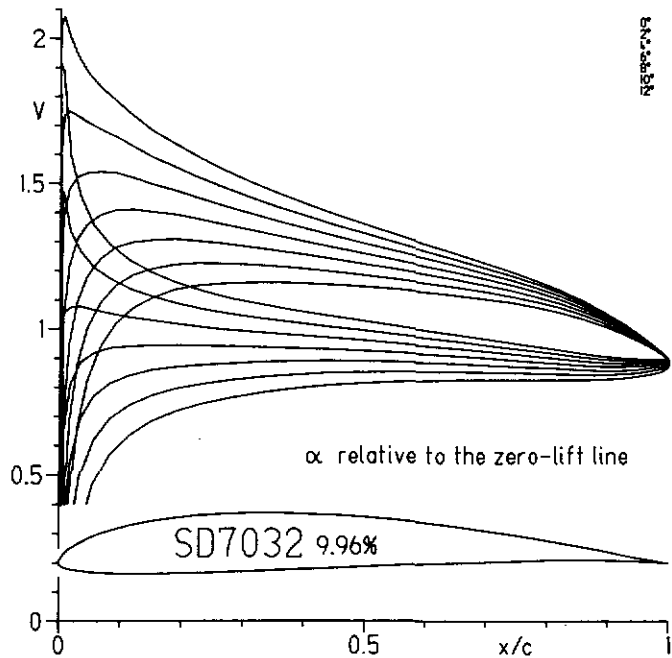
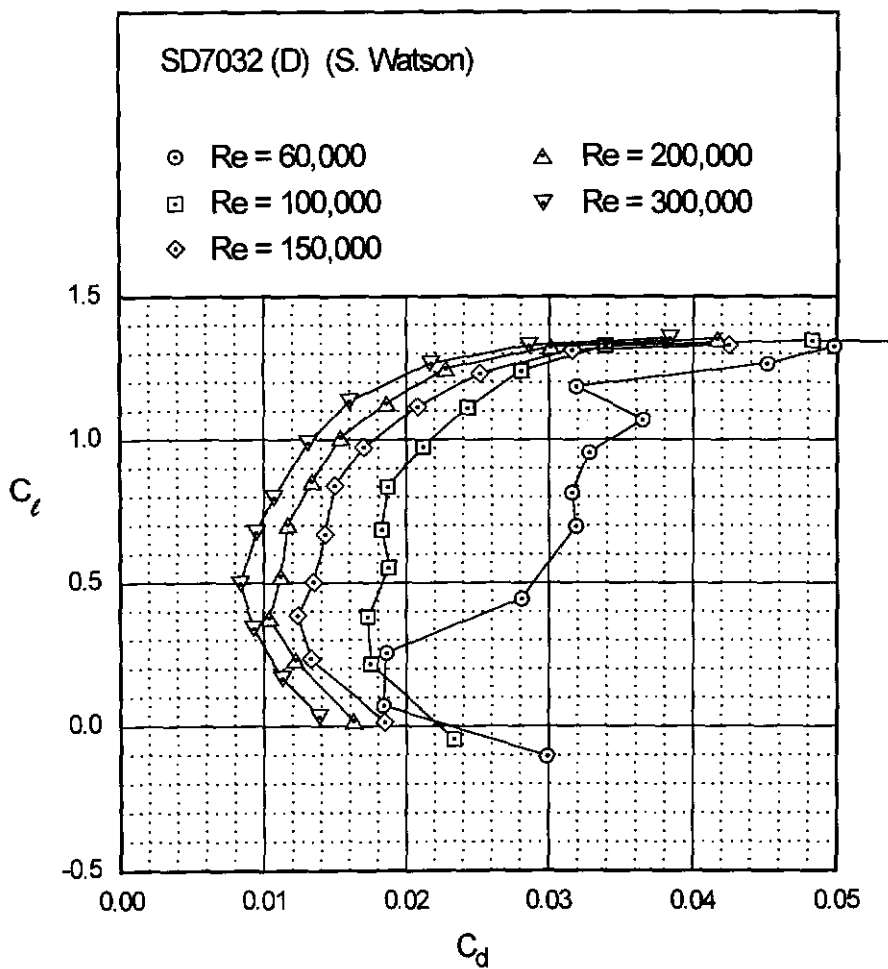
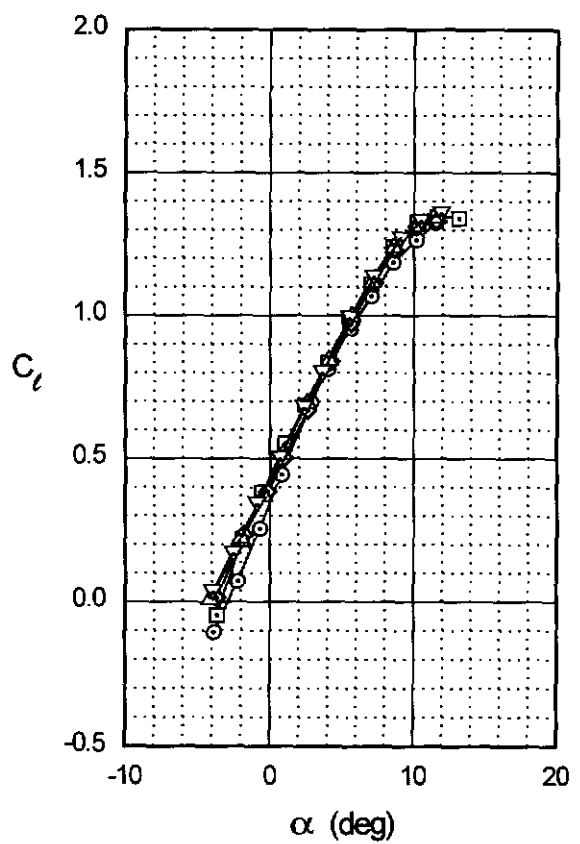


Fig. 4.125

Chapter 4: Airfoil Profiles and Performance Plots 211

SD7032 (D)



SD7032 (D)

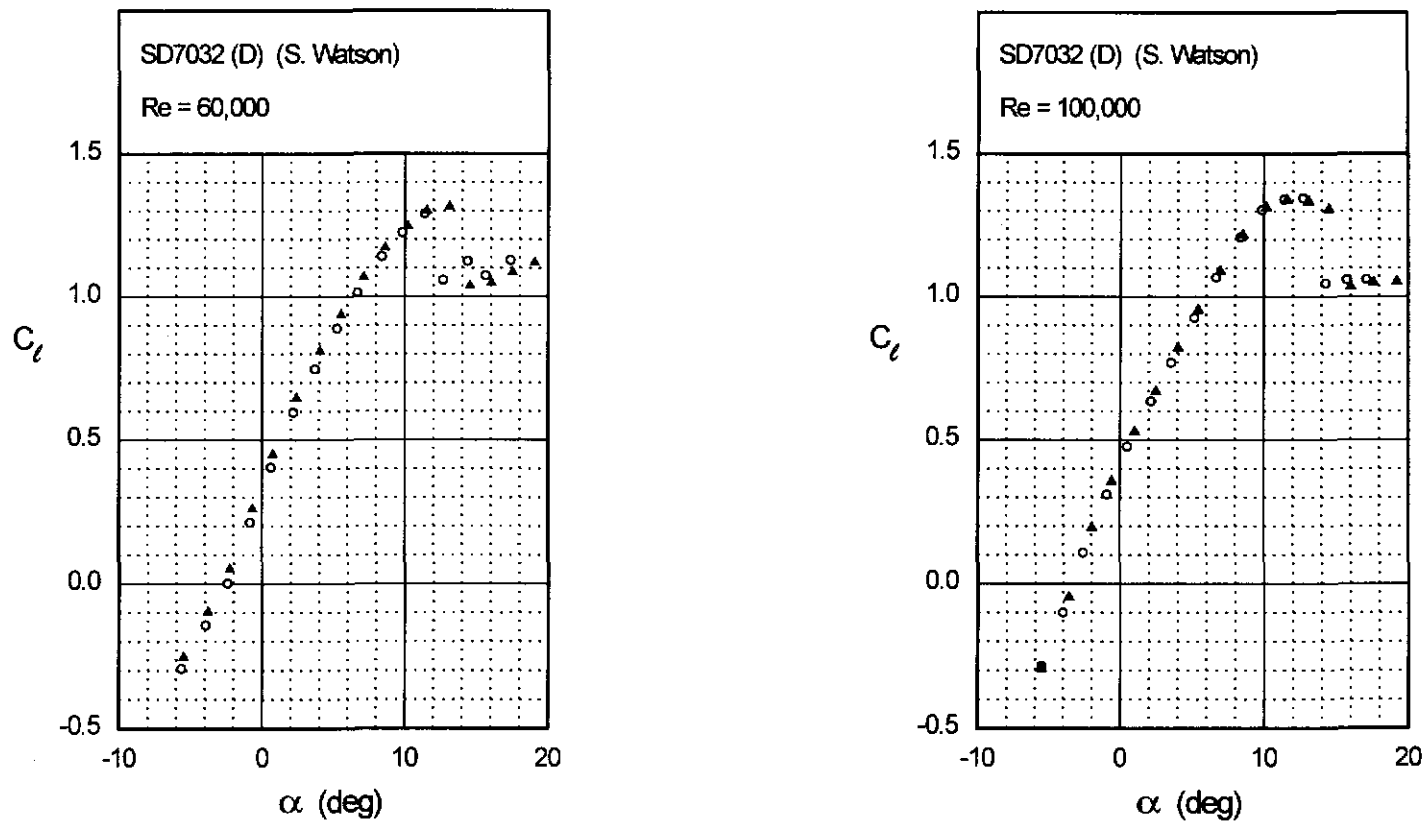
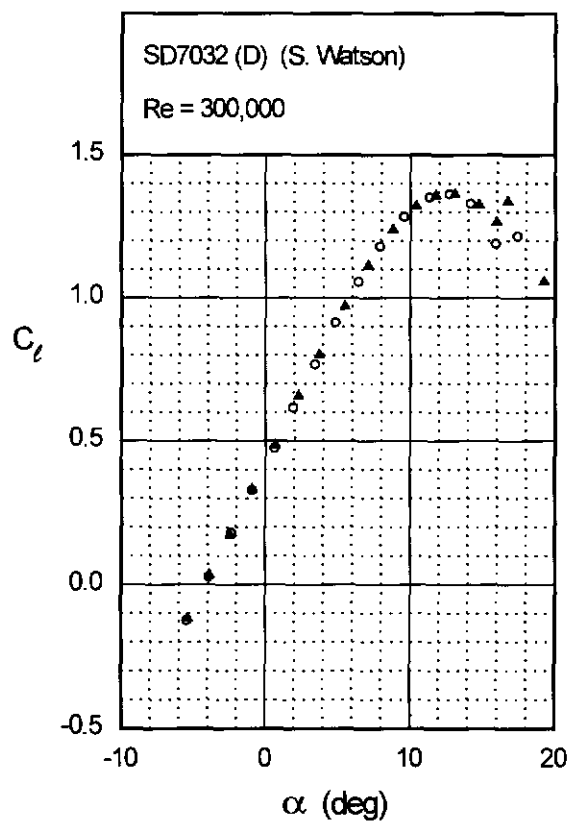
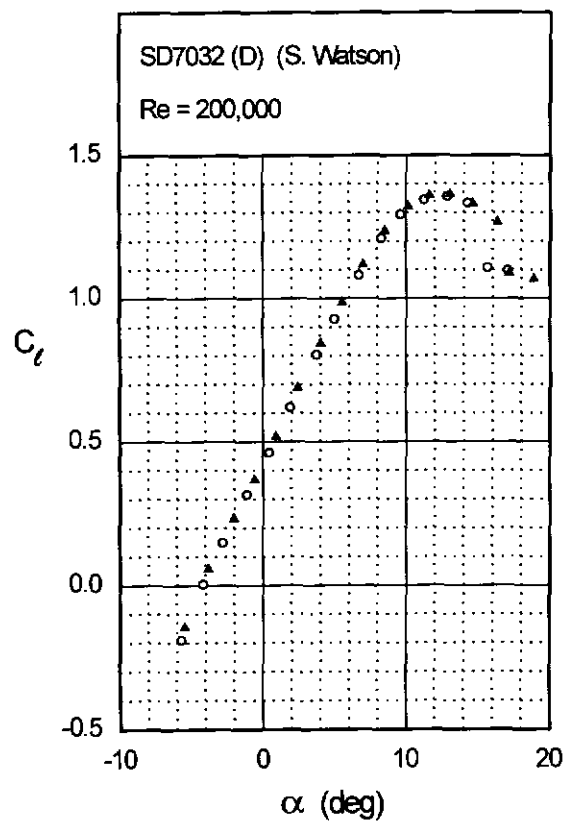


Fig. 4.126

Fig. 4.126 (continued)

Chapter 4: Airfoil Profiles and Performance Plots 213

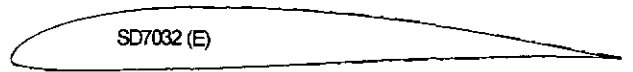
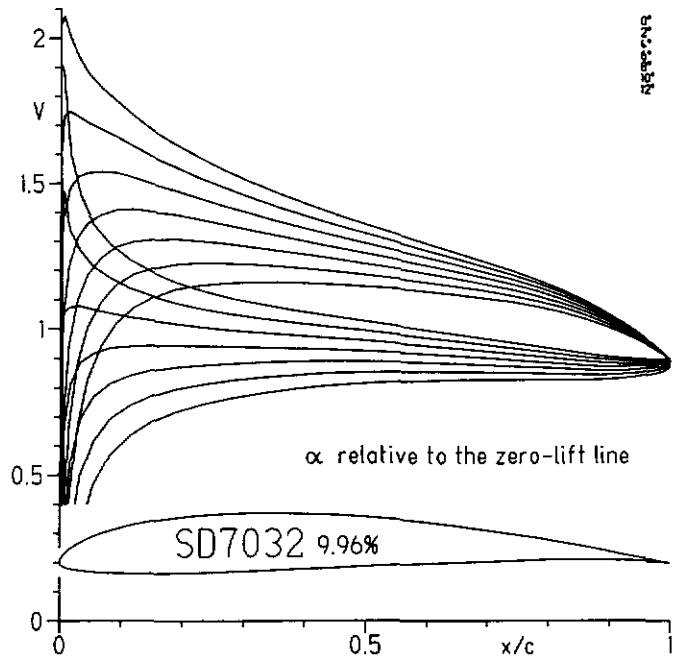
SD7032 (D)



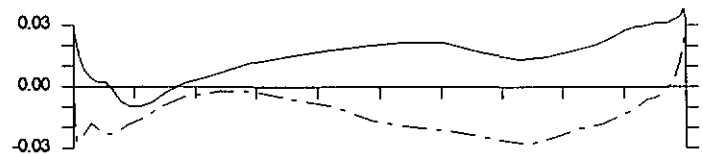
21.4 Summary of Low-Speed Airfoil Data

Figs. 4.127 & 4.128

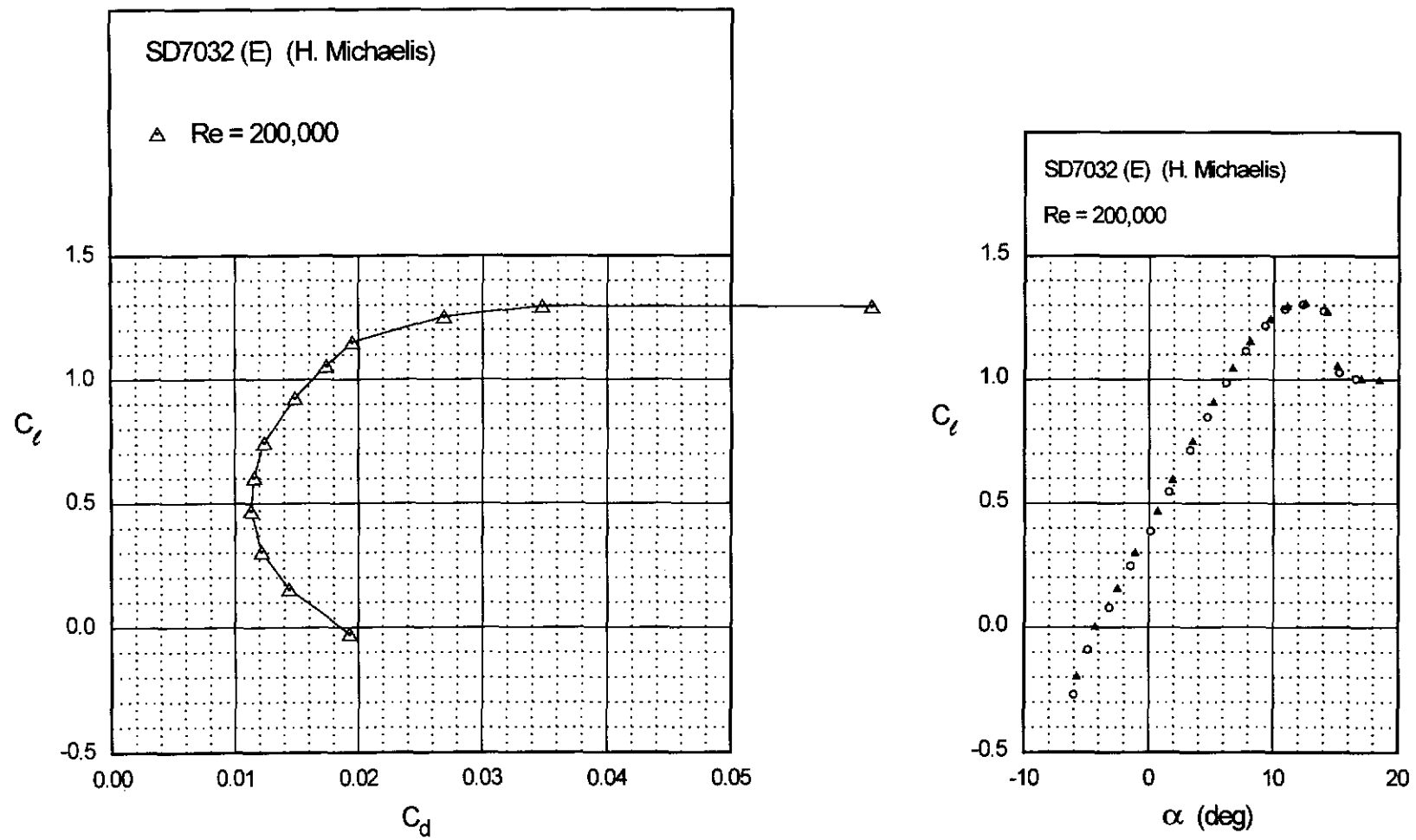
SD7032 (E)



Avg. Difference = 0.0152 in



SD7032 (E)



SD7037 (A)

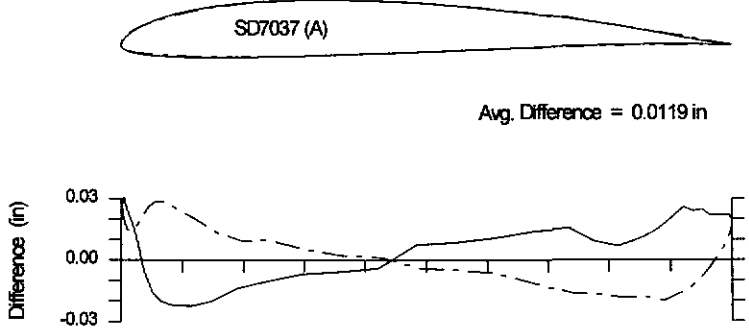
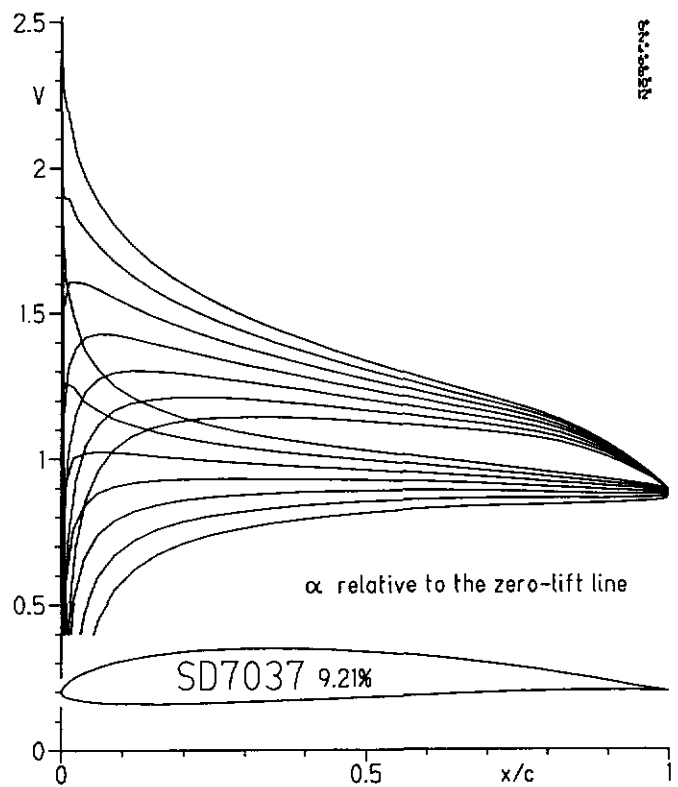


Fig. 4.133

Chapter 4: Airfoil Profiles and Performance Plots 217

SD7037 (A)

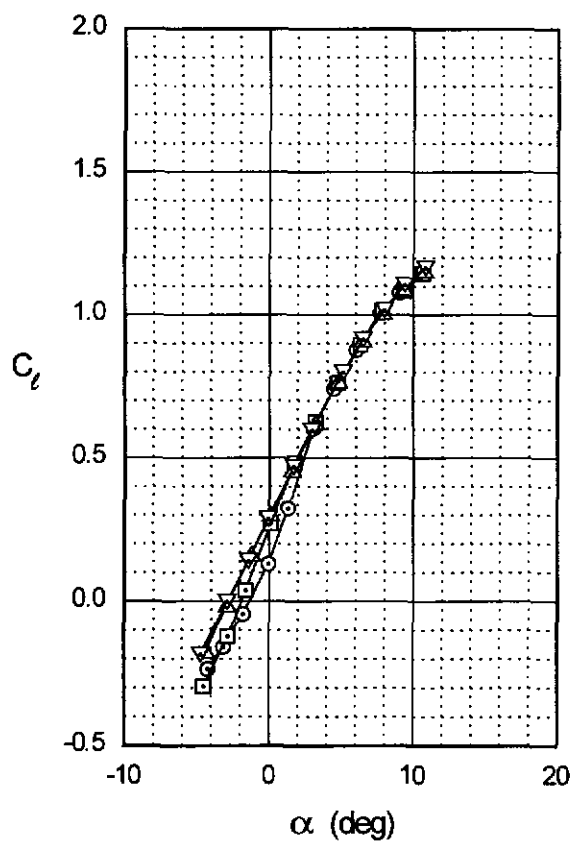
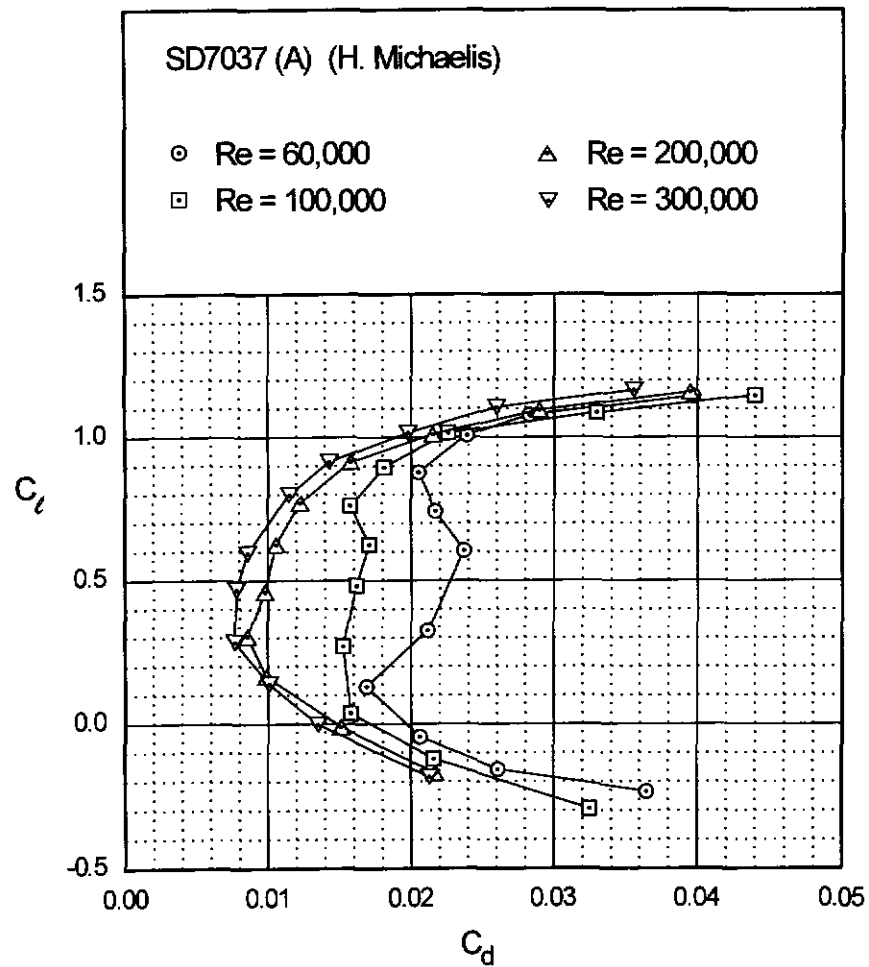


Fig. 4.134

SD7037 (A)

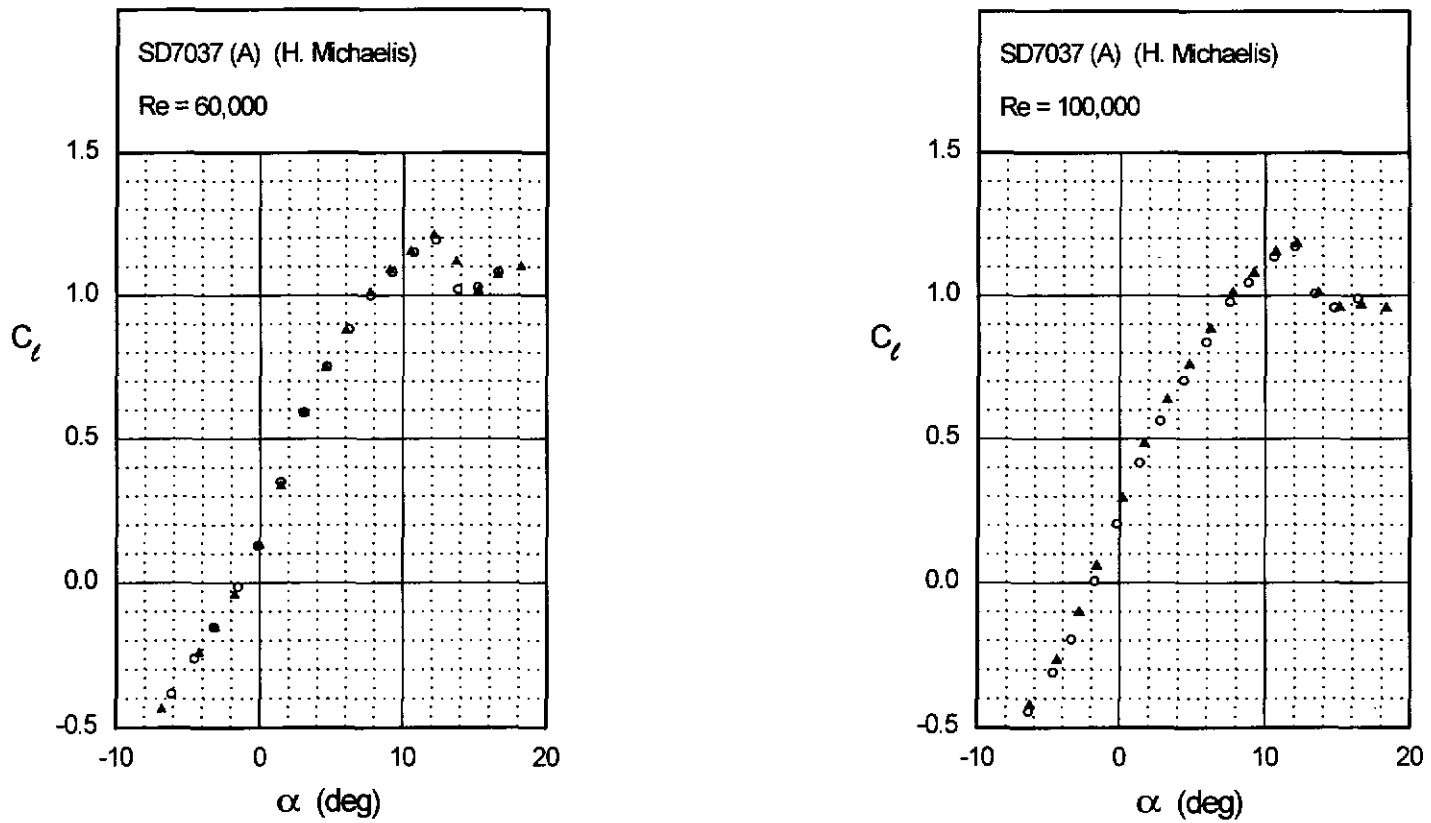
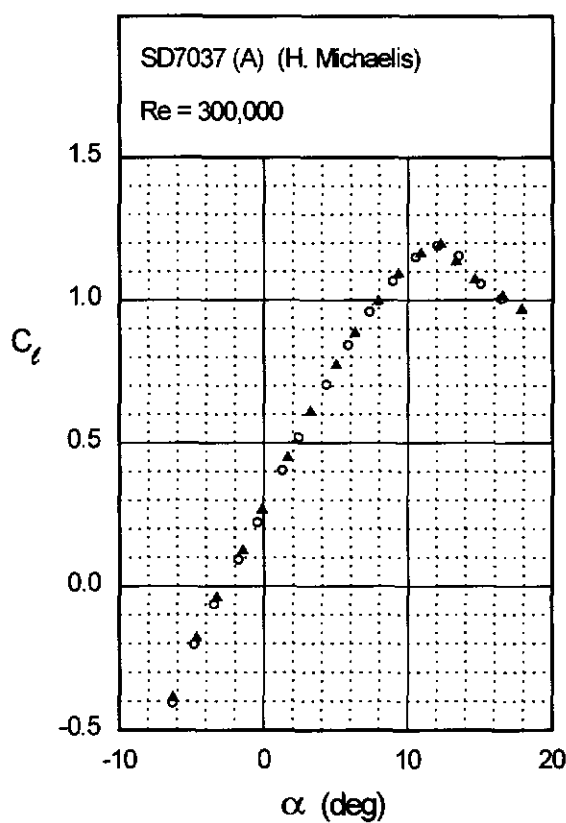
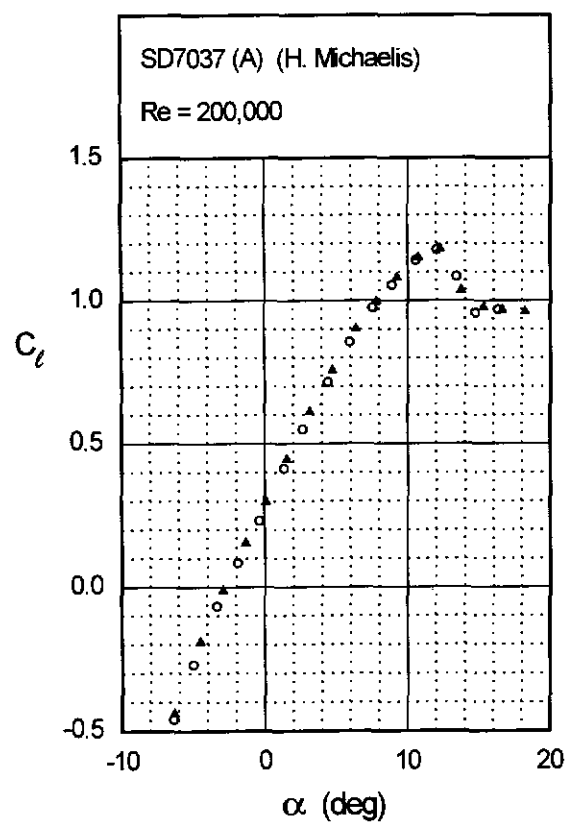


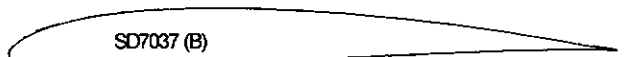
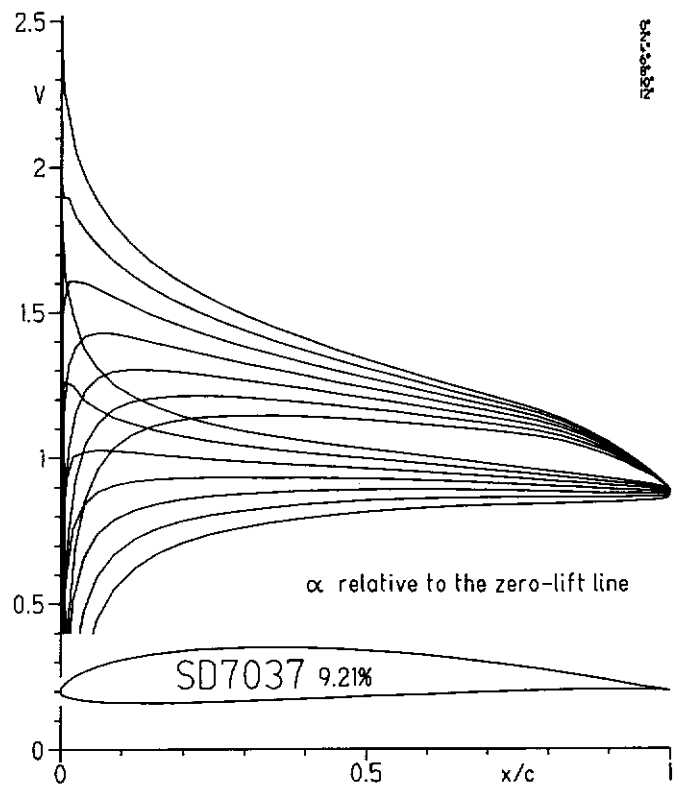
Fig. 4.134 (continued)

Chapter 4: Airfoil Profiles and Performance Plots 219

SD7037 (A)



SD7037 (B)



Avg. Difference = 0.0081 in

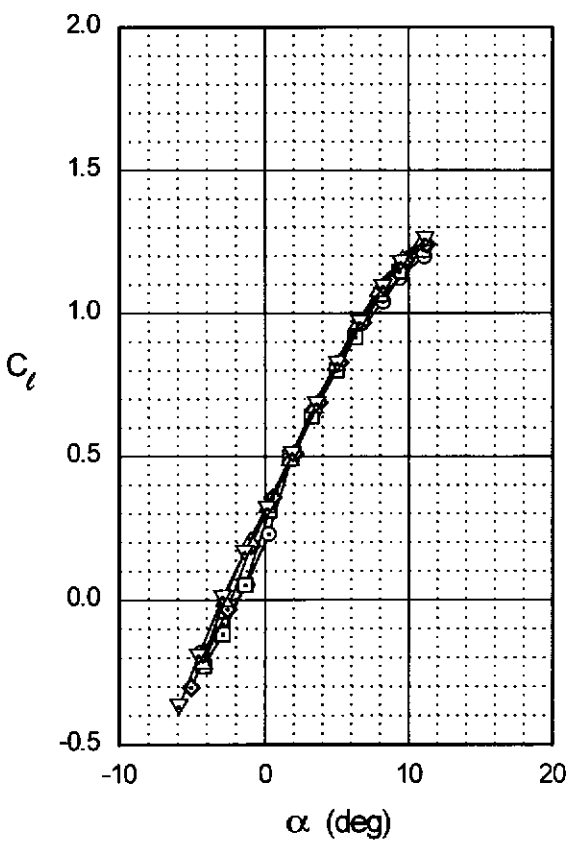
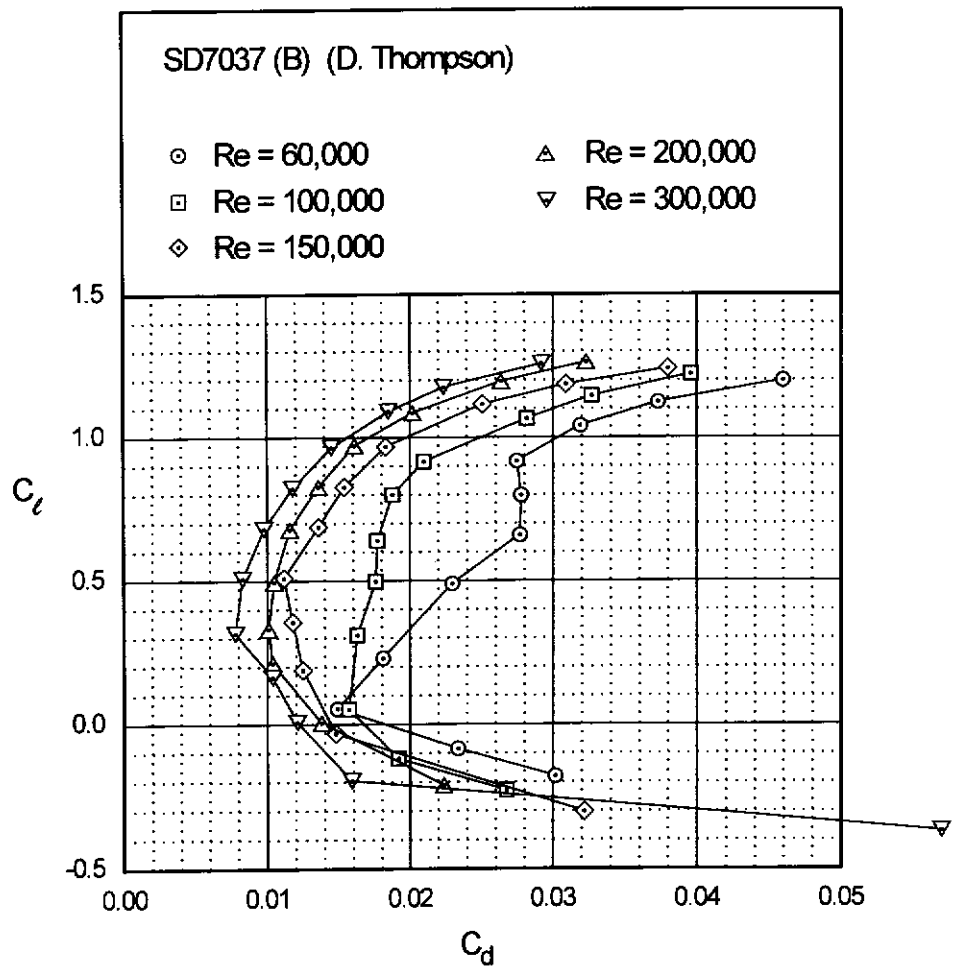


Fig. 4.137

Chapter 4: Airfoil Profiles and Performance Plots

221

SD7037 (B)



SD7037 (B)

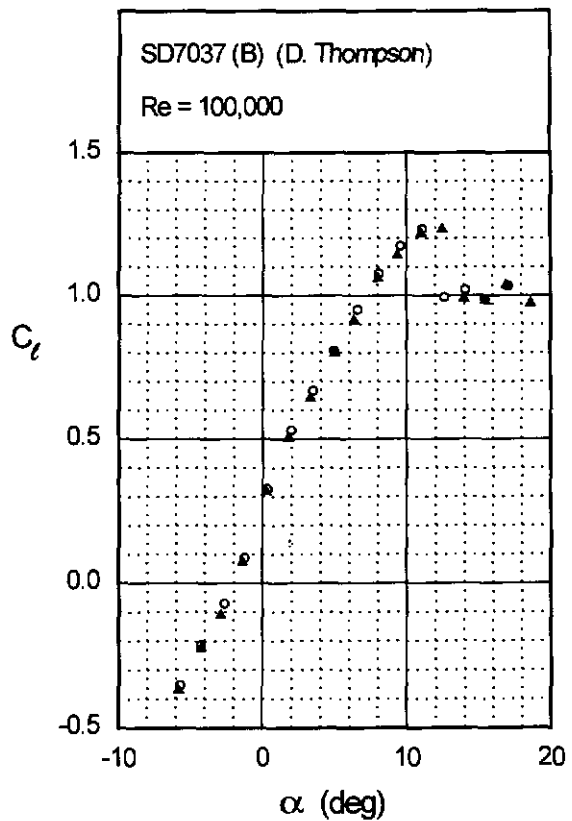
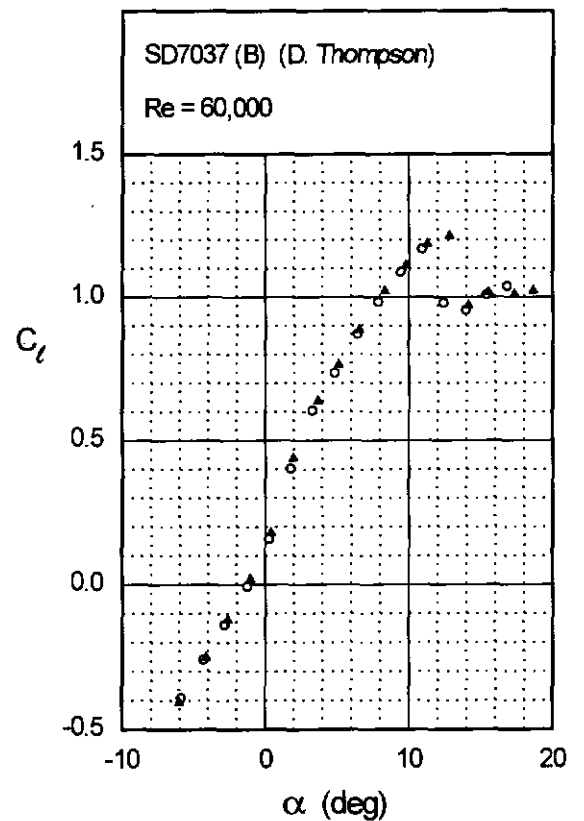


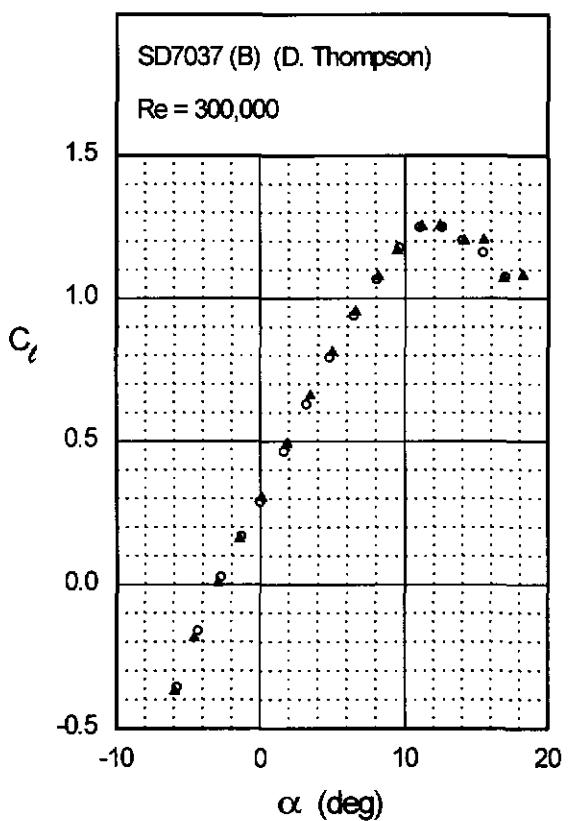
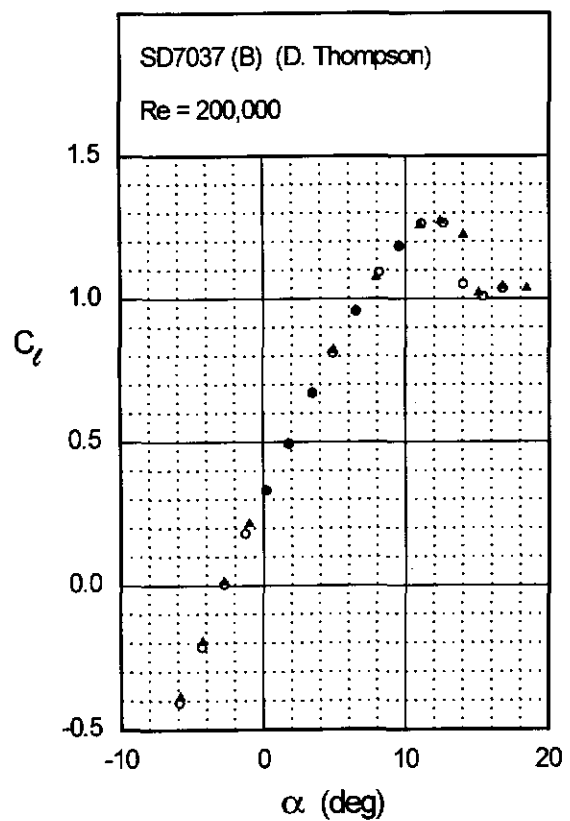
Fig. 4.138

Fig. 4.138 (continued)

Chapter 4: Airfoil Profiles and Performance Plots

223

SD7037 (B)



SD8000

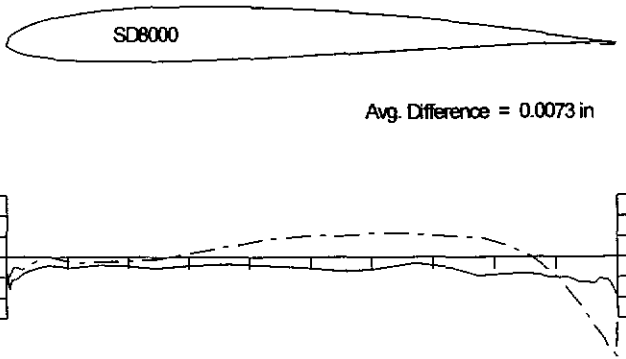
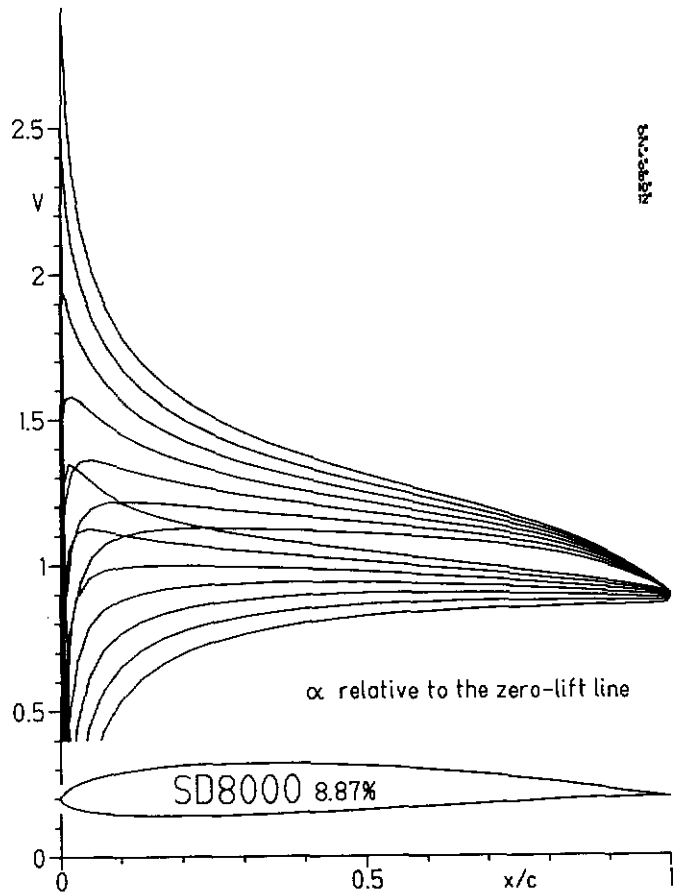
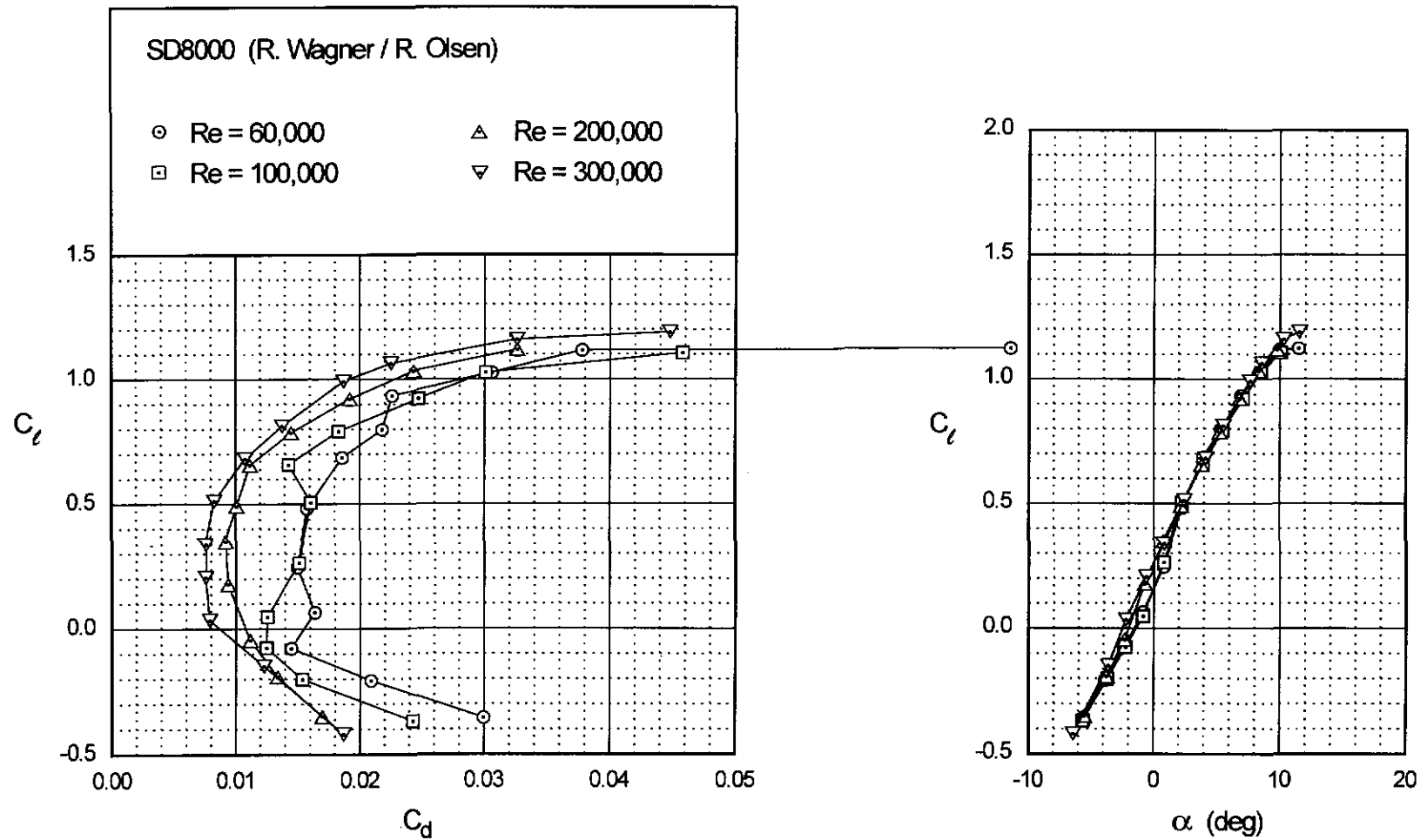


Fig. 4.141

Chapter 4: Airfoil Profiles and Performance Plots 225



SD8000

SD8000

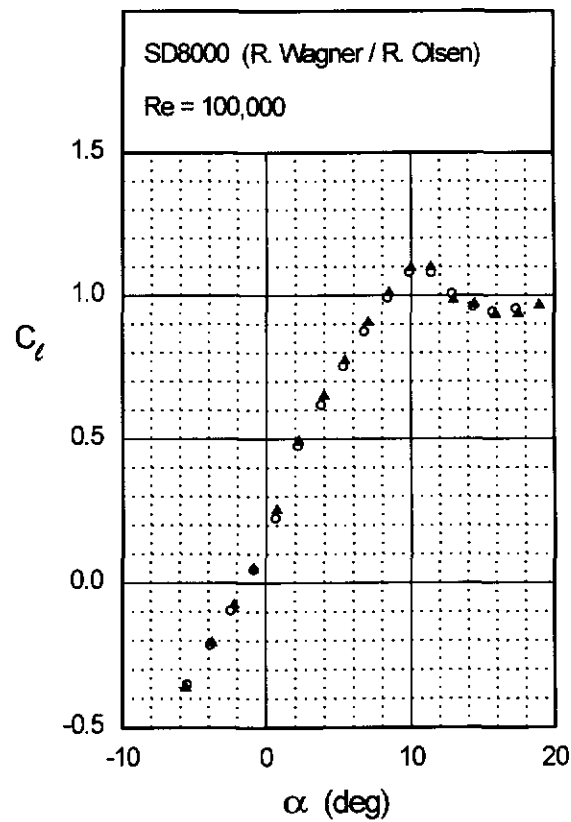
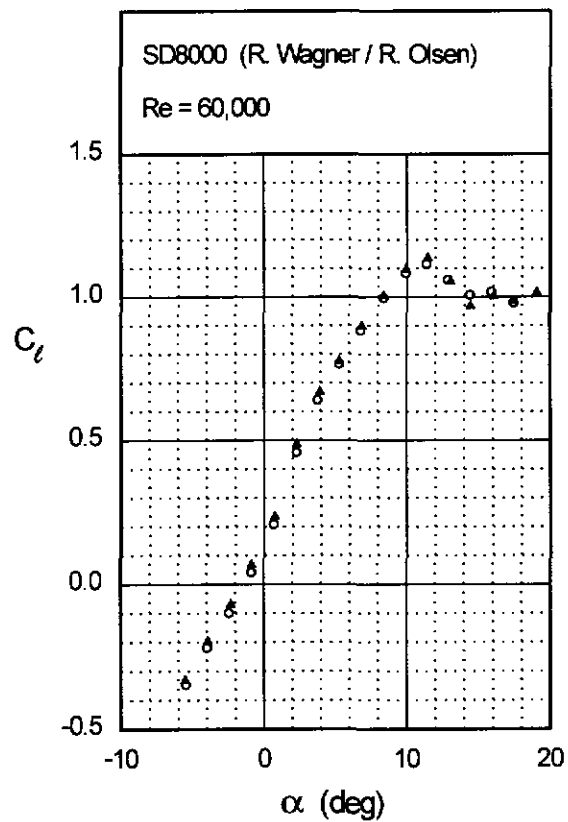
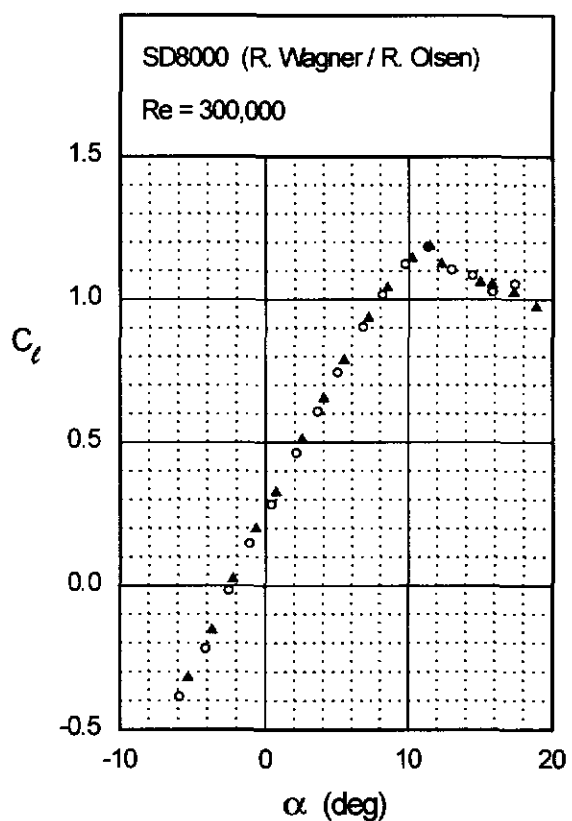
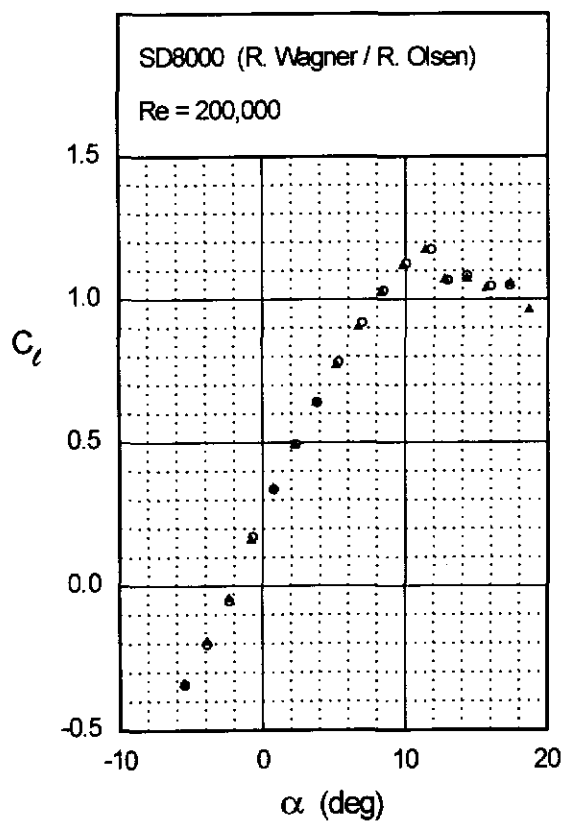


Fig. 4.142 (continued)

SD8000



SD8020

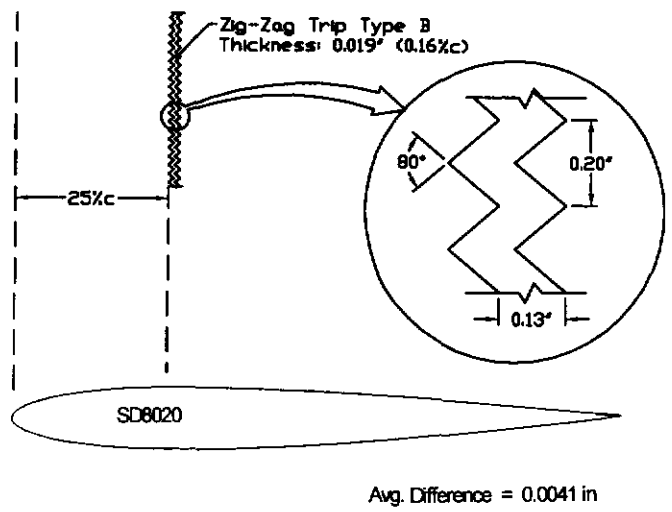
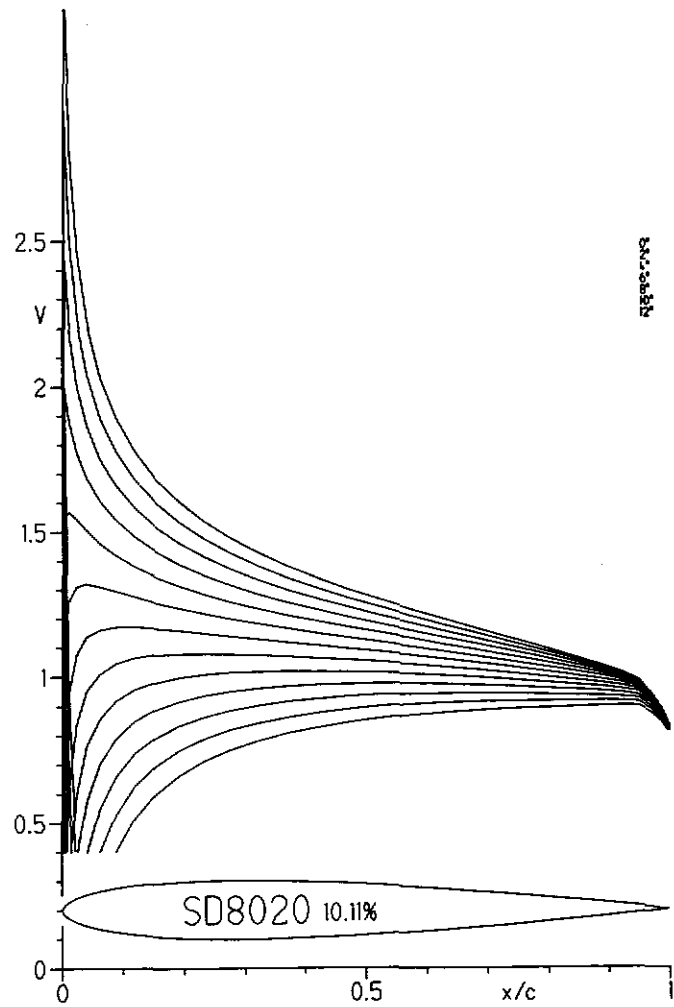
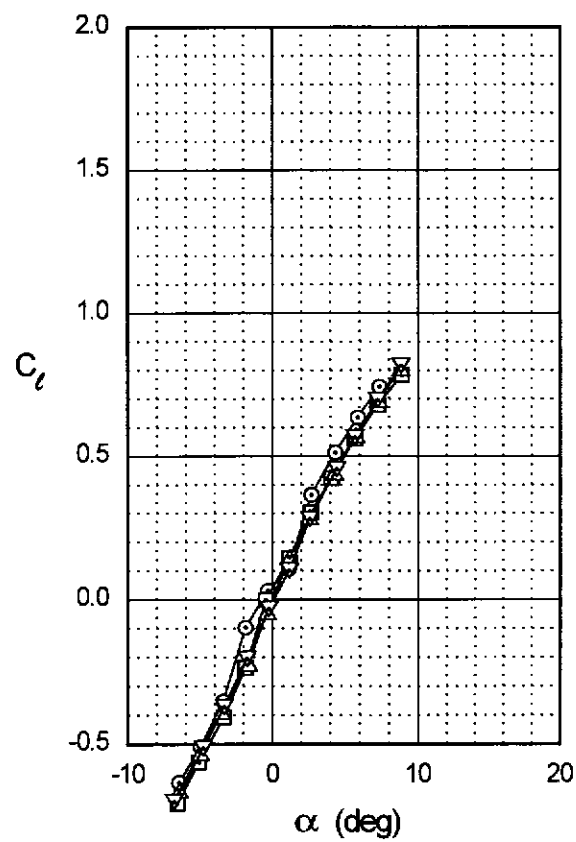
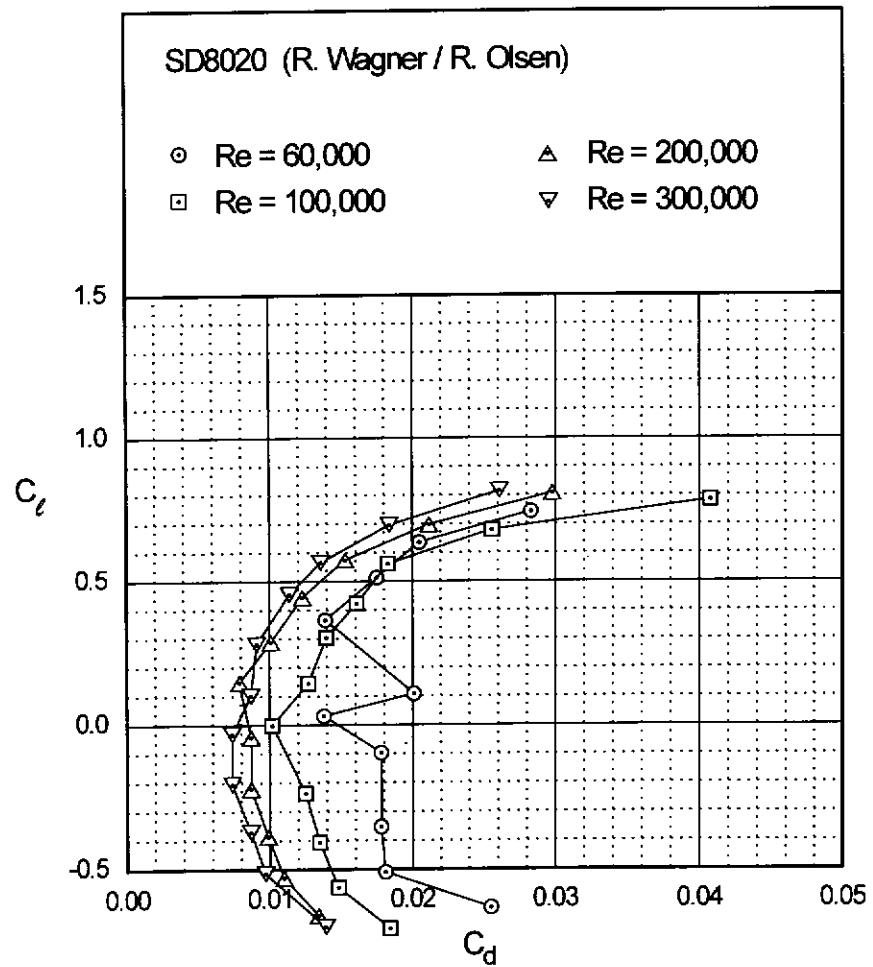


Fig. 4.145

Chapter 4: Airfoil Profiles and Performance Plots 229



SD8020

SD8020

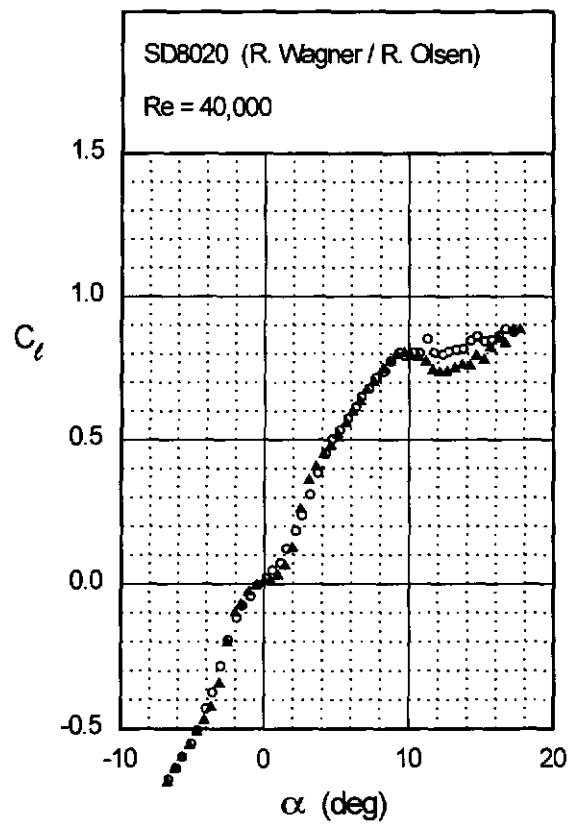
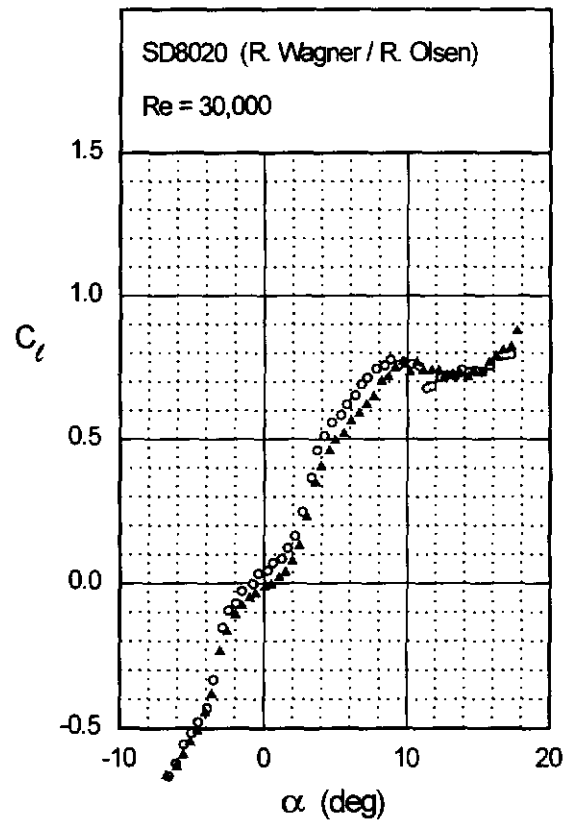


Fig. 4.146 (continued)

Chapter 4: Airfoil Profiles and Performance Plots 231

SD8020

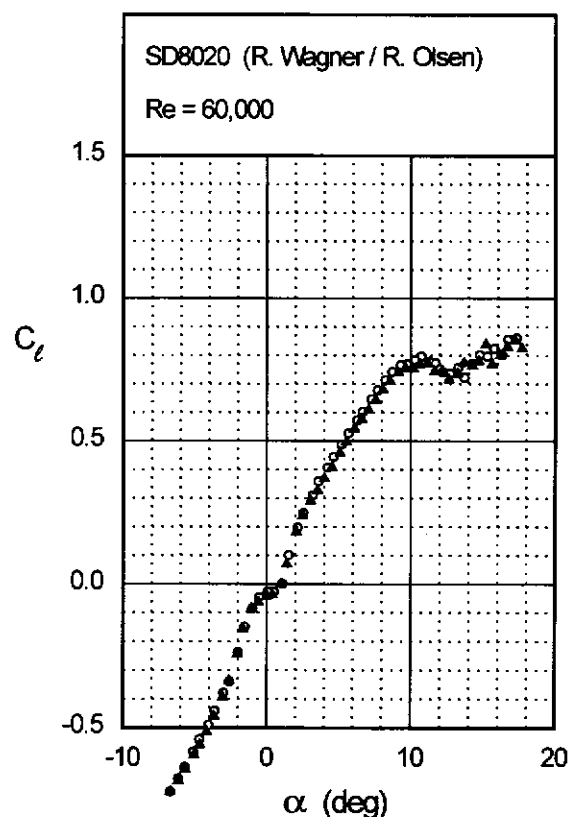
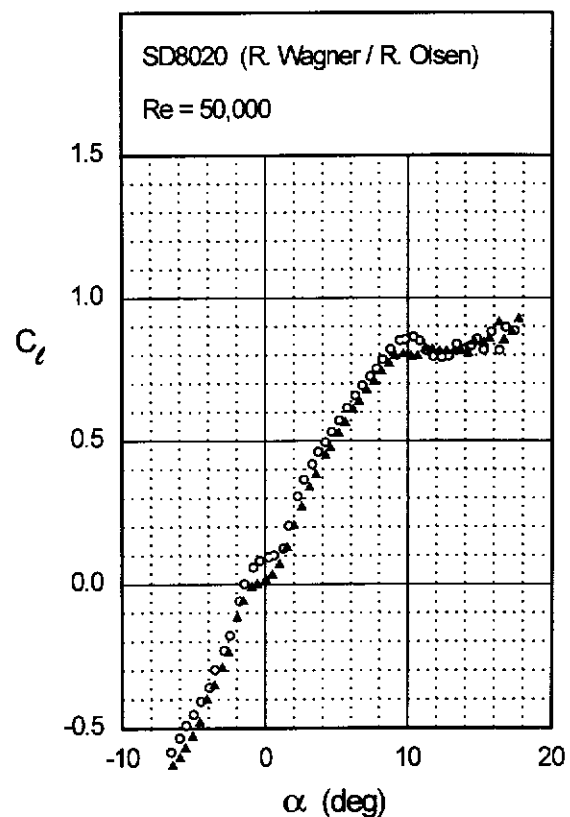


Fig. 4.146 (continued)

SD8020

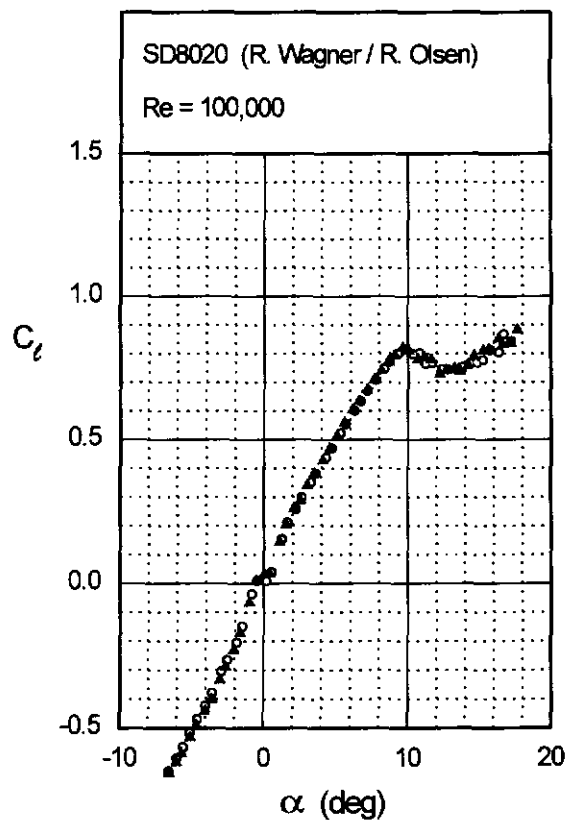
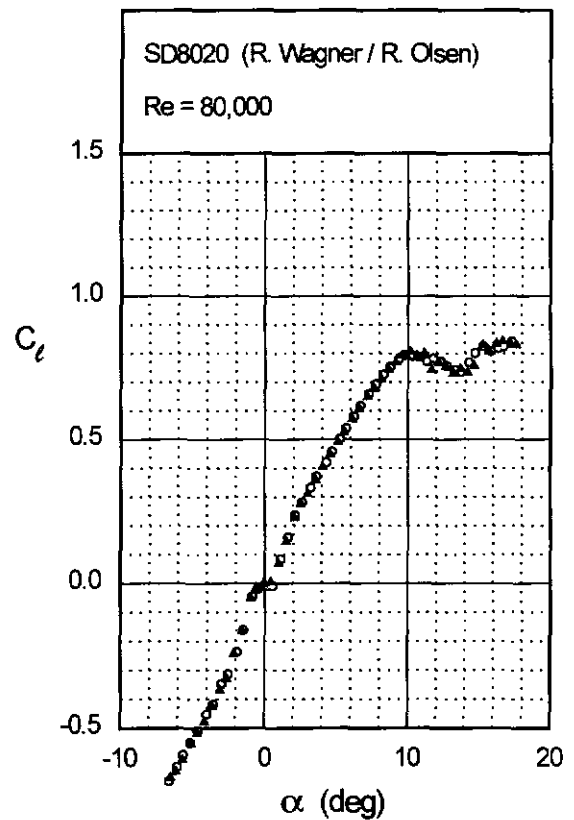


Fig. 4.146 (continued)

Chapter 4: Airfoil Profiles and Performance Plots 233

SD8020

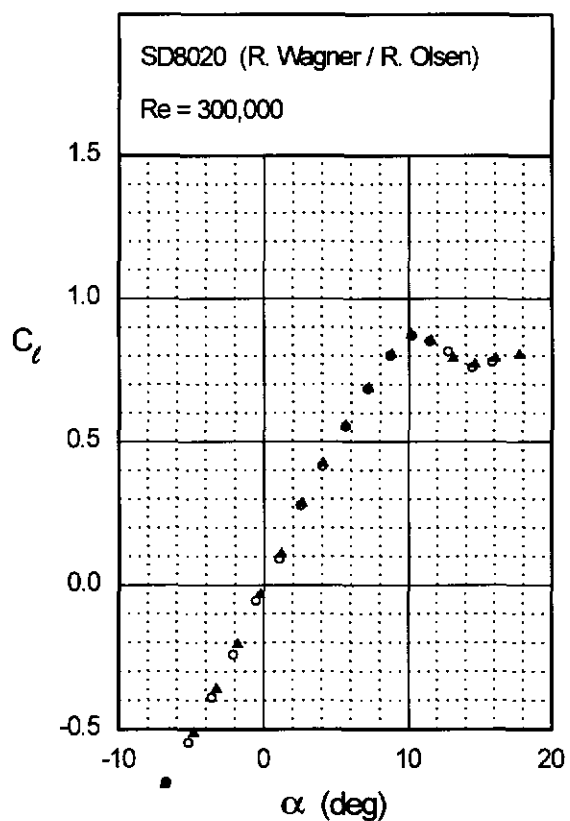
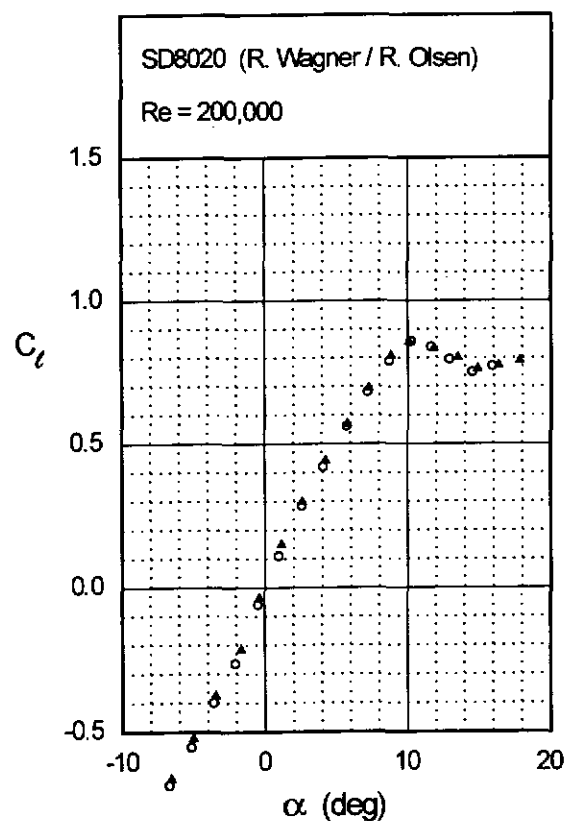


Fig. 4.147

SD8020

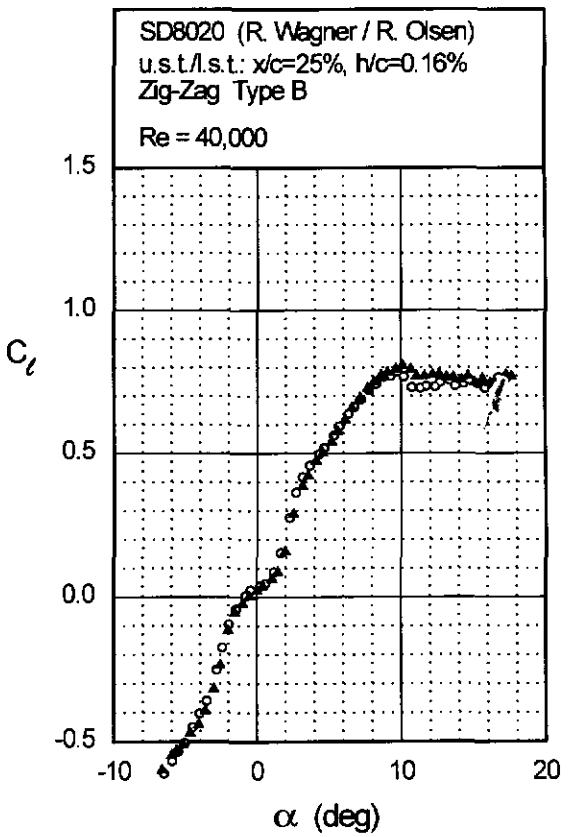
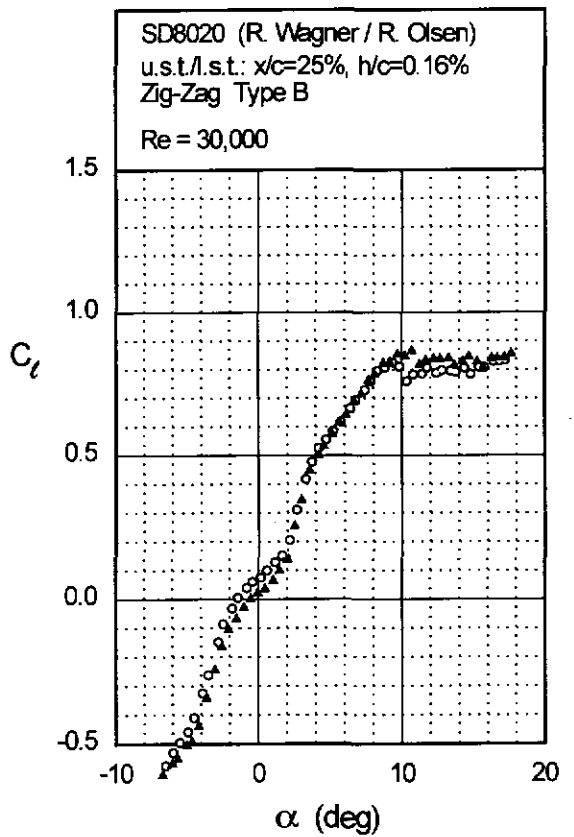
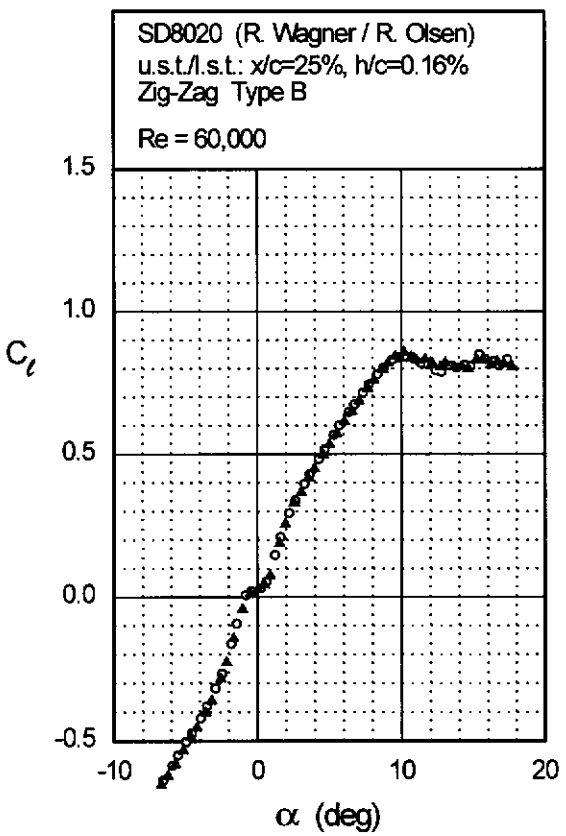
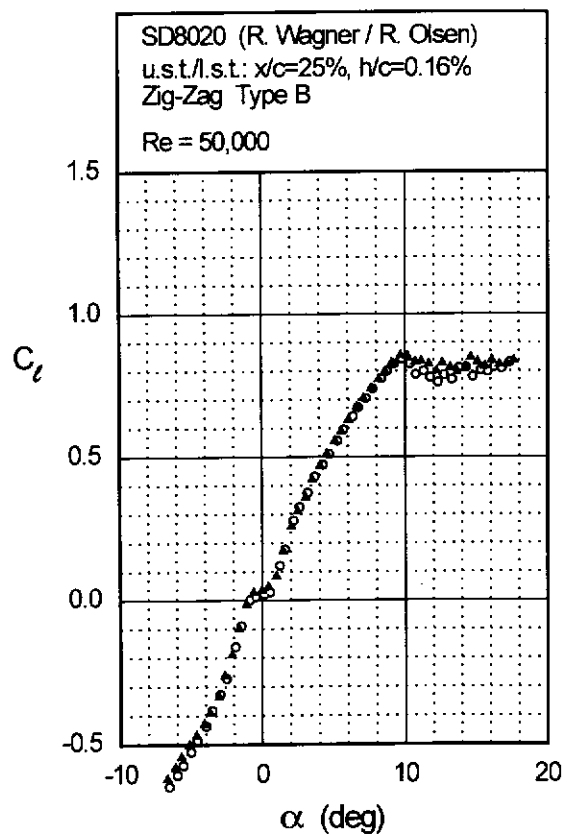


Fig. 4.147 (continued)

SD8020



SD8020

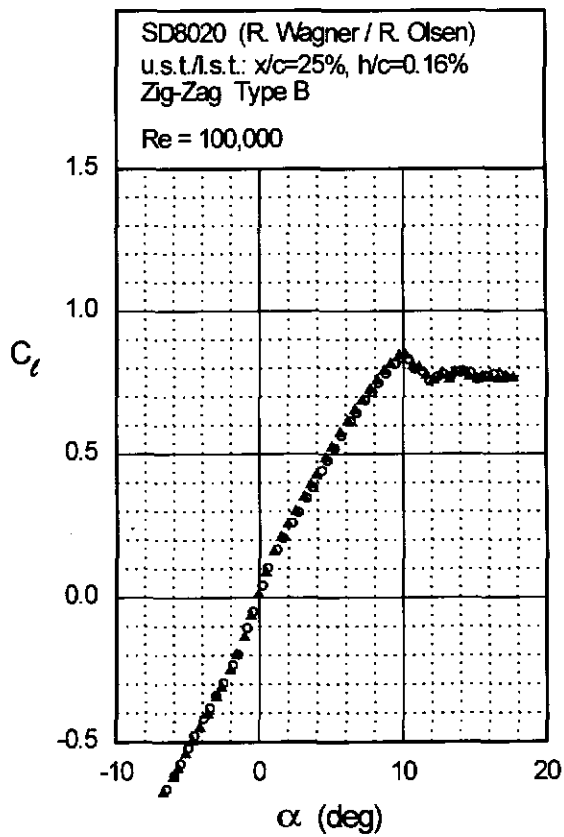
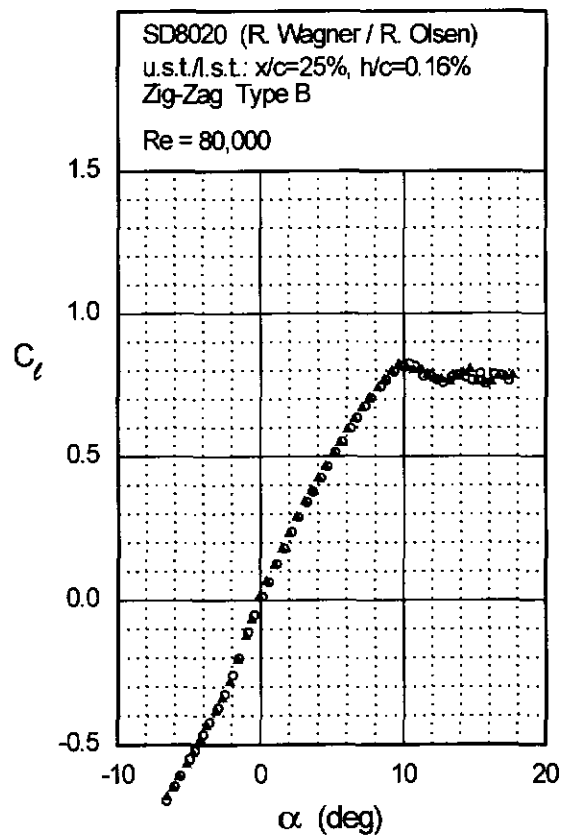
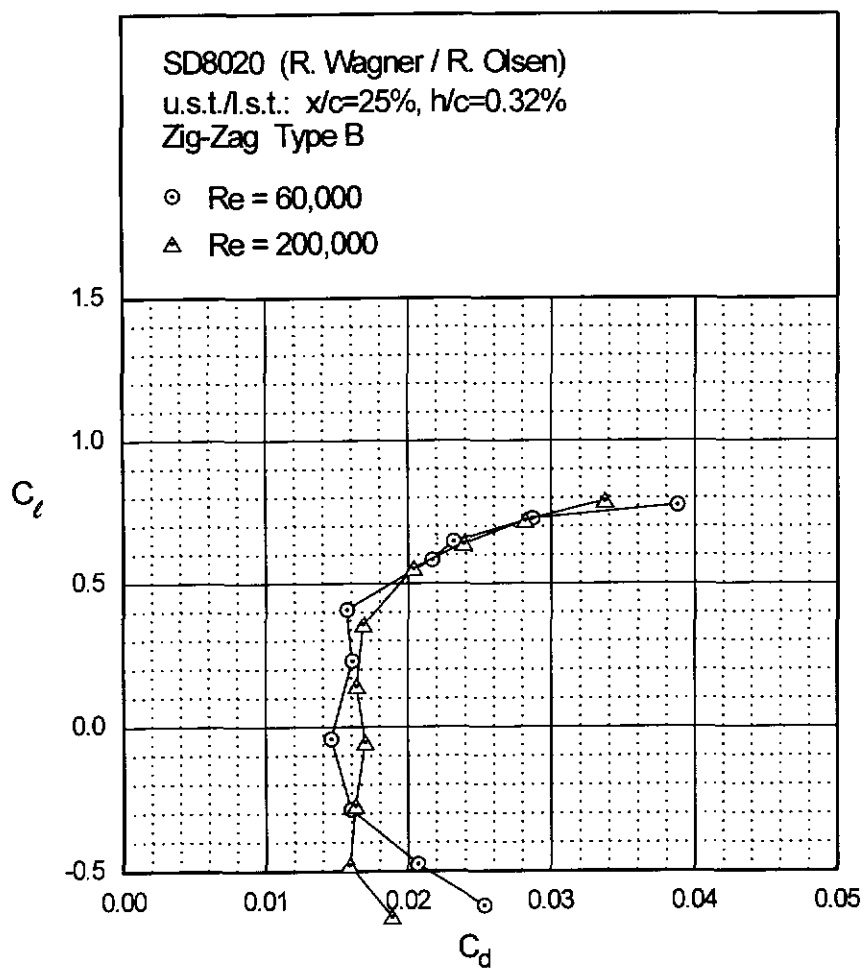
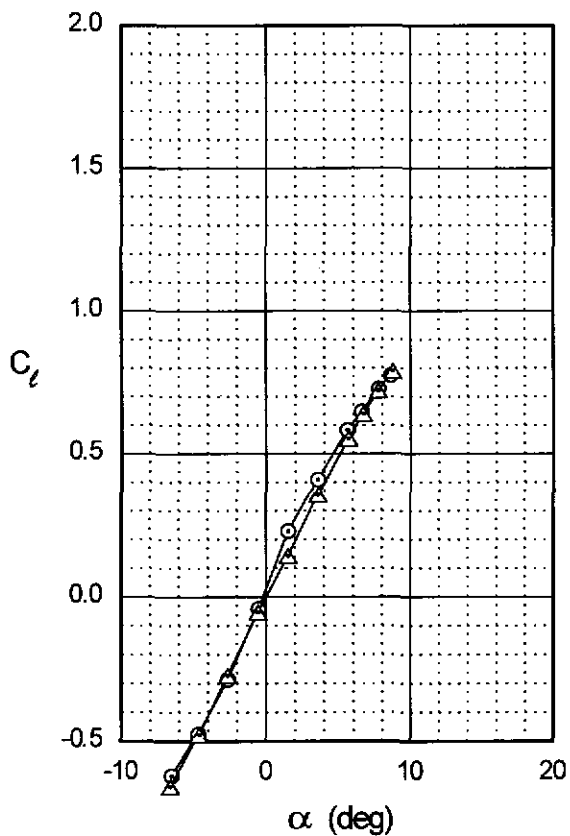


Fig. 4.148

Chapter 4: Airfoil Profiles and Performance Plots 237

SD8020



SD8020

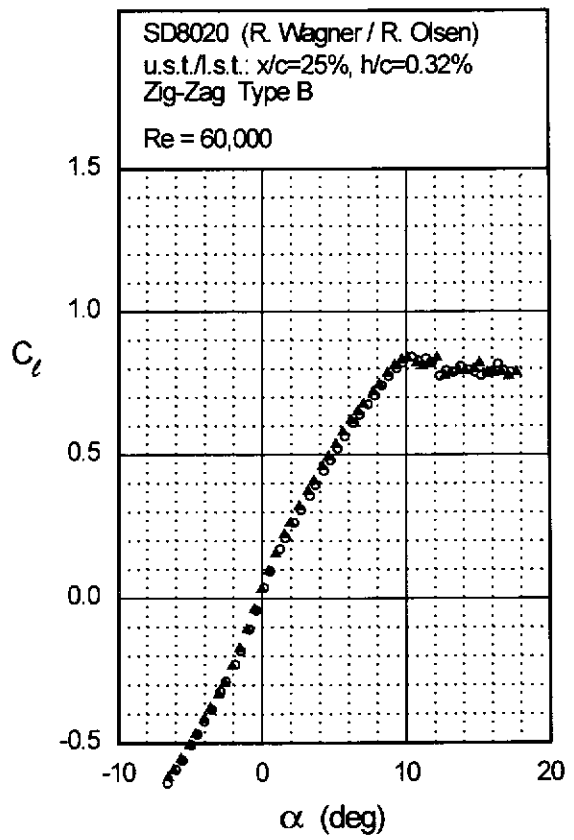
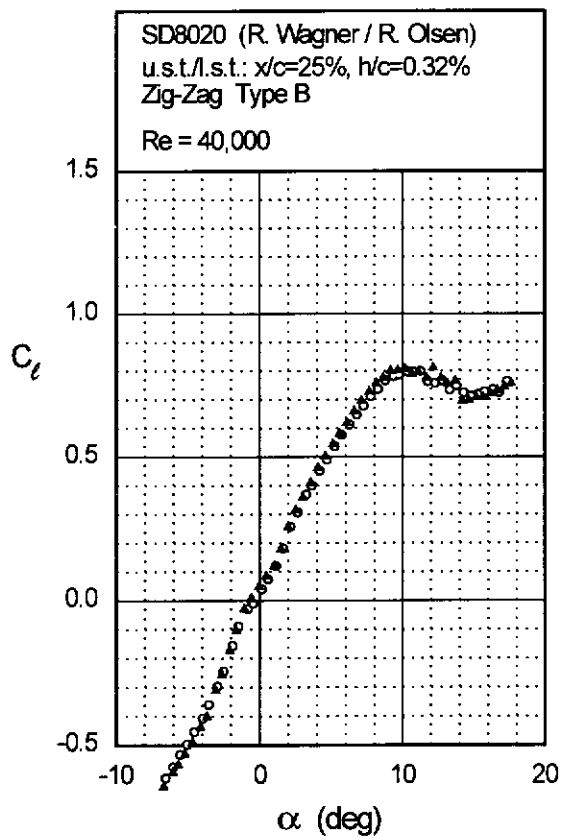
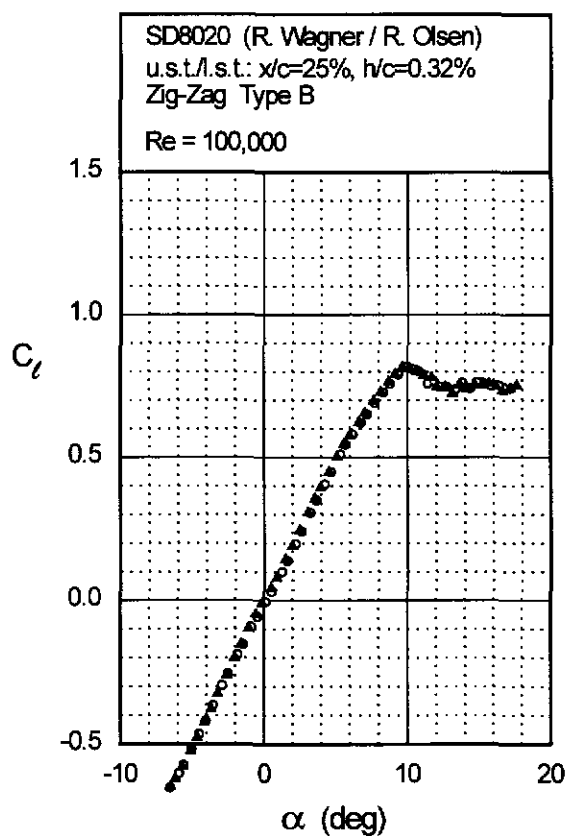
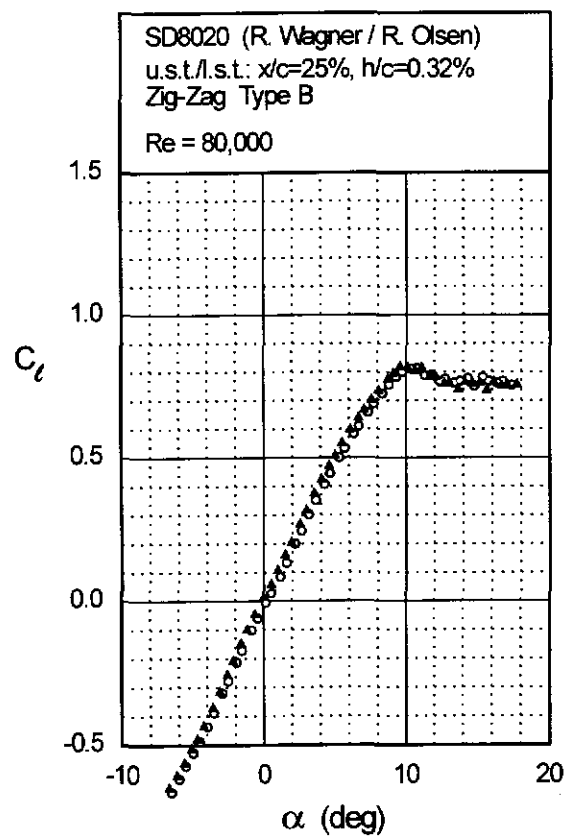


Fig. 4.148 (continued)

Chapter 4: Airfoil Profiles and Performance Plots

239

SD8020



WASP

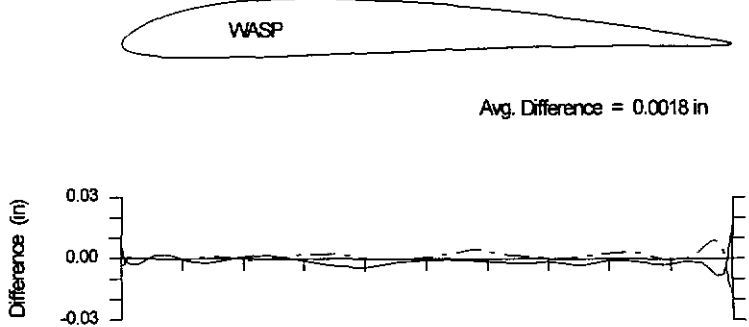
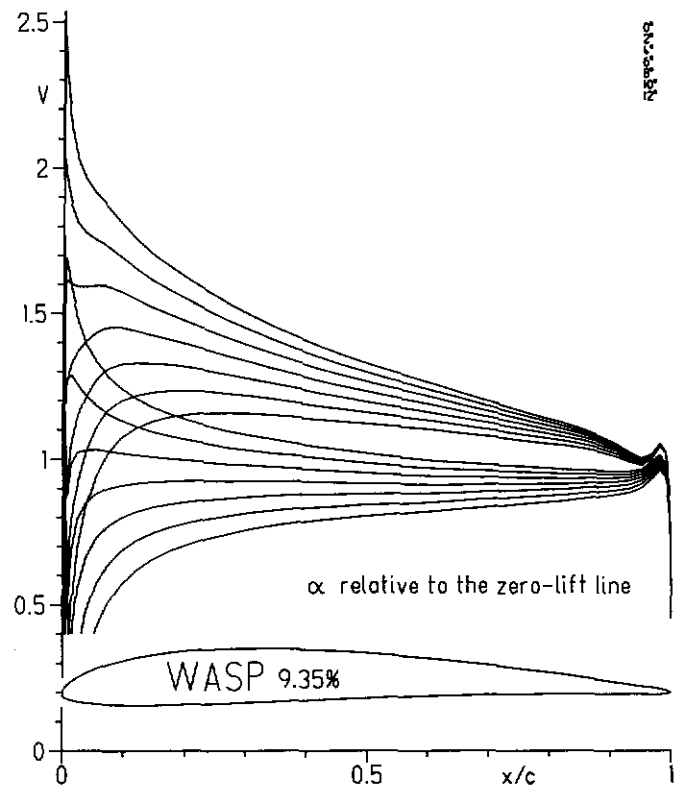


Fig. 4.152

Chapter 4: Airfoil Profiles and Performance Plots 241

WASP

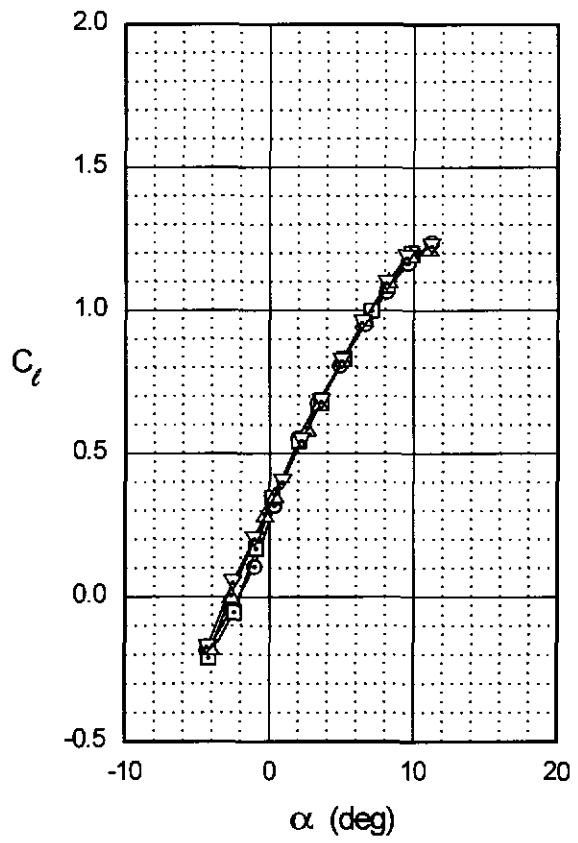
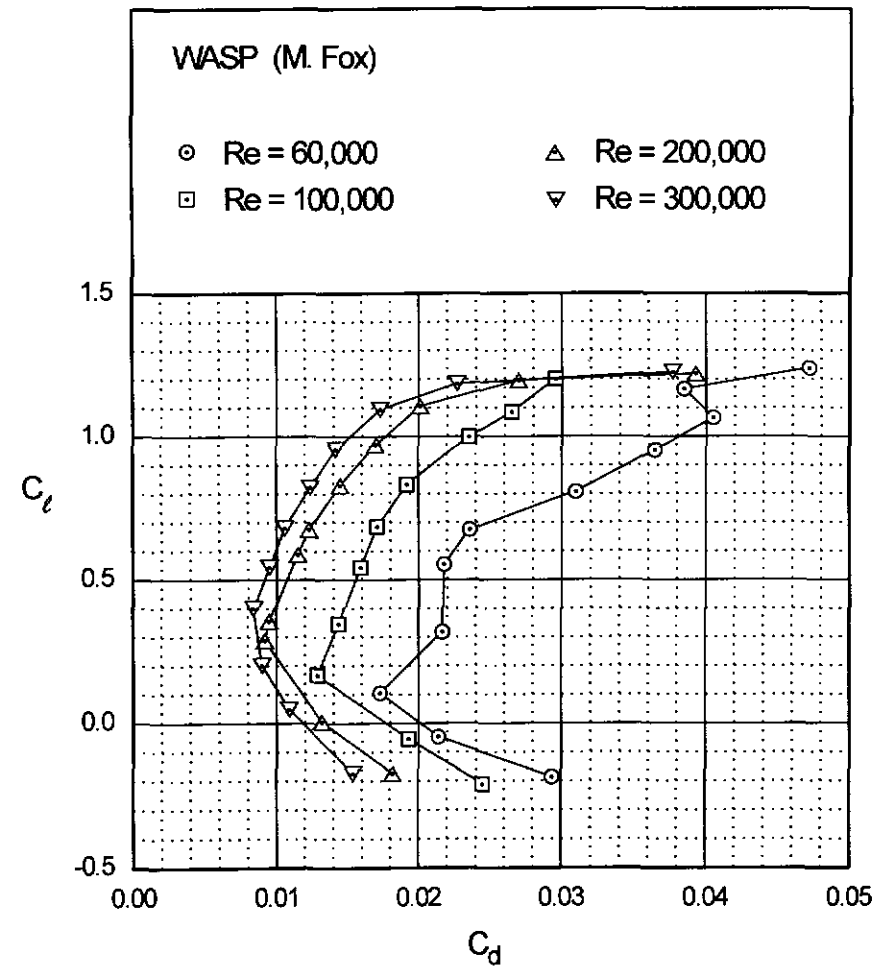


Fig. 4.153

WASP

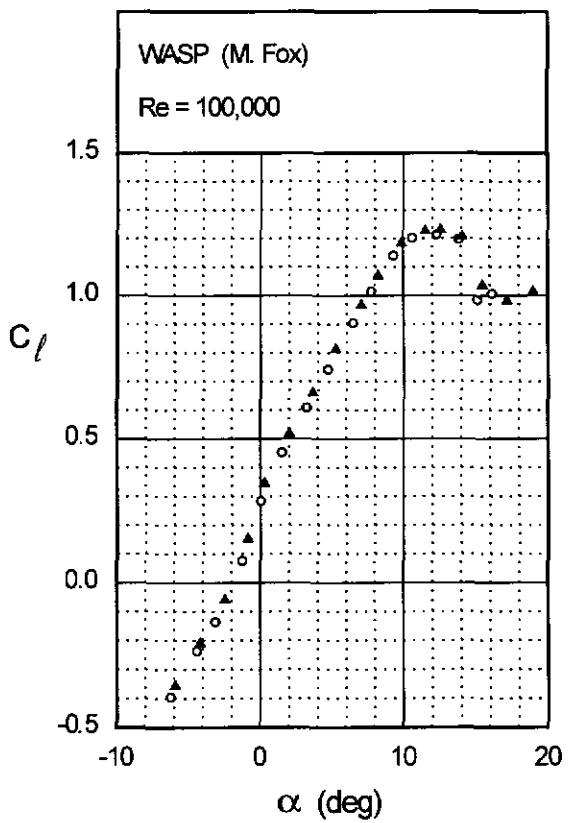
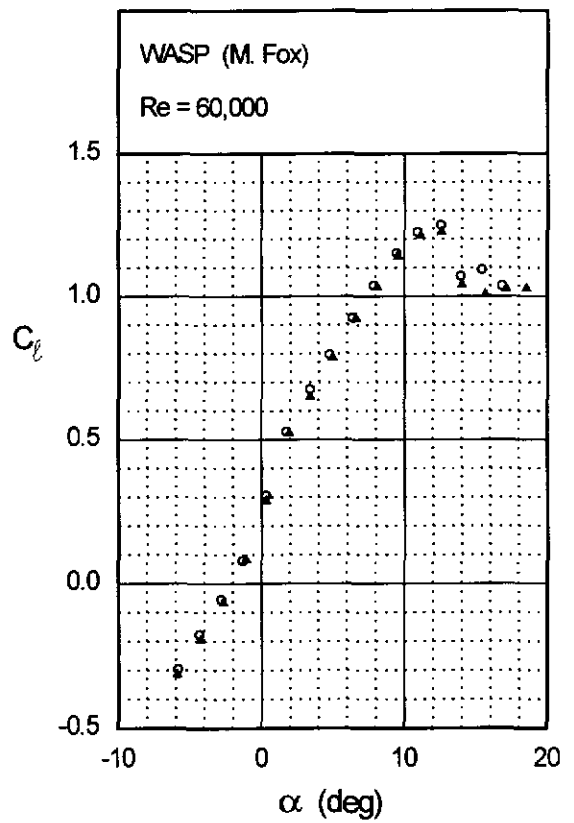
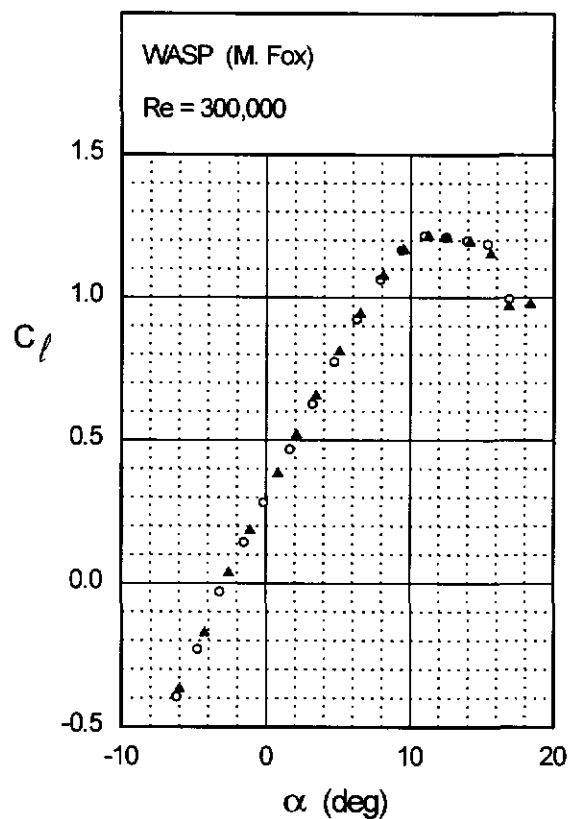
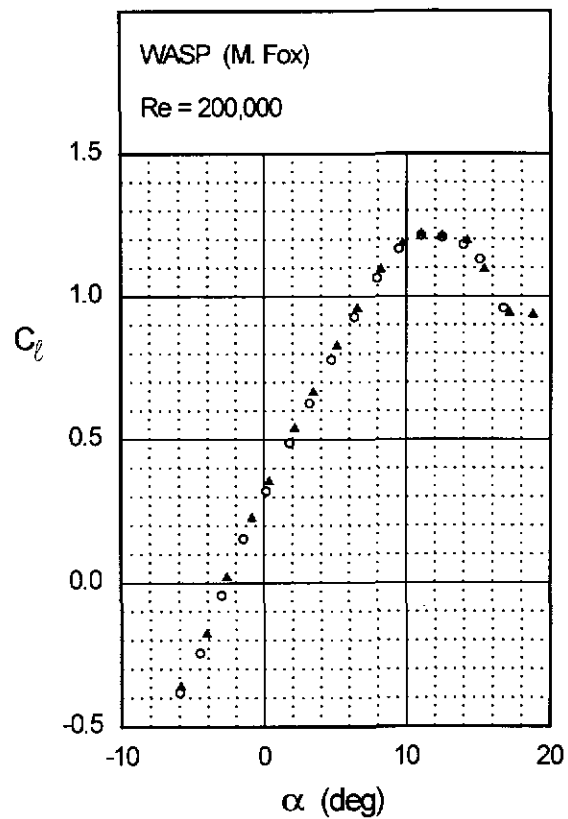


Fig. 4.153 (continued)

Chapter 4: Airfoil Profiles and Performance Plots 243

WASP



Extended Notes to the Text

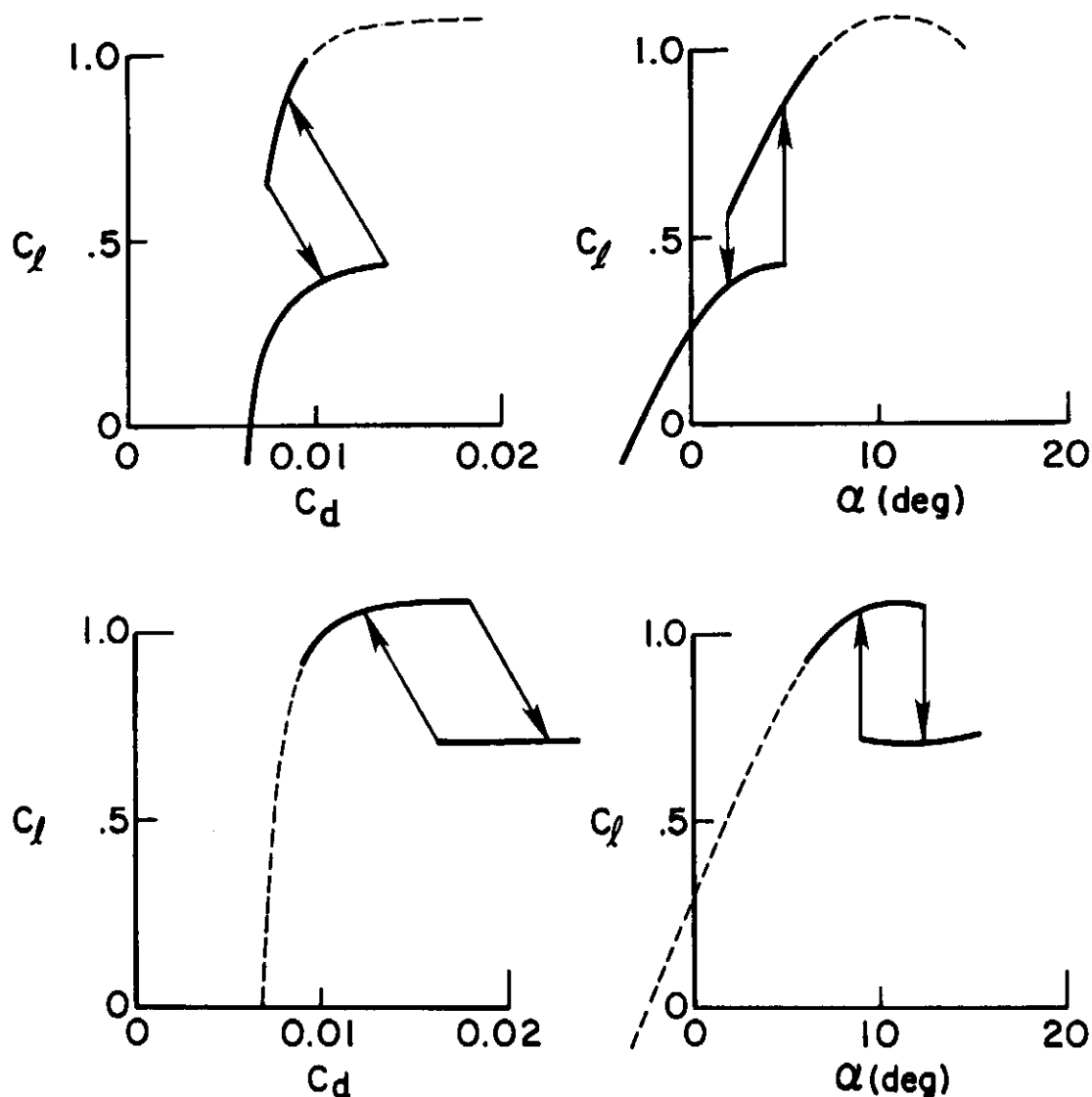
- n1. The “bunt,” as applied to F1C free-flight models, is a term used to describe a flight maneuver from the straight-up power position to a horizontal glide. The stabilizer is momentarily deflected after the engine stops to dive the model 90 deg from vertical straight-up to horizontal and in so doing optimize the model’s kinetic energy into the highest possible altitude for glide. The familiar corkscrew roll-out from power-to-glide does not work well on long winged models. High aspect ratio wings resist rolling about the longitudinal axis. The bunt allows the wing to roll about the lateral axis which long wings do with grace.

- Gilbert Morris

- n2. Some airfoils at low Reynolds numbers behave differently depending on whether the angle of attack is increasing or decreasing. Such airfoils are said to have hysteresis, which appears in the lift, drag and moment characteristics. In the current work, hysteresis is seen in the lift data but not the drag data since the drag was only measured for increasing angles of attack.

As depicted in the figures on the following page, two common types of airfoil hysteresis are found at low Reynolds numbers. The first type is initiated by a long laminar separation bubble present on the airfoil in the mid-lift range. As the angle of attack increases, the bubble grows larger. As this happens the drag rises dramatically to form a high-drag knee, and the lift falls-off to form a plateau—a process that is similar to trailing-edge stall. Further increasing the angle of attack “unstalls” the airfoil and causes the long bubble to collapse into a short bubble near the airfoil leading edge, resulting in markedly lower drag. Through decreasing angles of attack, a sharp decrease in lift occurs due to the return of the long bubble at an angle of attack lower than that at which the increase occurred. For some airfoils the collapse and return of the long bubble happens at the same angle of attack. This type of hysteresis can be called “long-bubble hysteresis,” although other names have been applied.^{32,33}

A second type of hysteresis is caused by a short laminar separation bubble. In this case, before stall near $C_{l_{max}}$ a short bubble exists on the airfoil leading edge. As the angle of attack increases, the airfoil stalls either by the bursting of a bubble (a leading edge stall). Through decreasing angle of attack from stall, the short bubble reattaches, identified by a sharp increase in the lift, at an angle of attack lower than that of stall for increasing angle of attack. This type of hysteresis can be called “short-bubble hysteresis.”



Long-bubble and short-bubble hysteresis.

As discussed, the type of hysteresis depends on the behavior of either a long-bubble present near the airfoil mid-chord or a short-bubble near the leading edge. (A description of how these two types of hysteresis are related to the airfoil velocity distribution can be found in Ref. 32.) Since the two types of hysteresis tend to be associated with different parts of the airfoil, it is possible for a single airfoil to exhibit both types of hysteresis, such as that seen on the FX 63-137 at Re of 90k. Finally, it should be noted that some airfoils cannot be classified by the two types of hysteresis discussed (see the FX 74-CL5-140 MOD and CH 10-48-13 characteristics).

- n3. The *reduced* Reynolds number for an aircraft can be obtained by starting with the definition of the airfoil chord Reynolds number given by

$$Re = \frac{\rho V c}{\mu}$$

For an aircraft in steady level flight, the aircraft speed is expressed as

$$V = \sqrt{\frac{2W/S}{\rho C_L}}$$

These two equations can be combined to yield

$$Re \sqrt{C_L} = \frac{c}{\mu} \sqrt{2\rho W/S}$$

For an aircraft at any given time in flight, the right-hand side of this equation is a constant. Consequently, the left-hand side is also a constant—an increase in the Re occurs through a decrease in C_L . It is this constant that is termed the reduced Reynolds number, that is,

$$\mathcal{R} = Re \sqrt{C_L}$$

Although this parameter has been given various names, the terminology used here is that due to Drela.³⁴ The reduced Reynolds number \mathcal{R} is most useful when comparing airfoil data since \mathcal{R} is constant for a given aircraft; whereas, the Re is not constant. Thus, when the airfoil data is plotted for various values of \mathcal{R} , airfoils can be more easily compared for aircraft applications.

- n4. The S1223 as well as the other new Selig airfoils were designed through the use of several low-speed airfoil design and analysis codes, in particular, the PROFOIL code,^{35–38} the Eppler code,^{10,11} and either the ISES^{12,13} or XFOIL code.¹⁴ The general design methodology is as follows. First, PROFOIL is used for rapid interactive design. A new airfoil that appears to meet the performance objectives is then screened through the use of two analysis codes, beginning with the Eppler code, and ending with either the ISES or XFOIL code. If at any state the candidate airfoil fails to meet the design goals, the experience is used to redesign the airfoil to more closely match the desired performance. This iterative process continues until a successful airfoil is designed.

The PROFOIL code, like the Eppler code, embodies an inverse airfoil design method and an integral boundary-layer method for rapid analysis at the design points. PROFOIL, however, differs from the Eppler code in that laminar and turbulent boundary-layer developments can be prescribed. For example, the laminar boundary layer can be directly specified to approach

transition in a favorable way for low Reynolds numbers. Such an ability, for instance, allows for control over the design of the bubble ramp. Beyond transition, the turbulent boundary-layer development can be specified to avoid turbulent separation by a desired margin. This capability is especially useful when designing for maximum lift. The method also allows for control over geometric characteristics like local geometry, maximum thickness, thickness distribution, etc.

The Eppler code is used for first stage screening of candidate airfoils. In the analysis mode, the inviscid velocity distributions are determined by a panel method. Performance is then done through the use of an integral boundary-layer method. In the drag calculation, the drag due to a laminar separation bubble is not determined. If the bubble is predicted to be longer than $0.03c$, however, a warning is issued to indicate that the bubble drag is probably large, and consequently the predicted drag is probably in error. Although the magnitude of the bubble drag is not determined, the method is invaluable when the user has had experience comparing its predictions with experiments.

The ISES code solves the two-dimensional Euler equations coupled with an integral boundary-layer formulation through a global Newton iteration method. Over the Reynolds number range considered here, the agreement between predicted and experimentally measured results is often good, although some discrepancies do exist. Since the ISES code is computationally intensive, it is only used in the later stages of design. It should be mentioned that the XFOIL code is more computationally efficient than the ISES code; however, XFOIL does not converge as readily as ISES for cases where there is significant separation, e.g., that found during the initiation and development of airfoil stall and that due to the presence of a large laminar separation bubble. Thus, ISES is preferred for its overall robustness, albeit at the cost of considerably more computation time. Neither code is capable of predicting airfoil stall characteristics or hysteresis.

References

- [1] Selig, M.S., Donovan, J.F. and Fraser, D.B., *Airfoils at Low Speeds*, Soartech 8, SoarTech Publications, 1504 N. Horseshoe Circle, Virginia Beach, VA, 23451, 1989.
- [2] Khodadoust, A., "An Experimental Study of the Flowfield on a Semispan Rectangular Wing with a Simulated Glaze Ice Accretion," Ph.D. Thesis, University of Illinois at Urbana-Champaign, Dept. of Aeronautical and Astronautical Engineering, 1993.
- [3] Jones, B.M., "The Measurement of Profile Drag by the Pitot Traverse Method," Aeronautical Research Council, R&M 1688, 1936.
- [4] Schlichting, H., *Boundary Layer Theory*, McGraw-Hill Book Company, New York, 1979.
- [5] Guglielmo, J.J. and Selig, M.S., "Large Spanwise Variations in Profile Drag for Airfoils at Low Reynolds Numbers," AIAA Paper 95-1783, June 1995.
- [6] Guglielmo, J.J., "Spanwise Variations in Profile Drag for Airfoils at Low Reynolds Numbers," Master's Thesis, University of Illinois at Urbana-Champaign, Dept. of Aeronautical and Astronautical Engineering, 1995.
- [7] White, F.M., *Viscous Fluid Flow*, McGraw-Hill, Inc., New York, 1991.
- [8] Giguère, P, "Two-Dimensional Wind Tunnel Boundary Layer Corrections for Low-Speed Testing in a Rectangular Test Section," University of Illinois, Report number to be assigned, 1995.
- [9] Rae, W.H., Jr. and Pope, A., *Low-speed Wind Tunnel Testing*, John Wiley and Sons, New York, 1984.
- [10] Eppler, R. and Somers, D.M., "A Computer Program for the Design and Analysis of Low-Speed Airfoils, Including Transition," NASA TM 80210, August 1980.
- [11] Eppler, R., *Airfoil Design and Data*, Springer-Verlag, New York, 1990.
- [12] Drela, M. and Giles, M.B., "Two-Dimensional Transonic Aerodynamic Design Method," *AIAA Journal*, Vol. 25, No. 9, September 1987, pp. 1199–1206.
- [13] Drela, M. and Giles, M.B., "ISES: A Two-Dimensional Viscous Aerodynamic Design and Analysis Code," AIAA Paper 87-0424, January 1987.
- [14] Drela, M., "XFOIL: An Analysis and Design System for Low Reynolds Number Airfoils," *Lecture Notes in Engineering: Low Reynolds Number Aerodynamics*, T.J. Mueller (ed.), Vol. 54, Springer-Verlag, New York, June 1989.

- [15] Coleman, H.W. and Steele, W.G., Jr., *Experimentation and Uncertainty Analysis For Engineers*, John Wiley and Sons, New York, 1989.
- [16] McGhee, R.J., Walker, B.S. and Millard, B.F., "Experimental Results for the Eppler 387 Airfoil at Low Reynolds Numbers in the Langley Low-Turbulence Pressure Tunnel," NASA TM 4062, October 1988.
- [17] Althaus, D., *Profilpolaren fur den Modellflug*, Neckar-Verlag VS-Villingen, 1980.
- [18] Morgan, H.L., Jr., "Computer Program for Smoothing and Scaling Airfoil Coordinates," NASA TM 84666, July 1983.
- [19] Archer, Randy, "Number Fifteen, F1C," Twenty-Fifth Annual Report, National Free Flight Society, 1992, pp. 105–106.
- [20] Kuhlman, B. and Kuhlman, B., *Understanding Polars without Math*, B² Streamlines, P.O. Box 976, Olalla, WA 98359-0976.
- [21] Donovan, J.F. and Selig, M.S., "Low Reynolds Number Airfoil Design and Wind Tunnel Testing at Princeton University," *Lecture Notes in Engineering: Low Reynolds Number Aerodynamics*, T.J. Mueller (ed.), Vol. 54, Springer-Verlag, New York, June 1989.
- [22] Mueller, T.J. and Batill, S.M., "Experimental Studies of the Laminar Separation Bubble on a Two-Dimensional Airfoil at Low Reynolds Numbers," AIAA Paper 80-1440, July 1980.
- [23] Foch, J.R. and Ailinger, K.G., "Low Reynolds Number, Long Endurance Aircraft Design," AIAA Paper 92-1263, February 1992.
- [24] Foch, J.R. and Toot, P.L., "Flight Testing Navy Low Reynolds Number (LRN) Unmanned Aircraft," *Lecture Notes in Engineering: Low Reynolds Number Aerodynamics*, T.J. Mueller (ed.), Vol. 54, Springer-Verlag, New York, June 1989.
- [25] Miley, S.J., "On the Design of Airfoils for Low Reynolds Numbers," *Proceedings of the Second International Symposium of the Technology and Science of Low-Speed and Motorless Flight*, Soaring Society of America, Los Angeles, CA, September 1974.
- [26] Wortmann, F.X., "The Quest for High Lift," *Proceedings of the Second International Symposium of the Technology and Science of Low-Speed and Motorless Flight*, Soaring Society of America, Los Angeles, CA, September 1974.
- [27] Selig, M.S. and Guglielmo, J.J., "High-Lift Low Reynolds Number Airfoil Design," AIAA Paper 94-1866, June 1994.
- [28] Boermans, L.M.M., Donker Duyvis, F.J., Ingen, J.L. van and Timmer, W.A., "Experimental Aerodynamic Characteristics of the Airfoils LA 5055 and DU

- 86-084/18 at Low Reynolds Numbers," *Lecture Notes in Engineering: Low Reynolds Number Aerodynamics*, T.J. Mueller (ed.), Vol. 54, Springer-Verlag, New York, June 1989.
- [29] Giguère, P., Lemay, J. and Dumas, G., "Gurney Flap Effects and Scaling for Low-Speed Airfoils," AIAA Paper 95-1881, June 1995.
 - [30] Liebeck, R.H. and Ormsbee, A.I., "Optimization of Airfoils for Maximum Lift," *J. Aircraft*, Vol. 7, No. 5, Sept-Oct 1970, pp. 409-415.
 - [31] Tangler, J.L. and Somers, D.M., "NREL Airfoil Families for HAWTs," AWEA WINDPOWER Conference, Washington, DC, March 1995.
 - [32] Selig, M.S., "The Design of Airfoils at Low Reynolds Numbers," AIAA Paper 85-0074, January 1985.
 - [33] Mueller, T.J., *Low Reynolds Number Vehicles*, AGARDograph No. 288, February 1985.
 - [34] Drela, M., "Transonic Low-Reynolds Number Airfoils," *J. of Aircraft*, Vol. 29, No. 6, Nov-Dec 1992, pp. 1106-1113.
 - [35] Selig, M.S. and Maughmer, M.D., "Multipoint Inverse Airfoil Design Method Based on Conformal Mapping," *AIAA J.*, Vol. 30, No. 5, May 1992, pp. 1162-1170.
 - [36] Selig, M.S. and Maughmer, M.D., "Generalized Multipoint Inverse Airfoil Design," *AIAA J.*, Vol. 30, No. 11, November 1992, pp. 2618-2625.
 - [37] Selig, M.S., "Multipoint Inverse Design of an Infinite Cascade of Airfoils," *AIAA J.*, Vol. 32, No. 4, April 1994, pp. 774-782.
 - [38] Saeed, F. and Selig, M.S., "A Multipoint Inverse Airfoil Design Method for Slot-Suction Airfoils," AIAA Paper 95-1857, June 1995.

Appendix A

Airfoil Coordinates

This appendix lists the airfoil coordinates. For any given airfoil, the true airfoil coordinates, if provided, are listed first. If the original coordinates were not ‘mathematically’ smooth or when there were too few points defining the airfoil (especially in the vicinity of the leading and trailing edges), the airfoil coordinates were smoothed with the program AFSMO¹⁸ developed at NASA Langley. Following the true coordinates and (if generated) smoothed coordinates, the actual wind-tunnel model coordinates are given. For the CH 10-48-13, FX 74-CL5-140 MOD, GEMINI, GM15, K3311 and WASP airfoils the smoothed coordinates were determined by smoothing the actual coordinates. As to be expected in these cases, the average difference between the smoothed airfoil and actual airfoil seen in the profile plots in Chapter 4 is quite small (~ 0.003 in) and is due to the model surface waviness and measurement error. Finally, coordinates for the NREL S822 and S823 airfoils designed by D.M. Somers (Airfoils, Inc.) can be acquired from NREL under a licensing agreement.

A18		0.60778	0.06160	A18		0.45970	0.00579
<i>x/c</i>	<i>y/c</i>	0.56937	0.06458	actual model		0.51571	0.00740
1.00000	0.00614	0.53099	0.06710			0.57735	0.00844
0.95000	0.01817	0.49265	0.06911			0.63480	0.00884
0.90000	0.02858	0.45435	0.07058	1.00000	0.00033	0.67858	0.00911
0.80000	0.04624	0.41638	0.07143	0.99690	0.00099	0.71898	0.00854
0.70000	0.06056	0.37887	0.07157	0.99191	0.00224	0.76508	0.00691
0.60000	0.07197	0.34204	0.07094	0.98482	0.00374	0.80917	0.00532
0.55000	0.07612	0.30609	0.06951	0.97861	0.00511	0.83733	0.00423
0.50000	0.07975	0.27120	0.06733	0.96785	0.00735	0.87102	0.00289
0.45000	0.08293	0.23760	0.06451	0.95536	0.00972	0.90385	0.00148
0.40000	0.08376	0.20549	0.06114	0.94364	0.01198	0.92078	0.00075
0.35000	0.08466	0.17504	0.05734	0.93398	0.01379	0.93589	0.00012
0.30000	0.08383	0.14648	0.05315	0.92071	0.01632	0.95129	-0.00055
0.25000	0.08065	0.11999	0.04860	0.90411	0.01925	0.96349	-0.00080
0.20000	0.07601	0.09576	0.04368	0.89181	0.02141	0.97274	-0.00121
0.15000	0.07026	0.07395	0.03839	0.86400	0.02621	0.98152	-0.00116
0.10000	0.06234	0.05468	0.03277	0.83715	0.03060	0.98959	-0.00119
0.07500	0.05660	0.03811	0.02694	0.80818	0.03498	0.99507	-0.00100
0.05000	0.04923	0.02433	0.02103	0.76407	0.04104	1.00000	0.00033
0.02500	0.03947	0.01338	0.01513				
0.01250	0.03239	0.00548	0.00932	0.71992	0.04669		
0.00000	0.01865	0.00098	0.00376	0.66487	0.05312		
		0.00000	0.00000	0.60663	0.05896		
		0.00000	0.00000	0.54910	0.06333		
0.01250	0.00781	0.00098	-0.00348	0.49645	0.06654		
0.02500	0.00357	0.00548	-0.00770	0.43814	0.06926		
0.05000	0.00075	0.01338	-0.01118	0.38347	0.06938		
0.07500	0.00000	0.02433	-0.01388	0.33236	0.06958		
0.10000	0.00006	0.03811	-0.01581	0.29351	0.06837		
0.15000	0.00200	0.05468	-0.01699	0.24769	0.06500		
0.20000	0.00475	0.07395	-0.01740	0.20920	0.06121		
0.25000	0.00806	0.09576	-0.01708	0.17697	0.05768		
0.30000	0.01038	0.11999	-0.01611	0.14758	0.05409		
0.35000	0.01353	0.14648	-0.01461	0.11892	0.04994		
0.40000	0.01657	0.17504	-0.01269	0.10641	0.04776		
0.45000	0.01780	0.20549	-0.01047	0.09459	0.04542		
0.50000	0.01884	0.23760	-0.00805	0.08092	0.04235		
0.55000	0.01980	0.27120	-0.00550	0.07075	0.03975		
0.60000	0.01998	0.30609	-0.00290	0.06073	0.03692		
0.70000	0.01924	0.34204	-0.00033	0.04549	0.03203		
0.80000	0.01452	0.37887	0.00209	0.03643	0.02853		
0.90000	0.00813	0.41638	0.00429	0.02720	0.02440		
0.95000	0.00434	0.45435	0.00617	0.02028	0.02095		
1.00000	0.00000	0.49265	0.00773	0.01302	0.01674		
		0.53099	0.00895	0.00710	0.01159		
		0.56937	0.00984	0.00109	0.00346		
A18		0.60778	0.01042	0.00000	-0.00001	0.00000	0.01271
smoothed		0.64594	0.01067	0.00489	-0.00732	0.01000	0.00400
		0.68359	0.01060	0.01059	-0.01050	0.01500	0.00274
		0.72043	0.01022	0.01487	-0.01187	0.02500	0.00156
1.00000	0.00307	0.75616	0.00954	0.02173	-0.01345	0.05000	0.00003
0.99754	0.00365	0.79048	0.00858	0.02945	-0.01488	0.07500	0.00000
0.99070	0.00530	0.82309	0.00738	0.04403	-0.01646	0.10000	0.00053
0.98037	0.00771	0.85370	0.00600	0.05870	-0.01696	0.15000	0.00294
0.96698	0.01070	0.88202	0.00450	0.07258	-0.01694	0.20000	0.00571
0.95044	0.01421	0.90775	0.00297	0.08798	-0.01669	0.25000	0.00812
0.93064	0.01819	0.93064	0.00149	0.10106	-0.01628	0.30000	0.01048
0.90775	0.02253	0.95044	0.00015	0.11648	-0.01556	0.35000	0.01310
0.88202	0.02712	0.96698	-0.00098	0.14251	-0.01381	0.40000	0.01617
0.85370	0.03185	0.98037	-0.00187	0.16858	-0.01185	0.45000	0.01847
0.82309	0.03661	0.99070	-0.00252	0.19992	-0.00957	0.50000	0.02021
0.79048	0.04132	0.99754	-0.00292	0.24110	-0.00652	0.55000	0.02136
0.75616	0.04591	1.00000	-0.00306	0.28536	-0.00401	0.60000	0.02129
0.72043	0.05029			0.34013	-0.00031	0.70000	0.01936
0.68359	0.05440			0.40095	0.00398	0.80000	0.01492
0.64594	0.05819					0.90000	0.00856

0.95000	0.00471	0.45435	0.01002	0.00029	0.00215	0.45435	0.16176		
1.00000	0.00000	0.49265	0.01177	0.00057	-0.00307	0.41638	0.16240		
		0.53099	0.01310	0.00440	-0.00796	0.37887	0.16133		
BE50									
		0.56937	0.01397	0.00934	-0.00977	0.34204	0.15862		
smoothed									
		0.60778	0.01440	0.01555	-0.01123	0.30609	0.15434		
		0.64594	0.01440	0.02299	-0.01267	0.27120	0.14859		
		0.68359	0.01402	0.03451	-0.01425	0.23760	0.14148		
		0.72043	0.01331	0.04815	-0.01526	0.20549	0.13310		
		0.75616	0.01233	0.06087	-0.01566	0.17504	0.12355		
		0.79048	0.01114	0.07498	-0.01579	0.14648	0.11291		
		0.82309	0.00980	0.08891	-0.01563	0.11999	0.10132		
		0.85370	0.00836	0.10403	-0.01514	0.09576	0.08896		
		0.88202	0.00688	0.11790	-0.01446	0.07395	0.07611		
		0.90775	0.00540	0.15101	-0.01252	0.05468	0.06312		
		0.93064	0.00398	0.18500	-0.01058	0.03811	0.05032		
		0.95044	0.00265	0.21545	-0.00896	0.02433	0.03793		
		0.96698	0.00146	0.25632	-0.00682	0.01338	0.02615		
		0.98037	0.00041	0.29934	-0.00459	0.00548	0.01531		
		0.99048	-0.00046	0.34231	-0.00201	0.00098	0.00586		
		0.99754	-0.00107	0.38434	0.00084	0.00000	0.00014		
		1.00000	-0.00130	0.43953	0.00402	0.00098	-0.00450		
		0.68359	0.05058	0.49864	0.00658	0.00548	-0.00914		
		0.64594	0.05463	0.55247	0.00811	0.01338	-0.01179		
		0.60778	0.05835	0.60994	0.00850	0.02433	-0.01269		
		0.56937	0.06171	0.67034	0.00809	0.03811	-0.01209		
		BE50							
		actual model							
				0.72948	0.00695	0.05468	-0.01028		
				0.77737	0.00545	0.07395	-0.00759		
				0.82030	0.00394	0.09576	-0.00435		
				0.84965	0.00292	0.11999	-0.00076		
				0.87774	0.00172	0.14648	0.00320		
				0.90758	0.00081	0.17504	0.00748		
				0.92014	0.00047	0.20549	0.01201		
				0.93617	0.00002	0.23760	0.01667		
				0.95086	-0.00034	0.27120	0.02136		
				0.96493	-0.00092	0.30609	0.02597		
				0.97271	-0.00111	0.34204	0.03040		
				0.98126	-0.00114	0.37887	0.03457		
				0.98898	-0.00119	0.41638	0.03839		
				0.99652	-0.00090	0.45435	0.04178		
				1.00000	-0.00003	0.49265	0.04466		
						0.53099	0.04693		
		CH 10-48-13							
		smoothed							
				0.56937	0.04851				
				0.60778	0.04933				
				0.64594	0.04932				
				0.68359	0.04845				
				0.72043	0.04672				
				0.75616	0.04423				
				0.79048	0.04108				
				0.82309	0.03739				
				0.85370	0.03322				
				0.88202	0.02867				
				0.90775	0.02386				
				0.93064	0.01896				
				0.95044	0.01410				
				0.96698	0.00936				
				0.98037	0.00516				
				0.99070	0.00212				
				0.99754	0.00044				
				1.00000	-0.00006				
		CH 10-48-13							
		actual model							
				0.53099	0.15538				
				0.49265	0.15942				
				1.00000	-0.00095				

0.99773	0.00103	0.75665	0.04350	0.41320	-0.03163	0.00958	-0.01000
0.99274	0.00376	0.79719	0.03978	0.46580	-0.03064	0.01319	-0.01157
0.98612	0.00720	0.82374	0.03675	0.51877	-0.02931	0.02096	-0.01420
0.97773	0.01108	0.85452	0.03249	0.57150	-0.02767	0.03009	-0.01668
0.96741	0.01590	0.87977	0.02835	0.62336	-0.02569	0.03948	-0.01882
0.95938	0.01968	0.90587	0.02328	0.67382	-0.02333	0.05464	-0.02171
0.94945	0.02417	0.91595	0.02132	0.72243	-0.02059	0.06817	-0.02379
0.94049	0.02810	0.92632	0.01912	0.76873	-0.01760	0.08950	-0.02626
0.93053	0.03234	0.94087	0.01579	0.81228	-0.01450	0.10662	-0.02784
0.91837	0.03745	0.95096	0.01325	0.85254	-0.01153	0.13833	-0.02995
0.90484	0.04316	0.96104	0.01044	0.88892	-0.00882	0.16421	-0.03111
0.88927	0.04968	0.96873	0.00815	0.92085	-0.00643	0.19316	-0.03200
0.86246	0.06072	0.97791	0.00530	0.94783	-0.00432	0.23635	-0.03279
0.82116	0.07729	0.98464	0.00318	0.96958	-0.00241	0.29760	-0.03315
0.78669	0.09023	0.99005	0.00140	0.98594	-0.00091	0.35915	-0.03278
0.75894	0.09990	0.99706	-0.00102	0.99637	-0.00016	0.42077	-0.03187
0.71822	0.11315	1.00000	-0.00095	1.00000	0.00000	0.48279	-0.03053
0.67728	0.12511					0.54271	-0.02895
0.63478	0.13591					0.60527	-0.02673
0.59270	0.14512					0.66857	-0.02379
0.53610	0.15463					0.73107	-0.02022
0.48363	0.16010					0.77240	-0.01746
0.42576	0.16241					0.81508	-0.01434
0.36667	0.16034					0.85142	-0.01141
0.31014	0.15444					0.87900	-0.00911
0.25403	0.14510					0.89676	-0.00765
0.21164	0.13517					0.91943	-0.00589
0.17178	0.12297					0.93686	-0.00452
0.14292	0.11171					0.95206	-0.00329
0.11299	0.09782					0.96402	-0.00250
0.08917	0.08514					0.97295	-0.00191
0.07757	0.07841					0.98200	-0.00151
0.06804	0.07248					0.99124	-0.00145
0.05601	0.06428					0.99865	-0.00133
0.04474	0.05577					1.00000	-0.00002
0.03043	0.04364						
0.02142	0.03505						
0.01041	0.02255						
0.00564	0.01550						
0.00071	0.00437						
0.00012	-0.00139						
0.00159	-0.00510						
0.00676	-0.00971						
0.01569	-0.01228						
0.02641	-0.01266						
0.03736	-0.01212						
0.04974	-0.01093						
0.06196	-0.00933						
0.07896	-0.00678						
0.09346	-0.00465						
0.10898	-0.00239						
0.11417	-0.00165						
0.14760	0.00324						
0.17333	0.00696						
0.20376	0.01158						
0.24943	0.01827						
0.28349	0.02298						
0.34683	0.03087						
0.39967	0.03646						
0.45729	0.04165						
0.51585	0.04599						
0.57726	0.04824						
0.63124	0.04907						
0.67481	0.04828						
0.71300	0.04657						

E374*x/c y/c*

1.00000 0.00000

0.99931 0.00133

0.99547 0.00193

0.99075 0.00259

0.98553 0.00323

0.97942 0.00403

0.97449 0.00478

0.96606 0.00620

0.95897 0.00737

0.95051 0.00873

0.94089 0.01035

0.92731 0.01261

0.91006 0.01542

0.88922 0.01879

0.87081 0.02175

0.84125 0.02638

0.80842 0.03160

0.76422 0.03834

0.72768 0.04383

0.66531 0.05294

0.60199 0.06157

0.54234 0.06862

0.41405 0.07751

0.34811 0.07769

0.28951 0.07547

0.22319 0.07015

0.17954 0.06464

0.14136 0.05815

0.11425 0.05246

0.09448 0.04762

0.08072 0.04382

0.06739 0.03970

0.05486 0.03534

0.04468 0.03137

0.03449 0.02693

0.02480 0.02219

0.01653 0.01759

0.00821 0.01213

0.00459 0.00912

0.00059 0.00354

0.00544 -0.00769

E374*actual model B**x/c y/c*

1.00000 -0.00002

0.99931 0.00133

0.99547 0.00193

0.99075 0.00259

0.98553 0.00323

0.97942 0.00403

0.97449 0.00478

0.96606 0.00620

0.95897 0.00737

0.95051 0.00873

0.94089 0.01035

0.92731 0.01261

0.91006 0.01542

0.88922 0.01879

0.87081 0.02175

0.84125 0.02638

0.80842 0.03160

0.76422 0.03834

0.72768 0.04383

0.66531 0.05294

0.60199 0.06157

0.54234 0.06862

0.41405 0.07751

0.34811 0.07769

0.28951 0.07547

0.22319 0.07015

0.17954 0.06464

0.14136 0.05815

0.11425 0.05246

0.09448 0.04762

0.08072 0.04382

0.06739 0.03970

0.05486 0.03534

0.04468 0.03137

0.03449 0.02693

0.02480 0.02219

0.01653 0.01759

0.00821 0.01213

0.00459 0.00912

0.00059 0.00354

0.00544 -0.00769

E387*x/c y/c*

1.00000 0.00000

0.99677 0.00043

0.98729 0.00180

0.97198 0.00423

0.95128 0.00763

0.92554 0.01184

0.89510 0.01679

0.86035 0.02242

0.82183 0.02866

0.78007 0.03540

0.73567 0.04249

0.68922 0.04975

0.64136 0.05696

0.59272 0.06390

0.54394 0.07020

0.49549 0.07546

0.44767 0.07936

0.40077 0.08173

0.35505 0.08247

0.31078 0.08156

0.26813 0.07908

0.22742 0.07529

0.18906 0.07037

0.15345 0.06448

0.12094 0.05775

0.09185 0.05033

0.06643	0.04238	0.18765	0.06751	0.50000	0.11562	0.98879	0.00563
0.04493	0.03408	0.15252	0.06202	0.43474	0.12031	0.98146	0.00870
0.02748	0.02562	0.12592	0.05690	0.37059	0.12180	0.97492	0.01125
0.01423	0.01726	0.10024	0.05108	0.33928	0.12130	0.97500	0.01122
0.00519	0.00931	0.08543	0.04710	0.30866	0.11998	0.95693	0.01772
0.00044	0.00234	0.07148	0.04284	0.27886	0.11785	0.94531	0.02170
0.00091	-0.00286	0.05827	0.03825	0.25000	0.11492	0.93349	0.02551
0.00717	-0.00682	0.04699	0.03386	0.22221	0.11122	0.92051	0.02950
0.01890	-0.01017	0.03772	0.02981	0.19562	0.10680	0.90331	0.03452
0.03596	-0.01265	0.02835	0.02503	0.17033	0.10168	0.88636	0.03932
0.05827	-0.01425	0.02078	0.02043	0.14645	0.09591	0.86782	0.04434
0.08569	-0.01500	0.01472	0.01639	0.12408	0.08955	0.84997	0.04899
0.11800	-0.01502	0.00861	0.01171	0.10332	0.08270	0.82203	0.05604
0.15490	-0.01441	0.00180	0.00468	0.08427	0.07552	0.79002	0.06384
0.19599	-0.01329	0.00267	-0.00568	0.06699	0.06812	0.74876	0.07337
0.24083	-0.01177	0.00683	-0.00775	0.05156	0.06052	0.70670	0.08250
0.28892	-0.00998	0.01289	-0.00957	0.03806	0.05264	0.64448	0.09460
0.33968	-0.00804	0.01923	-0.01107	0.02653	0.04430	0.58299	0.10468
0.39252	-0.00605	0.02737	-0.01261	0.01704	0.03548	0.52087	0.11253
0.44679	-0.00410	0.03552	-0.01390	0.00961	0.02636	0.45837	0.11780
0.50182	-0.00228	0.04178	-0.01472	0.00428	0.01742	0.39446	0.11992
0.55694	-0.00065	0.05075	-0.01564	0.00107	0.00926	0.33408	0.11893
0.61147	0.00074	0.06433	-0.01656	0.00000	0.00241	0.26817	0.11430
0.66472	0.00186	0.08169	-0.01728	0.00107	-0.00296	0.21284	0.10703
0.71602	0.00268	0.10196	-0.01767	0.00428	-0.00702	0.16606	0.09778
0.76475	0.00320	0.13171	-0.01766	0.00961	-0.01016	0.13272	0.08908
0.81027	0.00342	0.16440	-0.01716	0.01704	-0.01275	0.11672	0.08415
0.85202	0.00337	0.20232	-0.01623	0.02653	-0.01503	0.09989	0.07839
0.88944	0.00307	0.24433	-0.01495	0.03806	-0.01706	0.08201	0.07147
0.92205	0.00258	0.30493	-0.01288	0.05156	-0.01879	0.06895	0.06576
0.94942	0.00196	0.36410	-0.01068	0.06699	-0.02018	0.05624	0.05945
0.97118	0.00132	0.42605	-0.00820	0.08427	-0.02123	0.04500	0.05306
0.98705	0.00071	0.48404	-0.00599	0.10332	-0.02199	0.03324	0.04519
0.99674	0.00021	0.54791	-0.00384	0.12408	-0.02248	0.02382	0.03770
1.00000	0.00000	0.61294	-0.00200	0.14645	-0.02272	0.01858	0.03276
<hr/>							
E387							
actual model A							
<i>x/c</i>		<i>y/c</i>					
1.00000	0.00009	0.81865	0.00199	0.25000	-0.02043	0.00152	0.00669
0.99504	0.00095	0.85388	0.00216	0.27886	-0.01884	0.00081	0.00488
0.98857	0.00194	0.90937	0.00192	0.30866	-0.01675	0.00291	-0.00946
0.98221	0.00295	0.92880	0.00148	0.33928	-0.01418	0.00702	-0.01301
0.97326	0.00432	0.94537	0.00117	0.37059	-0.01118	0.01268	-0.01618
0.96536	0.00547	0.96059	0.00074	0.43474	-0.00421	0.01865	-0.01839
0.95657	0.00679	0.97265	0.00047	0.50000	0.00341	0.02609	-0.02033
0.94747	0.00807	0.98401	0.00019	0.56526	0.01092	0.03367	-0.02177
0.93717	0.00960	0.99037	-0.00006	0.62941	0.01760	0.04433	-0.02320
0.92293	0.01174	1.00000	0.00009	0.69134	0.02287	0.06261	-0.02489
0.90675	0.01418	<hr/>		0.75000	0.02629	0.08313	-0.02614
0.88693	0.01708	<hr/>		0.80438	0.02758	0.11482	-0.02708
0.86653	0.02009	<hr/>		0.85355	0.02661	0.14881	-0.02720
0.83877	0.02424	<hr/>		0.89668	0.02343	0.19042	-0.02643
0.80202	0.02969	<hr/>		0.93301	0.01841	0.23870	-0.02454
0.76503	0.03515	<hr/>		0.96194	0.01229	0.30207	-0.02062
0.72297	0.04144	<hr/>		0.98296	0.00822	0.36557	-0.01479
0.66059	0.05062	<hr/>		0.96194	0.01642	0.42496	-0.00814
0.60074	0.05897	<hr/>		0.93301	0.02581	0.48817	-0.00064
0.54060	0.06640	<hr/>		0.89668	0.03615	0.54911	0.00654
0.47469	0.07305	<hr/>		0.85355	0.04757	0.61046	0.01349
0.41020	0.07733	<hr/>		0.80438	0.06001	0.67309	0.01971
0.35069	0.07854	<hr/>		0.75000	0.07305	0.73663	0.02402
0.28881	0.07694	<hr/>		0.69134	0.08596	0.77968	0.02563
0.22593	0.07209	<hr/>		0.62941	0.09788	0.81868	0.02589
		<hr/>		0.56526	0.10799	0.9932	0.00044
		<hr/>		0.99504	0.00274	0.87115	0.02390

						GEMINI	
						smoothed model	
						<i>x/c</i>	<i>y/c</i>
0.88864	0.02243	0.09576	0.00270	0.40939	0.15502	1.00000	0.00014
0.90527	0.02047	0.11999	0.00584	0.35552	0.15787	0.99754	0.00151
0.91935	0.01849	0.14648	0.00921	0.29881	0.15647	0.99070	0.00419
0.93295	0.01621	0.17504	0.01279	0.24982	0.15052	0.98037	0.00623
0.94633	0.01363	0.20549	0.01651	0.21251	0.14297	0.96698	0.00919
0.95557	0.01169	0.23760	0.02030	0.14857	0.12269	0.95044	0.01300
0.96543	0.00937	0.27120	0.02410	0.13038	0.11492	0.93064	0.01720
0.97486	0.00695	0.30609	0.02786	0.10868	0.10440	0.90775	0.02213
0.98453	0.00421	0.34204	0.03152	0.08477	0.09084	0.88202	0.02757
0.99236	0.00182	0.37887	0.03503	0.07267	0.08299	0.85370	0.03335
0.99933	-0.00044	0.41638	0.03832	0.05717	0.07159	0.82309	0.03944
1.00000	0.00031	0.45435	0.04134	0.04571	0.06209	0.79048	0.04581
FX 74-CL5-140						0.75616	0.05236
MOD						0.72043	0.05893
smoothed model						0.68359	0.04997
<i>x/c</i>	<i>y/c</i>	0.68359	0.04997	0.00348	0.01099	0.68359	0.06539
1.00000	0.00009	0.72043	0.04936	0.00088	0.00462	0.64594	0.07161
0.99754	0.00189	0.75616	0.04807	0.00021	0.00186	0.60778	0.07745
0.99070	0.00624	0.79048	0.04608	0.00010	-0.00128	0.56937	0.08278
0.98037	0.01150	0.82309	0.04334	0.00200	-0.00571	0.53099	0.08745
0.96698	0.01741	0.85370	0.03978	0.00668	-0.00833	0.49265	0.09138
0.95044	0.02402	0.88202	0.03537	0.01274	-0.00872	0.45435	0.09455
0.93064	0.03188	0.90775	0.03013	0.02070	-0.00783	0.41638	0.09689
0.90775	0.04001	0.93064	0.02434	0.03086	-0.00640	0.37887	0.09835
0.88202	0.04848	0.95044	0.01851	0.04204	-0.00485	0.34204	0.09886
0.85370	0.05718	0.96698	0.01290	0.04204	-0.00485	0.30609	0.09832
0.82309	0.06616	0.98037	0.00756	0.06956	-0.00104	0.27120	0.09666
0.79048	0.07549	0.99070	0.00319	0.08794	0.00136	0.23760	0.09383
0.75616	0.08510	0.99754	0.00068	0.09851	0.00269	0.20549	0.08982
0.72043	0.09482	1.00000	-0.00003	0.11525	0.00476	0.17504	0.08469
0.68359	0.10446			0.14318	0.00820	0.14648	0.07851
0.64594	0.11385			0.17209	0.01174	0.11999	0.07137
0.60778	0.12287			0.19558	0.01447	0.09576	0.06334
0.56937	0.13137			0.24186	0.01984	0.07395	0.05453
0.53099	0.13916			0.28294	0.02443	0.05468	0.04523
FX 74-CL5-140						0.40135	0.03567
MOD						0.45829	0.04028
actual model						0.51318	0.04381
<i>x/c</i>	<i>y/c</i>	0.34451	0.03054	0.57902	0.04675	0.66945	0.04838
1.00000	-0.00141	0.38451	0.03054	0.63677	0.04815	0.70611	0.04792
0.45435	0.15177	0.40135	0.03567	0.66945	0.04838	0.75147	0.04660
0.41638	0.15606	0.45829	0.04028	0.70611	0.04792	0.79027	0.04442
0.37887	0.15868	0.51318	0.04381	0.75147	0.04660	0.82706	0.04129
0.34204	0.15944	0.57902	0.04675	0.79027	0.04442	0.82706	0.04129
0.30609	0.15820	0.63677	0.04815	0.82706	0.04129	0.85262	0.03834
0.27120	0.15493	0.66945	0.04838	0.85262	0.03834	0.87659	0.03477
0.23760	0.14964	0.70611	0.04792	0.87659	0.03477	0.90458	0.03288
0.20549	0.14243	0.75147	0.04660	0.90458	0.03150	0.9395	0.03724
0.17504	0.13344	0.79027	0.04442	0.91070	0.02793	0.95576	0.04136
0.14648	0.12292	0.82706	0.04129	0.92553	0.02425	0.96875	0.02187
0.11999	0.11110	0.85262	0.03834	0.93432	0.02187	0.97504	0.01870
0.09576	0.09826	0.87659	0.03477	0.94510	0.01870	0.98026	0.00665
0.07395	0.08459	0.89444	0.03150	0.95758	0.01480	0.98685	0.00377
0.05468	0.07030	0.91070	0.02793	0.99646	-0.00076	0.99646	-0.00076
0.03811	0.05576	0.92553	0.02425	1.00000	-0.00141	0.96875	0.01103
0.02433	0.04145	0.93432	0.02187			0.98026	0.00665
0.01338	0.02769	0.94510	0.01870			0.98685	0.00377
0.00548	0.01518	0.95758	0.01480			0.99646	-0.00076
0.00098	0.00518	0.96875	0.01103			1.00000	-0.00141
0.00000	-0.00021	0.97501	0.07760				
0.00098	-0.00435	0.77501	0.07760				
0.00548	-0.00787	0.74687	0.08540				
0.01338	-0.00871	0.70547	0.09655				
0.02433	-0.00754	0.66612	0.10668				
0.03811	-0.00539	0.61967	0.11797				
0.05468	-0.00292	0.57861	0.12719				
0.07395	-0.00022	0.52217	0.13872				
		0.46313	0.14873				

0.56937	-0.04430	0.00138	0.00573	0.45435	0.07172	0.99539	0.00116
0.60778	-0.04124	0.00224	-0.00749	0.41638	0.07295	0.98862	0.00264
0.64594	-0.03798	0.00576	-0.01212	0.37887	0.07352	0.98057	0.00402
0.68359	-0.03461	0.00958	-0.01550	0.34204	0.07339	0.97155	0.00594
0.72043	-0.03121	0.01818	-0.02044	0.30609	0.07255	0.95658	0.00878
0.75616	-0.02782	0.02489	-0.02351	0.27120	0.07097	0.94418	0.01143
0.79048	-0.02446	0.03421	-0.02702	0.23760	0.06866	0.93171	0.01364
0.82309	-0.02118	0.04612	-0.03060	0.20549	0.06561	0.91581	0.01630
0.85370	-0.01802	0.06079	-0.03431	0.17504	0.06182	0.89757	0.01997
0.88202	-0.01506	0.07669	-0.03771	0.14648	0.05731	0.88410	0.02301
0.90775	-0.01233	0.09104	-0.04043	0.11999	0.05210	0.85174	0.02964
0.93064	-0.00987	0.10322	-0.04255	0.09576	0.04629	0.82229	0.03442
0.95044	-0.00778	0.12623	-0.04588	0.07395	0.04003	0.79060	0.03884
0.96698	-0.00638	0.14307	-0.04789	0.05468	0.03354	0.74898	0.04494
0.98037	-0.00522	0.17180	-0.05041	0.03811	0.02698	0.70735	0.05047
0.99070	-0.00344	0.20230	-0.05225	0.02433	0.02052	0.66514	0.05535
0.99754	-0.00117	0.24452	-0.05360	0.01338	0.01433	0.62046	0.05914
1.00000	-0.00001	0.28864	-0.05443	0.00548	0.00852	0.56279	0.06420
<hr/>							
GEMINI							
<hr/>							
actual model		0.51287	-0.04801	0.00548	-0.00634	0.33961	0.07258
<hr/>		<i>x/c</i>		<i>y/c</i>			
1.00000	0.00075	0.57232	-0.04378	0.01338	-0.00868	0.28096	0.07109
0.99908	0.00273	0.62644	-0.03936	0.02433	-0.01036	0.23556	0.06865
0.99605	0.00405	0.66966	-0.03551	0.03811	-0.01150	0.18840	0.06385
0.99168	0.00502	0.71376	-0.03145	0.05468	-0.01210	0.15957	0.05955
0.98664	0.00622	0.75569	-0.02757	0.07395	-0.01207	0.13405	0.05505
0.97874	0.00822	0.79793	-0.02342	0.09576	-0.01136	0.10701	0.04930
0.96932	0.01028	0.82795	-0.02034	0.11999	-0.00996	0.09233	0.04536
0.96083	0.01213	0.86258	-0.01677	0.14648	-0.00785	0.07702	0.04098
0.94912	0.01471	0.89339	-0.01359	0.17504	-0.00510	0.06153	0.03601
0.93709	0.01726	0.91038	-0.01176	0.20549	-0.00179	0.05063	0.03216
0.92481	0.01978	0.92357	-0.01031	0.23760	0.00191	0.04017	0.02804
0.90932	0.02328	0.93966	-0.00865	0.27120	0.00586	0.02829	0.02250
0.89417	0.02643	0.95225	-0.00734	0.30609	0.00988	0.02132	0.01883
0.87998	0.02942	0.96343	-0.00624	0.34204	0.01379	0.01500	0.01537
0.84901	0.03568	0.97683	-0.00492	0.37887	0.01741	0.00842	0.01098
0.81705	0.04191	0.98975	-0.00378	0.41638	0.02060	0.00385	0.00725
0.78888	0.04740	0.99921	-0.00273	0.45435	0.02324	0.00167	0.00406
0.74459	0.05575	1.00000	0.00075	0.49265	0.02526	0.00000	-0.00011
0.70218	0.06344	<hr/>		0.53099	0.02661	0.00399	-0.00628
0.65948	0.07063	<hr/>		0.56937	0.02732	0.00781	-0.00744
0.61604	0.07737	<hr/>		0.60778	0.02740	0.01570	-0.00888
0.56044	0.08502	<hr/>		0.64594	0.02692	0.02268	-0.01002
0.50545	0.09148	1.00000	0.00006	0.68359	0.02594	0.03116	-0.01102
0.44769	0.09629	0.99754	0.00114	0.72043	0.02456	0.04716	-0.01198
0.38932	0.09870	0.99070	0.00356	0.75616	0.02287	0.06033	-0.01208
0.33216	0.09991	0.98037	0.00616	0.79048	0.02088	0.07504	-0.01193
0.27457	0.09810	0.96698	0.00865	0.82309	0.01858	0.08895	-0.01171
0.23045	0.09380	0.95044	0.01149	0.85370	0.01598	0.10477	-0.01108
0.19098	0.08847	0.93064	0.01516	0.88202	0.01317	0.12022	-0.01004
0.16333	0.08320	0.90775	0.01969	0.90775	0.01033	0.14641	-0.00794
0.13497	0.07639	0.88202	0.02474	0.93064	0.00765	0.17578	-0.00523
0.10705	0.06800	0.85370	0.03001	0.95044	0.00528	0.20395	-0.00226
0.09455	0.06359	0.82309	0.03524	0.96698	0.00332	0.24788	0.00282
0.08178	0.05860	0.79048	0.04030	0.98037	0.00179	0.29626	0.00853
0.06854	0.05269	0.75616	0.04511	0.99070	0.00075	0.34919	0.01424
0.05628	0.04664	0.72043	0.04963	0.99754	0.00017	0.40288	0.01903
0.04304	0.03937	0.68359	0.05386	1.00000	-0.00001	0.46307	0.02355
0.02848	0.03051	0.64594	0.05779	<hr/>		0.51862	0.02613
0.02029	0.02517	0.60778	0.06140	<hr/>		0.57584	0.02678
0.01347	0.02022	0.56937	0.06467	<hr/>		0.63110	0.02605
0.00665	0.01355	0.53099	0.06751	<hr/>		0.67619	0.02462
0.00347	0.00914	0.49265	0.06988	<hr/>		0.72014	0.02343
<hr/>		<i>x/c</i>		<i>y/c</i>			
<hr/>		GM15					
<hr/>		smoothed model					
<hr/>		<i>x/c</i>		<i>y/c</i>			
<hr/>		GM15					
<hr/>		actual model					
<hr/>		<i>x/c</i>		<i>y/c</i>			
<hr/>		1.00000		-0.00153		0.76444	

0.80748	0.01935	0.07130	-0.01468	0.00274	-0.00814	0.03116	0.02492
0.83766	0.01578	0.08313	-0.01522	0.01093	-0.01612	0.02167	0.02092
0.86986	0.01314	0.09799	-0.01544	0.02447	-0.02380	0.01453	0.01745
0.90304	0.00973	0.11476	-0.01532	0.04323	-0.03102	0.00688	0.01256
0.91751	0.00771	0.14018	-0.01471	0.06699	-0.03766	0.00164	0.00605
0.93202	0.00616	0.17005	-0.01340	0.09549	-0.04359	0.00038	-0.00286
0.95024	0.00412	0.20018	-0.01164	0.12843	-0.04871	0.00304	-0.00814
0.96279	0.00217	0.24453	-0.00875	0.16543	-0.05294	0.00744	-0.01239
0.97394	0.00103	0.29261	-0.00535	0.20611	-0.05621	0.01340	-0.01656
0.98610	-0.00010	0.34669	-0.00214	0.25000	-0.05849	0.01769	-0.01911
0.99283	-0.00114	0.40380	0.00016	0.29663	-0.05975	0.02600	-0.02334
1.00000	-0.00153	0.46250	0.00185	0.34549	-0.06000	0.03675	-0.02786
<hr/>							
GM15 (reflexed flap)		0.51368	0.00160	0.39604	-0.05928	0.05076	-0.03222
actual model		0.57249	-0.00017	0.44774	-0.05763	0.06808	-0.03608
reflexed flap		0.62846	-0.00386	0.50000	-0.05514	0.08714	-0.03943
<hr/>		0.67683	-0.00687	0.55226	-0.05189	0.11804	-0.04439
<hr/>		0.71743	-0.00421	0.60396	-0.04800	0.14686	-0.04810
<hr/>		0.75938	-0.00197	0.65451	-0.04359	0.18075	-0.05138
<hr/>		0.80531	0.00043	0.70337	-0.03880	0.23136	-0.05512
1.00000	-0.00108	0.83507	0.00051	0.75000	-0.03377	0.28906	-0.05784
0.99768	0.00163	0.86859	0.00083	0.79389	-0.02864	0.35629	-0.05804
0.99175	0.00226	0.90278	0.00027	0.83456	-0.02357	0.41865	-0.05705
0.98572	0.00287	0.91757	-0.00014	0.87157	-0.01870	0.48118	-0.05473
0.97308	0.00411	0.93247	-0.00034	0.90451	-0.01416	0.54428	-0.05096
0.95989	0.00541	0.94659	-0.00058	0.93301	-0.01009	0.60641	-0.04598
0.94798	0.00634	0.96192	-0.00100	0.95677	-0.00659	0.66791	-0.04046
0.93450	0.00746	0.97236	-0.00112	0.97553	-0.00377	0.72858	-0.03435
0.91824	0.00877	0.98319	-0.00154	0.98907	-0.00169	0.77346	-0.02874
0.90389	0.00998	0.99262	-0.00162	0.99726	-0.00043	0.81109	-0.02476
0.88952	0.01163	1.00000	-0.00108	1.00000	0.00000	0.84578	-0.01999
<hr/>		J5012		J5012		<hr/>	
<hr/>		x/c y/c		actual model		<hr/>	
<hr/>		1.00000	0.00000	1.00000	0.00043	0.94686	-0.00851
0.70598	0.02216	0.99726	0.00043	0.99683	0.00325	0.95756	-0.00780
0.66364	0.02436	0.98907	0.00169	0.99236	0.00410	0.96603	-0.00721
0.61958	0.03012	0.97553	0.00377	0.98621	0.00473	0.97488	-0.00634
0.56287	0.03802	0.95677	0.00659	0.97933	0.00565	0.98317	-0.00510
0.50630	0.04505	0.93301	0.01009	0.97334	0.00642	0.99140	-0.00347
0.45206	0.05049	0.90451	0.01416	0.96802	0.00702	0.99921	-0.00151
0.39478	0.05465	0.87157	0.01870	0.96016	0.00805	1.00000	0.00043
0.33826	0.05690	0.83457	0.02357	0.95092	0.00920	<hr/>	
0.28324	0.05801	0.79389	0.02864	0.93935	0.01065	<hr/>	
0.23720	0.05776	0.75000	0.03377	0.91244	0.01407	<hr/>	
0.19531	0.05558	0.70337	0.03880	0.89213	0.01708	<hr/>	
0.16463	0.05260	0.65451	0.04359	0.87168	0.02010	<hr/>	
0.13575	0.04900	0.60396	0.04800	0.84330	0.02397	<hr/>	
0.10962	0.04475	0.55226	0.05189	0.80711	0.02853	<hr/>	
0.09613	0.04188	0.50000	0.05514	0.72530	0.03722	<hr/>	
0.08282	0.03866	0.44774	0.05763	0.66130	0.04362	<hr/>	
0.06530	0.03414	0.39604	0.05928	0.59952	0.04832	<hr/>	
0.05167	0.03007	0.34549	0.06000	0.53716	0.05309	<hr/>	
0.04019	0.02614	0.29663	0.05975	0.47185	0.05714	<hr/>	
0.02474	0.01961	0.25000	0.05849	0.41102	0.05843	<hr/>	
0.01699	0.01587	0.20611	0.05621	0.34700	0.05953	<hr/>	
0.00813	0.01062	0.16544	0.05294	0.28532	0.05833	<hr/>	
0.00123	0.00324	0.12843	0.04871	0.22125	0.05623	<hr/>	
0.00000	0.00008	0.09549	0.04359	0.18379	0.05339	<hr/>	
0.00440	-0.00611	0.06699	0.03766	0.14666	0.05010	<hr/>	
0.01068	-0.00817	0.04323	0.03102	0.11503	0.04572	<hr/>	
0.01743	-0.00963	0.02447	0.02380	0.08233	0.03939	<hr/>	
0.02538	-0.01110	0.01093	0.01612	0.05940	0.03400	<hr/>	
0.03147	-0.01204	0.00274	0.00814	0.04376	0.02942	<hr/>	
0.04506	-0.01353	0.00000	0.00000	0.00000	0.00000	<hr/>	
0.05847	-0.01439	K3311		x/c y/c		<hr/>	
1.00000	0.00000	1.00000	0.01043	0.95000	0.02009	<hr/>	
0.95000	0.01043	0.90000	0.02931	0.85000	0.03842	<hr/>	
0.90000	0.02009	0.80000	0.04670	0.75000	0.05476	<hr/>	
0.85000	0.02931	0.70000	0.06170	0.65000	0.06895	<hr/>	
0.80000	0.03842	0.60000	0.07485	0.55000	0.08595	<hr/>	
0.75000	0.04670	0.50000	0.07966	0.50000	0.08347	<hr/>	
0.70000	0.05476	0.45000	0.08618	0.40000	0.08618	<hr/>	
0.65000	0.06170	0.35000	0.08702	0.30000	0.08595	<hr/>	
0.60000	0.06895	0.25000	0.08310	0.20000	0.07776	<hr/>	
0.55000	0.07485	0.15000	0.06966	0.10000	0.05748	<hr/>	

M06-13-128						
					<i>x/c</i>	<i>y/c</i>
0.08000	0.05130	0.11999	0.06267	0.92927	0.01326	
0.06000	0.04412	0.09576	0.05609	0.91421	0.01626	
0.04000	0.03498	0.07395	0.04899	0.88981	0.02080	
0.02000	0.02327	0.05468	0.04147	0.87119	0.02451	
0.01000	0.01563	0.03811	0.03372	0.84401	0.02951	
0.00000	0.00000	0.02433	0.02593	0.80879	0.03576	
0.01000	-0.01036	0.01338	0.01829	0.76896	0.04246	
0.02000	-0.01285	0.00548	0.01100	0.72532	0.04963	
0.04000	-0.01635	0.00098	0.00432	0.65974	0.05985	
0.06000	-0.01896	0.00000	0.00000	0.60050	0.06780	
0.08000	-0.02045	0.00098	-0.00381	0.54235	0.07445	
0.10000	-0.02169	0.00548	-0.00822	0.47337	0.08056	
0.15000	-0.02387	0.01338	-0.01171	0.41661	0.08425	
0.20000	-0.02492	0.02433	-0.01444	0.35294	0.08572	
0.25000	-0.02468	0.03811	-0.01666	0.28951	0.08457	
0.30000	-0.02405	0.05468	-0.01859	0.22964	0.08037	
0.35000	-0.02260	0.07395	-0.02033	0.18578	0.07492	
0.40000	-0.02113	0.09576	-0.02189	0.14442	0.06769	
0.45000	-0.01883	0.11999	-0.02320	0.11920	0.06178	
0.50000	-0.01608	0.14648	-0.02422	0.09024	0.05352	
0.55000	-0.01327	0.17504	-0.02491	0.07182	0.04722	
0.60000	-0.01053	0.20549	-0.02525	0.05559	0.04064	
0.65000	-0.00812	0.23760	-0.02524	0.04140	0.03416	
0.70000	-0.00592	0.27120	-0.02490	0.03141	0.02924	
0.75000	-0.00396	0.30609	-0.02424	0.02214	0.02376	
0.80000	-0.00232	0.34204	-0.02329	0.01532	0.01912	
0.85000	-0.00121	0.37887	-0.02207	0.00759	0.01280	
0.90000	-0.00051	0.41638	-0.02057	0.00303	0.00794	
0.95000	-0.00054	0.45435	-0.01879	0.00009	0.00133	
1.00000	0.00000	0.49265	-0.01679	0.00082	-0.00414	
<hr/>						
K3311						
smoothed						
<i>x/c</i>	<i>y/c</i>					
1.00000	0.00000	0.68359	-0.00686	0.04276	-0.01744	
0.99754	0.00055	0.72043	-0.00531	0.05520	-0.01904	
0.99070	0.00206	0.75616	-0.00396	0.07022	-0.02053	
0.98037	0.00428	0.79048	-0.00283	0.09125	-0.02225	
0.96698	0.00706	0.82309	-0.00195	0.12022	-0.02396	
0.95044	0.01040	0.85370	-0.00132	0.15193	-0.02512	
0.93064	0.01430	0.88202	-0.00094	0.19496	-0.02572	
0.90775	0.01871	0.90775	-0.00074	0.23624	-0.02561	
0.88202	0.02357	0.93064	-0.00067	0.30577	-0.02450	
0.85370	0.02879	0.95044	-0.00063	0.36754	-0.02317	
0.82309	0.03430	0.96698	-0.00057	0.42753	-0.02084	
0.79048	0.03999	0.98037	-0.00044	0.48901	-0.01772	
0.75616	0.04575	0.99070	-0.00026	0.55276	-0.01393	
0.72043	0.05150	0.99754	-0.00008	0.61363	-0.01064	
0.68359	0.05713	1.00000	0.00000	0.67612	-0.00737	
<hr/>						
K3311						
actual model						
<i>x/c</i>	<i>y/c</i>					
0.56937	0.07246	0.88673	-0.00146	0.85742	-0.00167	
0.53099	0.07666	1.00000	0.00003	0.90460	-0.00132	
0.49265	0.08025	0.99939	0.00056	0.92704	-0.00119	
0.45435	0.08315	0.99529	0.00107	0.94406	-0.00115	
0.41638	0.08525	0.99173	0.00173	0.95318	-0.00120	
0.37887	0.08647	0.98800	0.00241	0.96388	-0.00112	
0.34204	0.08674	0.98235	0.00350	0.97228	-0.00108	
0.30609	0.08604	0.97586	0.00452	0.98062	-0.00091	
0.27120	0.08436	0.96889	0.00574	0.98641	-0.00080	
0.23760	0.08174	0.96170	0.00711	0.99166	-0.00084	
0.20549	0.07821	0.95409	0.00856	0.99800	-0.00056	
0.17504	0.07381	0.94155	0.01100	1.00000	0.00003	
0.14648	0.06861					0.99393 -0.00073

0.99942	-0.00014	0.74706	-0.00844	MA409	0.56937	0.00754
1.00000	0.00000	0.78928	-0.00765	smoothed	0.60778	0.00808
		0.82743	-0.00701		0.64594	0.00837
M06-13-128		0.85713	-0.00651		0.68359	0.00844
actual model B		0.89265	-0.00579	<i>x/c</i>	<i>y/c</i>	
		0.91175	-0.00536	1.00000	0.00034	0.72043
<i>x/c</i>	<i>y/c</i>	0.93322	-0.00478	0.99754	0.00094	0.00830
1.00000	0.00013	0.94441	-0.00440	0.99070	0.00259	0.00798
0.99991	0.00090	0.95421	-0.00399	0.98037	0.00498	0.00749
0.99740	0.00124	0.96515	-0.00344	0.96698	0.00793	0.00687
0.99257	0.00149	0.97685	-0.00279	0.95044	0.01136	0.00613
0.98566	0.00162	0.98503	-0.00227	0.93064	0.01521	0.00529
0.97902	0.00196	0.99239	-0.00166	0.90775	0.01937	0.00439
0.96956	0.00242	0.99927	-0.00090	0.88202	0.02373	0.00347
0.96139	0.00305	1.00000	0.00013	0.85370	0.02817	0.00256
0.95256	0.00383			0.82309	0.03261	0.00170
0.94342	0.00472			0.79048	0.03694	0.00093
0.93006	0.00616			0.75616	0.04112	0.00028
0.91687	0.00765	MA409		0.72043	0.04505	0.99754
0.90392	0.00925	<i>x/c</i>	<i>y/c</i>	0.68359	0.04869	1.00000
0.88712	0.01146	1.00000	0.00070	0.64594	0.05198	-0.00036
0.86530	0.01451	0.95000	0.01246	0.60778	0.05486	MA409
0.84546	0.01744	0.90000	0.02308	0.56937	0.05732	actual model
0.81718	0.02197	0.80000	0.04015	0.53099	0.05933	
0.78112	0.02819	0.70000	0.05236	0.49265	0.06089	
0.74243	0.03529	0.65000	0.06154	0.45435	0.06202	
0.69893	0.04428	0.55000	0.06543	0.41638	0.06270	
0.64065	0.05777	0.50000	0.06945	0.37887	0.06291	
0.58100	0.07280	0.45000	0.07186	0.34204	0.06260	
0.51924	0.09047	0.40000	0.07391	0.30609	0.06172	
0.46121	0.10537	0.35000	0.07434	0.27120	0.06025	
0.39966	0.11277	0.30000	0.07398	0.23760	0.05819	
0.32971	0.11417	0.25000	0.07302	0.20549	0.05555	
0.26768	0.11073	0.20000	0.06925	0.17504	0.05234	
0.20710	0.10258	0.15000	0.06421	0.14648	0.04859	
0.17032	0.09508	0.10000	0.05673	0.11999	0.04433	
0.14567	0.08875	0.07500	0.05132	0.09576	0.03961	
0.12535	0.08252	0.05000	0.04479	0.07395	0.03450	
0.10647	0.07575	0.02500	0.03500	0.05468	0.02913	
0.08239	0.06552	0.01250	0.02831	0.03811	0.02369	
0.06396	0.05623	0.001250	0.01749	0.02433	0.01831	
0.05228	0.04960	0.01250	0.00878	0.01338	0.01305	
0.03982	0.04178	0.01250	0.00437	0.00548	0.00797	
0.03050	0.03527	0.01250	0.00082	0.00098	0.00318	
0.02092	0.02762	0.01250	0.00022	0.00000	-0.00004	
0.01126	0.01820	0.01250	0.00000	0.00098	-0.00302	
0.00491	0.01044	0.01250	0.00122	0.00548	-0.00664	
0.00032	0.00263	0.01250	0.00280	0.01338	-0.00968	
0.00347	-0.00885	0.01250	0.00514	0.02433	-0.01213	
0.00859	-0.01029	0.01250	0.00789	0.03811	-0.01400	
0.01784	-0.01219	0.01250	0.01031	0.05468	-0.01527	
0.03226	-0.01399	0.01250	0.01229	0.07395	-0.01590	
0.05462	-0.01559	0.01250	0.01424	0.09576	-0.01589	
0.08276	-0.01664	0.01250	0.01499	0.11999	-0.01527	
0.11168	-0.01712	0.01250	0.01525	0.14648	-0.01416	
0.16316	-0.01750	0.01250	0.01536	0.17504	-0.01264	
0.22105	-0.01733	0.01250	0.01384	0.20549	-0.01081	
0.27285	-0.01695	0.01250	0.01107	0.23760	-0.00875	
0.33585	-0.01621	0.01250	0.00704	0.27120	-0.00653	
0.39924	-0.01526	0.01250	0.00000	0.30609	-0.00421	
0.46002	-0.01418	0.01250	0.00000	0.34204	-0.00186	
0.52606	-0.01287	0.01250	0.00000	0.37887	0.00039	
0.58351	-0.01167	0.01250	0.00000	0.41638	0.00245	
0.64698	-0.01036	0.01250	0.00000	0.45435	0.00422	
0.70823	-0.00913	0.01250	0.00000	0.49265	0.00565	

MH45						
					<i>x/c</i>	<i>y/c</i>
0.00328	-0.00600	0.17500	0.08410	0.75958	0.04923	
0.00830	-0.00907	0.15000	0.07844	0.71819	0.05753	
0.01423	-0.01167	0.12500	0.07146	0.65931	0.06879	
0.01996	-0.01369	0.10000	0.06296	0.59687	0.07943	
0.02550	-0.01504	0.08750	0.05807	0.53642	0.08808	1.00000 0.00000
0.03360	-0.01635	0.07500	0.05274	0.47578	0.09452	0.99669 -0.00010
0.04220	-0.01731	0.06250	0.04696	0.41397	0.09840	0.98669 -0.00021
0.05421	-0.01795	0.05000	0.04072	0.34916	0.09961	0.97013 0.00016
0.06552	-0.01827	0.03750	0.03393	0.28574	0.09767	0.94746 0.00130
0.08973	-0.01834	0.02500	0.02636	0.22234	0.09218	0.91917 0.00332
0.10067	-0.01821	0.01000	0.01521	0.18314	0.08621	0.88574 0.00629
0.11201	-0.01798	0.00000	-0.00041	0.15247	0.07959	0.84775 0.01028
0.13732	-0.01725	0.01000	-0.01223	0.13478	0.07485	0.80590 0.01536
0.16378	-0.01619	0.02500	-0.01809	0.11301	0.06803	0.76107 0.02140
0.19399	-0.01505	0.03750	-0.02159	0.09509	0.06148	0.71405 0.02803
0.23873	-0.01281	0.05000	-0.02461	0.07437	0.05274	0.66547 0.03488
0.28061	-0.01034	0.06250	-0.02739	0.05843	0.04511	0.61587 0.04154
0.33952	-0.00702	0.07500	-0.03001	0.05001	0.04073	0.56569 0.04768
0.39707	-0.00433	0.08750	-0.03246	0.04097	0.03571	0.51532 0.05306
0.45727	-0.00184	0.10000	-0.03472	0.03239	0.03061	0.46516 0.05755
0.51627	-0.00082	0.12500	-0.03861	0.02467	0.02569	0.41564 0.06108
0.57355	-0.00006	0.15000	-0.04175	0.01653	0.02010	0.36723 0.06358
0.62624	0.00021	0.17500	-0.04425	0.01034	0.01534	0.32039 0.06498
0.67937	0.00048	0.20000	-0.04622	0.00788	0.01322	0.27558 0.06523
0.72125	0.00013	0.22500	-0.04776	0.00339	0.00843	0.23318 0.06425
0.76715	-0.00014	0.25000	-0.04892	0.00107	0.00457	0.19353 0.06203
0.81282	-0.00015	0.27500	-0.04974	0.00085	-0.00400	0.15691 0.05862
0.84246	-0.00012	0.30000	-0.05026	0.00374	-0.00842	0.12363 0.05410
0.87766	-0.00015	0.32500	-0.05052	0.00764	-0.01150	0.09395 0.04858
0.91173	-0.00071	0.35000	-0.05054	0.01331	-0.01442	0.06813 0.04218
0.92537	-0.00084	0.37500	-0.05035	0.01999	-0.01703	0.04634 0.03500
0.94213	-0.00111	0.40000	-0.04997	0.02801	-0.01969	0.02867 0.02722
0.95522	-0.00122	0.42500	-0.04941	0.03626	-0.02207	0.01520 0.01906
0.96880	-0.00129	0.45000	-0.04866	0.04648	-0.02474	0.00588 0.01088
0.97824	-0.00111	0.50000	-0.04660	0.05763	-0.02737	0.00079 0.00326
0.98517	-0.00084	0.55000	-0.04383	0.06963	-0.02994	0.00000 0.00000
0.99321	-0.00043	0.60000	-0.04036	0.08657	-0.03320	0.00068 -0.00279
1.00000	-0.00018	0.65000	-0.03628	0.11740	-0.03817	0.00641 -0.00788
MB253515						
smoothed						
<i>x/c</i>	<i>y/c</i>					
1.00000	0.00000	0.75000	-0.02669	0.18899	-0.04588	0.03421 -0.01814
0.95000	0.01032	0.80000	-0.02144	0.23249	-0.04847	0.05531 -0.02277
0.90000	0.02033	0.85000	-0.01606	0.29430	-0.05009	0.08085 -0.02678
0.85000	0.03052	0.90000	-0.01070	0.35640	-0.05059	0.11065 -0.02991
0.80000	0.04079	0.95000	-0.00544	0.41879	-0.04988	0.14460 -0.03206
0.75000	0.05095	1.00000	0.00000	0.48450	-0.04778	0.18252 -0.03329
0.70000	0.06078			0.54388	-0.04475	0.22408 -0.03366
0.65000	0.07005			0.60626	-0.04041	0.26891 -0.03330
0.60000	0.07849	1.00000	0.00039	0.66912	-0.03497	0.31654 -0.03229
0.55000	0.08582	0.99967	0.00028	0.72901	-0.02908	0.36646 -0.03073
0.50000	0.09174	0.99635	0.00105	0.77184	-0.02465	0.41816 -0.02875
0.45000	0.09602	0.99240	0.00188	0.84465	-0.01688	0.47104 -0.02646
0.42500	0.09748	0.98505	0.00339	0.87527	-0.01358	0.52449 -0.02399
0.40000	0.09847	0.96759	0.00686	0.89709	-0.01126	0.57786 -0.02143
0.37500	0.09898	0.95867	0.00870	0.91763	-0.00905	0.63049 -0.01888
0.35000	0.09904	0.94980	0.01051	0.93436	-0.00715	0.68174 -0.01640
0.32500	0.09868	0.94010	0.01252	0.95750	-0.00279	0.73095 -0.01403
0.30000	0.09788	0.92969	0.01462	0.96817	-0.00367	0.77754 -0.01179
0.27500	0.09660	0.91530	0.01751	0.98410	-0.00189	0.82094 -0.00971
0.25000	0.09473	0.89377	0.02198	0.99163	-0.00108	0.86062 -0.00782
0.22500	0.09211	0.86433	0.02796	0.99875	-0.00028	0.89607 -0.00613
0.20000	0.08861	0.83562	0.03381	1.00000	0.00039	0.92686 -0.00465
		0.80168	0.04070			0.95259 -0.00334

MH45		0.21002	-0.03435	0.00107	-0.00349	0.18469	0.04365
actual model		0.24978	-0.03405	0.00428	-0.00767	0.15708	0.04208
		0.29382	-0.03321	0.00961	-0.01214	0.13481	0.04056
		0.35002	-0.03175	0.01704	-0.01646	0.11586	0.03882
x/c	y/c	0.40632	-0.03007	0.02653	-0.02039	0.09458	0.03635
1.00000	-0.00012	0.46453	-0.02806	0.03806	-0.02395	0.07376	0.03302
0.99827	0.00179	0.57671	-0.02373	0.05156	-0.02720	0.05901	0.02992
0.99520	0.00212	0.63115	-0.02151	0.06699	-0.03023	0.04663	0.02681
0.99240	0.00228	0.67494	-0.01962	0.08427	-0.03305	0.03764	0.02415
0.98841	0.00249	0.71782	-0.01783	0.10332	-0.03564	0.02896	0.02122
0.98497	0.00284	0.75959	-0.01606	0.12408	-0.03795	0.01889	0.01749
0.98013	0.00313	0.80331	-0.01402	0.14645	-0.03994	0.01131	0.01404
0.97530	0.00344	0.83434	-0.01230	0.17033	-0.04161	0.00493	0.00973
0.96638	0.00399	0.86386	-0.01047	0.19562	-0.04295	0.00024	0.00229
0.95793	0.00447	0.89378	-0.00855	0.22221	-0.04397	0.00016	-0.00186
0.94952	0.00495	0.91042	-0.00743	0.25000	-0.04466	0.00234	-0.00712
0.93930	0.00558	0.92210	-0.00656	0.27886	-0.04504	0.00552	-0.01011
0.92778	0.00656	0.93479	-0.00566	0.30866	-0.04509	0.01021	-0.01281
0.91818	0.00749	0.94721	-0.00491	0.33928	-0.04484	0.01601	-0.01515
0.90665	0.00855	0.95882	-0.00420	0.37059	-0.04431	0.02354	-0.01736
0.89505	0.00971	0.97087	-0.00347	0.43474	-0.04248	0.03397	-0.01983
0.87743	0.01142	0.98152	-0.00281	0.50000	-0.03978	0.04585	-0.02250
0.86049	0.01322	0.98921	-0.00236	0.56526	-0.03638	0.05700	-0.02476
0.82591	0.01754	0.99814	-0.00179	0.62941	-0.03247	0.07278	-0.02793
0.79821	0.02126	1.00000	-0.00012	0.69134	-0.02823	0.09495	-0.03167
0.75602	0.02736			0.75000	-0.02384	0.12545	-0.03591
0.71415	0.03362			0.80438	-0.01945	0.15443	-0.03857
0.58275	0.05127			0.85355	-0.01522	0.19641	-0.04115
0.51906	0.05841			0.89668	-0.01127	0.23971	-0.04292
0.46381	0.06373			0.93301	-0.00770	0.29860	-0.04391
x/c	y/c	1.00000	0.00000	0.96194	-0.00463	0.36369	-0.04298
0.40971	0.06769	0.99572	0.00057	0.98296	-0.00218	0.42318	-0.04107
0.35884	0.06985	0.98296	0.00218	0.99572	-0.00057	0.48687	-0.03833
0.29253	0.07056	0.96194	0.00463	1.00000	0.00000	0.55039	-0.03483
0.25072	0.06980	0.93301	0.00770			0.61023	-0.03131
0.20946	0.06760	0.89668	0.01127			0.67169	-0.02741
0.18011	0.06517	0.85355	0.01522			0.73278	-0.02369
0.15412	0.06223	0.80438	0.01945			0.77620	-0.02086
0.12930	0.05861	0.75000	0.02384			0.81736	-0.01802
0.11007	0.05512	0.69134	0.02823			0.85242	-0.01533
0.09501	0.05198	0.62941	0.03247			0.87831	-0.01306
0.08431	0.04948	0.56526	0.03638			0.89724	-0.01154
0.07168	0.04616	0.50000	0.03978			0.91881	-0.00944
0.06060	0.04275	0.43474	0.04248			0.93434	-0.00832
0.04926	0.03858	0.37059	0.04431			0.94931	-0.00701
0.03750	0.03343	0.33928	0.04484			0.96153	-0.00585
0.02705	0.02794	0.30866	0.04509			0.97091	-0.00518
0.02012	0.02358	0.27886	0.04504			0.98726	-0.00288
0.01364	0.01864	0.25000	0.04466			0.99218	-0.00166
0.00843	0.01365	0.22221	0.04397			1.00008	-0.00019
0.00477	0.00938	0.19562	0.04295			1.00000	-0.00050
0.00086	0.00247	0.17033	0.04161				
0.00004	0.00053	0.14645	0.03994				
0.00631	-0.00670	0.12408	0.03795				
0.01189	-0.00959	0.10332	0.03564				
0.01834	-0.01249	0.08427	0.03305				
0.02381	-0.01471	0.06699	0.03023				
0.03119	-0.01721	0.05156	0.02720				
0.03888	-0.01939	0.03806	0.02395				
0.05568	-0.02307	0.02653	0.02039				
0.07078	-0.02561	0.01704	0.01646				
0.08371	-0.02746	0.00961	0.01214				
0.09714	-0.02909	0.00428	0.00767				
0.11366	-0.03073	0.00107	0.00349				
0.12732	-0.03177	0.00000	0.00000				
0.15294	-0.03319						
0.18046	-0.03405						

NACA 0009		NACA 0009		NACA 6409			
x/c	y/c	x/c	y/c	x/c	y/c	x/c	y/c
0.00000	0.00000	0.99995	0.00019	1.00000	0.00050	0.81736	-0.01802
0.00000	0.00000	0.99964	0.00079	0.97609	0.00136	0.85242	-0.01533
0.00000	0.00000	0.98599	0.00056	0.94616	0.00178	0.87831	-0.01306
0.00000	0.00000	0.97854	0.00072	0.92414	0.00558	0.89724	-0.01154
0.00000	0.00000	0.93607	0.00430	0.90698	0.00748	0.91881	-0.00944
0.00000	0.00000	0.94678	0.00324	0.88511	0.00991	0.93434	-0.00832
0.00000	0.00000	0.93607	0.00430	0.86640	0.01188	0.94931	-0.00701
0.00000	0.00000	0.92414	0.00558	0.83604	0.01503	0.96153	-0.00585
0.00000	0.00000	0.90698	0.00748	0.76079	0.02237	0.97091	-0.00518
0.00000	0.00000	0.88511	0.00991	0.71497	0.02614	0.98726	-0.00288
0.00000	0.00000	0.86640	0.01188	0.65763	0.03029	0.99218	-0.00166
0.00000	0.00000	0.83604	0.01503	0.60092	0.03413	1.00008	-0.00019
0.00000	0.00000	0.76079	0.02237	0.53019	0.03828	1.00000	-0.00050
0.00000	0.00000	0.71497	0.02614	0.47423	0.04098		
0.00000	0.00000	0.65763	0.03029	0.40460	0.04382		
0.00000	0.00000	0.60092	0.03413	0.34168	0.04563		
0.00000	0.00000	0.53019	0.03828	0.28447	0.04619		
0.00000	0.00000	0.47423	0.04098	0.22228	0.04526		

0.75272	0.06283	0.92590	0.02077	0.94065	0.00233	0.00000	0.00000
0.70608	0.07153	0.91387	0.02419	0.95459	0.00137	0.00025	-0.00189
0.65710	0.07961	0.90369	0.02679	0.96742	0.00039	0.00050	-0.00268
0.60627	0.08684	0.89095	0.02985	0.97864	-0.00042	0.00075	-0.00327
0.55413	0.09302	0.87619	0.03339	0.98835	-0.00088	0.00100	-0.00377
0.50132	0.09796	0.84472	0.04098	1.00000	0.00049	0.00125	-0.00421
0.44840	0.10152	0.81153	0.04855			0.00150	-0.00459
0.39590	0.10360	0.78438	0.05442			0.00175	-0.00495
0.34367	0.10352	0.73987	0.06314			0.00200	-0.00528
0.29315	0.10086	0.69754	0.07091			x/c	y/c
0.24502	0.09584	0.65769	0.07766	1.00000	0.00000	0.00225	-0.00559
0.19988	0.08874	0.61251	0.08448	0.95000	0.00540	0.00250	-0.00588
0.15830	0.07992	0.56042	0.09112	0.90000	0.01063	0.00300	-0.00642
0.12080	0.06982	0.50220	0.09713	0.85000	0.01583	0.00350	-0.00690
0.08780	0.05889	0.44575	0.10148	0.80000	0.02102	0.00400	-0.00735
0.05968	0.04762	0.38914	0.10386	0.75000	0.02620	0.00450	-0.00776
0.03677	0.03646	0.33272	0.10332	0.70000	0.03124	0.00500	-0.00815
0.01920	0.02581	0.27353	0.09971	0.65000	0.03597	0.00600	-0.00886
0.00720	0.01603	0.23447	0.09569	0.60000	0.04021	0.00650	-0.00919
0.00080	0.00737	0.18910	0.08827	0.55000	0.04387	0.00700	-0.00950
0.00000	0.00000	0.16203	0.08230	0.50000	0.04683	0.00750	-0.00980
0.00467	-0.00573	0.13640	0.07561	0.45000	0.04893	0.00800	-0.01010
0.01467	-0.00956	0.11046	0.06759	0.40000	0.04995	0.00850	-0.01037
0.02973	-0.01157	0.09637	0.06281	0.35000	0.04968	0.00900	-0.01065
0.04970	-0.01192	0.08404	0.05832	0.30000	0.04837	0.00950	-0.01091
0.07428	-0.01080	0.07102	0.05295	0.25000	0.04608	0.01000	-0.01117
0.10317	-0.00844	0.05713	0.04639	0.20000	0.04274	0.02000	-0.01529
0.13607	-0.00513	0.04597	0.04041	0.18000	0.04106	0.03000	-0.01842
0.17257	-0.00119	0.03371	0.03331	0.16000	0.03918	0.04000	-0.02103
0.21235	0.00307	0.02399	0.02739	0.14000	0.03707	0.05000	-0.02331
0.25498	0.00729	0.01574	0.02162	0.12000	0.03471	0.06000	-0.02535
0.30012	0.01112	0.00813	0.01477	0.10000	0.03201	0.07000	-0.02720
0.34730	0.01425	0.00108	0.00498	0.09000	0.03052	0.08000	-0.02892
0.39618	0.01639	0.00004	0.00089	0.08000	0.02892	0.09000	-0.03052
0.44707	0.01772	0.00632	-0.00897	0.07000	0.02720	0.10000	-0.03201
0.49868	0.01871	0.01049	-0.01087	0.06000	0.02535	0.12000	-0.03471
0.55040	0.01925	0.01966	-0.01274	0.05000	0.02331	0.14000	-0.03707
0.60167	0.01929	0.02611	-0.01335	0.04000	0.02103	0.16000	-0.03918
0.65193	0.01880	0.03332	-0.01372	0.03000	0.01842	0.18000	-0.04106
0.70065	0.01780	0.05037	-0.01406	0.02000	0.01529	0.20000	-0.04274
0.74728	0.01634	0.06540	-0.01292	0.01000	0.01117	0.25000	-0.04608
0.79130	0.01451	0.08015	-0.01232	0.00950	0.01091	0.30000	-0.04837
0.83223	0.01241	0.09344	-0.01166	0.00900	0.01065	0.35000	-0.04968
0.86957	0.01017	0.10750	-0.01057	0.00850	0.01037	0.40000	-0.04995
0.90288	0.00791	0.12194	-0.00915	0.00800	0.01010	0.45000	-0.04893
0.93180	0.00576	0.14880	-0.00638	0.00750	0.00980	0.50000	-0.04683
0.95593	0.00383	0.17622	-0.00281	0.00700	0.00950	0.55000	-0.04387
0.97503	0.00221	0.20133	0.00043	0.00650	0.00919	0.60000	-0.04021
0.98883	0.00101	0.24547	0.00525	0.00600	0.00886	0.65000	-0.03597
0.99722	0.00025	0.28357	0.00872	0.00550	0.00851	0.70000	-0.03124
1.00000	0.00000	0.33882	0.01219	0.00500	0.00815	0.75000	-0.02620
<hr/>							
NACA 6409							
actual model							
<hr/>							
x/c		y/c					
1.00000	0.00049	0.67127	0.01619	0.00225	0.00559	0.80000	-0.02102
0.99074	0.00359	0.71437	0.01508	0.00200	0.00528	0.85000	-0.01583
0.98429	0.00559	0.75797	0.01355	0.00175	0.00495	0.90000	-0.01063
0.97730	0.00769	0.80075	0.01137	0.00150	0.00459	0.95000	-0.00540
0.97242	0.00909	0.83002	0.00970	0.00125	0.00421	1.00000	0.00000
0.96508	0.01099	0.86288	0.00739	0.00100	0.00377	<hr/>	
0.95596	0.01341	0.89353	0.00555	0.00075	0.00327	x/c	y/c
0.94591	0.01594	0.91073	0.00440	0.00050	0.00268	0.99992	0.00071
0.93629	0.01827	0.92427	0.00362	0.00025	0.00189	0.99608	0.00136
						0.99029	0.00194

0.98300	0.00256	0.95323	-0.00547	0.06261	-0.02609	0.52500	0.05891
0.97367	0.00324	0.96391	-0.00438	0.07652	-0.02957	0.50000	0.06081
0.96164	0.00442	0.97343	-0.00334	0.09043	-0.03131	0.47500	0.06242
0.94893	0.00598	0.98189	-0.00233	0.10348	-0.03391	0.45000	0.06367
0.94062	0.00705	0.98877	-0.00175	0.11739	-0.03565	0.42500	0.06448
0.93106	0.00812	0.99866	-0.00071	0.13304	-0.03826	0.40000	0.06482
0.91739	0.00965	1.00000	0.00038	0.14696	-0.04000	0.37500	0.06470
0.90021	0.01152			0.16174	-0.04174	0.35000	0.06414
0.88131	0.01346			0.17696	-0.04304	0.32500	0.06319
0.86043	0.01561			0.20000	-0.04570	0.30000	0.06191
0.82848	0.01885	<i>x/c</i>	<i>y/c</i>	0.22759	-0.04845	0.27500	0.06031
0.78218	0.02331	1.00000	0.00000	0.25517	-0.05107	0.25000	0.05840
0.73276	0.02762	0.97241	0.00414	0.28522	-0.05304	0.22500	0.05616
0.67337	0.03289	0.94482	0.00760	0.31035	-0.05397	0.20000	0.05353
0.60978	0.03816	0.91826	0.01182	0.33793	-0.05498	0.17500	0.05044
0.54964	0.04264	0.88965	0.01565	0.36552	-0.05529	0.15000	0.04676
0.48886	0.04635	0.86206	0.02015	0.39310	-0.05572	0.12500	0.04241
0.42787	0.04825	0.83448	0.02416	0.42068	-0.05526	0.10000	0.03747
0.36190	0.04894	0.80689	0.02709	0.44827	-0.05471	0.09000	0.03537
0.30447	0.04817	0.77931	0.03140	0.47586	-0.05384	0.08000	0.03318
0.24276	0.04568	0.75172	0.03485	0.50344	-0.05255	0.07000	0.03088
0.20023	0.04283	0.72413	0.03795	0.53043	-0.05130	0.06000	0.02842
0.16052	0.03945	0.69696	0.04130	0.55862	-0.04936	0.05000	0.02573
0.13601	0.03698	0.66957	0.04435	0.58621	-0.04695	0.04000	0.02269
0.11091	0.03407	0.64174	0.04761	0.61379	-0.04454	0.03000	0.01918
0.08643	0.03071	0.61391	0.05075	0.64130	-0.04174	0.02000	0.01499
0.07408	0.02883	0.58783	0.05308	0.66913	-0.03913	0.01000	0.00994
0.06265	0.02681	0.56174	0.05565	0.69655	-0.03668	0.00500	0.00676
0.05240	0.02467	0.53304	0.05826	0.72431	-0.03451	0.00250	0.00468
0.03856	0.02136	0.50435	0.06070	0.75172	-0.03134	0.00200	0.00416
0.02957	0.01878	0.47913	0.06174	0.77931	-0.02831	0.00150	0.00359
0.02001	0.01543	0.45217	0.06313	0.80870	-0.02435	0.00100	0.00292
0.01370	0.01286	0.42261	0.06456	0.83448	-0.02139	0.00075	0.00252
0.00695	0.00942	0.39304	0.06428	0.86206	-0.01781	0.00050	0.00205
0.00169	0.00466	0.36696	0.06450	0.88870	-0.01470	0.00025	0.00145
0.00063	0.00286	0.34087	0.06378	0.91724	-0.01128	0.00000	0.00000
0.00047	-0.00243	0.31035	0.06266	0.94482	-0.00760	0.00025	-0.00145
0.00227	-0.00537	0.28275	0.06067	0.97241	-0.00415	0.00050	-0.00205
0.00660	-0.00890	0.25517	0.05880	1.00000	0.00000	0.00075	-0.00251
0.01230	-0.01209	0.22759	0.05659			0.00100	-0.00290
0.02183	-0.01627	0.20000	0.05328			0.00150	-0.00357
0.03003	-0.01901	0.17783	0.05087			0.00200	-0.00413
0.04119	-0.02206	0.16087	0.04870			0.00250	-0.00463
0.05047	-0.02425	0.14435	0.04613	<i>x/c</i>	<i>y/c</i>	0.00500	-0.00664
0.06368	-0.02705	0.13103	0.04334	1.00000	0.00000	0.01000	-0.00966
0.08151	-0.03033	0.11724	0.04072	0.99000	0.00155	0.02000	-0.01422
0.10171	-0.03340	0.10345	0.03830	0.98000	0.00300	0.03000	-0.01781
0.13017	-0.03702	0.08965	0.03512	0.97000	0.00440	0.04000	-0.02076
0.15982	-0.04030	0.07586	0.03224	0.95000	0.00718	0.05000	-0.02332
0.19836	-0.04365	0.06207	0.02899	0.92500	0.01070	0.06000	-0.02562
0.23931	-0.04648	0.04826	0.02512	0.90000	0.01431	0.07000	-0.02774
0.30199	-0.04944	0.03448	0.02098	0.87500	0.01798	0.08000	-0.02972
0.36475	-0.05084	0.02759	0.01835	0.85000	0.02162	0.09000	-0.03157
0.42555	-0.05029	0.02069	0.01546	0.82500	0.02516	0.10000	-0.03330
0.55070	-0.04390	0.01379	0.01208	0.80000	0.02855	0.12500	-0.03710
0.61418	-0.03926	0.00690	0.00760	0.77500	0.03181	0.15000	-0.04035
0.67674	-0.03356	0.00348	0.00414	0.75000	0.03494	0.17500	-0.04330
0.73809	-0.02754	0.00000	0.00000	0.72500	0.03798	0.20000	-0.04603
0.78083	-0.02328	0.00348	-0.00415	0.70000	0.04095	0.22500	-0.04850
0.82019	-0.01922	0.00690	-0.00760	0.67500	0.04386	0.25000	-0.05066
0.85473	-0.01566	0.01379	-0.01160	0.65000	0.04668	0.27500	-0.05244
0.88422	-0.01252	0.02069	-0.01491	0.62500	0.04941	0.30000	-0.05384
0.90343	-0.01061	0.02759	-0.01753	0.60000	0.05202	0.32500	-0.05486
0.92075	-0.00880	0.03448	-0.01933	0.57500	0.05448	0.35000	-0.05551
0.93800	-0.00705	0.04826	-0.02278	0.55000	0.05679	0.37500	-0.05583

				RG15		RG15	
				<i>x/c</i>	<i>y/c</i>	<i>x/c</i>	<i>y/c</i>
0.40000	-0.05583	0.17673	0.05054	1.00000	0.00000	1.00000	-0.00033
0.42500	-0.05552	0.14442	0.04532	0.99671	0.00054	0.99956	0.00118
0.45000	-0.05493	0.12115	0.04101	0.98726	0.00229	0.99473	0.00194
0.47500	-0.05409	0.10240	0.03738	0.97237	0.00514	0.98944	0.00265
0.50000	-0.05300	0.08552	0.03371	0.95248	0.00865	0.98943	0.00265
0.52500	-0.05166	0.07159	0.03024	0.92764	0.01254	0.97727	0.00430
0.55000	-0.05001	0.05916	0.02677	0.89810	0.01685	0.97079	0.00511
0.57500	-0.04806	0.04793	0.02335	0.86427	0.02152	0.96327	0.00619
0.60000	-0.04588	0.03906	0.02045	0.82660	0.02644	0.95678	0.00708
0.62500	-0.04357	0.02693	0.01609	0.78557	0.03149	0.94778	0.00832
0.65000	-0.04126	0.01800	0.01249	0.74165	0.03654	0.93797	0.00973
0.67500	-0.03896	0.01165	0.00948	0.69537	0.04146	0.92548	0.01145
0.70000	-0.03665	0.00593	0.00579	0.64723	0.04612	0.91565	0.01286
0.72500	-0.03422	0.00248	0.00241	0.59778	0.05039	0.90042	0.01510
0.75000	-0.03160	0.00189	0.00211	0.54753	0.05414	0.88394	0.01737
0.77500	-0.02877	0.00254	-0.00246	0.49702	0.05727	0.74504	0.03408
0.80000	-0.02578	0.00689	-0.00647	0.44676	0.05966	0.67182	0.04179
0.82500	-0.02269	0.01002	-0.00871	0.39727	0.06123	0.60574	0.04798
0.85000	-0.01959	0.01449	-0.01105	0.34902	0.06190	0.54068	0.05272
0.87500	-0.01650	0.01978	-0.01340	0.30248	0.06162	0.47840	0.05632
0.90000	-0.01342	0.02778	-0.01636	0.25809	0.06036	0.42204	0.05880
0.92500	-0.01032	0.03482	-0.01871	0.21624	0.05810	0.36113	0.06010
0.95000	-0.00713	0.04838	-0.02261	0.17730	0.05486	0.29558	0.05989
0.97000	-0.00445	0.06221	-0.02592	0.14161	0.05068	0.24179	0.05839
0.98000	-0.00304	0.07400	-0.02835	0.10945	0.04564	0.19037	0.05533
0.99000	-0.00156	0.08696	-0.03065	0.08108	0.03985	0.14441	0.05079
1.00000	0.00000	0.10175	-0.03301	0.05673	0.03343	0.11430	0.04672
R140				0.03658	0.02654	0.08978	0.04230
actual model A				0.20600	-0.04610	0.06762	0.03708
<i>x/c</i>		<i>y/c</i>		0.02076	0.01935	0.05259	0.03266
1.00000	0.00059	0.23145	-0.04851	0.00932	0.01214	0.04127	0.02877
0.99965	0.00026	0.30230	-0.05302	0.00235	0.00526	0.02632	0.02257
0.99623	0.00163	0.35298	-0.05479	0.00000	0.00000	0.01572	0.01667
0.99185	0.00277	0.40558	-0.05535	0.00002	-0.00048	0.00896	0.01183
0.98676	0.00375	0.45837	-0.05471	0.00336	-0.00534	0.00504	0.00833
0.97845	0.00509	0.49218	-0.05349	0.01247	-0.01006	0.00553	0.00233
0.96744	0.00680	0.53051	-0.05156	0.02670	-0.01436	0.01793	-0.01259
0.95733	0.00860	0.57601	-0.04864	0.04596	-0.01811	0.02427	-0.01439
0.94609	0.01083	0.61836	-0.04519	0.07010	-0.02123	0.03202	-0.01614
0.92986	0.01394	0.66369	-0.04102	0.09896	-0.02372	0.04919	-0.02220
0.91258	0.01658	0.70022	-0.03732	0.13224	-0.02559	0.06704	-0.02003
0.88866	0.01996	0.73779	-0.03313	0.16963	-0.02688	0.07736	-0.01745
0.86201	0.02370	0.77187	-0.02916	0.21073	-0.02762	0.04919	-0.01900
0.83519	0.02732	0.81100	-0.02452	0.25509	-0.02785	0.05726	-0.02003
0.80907	0.03075	0.83916	-0.02115	0.30221	-0.02762	0.06704	-0.02116
0.78207	0.03434	0.86371	-0.01822	0.35156	-0.02696	0.07736	-0.02220
0.74293	0.03883	0.88391	-0.01581	0.40257	-0.02590	0.09648	-0.02387
0.71258	0.04263	0.89942	-0.01396	0.45463	-0.02446	0.12009	-0.02549
0.68103	0.04619	0.91718	-0.01189	0.50713	-0.02262	0.15500	-0.02702
0.65171	0.04922	0.92802	-0.01066	0.55944	-0.02025	0.19367	-0.02803
0.62178	0.05206	0.93542	-0.00975	0.61128	-0.01717	0.24011	-0.02865
0.58465	0.05577	0.94490	-0.00862	0.66244	-0.01366	0.30056	-0.02884
0.55078	0.05870	0.95722	-0.00676	0.71237	-0.01015	0.36303	-0.02793
0.52023	0.06093	0.96778	-0.00537	0.76037	-0.00691	0.42108	-0.02646
0.48449	0.06258	0.97684	-0.00417	0.80575	-0.00413	0.48527	-0.02469
0.44969	0.06408	0.98362	-0.00304	0.84779	-0.00192	0.19367	-0.02803
0.41973	0.06481	0.99007	-0.00197	0.88583	-0.00034	0.24011	-0.02865
0.38880	0.06494	0.99475	-0.00120	0.91925	0.00062	0.30056	-0.02884
0.33882	0.06440	0.99920	-0.00026	0.94748	0.00101	0.36303	-0.02793
0.30226	0.06308	1.00000	0.00059	0.97003	0.00097	0.42108	-0.02646
0.26226	0.06030			0.98652	0.00064	0.48527	-0.02469
0.23109	0.05745			0.99660	0.00021		
0.20504	0.05438			1.00000	0.00000		

0.55188	-0.02231	0.00626	0.01866	0.58116	0.09838	0.98075	0.01646
0.61282	-0.01943	0.00217	0.01030	0.51830	0.10638	0.97111	0.02250
0.67555	-0.01523	0.00016	0.00277	0.45991	0.11242	0.95884	0.02853
0.73370	-0.01074	0.00023	-0.00345	0.39930	0.11681	0.94389	0.03476
0.78255	-0.00729	0.00337	-0.00773	0.33861	0.11829	0.92639	0.04116
0.82186	-0.00512	0.01034	-0.01070	0.26775	0.11516	0.90641	0.04768
0.85361	-0.00373	0.02071	-0.01324	0.20457	0.10701	0.88406	0.05427
0.87921	-0.00283	0.03417	-0.01529	0.16745	0.09969	0.85947	0.06089
0.90302	-0.00227	0.05052	-0.01685	0.12519	0.08872	0.83277	0.06749
0.92365	-0.00197	0.06959	-0.01786	0.09391	0.07821	0.80412	0.07402
0.93681	-0.00188	0.09118	-0.01830	0.06982	0.06801	0.77369	0.08044
0.94866	-0.00170	0.11512	-0.01810	0.05786	0.06189	0.74166	0.08671
0.95838	-0.00153	0.14119	-0.01715	0.04457	0.05380	0.70823	0.09277
0.96695	-0.00119	0.16911	-0.01524	0.03633	0.04791	0.67360	0.09859
0.97573	-0.00126	0.19906	-0.01183	0.02944	0.04232	0.63798	0.10412
0.98606	-0.00145	0.23157	-0.00697	0.02202	0.03546	0.60158	0.10935
0.99231	-0.00145	0.26670	-0.00124	0.01391	0.02653	0.56465	0.11425
0.99920	-0.00118	0.30427	0.00504	0.00972	0.02090	0.52744	0.11881
1.00000	-0.00033	0.34404	0.01158	0.00362	0.00974	0.49025	0.12303
<hr/>							
S1210							
		0.42909	0.02446	0.00185	-0.00554	0.41721	0.13011
		0.47370	0.03032	0.00763	-0.01127	0.38193	0.13271
		<i>x/c</i>	<i>y/c</i>	0.51919	0.03551	0.01687	-0.01493
1.00000	0.00000	0.56515	0.03986	0.02535	-0.01671	0.31488	0.13526
0.99837	0.00101	0.61113	0.04320	0.03157	-0.01762	0.28347	0.13505
0.99398	0.00397	0.65666	0.04543	0.04450	-0.01902	0.25370	0.13346
0.98753	0.00832	0.70127	0.04646	0.05676	-0.01987	0.22541	0.13037
0.97908	0.01317	0.74446	0.04625	0.08545	-0.02075	0.19846	0.12594
0.96811	0.01811	0.78575	0.04479	0.10512	-0.02075	0.17286	0.12026
0.95437	0.02328	0.82465	0.04214	0.13856	-0.01978	0.14863	0.11355
0.93796	0.02874	0.86071	0.03837	0.16539	-0.01790	0.12591	0.10598
0.91898	0.03443	0.89349	0.03364	0.20815	-0.01272	0.10482	0.09770
0.89754	0.04032	0.92255	0.02809	0.24922	-0.00626	0.08545	0.08879
0.87376	0.04637	0.94754	0.02192	0.30895	0.00352	0.06789	0.07940
0.84779	0.05254	0.96791	0.01530	0.36788	0.01310	0.05223	0.06965
0.81980	0.05879	0.98299	0.00890	0.43344	0.02266	0.03855	0.05968
0.78997	0.06506	0.99284	0.00390	0.49644	0.03030	0.02694	0.04966
0.75851	0.07130	0.99828	0.00095	0.55937	0.03653	0.01755	0.03961
0.72561	0.07747	1.00000	0.00000	0.61487	0.04070	0.01028	0.02954
0.69151	0.08349			0.67785	0.04314	0.00495	0.01969
0.65642	0.08932			0.73767	0.04325	0.00155	0.01033
0.62058	0.09490			0.77928	0.04170	0.00005	0.00178
0.58423	0.10016			0.81769	0.03910	0.00044	-0.00561
0.54763	0.10505			0.83794	0.03725	0.00264	-0.01120
0.51105	0.10948	1.00000	-0.00013	0.85523	0.03546	0.00789	-0.01427
0.47473	0.11335	0.99811	0.00094	0.87291	0.03326	0.01718	-0.01550
0.43891	0.11653	0.99327	0.00382	0.89185	0.03042	0.03006	-0.01584
0.40378	0.11892	0.98860	0.00623	0.90942	0.02729	0.04627	-0.01532
0.36955	0.12046	0.98320	0.00875	0.92714	0.02352	0.06561	-0.01404
0.33652	0.12091	0.97511	0.01220	0.94273	0.01954	0.08787	-0.01202
0.30456	0.12000	0.96703	0.01544	0.95734	0.01512	0.11282	-0.00925
0.27347	0.11784	0.95475	0.02010	0.96766	0.01155	0.14020	-0.00563
0.24341	0.11462	0.94579	0.02318	0.97714	0.00798	0.17006	-0.00075
0.21445	0.11047	0.93445	0.02695	0.98589	0.00448	0.20278	0.00535
0.18681	0.10556	0.92541	0.02975	0.99269	0.00165	0.23840	0.01213
0.16069	0.09994	0.91267	0.03349	1.00099	-0.00094	0.27673	0.01928
0.13622	0.09362	0.89739	0.03771	1.00000	-0.00013	0.31750	0.02652
0.11351	0.08672	0.88726	0.04036			0.36044	0.03358
0.09269	0.07932	0.86978	0.04470			0.40519	0.04021
0.07388	0.07149	0.84462	0.05056			0.45139	0.04618
0.05719	0.06332	0.81905	0.05619			0.49860	0.05129
0.04282	0.05484	0.78199	0.06393	1.00000	0.00000	0.54639	0.05534
0.03068	0.04593	0.74332	0.07152	0.99838	0.00126	0.59428	0.05820
0.02054	0.03672	0.70412	0.07876	0.99417	0.00494	0.64176	0.05976
0.01239	0.02755	0.64019	0.08959	0.98825	0.01037	0.68832	0.05994

0.73344	0.05872	0.01503	0.03884	0.58788	0.04408	0.89484	0.01595
0.77660	0.05612	0.01082	0.03257	0.53767	0.04783	0.87825	0.01823
0.81729	0.05219	0.00706	0.02587	0.48734	0.05093	0.85084	0.02165
0.85500	0.04706	0.00482	0.02100	0.43737	0.05323	0.83656	0.02334
0.88928	0.04088	0.00221	0.01365	0.38823	0.05467	0.81613	0.02577
0.91966	0.03387	0.00080	0.00745	0.34037	0.05520	0.80349	0.02728
0.94573	0.02624	0.00019	0.00286	0.29424	0.05479	0.79097	0.02869
0.96693	0.01822	0.00005	-0.00138	0.25026	0.05344	0.76233	0.03191
0.98255	0.01060	0.00083	-0.00593	0.20882	0.05117	0.74745	0.03352
0.99268	0.00468	0.00139	-0.00690	0.17033	0.04804	0.72867	0.03555
0.99825	0.00115	0.00312	-0.00872	0.13513	0.04409	0.71127	0.03747
1.00000	0.00000	0.00790	-0.01068	0.10353	0.03938	0.68297	0.04031
<hr/>							
S1223							
<u>actual model</u>							
<i>x/c</i>		<i>y/c</i>		0.06389		-0.01040	
1.00000	0.00013	0.08117	-0.00888	0.00107	0.00295	0.51966	0.05257
0.99720	0.00333	0.10354	-0.00663	0.00045	-0.00181	0.49053	0.05397
0.99187	0.00839	0.12948	-0.00369	0.00563	-0.00607	0.45887	0.05522
0.98689	0.01260	0.16404	0.00134	0.01601	-0.01033	0.42424	0.05619
0.98075	0.01692	0.20100	0.00781	0.03144	-0.01419	0.39420	0.05666
0.97339	0.02127	0.25115	0.01690	0.05180	-0.01752	0.36300	0.05675
0.96293	0.02660	0.29610	0.02479	0.07696	-0.02024	0.32813	0.05627
0.95370	0.03080	0.33392	0.03100	0.10672	-0.02234	0.29729	0.05528
0.94176	0.03581	0.38160	0.03816	0.14083	-0.02382	0.27385	0.05417
0.92548	0.04204	0.43006	0.04455	0.17897	-0.02471	0.23959	0.05204
0.91053	0.04728	0.47940	0.05004	0.22075	-0.02507	0.21505	0.05024
0.88969	0.05399	0.52654	0.05432	0.26575	-0.02494	0.18806	0.04784
0.87178	0.05924	0.57684	0.05747	0.31346	-0.02440	0.16310	0.04515
0.84496	0.06638	0.63172	0.05939	0.36335	-0.02349	0.13883	0.04209
0.81744	0.07305	0.67649	0.05980	0.41486	-0.02225	0.12001	0.03941
0.78334	0.08061	0.71559	0.05921	0.46742	-0.02074	0.10503	0.03710
0.74802	0.08779	0.73675	0.05844	0.52041	-0.01900	0.09032	0.03456
0.71868	0.09328	0.76333	0.05703	0.57326	-0.01706	0.07110	0.03058
0.68153	0.09976	0.78942	0.05506	0.62537	-0.01496	0.05662	0.02684
0.65038	0.10483	0.80947	0.05310	0.67617	-0.01273	0.04802	0.02436
0.61072	0.11087	0.83028	0.05062	0.72513	-0.01044	0.03936	0.02162
0.59071	0.11368	0.86994	0.04446	0.77171	-0.00816	0.02960	0.01831
0.56407	0.11720	0.89924	0.03838	0.81540	-0.00600	0.02130	0.01526
0.53542	0.12074	0.92149	0.03274	0.85566	-0.00409	0.01444	0.01217
0.50578	0.12419	0.94479	0.02561	0.89194	-0.00252	0.00802	0.00838
0.47863	0.12718	0.95707	0.02117	0.92370	-0.00135	0.00432	0.00562
0.44641	0.13039	0.97177	0.01493	0.95045	-0.00056	0.00072	-0.00228
0.41610	0.13304	0.98900	0.00570	0.97178	-0.00012	0.00106	-0.00277
0.38752	0.13509	0.99231	0.00363	0.98733	0.00004	0.00373	-0.00688
0.35962	0.13665	0.99800	-0.00013	0.99681	0.00003	0.00585	-0.00892
0.32854	0.13771	1.00000	-0.00178	1.00000	0.00000	0.00907	-0.01074
0.29648	0.13794					0.01530	-0.01336
0.26356	0.13679					0.02055	-0.01486
0.23263	0.13393					0.02545	-0.01591
0.21283	0.13114					0.03810	-0.01816
0.19561	0.12802	1.00000	0.00000			0.05334	-0.02016
0.17473	0.12336	0.99680	0.00020	1.00000	-0.00092	0.07060	-0.02192
0.15733	0.11868	0.98733	0.00088	0.99997	0.00020	0.08929	-0.02339
0.14032	0.11348	0.97184	0.00225	0.99555	0.00067	0.11283	-0.02480
0.12497	0.10819	0.95072	0.00438	0.99025	0.00168	0.14143	-0.02602
0.11009	0.10247	0.92441	0.00730	0.98554	0.00280	0.17509	-0.02667
0.09550	0.09613	0.89341	0.01095	0.98014	0.00351	0.21077	-0.02666
0.08018	0.08863	0.85821	0.01522	0.97341	0.00458	0.24782	-0.02619
0.06800	0.08199	0.81934	0.01994	0.96579	0.00571	0.30981	-0.02468
0.04897	0.07000	0.77733	0.02496	0.95450	0.00743	0.36414	-0.02279
0.03568	0.05999	0.73267	0.03005	0.94397	0.00897	0.41468	-0.02087
0.02846	0.05369	0.68588	0.03506	0.92361	0.01213	0.47090	-0.01854
0.01989	0.04487	0.63746	0.03978	0.91191	0.01364	0.52194	-0.01630

0.57581	-0.01355	0.01208	-0.00918	0.23934	0.05963	0.91539	0.01470
0.63128	-0.01072	0.02223	-0.01220	0.19735	0.05688	0.89155	0.01924
0.67090	-0.00877	0.03523	-0.01495	0.15534	0.05266	0.86543	0.02431
0.71094	-0.00702	0.05102	-0.01739	0.12433	0.04829	0.83728	0.02981
0.75430	-0.00509	0.06952	-0.01950	0.10986	0.04572	0.80738	0.03565
0.79276	-0.00317	0.09065	-0.02126	0.09582	0.04289	0.77601	0.04169
0.83080	-0.00144	0.11428	-0.02265	0.08643	0.04080	0.74337	0.04770
0.87524	0.00005	0.14032	-0.02368	0.07630	0.03837	0.70958	0.05354
0.90758	0.00110	0.16861	-0.02436	0.05400	0.03204	0.67484	0.05920
0.92690	0.00138	0.19900	-0.02471	0.04526	0.02901	0.63934	0.06454
0.94413	0.00165	0.23131	-0.02474	0.03654	0.02564	0.60327	0.06949
0.95833	0.00182	0.26535	-0.02448	0.02727	0.02166	0.56688	0.07399
0.96951	0.00163	0.30091	-0.02396	0.02128	0.01884	0.53032	0.07791
0.97956	0.00151	0.33778	-0.02318	0.01711	0.01665	0.49374	0.08125
0.98827	0.00133	0.37572	-0.02220	0.01203	0.01351	0.45740	0.08391
0.99585	0.00133	0.41449	-0.02101	0.00697	0.00952	0.42142	0.08584
1.00000	-0.00092	0.45383	-0.01965	0.00469	0.00711	0.38601	0.08706
<hr/>							
S7012							
<hr/>							
	<i>x/c</i>	<i>y/c</i>					
1.00000	0.00000	0.65044	-0.00978	0.01468	-0.01158	0.22311	0.08132
0.99819	0.00024	0.68859	-0.00732	0.01962	-0.01322	0.19440	0.07787
0.99294	0.00104	0.72582	-0.00504	0.02676	-0.01520	0.16729	0.07370
0.98451	0.00231	0.76182	-0.00300	0.03620	-0.01736	0.14189	0.06891
0.97296	0.00392	0.79628	-0.00128	0.04772	-0.01941	0.11833	0.06352
0.95833	0.00586	0.82889	0.00010	0.04752	-0.01938	0.09668	0.05760
0.94077	0.00817	0.85936	0.00112	0.07539	-0.02251	0.07705	0.05125
0.92044	0.01080	0.88743	0.00178	0.09520	-0.02407	0.05952	0.04455
0.89749	0.01372	0.91283	0.00211	0.12888	-0.02592	0.04413	0.03761
0.87210	0.01689	0.93533	0.00214	0.15977	-0.02698	0.03097	0.03054
0.84445	0.02029	0.95473	0.00192	0.19904	-0.02753	0.02008	0.02346
0.81474	0.02386	0.97084	0.00153	0.23819	-0.02729	0.01148	0.01655
0.78318	0.02757	0.98352	0.00105	0.30247	-0.02631	0.00524	0.00998
0.74999	0.03138	0.99266	0.00055	0.36215	-0.02488	0.00139	0.00398
0.71540	0.03524	0.99816	0.00016	0.42815	-0.02294	0.00007	-0.00091
0.67965	0.03909	1.00000	0.00000	0.49299	-0.02065	0.00214	-0.00493
0.64298	0.04287			0.55294	-0.01787	0.00762	-0.00871
0.60563	0.04654			0.61399	-0.01442	0.01587	-0.01193
0.56785	0.05002			0.67478	-0.01052	0.02720	-0.01436
0.52988	0.05324			0.73552	-0.00680	0.04175	-0.01620
<hr/>							
S7012							
<hr/>							
	<i>x/c</i>	<i>y/c</i>					
	1.00000	0.00024					
0.49193	0.05615			0.78148	-0.00428	0.05938	-0.01763
0.45426	0.05870			0.82002	-0.00242	0.07995	-0.01870
0.41710	0.06081			0.85315	-0.00103	0.10333	-0.01944
0.38070	0.06241			0.88282	-0.00019	0.12935	-0.01989
0.34520	0.06335			0.90308	0.00026	0.15784	-0.02009
0.31071	0.06360			0.92552	0.00047	0.18857	-0.02006
0.27741	0.06319			0.95235	0.00069	0.22132	-0.01980
0.24543	0.06209			0.96396	0.00054	0.25590	-0.01927
0.21486	0.06033			0.97523	0.00034	0.29218	-0.01849
0.18590	0.05795			0.98339	-0.00005	0.32993	-0.01757
0.15865	0.05496			0.99099	-0.00036	0.36889	-0.01656
0.13326	0.05143			0.99862	-0.00045	0.40878	-0.01551
0.10983	0.04738			1.00000	0.00024	0.44933	-0.01445
0.08846	0.04287					0.49021	-0.01338
0.06926	0.03798					0.53116	-0.01230
0.05229	0.03274					0.57188	-0.01123
0.03759	0.02728					0.61212	-0.01018
0.02525	0.02167					0.65160	-0.00914
0.01528	0.01605					0.69009	-0.00813
0.00773	0.01058					0.72734	-0.00716
0.00266	0.00542					0.76303	-0.00622
0.00007	0.00087					0.79681	-0.00533
0.00069	-0.00278					0.82841	-0.00450
0.00486	-0.00600					0.85793	-0.00373

0.88544	-0.00301	0.07697	-0.02144	0.09956	0.05510	0.63091	0.05177
0.91063	-0.00235	0.09621	-0.02215	0.07907	0.05012	0.58174	0.05738
0.93322	-0.00175	0.12762	-0.02249	0.06085	0.04458	0.53222	0.06225
0.95293	-0.00124	0.15810	-0.02285	0.04493	0.03864	0.48283	0.06606
0.96949	-0.00080	0.19891	-0.02277	0.03140	0.03234	0.43386	0.06866
0.98266	-0.00046	0.24187	-0.02203	0.02025	0.02579	0.38566	0.07003
0.99224	-0.00020	0.30328	-0.01968	0.01165	0.01916	0.33862	0.07020
0.99805	-0.00005	0.36843	-0.01772	0.00552	0.01240	0.29316	0.06922
1.00000	0.00000	0.43049	-0.01599	0.00163	0.00569	0.24976	0.06715
<hr/>							
S7055		0.55200	-0.01265	0.00147	-0.00540	0.17076	0.05988
actual model		0.61392	-0.01127	0.00651	-0.00985	0.13589	0.05480
<hr/>		0.67063	-0.00971	0.01471	-0.01427	0.10456	0.04887
<i>x/c</i>		0.73894	-0.00781	0.02583	-0.01860	0.07700	0.04218
1.00000	0.00040	0.78119	-0.00628	0.03977	-0.02271	0.05344	0.03486
0.99562	0.00203	0.82139	-0.00528	0.05642	-0.02654	0.03399	0.02710
0.99010	0.00284	0.85601	-0.00448	0.07569	-0.03003	0.01879	0.01913
0.98345	0.00397	0.88476	-0.00359	0.09749	-0.03316	0.00790	0.01132
0.97668	0.00506	0.90230	-0.00292	0.12169	-0.03590	0.00148	0.00411
0.96982	0.00632	0.92436	-0.00225	0.14818	-0.03824	0.00025	-0.00159
0.96240	0.00763	0.93865	-0.00180	0.17678	-0.04018	0.00495	-0.00647
0.95470	0.00905	0.95219	-0.00156	0.20735	-0.04171	0.01525	-0.01148
0.94683	0.01044	0.96302	-0.00127	0.23970	-0.04283	0.03068	-0.01612
0.93714	0.01212	0.97314	-0.00124	0.27364	-0.04354	0.05114	-0.02025
0.92450	0.01445	0.98332	-0.00121	0.30896	-0.04385	0.07648	-0.02381
0.91234	0.01666	0.99112	-0.00125	0.34545	-0.04377	0.10645	-0.02678
0.90178	0.01871	0.99936	-0.00105	0.38288	-0.04331	0.14078	-0.02919
0.88154	0.02256	1.00000	0.00040	0.42100	-0.04248	0.17909	-0.03105
0.86177	0.02643	<hr/>		0.45957	-0.04127	0.22096	-0.03238
0.83545	0.03185	S8052		0.49834	-0.03967	0.26592	-0.03321
0.79854	0.03912	<hr/>		0.53702	-0.03758	0.31347	-0.03354
0.76066	0.04651	<hr/>		0.57556	-0.03494	0.36306	-0.03338
0.72058	0.05398	1.00000	0.00000	0.61389	-0.03185	0.41413	-0.03273
0.66018	0.06405	0.99803	0.00018	0.65181	-0.02843	0.46614	-0.03159
0.60023	0.07286	0.99231	0.00079	0.68916	-0.02481	0.51852	-0.02995
0.53588	0.07980	0.98301	0.00181	0.72568	-0.02116	0.57073	-0.02784
0.47323	0.08473	0.97022	0.00330	0.76113	-0.01762	0.62223	-0.02527
0.41034	0.08802	0.95412	0.00533	0.79518	-0.01433	0.67254	-0.02231
0.34779	0.08827	0.93491	0.00790	0.82751	-0.01136	0.72116	-0.01906
0.28557	0.08628	0.91280	0.01104	0.85782	-0.00876	0.76761	-0.01568
0.22639	0.08189	0.88804	0.01472	0.88581	-0.00656	0.81133	-0.01236
0.18440	0.07689	0.86087	0.01891	0.91121	-0.00475	0.85176	-0.00922
0.14489	0.07040	0.83155	0.02357	0.93377	-0.00330	0.88838	-0.00638
0.12239	0.06522	0.80036	0.02863	0.95325	-0.00218	0.92070	-0.00399
0.10318	0.05983	0.76759	0.03400	0.96950	-0.00128	0.94818	-0.00214
0.08536	0.05384	0.73351	0.03957	0.98246	-0.00056	0.97032	-0.00090
0.07289	0.04896	0.69841	0.04524	0.99204	-0.00011	0.98661	-0.00024
0.06069	0.04381	0.66259	0.05083	0.99798	0.00002	0.99662	-0.00002
0.04943	0.03870	0.62635	0.05617	1.00000	0.00000	1.00000	0.00000
0.03860	0.03320	<hr/>		SD6060		SD6060	
0.02930	0.02774	0.58984	0.06088	<hr/>		<hr/>	
0.02098	0.02225	0.55299	0.06482	<hr/>		<hr/>	
0.01432	0.01724	0.51588	0.06814	<hr/>		<hr/>	
0.00716	0.01110	0.47873	0.07081	1.00000	0.00000	<hr/>	
0.00294	0.00641	0.44169	0.07283	0.99661	0.00023	<hr/>	
0.00005	-0.00085	0.40501	0.07423	0.98660	0.00108	<hr/>	
0.00025	-0.00185	0.36887	0.07498	0.97033	0.00283	<hr/>	
0.00422	-0.00712	0.33344	0.07511	0.94829	0.00559	<hr/>	
0.00819	-0.00946	0.29896	0.07461	0.92100	0.00941	<hr/>	
0.01368	-0.01173	0.26560	0.07351	0.88905	0.01419	<hr/>	
0.01940	-0.01365	0.23357	0.07182	0.85301	0.01977	<hr/>	
0.02561	-0.01527	0.20304	0.06957	0.81346	0.02595	<hr/>	
0.03578	-0.01721	0.17422	0.06676	0.77096	0.03248	<hr/>	
0.04885	-0.01892	0.14727	0.06341	0.72602	0.03912	<hr/>	
0.05964	-0.02005	0.12234	0.05951	0.67917	0.04563	<hr/>	
actual model		<hr/>		<hr/>		<hr/>	
<hr/>		<hr/>		<hr/>		<hr/>	
<i>x/c</i>		<i>y/c</i>		<i>x/c</i>		<i>y/c</i>	
<hr/>		<hr/>		<hr/>		<hr/>	
1.00000		-0.00005		1.00000		0.00158	
0.99445		0.00189		0.98915		0.00233	
0.98915		0.00189		0.98274		0.00280	
0.98274		0.00233		0.97632		0.00349	
0.97632		0.00280		0.96840		0.00427	
0.96840		0.00349		0.96021		0.00427	
0.96021		0.00427		0.95108		0.00523	
0.95108		0.00523		0.93972		0.00652	
0.93972		0.00652		0.92543		0.00819	
0.92543		0.00819		0.90947		0.01034	

		SD7003		SD7003			
		actual model		x/c		y/c	
0.88641	0.01350			1.00000	0.00000	0.49027	-0.02195
0.86803	0.01621			0.99681	0.00031	0.55287	-0.01896
0.83804	0.02061	x/c	y/c	0.98745	0.00132	0.61685	-0.01558
0.80333	0.02566	1.00000	0.00000	0.97235	0.00310	0.67653	-0.01223
0.76548	0.03134	0.99681	0.00031	0.95193	0.00547	0.74123	-0.00858
0.72844	0.03684	0.98745	0.00132	0.92210	0.00008	0.78341	-0.00630
0.66218	0.04601	0.97235	0.00310	0.94952	0.00052	0.82176	-0.00428
0.60211	0.05343	0.95193	0.00547	0.98973	0.00282	0.85838	-0.00238
0.54017	0.05990	0.92639	0.00824	0.98540	0.00319	0.88440	-0.00133
0.47817	0.06478	0.89600	0.01139	0.98022	0.00377	0.90074	-0.00064
0.41464	0.06785	0.86112	0.01494	0.97396	0.00438	0.91928	-0.00014
0.35251	0.06896	0.82224	0.01884	0.96788	0.00494	0.93834	0.00002
0.29323	0.06788	0.77985	0.02304	0.96124	0.00560	0.95147	-0.00006
0.22973	0.06474	0.73449	0.02744	0.94962	0.00669	0.96668	-0.00043
0.18531	0.06100	0.68673	0.03197	0.93592	0.00810	0.97836	-0.00097
0.14689	0.05603	0.63717	0.03649	0.92019	0.00954	0.98828	-0.00152
0.11633	0.05056	0.58641	0.04086	0.89956	0.01165	0.99431	-0.00177
0.08752	0.04407	0.53499	0.04494	0.87889	0.01356	1.00002	-0.00181
0.06241	0.03708	0.48350	0.04859	0.84842	0.01648	1.00000	-0.00009
0.04904	0.03258	0.43249	0.05171	0.81369	0.01979		
0.04040	0.02962	0.38250	0.05415	0.77486	0.02353		
0.02969	0.02475	0.33405	0.05581	0.73262	0.02755		
0.02245	0.02092	0.28760	0.05658	0.67067	0.03331	x/c	y/c
0.01453	0.01602	0.24358	0.05639	0.60737	0.03899	1.00000	0.00000
0.00633	0.00922	0.20240	0.05518	0.54734	0.04392	0.99674	0.00048
0.00062	0.00191	0.16442	0.05292	0.48510	0.04838	0.98712	0.00204
0.00047	-0.00164	0.12993	0.04961	0.42437	0.05202	0.97155	0.00485
0.00103	-0.00245	0.09921	0.04526	0.36209	0.05478	0.95054	0.00894
0.00459	-0.00592	0.07244	0.03993	0.30006	0.05629	0.92464	0.01420
0.01135	-0.01002	0.04978	0.03372	0.23709	0.05612	0.89436	0.02041
0.01901	-0.01298	0.03130	0.02677	0.19703	0.05464	0.86021	0.02731
0.02524	-0.01491	0.01702	0.01932	0.17634	0.05336	0.82264	0.03460
0.03464	-0.01737	0.00697	0.01172	0.15254	0.05138	0.78208	0.04199
0.04704	-0.01998	0.00127	0.00438	0.12780	0.04869	0.73892	0.04925
0.05625	-0.02151	0.00025	-0.00186	0.11036	0.04624	0.69356	0.05620
0.07464	-0.02396	0.00457	-0.00741	0.09384	0.04344	0.64646	0.06270
0.09503	-0.02628	0.01408	-0.01285	0.07961	0.04058	0.59812	0.06861
0.12572	-0.02867	0.02839	-0.01759	0.06546	0.03722	0.54902	0.07381
0.15720	-0.03022	0.04763	-0.02141	0.05047	0.03289	0.49967	0.07816
0.19690	-0.03144	0.07182	-0.02438	0.04069	0.02953	0.45058	0.08154
0.23471	-0.03216	0.10073	-0.02660	0.03243	0.02625	0.40222	0.08385
0.29580	-0.03320	0.13407	-0.02809	0.02599	0.02342	0.35506	0.08500
0.36138	-0.03322	0.17150	-0.02888	0.02034	0.02069	0.30953	0.08493
0.42232	-0.03252	0.21268	-0.02900	0.01552	0.01802	0.26604	0.08359
0.48560	-0.03125	0.25719	-0.02852	0.01027	0.01445	0.22499	0.08096
0.54849	-0.02919	0.30456	-0.02752	0.00624	0.01081	0.18671	0.07703
0.60979	-0.02634	0.35426	-0.02608	0.00244	0.00612	0.15146	0.07182
0.67166	-0.02206	0.40572	-0.02428	0.00104	0.00377	0.11948	0.06548
0.73181	-0.01757	0.45837	-0.02217	0.00031	-0.00204	0.09105	0.05809
0.77283	-0.01466	0.51161	-0.01980	0.00347	-0.00683	0.06627	0.04976
0.81335	-0.01179	0.56484	-0.01723	0.00885	-0.01060	0.04524	0.04078
0.84864	-0.00910	0.61748	-0.01450	0.01755	-0.01436	0.02812	0.03145
0.87676	-0.00685	0.66898	-0.01167	0.02766	-0.01756	0.01502	0.02206
0.89785	-0.00525	0.71883	-0.00887	0.03904	-0.02054	0.00606	0.01293
0.91888	-0.00360	0.76644	-0.00628	0.05200	-0.02324	0.00115	0.00448
0.93566	-0.00252	0.81118	-0.00403	0.06315	-0.02501	0.00038	-0.00223
0.94851	-0.00172	0.85241	-0.00220	0.07902	-0.02678	0.00532	-0.00701
0.96113	-0.00127	0.88957	-0.00082	0.10100	-0.02841	0.01649	-0.01088
0.97256	-0.00092	0.92210	0.00008	0.12878	-0.02970	0.03308	-0.01403
0.98297	-0.00083	0.94952	0.00052	0.16084	-0.03050	0.05491	-0.01635
0.98875	-0.00080	0.97134	0.00057	0.19924	-0.03067	0.08180	-0.01787
0.99902	-0.00080	0.98718	0.00037	0.24389	-0.03013	0.11351	-0.01862
1.00000	-0.00005	0.99679	0.00011	0.30555	-0.02867	0.14974	-0.01867
		1.00001	0.00000	0.36704	-0.02680	0.19010	-0.01810
				0.43136	-0.02445	0.23420	-0.01699

0.28153	-0.01547	0.01227	0.01814	0.66868	0.05901	0.82261	0.03141
0.33154	-0.01363	0.00787	0.01368	0.60720	0.06737	0.78201	0.03788
0.38364	-0.01152	0.00240	0.00633	0.54130	0.07453	0.73865	0.04413
0.43724	-0.00922	0.00023	-0.00192	0.47884	0.07969	0.69294	0.05011
0.49176	-0.00678	0.00280	-0.00679	0.41734	0.08315	0.64539	0.05572
0.54659	-0.00430	0.00928	-0.01148	0.35286	0.08482	0.59655	0.06085
0.60112	-0.00190	0.01264	-0.01250	0.29265	0.08421	0.54693	0.06538
0.65469	0.00030	0.01846	-0.01399	0.22164	0.07990	0.49706	0.06917
0.70664	0.00224	0.02881	-0.01573	0.18166	0.07543	0.44745	0.07211
0.75634	0.00379	0.04723	-0.01785	0.15363	0.07095	0.39862	0.07410
0.80313	0.00485	0.06062	-0.01903	0.12851	0.06583	0.35101	0.07504
0.84635	0.00535	0.07656	-0.02001	0.10848	0.06109	0.30508	0.07488
0.88534	0.00526	0.09187	-0.02064	0.09024	0.05614	0.26125	0.07358
0.91942	0.00458	0.10349	-0.02099	0.07700	0.05214	0.21989	0.07113
0.94797	0.00350	0.12003	-0.02144	0.06371	0.04780	0.18137	0.06754
0.97054	0.00226	0.14868	-0.02176	0.05270	0.04356	0.14601	0.06286
0.98684	0.00113	0.17685	-0.02145	0.03901	0.03705	0.11410	0.05715
0.99670	0.00030	0.20472	-0.02073	0.02749	0.03063	0.08586	0.05049
1.00000	0.00000	0.24431	-0.01943	0.01674	0.02342	0.06146	0.04300
<hr/>							
SD7032							
actual model D							
<i>x/c</i>		<i>y/c</i>					
1.00000	-0.00035	0.51631	-0.00740	0.01247	-0.01281	0.00021	0.00185
0.99864	0.00040	0.57476	-0.00438	0.02075	-0.01447	0.00127	-0.00393
0.99665	0.00110	0.62875	-0.00132	0.02898	-0.01573	0.00806	-0.00839
0.99353	0.00185	0.67810	0.00055	0.05026	-0.01875	0.02038	-0.01227
0.98888	0.00276	0.71802	0.00157	0.06704	-0.01997	0.03800	-0.01541
0.98259	0.00379	0.75935	0.00282	0.08723	-0.02055	0.06074	-0.01777
0.97541	0.00481	0.80501	0.00420	0.11218	-0.02087	0.08844	-0.01934
0.96809	0.00616	0.83600	0.00481	0.14554	-0.02052	0.12084	-0.02017
0.96252	0.00712	0.86820	0.00511	0.18027	-0.01982	0.15765	-0.02032
0.94859	0.00980	0.89605	0.00491	0.23716	-0.01833	0.19850	-0.01987
0.93704	0.01181	0.90948	0.00457	0.29788	-0.01643	0.24296	-0.01891
0.92652	0.01367	0.92313	0.00380	0.36224	-0.01440	0.29055	-0.01754
0.91821	0.01508	0.94075	0.00277	0.42552	-0.01213	0.34071	-0.01586
0.90582	0.01711	0.95357	0.00173	0.48858	-0.01002	0.39288	-0.01396
0.89075	0.01972	0.96655	0.00116	0.54975	-0.00763	0.44643	-0.01190
0.85677	0.02607	0.97922	0.00045	0.61762	-0.00501	0.50074	-0.00976
0.82499	0.03159	0.99036	-0.00013	0.67933	-0.00296	0.55519	-0.00760
0.79355	0.03686	0.99484	-0.00029	0.74312	-0.00116	0.60914	-0.00549
0.75266	0.04431	0.99844	-0.00040	0.78526	0.00013	0.66197	-0.00349
0.71060	0.05136	1.00000	-0.00035	0.82732	0.00111	0.71305	-0.00168
0.66862	0.05770	<hr/>		0.86321	0.00139	0.76178	-0.00014
0.62429	0.06346	SD7032		0.89349	0.00146	0.80752	0.00104
0.56871	0.06980	actual model E		0.91412	0.00119	0.84964	0.00182
0.51073	0.07533	<hr/>		0.93708	0.00083	0.88756	0.00220
0.45314	0.07952	<i>x/c</i>	<i>y/c</i>	0.95104	0.00026	0.92071	0.00218
0.39660	0.08205	1.00000	-0.00002	0.96729	-0.00036	0.94859	0.00185
0.34046	0.08289	0.99604	0.00103	0.98134	-0.00078	0.97077	0.00132
0.28613	0.08208	0.99174	0.00144	0.99034	-0.00083	0.98690	0.00071
0.24396	0.07994	0.98543	0.00239	0.99826	-0.00055	0.99671	0.00021
0.19704	0.07609	0.97848	0.00360	1.00000	-0.00002	1.00000	0.00000
0.17147	0.07271	0.97068	0.00492	<hr/>		SD7037	
0.14238	0.06773	0.96224	0.00654	<i>x/c</i>	<i>y/c</i>	<hr/>	
0.11459	0.06170	0.95405	0.00821	1.00000	0.00000	<i>x/c</i>	<i>y/c</i>
0.09965	0.05761	0.94438	0.01010	0.99672	0.00042	1.00000	0.00010
0.08841	0.05421	0.93313	0.01232	0.98707	0.00180	0.99939	0.00020
0.07620	0.05025	0.91812	0.01539	0.97146	0.00436	0.99527	0.00090
0.06239	0.04531	0.90203	0.01859	0.95041	0.00811	0.99014	0.00163
0.04837	0.03948	0.87770	0.02327	0.92450	0.01295	0.98353	0.00263
0.03818	0.03453	0.85205	0.02816	0.89425	0.01865	0.97403	0.00417
0.02912	0.02965	0.81421	0.03526	0.86015	0.02490	0.96261	0.00617
0.01986	0.02401	0.77184	0.04269				
		0.72898	0.04973				

0.95155	0.00837	0.99745	-0.00020	0.36946	-0.01644	0.25477	-0.02969
0.93611	0.01114	1.00000	0.00010	0.43210	-0.01382	0.30202	-0.02864
0.92040	0.01426			0.49408	-0.01144	0.35163	-0.02710
0.89570	0.01832			0.55674	-0.00899	0.40307	-0.02514
0.87523	0.02168	SD7037		0.61627	-0.00666	0.45576	-0.02284
0.84954	0.02595	actual model B		0.68273	-0.00401	0.50913	-0.02024
0.81473	0.03151	<i>x/c</i>	<i>y/c</i>	0.74376	-0.00163	0.56263	-0.01744
0.77445	0.03798	1.00000	0.00024	0.78840	-0.00022	0.61566	-0.01459
0.73371	0.04426	0.99970	0.00101	0.82871	0.00066	0.66757	-0.01179
0.67283	0.05179	0.99598	0.00202	0.86231	0.00116	0.71773	-0.00910
0.60966	0.05842	0.99205	0.00266	0.89094	0.00125	0.76556	-0.00662
0.54617	0.06407	0.98502	0.00365	0.90746	0.00133	0.81047	-0.00445
0.48282	0.06857	0.97716	0.00484	0.92920	0.00109	0.85185	-0.00268
0.42115	0.07073	0.96931	0.00617	0.94526	0.00087	0.88910	-0.00132
0.35717	0.07218	0.96189	0.00740	0.95938	0.00051	0.92170	-0.00040
0.29557	0.07174	0.95176	0.00908	0.97400	0.00017	0.94916	0.00013
0.23162	0.06859	0.93747	0.01138	0.98276	-0.00013	0.97105	0.00032
0.18963	0.06476	0.92491	0.01353	0.99226	-0.00073	0.98700	0.00026
0.14693	0.05875	0.90813	0.01654	0.99963	-0.00101	0.99673	0.00009
0.11775	0.05343	0.89082	0.01969	1.00000	0.00024	1.00001	0.00000
0.08713	0.04632	0.87337	0.02265				
0.06452	0.03971	0.84839	0.02689				
0.05084	0.03504	0.82124	0.03133				
0.03697	0.02983	0.77629	0.03808	SD8000			
0.02726	0.02581	0.73714	0.04373	<i>x/c</i>	<i>y/c</i>		
0.01915	0.02154	0.67533	0.05168	1.00000	0.00000		
0.01227	0.01678	0.61304	0.05864	0.99674	0.00030		
0.00792	0.01314	0.55026	0.06448	0.98711	0.00130		
0.00381	0.00873	0.48609	0.06920	0.97148	0.00321		
0.00201	0.00608	0.42380	0.07261	0.95032	0.00607		
0.00106	0.00411	0.36212	0.07430	0.92413	0.00984		
0.00000	-0.00114	0.29770	0.07411	0.89343	0.01434		
0.00104	-0.00405	0.23632	0.07153	0.85871	0.01936		
0.00523	-0.00834	0.19389	0.06803	0.82042	0.02466		
0.01049	-0.01095	0.15198	0.06297	0.77899	0.03000		
0.01641	-0.01278	0.12033	0.05764	0.73481	0.03521		
0.02217	-0.01413	0.09461	0.05214	0.68831	0.04017		
0.03130	-0.01547	0.07954	0.04827	0.63998	0.04478		
0.04393	-0.01670	0.06942	0.04532	0.59034	0.04894		
0.05396	-0.01754	0.05672	0.04144	0.53991	0.05256		
0.07175	-0.01882	0.04558	0.03723	0.48921	0.05553		
0.09250	-0.02009	0.03513	0.03261	0.43875	0.05780		
0.12402	-0.02118	0.02605	0.02761	0.38905	0.05929		
0.15728	-0.02178	0.01987	0.02350	0.34062	0.05996		
0.19785	-0.02160	0.01370	0.01882	0.29395	0.05978		
0.23954	-0.02063	0.01022	0.01598	0.24951	0.05872		
0.30173	-0.01914	0.00719	0.01306	0.20775	0.05675		
0.36573	-0.01710	0.00167	0.00588	0.16906	0.05389		
0.42758	-0.01477	0.00022	0.00212	0.13380	0.05012		
0.48907	-0.01271	0.00211	-0.00668	0.10229	0.04548		
0.55079	-0.01026	0.00487	-0.00914	0.07476	0.04000		
0.61275	-0.00788	0.01007	-0.01186	0.05142	0.03377		
0.67713	-0.00581	0.01523	-0.01365	0.03238	0.02686		
0.74024	-0.00400	0.02322	-0.01605	0.01766	0.01948		
0.78350	-0.00276	0.02997	-0.01761	0.00729	0.01194		
0.82467	-0.00189	0.04075	-0.01936	0.00136	0.00460		
0.86111	-0.00124	0.05077	-0.02039	0.00022	-0.00175		
0.89018	-0.00112	0.06403	-0.02134	0.000440	-0.00749		
0.91028	-0.00083	0.07854	-0.02223	0.01370	-0.01315		
0.93140	-0.00068	0.09895	-0.02280	0.02780	-0.01814		
0.94733	-0.00051	0.13065	-0.02300	0.04677	-0.02225		
0.96292	-0.00036	0.15845	-0.02281	0.07058	-0.02544		
0.97465	-0.00027	0.20002	-0.02238	0.09914	-0.02776		
0.98378	-0.00029	0.24292	-0.02137	0.13219	-0.02929		
0.99008	-0.00028	0.30574	-0.01912	0.16941	-0.03008		
				0.21041	-0.03020		

0.00064	-0.00310	0.11789	0.04233	0.29098	0.05021	0.93064	0.01373
0.00268	-0.00638	0.08774	0.03802	0.23096	0.04966	0.90775	0.01754
0.00629	-0.00936	0.06179	0.03287	0.19250	0.04838	0.88202	0.02173
0.01227	-0.01252	0.04024	0.02697	0.16513	0.04683	0.85370	0.02616
0.01719	-0.01468	0.02318	0.02041	0.14181	0.04497	0.82309	0.03071
0.02222	-0.01655	0.01065	0.01345	0.11555	0.04230	0.79048	0.03534
0.02657	-0.01790	0.00276	0.00645	0.09471	0.03947	0.75616	0.04001
0.03833	-0.02054	0.00000	0.00000	0.07409	0.03594	0.72043	0.04467
0.04884	-0.02230	0.00276	-0.00645	0.05620	0.03208	0.68359	0.04923
0.06105	-0.02386	0.01066	-0.01345	0.04384	0.02876	0.64594	0.05362
0.07541	-0.02541	0.02319	-0.02041	0.03327	0.02534	0.60778	0.05775
0.09852	-0.02727	0.04024	-0.02697	0.02199	0.02080	0.56937	0.06154
0.12534	-0.02862	0.06180	-0.03287	0.01428	0.01681	0.53099	0.06495
0.15997	-0.02940	0.08774	-0.03802	0.00757	0.01239	0.49265	0.06796
0.19782	-0.02955	0.11790	-0.04233	0.00311	0.00799	0.45435	0.07055
0.24327	-0.02902	0.15204	-0.04574	0.00147	0.00536	0.41638	0.07265
0.30405	-0.02732	0.18987	-0.04824	0.00047	-0.00298	0.37887	0.07421
0.36741	-0.02485	0.23107	-0.04982	0.00096	-0.00428	0.34204	0.07514
0.42792	-0.02195	0.27524	-0.05051	0.00279	-0.00745	0.30609	0.07537
0.49041	-0.01878	0.32197	-0.05034	0.00737	-0.01163	0.27120	0.07482
0.55391	-0.01531	0.37077	-0.04938	0.01322	-0.01524	0.23760	0.07345
0.61699	-0.01167	0.42117	-0.04769	0.01678	-0.01716	0.20549	0.07122
0.67610	-0.00841	0.47262	-0.04536	0.02298	-0.02022	0.17504	0.06813
0.73884	-0.00504	0.52457	-0.04246	0.02831	-0.02247	0.14648	0.06419
0.78108	-0.00282	0.57648	-0.03908	0.03865	-0.02621	0.11999	0.05944
0.82102	-0.00116	0.62778	-0.03534	0.05296	-0.03047	0.09576	0.05388
0.85989	0.00010	0.67790	-0.03135	0.06671	-0.03381	0.07395	0.04750
0.88821	0.00066	0.72629	-0.02722	0.09061	-0.03838	0.05468	0.04040
0.90521	0.00087	0.77238	-0.02308	0.12098	-0.04271	0.03811	0.03288
0.92671	0.00075	0.81561	-0.01907	0.14971	-0.04583	0.02433	0.02528
0.94213	0.00062	0.85539	-0.01532	0.19223	-0.04893	0.01338	0.01779
0.95687	0.00028	0.89119	-0.01188	0.23731	-0.05068	0.00548	0.01060
0.96956	0.00001	0.92248	-0.00876	0.29757	-0.05124	0.00098	0.00395
0.97878	-0.00029	0.94886	-0.00591	0.36030	-0.05009	0.00000	-0.00042
0.98453	-0.00065	0.97018	-0.00330	0.42266	-0.04822	0.00098	-0.00434
0.99052	-0.00077	0.98626	-0.00131	0.48291	-0.04564	0.00548	-0.00897
0.99846	-0.00127	0.99647	-0.00027	0.55072	-0.04195	0.01338	-0.01273
1.00000	0.00051	1.00000	0.00000	0.61223	-0.03786	0.02433	-0.01570
SD8020		SD8020		SD8020		SD8020	
<i>x/c</i>	<i>y/c</i>	<i>x/c</i>	<i>y/c</i>	<i>x/c</i>	<i>y/c</i>	<i>x/c</i>	<i>y/c</i>
1.00000	0.00000	1.00000	0.00011	0.85535	-0.01637	0.11999	-0.02197
0.99646	0.00027	0.98625	0.00131	0.88453	-0.01350	0.14648	-0.02189
0.97017	0.00330	0.94885	0.00591	0.90299	-0.01163	0.17504	-0.02147
0.92247	0.00876	0.92247	0.00239	0.92111	-0.00969	0.20549	-0.02077
0.89118	0.01188	0.98111	0.00284	0.93656	-0.00809	0.23760	-0.01984
0.85538	0.01532	0.97326	0.00346	0.95033	-0.00657	0.27120	-0.01872
0.81560	0.01908	0.96549	0.00406	0.96385	-0.00508	0.30609	-0.01746
0.77237	0.02308	0.95378	0.00509	0.97644	-0.00373	0.34204	-0.01608
0.72627	0.02722	0.93947	0.00648	0.98576	-0.00269	0.37887	-0.01462
0.67789	0.03135	0.90064	0.01003	0.99371	-0.00177	0.41638	-0.01309
0.62777	0.03535	0.88305	0.01164	0.99930	-0.00111	0.45435	-0.01154
0.57647	0.03909	0.85620	0.01421	1.00000	0.00011	0.49265	-0.01002
0.52456	0.04246	0.81837	0.01774	WASP		0.53099	-0.00856
0.47261	0.04536	0.77897	0.02135	smoothed model		0.56937	-0.00723
0.42116	0.04770	0.73462	0.02528	<i>x/c</i>	<i>y/c</i>	0.60778	-0.00604
0.37077	0.04938	0.67566	0.03030	1.00000	0.00007	0.64594	-0.00503
0.32196	0.05034	0.61081	0.03524	0.99754	0.00132	0.68359	-0.00420
0.27523	0.05051	0.55035	0.03943	0.99070	0.00392	0.72043	-0.00353
0.23106	0.04982	0.48701	0.04337	0.98037	0.00632	0.75616	-0.00299
0.18987	0.04824	0.41960	0.04683	0.96698	0.00831	0.79048	-0.00258
0.15203	0.04574	0.35578	0.04908	0.95044	0.01060	0.82309	-0.00231
						0.85370	-0.00220
						0.88202	-0.00223

0.90775	-0.00237	0.17424	-0.02130
0.93064	-0.00258	0.20582	-0.02070
0.95044	-0.00291	0.24853	-0.01931
0.96698	-0.00323	0.28925	-0.01776
0.98037	-0.00313	0.35038	-0.01538
0.99070	-0.00225	0.40203	-0.01347
0.99754	-0.00088	0.46036	-0.01114
1.00000	-0.00016	0.51593	-0.00881
		0.57793	-0.00632
<hr/>			
WASP			
<hr/>			
actual model		0.63048	-0.00502
		0.67423	-0.00409
		0.71664	-0.00333
		0.75867	-0.00260
<i>x/c</i>		0.80236	-0.00197
1.00000	0.00022	0.83345	-0.00170
0.99989	0.00203	0.86509	-0.00178
0.99585	0.00302	0.89302	-0.00204
0.99190	0.00379	0.90911	-0.00212
0.98579	0.00488	0.92227	-0.00220
0.97399	0.00695	0.94096	-0.00227
0.96060	0.00911	0.95520	-0.00219
0.94952	0.01089	0.96798	-0.00221
0.93443	0.01328	0.97706	-0.00222
0.91987	0.01570	0.98496	-0.00219
0.90601	0.01794	0.99773	-0.00203
0.89170	0.02022	1.00000	0.00022
0.85854	0.02554		
0.82573	0.03052		
0.79503	0.03488		
0.75211	0.04053		
0.70872	0.04628		
0.66522	0.05145		
0.62163	0.05638		
0.56465	0.06215		
0.50733	0.06700		
0.45447	0.07061		
0.39619	0.07338		
0.34099	0.07507		
0.28274	0.07524		
0.23843	0.07380		
0.19210	0.07018		
0.16650	0.06712		
0.13833	0.06281		
0.10969	0.05728		
0.09819	0.05462		
0.08388	0.05084		
0.07039	0.04660		
0.05665	0.04146		
0.04371	0.03570		
0.02744	0.02701		
0.01496	0.01888		
0.00498	0.01006		
0.00027	0.00234		
0.00073	-0.00390		
0.00431	-0.00827		
0.00993	-0.01125		
0.01686	-0.01374		
0.02494	-0.01574		
0.03330	-0.01723		
0.04439	-0.01867		
0.06175	-0.02015		
0.07602	-0.02094		
0.09099	-0.02147		
0.10561	-0.02174		
0.11860	-0.02182		
0.14807	-0.02164		

Appendix B

Airfoil Polar Data

All of the polar data shown in Chapter 4 is listed in this appendix and identified by airfoil name, figure number, and run number. This same data in addition to the four spanwise C_d values used to obtain the average C_d are included with the data distribution disk. Also included on the disk but not listed here is the lift data plotted in the C_l - α curves shown in Chapter 4.

A18	5.75	0.908	0.0152	7.73	1.049	0.0174	9.98	1.002	0.0452
Fig. 4.3	7.87	1.064	0.0214	9.17	1.140	0.0226	Run: 503		
	9.25	1.138	0.0260	10.47	1.200	0.0307	$Re = 102200$		
	10.21	1.171	0.0328						
Run: 278									
$Re = 40400$									
α	C_l	C_d		α	C_l	C_d	α	C_l	C_d
-1.20	0.120	0.0257		-5.39	-0.338	0.0613	-6.38	-0.468	0.0320
0.88	0.329	0.0213		-3.63	-0.058	0.0139	-5.39	-0.425	0.0252
2.77	0.543	0.0371					-4.36	-0.337	0.0203
5.00	0.839	0.0438							
6.98	1.002	0.0346							
9.01	1.101	0.0315							
11.03	1.133	0.0632							
Run: 161									
$Re = 61300$									
α	C_l	C_d		α	C_l	C_d	α	C_l	C_d
-2.11	0.028	0.0235		-1.74	0.032	0.0206	1.30	0.949	0.0202
-0.22	0.220	0.0190		-0.13	0.192	0.0165	2.30	1.040	0.0197
1.09	0.412	0.0212		1.35	0.442	0.0148	3.41	1.139	0.0194
2.39	0.594	0.0230		2.98	0.623	0.0196	5.17	1.283	0.0210
4.11	0.809	0.0251		4.51	0.763	0.0244	7.26	1.467	0.0242
5.96	0.964	0.0229		5.78	0.867	0.0214	9.52	1.647	0.0292
7.55	1.049	0.0268		7.45	0.993	0.0301	11.67	1.806	0.0363
9.08	1.127	0.0353		9.03	1.108	0.0326			
10.34	1.166	0.0439		10.51	1.188	0.0386			
Run: 163									
$Re = 101700$									
α	C_l	C_d		α	C_l	C_d	α	C_l	C_d
-1.57	0.085	0.0188		-3.48	-0.132	0.0274	-6.39	-0.439	0.0338
-0.41	0.270	0.0146		-1.75	0.020	0.0178	-5.31	-0.384	0.0287
1.05	0.472	0.0156		-0.28	0.238	0.0130	-4.28	-0.324	0.0224
2.77	0.655	0.0172		1.42	0.467	0.0131	-3.29	-0.237	0.0167
4.32	0.787	0.0166		3.45	0.655	0.0157	-2.32	-0.159	0.0168
5.88	0.917	0.0181		4.29	0.731	0.0171	-1.21	-0.015	0.0191
7.54	1.014	0.0264		5.97	0.876	0.0211	-0.19	0.105	0.0222
8.94	1.090	0.0332		7.31	0.987	0.0247	0.88	0.256	0.0264
10.11	1.126	0.0404		9.21	1.131	0.0301	1.84	0.364	0.0288
Run: 165				10.37	1.179	0.0367	2.96	0.429	0.0332
$Re = 203800$							3.90	0.521	0.0357
α	C_l	C_d					4.93	0.669	0.0354
-1.60	0.201	0.0131		-5.41	-0.370	0.0690	5.99	0.786	0.0351
0.12	0.389	0.0098		-3.12	-0.091	0.0188	6.98	0.883	0.0302
1.48	0.528	0.0095		-1.73	0.102	0.0127	7.97	0.952	0.0293
2.88	0.674	0.0107		-0.44	0.247	0.0103	8.97	0.980	0.0318
4.32	0.807	0.0127		1.28	0.437	0.0092	9.98	1.013	0.0400
5.54	0.900	0.0152		2.80	0.591	0.0104			
7.44	1.033	0.0215		4.37	0.738	0.0129			
8.86	1.117	0.0276		5.71	0.860	0.0159			
10.15	1.169	0.0351		7.55	1.020	0.0191			
Run: 521				8.82	1.114	0.0226			
$Re = 203800$				10.37	1.186	0.0335			
α	C_l	C_d							
-5.33	-0.380	0.0668							
-3.43	-0.095	0.0180							
Run: 167									
$Re = 303300$									
α	C_l	C_d							
-2.42	0.124	0.0111		-5.10	-0.326	0.0608	1.83	0.400	0.0262
-0.49	0.330	0.0104		-3.44	-0.089	0.0172	2.82	0.492	0.0284
0.89	0.476	0.0084		-2.19	0.069	0.0120	3.98	0.608	0.0291
2.34	0.623	0.0088		-0.34	0.264	0.0095	5.00	0.709	0.0242
4.22	0.789	0.0107		1.23	0.430	0.0080	5.94	0.802	0.0213
				2.90	0.597	0.0093	6.99	0.900	0.0200
				4.32	0.734	0.0112	7.99	0.942	0.0264
				6.20	0.917	0.0145	8.92	0.967	0.0340

6.93	0.891	0.0164
8.00	0.940	0.0228
9.08	0.986	0.0289
10.10	1.016	0.0374

E387 (A)

Fig. 4.19

Run: 209
 $Re = 61500$

α	C_l	C_d
-5.36	-0.255	0.0425
-3.71	-0.127	0.0248
-2.12	0.059	0.0240
-0.68	0.250	0.0237
0.92	0.439	0.0296
2.58	0.611	0.0346
4.17	0.769	0.0400
5.40	0.880	0.0421
6.98	1.026	0.0415
8.80	1.183	0.0287
10.13	1.201	0.0437

Run: 211
 $Re = 101800$

α	C_l	C_d
-5.37	-0.294	0.0471
-3.61	-0.067	0.0229
-2.04	0.146	0.0167
-0.49	0.311	0.0170
0.81	0.436	0.0195
2.45	0.590	0.0221
3.85	0.721	0.0229
5.60	0.890	0.0229
6.91	1.014	0.0226
8.68	1.150	0.0251
10.10	1.169	0.0422

Run: 555
 $Re = 152700$

α	C_l	C_d
-5.30	-0.296	0.0491
-3.46	-0.030	0.0191
-2.11	0.103	0.0141
-0.50	0.258	0.0120
0.83	0.398	0.0132
2.53	0.577	0.0157
4.06	0.732	0.0179
5.64	0.887	0.0182
7.05	1.018	0.0184
8.63	1.126	0.0245
10.02	1.159	0.0385

Run: 213
 $Re = 203800$

α	C_l	C_d
-4.65	-0.145	0.0237
-3.35	-0.010	0.0158
-1.97	0.121	0.0119
-0.37	0.281	0.0104
1.27	0.454	0.0116
2.67	0.599	0.0130
4.23	0.761	0.0142
5.59	0.893	0.0149
7.23	1.042	0.0163
8.77	1.127	0.0259

10.16	1.164	0.0378
Run:	215	
	$Re = 305200$	

α	C_l	C_d
-5.45	-0.235	0.0406
-3.92	-0.077	0.0163
-2.24	0.085	0.0116
-0.24	0.289	0.0085
1.04	0.429	0.0092
2.53	0.587	0.0100
4.07	0.748	0.0113
5.93	0.931	0.0125
6.93	1.013	0.0140
8.44	1.103	0.0212
9.91	1.156	0.0322

FX 63-137 (B)
Fig. 4.23

Run: 159
 $Re = 102100$

α	C_l	C_d
----------	-------	-------

-5.05	-0.019	0.0481
-3.74	0.174	0.0382
-2.87	0.289	0.0364
-1.91	0.398	0.0364
-0.58	0.494	0.0441
0.36	0.563	0.0510
1.28	0.619	0.0538
2.26	0.677	0.0590
3.46	0.772	0.0657
4.39	1.007	0.0498
5.62	1.211	0.0378
6.50	1.304	0.0351
7.49	1.397	0.0336
8.31	1.459	0.0336
9.68	1.558	0.0337
10.53	1.608	0.0365
11.40	1.646	0.0403
12.96	1.677	0.0513

Run: 154
 $Re = 204000$

α	C_l	C_d
----------	-------	-------

-5.79	0.144	0.0265
-4.74	0.264	0.0203
-3.65	0.379	0.0175
-2.54	0.509	0.0155
-1.62	0.604	0.0159
-0.43	0.725	0.0173
0.85	0.854	0.0183
1.40	0.907	0.0185
2.61	1.024	0.0192
3.97	1.155	0.0194
4.65	1.213	0.0194
5.86	1.318	0.0194
6.74	1.401	0.0201
8.25	1.518	0.0217
9.10	1.574	0.0237
10.47	1.641	0.0284
10.66	1.647	0.0297
11.93	1.672	0.0366
12.82	1.671	0.0456

Run: 506

 $Re = 254900$

α	C_l	C_d
----------	-------	-------

-6.29	0.084	0.0312
-4.91	0.241	0.0184
-3.88	0.355	0.0158
-2.75	0.483	0.0135
-1.82	0.587	0.0136
-0.75	0.694	0.0144
0.23	0.790	0.0151
1.23	0.886	0.0158
2.32	0.995	0.0164
3.34	1.094	0.0167
4.32	1.183	0.0171
5.33	1.271	0.0173
6.46	1.363	0.0176
7.47	1.446	0.0186
8.30	1.503	0.0199
9.46	1.574	0.0233
10.47	1.625	0.0267

GEMINI
Fig. 4.31

Run: 511
 $Re = 306300$

α	C_l	C_d
----------	-------	-------

-5.82	0.144	0.0207
-4.87	0.249	0.0167
-3.85	0.363	0.0146
-2.80	0.481	0.0127
-1.75	0.599	0.0123
-0.73	0.704	0.0129
0.32	0.807	0.0136
1.33	0.907	0.0143
2.33	1.008	0.0147
3.34	1.104	0.0151
4.42	1.212	0.0156
5.43	1.300	0.0163
6.39	1.371	0.0163
7.46	1.454	0.0175
8.49	1.522	0.0195
9.53	1.583	0.0225
10.51	1.628	0.0262
11.49	1.657	0.0321

FX 74-CL5-140

MOD
Fig. 4.27

Run: 185
 $Re = 202800$

α	C_l	C_d
----------	-------	-------

-1.81	0.607	0.0401
-0.49	0.852	0.0279
1.18	1.036	0.0246
2.68	1.181	0.0235
4.23	1.320	0.0264
5.57	1.433	0.0288
7.38	1.576	0.0328
9.00	1.692	0.0369
10.43	1.784	0.0410

GM15

Fig. 4.36

Run: 217

 $Re = 102300$

α	C_l	C_d
----------	-------	-------

-7.00	-0.521	0.0270
-3.28	-0.074	0.0156
-2.71	-0.028	0.0170
-1.08	0.101	0.0171
0.55	0.360	0.0203
2.07	0.504	0.0186
3.63	0.624	0.0196
5.12	0.755	0.0240
6.43	0.859	0.0261
8.27	1.007	0.0289
9.60	1.111	0.0299
11.02	1.197	0.0324
12.63	1.179	0.0409

Run: 219

 $Re = 204100$

α	C_l	C_d
----------	-------	-------

-7.04	-0.391	0.0189
-5.60	-0.269	0.0148
-3.85	-0.138	0.0119
-2.47	-0.022	0.0119
-1.14	0.103	0.0120
0.38	0.251	0.0124
2.10	0.477	0.0125
3.55	0.641	0.0137
5.14	0.773	0.0160
7.03	0.937	0.0200
8.19	1.033	0.0217
9.76	1.137	0.0229
11.10	1.136	0.0342
12.65	1.093	0.0538

Run: 221

 $Re = 306100$

α	C_l	C_d
----------	-------	-------

-5.76	-0.291	0.0146
-4.53	-0.193	0.0122
-2.47	-0.020	0.0106
-1.29	0.093	0.0103
0.76	0.310	0.0103
2.07	0.452	0.0114
3.58	0.634	0.0134
5.22	0.793	0.0136
6.85	0.938	0.0163
8.25	1.056	0.0178
9.57	1.113	0.0200
11.22	1.111	0.0351

GM15

Fig. 4.36

Run: 404

 $Re = 40900$

α	C_l	C_d
----------	-------	-------

-3.61	-0.072	0.0504
-1.52	0.160	0.0271
0.66	0.368	0.0235
2.60	0.594	0.0233
4.59	0.869	0.0320

7.96	0.925	0.0316	Run: 526	Run: 530	Run: 246	
9.56	0.998	0.0462	$Re = 61200$	$Re = 304700$	$Re = 101700$	
Run: 179			α	C_l	C_d	
$Re = 102100$	-6.20	-0.466	0.0321	-6.07	-0.502	0.0190
	-4.66	-0.314	0.0209	-4.49	-0.355	0.0145
α	C_l	C_d				
-4.38	-0.255	0.0264	Run: 114			
-2.61	-0.106	0.0186	$Re = 102000$			
-1.24	0.021	0.0147	α	C_l	C_d	
0.31	0.173	0.0109	-2.94	-0.153	0.0124	
1.81	0.417	0.0139	-1.40	0.081	0.0135	
3.29	0.581	0.0148	0.16	0.224	0.0171	
5.06	0.734	0.0155	1.48	0.341	0.0196	
6.41	0.841	0.0197	3.33	0.516	0.0181	
8.23	0.945	0.0315	4.68	0.650	0.0183	
9.43	0.998	0.0432	6.16	0.789	0.0207	
Run: 181			7.62	0.910	0.0250	
$Re = 203100$			9.26	1.025	0.0309	
	-4.40	-0.251	10.66	1.093	0.0401	
	-2.82	-0.118	12.34	1.099	0.0474	
α	C_l	C_d	Run: 527			
-4.40	-0.251	0.0175	$Re = 101900$			
-2.82	-0.118	0.0145	α	C_l	C_d	
-1.45	0.038	0.0113	-6.11	-0.488	0.0260	
-0.03	0.226	0.0092	-4.67	-0.352	0.0176	
1.71	0.414	0.0092	Run: 116			
3.29	0.574	0.0102	$Re = 203500$			
4.70	0.703	0.0122	α	C_l	C_d	
6.12	0.819	0.0164	1.97	0.729	0.0203	
7.57	0.917	0.0232	3.32	0.858	0.0214	
9.22	1.006	0.0375	5.07	1.009	0.0235	
Run: 183			-3.00	-0.168	0.0123	
$Re = 304300$			6.45	1.132	0.0243	
	-4.68	-0.280	8.10	1.265	0.0255	
	-3.14	-0.140	-0.04	0.151	0.0109	
	-1.43	0.070	9.70	1.383	0.0285	
α	C_l	C_d	Run: 191			
-4.68	-0.280	0.0145	$Re = 203100$			
-3.14	-0.140	0.0142	α	C_l	C_d	
-1.43	0.070	0.0087	-2.89	0.285	0.0193	
0.00	0.240	0.0081	-1.38	0.437	0.0150	
1.61	0.407	0.0072	0.21	0.602	0.0145	
3.48	0.590	0.0092	1.66	0.744	0.0135	
4.77	0.702	0.0113	3.32	0.903	0.0147	
6.20	0.820	0.0149	Run: 528			
7.99	0.950	0.0233	$Re = 203700$			
9.38	1.023	0.0352	α	C_l	C_d	
Run: 523			-4.63	-0.335	0.0148	
$Re = 303500$			Run: 529			
	-6.08	-0.447	$Re = 202800$			
	-6.17	-0.508	α	C_l	C_d	
MH45			-6.17	-0.508	0.0209	
Fig. 4.60			Run: 118			
Run: 112			$Re = 304800$			
$Re = 61300$			α	C_l	C_d	
	-2.92	-0.178	0.0114	-6.06	-0.577	0.0226
	-1.45	-0.031	0.0096	-4.30	-0.445	0.0174
	0.14	0.164	0.0089	-2.72	-0.333	0.0177
	1.48	0.317	0.0089	-1.17	-0.043	0.0196
	3.02	0.490	0.0099	0.32	0.031	0.0116
	4.49	0.648	0.0113	1.84	0.145	0.0179
	6.27	0.832	0.0138	3.17	0.388	0.0171
	7.65	0.959	0.0168	4.69	0.519	0.0195
	9.34	1.097	0.0219	6.50	0.650	0.0289
	10.72	1.163	0.0274	7.90	0.732	0.0434

Run: 205 <i>Re</i> = 203500	α	C_l	C_d	Run: 550 <i>Re</i> = 152500	α	C_l	C_d	3.19	0.187	0.0441	Run: 420 <i>Re</i> = 509100			
-5.62 -0.548	0.0198	-6.07 -0.430	0.0309	-5.10 -0.348	0.0217	-4.64	0.338	0.0533	6.38	0.751	0.0329	-2.84 -0.028	C_d	0.0100
-4.07 -0.432	0.0147	-4.13 -0.264	0.0169	-4.13 -0.264	0.0169	7.89	0.964	0.0221	9.44	1.062	0.0261	Run: 421 <i>Re</i> = 506800		
-2.70 -0.273	0.0105	-3.25 -0.186	0.0138	-3.25 -0.186	0.0138	10.93	1.074	0.0396	Run: 417 <i>Re</i> = 102500					
-0.96 -0.092	0.0107	-2.02 -0.082	0.0127	-2.02 -0.082	0.0127	12.42	1.115	0.0510	12.42	1.115	C_d	-1.20 0.154	0.0098	
0.36 0.024	0.0106	-1.28 -0.015	0.0122	-1.28 -0.015	0.0122	Run: 419 <i>Re</i> = 204500	α	C_l	C_d	Run: 422 <i>Re</i> = 510700				
2.01 0.211	0.0124	0.04 0.174	0.0110	0.04 0.174	0.0110	0.52 0.350	0.0096	0.52 0.350	0.0096	0.52 0.350	0.0096	Run: 423 <i>Re</i> = 511500		
3.84 0.465	0.0130	5.12 0.564	0.0172	5.12 0.564	0.0172	1.67 0.474	C_d	1.67 0.474	0.0095	1.67 0.474	0.0095	Run: 424 <i>Re</i> = 511400		
6.46 0.626	0.0217	6.46 0.626	0.0109	6.46 0.626	0.0109	3.56 0.683	0.0097	3.56 0.683	0.0097	3.56 0.683	0.0097	Run: 426 <i>Re</i> = 509500		
8.28 0.715	0.0319	9.54 0.786	0.0489	9.54 0.786	0.0489	6.20 0.911	C_d	6.20 0.911	0.0115	6.20 0.911	0.0115	Run: 428 <i>Re</i> = 509600		
9.54 0.786	0.0489	4.06 0.626	0.0126	4.06 0.626	0.0126	4.19 0.638	0.0115	4.19 0.638	0.0115	4.19 0.638	0.0115	Run: 429 <i>Re</i> = 508300		
Run: 207 <i>Re</i> = 305200	5.10 0.723	5.10 0.723	0.0143	5.10 0.723	0.0143	5.94 0.793	0.0169	5.94 0.793	0.0169	5.94 0.793	0.0169	Run: 430 <i>Re</i> = 509900		
α	C_l	C_d		α	C_l	C_d	7.14 0.888	0.0213	7.14 0.888	0.0213	7.14 0.888	0.0213	Run: 431 <i>Re</i> = 511200	
-5.71 -0.558	0.0189	8.19 0.954	0.0243	8.19 0.954	0.0243	8.96 0.997	0.0304	8.96 0.997	0.0304	8.96 0.997	0.0304	Run: 432 <i>Re</i> = 510400		
-3.85 -0.358	0.0120	9.98 1.040	0.0415	9.98 1.040	0.0415	10.80 1.101	0.0308	10.80 1.101	0.0308	10.80 1.101	0.0308	Run: 433 <i>Re</i> = 506700		
-2.65 -0.243	0.0096	Run: 81 <i>Re</i> = 203500	-0.44 -0.047	0.0090	-0.44 -0.047	0.0090	-0.44 -0.047	0.0090	-0.44 -0.047	0.0090	-0.44 -0.047	0.0090	Run: 434 <i>Re</i> = 509100	
0.59 0.044	0.0089	1.53 0.340	0.0240	1.53 0.340	0.0240	1.53 0.340	0.0240	1.53 0.340	0.0240	1.53 0.340	0.0240	Run: 435 <i>Re</i> = 306500		
2.13 0.204	0.0092	3.02 0.493	0.0228	3.02 0.493	0.0228	3.02 0.493	0.0228	3.02 0.493	0.0228	3.02 0.493	0.0228	Run: 436 <i>Re</i> = 308100		
3.39 0.362	0.0101	4.57 0.652	0.0195	4.57 0.652	0.0195	4.57 0.652	0.0195	4.57 0.652	0.0195	4.57 0.652	0.0195	Run: 437 <i>Re</i> = 310700		
5.10 0.559	0.0165	6.11 0.836	0.0165	6.11 0.836	0.0165	6.11 0.836	0.0165	6.11 0.836	0.0165	6.11 0.836	0.0165	Run: 438 <i>Re</i> = 313300		
6.45 0.629	0.0199	7.75 0.966	0.0166	7.75 0.966	0.0166	7.75 0.966	0.0166	7.75 0.966	0.0166	7.75 0.966	0.0166	Run: 439 <i>Re</i> = 315900		
8.03 0.705	0.0282	9.08 1.032	0.0226	9.08 1.032	0.0226	9.08 1.032	0.0226	9.08 1.032	0.0226	9.08 1.032	0.0226	Run: 440 <i>Re</i> = 318500		
9.60 0.803	0.0526	10.64 1.075	0.0336	10.64 1.075	0.0336	10.64 1.075	0.0336	10.64 1.075	0.0336	10.64 1.075	0.0336	Run: 441 <i>Re</i> = 321100		
RG15 (B)		12.10 1.107	0.0467	12.10 1.107	0.0467	12.10 1.107	0.0467	12.10 1.107	0.0467	12.10 1.107	0.0467	Run: 442 <i>Re</i> = 323700		
Fig. 4.80		Run: 437 <i>Re</i> = 306500		Run: 79 <i>Re</i> = 304200		Run: 438 <i>Re</i> = 310700		Run: 439 <i>Re</i> = 313300		Run: 440 <i>Re</i> = 315900		Run: 441 <i>Re</i> = 318500		
Run: 85 <i>Re</i> = 614000	α	C_l	C_d	7.26 0.891	0.0193	7.26 0.891	0.0193	7.26 0.891	0.0193	7.26 0.891	0.0193	Run: 442 <i>Re</i> = 323700		
Run: 85 <i>Re</i> = 614000	8.75 0.979	0.0270	10.29 1.040	0.0421	10.29 1.040	0.0421	10.29 1.040	0.0421	10.29 1.040	0.0421	10.29 1.040	0.0421	Run: 443 <i>Re</i> = 326300	
α	C_l	C_d		Run: 79 <i>Re</i> = 304200	α	C_l	C_d	1.38 0.415	0.0145	1.38 0.415	0.0145	1.38 0.415	0.0145	Run: 444 <i>Re</i> = 328900
-6.86 -0.454	0.0526	-6.49 -0.458	0.0336	-6.49 -0.458	0.0336	2.75 0.563	0.0148	2.75 0.563	0.0148	2.75 0.563	0.0148	Run: 445 <i>Re</i> = 331500		
-4.98 -0.310	0.0284	-5.13 -0.345	0.0155	-5.13 -0.345	0.0155	4.63 0.753	0.0140	4.63 0.753	0.0140	4.63 0.753	0.0140	Run: 446 <i>Re</i> = 334100		
-3.58 -0.197	0.0199	-3.66 -0.204	0.0127	-3.66 -0.204	0.0127	5.95 0.864	0.0136	5.95 0.864	0.0136	5.95 0.864	0.0136	Run: 447 <i>Re</i> = 336700		
-1.93 -0.074	0.0155	-2.16 -0.015	0.0093	-2.16 -0.015	0.0093	7.55 0.956	0.0156	7.55 0.956	0.0156	7.55 0.956	0.0156	Run: 448 <i>Re</i> = 339300		
-0.34 0.089	0.0147	-0.56 0.162	0.0085	-0.56 0.162	0.0085	8.89 1.027	0.0205	8.89 1.027	0.0205	8.89 1.027	0.0205	Run: 449 <i>Re</i> = 341900		
1.12 0.255	0.0175	0.93 0.321	0.0077	0.93 0.321	0.0077	10.39 1.089	0.0293	10.39 1.089	0.0293	10.39 1.089	0.0293	Run: 450 <i>Re</i> = 344500		
2.75 0.519	0.0187	2.56 0.500	0.0082	2.56 0.500	0.0082	12.12 1.141	0.0414	12.12 1.141	0.0414	12.12 1.141	0.0414	Run: 451 <i>Re</i> = 347100		
4.23 0.674	0.0200	4.05 0.652	0.0101	4.05 0.652	0.0101	Run: 435 <i>Re</i> = 408100	α	C_l	C_d	12.85 1.161	0.0435	12.85 1.161	0.0435	Run: 452 <i>Re</i> = 350700
5.65 0.786	0.0212	5.59 0.790	0.0131	5.59 0.790	0.0131	8.07 -0.555	0.0135	8.07 -0.555	0.0135	8.07 -0.555	0.0135	Run: 453 <i>Re</i> = 353300		
7.29 0.901	0.0273	7.14 0.916	0.0164	7.14 0.916	0.0164	6.53 -0.417	0.0119	6.53 -0.417	0.0119	6.53 -0.417	0.0119	Run: 454 <i>Re</i> = 355900		
8.84 0.991	0.0357	8.75 1.023	0.0240	8.75 1.023	0.0240	-5.16 -0.281	0.0110	-5.16 -0.281	0.0110	-5.16 -0.281	0.0110	Run: 455 <i>Re</i> = 358500		
10.23 1.046	0.0493	10.34 1.093	0.0380	10.34 1.093	0.0380	-3.49 -0.107	0.0110	-3.49 -0.107	0.0110	-3.49 -0.107	0.0110	Run: 456 <i>Re</i> = 361100		
S822		1.15 0.407	0.0113	1.15 0.407	0.0113	-1.97 0.058	0.0110	-1.97 0.058	0.0110	-1.97 0.058	0.0110	Run: 457 <i>Re</i> = 363700		
Fig. 4.84		2.58 0.564	0.0113	2.58 0.564	0.0113	-0.52 0.221	0.0112	-0.52 0.221	0.0112	-0.52 0.221	0.0112	Run: 458 <i>Re</i> = 366300		
Run: 416 <i>Re</i> = 102400	α	C_l	C_d	4.22 0.736	0.0115	4.22 0.736	0.0115	4.22 0.736	0.0115	4.22 0.736	0.0115	Run: 459 <i>Re</i> = 368900		
Run: 416 <i>Re</i> = 102400	-7.19 -0.710	0.0249	5.87 0.884	0.0119	7.88 0.975	0.0172	7.88 0.975	0.0172	7.88 0.975	0.0172	Run: 460 <i>Re</i> = 371500			
4.10 0.654	0.0158	-4.28 -0.385	0.0242	-4.28 -0.385	0.0242	9.42 1.044	0.0231	9.42 1.044	0.0231	9.42 1.044	0.0231	Run: 461 <i>Re</i> = 374100		
5.65 0.793	0.0183	-2.75 -0.267	0.0284	-2.75 -0.267	0.0284	10.80 1.101	0.0308	10.80 1.101	0.0308	10.80 1.101	0.0308	Run: 462 <i>Re</i> = 376700		
7.21 0.907	0.0241	-1.39 -0.212	0.0315	-1.39 -0.212	0.0315	12.34 1.145	0.0413	12.34 1.145	0.0413	12.34 1.145	0.0413	Run: 463 <i>Re</i> = 379300		
8.75 0.994	0.0319	0.09 -0.112	0.0336	0.09 -0.112	0.0336	-7.99 -0.578	0.0126	-7.99 -0.578	0.0126	-7.99 -0.578	0.0126	Run: 464 <i>Re</i> = 381900		
10.26 1.055	0.0505	1.60 0.035	0.0357	1.60 0.035	0.0357	-8.77 -0.642	0.0140	-8.77 -0.642	0.0140	-8.77 -0.642	0.0140	Run: 465 <i>Re</i> = 384500		

S823
Fig. 4.88

Run: 454	-6.34	-0.413	0.0154
$Re = 103000$	-4.79	-0.271	0.0148
	-3.27	-0.123	0.0148
	-1.76	0.043	0.0145
	-0.22	0.222	0.0141
	1.38	0.407	0.0134
	2.82	0.574	0.0133
	4.43	0.748	0.0137
	5.95	0.898	0.0147
	1.54	0.289	0.0435
	2.97	0.429	0.0448
	4.35	0.603	0.0406
	5.98	0.770	0.0384
	7.56	0.917	0.0332
	9.21	1.064	0.0319
	10.56	1.159	0.0306
	12.21	1.166	0.0436
Run: 457	α	C_l	C_d
$Re = 204900$	-3.19	-0.096	0.0214
	-1.46	0.079	0.0199
	0.40	0.283	0.0191
	1.53	0.409	0.0196
	3.05	0.579	0.0205
	4.67	0.750	0.0205
	6.12	0.891	0.0214
	7.66	1.029	0.0215
	9.31	1.151	0.0239
	10.67	1.180	0.0341
	12.17	1.151	0.0658
Run: 458	α	C_l	C_d
$Re = 205800$	-4.74	-0.229	0.0230
Run: 461	α	C_l	C_d
$Re = 307400$	-4.90	-0.269	0.0172
	-3.28	-0.114	0.0168
	-1.85	0.040	0.0163
	-0.21	0.223	0.0159
	1.30	0.397	0.0154
	2.84	0.571	0.0155
	4.44	0.742	0.0162
	5.97	0.895	0.0169
	7.50	1.029	0.0183
	9.21	1.140	0.0219
	10.79	1.161	0.0369
Run: 462	α	C_l	C_d
$Re = 306400$	-5.85	-0.357	0.0177
Run: 465	α	C_l	C_d
$Re = 408800$	-7.86	-0.563	0.0182
Run: 464	α	C_l	C_d
$Re = 410100$	-7.83	-0.562	0.0181

S1210
Fig. 4.92

Run: 129	10.43	1.737	0.0304
$Re = 102600$	11.61	1.759	0.0370
Run: 490	Run: 490		
$Re = 254400$	α	C_l	C_d
	-4.14	0.428	0.0178
	-3.13	0.572	0.0136
	-2.17	0.685	0.0134
	-1.11	0.787	0.0146
	-0.06	0.890	0.0157
	1.00	0.995	0.0165
	1.08	0.972	0.0307
	2.02	1.061	0.0305
	3.07	1.161	0.0319
	4.22	1.248	0.0322
	5.19	1.322	0.0348
	6.32	1.414	0.0377
	7.12	1.473	0.0391
	8.24	1.563	0.0387
	9.35	1.639	0.0399
	10.16	1.687	0.0388
	11.18	1.735	0.0391
Run: 491	Run: 491		
$Re = 253400$	α	C_l	C_d
	12.26	1.774	0.0393
Run: 495	Run: 495		
$Re = 305500$	α	C_l	C_d
	-5.10	0.297	0.0211
	-4.11	0.449	0.0156
	-3.06	0.587	0.0124
	-2.04	0.697	0.0125
	-1.04	0.793	0.0136
	0.00	0.898	0.0147
	0.99	0.995	0.0152
	2.07	1.102	0.0162
	3.07	1.198	0.0168
	4.12	1.263	0.0248
	5.30	1.356	0.0269
	6.32	1.435	0.0286
	7.32	1.510	0.0300
	8.14	1.567	0.0308
	9.45	1.656	0.0321
	10.28	1.703	0.0334
	11.23	1.735	0.0366
	12.27	1.752	0.0436
Run: 131	Run: 131		
$Re = 204100$	α	C_l	C_d
	-4.15	0.451	0.0197
	-3.16	0.590	0.0149
	-2.19	0.694	0.0148
	-1.16	0.792	0.0160
	-0.03	0.903	0.0173
	0.90	0.991	0.0182
	1.93	1.092	0.0190
	2.91	1.182	0.0200
	3.97	1.276	0.0210
	5.07	1.362	0.0214
	6.13	1.451	0.0229
	7.12	1.530	0.0242
	8.13	1.602	0.0255
	9.33	1.685	0.0274

S1223
Fig. 4.96

Run: 134	-3.30	0.384	0.0687
$Re = 102100$	-2.53	0.752	0.0355
	-1.01	0.937	0.0247
	-0.03	1.037	0.0269
	0.89	1.120	0.0311
	1.73	1.193	0.0324
	2.56	1.267	0.0341
	3.69	1.343	0.0375
	4.82	1.423	0.0426
	5.70	1.485	0.0475

6.68	1.536	0.0548	2.02	1.259	0.0209	Run: 532	6.69	0.864	0.0171		
Run: 590			3.57	1.398	0.0226	$Re = 203000$	8.03	0.956	0.0252		
$Re = 152600$			5.07	1.510	0.0242		9.57	1.039	0.0383		
α	C_l	C_d	6.57	1.624	0.0268	α	C_l	C_d			
-2.31	0.779	0.0275	8.17	1.743	0.0300	-4.21	-0.242	0.0156	Run: 90		
-0.83	0.948	0.0219	9.65	1.844	0.0330	8.68	0.989	0.0460	$Re = 203200$		
0.73	1.115	0.0246	11.17	1.939	0.0363	Run: 138	α	C_l	C_d		
2.89	1.313	0.0291	12.79	2.029	0.0401	$Re = 305100$	-5.93	-0.450	0.0229		
Run: 598			14.68	2.080	0.0445		-4.42	-0.310	0.0159		
$Re = 152900$			16.32	2.114	0.0544	α	C_l	C_d			
α	C_l	C_d	S1223				-2.88	-0.157	0.0112		
3.91	1.399	0.0311	Fig. 4.98				-1.40	0.007	0.0091		
5.22	1.502	0.0360					0.33	0.196	0.0077		
6.83	1.617	0.0413					1.75	0.351	0.0096		
8.60	1.729	0.0493	Run: 370				3.34	0.525	0.0111		
9.89	1.803	0.0556	$Re = 203800$				4.74	0.671	0.0124		
11.41	1.883	0.0623	α	C_l	C_d		6.41	0.836	0.0146		
Run: 136			-0.45	0.962	0.0329	α	C_l	C_d			
$Re = 203800$			1.75	1.161	0.0372	-5.55	-0.344	0.0179	7.91	0.949	0.0223
α	C_l	C_d	3.75	1.319	0.0406	-3.93	-0.197	0.0131	9.44	1.036	0.0343
-2.84	0.587	0.0437	5.81	1.475	0.0465	-2.57	-0.039	0.0093	10.94	1.071	0.0588
-1.47	0.903	0.0207	7.66	1.595	0.0520	0.83	0.178	0.0074	Run: 88		
-0.02	1.070	0.0211	9.87	1.727	0.0608	0.59	0.325	0.0069	$Re = 304700$		
0.64	1.129	0.0221	S1223				3.74	0.641	0.0093		
1.80	1.235	0.0237	Fig. 4.101				5.73	0.794	0.0168		
2.96	1.341	0.0252					7.22	0.906	0.0248		
3.74	1.396	0.0257	Run: 517				8.60	0.997	0.0494		
4.72	1.473	0.0280	$Re = 203500$				Run: 94	S7012			
6.22	1.582	0.0318	α	C_l	C_d		$Re = 61400$	α	C_l	C_d	
6.86	1.627	0.0333	-0.42	1.243	0.0270			-5.83	-0.432	0.0394	
7.88	1.696	0.0364	3.59	1.589	0.0332			-4.33	-0.308	0.0252	
Run: 588			7.78	1.842	0.0426			-2.80	-0.167	0.0171	
$Re = 203600$			S6062					-1.31	-0.036	0.0127	
α	C_l	C_d	Fig. 4.105					0.10	0.109	0.0113	
8.86	1.765	0.0391						1.72	0.393	0.0180	
10.12	1.840	0.0422	Run: 142					3.48	0.579	0.0245	
11.05	1.892	0.0450	$Re = 101800$					4.81	0.696	0.0189	
11.81	1.935	0.0465	α	C_l	C_d			6.32	0.827	0.0243	
13.11	2.003	0.0491	-3.98	-0.216	0.0186			7.84	0.949	0.0274	
13.90	2.042	0.0509	-2.17	-0.048	0.0124			9.54	1.048	0.0387	
15.13	2.091	0.0542	-0.61	0.090	0.0107			10.94	1.081	0.0588	
Run: 594			Run: 92					Run: 152	S7055		
$Re = 254600$			$Re = 101700$					$Re = 61200$	Fig. 4.113		
α	C_l	C_d	α	C_l	C_d			α	C_l	C_d	
-3.05	0.443	0.0573	0.75	0.244	0.0135	-5.88	-0.468	0.0348			
-1.08	0.936	0.0185	2.38	0.510	0.0146	-4.40	-0.331	0.0201			
0.45	1.105	0.0194	3.52	0.621	0.0145	-2.91	-0.190	0.0144			
1.92	1.240	0.0221	5.31	0.773	0.0166	-1.31	-0.049	0.0104			
3.45	1.376	0.0237	7.00	0.876	0.0293	0.23	0.188	0.0122			
5.09	1.497	0.0259	8.28	0.951	0.0424	1.76	0.373	0.0142			
6.60	1.610	0.0290	Run: 140					3.28	0.524	0.0160	
8.14	1.719	0.0320	$Re = 202900$					4.75	0.670	0.0173	
9.53	1.811	0.0353	α	C_l	C_d			6.38	0.832	0.0186	
11.34	1.920	0.0398	-6.86	-0.480	0.0567			7.94	0.959	0.0249	
12.87	2.003	0.0425	-2.91	-0.108	0.0123			9.48	1.039	0.0414	
14.52	2.076	0.0473	-2.59	-0.072	0.0113			10.97	1.079	0.0659	
Run: 597			-0.77	0.140	0.0093			Run: 565	S7055		
$Re = 305300$			0.56	0.311	0.0084			$Re = 152800$	Fig. 4.113		
α	C_l	C_d	2.44	0.519	0.0091			α	C_l	C_d	
-2.69	0.638	0.0425	3.73	0.651	0.0105			-5.95	-0.447	0.0276	
-1.03	0.953	0.0184	5.48	0.780	0.0169			-4.15	-0.280	0.0167	
0.46	1.116	0.0182	6.72	0.866	0.0237			-2.55	-0.128	0.0113	

5.39	0.909	0.0204	α	C_l	C_d	2.18	0.383	0.0135	6.07	0.787	0.0209
6.66	1.023	0.0224	-6.14	-0.440	0.0293	3.26	0.495	0.0141	7.71	0.916	0.0289
7.96	1.130	0.0259	-5.15	-0.363	0.0228	4.29	0.598	0.0139	9.18	1.019	0.0339
9.89	1.227	0.0346	-4.24	-0.296	0.0208	5.21	0.691	0.0145			
Run: 537			-3.21	-0.213	0.0150	6.25	0.787	0.0155	Run: 171		
$Re = 153200$			-2.15	-0.119	0.0130	7.43	0.887	0.0192	$Re = 102200$		
α	C_l	C_d	-1.17	-0.035	0.0123	8.21	0.936	0.0235	α	C_l	C_d
-4.63	-0.079	0.0216	-0.10	0.117	0.0191	9.28	0.981	0.0332	-4.76	-0.343	0.0180
-2.65	0.103	0.0165	0.97	0.280	0.0221	10.70	1.013	0.0500	-3.20	-0.192	0.0144
-1.04	0.261	0.0143	1.87	0.406	0.0242				-1.54	-0.053	0.0101
0.44	0.400	0.0146	3.10	0.543	0.0299	Run: 73			0.01	0.106	0.0091
1.91	0.549	0.0156	4.05	0.637	0.0290	$Re = 203700$			1.33	0.326	0.0119
3.47	0.710	0.0165	4.95	0.710	0.0274	α	C_l	C_d	3.11	0.494	0.0145
5.01	0.869	0.0175	6.01	0.805	0.0248	-6.08	-0.436	0.0198	4.41	0.619	0.0158
6.51	1.011	0.0190	7.05	0.901	0.0247	-5.26	-0.371	0.0176	6.17	0.788	0.0197
8.06	1.128	0.0218	8.02	0.967	0.0252	-4.36	-0.253	0.0149	7.55	0.907	0.0254
9.73	1.206	0.0322	9.09	1.023	0.0328	-3.20	-0.126	0.0116	9.23	1.017	0.0387
			10.06	1.068	0.0434	-2.26	-0.054	0.0107	10.55	1.066	0.0603
Run: 148						-1.17	0.035	0.0096	Run: 173		
$Re = 203900$			Run: 75			-0.22	0.120	0.0087	$Re = 203400$		
α	C_l	C_d	$Re = 102300$			0.96	0.267	0.0111	α	C_l	C_d
-2.08	0.163	0.0133	α	C_l	C_d	2.02	0.378	0.0112	-4.65	-0.326	0.0138
-0.82	0.279	0.0114	-6.07	-0.451	0.0256	2.84	0.461	0.0114	-2.85	-0.144	0.0108
0.48	0.417	0.0122	-5.29	-0.396	0.0211	3.89	0.573	0.0113	-1.67	-0.032	0.0093
2.42	0.621	0.0128	-4.17	-0.316	0.0173	5.09	0.700	0.0124	0.02	0.162	0.0076
3.74	0.758	0.0136	-3.24	-0.235	0.0158	6.00	0.785	0.0133	1.53	0.321	0.0090
5.21	0.907	0.0144	-2.32	-0.137	0.0153	7.04	0.876	0.0169	3.05	0.479	0.0107
7.10	1.076	0.0176	-1.20	0.043	0.0162	8.01	0.942	0.0220	4.66	0.645	0.0130
8.30	1.160	0.0214	-0.09	0.203	0.0171	9.02	0.988	0.0300	5.97	0.773	0.0156
9.59	1.195	0.0304	0.85	0.297	0.0189	10.08	1.018	0.0402	7.49	0.909	0.0204
Run: 535			1.94	0.402	0.0204	Run: 71			9.04	1.022	0.0288
$Re = 203700$			2.93	0.491	0.0213	$Re = 305000$			10.50	1.101	0.0411
α	C_l	C_d	3.94	0.582	0.0197	α	C_l	C_d	Run: 175		
-4.49	-0.079	0.0190	5.05	0.690	0.0181	-6.10	-0.433	0.0184	$Re = 304700$		
			6.00	0.775	0.0189	-4.61	-0.277	0.0135	α	C_l	C_d
Run: 548			7.05	0.869	0.0199	-3.96	-0.218	0.0123	-4.27	-0.290	0.0114
$Re = 203000$			8.00	0.939	0.0235	-2.88	-0.124	0.0103	-2.96	-0.154	0.0100
α	C_l	C_d	9.02	0.987	0.0328	-1.89	-0.038	0.0093	-1.67	-0.021	0.0080
-2.92	0.072	0.0151	10.04	1.015	0.0404	-0.89	0.049	0.0089	0.24	0.173	0.0073
Run: 146			Run: 442			0.07	0.134	0.0082	1.72	0.335	0.0080
$Re = 304700$			$Re = 152800$			1.23	0.292	0.0087	3.24	0.503	0.0098
α	C_l	C_d	α	C_l	C_d	2.25	0.400	0.0088	4.70	0.657	0.0117
-1.06	0.242	0.0097	-6.22	-0.460	0.0238	3.18	0.500	0.0092	6.06	0.788	0.0138
0.37	0.397	0.0094	-4.31	-0.313	0.0184	4.18	0.605	0.0097	7.77	0.941	0.0193
2.11	0.583	0.0100	-3.05	-0.147	0.0135	5.20	0.709	0.0104	9.07	1.040	0.0250
4.00	0.784	0.0112	-1.44	0.001	0.0133	6.21	0.803	0.0131	10.59	1.122	0.0362
5.19	0.900	0.0123	-0.05	0.188	0.0137	7.31	0.892	0.0174	Run: 533		
6.43	1.011	0.0140	1.65	0.342	0.0136	8.36	0.957	0.0230	$Re = 303400$		
8.11	1.136	0.0189	3.28	0.511	0.0141	9.26	0.997	0.0293	α	C_l	C_d
10.10	1.177	0.0375	4.72	0.656	0.0143	10.27	1.020	0.0397	-6.28	-0.506	0.0167
Run: 534			6.27	0.806	0.0158	SD7003			Run: 235		
$Re = 304700$			7.76	0.927	0.0208	Fig. 4.121			$Re = 60900$		
α	C_l	C_d	9.17	0.993	0.0325				α	C_l	C_d
-4.49	-0.111	0.0166	10.72	1.025	0.0502				-4.84	-0.304	0.0250
Run: 577			Run: 540						-2.92	-0.151	0.0155
$Re = 305100$			$Re = 153000$						-1.61	-0.041	0.0128
α	C_l	C_d	α	C_l	C_d				-0.10	0.111	0.0135
-2.96	0.054	0.0131	-6.02	-0.462	0.0233				1.66	0.374	0.0137
SD6060			-5.03	-0.398	0.0191				3.02	0.517	0.0140
Fig. 4.117			-4.07	-0.303	0.0179				4.59	0.656	0.0181
Run: 77			-2.80	-0.130	0.0133						
$Re = 61300$			-1.78	-0.028	0.0132						
			-0.96	0.026	0.0138						
			0.12	0.196	0.0133						
			1.13	0.280	0.0129						

Run: 329
 $Re = 202800$

α	C_l	C_d
-5.50	-0.349	0.0170
-3.76	-0.191	0.0134
-2.30	-0.046	0.0112
-0.72	0.177	0.0094
0.79	0.349	0.0092
2.20	0.491	0.0101
3.83	0.655	0.0112
5.24	0.785	0.0145
6.83	0.921	0.0192
8.34	1.032	0.0243
9.80	1.117	0.0326

Run: 331
 $Re = 304300$

α	C_l	C_d
-6.39	-0.420	0.0187
-3.59	-0.149	0.0123
-2.19	0.034	0.0079
-0.59	0.206	0.0076
0.82	0.338	0.0076
2.47	0.512	0.0083
4.16	0.681	0.0108
5.56	0.812	0.0138
7.65	0.992	0.0187
8.59	1.063	0.0225
10.32	1.159	0.0326
11.54	1.189	0.0448

SD8020

Fig. 4.145

Run: 252

 $Re = 61400$

α	C_l	C_d
-6.45	-0.633	0.0255
-4.93	-0.509	0.0181
-3.36	-0.352	0.0178
-1.81	-0.097	0.0178
-0.29	0.031	0.0138
1.17	0.107	0.0201
2.72	0.366	0.0139
4.37	0.513	0.0175
5.88	0.635	0.0205
7.39	0.743	0.0283

Run: 254

 $Re = 101700$

α	C_l	C_d
-6.55	-0.704	0.0184
-5.03	-0.562	0.0148
-3.32	-0.407	0.0135
-1.81	-0.237	0.0125
-0.41	-0.001	0.0102
1.21	0.144	0.0127
2.69	0.303	0.0140
4.10	0.423	0.0161
5.68	0.561	0.0183
7.27	0.679	0.0256
8.89	0.783	0.0408

Run: 256
 $Re = 203500$

α	C_l	C_d
-6.41	-0.659	0.0134
-4.95	-0.529	0.0110
-3.43	-0.387	0.0099
-1.62	-0.221	0.0087
-0.33	-0.042	0.0087
1.21	0.147	0.0079
2.58	0.287	0.0101
4.30	0.444	0.0123
5.77	0.574	0.0153
7.30	0.697	0.0212
8.86	0.807	0.0298

Run: 258
 $Re = 305200$

α	C_l	C_d
-6.77	-0.699	0.0139
-4.75	-0.514	0.0097
-3.27	-0.371	0.0087
-1.73	-0.206	0.0074
-0.22	-0.033	0.0074
1.18	0.101	0.0087
2.61	0.280	0.0091
4.45	0.454	0.0114
5.69	0.565	0.0136
7.24	0.696	0.0184
8.86	0.815	0.0261

WASP
 Fig. 4.152

Run: 229
 $Re = 61200$

α	C_l	C_d
-4.30	-0.187	0.0294
-2.62	-0.047	0.0214
-1.01	0.106	0.0173
0.38	0.318	0.0217
1.99	0.554	0.0218
3.34	0.676	0.0236
4.92	0.807	0.0310
6.68	0.952	0.0365

Run: 258
 $Re = 305200$

α	C_l	C_d
-4.18	-0.211	0.0245
-2.44	-0.054	0.0193
-0.87	0.167	0.0129
0.23	0.346	0.0144
2.05	0.543	0.0159
3.63	0.685	0.0171
5.23	0.832	0.0192
7.07	0.999	0.0235
8.20	1.085	0.0265
9.87	1.201	0.0296

Run: 231

 $Re = 203300$

α	C_l	C_d
-4.02	-0.175	0.0182
-2.65	0.006	0.0132
-0.29	0.288	0.0092
0.40	0.355	0.0095
2.63	0.588	0.0115
3.50	0.675	0.0123
5.11	0.830	0.0145
6.63	0.971	0.0170
8.26	1.106	0.0201
9.79	1.195	0.0270
11.09	1.219	0.0393

Run: 233

 $Re = 305100$

α	C_l	C_d
-4.31	-0.175	0.0154
-2.53	0.049	0.0109
-1.03	0.201	0.0090
0.90	0.400	0.0084
2.22	0.543	0.0095
3.60	0.680	0.0106
5.06	0.822	0.0124
6.46	0.956	0.0142
8.11	1.094	0.0173
9.51	1.184	0.0227
11.24	1.224	0.0377

Appendix C

UIUC Low-Speed Airfoil Tests Manifesto

The UIUC Low-Speed Airfoil Tests Manifesto which appears below is a modified version of the initial announcement of the wind-tunnel test program written in December 1993. At the risk of being redundant with respect to what was included in the Preface, most of the original content of the announcement is retained. For recent information on the UIUC LSATs, please see the latest bulletin available from either the coordinator at the address given or from <http://uxh.cso.uiuc.edu/~selig> on the World Wide Web.

We are searching for a group of experienced modelers to build a variety of airfoil wind-tunnel models for tests at the University of Illinois at Urbana-Champaign (UIUC). A low-speed, low-turbulence wind tunnel has been instrumented to take lift and drag measurements on airfoils at low speeds over the Reynolds number range from 40,000 to 500,000 (40k to 500k). The scope of the airfoil wind-tunnel tests will be limited only by the number of wind-tunnel models provided and the amount of funding received. Hopefully, the proposed modeler-supported airfoil test program will become self-sustaining. Your support and help of any kind will be acknowledged in reports on the project to be published through SoarTech Publications (Herk Stokely). We plan to publish the results through SoarTech frequently—possibly twice per year.

A similar undertaking (with substantial support from modelers) was started by Michael Selig, John Donovan and the late David Fraser in 1987 at Princeton University. In a two year period, over 60 various low-speed airfoils were wind-tunnel tested, involving over 1200 hours of wind-tunnel test time. The results were published in SoarTech 8 in 1989, and many of the new airfoil designs produced and tested during the program are now widely used on R/C sailplanes. As of November 1993, over 2200 copies of SoarTech 8 are in circulation worldwide. SoarTech 8 is available from

SoarTech Publications
c/o H.A. Stokely
1504 N. Horseshoe Circle
Virginia Beach, VA 23451
e-mail: herkstok@aol.com

At the present time, there is a need for new airfoils for R/C sailplanes. For example, R/C handlaunch soaring is booming, but few good airfoils (e.g., E387 and SD7037) presently exist for such sailplanes. Sailplanes for the new F3J competition are just beginning to evolve, and new airfoils will probably be required. What will they look like? In the past, only a few airfoils (e.g., HQ 1.5/8.5, RG15 and SD7003) have been favored for F3B competition. In shape, handling and performance the SD7003 is quite different from the other airfoils mentioned. These significant differences suggest that it may be possible to design new airfoils that have better overall characteristics for F3B competition. In addition to the design and wind-tunnel testing of new airfoils, several existing airfoils should be tested. The SD7037 and RG15 are quite popular and often used with flaps. The flap effectiveness of these airfoils should be quantified through wind-tunnel tests, and the results should be used in the design of new airfoils.

There is also a need for new airfoils for R/C sport, aerobatic, and electric planes, as well as R/C helicopters. Often, NACA airfoils are used for these applications, but as compared with airfoils that could be designed today, many of the NACA airfoils (which were designed decades ago mostly by trial and error) are inferior. At the time the NACA airfoils were designed, little was known about the complex aerodynamics of airfoils operating at low Reynolds numbers. (Airfoils with small chords at low speeds, such as those on model aircraft, are said to operate in the low Reynolds number flight regime). In recent years, much has been learned about low Reynolds number aerodynamics, and this knowledge has successfully been applied to the design of new airfoils for R/C sailplanes, ushering in a new era in R/C soaring. Overall, R/C sailplane performance has improved dramatically. Older airfoils are no longer used. R/C power aircraft performance could likewise be dramatically improved through the use of newly designed, specially tailored airfoils.

Unique airfoil design requirements also exist for other categories of model aircraft. For example, FAI free flight aircraft (which incorporate both a powered launch segment and gliding flight) operate over a wide range of speeds. In the past, many airfoils with good performance characteristics have been designed for FAI free flight. These airfoils should be wind-tunnel tested to quantify their performance. The results gleaned from the tests could then be applied in the design process in an effort to develop new airfoils with improved performance. Also, the Society of Automotive Engineers (SAE) sponsors an annual model airplane design competition in which university student teams design, build and fly an R/C cargo aircraft. The record cargo weight that has been carried now stands at 24 3/4 lb for a model with a 60-size engine and 1200 in² total projected area. Conceivably, this record could be broken by an aircraft with an airfoil (or airfoils) specifically designed for the competition. Clearly, the need for new airfoils and data on existing airfoils is not limited just to R/C sailplanes, but applies to any type of model aircraft where better handling qualities and overall performance are desired.

Other topics of interest include the effects of turbulators and contour accuracy. Are boundary layer trips simply “repairs” to otherwise bad airfoils, or can trips be integrated with the airfoil and result in improvements over, say, the SD7037? The Princeton tests began to address this issue, but many questions still remain. For example, what is the best trip height for a given airfoil? Also, what is the best trip geometry, where should the trip be located for best performance, and what type of airfoils respond best to trips? The Princeton tests also shed some light on how accurate airfoils must be in order to achieve expected performance, but a more systematic effort should be made to test the best airfoils for sensitivity to contour accuracy. Also, we are interested in designing and testing families of airfoils for use in, say, transitioning from one airfoil at the root to a different airfoil at the tip. It is unlikely that the best performance can be obtained from a single airfoil used along the entire wing span. This is especially true for flying wings. Companion airfoils for blending should be designed for use with the most popular existing airfoils, e.g., SD7037 and RG15. It is expected that the practice of blending airfoils along the span will become much more popular than it is today. In an effort to maximize low Reynolds number airfoil performance for model aircraft, all of these topics should be addressed.

Overall, the UIUC test objectives will be to design and wind-tunnel test new airfoils for each category of aircraft listed above and also to examine the effects of flaps, turbulators and contour accuracy. We are especially interested in testing existing airfoils that are known to have superior performance. Wind-tunnel data on such airfoils will be used during the design of new and better airfoils. If you believe that we have overlooked an important area, we would be interested in your input and may consider expanding the scope of the project. The number of airfoil models to be tested has not been predefined; rather, it will be depend on the level of interest and support from the modeling community.

The wind-tunnel models should have a 33 5/8 in span with a 12 in chord and can either be built-up or foam core. To insure a uniform contour, the built-up models need to be fully sheeted. For the foam core models, we may be able to supply two 12 inch chord wing templates. The surface finish can either be fiberglass or monokote; however, we are interested in the effects of surface finish and will consider testing models with non-smooth surfaces. The models will be attached to the wind-tunnel balance by standard model wing rods. Standard model construction techniques should provide the necessary strength (supporting 15–20 lb of lift when pinned at both ends). The brass tubing and collars for the models will be supplied along with full-scale plots and/or coordinates of the airfoil, if requested. (Please contact us before starting any construction on a wind-tunnel model.)

The airfoils will be tested in the UIUC open-circuit 3 × 4 ft subsonic wind tunnel. The turbulence intensity level is minimal and more than sufficient to ensure good flow integrity at low Reynolds numbers. The experimental apparatus

used at Princeton will be modified for the UIUC tests. Lift and drag measurements for each airfoil will be taken at Reynolds numbers of 60k, 100k, 200k and 300k. In some instances, it may be possible to take limited data over an expanded range (40k–500k). The lift characteristics will be determined through force-balance measurements, while the drag will be evaluated by the momentum method through the use of pitot-static probes traversed through the airfoil wake at several spanwise locations. We are also interested in airfoil pitching moment measurements, but the current apparatus does not have such a capability. However, a pitching moment balance has been recently designed and should provide pitching moment data in the near future.

If you are interested in building wind-tunnel models for the tests or wish to request information, please write, fax or send e-mail to the coordinator

UIUC LSATs Coordinator
c/o Prof. Michael Selig
Dept. of Aeronautical and Astronautical Eng.
University of Illinois at Urbana-Champaign
306 Talbot Laboratory, 104 S. Wright St.
Urbana, IL 61801-2935
e-mail: uiuclsats@opus.aae.uiuc.edu
fax: (217) 244-0720

The program will be self-sustaining so long as funds are made available for equipment maintenance/upgrades and graduate student stipend support and tuition and fees (approximately \$16,000/yr per student). The initial goal is to raise enough money to support at least two graduate students for a three year period. It is envisioned that a small level of support from a large number of modeling enthusiasts could sustain the airfoil design wind-tunnel test program indefinitely. The impact on model aviation could be tremendous. Donations can be mailed to

Prof. Michael Selig
Dept. of Aeronautical and Astronautical Eng.
University of Illinois at Urbana-Champaign
306 Talbot Laboratory, 104 S. Wright St.
Urbana, IL 61801-2935
e-mail: m-selig@uiuc.edu

Please make checks payable to “University of Illinois, AAE Dept.” Also, please write on the check “Selig — Wind Tunnel Testing/AE Unrestricted Funds,” and provide a letter stating that your contribution is to be used by Prof. Selig and his group of students (both undergraduate and graduate) in support of the airfoil wind-tunnel tests. Finally, for a suggested donation of \$18 in US, Canada, and Mexico (or \$22 in other countries) you can receive a UIUC LSATs white short-sleeve shirt. All proceeds will go toward the continuation of the project.